強磁場新機能の開発

-強磁場印加による新プロセスと高機能ナノ材料の創製-

平成 15 年度～平成 17 年度

文部科学省 科学研究費補助金 特定領域研究

(領域番号 767)

研究成果報告書

課題番号:15085101

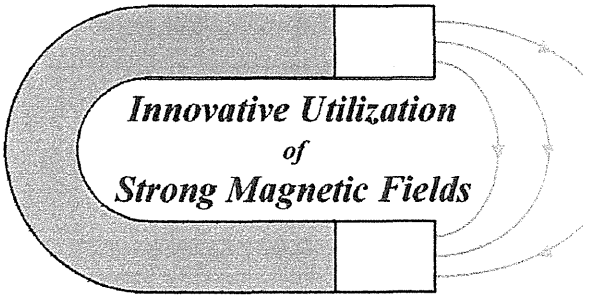

平成 18 年 5 月

領域代表者 山口益弘

(横浜国立大学・大学院工学研究院・教授)

はしがき

平成18年5月
領域代表 山口益弘

本冊子は，平成15年度から平成17年度の3年間にわたり実施された文部科学省科学研究費補助金特定領域研究「強磁新機能の開発―強磁場印加による新プロセスと高機能ナノ材料の創製―」(領域番号 767)の研究成果を報告するものである．本特定領域研究は，反磁性体・常磁性体などの弱磁性物質を主な対象として強い静磁場を印加する新しい材料プロセスを開発し、それにより高機能ナノ材料を創製することを目的とした．本領域の班員らが世界に先駆けて始めた研究により，化学反応，非磁性物質・結晶の組織，相転移などに対する磁場の影響が存在することは確認していた．これを発展させて「強磁場で新規の物質・材料を創り、その機能を制御する」という新たな科学分野（Magneto-Science と称する）を確立することをめざした．

すでに確固たる研究基盤が存在したので本領域研究は効果的に進捗した．「高磁気力場による材料制御」としては擬似無重力状態での高純度な結晶成長を実現し，宇宙環境実験に比して経費・機会・時間などあらゆる点で有利であることを示した．これにともない磁場環境での物質対流・化学反応の物理・化学が解き明かした．「磁場印加による組織制御」に関連した課題では，有機高分子・無機固体・金属・合金・生体物質など広範囲の物質系において共通の基礎学理に基づく取り扱いができるまでに進展した．その結果，磁場印加でしかなしえない3次元的な立体配向まで可能とし，加えて磁場配向の一般論を構築した．本特定領域研究の重要な目標であった基礎から応用へ「学理の体系化」が実現したといえる．「磁場印加によるナノ材料の創製と機能」に関連してナノサイズ粒子集団の整列を実現しり，DNA の高度分離法を生み出した．これらは本領域の研究によって新規に見出された磁場効果に基づいていることを強調したい．しかしながら，磁場効果は未知の面も多い．「水に対する磁場効果」の解明は，生命現象としても科学技術としても重要な課題である．本特定領域研究で初めて科学的にこの課題に向きあい，水の物性が磁場により影響を受けることを実証した．このほか本領域の研究成果から次世代の Magneto-Science へと展開する新しい課題が多々生み出されている．

本領域は，我が国で生まれ，わが国で育ったこの独創的な研究分野をさらに発展させて国内外に知らしめるという使命を帯びていた．研究会・国際シンポジウムの開催，ウエブサイトの公開，ニュースレターの刊行，英文テキスト”Magneto-Science”の発刊，関連する国際会議への参加，国内外研究機関との共同研究を行い，本領域の成果を国内外に周知し，かつ学問的な刺激を与えた．この新しい科学分野が世界的に認知されて，本領域を申請した際のキーワード「日本から世界へ」に添えたものと自負している．なお，本特定領域研究の遂行にあたり、評価委員ならびに外部学識者には研究の指針について貴重なご助言をいただいたことを感謝いたします．

平成18年5月
領域代表 山口益弘

目次

１．研究領域名

強磁場新機能の開発―強磁場印加による新プロセスと高機能ナノ材料の創製―

２．代表者名

山口益弘（横浜国立大学大学院工学研究院・教授）

３．研究期間

平成15年度～平成17年度

４．研究経費

交付決定額（配分額）　（単位：千円）

年度	直接経費	間接経費	合計
平成15年	136,400	0	136,400
平成16年	111,500	0	111,500
平成17年	57,600	0	57,600
総計	305,500	0	305,500

５．研究組織

総括班「強磁場新機能の開発―強磁場印加による新プロセスと高機能ナノ材料の創製―の総括」

研究代表者　山口益弘（横浜国立大学・大学院工学研究院・教授）

研究分担者　谷本能文（広島大学・大学院理学研究科・教授）

尾関寿美男（信州大学・理学部・教授）

木村恒久（首都大学東京・都市環境学部・教授）

評価担当者　長倉三郎（日本学士院・院長）

北沢宏一（科学技術振興機構・理事）

本河光博（東北大学・名誉教授）

林　久治（学習院大学・客員教授）

研究協力者(外部学識者)

青柿良一（職業能力開発総合大学校・教授）

浅井滋生（名古屋大学・大学院工学研究科・教授）

安宅光雄（産業総合研究所・人間系特別研究体・グループリーダー）

上野照剛（東京大学・大学院医学系研究科・教授）

岸尾光二（東京大学・大学院工学系研究科・教授）

北原和夫（国際基督教大学・理学科・教授）

三浦　登（東京大学・名誉教授）

宮越順二（弘前大学・医学部・教授）

和田　仁（東京大学・大学院新領域創成科学研究科・教授）

渡辺和雄（東北大学・金属材料研究所・教授）
渡辺恒雄（首都大学東京・都市教養学部・教授）
渡会　仁（大阪大学・大学院理学研究科・教授）

計画研究班

研究課題ア「磁気浮上炉による材料プロセスの開発」
研究代表者　茂木　巖（東北大学・金属材料研究所・助手）
研究分担者　高橋弘紀（東北大学・金属材料研究所・助手）

研究課題イ「高磁気力による微小重力場の生成と高機能性材料の創製」
研究代表者　谷本能文（広島大学・大学院理学研究科・教授）
研究分担者　藤原昌夫（広島大学・大学院理学研究科・助手）
大庭　亨（宇都宮大学・工学部・助手）
藤原好恒（広島大学・大学院理学研究科・助教授）
岡崎正治（産業技術総合研究所・総括研究員）
中垣良一（金沢大学・大学院自然科学研究科・教授）

研究課題ウ「強磁場を用いた高分子材料の構造制御」
研究代表者　木村恒久（首都大学東京・都市環境学部・教授）
研究分担者　山登正文（首都大学東京・都市環境学部・准教授）
櫻井伸一（京都工芸繊維大学・繊維学部・助教授）
斎藤　拓（東京農工大学・工学部・助教授）

研究課題エ「強磁場による自己構造構築と機能操作」
研究代表者　尾関寿美男（信州大学・理学部・教授）
研究分担者　藤尾克彦（信州大学・理学部・助手）
飯山　拓（信州大学・理学部・助手）
勝木明夫（信州大学・教育学部・助教授）

研究課題オ「強磁場を用いた新しい物質分離法の開発」
研究代表者　山口益弘（横浜国立大学・大学院工学研究院・教授）
研究分担者　島津佳弘（横浜国立大学・大学院工学研究院・助教授）
山本　勲（横浜国立大学・大学院工学研究院・助教授）
広田憲之（物質・材料研究機構・研究員）
木吉　司（物質・材料研究機構・副センター長）
阿部晴雄（物質・材料研究機構・主席研究員）

研究課題カ「強磁場印加プロセスによる金属・酸化物の組織制御と新機能性材料の創製」
研究代表者　掛下知行（大阪大学・大学院工学研究科・教授）

研究分担者　植田千秋（大阪大学・大学院理学研究科・助教授）
福田　隆（大阪大学・大学院工学研究科・講師）
寺井智之（大阪大学・大学院工学研究科・助手）

研究課題キ「磁場印加プロセスによる有機・無機複合ナノ粒子の創製と機能性ナノ素子の開発」
研究代表者　森田　浩（千葉大学・工学部・教授）
研究分担者　稲場秀明（千葉大学・教育学部・教授）
米村弘明（九州大学・大学院工学研究院・助教授）

研究課題ク「強磁場が誘起する液体の構造転移と新機能の創製」
研究代表者　中林誠一郎（埼玉大学・理学部・教授）
研究分担者　坂口浩司（静岡大学・電子工学研究所・助教授）

６．研究成果の概要

磁気浮上炉による材料プロセスの開発

茂木　巖，高橋弘紀
東北大学金属材料研究所

概要

30T級ハイブリッドマグネットを用いて反磁性物質を浮上させ，材料の無容器溶融凝固を可能にする磁気浮上炉の開発に成功した．磁気浮上炉での物質合成を行うために反磁性物質の熱的挙動の観察を行い，反磁性流体においても熱対流を勾配磁場により制御せきること，磁気浮上した高分子試料が不均一加熱により激しく回転運動することなどの新しい現象を見出した．　これらの結果から磁気浮上状態に対する理解を深め，様々な物質の無容器溶融凝固を可能にする均一加熱磁気浮上炉を開発し，高分子の球状試料の作製することができた．

1. はじめに

反磁性物質が磁場から受ける斥力が重力とバランスするほど大きくなると，物質は浮上する．これが磁気浮上である（図1）．地上でできるこの擬似無重力状態を材料プロセスに応用することは極めて有意義である．本研究は，30T級ハイブリッドマグネット（図2）[1]を用いて反磁性物質を浮遊させ，無容器での材料の溶融凝固プロセスを開発するものである．磁気浮上状態での物質の加熱に際し，自然対流や磁気対流，配向や運動などの熱的挙動に関する基礎データを蓄積し磁気浮上状態に対する理解を深め，それを礎に磁気浮上の特徴を活かした最適の溶融凝固プロセスを提案する．

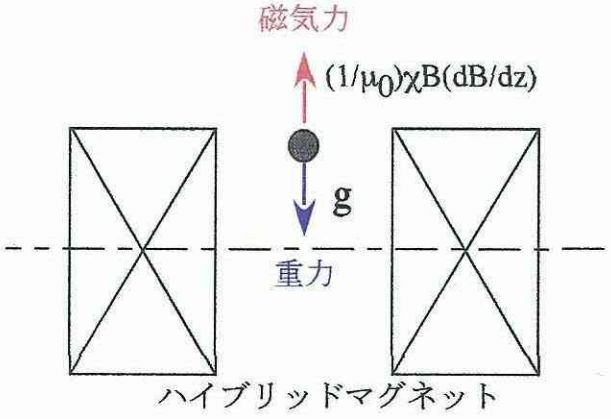

図1　反磁性物質の磁気浮上

図2　東北大学の無冷媒型ハイブリッドマグネット．無冷媒型超伝導マグネットの内側に大電力水冷マグネットが組みこまれている

2. 磁気浮上状態における物質の挙動

2.1 熱対流の制御

磁気浮上を材料プロセスに応用する上で，勾配強磁場下における物質の挙動を理解することは重要である．そこで，材料プロセスに重要な液体の熱輸

送と対流の様子を勾配強磁場下で調べてみた．[2] マイクログラビティ環境では，密度差に起因する液体の自然対流は消失するため，良質の結晶を育成する実験が行われている．同様の効果を期待して，勾配強磁場下で結晶成長の実験が行われているが，対流の様子を直接観察した例はなかった．

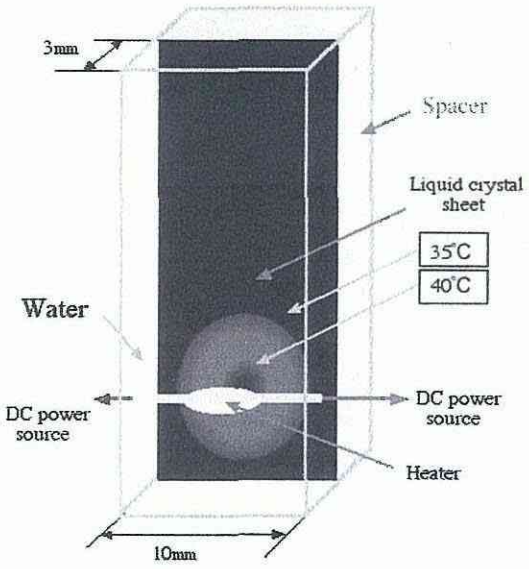

図３　水の熱対流を観察するためのセル

水を薄型セルに入れ，セル内に設置したヒーターにより加熱する．そのときの熱輸送の様子を，特定の温度（20–25, 35–40, 40–45℃）に反応して変色する液晶シートを用いて可視化した（図３）．反磁性の水に磁気浮上に相当する磁気力場 $B(\mathrm{d}B/\mathrm{d}z) = -1360\ \mathrm{T^2 \cdot m^{-1}}$ を印加した状態でヒーターを加熱すると，熱対流は通常とは著しく異なる様相を呈した．ゼロ磁場においてヒーター上方へと立ち上る熱対流は，磁気浮上状態ではほとんどみられなくなり，35–40℃の温度域ではマイクログラビティ状態で生じる熱伝導に近い振る舞いが観察された（図４(a)）．しかしよく見ると，上下の変色域が非対称になっており，熱対流が完全には消失していないことも確認された．同じ実験を20–25℃で変色する液晶シートで行うと，より明瞭に熱対流が観察された．[3]

温度 t_1 の液体の中で，温度 t_2 に温められた液体にかかる力は，体積磁化率 χ_v と密度 ρ を用いて

$$F = (1/\mu_0)\{\chi_v(t_2) - \chi_v(t_1)\}B(dB/dz) - \{\rho(t_2) - \rho(t_1)\}g, \qquad (t_2 > t_1) \qquad (1)$$

と書くことができる．ここで，B は位置 z における磁束密度，μ_0 は真空の透磁率である．もし液体の質量磁化率 χ_g に温度依存性がないとすると，磁気浮上状態では $F=0$ となり，たしかに熱対流は消失する．ところが，水の場合 $|\chi_g|$ は温度上昇に伴いわずかに大きくなることが報告されている．$t_2 - t_1 = 1$℃の仮定のもと $F=0$ となるような磁気力場の値を求めてみると，実験の温度域20

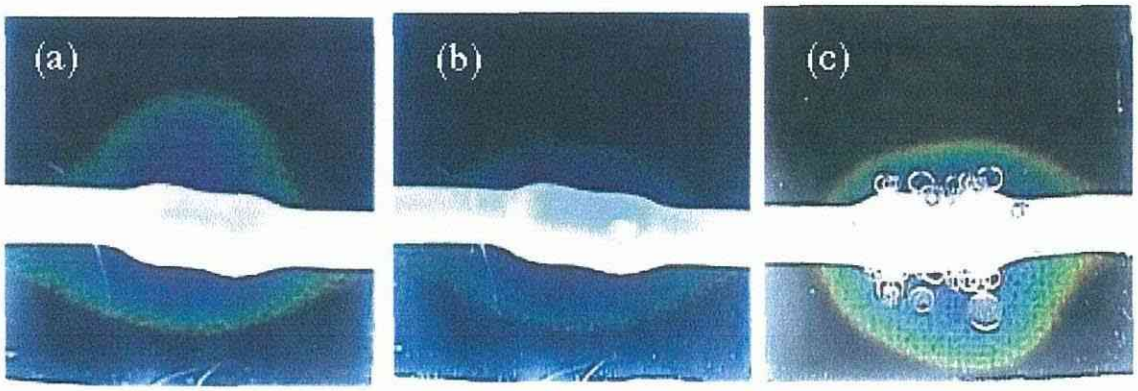

図４　勾配磁場中での水の熱輸送. (a)磁気力場 $B(\mathrm{d}B/\mathrm{d}z) = -1360\ \mathrm{T^2 \cdot m^{-1}}$, 温度35–40℃, (b) 磁気力場が $-2880\ \mathrm{T^2 \cdot m^{-1}}$, 温度35–40℃, (c) 磁気力場が $-2880\ \mathrm{T^2 \cdot m^{-1}}$, 温度40–45℃.

～45℃ではおよそ–2000 ～ –4000 $T^2 \cdot m^{-1}$ という値になる．このことは，磁気浮上状態ではマイクログラビティとは異なり，水の熱対流はなくならないことを意味している．さらに，20℃付近では体積磁化率の変化が小さいことから，より大きな磁気力場が必要なこともわかる．このことは，20–25℃でより明瞭に熱対流が観察されたこととよい一致を示している．

さらに磁場を強くして，磁気力場が–2880 $T^2 \cdot m^{-1}$ になったとき，35–40℃でほぼ完全に対流が消失し，熱伝導の状態が観察された（図4(b)）．また同じ勾配磁場下で温度を40–45℃にすると，こんどは下向きに対流が発生することが確認された（図4(c)）．F=0 とするための磁気力場の絶対値は温度上昇とともに小さくなるため，高温では磁気力項が重力項よりも大きくなり，下向きの磁気対流が発生したことがわかる．

これらの結果は，磁気浮上状態がマイクログラビティとは等価ではないが，勾配磁場により液体の熱対流を制御できることを示しており，物質合成にとって大きなメリットとなるはずである．

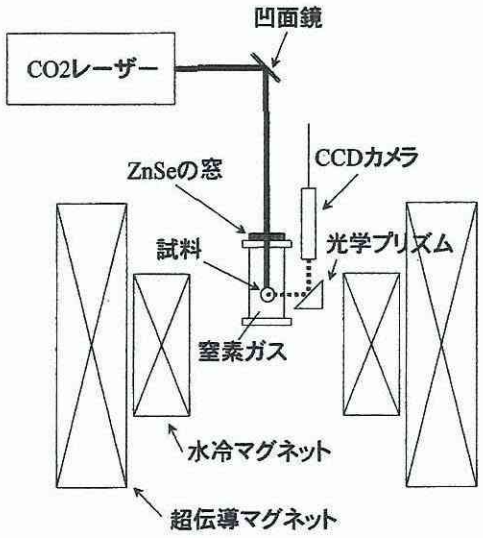

図5　CO_2 レーザー加熱磁気浮上炉

2.2 加熱により誘起される運動

炭酸ガスレーザー加熱の磁気浮上炉（図5）を用いて，数種類の有機ポリマーや分子性結晶の浮遊溶融を試みた．多くの物質で加熱により上下動や回転運動が観察された．特に激しい運動を示したのが PMMA（ポリメチルメタクリレート）の円柱状のペレットである．レーザー光が浮上試料の重心付近に照射されたときには試料はまず上昇し，水平方向のポテンシャルエネルギーに安定点がなくなると壁に向かって移動する．レーザー照射がはずれると温度が下がり，元の浮上位置に戻る．レーザーを照射している間はこの運動を繰り返す．この結果は，PMMA の反磁性磁化率が温度上昇とともに大きくなることを意味している．マグネットの磁気力場分布を考慮すると，2%程度磁化率が変化するだけでこのような運動が起こるものと推察された．また，レーザー光が

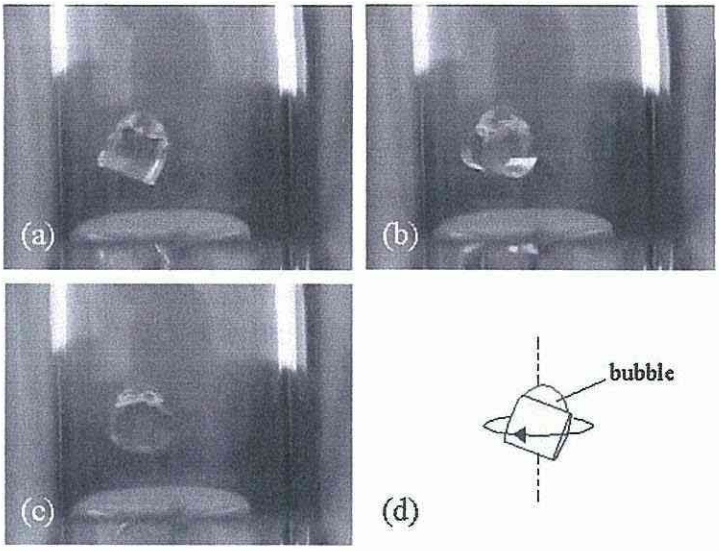

図6　レーザー照射による磁気浮上物質の回転運動．試料はPMMA（ポリメチルメタクリレート）．

不均一に照射された場合には，水平面内での回転運動が観察された（図6）．さらに，レーザー光の照射位置が変わると，円柱の軸を中心とする回転運動なども観察された．いずれも，反磁性磁化率の増加と，不均一加熱による試料内の温度分布に起因しており，磁化率変化によるポテンシャルエネルギーの増大が運動エネルギーに変換された結果生じたものである．従来，反磁性磁化率の温度依存性はほとんど無視されてきたが，数パーセント程度の磁化率の変化であっても，磁気浮上状態では大きな浮上位置の変化をもたらすので，磁気浮上炉の設計には重要となる．

また，熱伝導率の小さな高分子試料をレーザー加熱すると，図6の気泡の発生からもわかるように，局所加熱により高分子が分解してしまう．このような問題を解決するためには，より穏やかに均一加熱できる磁気浮上炉を開発をする必要がある．

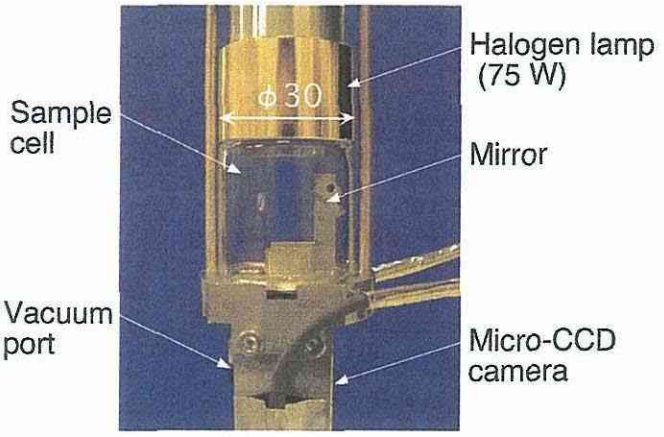

図7　赤外線ランプ磁気浮上炉

3. 磁気浮上炉の開発と物質合成

3.1 均一加熱の磁気浮上炉の開発

上述の観察結果をもとに，新たに二種類の磁気浮上炉の開発を試みた．小型の赤外線ランプを直接マグネットボア内に挿入する形式の赤外線ランプ炉の開発と，白金ヒーターを用いた電気炉の磁気浮上炉としての使用を試みた．

図7に示した赤外線ランプ炉は，マグネットのボア内に設置した小型ハロゲンランプで浮上試料を直接照射するタイプのもので，単純な構造ゆえに極めて操作しやすく，しかも安価に製作できる磁気浮上炉となった．これは高分子や分子性結晶を扱うために開発したもので，レーザー光に比べより均一に光を照射し，より穏やかな加熱ができ，また，白色光であるためより多くの種類の物質を対象にできるという利点がある．

高分子の無容器溶融にはさらに均一

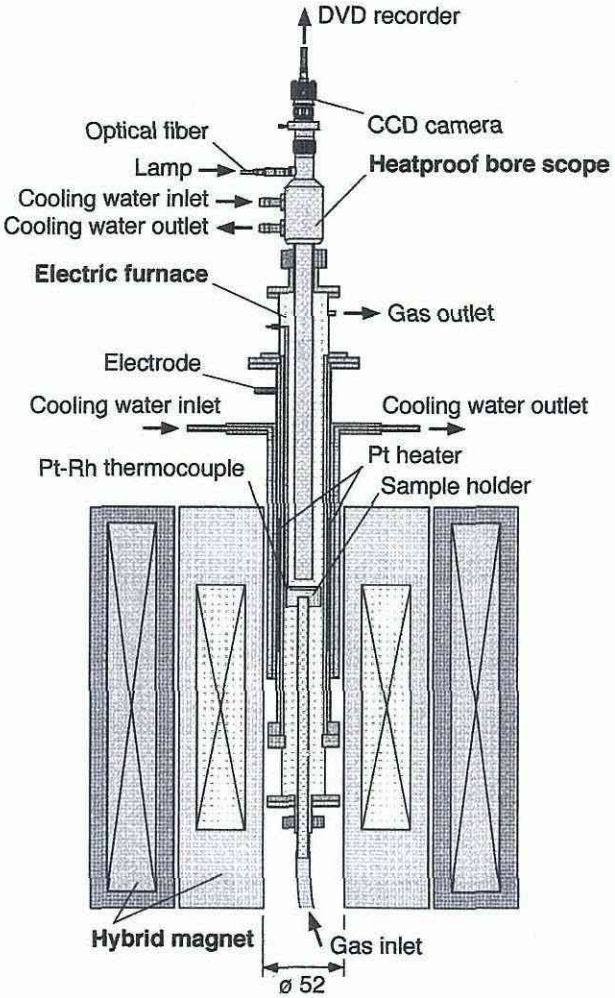

図8　均一加熱磁気浮上炉．白金ヒーターを用いた電気炉に耐熱ボアスコープを組み合わせ，30T，800℃までの加熱挙動の観察が可能になった．

な加熱を必要とするために，電気炉を用いた磁気浮上炉の開発を行った．[4]白金ヒーターを用いて1200℃まで加熱できる電気炉は，これまでに様々な試料の磁場中熱処理に用いられてきたが，試料空間全体が高温となるため観察系を組み込むのが困難であった．そこで我々は800℃まで使用できる耐熱ボアスコープを電気炉上部から挿入することにより，この問題を解決した．図８がその模式図である．この磁気浮上炉を用いることにより，レーザー炉では局所加熱が起こるために試料全体を溶融できなかった高分子試料や粉体試料などの加熱と溶融状態の観察が可能となった．

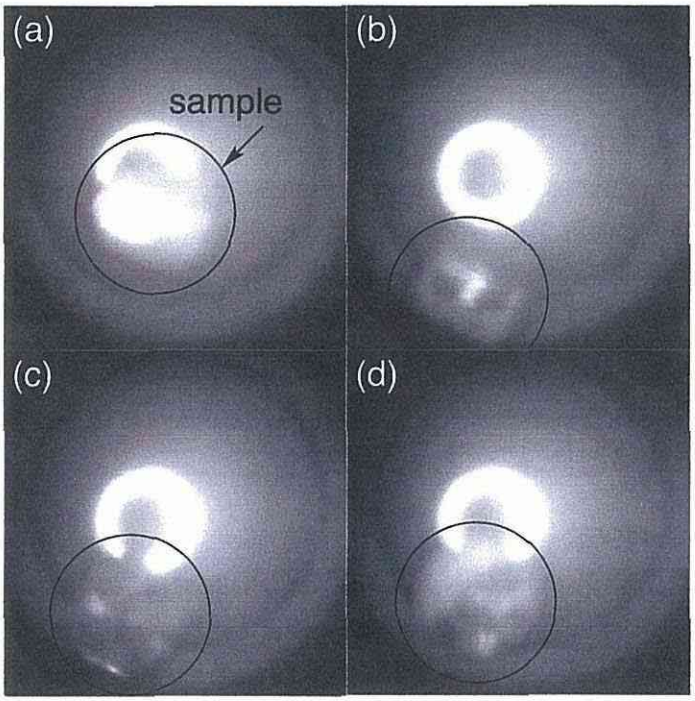

図９　均一加熱磁気浮上炉を用いたシクロオレフィンポリマーの無容器溶融凝固．中心磁場 18T．(a)18℃，(b)147℃，(c)213℃，(d)226℃．

3.2 浮上物質に働く磁気力解析

磁化率のより小さい物質を浮上させる場合，マグネットが発生する磁場分布のみならず磁気浮上炉内における試料近傍の磁場分布をより詳細に検討する必要があることが分かった．試料を安定に浮上させるためには，試料近傍の磁場分布を必要以上に乱さないことが重要であり，磁気浮上炉においてはよりシンプルな構造が求められる．電気炉を用いた際に，径方向の安定点がマグネットの中心からずれているような試料の挙動が観察されている．これを検証するためには，磁場中に設置された電気炉も含めた磁場分布を詳細に検討する必要あり，今後の検討課題である．

3.3 球状配向ポリマーの合成

均一加熱磁気浮上炉を用いて，２種類の透明プラスチック試料の球状試料作製を試みた．[3] 試料はPMMAとシクロオレフィンポリマーZEONEX（日本ゼオン）である．図９は磁気浮上炉内でシリンダー状の ZEONEX 試料（図９(a)）が，213℃で溶融し始め（図９(c)），226℃で球状になる様子（図９(d)）を示したものである．図10(a)は得られた球状試料の写真である．ゼロ磁場で同様に作製したもの（図 10(b)）が重力により偏平な形をしているのに比べると，磁気浮上炉では明らかに重力の相殺効果がみられる．今後，歪みのない高品位の光学材料の作

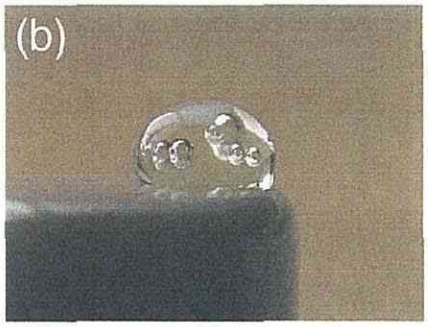

図 10　(a)磁気浮上炉で作製したZEONEX の球状試料，(b)ゼロ磁場で作製した試料

製に応用が期待される．ただし，試料内に気泡が見られることから，より高品質の試料作製を目指す上では溶融凝固条件の最適化が必要である．

4. おわりに

反磁性物質の磁化率の温度依存性は，磁気浮上状態での物質の熱的挙動を左右する重要な因子となることがわかった．このことを利用して，磁気浮上状態での反磁性磁化率の精密測定装置の開発が期待できる．反磁性物質の磁化率は，電子状態や化学結合の状態を反映しているはずであるから，その温度依存性の解明は重要である．今後，「反磁性物質の磁性と磁気化学」という新たな分野にまで発展することを期待したい．また，ここで開発した磁気浮上炉を，ボールテクノロジーのための球状試料作製や，過冷却状態からの球状単結晶析出などに応用し，機能性物質合成の新しい材料プロセスに展開させたい．

参考文献

[1] K. Watanabe, G. Nishijima, S. Awaji, K. Takahashi, K. Koyama, M. Motokawa, M. Ishizuka, T. Hasebe and J. Sakuraba, Advances in the first cryogen-free hybrid magnet, IEEE Trans. on Appl. Supercond. 14 (2004) 388-392.

[2] I. Mogi, C. Umeki, K. Takahashi, S. Awaji, K. Watanabe and M. Motokawa, Control of Thermal Convection in Water by Strong Gradient Magnetic Fields. Jpn. J. Appl. Phys. 42 (2003) L715 - L717.

[3] I. Mogi, C. Umeki, K. Takahashi, S. Awaji, K. Watanabe and M. Motokawa, Heat Transfer in Water under Strong Gradient Magnetic Fields, IEEE Trans. On Applied Superconductivity, 14 (2004) 1682-1684.

[4] K. Takahashi, I. Mogi, T. Onogi, S. Awaji, M. Motokawa and K. Watanabe, Materials processing in magnetic levitation furnaces, Sci. Tech. Adv. Mat.(2006) (in print)

高磁気力による微小重力の生成と機能性材料の創製

谷本能文[1]，藤原好恒[1]，藤原昌夫[1]，中垣良一[2]，岡嵜正治[3]，大庭　亨[4]
1広島大学・大学院理学研究科，2金沢大学・大学院自然科学研究科
3産業技術総合研究所・計測フロンティア研究部門，4宇都宮大学・工学部

概要

本研究では，最大15Tの強磁場，1500 T^2/m の高磁気力により作り出された擬似微小重力場・過重力場のキャラクタリゼーションとその応用について研究するとともに，強磁場・高磁気力による機能性物質のマクロ構造・形態の制御，ナノ構造制御の新手法の開拓，高機能性材料の創製にチャレンジした。

1. はじめに

物質はそれぞれ固有の磁性（反磁性・常磁性・強磁性）をもっている。この物質固有の特性を使って化学反応や物理変化を制御できたらというのは多くの科学者の夢であった。最近超伝導磁石が容易に使えるようになり，ごく普通の反磁性物質でも顕著な磁場効果が得られることから特に注目を集めるようになった。磁場は，クリーンで低コスト・環境にやさしい新しい物理環境場であり，磁場効果の研究と応用技術の開発は２１世紀の新産業を支える基盤のひとつとして重要な位置を占めるものと期待される。ここでは，誰でも自由に使うことのできる強度の磁場—最大15T，1500 T^2/m の強磁場—によって引き起こされる新規物理環境の特性の解明とその応用について研究を行った。

2. 高磁気力場のキャラクタリゼーション

図１に本研究に用いた高磁気力用超伝導磁石を示す。本超伝導磁石は直径40 mmの空間に，最大15 T，1500 T^2/m の垂直強磁場を１年以上連続して発生できるところに特色があり，水・ミニトマト・カエルなどの反磁性物質の磁気浮上が可能である。そこで本超伝導磁石を用いて種々の研究を行った。

図１．高磁気力用超伝道磁石

光反応を利用した熱対流の磁場中その場観察：ある種の有機化合物に紫外光照射すると，光反応が起こり光を吸収した部分が着色する。と同時に，光エネルギーの一部は熱となり，着色溶液の温度上昇を引き起こす。熱対流の観察に好都合である。そこで，先ずベンゼン溶液の熱対流について研究した。Diarylethene 誘導体 (D) のベンゼン溶液（無色）の入った石英セルの底を数秒間レーザー照射すると，光異性化反応によりセルの底に赤紫色の着色溶液が生成する(図２)。

ゼロ磁場では照射５秒後に底から離れ，上昇する。$-1500T^2/m$ の磁場中では約９秒後に底から離れ，その後速やかに上昇した。一方 $+1200T^2/m$ の磁場中では，着色溶液は約２秒後に底からはなれ，ゆっく

りと上昇した。そして，今度は逆にゆっくりと下降した（Uターン現象）。Dが吸収した光エネルギーは，一部は異性化反応に使われ，残りは熱エネルギーとなりベンゼン溶媒の温度上昇(体積膨張)に使われる。

温度上昇した着色溶液の容器底での滞留時間は着色溶液にかかる圧力 ΔP に比例する。

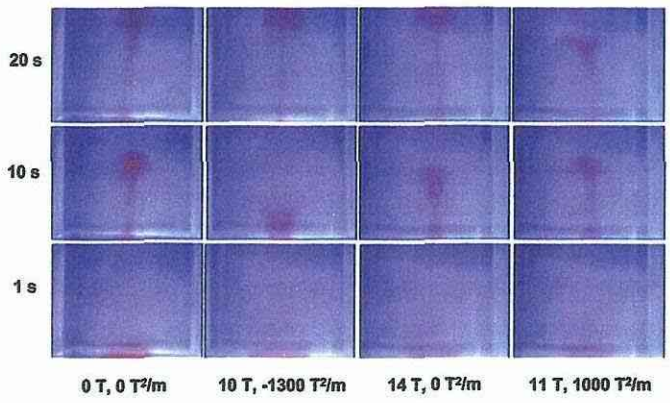

図２．ベンゼン溶液の熱対流　時間は，光照射後の時間を示す（側視）

$$\Delta P = (\Delta\rho_{solution})gh + (\Delta\chi_{benzene})(1/\mu_0)hB\partial B/\partial z + (\chi_{PI} - \chi_{CMTE})\,c(1/\mu_0)hB\partial B/\partial z \quad (1)$$

(1)式の右辺第一項は溶液の体積膨張による密度変化による浮力，第二項は溶媒の体積膨張による磁化率変化による磁気力，第三項は溶質の光異性化による磁化率変化による磁気力である。ゼロ磁場では(1)式右辺第一項の浮力により着色溶液が容器底からはく離するが，磁場中では第二項，第三項による磁気力が作用する。-1500T²/m では第二項の値の大きさは第一項と同程度で方向は逆となり，ΔP がほぼゼロのためはく離に時間を要する。逆に+1200T²/m では第二項の値が第一項と同程度で同じ方向になるため高圧力となり，はく離が促進されたものである。第三項の値は時間に依存しないのに対し，第一項と第二項は時間とともにその値は小さくなる。このことから，Uターン現象は値の小さな第三項により引き起こされたものと推測された。[1]

ジフェニルアミンと四臭化炭素の光反応を利用してベンゼン溶液の熱対流のその場観察をしたところ，溶質の濃度に依存したさまざまな対流パターンが観察され，溶質濃度が高いときはその磁化率変化が対流に大きな寄与をすること，垂直磁場勾配のみならず半径方向の磁場勾配が大きな影響を及ぼすことなどが分かった。[2]

<u>プラスチックの磁気浮上・磁気分離</u>：勾配磁場中に反磁性物体を置くと磁気力（$F_m = (m\chi/\mu_0)B\partial B/\partial z$）が作用する。この磁気力と重力（mg）が物体全体として釣り合うとき，物体は浮上する（磁気浮上）。

$$(m\chi/\mu_0)\,B\partial B/\partial z = mg \quad (2)$$

ポリエチレンなどのプラスチックチップの磁気浮上を図１の超伝導磁石中で行なった（図３）。プラスチックの種類によりその磁化率は異なる。本超伝導磁石では，ポリエチレンやポリアミドなどは磁気浮上するが，ポリ（エチレンテレフタレート）は磁気浮上しない。さらに，超伝導磁石中の $B\partial B/\partial z$ の値は場

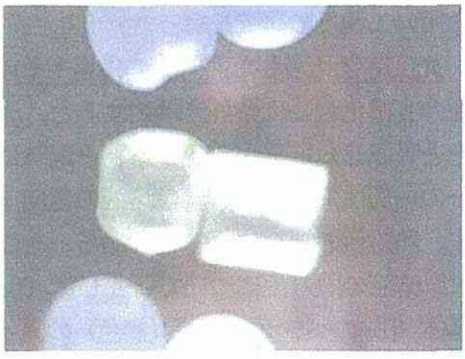

図３．プラスチックチップの磁気浮上（側視）　上から順にポリエチレン，ポリスチレン，ポリアミド

所により異なるため，プラスチックの種類により磁気浮上位置が異なる。プラスチックチップの磁気浮上位置から，逆にその磁化率が直読できることが分かった。つぎに，磁気浮上を利用して，ポリプロピレン，ポリアミド，ポリ（エチレンテレフタレート）チップの磁気分離を行い，それらの分離に成功した。[3]

高磁気力によるたんぱく質結晶の高品位化：宇宙では無重力のため重力による対流がないためX線結晶学的に高品位のたんぱく質結晶を作成できることが知られている。磁気力と重力が物体の任意の点で釣り合う時，擬似的にその物体は微小重力状態となる。そこで磁気力を利用した擬似微小重力場で，宇宙と同様に高品位な結晶をつくることができるかどうかリゾチームたんぱく質結晶を例に検討した。磁場中とゼロ磁場で作成した結晶のX線構造解析を行ない，B因子を求め比較した。図4に示すように，ゼロ磁場で作成した結晶のB因子の値は約16.0であったが，磁場による擬似微小重力場（μG）で作成した結晶では約15.0，1.8Gの擬似過重力場下で作成した結晶は約15.8となり，磁場による擬似微小重力場を用いることにより高品位なたんぱく質結晶をつくることが可能なことが，世界ではじめて実証された。[4]

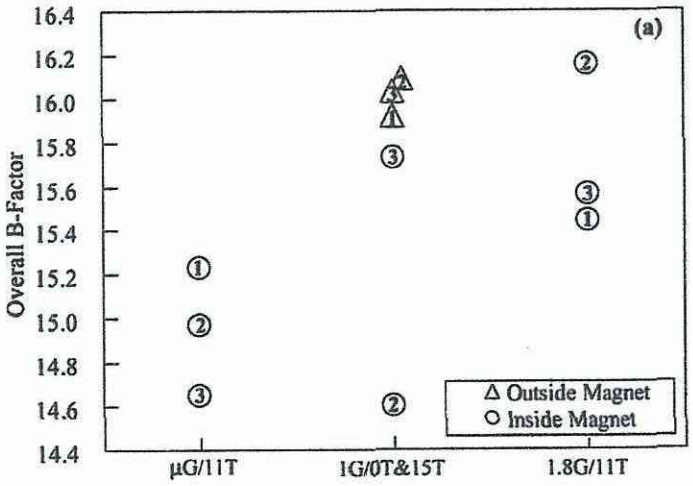

図4．リゾチーム結晶のB因子に及ぼす磁場・重力の影響　△，磁石の外；　○，磁石の中

形態的キラリティーの磁気誘導：ケイ酸ナトリウムと重金属塩の反応により生成するケイ酸金属の半透膜チューブの形態の磁場効果について検討した。その結果，図5a,bに示すように，硫酸亜鉛結晶を使った場合，右巻きの半透膜チューブができ、3次元形態的キラリティーの磁気誘導に世界で初めて成功した。すなわち3 T ～15 Tの垂直強磁場により右巻きまたは左巻き螺旋の半透膜チューブを選択的につくることができることがわかった。この磁場効果は，水溶液中のイオンに対するローレンツ力が原因と推定される。この新規現象が一般性のある現象かどうか，またメカニズムの詳細について解明するため，他の反磁性・常磁性金属塩結晶についての研究を行った。その結果反磁性の塩化マグネシウムや常磁性の硫酸銅の場合も，硫酸亜鉛の場合と同様に右巻き・左巻きのチューブを磁場で自由に

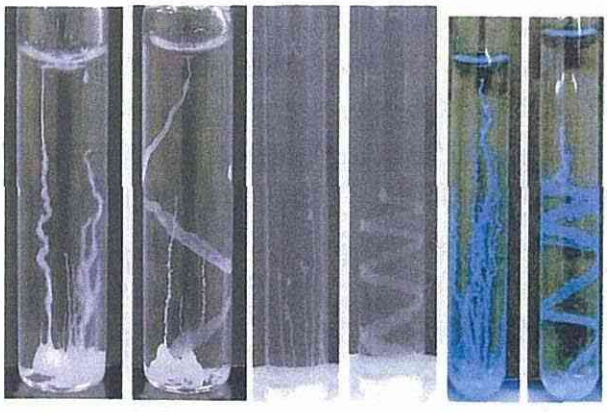

図5．シリケートガーデン反応の磁場効果　(a)，(b)は$ZnSO_4$，(c)，(d)は$MgCl_2$，(e)，(f)は$CuSO_4$塩の場合，それぞれ前者はゼロ磁場，後者は15Tの磁場中で作成した半透膜チューブ

誘導できることが分かった。また，容器壁から離れたチューブは，磁場の印加により捩れて成長することが分かった。すなわち，３次元形態的キラリティーの磁気誘導はシリケートガーデン反応（ケミカルガーデン反応）に一般的な現象であることがわかった。これらの結果は，反応中の溶液の磁場中その場観察の結果から，半透膜チューブ先端からの内溶液の噴出流中のイオンに対するローレンツ力によるが，その方向はチューブと周囲との相対条件により決まるという，Boundary-assisted MHD 機構によることが解明された。[5]

さらに硝酸銀イオンと金属銅により析出する銀樹の２次元パターンに対する垂直磁場効果を検討し，銀樹パターンに対する磁場効果は上記機構によることを確認した。さらに，高磁場中の反応では，磁化率勾配力（$(1/2\mu_0)\ (\partial\chi/\partial r)B^2$）が反応に大きな影響を持つことを示すことができた。電気化学反応では常磁性物質の場合このような力が作用することが知られているが，強磁場では反磁性物質でも磁化率勾配（濃度勾配）による力の影響が大きいことが明らかとなった。[6]

3. ビニルカルバゾールの高機能化

ポリビニルカルバゾール（PVC）を用い，その溶液から薄膜を作製して高機能化を検討した。結果を図６に示す。11 T（微小重力），最大中心磁場 15 T（通常重力），12 T（過重力），磁石外 0 T（通常重力）のそれぞれにおいて，PVC のクロロホルム溶液から石英基盤を磁場方向と同じ鉛直方向へ引き上げて PVC 薄膜を作製したところ，強磁気力存在下つまり微小重力と過重力環境において，膜表面に種々の大きさのナノホール（例えば直径 222nm x 深さ 33nm）の出現が確認された。これは予想外の効果であり，今のところメカニズムは明らかではない。しかし，おそらく固液界面もしくはできたばかりのウエットな薄膜表面から気化したクロロホルム蒸気拡散に対する磁気力の効果と考えられる。0 T と 15 T の通常重力下においては，膜表面は一様になだらかであった。

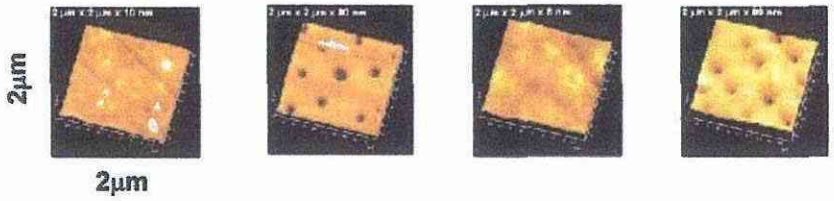

図６．ポリビニルカルバゾール薄膜の磁場効果
(a) 0 T, (b) 11T, −1500 T^2/m (c) 15 T, $0T^2/m$ (d)12 T, $+1200T^2/m$

次に，ガラス基盤を水平から少し傾けて PVC のクロロホルム溶液に浸し，上記の４カ所の磁場（磁場方向は基盤にほぼ垂直になる）において溶媒蒸発法によって薄膜を作製したところ，縞様パターンが形成され，その縞様パターンの間隔に磁場強度による違いが観察された（図７）。つまり，０ T では縞様パターンの幅・間隔共に 40μm 前後であったものが，微小重力では幅は約 15 μm と狭く間隔は約 70 μm と広がった。過重力では幅は約 70 μm

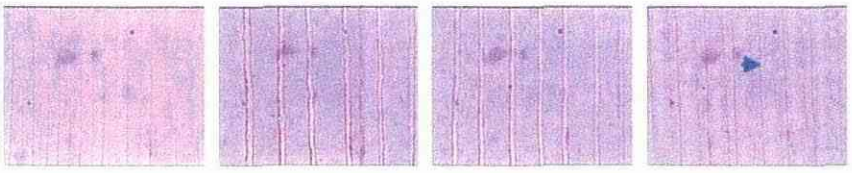

図７．ポリビニルカルバゾール薄膜の磁場効果
(a) 0 T, (b) 11T, −1500 T^2/m (c) 15 T, $0T^2/m$ (d)12 T, $+1200T^2/m$

と広く間隔はやや狭くなった。このパターン形成は非線形現象であるが，クロロホルムの蒸発方向とその速度に対する磁気力の効果と推定された。以上２つの薄膜形成時の磁場効果は，磁場中で作製したPVC薄膜に一様な平滑な表面しかもたない薄膜には無い機能を与えていることを示す。しかもそれが強磁気力を用いた微小重力や過重力で獲得できるので，PVC膜に新機能の発現の下地を強磁場によって作ることができたといえる。

さらに，ポルフィリンナノロッドの磁気配向を試みた。８Ｔの水平磁場により長さ約10μｍのナノロッドは磁場により配向したが，長さ約１μｍのナノロッドは配向しなかった。そこで，図１の磁石を使い垂直磁場による長さ約１μｍのナノロッドの配向を試みたところ，+1200 T^2/m の過重力場中でのみロッドの配向を示唆する結果が得られた。この結果は磁気力によるロッドの沈降速度の増加と推察された。

4. 機能性有機結晶の高品位化

導電性有機材料であるの結晶性の有機化合物（ペンタセン）と非結晶性の高分子化合物（ポリチオフェン誘導体）の２種類について，強磁場印加の効果を検討した。

まず，ペンタセンに対して，鉛直強磁場下（15T）で真空蒸着によってその結晶の薄膜を基盤上に調製した。蒸着方向は磁場と平行である。基盤平面の角度を磁場と90°（垂直），30°（平行に近く傾けた）の場合について実験を行った。成長した結晶のAFM像を比較すると，結晶はさまざまな方向を向き，磁場印加によって配向は観測できなかった。気体ペンタセン分子の磁気配向エネルギーが熱エネルギーと比べ著しく小さいため，配向が起こらなかったものと推定された。

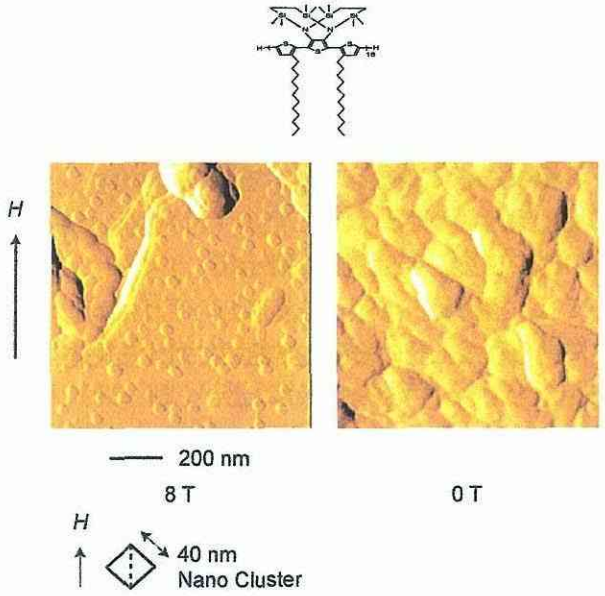

図８．ポリチオフェン誘導体ナノクラスターの磁気配向

次に，ポリチオフェン誘導体（図８上）に対して，水平強磁場下（8T）でその有機溶液を蒸発させて，薄膜を基板上に調製した。基盤は水平面内に置いた。単層程度の薄い膜を作成して，表面の形状をAFMによって観察した。試料が基板にまばらに付着している箇所を調べたところ，直径50nm程度の部分に，磁気配向を示唆する結果が得られた（図８）。また，試料が基板に重なって付着している箇所においても，直径200nm程度の部分が磁場と平行に配向することが分かった。

5. 無機光触媒の高機能化

光触媒は，光エネルギーの有効利用のために大変注目されている触媒のひとつである。本研究では，溶液中（湿式）における光電着法により光触媒の表面に白金または銀を担持させる際，強磁場中での助触媒の形態，結晶形，及び光触媒活性に対してどのような効果が認められるかなどを検討した。

中心磁場約１５Ｔの超伝導磁石中において，TiO_2表面への白金，金，銀，銅，コバルトなどの金属微粒子の光担持効果を検討した。コバルトの場合，磁気力が強く作用する条件下で担持すると，地球磁場や磁場勾配のない中心磁場よりも，３価より２価コバルトが多く存在する傾向がＸ線光電子分光法による表面化学分析の結果から認められた(図９)。この結果は，溶液中のCo^{2+}（常磁性）の磁気対流が，光担持に影響したものと考えられる。このように，担持されたコバルト表面の化学組成において，高磁気力場での磁場効果が観測された。一方，担持したコバルトの量・形態・結晶形に対する磁場効果は観測されなかった。その他の白金，金，銀，銅については，担持量・形態・結晶形のいずれに対しても磁場効果は観測されなかった。また，コバルトに見られた上記の表面化学組成に対する磁場効果も見られなかった。

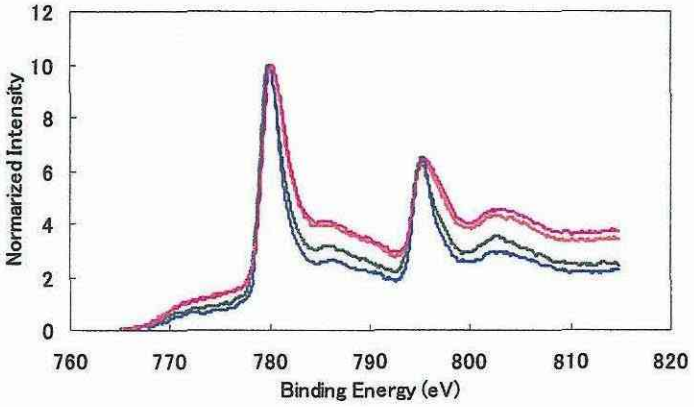

図９．コバルトのＸ線光電子スペクトル
—，０Ｔ；—，15T，０T^2/m；—，11T，-1500T^2/m；—，12T，+1200 T^2/m

6. メソポーラスシリカの高機能化

物質分離の材料として重要であるメソポーラスシリカ MCM-41 について研究を行った。先にメソポーラスシリカの機能の特徴を探索するためにメソポーラスシリカ中の光反応について研究している。図１０に示すように，メソポーラスシリカを充填した溶液中の光反応において散逸生成物の収量が０.５Ｔの磁場により約20%増加することを見出していた。このことはMCM-41 中のナノポアがミセルのかご効果と同様の性質を示すということを意味する。磁場によりメゾポーラスシリカの特性を変えることができるのではないかと考え，磁場下でメソポーラスシリカを合成し，その構造や充填されたカラムへの影響を検討したが，有意な効果はほとんど観測されなかった。

そこで，光反応の磁場効果の研究により見出されたメソポーラスシリカのナノポアの特異性の解明に力を注ぐこととした。その結果，メソポーラスシリカと液体との相互作用に関しては，多くの新規ナノポア効果を発見した。具体的には，a. 巨視的世界では均一な 2-propanol と cyclohexane の溶液は，ナノポア内で相分離すること；b. 狭いナノ空間内での 2-Propanol の拡散が予想に反して非常に速いこと；c. ナノポア内をアルコールがポアズイユの法則に反して速く流れる；d．ナノポア内で，ア

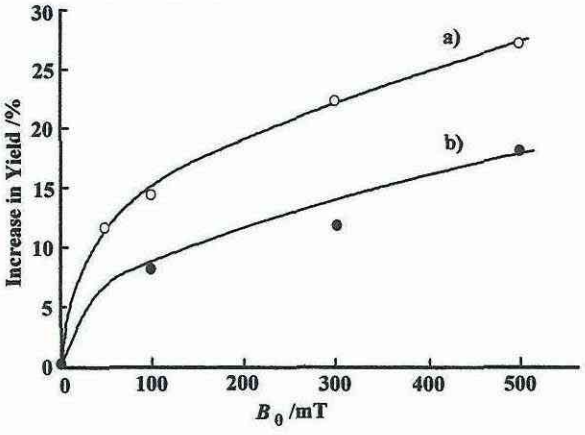

図１０．メソポーラスシリカ中の光反応の磁場効果　縦軸は散逸生成物の相対収量，ポアサイズは(a) 2.5nm，(b)3.4 nm

ルコールは液晶的である，e.水内の不純物有機分子をナノポア内の水分子ネットが取り込む，などの新奇な現象を見いだした。[7]

7. 生物分子素子の高機能化

本研究では，強磁場を利用して担当者らが開発してきた生物分子素子「機能化微小管」を集積・組織化し，ナノ素子としての機能向上や高次機能の発現を図ることを目的とした。そのためにまず，微小管そのものの磁気配向について，次に 機能化微小管」の磁気配向構造の制御，および集積化・組織化による機能の変化を検討した。

微小管の磁気配向に適した実験条件・実験手順を決めるのに困難を極めたが，試行錯誤を繰り返すことにより，漸くその条件を決めることができた。そして，その条件下で微小管の磁気配向を試みた。結果を図１１に示す。図から明らかなように，微小管は磁場から少し傾いて配向した。

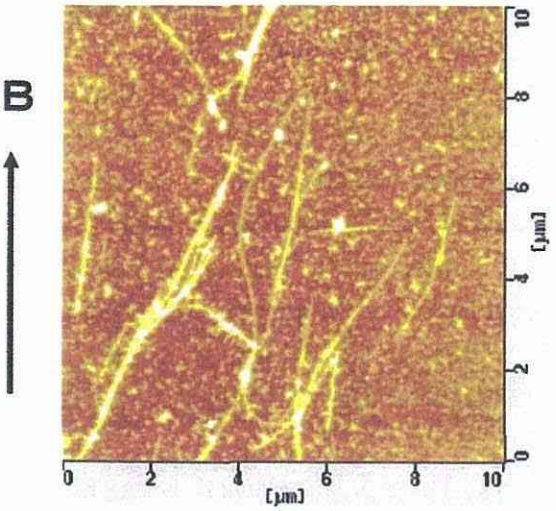

図１１．微小管の磁気配向（６T）

さらに，「機能化微小管」の集積化・組織化のために，微小管上に素子を集積する新たな方法を開発した。これは新たに設計・合成した微小管結合性ペプチドを利用するもので，これにより微小管の変性を抑えるとともに，複合化可能な素子の範囲を広げることができた。

微小管磁気配向のための実験系を構築できたこと，微小管の濃度・長さ・磁場強度による「機能化微小管」の配向・集積度・組織度の変化（すなわち構造制御の方法論）を見出すことができた。

8. おわりに

本研究では，15 T，1500 T^2/m の強磁場のキャラクタリゼーションと強磁場のマテリアルサイエンスへの応用について基礎的研究を行った。

強磁場により擬似微小重力場，1.8G の擬似過重力場を作ることができた。擬似微小重力場によりリゾチームたんぱく質結晶の高品位化が可能であることが世界ではじめて実証された。このことは，擬似微小重力場が，たんぱく質の結晶化などの宇宙実験の地上予備実験やある種の宇宙実験成果の実用化（地上化）に利用できることを明確に示したものである。

熱対流の磁場中その場観察や３次元形態的キラリティーの磁気誘導などの研究から明らかなように，強磁場は，磁気力（$\chi BdB/dz$），磁化率勾配力（$(d\chi/dr)B^2$）やローレンツ力（$qv \times B$）という種々の力の作用する場であり，同時に磁気配向などの磁場効果の作用する場である。このように強磁場は，他に類をみない特徴を有する新規な場であることが分かった。この複雑な場を完全に理解するためには，今後さらに定量的に解明していく必要がある。

このような新規な場により，例えば，対流を加速・抑制するなどが可能であり，材料創製へのさまざまな応用が直ちに期待されるなど，今後マテリアルサイエンスの広い分野での応用が可能であることは間違いない。

強磁場のマテリアルサイエンスへの応用のひとつとして，ナノ材料に注目しその磁気配向にチャレンジした。ナノ材料の場合，熱運動が配向を妨げるため磁気配向を固定化するための工夫が必要であったが，今回の研究で幾つかの材料で磁気配向に成功した。しかしながら，現段階では各論にすぎず，一般的な方法論の確立が今後の課題である。

本研究により 15 T，1500 T^2/m の強磁場環境の特徴の概略を解明することができたが，引き続き更に研究の深化が必要である。

参考文献

[1] W. Duan, M. Fujiwara, and Y. Tanimoto, In situ observation of laser-induced convection of benzene solution of photochromic compound in high magnetic field, Jpn. J. Appl. Phys. 43, 8213 (2004).

[2] F. Koyama and Y. Tanimoto, Photo-induced convection of benzene solution of diphenyloamine and carbon tetrabromide in strong magnetic fields, Mol. Phys., in press.

[3] Y. Tanimoto, M. Fujiwara, M. Sueda, K. Inoue, and M. Akita, Magnetic levitation of plastic chips: Applications for magnetic susceptibility measurement and magnetic separation, Jpn. J. Appl. Phys. 44, 6801 (2005).

[4] D. C. Yin, N. I. Wakayama, K. Harata, M. Fujiwara, T. Kiyoshi, H. Wada, N. Niimura, S. Arai, W. D. Huang, and Y. Tanimoto, Formation of protein crystals (orthorhombic lysozyme) in quasi-microgravity environment obtained by superconducting magnet, J. Cryst. Growth, 270, 184 (2004).

[5] W. Duan, S. Kitamura, I. Uechi, A. Katsuki, and Y. Tanimoto, Three-dimensional morphological chirality induction using high magnetic fields in membrane tubes prepared by a silicate garden reaction, J. Phys. Chem., 109, 13445 (2005).

[6] F. Tang, A. Katsuki, and Y. Tanimoto, Effect of high magnetic field on a quasi-3D siliver dendrite growing system, Mol. Phys., in press.

[7] S. Anandam and M. Okazaki, Dynamic, flow motion and nanopore effect of molecules present in the MCM-41 nanopores —An overview, Microporous and Mesoporous Materials, 87, 77 (2005).

強磁場を用いた高分子材料の構造制御

木村恒久[1]，山登正文[1]，櫻井伸一[2]，斎藤　拓[3]
1首都大学東京・都市環境学部，2京都工芸繊維大学・繊維学部，3東京農工大学・工学部

概要
本研究では，結晶性高分子及びブロック共重合体の構造形成を磁場により制御する方法について検討した．従来磁場配向しなかった高分子量ポリプロピレンの超臨界二酸化炭素下での磁場配向，ブロック共重合体のミクロ相分離構造の磁場配向に成功した．又，透明性が高く，かつ高配向性の高分子フィルムの作製に成功した．更に，微粒子懸濁系の3次元磁場配向に成功し，ナノからミクロンサイズの微粒子の擬単化への道を拓いた．

1．はじめに

結晶性高分子が磁場配向することは現在では広く認識されているが，全ての結晶性高分子が配向するわけではない．汎用樹脂の isotactic polypropylene （iPP）は，磁場配向が達成されると大きな応用展開が期待できる．しかし，これまで低分子量重合体の配向は達成されているものの，実用に供される高分子量体のものは単一では配向に成功していない．今回は超臨界二酸化炭素下での特殊な結晶成長を利用することにより，初めて磁場配向に成功した．

ブロック共重合体はミクロ相分離構造を形成するので，磁場による構造制御の可能性が考えられるが，構造サイズおよび磁気異方性が小さいために，磁場配向は困難と考えられていた．しかし，本研究では強磁場下でシリンダー構造が磁場配向することが見出された．更にミクロ相分離の一方の相を選択的に常磁性化することによりラメラ配向が促進されたことから，形状異方性による配向メカニズムが示唆された．

高分子の配向制御により複屈折の制御が可能になるので，光学材料用のフィルムの作製に磁場配向が有効である．磁場配向のためにはサブミクロンオーダーの磁気異方性構造が必要であるが，このサイズの異方性構造は光を強く散乱するので，磁場配向と透明性とはトレイドオフの関係にある．本研究では液晶性ブロック共重合体を用いることによりこの困難を克服した．その結果1/4波長板程度のリタデーションを有する透明配向フィルムを作製することができた．

ミクロからナノサイズの微粒子を作製し，それを高分子マトリックス中に懸濁し磁場配向させることにより，配向複合材料を作製した．二軸性結晶の場合には，静磁場下では磁化容易軸が，回転磁場下では磁化困難軸が一軸配向するが，これまで，二軸を同時に配向させる手法は知られていなかった．本研究では，時間的に変動する特殊な磁場を用いることにより，初めて二軸配向を達成した．これにより，擬単結晶状複合材料を作り出す手法を確立した．

図1超臨界磁場印加システム

2．超臨界流体場での磁場印加による高分子の高次構造制御

高分子を超臨界二酸化炭素雰囲気下で磁場印加させることが可能な耐圧容器の試作を行った（図1）．耐圧容器として磁石内で使用可能で高温・高圧に耐えられるチタンを用

い，耐圧容器内に挿入した試料の温度コントロールはセラミックヒーターにより行った．試作した耐圧容器を超伝導磁石内に挿入して超臨界磁場印加システムを構築した．超臨界二酸化炭素雰囲気下で高分子試料をその溶融温度以上まで昇温して，その後，結晶化温度まで冷却して等温熱処理することで，高分子の結晶化に対する超臨界流体場での磁場印加を可能にした．

高分子量 iPP を大気圧下で磁場を印加して溶融結晶化させても配向した結晶構造を得ることができなかった．ところが，二酸化炭素雰囲気下で 8T の磁場を印加しながら溶融結晶化させることで，長軸方向が磁場の印加方向に沿って配列して，巨視的な光学異方性を有する針状結晶の得られることが見出された（図2）．実際に結晶内の分子鎖が配向していることは，広角 X 線回折像の方位角依存性と偏光フーリエ変換赤外吸収スペクトルから得られる赤外二色性の結果から確認できた．さらに，広角 X 線回折の一次元プロファイルが二酸化炭素雰囲気下で磁場を印加させながら溶融結晶化させることで大きく変化して，大気圧下ではα型であった結晶構造が，α＋γ型へと変化することがわかった．

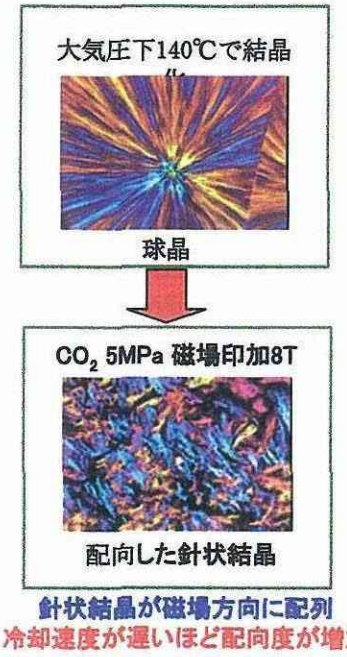

図2　ポリプロピレンの磁場配向

高分子量 PP を磁場印加させながら低温で溶融結晶化させることで，磁場配向の度合いが増加した．また，溶融後の冷却速度を遅くすることで結晶配向の度合いが増加した．これは，溶融させた温度が低いためにすべての履歴が消されず溶融状態で完全なランダムコイルにならず，二酸化炭素による秩序構造形成が容易になったことと，冷却速度が遅いために秩序構造が形成される結晶化誘導期が伸びたことで磁場の影響を受けやすくなり，秩序構造が磁場配向に必要な体積まで成長後，磁気トルクにより回転し，その後に成長する結晶も配向することにより磁場配向の度合いが増加したことを考えることで説明できた．

以上のように，超臨界磁場印加システムを構築することで，1）大気圧下では磁場配向できなかった高分子量 PP を磁場配向できるようになり，2）結晶構造・高次構造の制御も可能になり，3）磁場配向のための最適条件が見出され，当初の目標を十分に達成できた．

3. 磁場によるブロック共重合体のナノ構造制御

ブロック共重合体は，ブロック組成に応じ，図3に示すようなミクロ相分離構造を形成する．ポリスチレン-水添ポリブタジエン-ポリスチレン（SEBS）トリブロックコポリマーが形成するシリンダー状のミクロ相分離構造（ポリスチレンがシリンダーを形成している）の場合に，磁場配向する結果が得られた．しかし，その度合いはかなり小さく，30 T の磁場強度でも場合によってはさほど顕著な配向が得られないと言う結果もあった．磁場印加方向に対してシリンダー構造が平行に配向するのが一般的な結果となった．ポリスチレン-ポリブタジエン-ポリスチレン

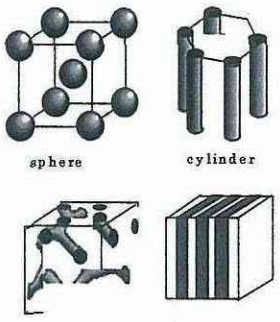

図3　ブロック共重合体におけるミクロ相分離構造

(SBS) トリブロックコポリマーが形成するラメラ状のミクロ相分離構造の場合には，磁場配向は確認できなかった．そこで，上記の磁場配向を，より顕著にするため，ナノシリンダーの直径程度の厚みを有する薄膜（膜厚約２０nm）について実験を行った．

シリコーンウェハ基板上にスピンキャストした薄膜について原子間力顕微鏡観察と視射角入射小角X線散乱実験を行った．現在も継続しているが，ナノシリンダーが磁場印加方向に対して平行に配向する結果が定量的に得られた．

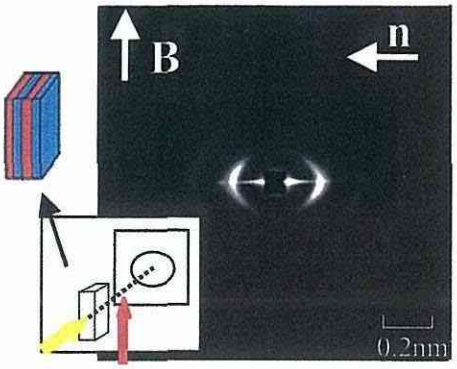

図４　配向ラメラのX線小角散乱像

以上のように，当初の予想通り，シリンダーについては磁場配向可能で，さらに基板上での表面パターンの磁場によるナノ・マニピュレーションが可能であることを示すことができた．残念ながら，ラメラ状のミクロ相分離構造については，配向に及ぼす磁場の有効性を示すことはできなかった．

そこで，片方の相に特異的に常磁性キレート化合物が取り込まれるような系を選択し磁場処理を行ったところ，図４に示すようにラメラの配向挙動が見られた．現在再現性試験を行っている．磁気異方性にもとづく磁場配向においては，常磁性の導入により配向が促進されることは考えにくいので，この結果は，構造異方性によるものと理解される．

4．磁場を用いた光学材料の創成

ポリエステルエーテルやポリブチレンテレフタレート/ポリカーボネート系アロイについては比較的透明な状態で（透過率65%～70%）配向させることに成功した．いずれも融点直上で溶融させ融点直下で結晶化させることが重要であった．しかしながら，これらの系は光学材料として利用するには不十分なものであった．アイソタクチックポリプロピレン（iPP）に核剤を添加した系では速い冷却速度で冷却結晶化させることにより透明で配向した試料を得ることに成功した．また核剤添加iPPにおいて不均一磁場を用いて傾斜配向材料について検討を行った．その結果，核剤添加iPPを不均一な磁場分布に従って傾斜配向させることにも成功した．最終的には液晶/非晶のブロック共重合体を磁場配向させることで優れた透明性と配向性を有するフィルムの作製に成功し，当初の透明配向体作製の目標は達成することが出来た（図５）．また，液晶/非晶のブロック共重合体を磁場配向させることで，ミクロ相分離構造の配向制御やミクロ相分離構造の周期性の制御が可能となるような新たな知見が得られた．磁気双極子相互作用などの影響が考えられるが，詳細は今後の検討課題といえる．

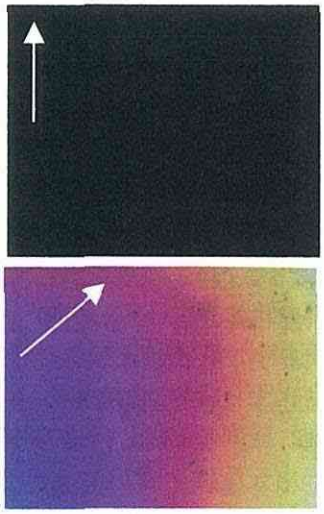
図５　配向試料の偏光顕微鏡写真．ほぼ1/4波長板の位相差を実現．矢印は印加磁場方向．

強磁性体周期構造を利用したパターン作製装置はその構造が複雑であるため幾つか問題点が見つかった．現状

でも250℃以上では使用時間が限られ，高分子の溶融結晶化プロセスへの応用は達成できなかった．微粒子の自己組織化のパターン化は複雑模様への応用，2種類の異なる粒子の同時パターン化など今後の応用展開の基礎となる結果が得られた．

サブテーマについては，磁場配向を磁場内FT-IRで観察した．アイソタクチックポリスチレンの場合，溶融状態での配向は確認できず，結晶化初期過程でのみ配向していることが明らかとなった．一方，ポリエチレンテレフタレートでは溶融中でわずかに配向していることを示唆するデータが得られた．しかしながら最終的な配向度はその後の結晶成長の初期過程に依存しており，磁場配向を制御するためには結晶化初期過程の制御が重要であることが明らかとなった．

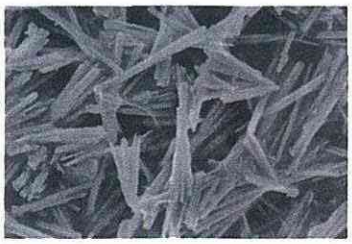

マイクロロッドのSEM写真

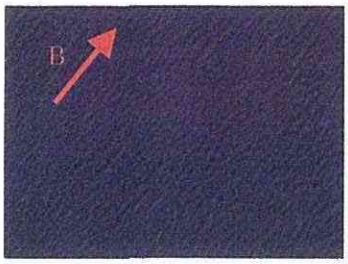

磁場配向サンプルの光学顕微鏡写真

図6　$Gd(OH)_3$マイクロロッドの磁場配向

5. 高分子／ナノ複合体の磁気プロセッシング

ナノ粒子分散系の磁場配向技術を確立し，光学材料への応用展開を目指した．無機水酸化物ナノロッド，セルロースナノファイバー，カーボンナノチューブ（CNT）の懸濁系に磁場印加し，これらの配向制御，及びその固定化を達成した．パターニングと配向が同時に達成できることが示された．

具体的には以下の事柄が達成された．（1）種々のナノ粒子を作製する方法を確立した．水熱処理による$Gd(OH)_3$ナノロッドの作製（図6）[1]，セルロース繊維の酸処理によるナノファイバー作製方法の確立，CNTの短繊維懸濁液の調製法の確立．（2）配向の固定化に関しては光硬化性樹脂を用る方法を確立した．（3）磁気モジュレーターを用いて，配向とパターニングを同時に行う方法を確立した．有機微結晶，CNTに対してこのプロセスを適用し，パターン化異方発光材料の作製，CNTの配向，線状パターニングを達成した．工業化を目指し，連続配向方法の検討も行ったが，具体化には至らなかった．

この他，配向の精密化手法の開拓を行い，微結晶の3次元配向を達成した[2,3]．二軸結晶（orthorhombic, monoclinic, triclinic）の磁化率の大きさは通常全て異なる．静磁場下では磁化容易軸が，回転磁場下では磁化困難軸が一軸配向するが，これまで二軸を同時に配向させることは不

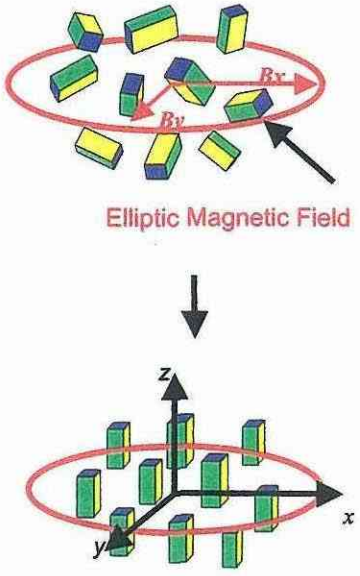

図7　楕円磁場を用いた二軸結晶の3次元磁場配向

可能であった．今回，二軸配向が楕円磁場を用いることにより可能であることを，理論的に示し(図7)，実験的検証を行った．20 μm程度の粒径の有機微結晶粉末を光硬化性樹脂に懸濁し，楕円磁場を印加し，二軸配向を達成した後，光照射により配向を固定した．得られた試料をXRD解析した所，スポットの半値幅は単結晶の5倍ほど広かったが，単結晶に比べ遜色のない分解能が得られた(図8)．この方法により微結晶粉末の擬単結晶化が可能となる．XRD，中性子，固体NMR等の分光学的測定において，粉末試料を用い，単結晶解析ができることを意味する．擬単結晶材料の創製にも有効である．

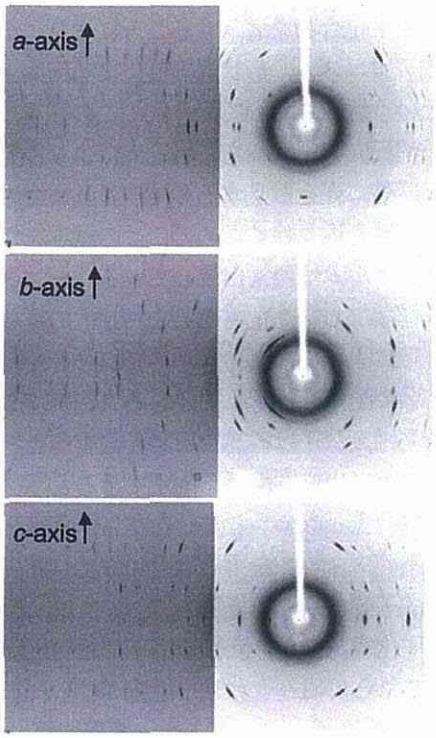

配向度は，磁気エネルギーと，熱エネルギー $k_{\mathrm{B}}T$ との競合により決まる．配向揺らぎは，

$$\Delta\theta^2 \approx \mu_0 k_{\mathrm{B}} T / (B^2 V \chi_a)$$

により評価できる．今回の結果では5 Tの磁場を用いて行った．$\Delta\theta$が元の単結晶の5倍程度であったが，上式からも分かるように，磁場強度を大きくすれば，容易に回折スポットの半値幅を小さくすることが可能である．

6. おわりに

本研究では高分子の磁場配向制御ための基礎研究，およびその応用展開を行った．結晶性高分子の磁場配向は，熱力学的優先配向メカニズムも提案されているが，多くの場合，結晶化の際に生じる異方構造が磁気トルクを受けて回転することにより生じる，というメカニズムで説明がなされている．しかし，その詳細は高分子の種類に依存する．結晶性高分子の中にも配向しないものもあるし，同一の高分子であっても，分子量に依存して配向したりしなかったりといった現象が知られている．また，熱履歴にも大きく依存する．このように，配向は個々の高分子の結晶化の特性に依存した，複雑な現象であることが示唆される．

実際，本研究で明らかにされたように，結晶化の機構が配向を大きく左右する．iPPは，球晶を作りやすい性質を持つ．球晶形成は配向を阻害するので，iPPは磁場配向が難しい．ところが超臨界二酸化炭素中で結晶化させると，球晶形成が抑えられて，針状結晶が生じることが知られていた．このことは磁場配向に有利であるので，磁場印加下，超臨界二酸化炭素下でiPPの結晶化を行ったところ，予想通りに磁場配向した．汎用の高分子量iPPの磁場配向は，応用面でも展開が期待される．

ブロック共重合体は，シリンダー，ラメラ等のミクロ相分離構造を取ることはよく知られている．これらの構造はナノサイズなので，磁場配向は困難と考えられる．また，相分離界面での高分子鎖の伸張による磁気異方性が期待されるが，結晶性高分子に比べれば，異方性ははるかに小さい．しかしながら，強磁場（30T）下では，これらの困難を克服できるのではないかと考え実験を行ったところ，シリンダー相が磁場に平行に配向する兆候が見出された．配向メカニズムが

回転タイプか，優先配向タイプかは現在のところ不明である．更に，片方の相に選択的に常磁性キレート化合物を導入することにより，ラメラ相の磁場配向の兆候が得られたことから，第３の配向メカニズム，形状異方性による配向メカニズムが示唆された．磁場配向の適用対象を拡大するという意味において，今回のこの発見は大きな意義があるといえる．

透明配向フィルムを磁場配向により作製することは，配向できる程度のサイズを有する異方構造が同時に光を散乱するので，これまでの様々な試みにも関わらず困難であった．今回は，これらの困難を取り除くための二つの試みを行った．iPP は結晶化速度が速く大きな球晶を生じるので，フィルムは通常白濁している．ところがいわゆる結晶化核剤と呼ばれる有機或いは無機の微結晶を添加し結晶化させると，iPP の結晶サイズを小さくできるため，透明性が増加する．核剤の種類によっては高分子がエピタキシャル結晶成長する系がある．そこで，核剤の磁場配向により iPP の配向を誘起したところ，透明性の高い iPP 配向フィルムを得ることに成功した．

液晶性高分子は容易に磁場配向することはよく知られている．磁場配向によりモノドメイン化することにより透明性を向上できると期待されるが，市販の液晶性高分子は磁場配向させても透明性は向上しない．しかしながら，今回液晶性ブロック共重合体を磁場配向させたところ，高配向の透明フィルムを得ることに成功した．

微粒子懸濁系の磁場配向については，擬単結晶化技術という新たな展開が得られた．静磁場下では磁化容易軸が，回転磁場下では磁化困難軸が一軸配向することはよく知られている．本研究ではこれらの組み合わせと位置づけられる方法により，二軸結晶（斜方，単斜，三斜）の二軸配向（３次元配向）に成功した．実際に用いた磁場は，強度変調型（AM）および周波数変調型（FM）の回転磁場である．この手法により，懸濁微結晶を３次元配向させた複合材料，３次元配向した結晶性高分子材料の創成に道が開かれた．今後の展開が期待される．

参考文献

[1] C. Chang, F. Kimura, T. Kimura, and H. Wada, Preparation and characterization of rod-like Eu:Gd2O3 phosphor through a hydrothermal routine, *Material Letters*, **59 (8-9)**, 1037-1041 (2005).

[2] T. Kimura and M. Yoshino, Three-Dimensional Crystal Alignment Using Time-Dependent Elliptic Magnetic Field, *Langmuir*, **21**, 4805-4808 (2005).

[3] T. Kimura, F. Kimura, and M. Yoshino, Magnetic Alteration of Crystallite Alignment Converting Powder to a Pseudo Single Crystal, *Langmuir*, **22**, 3464-3466 (2006)

強磁場によるナノ構造構築と機能操作

尾関寿美男[1]、藤尾克彦[1]、飯山　拓[1]、勝木明夫[2]
1信州大学・理学部、2信州大学・教育学部

概要

非磁性のハイドロゲル，脂質ベシクル，コアセルベート，トリブロックコポリマー/シリケートハイブリッド，メソポーラスシリカや弱磁性の有機金属錯体や金属樹のコロイド次元集合体を磁場下で組織化および機能化した。磁場応答性部位に注目して，細孔性固体や生体モデル物質を中心に磁場の作用を探索的に研究した。構造の磁場による自己組織化，磁気異方性添加物による機能の磁場敏感化を検証し，これらによって，弱磁性系の異方性ナノテクスチャーやナノ構造を，磁性をベースに簡便に，内部から組み上げる新しい方法論の端緒を得た。また，磁場による反応や機能・物性の制御の例として，水の磁気処理効果や溶液中の濃度ゆらぎの磁気力場制御を検証するとともに，水素の低温での吸着・反応や電気化学における非線形化学反応に伴う構造形成の磁場応答を調べた。

1. はじめに

材料に望まれる機能は自己集合や自律反応で自然に生まれる物質の構造に由来するそれらだけでは対応できなくなっている。ミクロスケールで発現する特性を統計的平均化によって失わせず，マクロな単位で発揮させることが重要である。これらを実現する手段の一つに磁場があり，(i) 磁場中での物質合成による構造制御，(ii) 物質中の第2物質の磁場による選択的配向・構造制御，(iii) 物質の磁場による構造―物性制御に利用され，物質・材料開発の有用なエネルギーであることが確かめられつつある。磁場は極めてマイルドかつクリーンなエネルギーで，物質透過性や小さな界面効果などの特徴をもつ[1]。そのため，表面から深部まで同じように磁場効果を及ぼすことができ，電場や流れなどの他のエネルギー源とは異なる際立った特徴を有している。

このような磁場効果は物質のもつ磁気的性質と磁場の種類の組み合わせによって制御される。物質は普遍的に反磁性磁化をもつために，すべての物質が磁場と相互作用する。たとえば，磁気異方性が$\Delta\chi$ の N 個の分子を含むドメイン(体積 N_v)のもつ磁気配向エネルギーE_r は，分子の長軸と磁場のなす角度をϕ とすると，

$$E_r = -\frac{H^2}{2}(\chi_\perp + \Delta\chi\cos^2\phi)N_v \qquad (1)$$

で与えられる。N あるいは H が熱エネルギーよりも十分大きければ，分子の長軸は磁場と直交するようになる。10T 超級の液体ヘリウムフリー超伝導マグネットが安価に入手できるようになって，非磁性かつ絶縁性の無機・有機物質にまで磁場の適用範囲は広がり，実験室レベルで磁気浮上を可能になった。磁場は空間的・時間的にゆらぐので，磁場効果は均一磁場，不均一磁場（勾配磁場と局所磁場），交番磁場などの種々の効果が重畳してあらわれ，メカニズムを推察する際に注意を要するが，それだけに思わぬ相乗効果が期待できる。また，磁場は反応物質，応答物質に直接に作用するば

かりでなく，輸送，保持，方向性，無容器など環境，条件設定への展開も可能である。

本研究では，弱磁性の高分子や分子ネットワーク，分子集合体構造やそれらの物性・機能を磁場を利用して制御することを目指した。

2. ゲルの構造と機能の外部磁場制御

化学架橋ゲルであるポリ(*N* -イソプロピルアクリルアミド)ゲル（NIPA ゲル）は低温の純水中ではネットワークに水分子を取り込んで膨潤しているが，温度上昇に伴って徐々に脱水和し，34℃付近で急激に収縮する。この不連続な体積変化を体積相転移と呼ぶ。モノマーから高分子への成長と架橋生成を内径 0.4mm のガラス毛細管中で磁場下で行うと，調製したゲルは膨潤相での直径が増加し，収縮相は幾分減少したので，磁場中で調製したゲルの体積相転移点における不連続性は顕著になった。25℃での膨潤状態のゲルの直径は調製磁場強度の増加に伴って単調に増大し，30T ではゼロ磁場のゲルに比べて約 40% 大きくなった[2]。また，高分子鎖が磁場に対して垂直に配向するために構造異方性を示し，磁場印加方向へのサイズ変化の方がかなり大きかった。このゲルの異方性は磁化率の異方性や偏光解消として観測された。

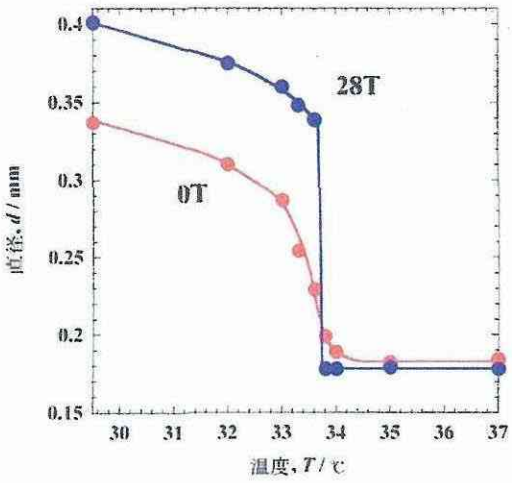

図 1. NIPA ゲルの不連続体積変化の磁場

28T で調製したゲルの磁場は見掛けの架橋度は仕込み時の約 4 分の 1 に減少し，ヤング率は 3 分の 1 になっており，架橋度の低下によってゲルがかなり柔らかくなっていることがわかった。これは，磁場配向した高分子鎖間が架橋されにくいため，高分子鎖の一端が架橋されていないダングリング鎖が生成するためであることが，張力緩和測定によって示唆された。

NIPA ゲルは調製温度の上昇とともに白濁するが，磁場中で調製すると透明度の高いゲルが生成した。これは調製温度の上昇に伴って生成する高分子の密集したドメインが，磁場中で調製すると光の波長に比べて十分小さくなったためと考えられる。熱分析により，磁場中調製ゲルは相転移熱が磁場強度の増加とともに大きくなり，水和量が増加したことがわかった。また，偏光顕微鏡観察から，同じ磁場強度でも相転移温度以上で調製したゲルの方が磁場配向が促進されたことがわかった。その他，磁場下で調製すると，体積相転移が誘起されること（図 1），不透明な高架橋度ゲルを透明化できること，高温調製ゲルの体積相転移現象を体積の大きい領域にシフトできること，調製時の磁場方向によってヨウ素拡散を制御できることなどを見出した[2,3]。

NIPA ゲルに外部磁場を印加すると膨潤し，30T で直径が約 20%増大した。熱分析の結果，磁場中では相転移熱が増加しており，直径の増大は水和量の増加に起因することがわかった。また，溶媒に添加物を加えた溶液中での体積相転移温度は磁場によってシフトした。磁場印加による温度シフトは添加物の種類と濃度に大きく依存し，最大±0.6K であった。磁場による収縮後の溶液中の添加物濃度減少は磁場による疎水性添加物のゲルへの結合量の増加が相転移温度シフトを誘起したことを示唆した。この磁場誘起体積相転移は分子結合に続いて脱水和が起こる点で，通常の温度誘起体積相転移（脱水和してから疎水性分子が結合）とは全く異なる。この温度シフトを利用すると，外部磁場刺激によってゲルを操作できる。図 2 は NIPA ゲルを水溶液中で膨潤させ，温度を一定に保って 10T の磁場を ON，OFF した際の体積変化を示したものである。このように，条件次第ではゲルは外部磁場によって意外に大きく歪むので，外部磁場によるゲルの網目や形状の制御が可能である。種々の条件を組み合わせると特徴あるゲルが調製可能である。

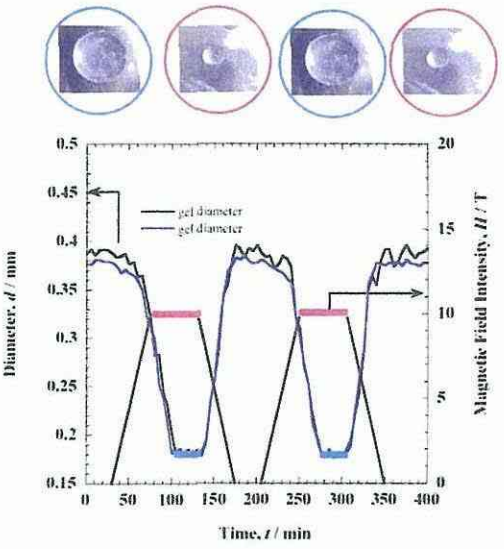

図 2. 磁場印加に伴うゲル直径の経時

無機ゲルとしてのシリカゲルも，ケイ酸ナトリウム水溶液をイオン交換し，ゲル化時に磁場を印加すると細孔構造を制御できた。磁場によって結晶性が良くなり，メソポアが発達して特徴ある細孔径分布となった。

3. 磁場による溶液構造・物性の変化の検証

脂質からなるリポソーム（ベシクル）膜への機能性分子の添加によって生体膜機能を模倣したり，ベシクルの内水相を細胞質とみなして機能化する試みが盛んである。薬物輸送担体や薬物徐放系としての応用も検討されている。通常の膜融合には物理的摂動として電場が用いられているが，穏やかな方法とはいえない。

磁気異方性分子からなるドメインの磁場配向は磁場方向に対して角度ϕ で起こるので，隣り合うドメイン間で異なる配向が許される。この配向欠陥を解消するために膜は曲率を持つように変形する。実際，磁気エネルギーが小さいときには球から楕円体へ変形した（図3)。一方，磁気エネルギーが大きいときには膜は波打つが，その際生じる弾性エネルギーは膜の不安定化に導く。これらのエネルギーバランスから磁場中でのベシクルの安定化条件を求めると，一つのベシクル内に含まれる分子数の許容数が，ρ を膜の局所的曲率半径として

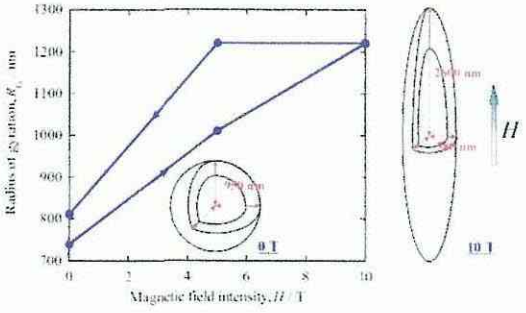

図 3. ベシクルの回転半径の磁場による

次式で求まる。

$$6(1-\underline{n})-r_0\rho^{-1}(n^{1/2}-n)\geq 0 \qquad (2)$$

磁場下にあるベシクルに含まれる分子数がゼロ磁場での粒径2 r_0 をもつベシクルの n 個分に相当するとき，$n>1$ を磁場融合，$n<1$ を磁場分裂，$n=1$ を安定と呼ぶことにする。与えられたρ に対して図示したところ，実測値は安定化条件の境界付近に沿って分布した[4]。同じ初期粒径から出発しても，添加物や磁場強度が異なると融合も分裂も誘起される（図 4)。また，ベシクルはパルス磁場や変動磁場を用いた短時間の磁場曝露でも粒径が変化した。しかし，安定な粒径分布ではないため，長時間曝露によって粒径分布は変化した。

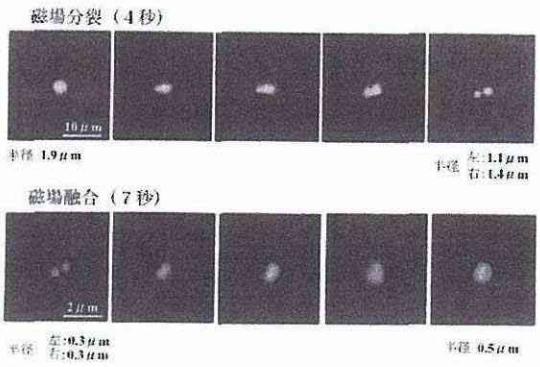

図 4. ベシクルの融合と分裂の光学顕

脂質膜は分子・イオンを通しにくいので，生体中での薬物輸送・放出システムとして利用する試みが盛んである。磁場はエネルギーが低いが，物質透過性の遠達力であるので，この目的には最適である。蛍光色素カルボキシフルオレッセインはベシクルの膜内分子磁場配向によって脂質膜を透過した。

磁場下で溶液からの光散乱強度が測定できる静的および動的光散乱計を開発した。これらを用いて，ミミズ状ミセルやひも状ミセルの会合状態の磁場による変化を検出した。屈曲した棒は伸び，ランダムコイルは球から楕円体に歪むことが示唆された。また，液液相分離に伴う濃度ゆらぎへの磁場効果を検討し，磁気力による擬似磁気浮上によってゆらぎの相関長が変化する兆候を得た。

水への磁場の効果を接触角と炭酸カルシウムの結晶形態および結晶構造変化から界面化学的に検討した[5]。接触角はわずかに減少し，ぬれ性が増大することがわかった（図 5)。また，炭酸カルシウムの結晶の形態や構造も磁場で変化した。磁場中を通過した水の機能が変化するという説の真偽を検証した。超純粋を真空蒸留するなど極めて慎重に検討した結果，酸素を溶存した純水は磁束変化によって構造および機能を変化させることがわかった。その原因を理解することは現在の理論的枠組みでは容易ではないので，なお，慎重に

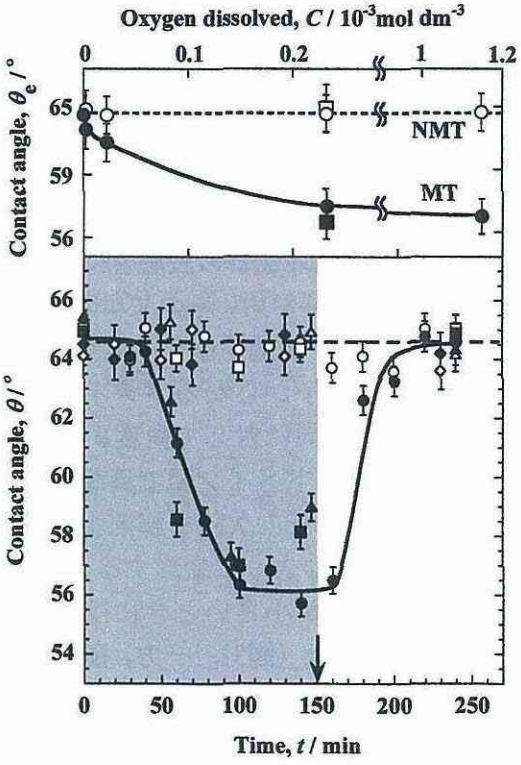

図 5. 水の接触角への磁気処理効果

検討を継続している。

4．有機/無機ハイブリッドの構造と機能の磁場制御

界面活性剤分子の分子軸は磁場と垂直に配向するので，これらが会合した棒状ミセルはその中心軸が磁場方向に一致するとき最も安定化する。この配向性を利用して間接的にシリカ骨格を並べることができる[1]。メソポーラスシリカは均一な細孔をもち，吸着，触媒，物性研究の分野で注目を集めている。この物質群は，界面活性剤やコポリマーが形成する棒状ミセルがシリケートイオンを含む溶媒を挟んで平行に並んだヘキサゴナル構造（H 構造）から界面活性剤を除去して得られる。ハニカム状に配列した均一な細孔は有機鋳型の長さに依存して 2～20nm となる。磁場下では H 構造ドメインの成長，究極的には単一ドメインの多孔体が期待される。臭化ヘキサデシルトリメチルアンモニウムの水溶液とテトラエトキシオルトシランのエタノール溶液とを混合したゾルを均一磁場下でゲル化させ，得られたハイブリッドを 823K の空気中で 5 時間処理してメソポーラスシリカとした。この細孔径は面間隔と同様に磁場強度の増大とともに小さくなり，細孔容量は大きくなった。メソ細孔が得られない塩基性条件で強磁場を印加すると H 構造が発達するために窒素吸着等温線にステップが現れる（図 6）。磁場によって典型的なメソポーラスシリカ MCM-41 が誘導された。また，トリブロックコポリマーを鋳型とした SBA-15 の細孔配向の磁場制御も可能になった。

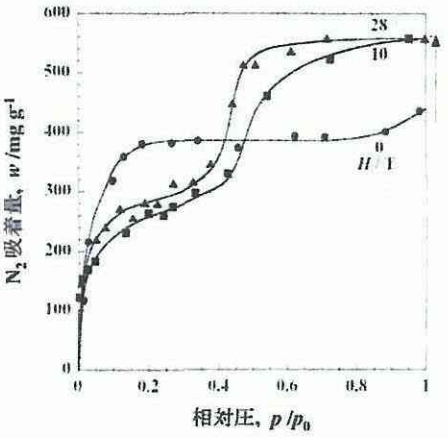

図 6. 異なる磁場強度で調製したメソポーラスシリカの 77K での窒素吸着等温線

ピラジンやフマル酸などを配位子にもつ 3 次元集積型有機金属錯体を磁場中で調製して，結晶のモルフォロジーや集合状態を変化させた。それらの熱安定性や細孔構造，吸着能に磁場効果を認めた。特に，同じ組成のピラジン/ピラジンジカルボン酸/過塩素酸銅水溶液から，6T の磁場を用いて 2 種の新規結晶構造を見出した（図 7）。

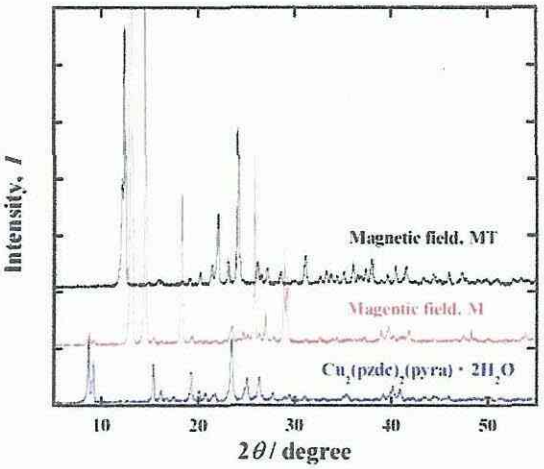

図 7. Cu/pzdc/pyra 錯体の X 線回折図

5．磁場による吸着相の状態と表面反応の制御

臨界温度周辺における水素吸着測定を行うために，高圧および強磁場に対応した装置を設計，製作した。測定装置には広い圧力範囲を高精度で測定できるように異なる圧力範囲が測定できる圧力計を取り付け，8MPa までの広い圧力範囲においての吸着測定を可能にした。多孔質固体と吸着平衡にある水素に磁場を印加して吸着量変化を見出した（図 8）。磁場による吸着量変化は超臨界状態においても起きるが，温度が低い

ほど変化量は大きくなることから温度が低いほど水素凝縮相の磁性は常磁性的な性質を示すことがわかった。気体及び液体の水素は反磁性物質であることから，凝縮相水素の磁性が固体表面との特異な相互作用によって変化したことが吸着への磁場効果の原因であると思われる。

トンネル現象への磁場効果を検証するために，典型的なトンネル反応である低温での水素/芳香族分子反応と電極上での脂質膜を介してのトンネル電子移動を調べた。前者については，圧力応答による水素吸着量検出と質量分析による反応の実証，および同位体効果を検討し，後者については，最適電極系の作成，イオン対複合膜の安定化，膜形成の実証などをデータを取りながら，検証した。超伝導マグネットによる磁場印加システムを構築し，強磁場印加効果を検討した。

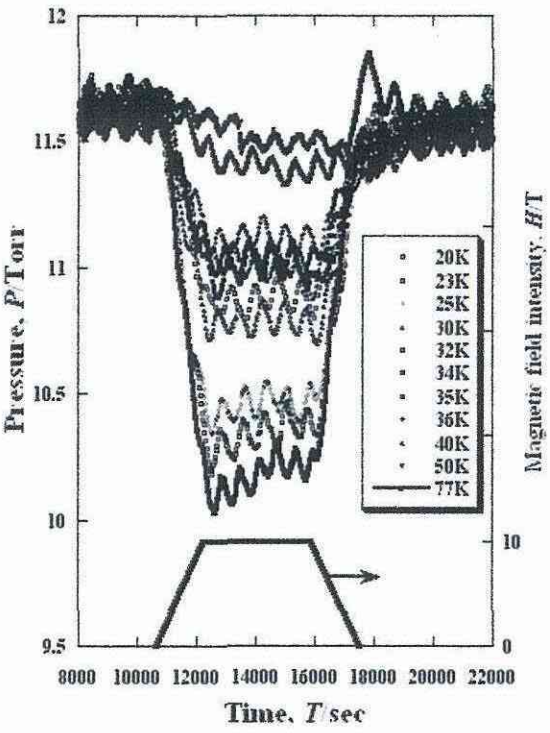

図 8. 磁場印加に伴う水素圧力の経時変化

反応性水素原子を水素分子から発生させるために紫外光と水素吸蔵合金を用いた。トンネル反応を追跡するために 15K 級クライオスタットにサファイア窓とガス導入部を設け，圧力変化を鋭敏にしかも温度ゆらぎの影響を避けるために差圧を検出し，質量分析器に接続して反応物を確認した。ベンゼン/水素/活性炭素繊維系，シクロヘキセン/水素/水素吸蔵合金系で水素付加反応の温度依存性と同位体効果を調べ，トンネル反応が進行することを見出した。磁場はこれらのトンネル反応の種類に依存して，抑制にも促進にも寄与することが判った（図 9）。

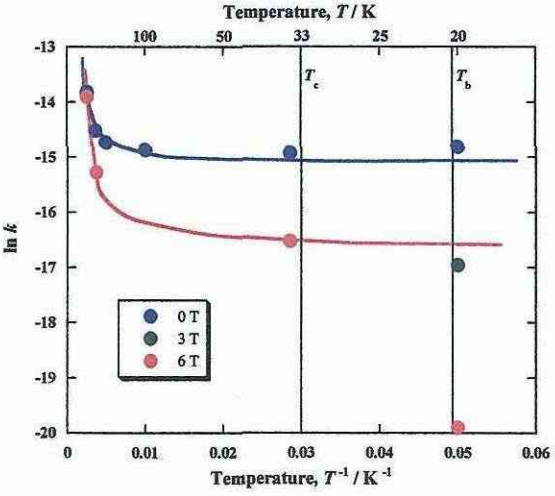

図 9. 6 T における $H_2/C_6H_{10}/SmCo_5$ 系の速度定数の温度依存性

電極上のカルボキシル基をもつ自己組織化膜上に陽イオン性脂質膜を自己組織的に複合化させ，イオン対を介した電子移動系（トンネル系）を構築した。鉄錯体水溶液－脂質複合膜―電極系でのレドックス反応への磁場効果をサイクリックボルタンメトリーによって検出した。特別な複合化手法によってのみトンネル電子移動系を構築でき，磁場によって電子移動を制御できることが分かった。

酸化チタンによるメチレンブルー吸着活性および光分解反応触媒活性は磁場によって促進された。微粒子効果やイオンドープによるバンドギャップの変化により，磁場による活性変化に大きな違いがみられ，不均一光触媒活性の磁場制御の端緒が得られた。

6. 非線形化学反応に伴う構造形成への磁場効果

平衡状態ではなく非平衡状態にある化学反応に対しては，制御できるほどの磁場摂動をあたえうる。非平衡状態の反応のひとつとして非線形化学反応は，生物の機能発現やパターン形成などと関連して近年大変興味が持たれている反応の一つである。本研究は，パターン形成反応および吸着現象などの非線形反応に対する磁場効果を解明することを目的とする。特に，典型的な非線形現象である金属樹成長の磁場効果および結晶の配向について検討を行った，これらの化学反応の制御は新機能材料の開発にもつながるものである。

固/液相間の酸化還元反応による金属樹の成長過程は非平衡状態における反応であるため，外部からの摂動の影響を受けやすい。本研究では，金属銅—銀イオン系，または金属亜鉛—銀イオン系から生成する銀樹について磁場によって顕著に形成パターンおよび収量が変化すること，およびその詳細について検討した。

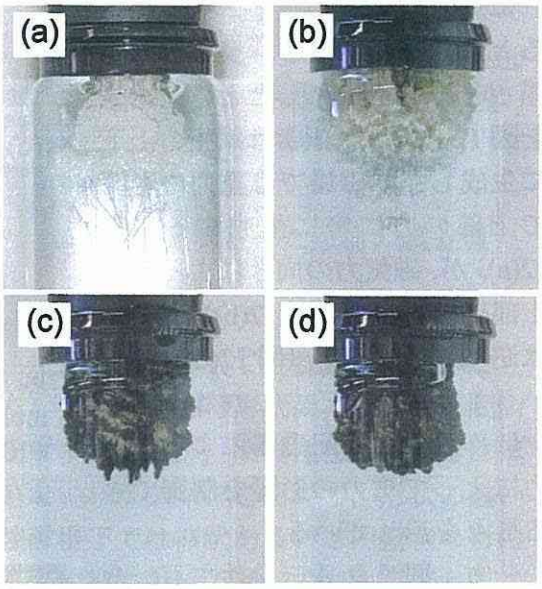

図 10. Cu-Ag^+ 系 ([$AgNO_3$] = 0.05 mol/dm^3) で生成した銀樹．(a) 零磁場, (b) 9.8 T, +1070 T^2/m, (c) 15.0 T, +50 T^2/m, (d) 5.6 T, -940 T^2/m.

金属銅—銀イオン系からの銀樹の成長過程を最大磁場強度 15 T の不均一磁場中で行った結果を図 10 に示す。零磁場の状態では，金属光沢を持った樹枝状結晶が成長している（図 10(a)）のに対し，磁場中ではいずれの磁場条件下においても金属光沢が失われ，全体の形状も球状になっている（図 10(b), (c) および(d)）ことから，明らかに磁場の影響が見られる。図 11 に銅イオ

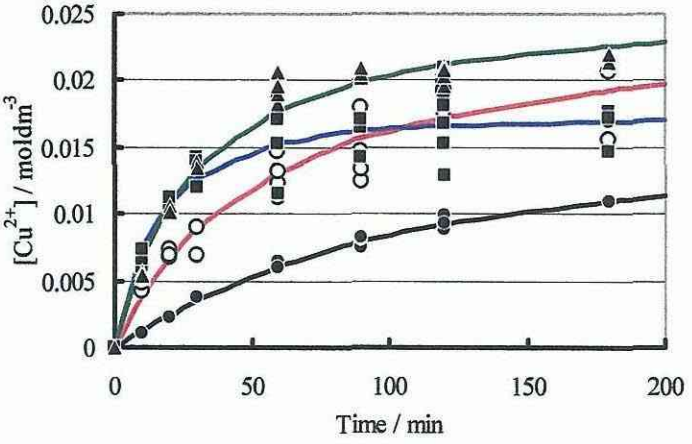

図 11. Cu^{2+}イオン濃度の時間変化: (●) 零磁場; (○) 9.8 T, +1070 T^2/m; (■) 15.0 T, +50 T^2/m; (▲) 5.6 T, -940 T^2/m.

ン濃度の時間変化を示す。いずれの磁場条件においても零磁場条件とくらべて立ち上がりが速く，収量も約 2 倍以上増加していることがわかる。イオン反応では，ローレンツ力が作用することに加えて，この反応系では常磁性イオン種である銅イオンが関与することから，勾配磁場による磁気力の影響も見られた。磁場によって形状および収量が顕著に変化することがわかった[6]。さらに銀樹の形状が球状になることについては，界面における磁化率勾配による磁気力によるものであることを明らかにした[7]。

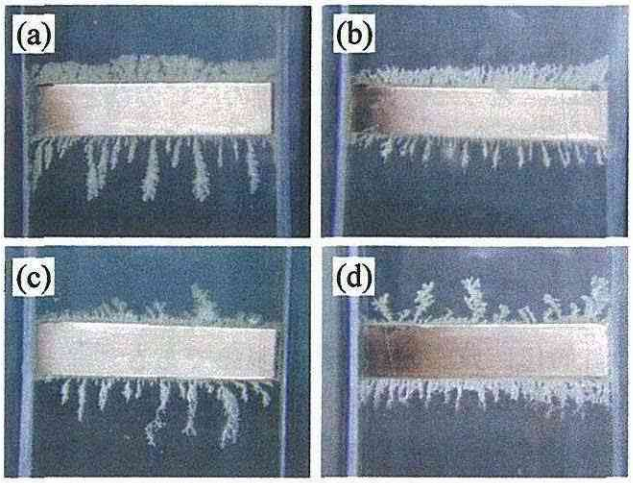

図 12. Cu-Ag^+ 系　板厚 0.1 mm ([$AgNO_3$] = 0.05 mol/dm^3) で生成した銀樹．(a) 零磁場, (b) 9.8 T, +1070 T^2/m, (c) 15.0 T, +50 T^2/m, (d) 5.6 T, -940 T^2/m．磁場の向きは下方向．

磁気力の影響は系を 2 次元にするとより顕著になる。反応溶液の厚さを 0.1 mm にしたときの結果を図 12 に示す。銀樹は銅板の上下に生成し，零磁場では重力の影響で上部の方に密に生成する（図 12(a)）が，磁気力の向きによって，上部により密集（図 12(b)）あるいは逆に下部に密集（図 12(d)）していることがわかる。これは銅イオンに作用する勾配磁場による磁気力によって重力の影響を制御できることを示している。

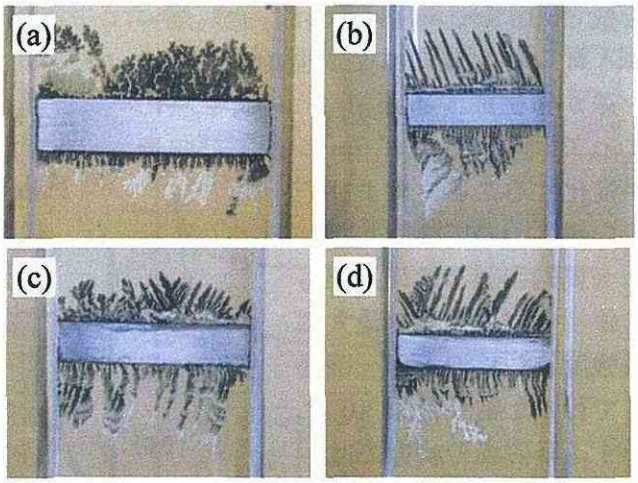

図 13. Zn-Ag^+ 系　板厚 0.4 mm ([$AgNO_3$] = 0.05 mol/dm^3) で生成した銀樹．(a) 零磁場, (b) 9.8 T, +1070 T^2/m, (c) 15.0 T, +50 T^2/m, (d) 5.6 T, -940 T^2/m．磁場の向きは下方向．

一方，同じ 2 次元条件でも，金属亜鉛—銀イオン系から生成する銀樹は前述の系の結果と非常に異なる。この反応系は反磁性種のみからなる系であり，磁場の影響は受けにくいと予想されていた.しかし，この系も著しい影響を受けることがわかった（図 13)。零磁場では，樹枝状結晶が成長している（図 13(a)）のに対し，磁場中では銀樹は直線的になり，磁場に対して約 30 度傾けて配向している（図 13(b), (c) および(d)）ことがわかる。また，その角度は磁場条件の違いにかかわらず，ほぼ同じであることがわかる。銀結晶は面心立方のため，結晶そのもの自身は磁気異方性がない。しかし，SEM および XRD の結果から銀結晶の形状および成長方向が異方的であることから，形状磁気異方性による配向であることがわかった[8]。

さらに銀樹成長の初期段階のその場観測を行うと，高さ約 0.5 mm の銀樹が磁場によ

って歳差運動をしていることがわかった（図 14）。歳差運動の回転速度は磁場強度および銀イオン濃度に依存することから，この現象はローレンツ力によるものであることがわかった。その回転速度の濃度依存性，磁場強度依存性から，磁場強度が 8 T で溶液中の銀イオン濃度が 0.04 mol/dm^3 のとき約 1 N/cm^3 の力が銀樹に作用していることがわかった。この現象は化学ポテンシャルが力学的エネルギーに変換しており，非常に興味深いものである[9]。

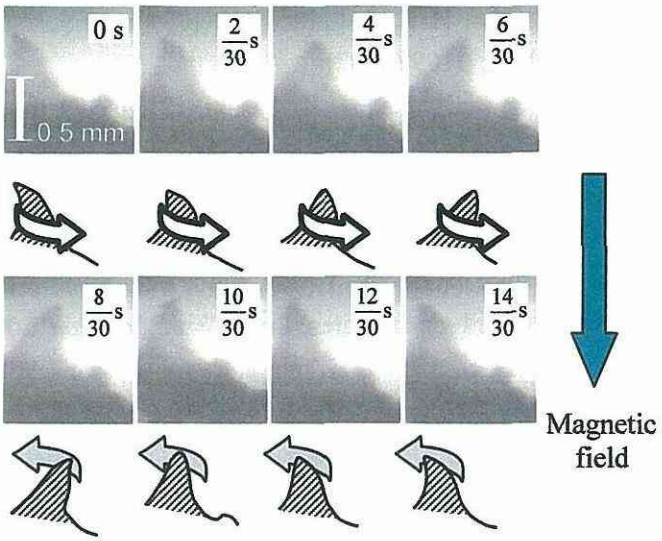

図 14. Zn-Ag$^+$ 系で観測された銀樹の歳差運動.

これまで反磁性種の磁場による配向は分子レベルまたは結晶の磁化率の異方性によるものとして定量的な説明がなされてきたが，アモルファスや磁気 Z 異方性がない無機化合物は形状異方性による配向が可能なのだろうか？強磁性体についての研究は多くあるが，反磁性種についてはほとんどない。そこで，分子的に全く配向していないパラフィンを用いて，形状の違いのみによる配向現象を検討した。その結果，強磁場下では棒状あるいは円盤状の形の違いによる配向の違いが観測された。また，磁場勾配によって配向の向きが変わることがわかった。この現象はこれまで見出されてきた無機結晶で磁化率の異方性では説明が困難な現象について説明が可能となり，あらゆる物体が磁場によって配向できることを示している。

7. おわりに

吸着現象に代表されるように，界面では相互作用を通じて磁気的性質を変え，思いもよらない極めて特殊な磁気状態が可能であり，局所的，異方的，トンネル的現象が磁場と相互作用するようになる。一方で，磁場分布をナノからマクロまで階層的に，空間的，時間的，エネルギー的にデザインすることで，磁場分布に基づく局所デザイン物質，磁気分布デザインされた物質，デザインされた磁場分布に応答する物質群をターゲットとする材料化学が有り得よう。磁場を新たな材料化学におけるエネルギー源として位置づけるだけでなく，さらにソフィスティケーティドには，他のエネルギーあるいはそれによって駆動される物性とシンクロナイズさせることによって，その複雑さに見合った統一性，複雑性，新奇性を期待すべきである。その先には，既存材料の高性能化に留まらず，超極限における未来材料化学が広がっている。

参考文献

[1] 北沢宏一監修，尾関寿美男，谷本能文，山口益弘編著：磁気科学、アイピーシー、2002.　尾関寿美男，未来材料，4（11），42（2004）.

[2] S. Ozeki, H. Kurashima: Encyclopedia of Surface and Colloid Science, Marcel Dekker, ed. A. Hubbard, 3109 (2002).
[3] S. Ozeki, I. Otsuka, H. Kawasaki, H. Maeda: the GelSympo 2003 Digital Proceedings, IIPc07.
[4] S. Ozeki, H. Kurashima and H. Abe: J. Phys. Chem. *J. Phys. Chem. B.* 104, 5657 (2000).
[5] I. Otsuka and S. Ozeki, J. Phys. Chem. B, 110, 1509 (2006).
[6] A. Katsuki, I. Uechi, Y. Tanimoto, Effects of a high magnetic field on the growth of 3-dimensional silver dendrites, *Bull. Chem. Soc. Jpn.* 2004, *77(2)*, 275-279.
[7] A. Katsuki, S. Aibara, Y. Tanimoto, Crystal morphology change by magnetic susceptibility force, *Science Technology of Advanced Materials, in print.*
[8] A. Katsuki, I. Uechi, Y. Tanimoto, The Magnetic Orientation of 2-Dimensional Silver Dendrites, *Bull. Chem. Soc. Jpn.* 2005, *78(7)*, 1251-1255.
[9] A. Katsuki, Y. Tanimoto, Precession of Silver Dendrites in a Magnetic Field Due to MHD Induced Convection, *Chem. Lett.* 2005, *34(5)*, 726-727.

強磁場を用いた新しい物質分離法の開発

山口益弘[1]、島津佳弘[1]、山本　勲[1]、廣田憲之[2]、木吉　司[2]、阿部晴雄[2]
1横浜国立大学・大学院工学研究院、2物質・材料研究機構・強磁場センター

概要

本研究では強磁場を用いて新しい物質分離法を開拓するとともに、その目的にふさわしい新型マグネットを開発した。強磁場印加により、水素同位体分離においては従来よりも同位体分離係数を上昇させることができ、DNA 分離ではその構造的な違いにより明瞭に分離することができ、また生体物質をその反磁性磁化率の違いに基づいて効率的に分離することができた。一方、物質分離に適した磁気力場を増強するマグネットを考案して実機を開発した。

1. はじめに

物質分離は重要な科学的テーマの一つである。本研究は、強磁場印加が引き起こす特有の効果である高磁気エネルギー，磁場配向，高磁気力などを利用して，従来法では分離能が小さかった物質，あるいは分離が困難であった物質を分離・分析する新しい方法を開拓することを目指した。分離すべき対象としたものは，現在および将来に重要である物質である水素同位体，DNA，生体物質である．DNA の新規分離法によりバイオ技術に寄与し，またガラス等の分離処理へ適用でき環境問題にも貢献する。それとともに物質分離のための基礎現象を解明する。その技術的な裏 du づけとなる，物質分離で必要とされる磁気力を効果的に提供できるマグネットを考案する．

2. 強磁場を用いた水素同位体分離

素吸蔵合金を用いる水素同位体（軽水素・重水素・三重水素）分離法は、同位体分離能は他の方法に比して必ずしも高いものではない。本研究では強磁場を印加することによって同位体分離能を向上させること、およびその機構を解明することを目的とした。実験では、強磁性金属水素（重水素）化物 $LaCo_5H(D)_x$ および常磁性金属水素（重水素）$LaNi_5H(D)_x$ を用い，13T までの磁場下で同位体分離実験を行った．分離前のガスは H_2:D_2=1:1 の組成に調整した．金属に H_2 と D_2 を吸収させた後に気相中に残ったガスの組成を分析した(図 1)．その結果，$LaCo_5H(D)_x$ においては零磁場よりも 13T では重水素濃度が 6.1%ほど増大した．一方，$LaNi_5H(D)_x$ を用いた場合には磁場による重水素濃度の増大は見られなかった．同位体分離係数 $\alpha=(D/H)_{gas}/(D/H)_{solid}$ は零磁場での 1.54 から 13T での 2.25 に向上した(図 2)．分離能の上昇は $LaCo_5H(D)_x$ の強磁性に起因して強磁場下で平衡圧の差が増大したことによることが分かった。[1]

さらに、磁場による物質分離の基礎を解明する目的で、水溶液中の単一イオンに対する磁気ミグレーション(Magneto-migration)の存在を

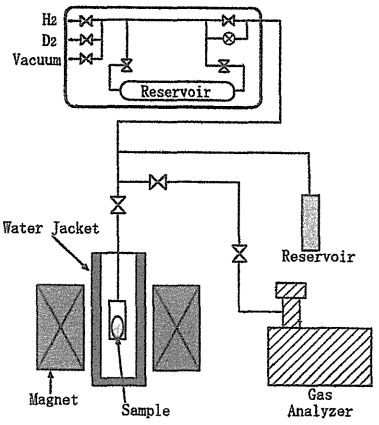

図 1.　水素同位体分離装置

実証した．通常、単一イオンにおける対する磁気力は熱擾乱よりもはるかに弱く、このような磁場効果は通常観測できない。本実験では磁気力をできるだけ大きくするために Dy^{3+}イオン（有効磁気モーメント10.6μ_B）を含む水溶液を13T級マグネットが作る勾配磁場中（磁気力場の大きさB(dB/dz)=588T^2/m）に2週間ほど静置した。その結果は溶液アンプルの両端で0.6%のイオン濃度差を得たものである．[2]

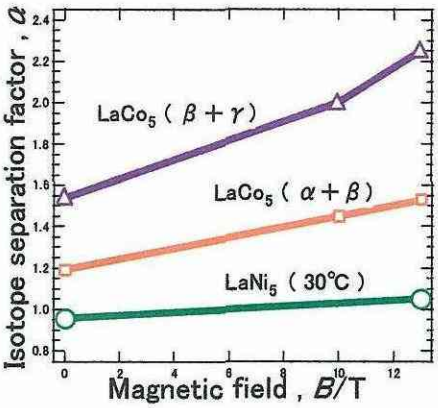

図2. 水素同位体分離能の磁場依存性

3. 磁場配向ゲルを用いたDNA電気泳動

DNAはアガロースゲル中を電気泳動すると長さによって泳動速度が異なるので分離される。DNA電気泳動に対する強磁場効果として、一つには、アガロースゲルを磁場中で作製し、異方的な構造のゲルを用いて泳動速度を測定した。もう一つは、電気泳動を強磁場中で行うことによってDNAを配向させ泳動速度の変化を測定した。いずれも泳動速度が顕著に変化するという結果を得て、磁場を利用した新しい泳動法を提唱した。

アガロースは寒天ゲルを形成するのに欠かせない主成分で、長いひも状の反磁性物質である。熱したアガロース水溶液を室温まで冷却することによってゲル化し、その網目構造はDNAの電気泳動の支持体として用いられる。アガロース分子は磁化率に異方性があるため、強磁場中でゲル化すると分子が配向したゲルが形成されることを見出した。強磁場中で冷却して作製したゲルは、光学的な異方性として10^{-7}程度の複屈折率が出現し、力学的な特性としては貯蔵弾性率に大きな異方性が出現し、磁力線方向に硬いゲルができた。このゲルはアセトン溶液中で異方的に収縮し、収縮し難い方向は硬い方向と一致した。強磁場によるアガロース分子の配向が、異方的なネットワーク構造を持つ配向ゲル中をDNAが移動すると異方的な速度増加が現れ、その変化は泳動電圧に依存した。DNAは、一般に知られる直鎖状の二重らせんDNAの他に、環状のDNAや一本鎖の形状のDNAなどがあり、特定の泳動速度を持つ。異なる形状であっても同等の泳動

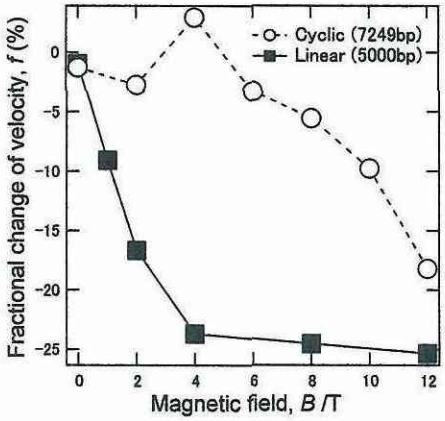

図3. DNAの泳動速度に対する磁場効果。白丸は環状DNA，黒丸は直鎖上DNAで無磁場ではほぼ同じ泳動速度を持つ．[3]

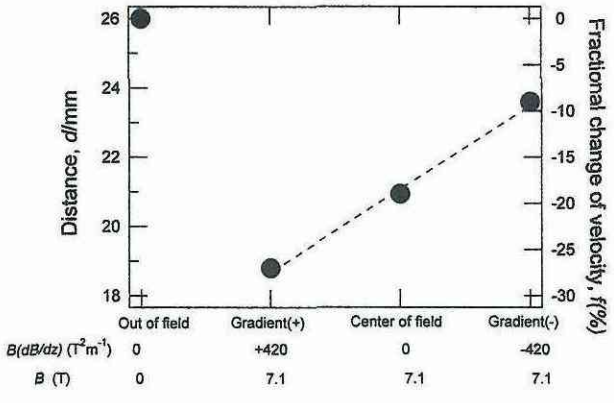

図4. 直鎖状DNAの泳動速度に対する磁場と磁場勾配の効果。無磁場下泳動に比較して、磁場下では泳動速度が減少した。正の磁場勾配はさらに速度が低下した。[4]

速度を持つために分離できないDNAがある。磁場配向ゲルを用いて適当な泳動電圧で電気泳動することで、これまでに分離できないDNAを分離することに成功した。気泳動を行うと、泳動速度の低下が起こる。DNAの電気泳動を12Tまでの磁場中で行い、泳動速度の減少を観測した。図3に結果の例を示した。縦軸は無磁場での平均泳動速度を基準とした速度の変化率であり、形状、長さによって速度低下の挙動は大きく異なった。

反磁性のDNAは不均一磁場（勾配磁場）中で、磁気力を受ける。DNAが電気泳動で陽極へ泳動するクーロン力に比較した磁気力の大きさを調査した。無磁場および7.1Tの均一磁場中、さらに7.1Tで±420T^2/mの勾配磁場中でそれぞれ3回、サブマリンゲル電気泳動を行った。支持体ゲルはTAEバッファー溶液を用いゲル濃度1.0wt.%のアガロースゲル（w70×d96×h34 mm^2）を作製して使用した。75.0mmの白金電極間にDNAとしてEZ Load HT Molecular Markers（Bio-Rad Lab.製）を電極間電圧50V、5.0℃で4時間泳動させた後、10kb長のDNAバンドを観測し、泳動距離および平均的な移動速度の変化率を算出した。ここで、電界の印加方向（泳動方向）は磁力線の向きと平行にした。結果を図4に示した。[4] 無磁場での泳動距離26.0mmに対し、7.1Tの均一磁場中では泳動距離が21.0mmまで短くなり、速度変化率は–19%であった。この減少は、これまでの研究により、DNAの配向に起因すると考えられる。正勾配磁場中では泳動距離はさらに短くなり19.0mm、負勾配では23.5mmを示した。正勾配磁場でDNAの泳動は加速され、負勾配で減速された。本実験条件では、磁気力はクーロン力の1割程度であると見積もることができる。さらに強い勾配磁場下、あるいは長時間の泳動を行うことで、電極を装着しない泳動槽による磁場のみによるDNAの泳動が可能になると考えられる。DNAを構成するA-TペアとG-Cペアでは水素結合の数が異なるので、DNAの磁化率は塩基対の比(A-T)/(G-C)に依存する。この強磁場を用いた手法は、従来の塩基対の数に対応するリン酸の数による分離と異なり、塩基対の構成比率に対応する磁化率による分離という全く新しいDNAの分離手法である。DNAの高精度分離が達成されることによりバイオ技術に貢献し，またDNA電気泳動の機構を解明することにつながる。

4. 弱磁性物質の重力制御環境と磁気分離

勾配磁場下では物質に対してその磁性に応じた磁気力が作用する。また、周囲媒体の制御によって、磁気力を増強することができる（磁気アルキメデス効果）。本研究では、磁気アルキメデス効果を利用することで得られる重力制御環境によって、生体物質分離など新規の物質分離プロセスの探索、及び、磁気アルキメデス浮上環境の材料プロセスの場としての評価を行なうことを目指した。

図5. 磁気アルキメデス法により分離されたヘモグロビン(上)とフィブリノーゲン(下).

磁気アルキメデス分離適用の対象としては、血液製剤やタンパク質などの生体関連物質のように付加価値の高い物質の他、ガラスリサイクルや、類似有機物間の分離など、工学的観点から実用の可能性のある対象が存在することがわかった。図5はヘモグロビンとフィブリノーゲンの混合物が加圧酸素中で磁気アルキメデス浮上して分離された状態である。[5] さらに、コラーゲンのように、基本構造は共通でも、分子を構成するアミノ酸配列のわずかな違いや、立体構造の違いに起因して、高感度分離が実現すること

も確認した。生体物質の分離については、これまで、磁気的性質の違いが分離パラメータとして利用された例はなかったが、本研究によって、磁気アルキメデス分離法が新たな分離手法として利用可能であることが実証された。

また、磁気アルキメデス浮上環境の材料プロセスの場としての利用に関しては、誘起磁気双極子間相互作用による弱磁性粒子集団の構造形成と、物質流れの制御について検討した。

まず、弱磁性物質であっても、条件を制御することで、自己組織的な構造形成が起こることを見出した。弱磁性物質粒子が多数存在する面に対し、磁場を水平な方向に印加した場合には、1次元のチェーン状構造が、垂直に印加した場合には三角格子構造の形成が観測された。図6は誘起磁気双極子間相互作用により、三角格子状に配列した直径1 mmの金粒子である。[6] 金粒子は、相互作用を増強する目的で、塩化マンガン水溶液に入れられており、磁気アルキメデス浮上によって、溶液表面に浮かんでいる。粒子の存在する面に垂直に印加された磁場によって、金粒子が磁化され、それらが相互に反発することで、互いに接触することなく、この構造を形成している。このような自己組織的構造形成が実験的に観測された粒径範囲は10 μm～1 mmの範囲であった。さらに、分子動力学法に基づくシミュレーションモデルの構築に成功し、多粒子系での構造形成に関する評価を行なった。シミュレーションにより予想された金粒子の2次元配列は、実験で観測されたものとよく一致した。このシミュレーションモデルを利用すれば、今後、さらなる高次構造制御に関する知見が得られると期待される。全ての物質は磁性を有するため、この相互作用による構造制御は非常に応用範囲の広いものである。原子や分子が結晶を構築するように、もっと大きな粒子群において自己組織的な構造形成を可能とする手段となりえ、材料分野などへ新たな磁場応用の展開を示すものとして興味深い現象である。

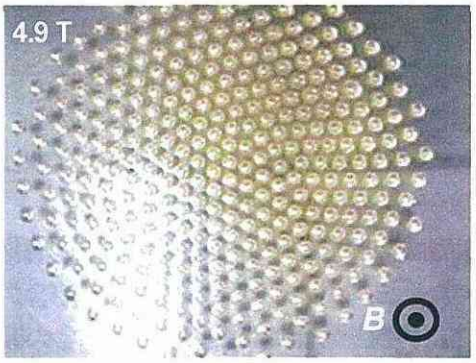

図6. 2次元面内で誘起磁気双極子相互作用により三角格子状に配列した金粒子群

反磁性物質の物質流れに対する磁場影響に関して、水の熱対流に及ぼす磁場効果の評価を、流れの可視化及び熱伝導測定により行なった。この結果、磁気力を作用させる方向に依存して、熱対流の制御が実現することを見出した。また、制御を行なう温度領域によっては、効果の逆転が起こることを見出し、体積磁化率の温度依存を考慮することで理解することができた。常磁性物質の含まれる系では、その磁化率が大きく、温度に依存して大きく変化するため、従来から多くの物質流れの制御に関する報告があったが、反磁性物質のみで構成される系では知られていなかった。水のように温度による磁化率の変化が小さな物質でも、磁気力の利用で流れを制御できると言う知見は、材料プロセスの磁場制御にも通じ、重要な知見であると考えられる。

5. 高機能を有する磁気力制御装置の考案

反磁性物質の磁気浮上、磁気アルキメデス効果の研究では磁気力の増大とその空間分布の制御が重要である。磁気力は磁場と磁場勾配の積に比例するため、強磁場中で大きな磁場勾配を作ることで、大きな磁気力を得ることができる。バルク超伝導体は強磁場中でも高い臨界電流密度を持っているため、これを磁気力の増強に適用することを行った。

図7のように市販の伝導冷却型超伝導マグネット（室温ボア直径100 mm）に挿入可能で、内

部に組み込んだバルク超伝導体を21 Kまで冷却できる磁気力制御装置を開発した。外部磁場11.5 Tを発生した状態でバルク超伝導体を冷却し、超伝導状態とした後で磁場を下げると、図7に示すようにバルク超伝導体内部の磁束がほぼ保存され、大きな磁場勾配が生じていることが確認された。8.5 Tでの磁場分布から計算される磁場×磁場勾配の大きさは-1029 T^2/m に達しており、使用したマグネットが12 Tで生じる-564 T^2/m の2倍近い値が得られている。[7]

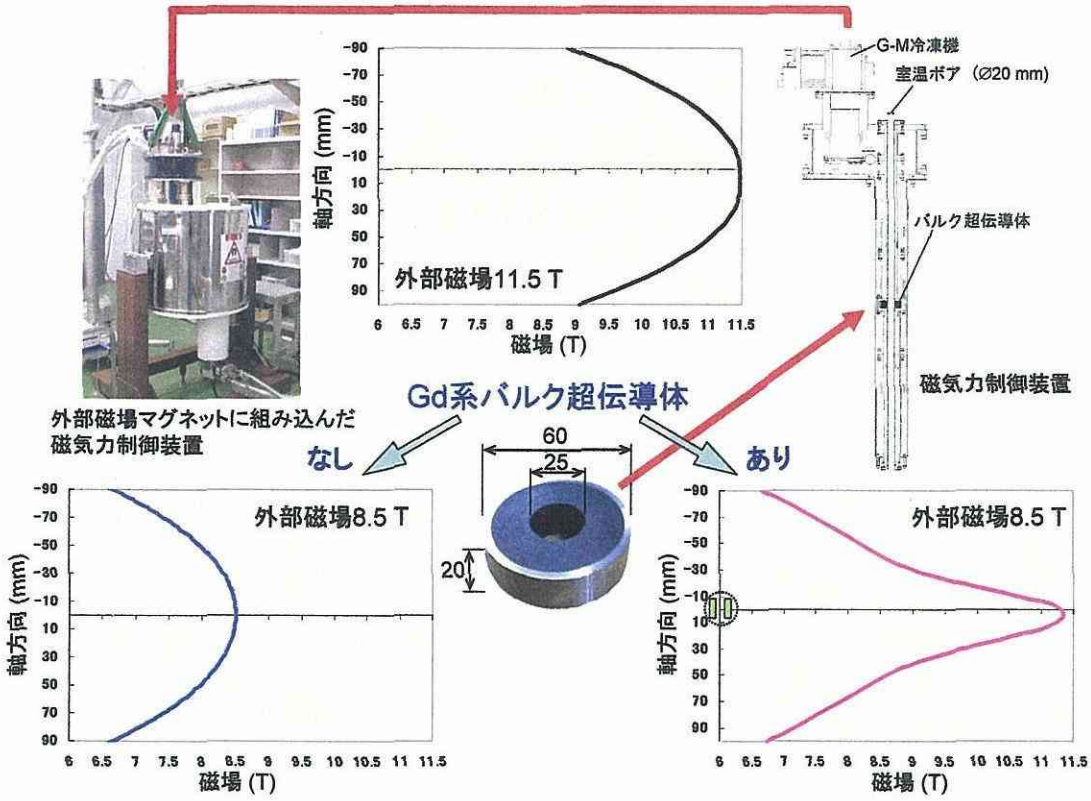

図7. 開発した磁気力制御装置による磁気力増強効果の実証

また全く別の磁気力制御装置として、端部の磁場を使用したWork bench-typeのマグネットも開発した (図8)。従来の超伝導マグネットとは異なり、片側が完全に開放された空間に磁場を発生することが可能である。最初に開発したマグネットは冷凍機のコールドヘッドに直接乗せる形で取り付けており、縦、横回転可能で、永久磁石では発生できない3.4 Tの磁場を発生した。本マグネットは所謂オープングラジエントを利用した物質分離の実験に大いに寄与すると期待している。

6. おわりに

本研究で見出した磁場中電気泳動は、DNA以外の物質群にも広範囲に適用できるであろう。生体物質では磁化率およびその異方性は構造に依存しているので、構造敏感な分離法として発展が期待できる。Work bench-type magnetは今後の利用が広がるものと見込まれる。

図8. 開発したWork bench-typeマグネット

参考文献

[1] Y. Ito, R. Takahashi, S. Mizusaki, I. Yamamoto and M. yamaguchi, Magnetic field effects on the hydrogen isotope separation with metal hydrides, Science and Technology of Advanced Materials, (in print).

[2] I. Yamamoto and M. Yamaguchi, Anisotropic Properties of Magnetic Ordered Gel, Proc. CD ISMS2005, 4O03 (2006).

[3] I. Yamamoto and M. Yamaguchi, Anisotropic Properties of Magnetically Ordered Gel, Science and Technology of Advanced Materials (2006) (in print).

[4] 吉田考平ほか、強磁場を利用したDNAの電気泳動、生体磁気学会誌特別号（2006）投稿中.

[5] N. Hirota, M. Kurashige, M. Iwasaka, M. Ikehata, H. Uetake, T. Takayama, H. Nakamura, Y. Ikezoe, S. Ueno, H. Wada, and K. Kitazawa, Magneto-Archimedes separation and its application to the separation of biological materials, Physica B 346-347, (2004) 267-271.

[6] N. Hirota, T. Takayama, E. Beaugnon, Y. Saito, T. Ando, H. Nakamura, S. Hara, Y. Ikezoe, H. Wada, K. Kitazawa, Control of structures of feeble magnetic particles by utilizing induced magnetic dipoles, Journal of Magnetism and Magnetic Materials, 293 (2005) 87-92.

[7] T. Kiyoshi, T. Koizumi, X. Liu and S. Matsumoto, Magnetic force enhancement using an HTS bulk cylinder, Proc. CD ISMS2005, 1O12 (2006).

強磁場印加プロセスによる金属・酸化物の組織制御と新機能性材料の創製

掛下知行[1]、植田千秋[2]、福田隆[1]、寺井智之[1]
1大阪大学・大学院工学研究科、2大阪大学・大学院理学研究科

概要

本研究では、スピンが関与した結晶磁気異方性とスピンが関与しない反磁性異方性を利用した新しい構造・組織・機能を有する材料の創製と目指した。そのひとつとして、強磁性形状記憶合金における磁場による双晶変形挙動を詳細に調べ、磁場によりバリアント再配列が起きる条件を定量的に評価した。また、反磁性異方性$(\Delta\chi)_{DIA}$を固体全般にわたって集積するシステムを、微小重力および永久磁石を用いた装置を導入することにより確立した。結晶固有の$(\Delta\chi)_{DIA}$は、個々の結合軌道に一定の異方性を仮定することで説明された。その値を用いた解析の結果、反磁性のミクロン粒子の大多数は、2テスラ以下の磁場で配向することが明らかとなった。

1. はじめに

物質の性質は、一般に磁場方向に対して等価ではなく、異方性を有している。この磁気異方性は、スピンが関与する結晶磁気異方性等とスピンが関与しない反磁性異方性があり、その起源の解明は物質内の磁気的相互作用を理解する上で重要であり、多くの研究がなされている。また、この異方性、特に、結晶磁気異方性は実際に使用される磁性材料（磁気メモリー、磁歪、磁石、電磁鋼板等）の中心的な役割を担う現象であることは衆知のとおりである。本研究では、スピンが関与する結晶磁気異方性とスピンが関与しない反磁性異方性を利用した新しい構造、組織、機能を有する材料の基礎物性と材料開発を目指した。（1）スピンが関与する磁気異方性については、磁場により結晶学的ドメインが配向する現象がこれまでに、強磁性の形状記憶合金であるFe_3Pt, Fe-Pd, Ni-Mn-Gaにおいて見出されている。この現象は、結晶磁気異方性により定性的には説明されているが、その定量評価についてはほとんどなされていない。本研究では、磁場による結晶学的ドメインの配向を定量的に説明できるモデルを構築した。ところで、磁場により結晶学的ドメインが制御されると、数%にも及ぶ巨大な歪みが磁場で制御できることになる。このように、磁場による結晶学的ドメイン制御は機能制御につながり、アクチュエータなどに応用できるものと期待されている。（2）スピンが関与しない磁気異方性に関しては、固体の大多数を占める反磁性体は自発磁化を有さず、その磁気的効果が検討されることはあまりなかった。しかし反磁性の固体は、反磁性磁化率の異方性$(\Delta\chi)_{DIA}$のために磁場配向する可能性を一般に有している。この特性に起因した新しい効果が、この特定領域研究でも数多く報告されている。しかし$(\Delta\chi)_{DIA}$は一般に微弱で既存の感度では検出が困難な場合が多い。このため配向には数テスラ以上の強磁場が必要と考えられてきた。またその研究は、機能性材料として関心が持たれる一部の物質に集中していた。そこで本研究では、新規の測定法を開発することにより、$(\Delta\chi)_{DIA}$の効率的な集積をめざした。

2. 強磁性形状記憶合金における巨大磁場誘起歪

物質の形状および体積は、温度・応力はもちろんのこと磁場付加よっても変化する。すなわち磁場により歪が生じる。磁場による代表的な歪発現の機構として、スピン・軌道相互作用を通した格子の弾性歪と磁気転移による体積磁歪がある。特に、前者は磁歪と呼ばれる。その代表的な

材料としてTerfenol-Dと称される$Tb_{0.3}Dy_{0.7}Fe_2$単結晶が挙げられ、磁場により0.1～0.2%もの歪が発生する。後者の例として、Fe-Rh合金の磁場誘起反強磁性-強磁性転移が挙げられる。この転移に伴い、約0.8%もの体積膨張が起きるが、転移磁場が高いため実用には至っていない。

最近になり、上述した機構とは全く異なる磁場誘起歪が強磁性を示すNi-Mn-Ga形状記憶合金の熱弾性型マルテンサイト相においてUllakkoらにより見出された。この歪は数%にも達し、かつ比較的弱い磁場で発生するため、その基礎ならびに応用に多くの関心が寄せられている。

この機構は磁場によるマルテンサイトの結晶学的ドメイン（バリアント）の再配列に起因する。形状記憶合金のマルテンサイト相は、幾つかのバリアントから構成されている。簡単のために、図1に示すように2種類のバリアントから構成されている場合を考える。温度を下げてマルテンサイト変態をさせると、全てのバリアントは、同じ量だけ生成し、変態に伴う外形変化ができるだけ小さくなるように配置する(図1 a→b)。これらバリアント間の界面は比較的容易に移動することが可能な双晶面になっている。したがって、外部から剪断応力τを加えると、双晶変形により大きな歪が現れる（図1 b→c)。この大きな歪は、高温相に戻すことにより消失する(図1 c→a)。これが、通常の形状記憶効果である。マルテンサイト相が強磁性の場合には、結晶学的ドメイン構造に加えて、磁区構造が存在する。磁気モーメント$\boldsymbol{m}$は、外部磁場が無い場合は、それぞれのバリアント内で図2(b)の矢印で示す磁化容易軸方向を向いていると考えられる。この状態において、一方のバリアントの磁化容易軸方向（他方にとっては磁化困難軸方向）に外部から磁場$\boldsymbol{H}$を印加すると、磁気モーメントが磁化困難軸方向を向いたバリアントは、磁気モーメントが容易軸を向いたバリアントに比べて、結晶磁気異方性エネルギーの分だけエネルギーの高い状態になり不安定となる。その結果、バリアント界面を介して磁気的な剪断応力(τ_{mag})が働き、このτ_{mag}が、双晶界面の移動に必要な応力(τ_{req})よりも大きいならば、バリアント再配列が起き、大きな歪が現れる(図1b→c)と考えることができる。

上述した機構を考慮すると、磁場によりバリアント再配列が起きるためには、大きな結晶磁気異方性を有すると同時に低いτ_{req}を持つことが必要条件と言える。本研究では、磁場によりバリアント再配列が起きるFe-Pd系、Fe-Pt系、ならびにNi_2MnGaにおいて上述した関係、すなわち$\tau_{mag}>\tau_{req}$が実際に成り立っていることを明らかにした。[1-7]

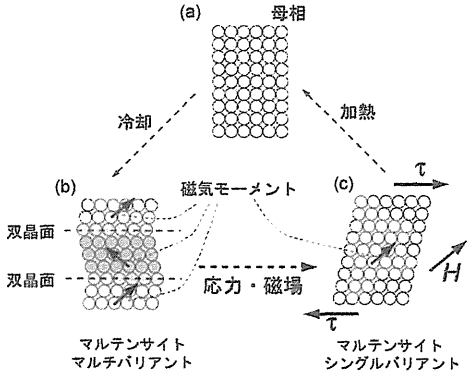

図1. 応力ならびに磁場によるバリアント再配列の概念図。

はじめに、巨大磁場誘起歪を示す3種の合金Fe-31.2Pd(at.%)、Fe_3PtならびにNi_2MnGaのマルテンサイト変態挙動ならびに磁気転移について概説する。Fe-31.2Pd合金は高温からの焼入れにより凍結したA1型構造の母相からf.c.t.と呼ばれる正方晶のマルテンサイトに変態する。Fe_3Ptのマ

ルテンサイト変態は規則度($L1_2$型)に依存するが、規則度が0.8程度の母相は$L6_0$型構造の正方晶へとマルテンサイト変態する。また、Ni_2MnGaは$L2_1$型構造の母相から、10M構造と呼ばれる擬正方晶のマルテンサイト相に変態する。これらの合金の変態温度はFe-31.2Pdが230K、Fe_3Ptが85K、Ni_2MnGaが202Kである。これら合金の格子定数の温度依存性を図2に示す。Fe-31.2PdとFe_3Ptのマルテンサイト相の格子定数は変態温度以下において徐々に変化するのに対して、Ni_2MnGaの格子定数は変態温度において大きく変化し、それ以下ではあまり変化しない。いずれの合金においても、マルテンサイト相における軸比は、77Kで(Fe_3Ptについては4.2Kで)約0.94程度であることが特徴である。磁化容易軸はFe-31.2Pd合金ではa軸であり、Fe_3PtとNi_2MnGaではc軸である。マルテンサイト相を正方晶として取り扱うと、マルテンサイト相には3種類の格子対応バリアントが存在することになる。これらのバリアント間の界面は$\{101\}_M$(Mはマルテンサイト相を表す)双晶面となっている。また、母相の$[001]_P$(Pは母相を表す)方向は、ひとつのバリアントではc軸であり、他の2つのバリアントではa軸となる。キュリー温度はFe-31.2Pdでは約650K、Fe_3Ptでは約450K、Ni_2MnGaでは約376Kであり、Fe-31.2PdならびにFe_3Ptはインバー合金としても良く知られている。

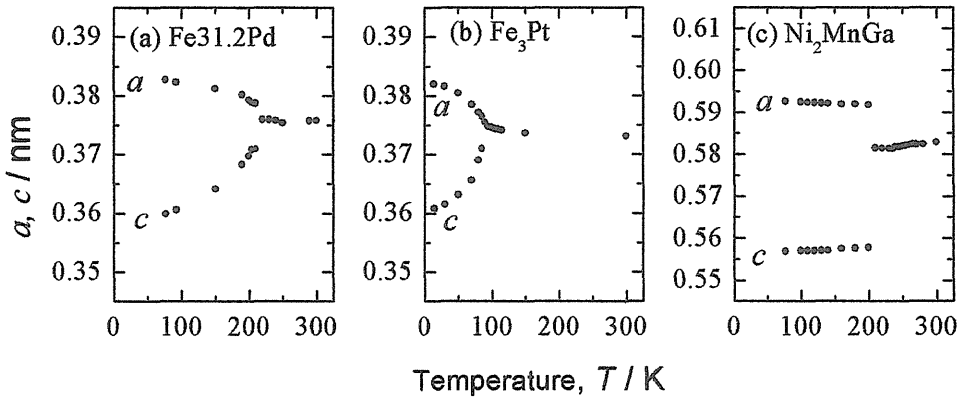

図2. Fe-31.2Pd, Fe_3PtならびにNi_2MnGaの格子定数。

これら合金単結晶を無磁場下で冷却しマルテンサイト単相にした後に、$[001]_P$方向に磁場を印加した際の$[001]_P$方向への歪をキャパシタンス法で測定した。それらの結果を、図3(a) (Fe-31.2Pd)、(b) (Fe_3Pt)、(c) (Ni_2MnGa)に示す。いずれの合金においても約0.25MA/m付近の磁場から試料の変形が始まっていることがわかる。すなわち、Fe-31.2Pd合金では磁場方向に伸び、Fe_3PtならびにNi_2MnGaでは磁場方向に収縮している。このように歪方向が合金により異なるのはそれらの磁化容易軸が異なるためである。この歪と格子定数から、Fe-31.2PdならびにNi_2MnGaでは結晶磁気異方性エネルギーが最も低いバリアントがほぼ完全に選択されていることがわる(Fe-31.2Pdでは磁化容易軸であるa軸が磁場方向を向いたバリアント、Ni_2MnGaでは容易軸であるc軸が磁場方向を向いたバリアント)。しかしながら、Fe_3Ptでは、容易軸であるc軸が磁場方向を向いたバリアントの割合は70%程度にしか達していない。また、この系の特徴的なこととして、Fe-31.2PdならびにNi_2MnGaの場合とは異なり、図3(b)の曲線Bからわかるように、0.6%もの歪が磁場除去に際して回復することが挙げられる。この歪はその後の磁場印加・除去により繰り返し現れ、その値は、超磁歪材料であるTerfenol-Dにおける磁歪の約3倍にもなる。このような歪みの回復は弾性エネルギーの蓄積によるものであると考えられるが、その起源については未だ明らかでは

ない。以上に述べたマルテンサイト変態温度、軸比、磁場によるバリアント再配列の結果を表1にまとめて示した。

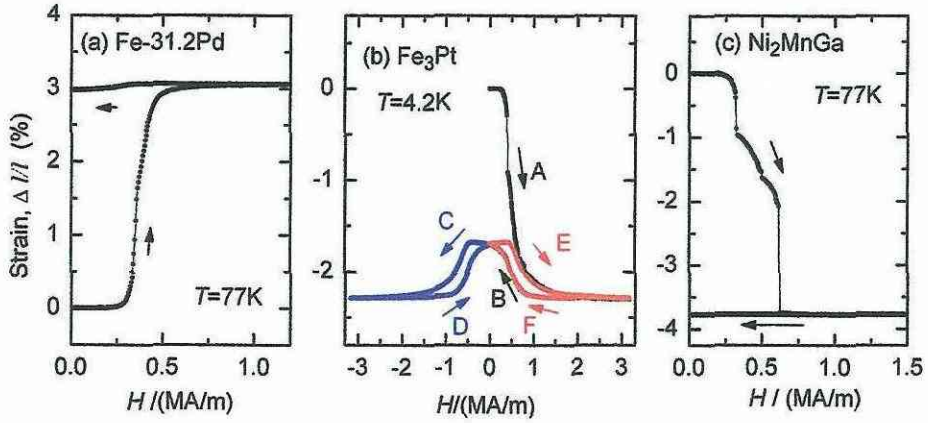

図3. Fe-31.2Pd, Fe3Pt ならびに Ni_2MnGa における磁場誘起歪。

表1　強磁性形状記憶合金の特性

	Fe-31.2Pd (at.%)	Fe_3Pt	Ni_2MnGa
マルテンサイト変態温度(K)	230	85	202
軸比 (c/a)	0.940 (77 K)	0.945 (14 K)	0.940 (77 K)
磁化容易軸	a 軸	c 軸	c 軸
$[001]_P$ 磁場下での $[001]_P$ 方向への歪	膨張	収縮	収縮
$[001]_P$ 磁場下における優位なバリアントの割合	100%	70% (14 K)	100%
磁場除去に際して回復する歪 (%)	0	0.6 (4.2 K)	0
結晶磁気異方性定数 K_u (kJ/m^3)	−180 (77 K)		420 (77 K)
磁気的剪断応力の最大値 τ_{mag}^m (MPa)	1.5 (77 K)		3.4 (77 K)
双晶変形応力 τ_{req} (MPa)	~1 (80 K)		~1.5 (77K)

つぎに、上述したように磁気的剪断応力τ_{mag}がバリアント再配列に必要な応力τ_{req}より大きくなっていることをFe-31.2Pd合金の場合について定量的に示す。その前に、磁気的剪断応力τ_{mag}と他の物理量との関係を示す。この値は、バリアント再配列前後の磁気的エネルギー差、ΔU_{mag}、と双晶変形の剪断量、s、($s=[1-(c/a)^2]/(c/a)$) で、$\tau_{mag}=\Delta U_{mag}/s$ と表される。ΔU_{mag}は主にゼーマンエネルギーと結晶磁気異方性エネルギーからなる。この値は、磁場を磁化容易軸に平行に印加した場合に最大値をとり、その値は、一軸結晶磁気異方性定数$|K_u|$となる。したがって、磁気的剪断応力τ_{mag}を評価するには$|K_u|$の値とsの値が必要となる。sの値は格子定数から算出され、Fe-31.2Pdでは77Kで0.124である。$|K_u|$の値は、磁化困難軸(c軸)方向の磁化曲線と磁化容易軸(a軸)方向の磁化曲線の囲む面積として求めることができる。磁化困難軸ならびに容易軸の磁化曲線を求めるためには磁化測定の間を通して単一バリアントとする必要がある（磁場によるバリアント再配列を

阻止しなければならない)。そこで、試料に一軸圧縮応力を加えて単一バリアントにして測定を行った。77K における測定結果を図4に示す。この磁化曲線の囲む面積より$|K_u|$を求めると、その値は約 180kJ/m^3 となる。求めた$|K_u|$と s の値を用いて、77K におけるτ_{mag} の最大値を算出すると 1.5MPa となる。一方、τ_{req} は単結晶を用いた引張試験により求めることができる。図5は Fe-31.2Pd の 80K における[001]方向への引張試験よりもとめた応力ー歪曲線の一例であり、この図では約 2MPa にステージが見られる。双晶変形のシュミット因子は0.5であるから、この場合τ_{req} は約1MPa となる。このようにして、τ_{mag} の最大値がτ_{req} より大きいことが確かめられる。他の温度においても、τ_{mag} とτ_{req} の値を求めることができ、その結果を図6に示す。この図より、調べた全温度範囲において、τ_{mag} の最大値(τ_{mag}^{m})はτ_{req} より大きいことが確かめられる。しがって、これらの温度範囲において、磁場下で優位なバリアントへと完全に再配列されることになる。

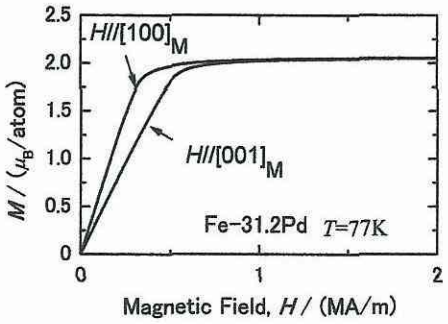

図4. Fe-31.2Pd の磁化曲線。

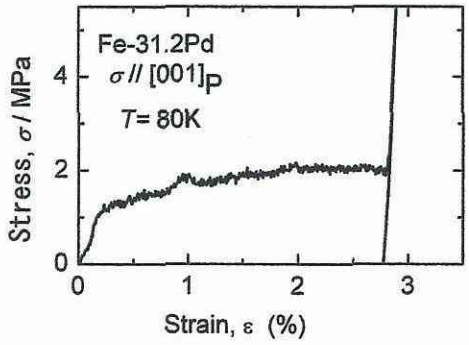

図5. Fe-31.2Pd の応力-歪曲線。

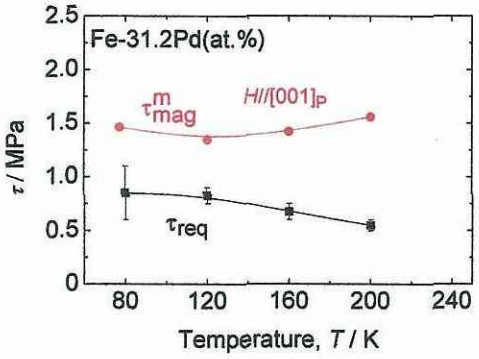

図6. Fe-31.2Pd におけるτ_{mag}^{m} とτ_{req} の関係。

ところで、結晶磁気異方性によるバリアント間のエネルギー差に基づく考え方では、磁場方向を変えることにより、バリアント間の磁気的なエネルギー差が変化するため、顕著な磁場方向の効果があると考えられる。たとえば、磁場を$[110]_P$ 方向に加えた場合には、τ_{mag}^{m} は$[001]_P$ 方向に加えた場合の 1/2 であり、τ_{req} と同程度となる。また、$[111]_P$ に加えた場合には、τ_{mag} は発生しないことになる。実際、これらの方向に磁場を印加してバリアント再配列を調べた結果、$[110]_P$ に磁場を加えた場合は一部でしかバリアント再配列が起きず、$[111]_P$ に印加した場合はほとんど起きないことが確認された。また、多結晶においては磁場によるバリアント再配列は単結晶に比べるとほとんど起きないが、このことは多結晶においては双晶変形応力が約 10MPa 以上となっており、

τ_{mag} に比べて非常に大きいためである。以上のように、磁場によるバリアント再配列においては結晶磁気異方性が主要な要因であると結論される。

なお、Ni_2MnGa についても Fe-31.2Pd と同様な磁化曲線が得られており、77K における K_u は約 420kJ/m^3 であり、これより求めたτ_{mag}の最大値は 3.4MPa である。一方、圧縮試験により求めたτ_{req}の値は 1.2 から 2.2MPa であり、この場合も、τ_{mag}の最大値はτ_{req}より大きいことが定量的に確かめられる。

3. 反磁性物質における磁気異方性の検出と磁場配向条件の検証

反磁性異方性$(\Delta\chi)_{DIA}$は固体中の電子の空間分布の異方性に起因するとされ、有機分子に関する議論が先行してきた。しかし無機結晶については測定値が少なく、未検討のままだった。当グループではこれまで、個々の化学結合に一軸性の$(\Delta\chi)_{DIA}$を仮定したモデルによる解析を行なってきた。今回、酸化結晶を構成する代表的な化学結合として、酸素 4 配位の T-O 結合、6 配位の M-O 結合および水素結合の 3 種類に着目し、各々個別に測定値と計算値の比較を進めた[10]。図 7 にその結果を示す。図中、縦軸は測定値、横軸は結合一本当の$(\Delta\chi)_{DIA}$を単位とした計算値で、個々の結合についてよい相関を得た。さらに各々の相関の傾きから結合一個の$(\Delta\chi)_{DIA}$値が、

- 水素結合：1.1x10^{-30} emu
- [TO_4]の結合：3.7x10^{-30}emu
- [MO_6]の結合：0.32x10^{-30} emu

と推定された。この結果から未測定の結晶の$(\Delta\chi)_{DIA}$値が推定できる。すなわち結晶構造から結合方向を算出し、これに上記の$(\Delta\chi)_{DIA}$を代入することで結晶の値が計算できる。それによると未測定の代表的な結晶構造の大多数は10^{-8}～10^{-10}emu/g の範囲の$(\Delta\chi)_{DIA}$を有する。

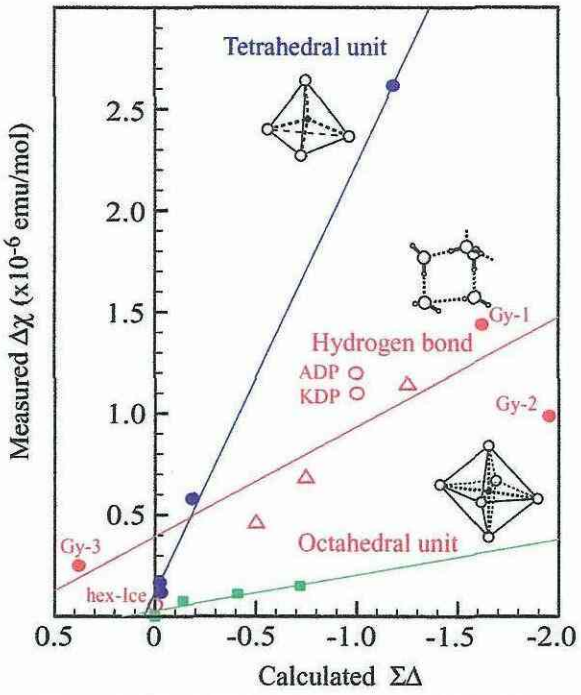

図 7 反磁性異方性の測定値と理論値[10]

ランジュバン&キュリーの古典的な解析に従うと、液体に分散した粒子の配向は粒子の磁気異方性エネルギー $(1/2)\Delta\chi B^2$ がブラウン運動 $(1/2)k_BT$ を 1 桁以上回った時にほぼ完了する。これに従うなら半径ϕ 1 μmの反磁性結晶は、$(\Delta\chi)_{DIA}$ 値が 10^{-9}emu/g を上回る場合、1 テスラ以下の磁場でほぼ配向することになる。この検証実験を、$(\Delta\chi)_{DIA}$既知のグラファイト、コランダム、KDP、セッコウ、フォルステライトについて行い、理論通り低磁場で配向することを確認した[10]。その結果を図 8 に示す。

$(\Delta\chi)_{DIA}$の起源に関する上記のモデルはあくまで古典的な描象に基づくもので、自明であるかどうか必ずしも明確ではない。また、軌道半径が極めて小さい水素結合が 6 配位結合より大きい$\Delta\chi$を持つなど、図 7 の結果に不明な点も多数存在する。これらは物性物理もしくは量子化学で、今後取り組むべき課題である。後述の馬蹄形磁石による単結晶の回転振動をみると、グラファイト、方解石、生石膏、フォルステライト、黒ウンモは同条件で全く異なる周期で振動する（図 12 参照）。その原因について、本質的な答えはまだ見出されていない。

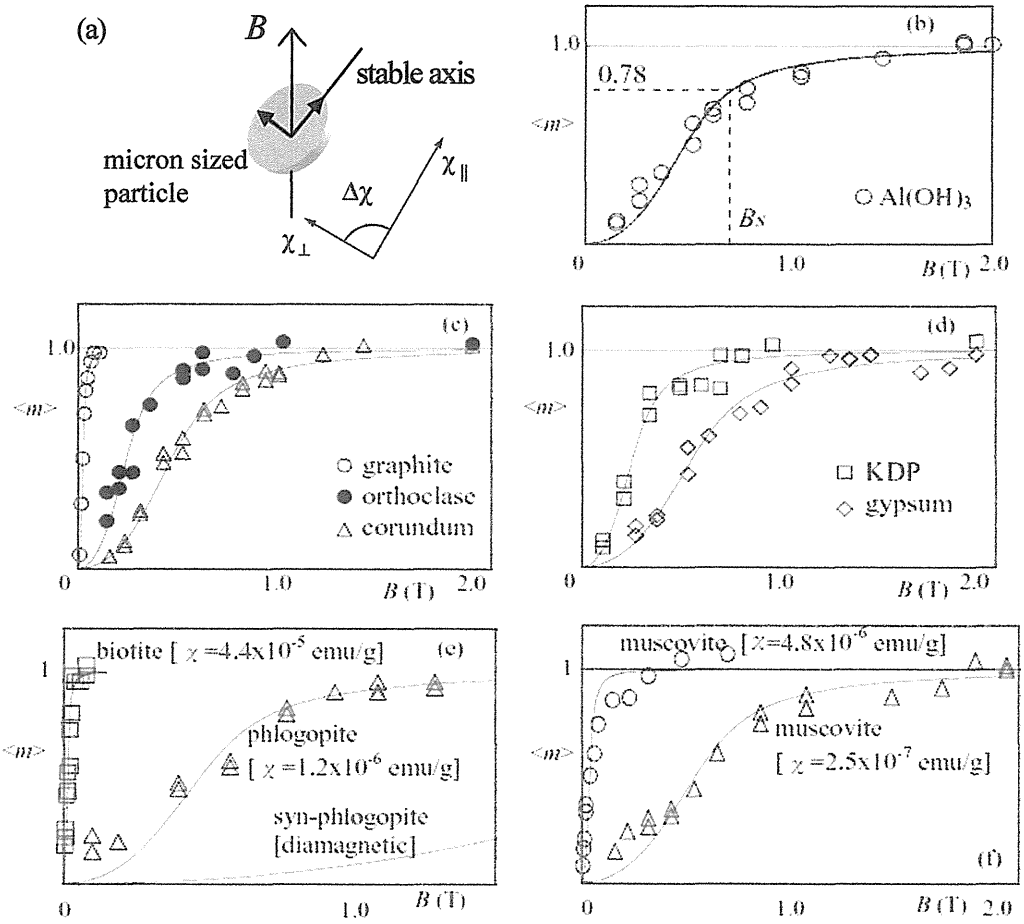

図8　反磁性粒子の磁場整列過程[10, 12]

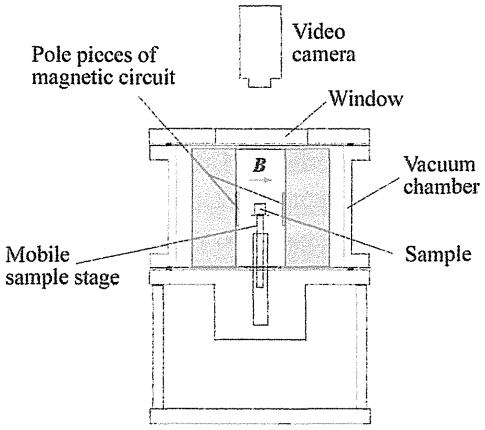

図9　微小重力実験で用いた装置[9]

現実の反磁性結晶は磁性イオンを含む場合が多く、これに起因する常磁性異方性$(\Delta\chi)_{para}$も配向の重要な要因となることが明らかとなった[12]。図 8-(e)(f)に見られるように、結晶に数パーセントの常磁性イオンが置換することで、配向に要する磁場は 0.01 テスラのレベルまで減少する。従って整列は馬蹄形磁石程度の弱磁場で実現することになる。なお$(\Delta\chi)_{para}$がキュリー則

に従って温度変化するため、低温において配向磁場の減少はさらに顕著となる。

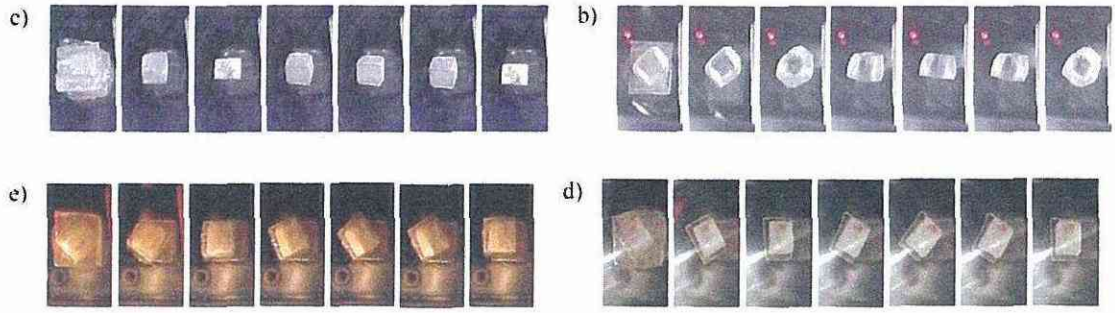

図１０ 微小重力実験の結果[9]

現存する膨大な種類の物質のほとんどについて、その反磁性異方性$(\Delta\chi)_{DIA}$は未測定であり、その集積が急務である。既存の$(\Delta\chi)_{DIA}$測定では、試料を固いファイバーで水平磁場中に吊す。試料には安定軸を磁場方向に回転させるトルクが働き、これとファイバーのネジレを復元しようとするトルクがつり合う。このバランスを利用するため、$(\Delta\chi)_{DIA}$の感度の上限は復元トルクで制限されていた。当グループではこれまでに、極細ファイバーを用いる事で復元トルクが無視できる条件を実現した。この時、安定軸は磁場方向を中心に回転振動し、その周期から復元トルクを用いずに$\Delta\chi$が検出された。この方法によって 10^{-9}emu/g のレベルの$(\Delta\chi)_{DIA}$を容易に測定することが可能となり、カンラン石、サファイア、正長石、魚眼石、生セッコウ、水酸化マグネシウム、KDP、など基本的な酸化物　の$(\Delta\chi)_{DIA}$値をあらたに得た。

ところで前述の考察によると、未測定の酸化物の中には$(\Delta\chi)_{DIA}$が 10^{-10}emu/g レベルのものが存在する。従って$(\Delta\chi)_{DIA}$の集積には、さらに高い感度を必要とする。感度を向上させる最もシンプルな方法は、ファイバー自体を除去することである。これを検証するために、図９に示す装置を日本無重量総合研究所(MGLAB)および産業技術総研究所・北海道センター(AIST) の落下カプセルに搭載し、微小重力下での実験を進めた。その結果、磁場中に浮遊させた結晶の磁気的安定軸が、磁場方向を基準にして回転振動することを確認した[9]。生セッコウ、方解石、尿素、酒石酸の観測結果を図 10 に示す。この実験の準備段階において、微小重力中に浮遊させた試は大きな併進運動をすると予想された。このため大きな均一磁場空間をヘルムホルツコイルで発生させ、試料が並進運動したとしても、均一磁場中に滞在するようにした。試料台を微少重力の達成直後に高速で引き抜く事で、併進運動が 0.5 cm 以下に抑えられた。実験パラメータを変えた時の周期は理論値と一致し、測定原理の有効性が確認された。

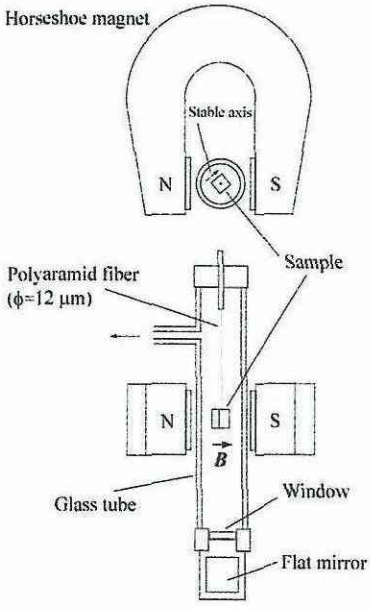

図 11. 馬蹄形磁石を用いた簡易型の測定装置。

現行よりさらに長い周期の実験（例えば航空機での 20 秒あるいは軌道実験での 100 秒レベル）が実現すれば、感度は桁違いに向上する。宇宙実験で得られる感度はこれまで達成されたことのない一種の未知領域であり、微小な電子分布の異方性に起因した

新たな研究の端緒となる可能性を有する。

先に述べたように、未測定の固体の多くは $1x10^{-8}$emu/g 以上の $(\Delta\chi)_{DIA}$ 値を持つことが予想される。そこで感度の向上と並行して、馬蹄形磁石を用いた簡易型の測定装置を地上重力条件で開発した（図 11 参照）。$\Delta\chi$ が 10^{-8} emu/g を上回り、さらに磁場中に試料を吊るすためのファイバーとして直径 12 ミクロンのポリアラミド細線を用いた場合、磁場強度が 0.01T レベルの弱磁場でも吊糸のネジレ復元力は無視でき、浮遊試料と同等の $\Delta\chi$ 測定が実現する。その測定例を図 12 に示す。検証実験の結果、10^{-5} ～10^{-8} emu/g の範囲の $(\Delta\chi)_{DIA}$ が測定可能であることが確認された[11]。

自発磁化の磁場的作用は、方位磁石が地磁気により回転振動するという直感的な現象によって、古くから広く認識されてきた。その認識が今日の数々の磁気デバイスを創出する要因となった。今回、同様の回転振動が図 10 および図 12 のように通常の結晶で観察されたことで、反磁性物質も日常的な磁場で活性である事が、ひろく認識されるようになると期待される。

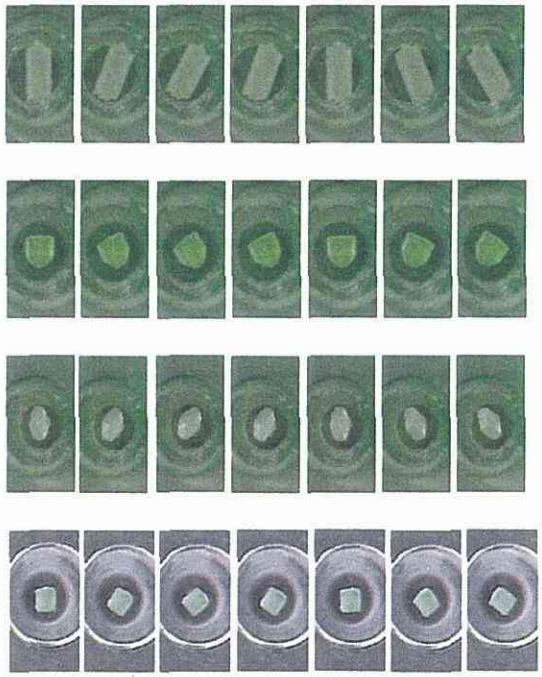

図 12. 馬蹄形磁石による反磁性結晶の回転振動の連続写真で、a) 尿素、 b) カンラン石、 c) 方解石、 d) タルクの例を示す。磁場(B=0.01T)は上下方向に印加されている[11]。

4. おわりに

本研究では、磁場を用いた組織制御による新機能性材料の創製を目的とし、磁気異方性の測定と、磁場による配向実験を２種類の物質について行った。

ひとつは、強磁性形状記憶合金であり、この場合、単一バリアントにした状態で磁化測定を行うことにより、結晶磁気異方性定数を測定し、この値をもとに磁場によるバリアント再配列の起きる機構を明確にすることに成功した。今回は、主に無拡散変態における磁場による組織制御の機構を明らかにしたが、拡散変態においても結晶磁気異方性により組織制御が可能であることを CoPt の規則化過程において確認した。今後は、拡散過程において磁場による組織制御が起きる条件を明らかにする予定である。

もうひとつは反磁性物質であり、今回、測定値に基づく解析により $(\Delta\chi)_{DIA}$ の大多数は 10^{-8}～10^{-10} emu/g の範囲にあることが推定された。これに対して、微小重力下で感度を向上させ、さらに簡易型システムを開発することにより、上の範囲の $(\Delta\chi)_{DIA}$ を効率的に集積する見通しが得られた。一方、検出した $\Delta\chi$ 値を用いることで、反磁性粒子を配向させるのに必要最低限の磁場強度が予測でき、効率的な配向プロセスを設計することが可能となる。一連の研究により、大多数の反磁性体が実用的な低磁場で磁気的に活性であることが明確となった。

参考文献

[1] T. Sakamoto, T. Fukuda, T. Kakeshita and K. Kishio, Rearrangement of martensite variants under magnetic field applied along [001], [011] and [111] directions in Fe-31.2mol%Pd

[2] 阪本辰顕、福田隆、掛下知行「強磁性形状記憶合金 Fe-31.2mol%Pd の一軸結晶磁気異方性定数ならびに双晶変形応力」日本金属学会誌 69 (2005) 649-653.

[3] N. Okamoto, T. Fukuda, T. Kakeshita and T. Takeuchi, Magnetocrystalline anisotropy and twinning stress of 10M and 2M martensites in Ni-Mn-Ga system, Materials Science Forum, 512 (2006) 195-200.

[4] N. Okamoto, T. Fukuda, T Kakeshita, T Takeuchi and K Kishio: Rearrangement of variants in Ni_2MnGa under magnetic field, Science and Technology of Advanced Materials 5 (2004) 29-34

[5] T. Sakamoto, T. Fukuda, T. Kakeshita, T. Takeuchi and K. Kishio : Giant magnetic field-induced strain due to rearrangement of variants in an ordered Fe_3Pt, Science and Technology of Advanced Materials 5 (2004) 35-40

[6] J-h Kim, T. Fukuda and T. Kakeshita, A new phase induced in Ni2MnGa by uniaxial stress, Scripta Materialia 54 (2006) 585-588.

[7] T. Sakamoto, T. Fukuda, T. Kakeshita, T. Takeuchi and K. Kishio, Magnetic field-induced strain in iron-based ferromagnetic shape memory alloys, J. Appl. Phys. 93 (2003), 8647-8649.

[8] C. Uyeda, K. Tanaka and R. Takashima, Stabilization of Position of a Solid Body Isolated in Micro-Gravity and Field-Induced Rotational-Oscillation Caused by Diamagnetic Anisotropy, Jpn. J. Appl. Phys. 42, L1226-L1228 (2006).

[9] C. Uyeda, M. Mamiya, R. Takashima, T. Abe, H. Nagai and T. Okutani, Diamagnetic anisotropy detected by a magnetic oscillation in a drop capsule without suspending crystals with fiber, Jpn. J. Appl. Phys. 45, L124-127, (2006).

[10] C. Uyeda, R. Takashima and K. Tanaka : Magneto-rotation of Nonmagnetic Micro-crystals Caused by Diamagnetic Anisotropy, Appl. Phys. Lett. 86, 094103-1-3, (2005).

[11] C. Uyeda, T. Abe and R. Takashima, Magnetic anisotropy of ordinary crystals without spontaneous magnetic moments detected by rotational oscillations in a reduced field produced by a horseshoe magnet, Jpn. J. Appl. Phys. 46, 1397-1399, (2006).

[12] C. Uyeda, K. Tanaka and R.T akashima, Magnetic Alignment of Non-ferromagnetic Particles Caused by Paramagnetic and Diamagnetic Anisotropy Achieved at Low Field Intensity Due to Reduction of Temperature, Jpn. J. Appl. Phys., 42, (Part 1) 980-984, (2004).

磁場印加プロセスによる有機・無機複合ナノ粒子の創製と機能性ナノ素子の開発

森田　浩[1]、米村弘明[2]、稲場秀明[3]
1 千葉大学工学部、2 九州大学大学院工学研究院、3 千葉大学教育学部

概要

本研究では気相光化学反応を利用して鉄やコバルトを含んだ有機・無機複合超微粒子を作製しその組成と化学構造、および形態が磁場を印加すると変化することを見いだし、また、鉄とコバルトの両成分を含んだ結晶状生成物が磁場配向することを見いだした。また、フラーレン誘導体と電子ドナーを連結した化合物からナノ集合体を作製する方法を考案し、ナノクラスターで修飾した電極の光電変換特性や発光特性が磁場の印加で大きく向上することを見いだした。さらに、導電性ポリマーをラッピングしたカーボンナノチューブを作製して磁場を印加すると溶液の滴下乾燥時に配向し、さらに高磁場下で特異な凝集状態となることを発見した。また、磁場下で測定できる高感度DSC装置を開発し、水や有機物質の融点が6Tの磁場を印加すると数十mKも上昇することを見いだした。

1. はじめに

新規なナノ粒子を創製しそれを利用して機能性ナノ素子を作製することは、急速に発展しているナノテクノロジーの分野において重要な技術となる。本研究では新規な有機・無機複合ナノ粒子を①気相光化学反応を利用した気相ナノ粒子作成法と②フラーレン誘導体と電子ドナーを連結した化合物を合成し、そのナノ凝集体から有機無機ハイブリッド構造を形成させる方法で作製する。第一の光化学反応を利用する方法では、二種類の金属を内包する複合超微粒子やケイ素化合物と有機金属化合物を含む複合超微粒子を作製し、複合超微粒子の化学構造とその粒径をレーザー光で制御し、さらに沈積物の形態と配向を磁場で制御することを試みる。また、第二の方法では有機分子(フラーレン)と無機化合物（希薄磁性半導体）を組織化させたナノ粒子の作製方法や構造を検討し、作製したナノ粒子の光特性（光電変換特性や発光特性）に及ぼす磁場の影響やナノ粒子の作製時に及ぼす磁場の影響を検討する。これによって、ナノ構造及び光特性を磁場によって制御する方法を探る。これらの方法で新規なナノ構造体やナノ素子を構築するための基礎技術が確立できる。また、ナノ粒子を強磁場下で集積すると新規な凝集状態が発現する場合がある。その基礎的な知見を得るために、反磁性および常磁性物質の熱力学的な精密物性測定を強磁場下で行い、物質の相転移における磁場の影響を解析する。そのために、強磁場中で測定可能な1mK程度の温度分解能を持つ高感度示差走査熱量計（DSC）を開発し，有機分子，水，反磁性金属などの相転移に対する磁場効果について測定しその機構について考察を行う。

2. 強磁場とレーザーによる有機･金属複合ナノ粒子の作製

金属元素を含む超微粒子やナノ粒子を作製するため、金属カルボニル化合物（鉄ペンタカルボニル（$Fe(CO)_5$）、またはコバルトトリカルボニルニトロシル($Co(CO)_3NO$)）と二硫化炭素（CS_2）との混合気体試料に水銀灯（313 nm）、または窒素ガスレーザー光（337 nm）を照射した結果、有機金属化合物を含む超微粒子を気相中で作製することができた。超微粒子を作製するための実験条件を検討するため、照射光の波長をArFエキシマーレーザー光を用いて193 nmに、また炭酸ガスレーザー光を用いて10.6 μmとして$Fe(CO)_5$/ CS_2混合気体試料に光照射した結果、光化学

反応は効率良く進行したが、固形生成物としては膜状物質が得られ超微粒子は形成されなかった。これらの実験結果より、気相中で超微粒子を形成するためには ①適度に抑制された粒子核の生成と ②比較的速い粒子の成長速度が必要であることが明らかとなった。

気相中の光反応で生成した粒子核はセル内を対流しながらナノ粒子、超微粒子へと成長し、下部に敷いたガラス基板と衝突して基板上に捕獲される。このため、セルの内径を変えることで対流時間、即ち、超微粒子1個の光化学反応時間が制御できると考えられる。そこで、内径の異なるシリンダー型照射セルを使用して超微粒子の粒径がどのように変化するのかを検討した。$Fe(CO)_5/CS_2$ 混合気体と $Co(CO)_3NO/CS_2$ 混合気体に 313 nm 光を照射した結果、セルの内径を 35mm から 20mm へと小さくすると平均粒径がそれぞれ 0.28μm から 0.19μm へ、また、0.35μm から 0.18μm へと小さくなった。[1] この実験結果から照射セルの内径を変えるという簡便な方法で粒径が制御できることが明らかとなった。

次に、複合超微粒子の形成時（即ち、光照射時）に超伝導磁石で5T までの磁場を印加し、形成された複合超微粒子の化学組成と粒径がどのように変化するのかを検討した。図1に $Fe(CO)_5/CS_2$ 混合気体から生成した超微粒子の FT-IR スペクトルを示す。FT-IR スペクトルを解析した結果、$Fe(CO)_5/CS_2$ 混合気体から生成した超微粒子では5Tの磁場を印加すると粒子中の Fe 成分が増加し、$Co(CO)_3NO_5/CS_2$ 混合気体から生成した超微粒子では5Tの磁場を印加すると粒子中の Co 成分が減少し、複合超微粒子の化学組成が磁場で制御できることが明らかとなった。[2] また、$Fe(CO)_5/CS_2$ 混合気体から沈積した複合超微粒子の平均粒径が 5T の磁場を印加すると約 12%小さくなるのに対して、$Co(CO)_3NO_5/CS_2$ 混合気体から生成した超微粒子の場合には図2 に示すように平均粒径が大きくなることも観測され、微粒子形成に関わ

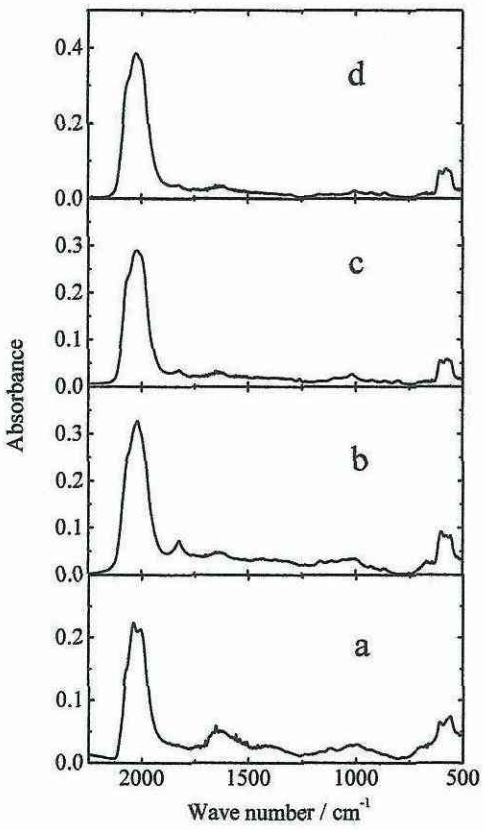

図1．$Fe(CO)_5/CS_2$ 混合気体から生成した超微粒子の FT-IR スペクトル (a) 0 T, (b) 1 T, (c) 3 T, (d) 5 T.

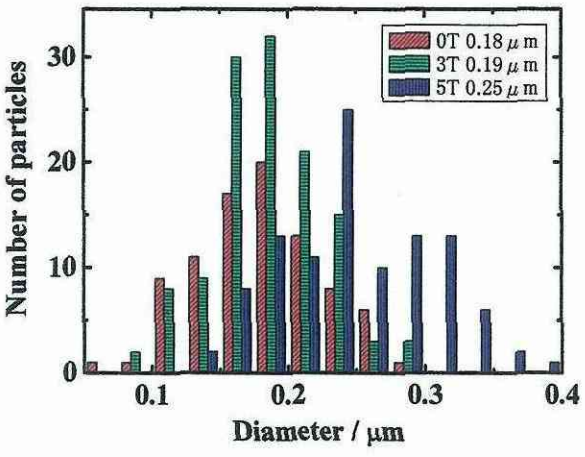

図 2. $Co(CO)_3NO_5/CS_2$ 混合気体から磁場を印加して生成した超微粒子の粒径分布 (赤) 0 T、(緑) 3 T, (青) 5 T.

る化学反応速度も磁場の影響を受けていることが示唆された。

二種類の金属元素を含む粒子を作製するため、$Fe(CO)_5$ と $Co(CO)_3NO$ の混合気体試料に水銀灯（313 nm）光を照射した結果、二種類の有機金属化合物を含む超微粒子（粒径 100～150nm）と有機鉄化合物を主成分とする結晶状物質（大きさ 8～16 μm）を作製することができた。1～5T の磁場を印加すると $Fe(CO)_5$ の光化学反応が促進されると同時に、結晶状の生成物の沈積方向が磁場の方向と垂直に揃うことが観測され、形状依存性による磁場配向を利用して沈積物を配向させることができた（図 3）。また、この混合気体試料に CS_2 を加えると鉄とコバルトを含む超微粒子のみが作製でき、合金超微粒子を作製する手段として CS_2 の化学反応性を利用することができた。また、5 T の磁場を印加すると Fe 成分が Co 成分よりも増加し、磁場を印加すると金属成分の化学組成が制御できることが判明した。

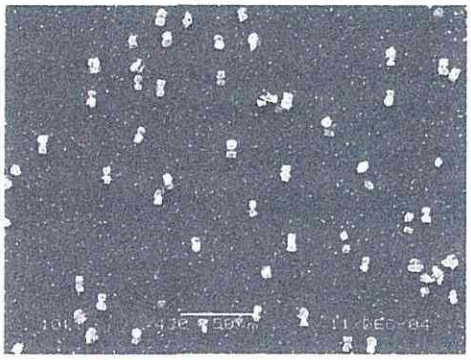

図 3. $Fe(CO)_5$ と $Co(CO)_3NO$ の混合気体から作製した結晶状の生成物。磁場は左右方向に印加されている。

超微粒子中での固相光化学反応を誘起して超微粒子の化学組成と粒径が制御できるのかどうかを検討した。即ち、$Fe(CO)_5$ と CS_2 の混合気体から作製した超微粒子を基板上に沈積させた後、沈積させた超微粒子に水銀灯（313 nm）光、または YAG レーザー光（532nm, 266nm）を光照射した（後露光）。水銀灯（313 nm）の後露光では鉄に配位している CO 基が脱離したが、高密度励起が可能な YAG レーザー光（532 nm）の後露光では 200nm の大きさの粒子が 70nm 程の大きさへと小さくなることが観測され、超微粒子生成後の光照射で化学組成と粒径が制御できることを見出した。

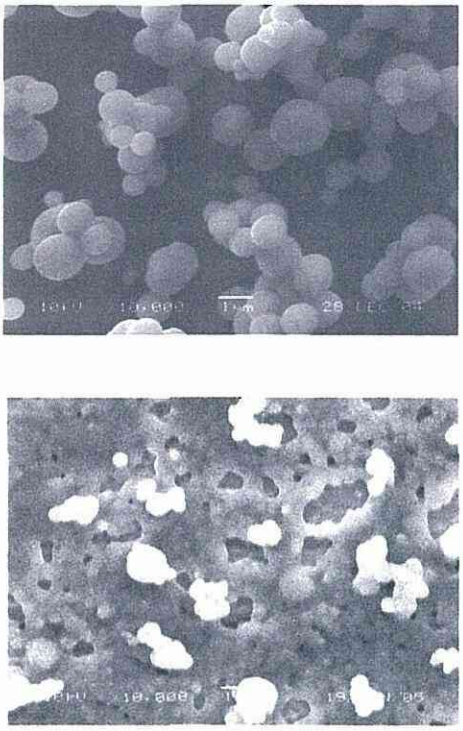

図 4. ATMeSi/$Fe(CO)_5$/CS_2 の混合気体から作製した超微粒子（上）と融着し薄膜化した超微粒子（下）

有機ケイ素化合物と $Fe(CO)_5$ の混合気体試料から複合粒子を作製することを試みた。アリルトリメチルシラン（ATMeSi）と $Fe(CO)_5$ の混合気体に水銀灯（313 nm）光を照射すると約 2.5μm の大きさの結晶状の生成物と 0.5μm の微粒子が形成できたが、混合気体試料に CS_2 を加えると三成分が取り込まれた超微粒子（平均粒径 0.31μm）のみが作製できた。[3] $Fe(CO)_5$ を微粒子化するためには二硫化炭素を加える方法が有効であることが確認できた。磁場（5 T）を印加すると平均粒径は大きくなり、$Fe(CO)_5$ の化学反応性が増大した。図 4 に示すように、この三成分混合気体試料では生成物の形態は ATMeSi と CS_2 の分圧に大きく依存し、ATMeSi を多くすると生成した微粒子が融着し始め膜状物質へと変化することがわかった。

さらに、有機ケイ素化合物としてトリメチルシリルアセチレンを使用し $Fe(CO)_5$ との混合気体試料から微粒子作製を試みた。水銀灯（313 nm）の光照射によりケイ素化合物を含んだ薄膜が形成できたが、3T の外部磁場を印加すると 90nm の大きさの超微粒子のみが形成できることを見い出した。磁場を強く（5 T）すると膜状の生成物が出来易くなり、強磁場により生成物の形態が変化することを見い出した。[4]

気相光化学反応を利用して超微粒子を形成する際に磁場を印加すると、超微粒子の化学組成と粒子サイズ、および生成物の形態が制御でき、さらに混合気体の分圧を最適化すると超微粒子が互いに結合した状態になることがわかった。これらの基礎技術を発展させると種々の化学組成と機能性をもった超微粒子とナノ粒子から様々な素子が組み立てられると期待できる。

3. 磁場印加プロセスによる新規光機能ナノ素子の創製

有機化合物のナノ構造における光特性の磁場制御については、正電荷を持つフラーレン誘導体（$C_{60}N^+$）クラスター－メチルフェノチアジン(MePH)系の溶液中における光誘起電子移動反応に対する磁場効果と $C_{60}N^+$－MePH ナノクラスターを固定化した修飾電極における光電気化学反応に対する磁場効果の研究を行った。C_{60} や C_{60} 誘導体は溶媒を選択することで、C_{60} 同士が会合したナノメーターサイズのクラスターを形成することが知られている。そこで、THF と水の混合溶媒を用いて、図 5 に示す正電荷を持った $C_{60}N^+$ を MePH とともにクラスター化させた。ダイナミック光散乱光度計（DLS）および原子間力顕微鏡（AFM）の観測結果(図 5)より、$C_{60}N^+$ が混合溶液中で約 100nm のナノクラスターを形成する事がわかった。Nd-YAG レーザーの第 3 高調波(355 nm)を用いて、この $C_{60}N^+$ - MePH ナノクラスターの過渡吸収スペクトルを測定した。レーザー光照射によって、MePH の励起 3 重項状態から $C_{60}N^+$ クラスターへの光誘起分子間電子移動反応が起こっている事がわかった。そして MePH ラジカルの散逸ラジカル収量（Δ= Abs(H T)/Abs(0 T)）が磁場の増加に伴って大きく増加する磁場効果が観測できた(図 6)。この磁場効果はナノクラスターによって発現していると考えられる。[5]

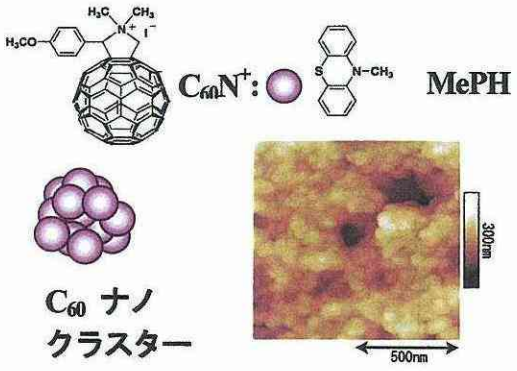

図 5. $C_{60}N^+$ と MePH の化学構造と MePH を含んだ C_{60} ナノクラスターの AFM 像

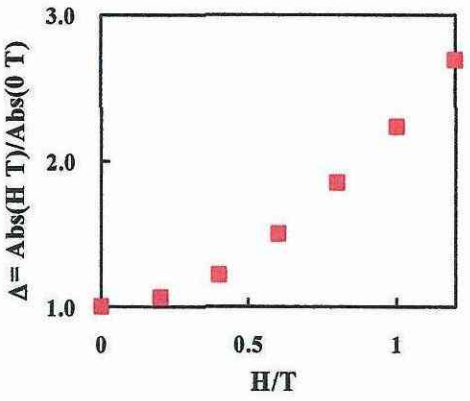

図 6. Δの磁場強度依存性

次に、$C_{60}N^+$－MePH ナノクラスターを固定した修飾電極を次の手順で作製した。金電極上にスルホン酸塩を末端にもつチオール化合物の自己組織化単分子膜（SAM）を形成させた。SAM 金電極を $C_{60}N^+$ -MePH ナノクラスター溶液に浸漬することで，静電相互作用でナノクラスターを修飾電極に

固定した。AFM 測定によってナノクラスターが固定されていることがわかった。光電極を動作極、対極を白金電極、参照極を Ag/AgCl 電極とした 3 極セルを構成し、バルク水相に犠牲試薬としてトリエタノールアミンを添加し、光照射を行うと、アノード方向の光電流が観測できた。アクションスペクトルの結果より、$C_{60}N^{+}$ナノクラスターの光励起によって光電流が起こっていることがわかった。次に、修飾電極の光電流を電磁石中で測定を行った（図 7）。Q 値(%)を Q(%) =(I(H)-I(0))/I(0)×100 と定義した。ここで、I(H)と I(0)はそれぞれ磁場(H；T)を印加した時としない時の光電流の値を示している。Q 値は磁場強度の増加に伴って増加した (0.5T:3%)。この様に$C_{60}N^{+}$−MePH ナノクラスター修飾電極における光電変換機能を磁場で制御することに成功した。[6]

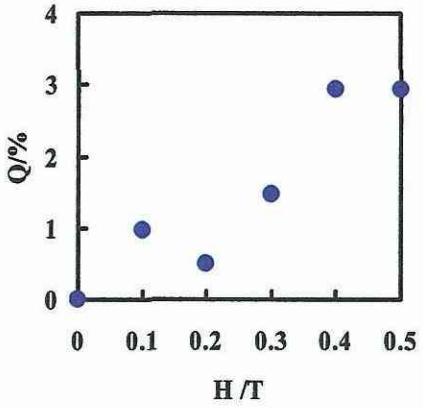

図 7. $C_{60}N^{+}$-MePH ナノクラスター光電極における光電流に及ぼす磁場の影響

次に、無機化合物のナノ構造については、希薄磁性半導体 ($Zn_{1-x}Mn_xS$) 固定化薄膜の発光特性に及ぼす磁場印加プロセスの影響を検討した。数 nm の $Zn_{1-x}Mn_xS$ ナノ粒子を AOT 逆ミセル法によって作製した (図 8)。$Zn_{1-x}Mn_xS$ ナノ粒子では 590nm 付近に発光ピークが観測された。この発光は ZnS からエネルギー移動した Mn^{2+}励起状態からの発光に帰属される。次に、$Zn_{1-x}Mn_xS$ ナノ粒子を石英基板上に SAM によって固定する際に、磁場を印加した場合としない場合の比較を行うことで、薄膜作製過程に及ぼす磁場印加プロセスの効果について検討を行った。W=5 のナノ粒子を用いた場合、磁場強度が増加するに伴って、薄膜の発光偏光度が増加した (表 1)。W=10 のナノ粒子を用いた場合についても同様な結果が得られた。従って、これらの発光偏光度の増加は磁場印加プロセスが原因であることがわかった。

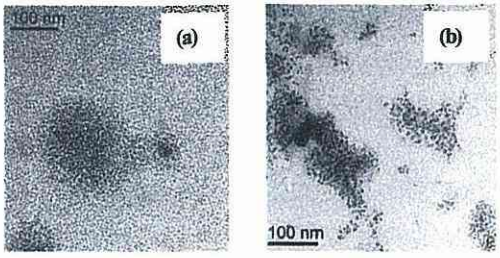

図 8. $Zn_{0.95}Mn_{0.05}S$ ナノ粒子の TEM 像
((a) W=5, (b) W=10)

表 1. $Zn_{0.9}Mn_{0.1}S$ (W=5, 10)のナノ粒子修飾膜の発光偏光度 (p) と磁場強度との関係

	0.2 T	0.6 T	0.8 T
W = 5	0.028	0.05	0.075
W = 10	0.029	0.06	0.076

さらに、同じ磁場強度 (0.8 T) で磁場印加プロセスの効果を比較すると、ナノ粒子中の磁性イオンである Mn^{2+}の成分比すなわち x の値が大きくなるほど、発光偏光度の値が大きくなった (表 2)。従って、この発光偏光度の増加には、ナノ粒子に散在する磁気モーメントを所有する Mn^{2+}が関与していることが明らかになった。

表 2. $Zn_{1-x}Mn_xS$ のナノ粒子修飾膜の組成比 (x) と発光偏光度 (p) との関係

組成比 (x)	発光偏光度 (p)
0.02	0.047
0.05	0.061
0.10	0.079

以上より、上記の結果は、薄膜作製時において磁場印加プロセスが薄膜における Mn^{2+} の発光偏光特性に影響を及ぼしたためと考えられる。言い換えれば、外部磁場がナノ粒子内部の Mn^{2+} と相互作用することで、ナノ粒子の発光偏光特性を増加させるように、配向しながらナノ粒子が基板上に固定化したと考えられる。[7]

次に、強磁場によるナノ構造の制御に関する検討を行った。近年脚光を浴びるカーボンナノチューブ（CNT）には単層カーボンナノチューブ（SWNT）と多層カーボンナノチューブ（MWNT）の２種類がある。これらのCNTは、高伝導性や構造に依存した電子状態の変化など他の物質にはない特異的な電子特性を示すため、次世代の光電変換素子や電子デバイスへの応用が期待されている。CNTの持つ異方的な特性を活かすには、CNTの配向制御を行う必要がある。配向制御の１つとして、強磁場を用いたCNTの磁場配向が注目されている。また、CNTは溶媒に溶けにくく凝集しやすいが、ポリマーで覆い包むことで溶媒に可溶化分散が可能なことが報告されている。そこで、導電性を示すポリマー(MEHPPV)（図9）を用いてSWNT/MEHPPV複合体を形成させた。基板に対して横向きの強磁場を印加した時のSWNT/ MEHPPV複合体の磁場配向について検討した。[8,9]

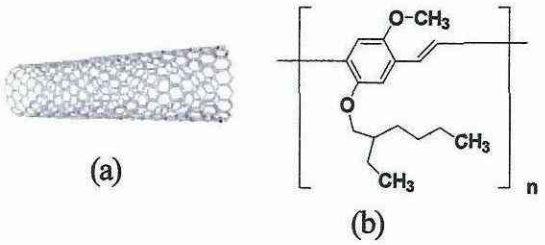

図9. SWNT(a)とMEHPPV(b)の化学構造

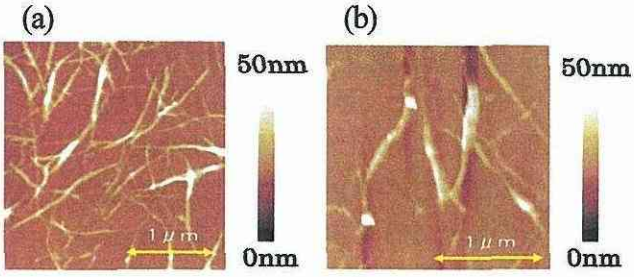

図10. SWNT/MEHPPV 複合体のAFM像（a）無磁場の場合、(b) 磁場（8 T）を印加した場合

SWNT/ MEHPPV 複合体の溶液をマイカ基板に滴下し、乾燥させる際に、横向きの超伝導磁石を用いて８Tの強磁場を印加した場合と無磁場の場合について比較を行った。AFM像を観察すると、無磁場の場合は SWNT/MEHPPV 複合体がランダムに配向していたが、８T の強磁場を印加した時は、外部磁場の向きと複合体の長軸が平行に配向していた(図10)。CNTはCNTの長軸と磁場の向きが平行に並ぶことが知られているが、新規光特性を示すことが期待できるナノスケールの複合体を強磁場によって配向させたことは非常に有意義である。

SWNTを強酸によって短く切断すると、SWNT が分散した水溶液を調製することができる。その水溶液を上記のSWNT/MEHPPV 複合体の場合と同様に横向きの磁場を印加すると、図10と同様にSWNTの長軸と外部磁場が平行に配向する磁場配向が AFM 像において確認できた。従って、SWNT/MEHPPV複合体の磁場配向はSWNTが原因で起こっていることがわかった。

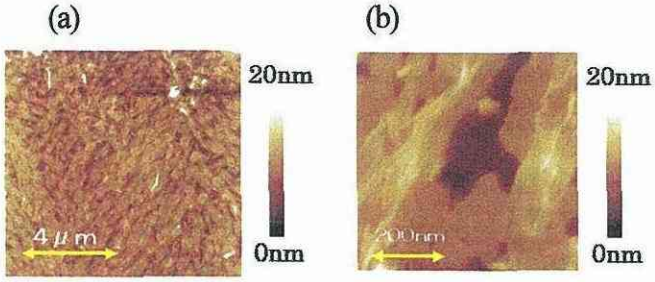

図11. SWNTのナノ構造（磁場強度 5.6 T：磁場勾配 -940 T^2/m）(a) AFM像と(b) 拡大図

次に、強磁場（15T）を用いて、重力と逆向きの磁気力が加わる特殊環境場に試料を置くと、数ナノメーターのファイバーが組織化した非常に興味深いナノ構造が観測できた（図 11)。無磁場や他の磁場環境ではこのナノ構造は観測できず、強磁場が生み出す特殊環境でのみ形成されるナノ構造である。使用した SWNT は 1μm 程度に切断されており、何らかの要因で SWNT がある程度の長さをもつナノファイバーを形成し、乾燥する過程でナノファイバー同士が集まり、網目状のナノ構造を形成したと考えられる。強磁場によって組織化するこの成果は非常に興味深く、詳しい機構については現在検討中である。[8, 9]

さらに、上記の $C_{60}N^{+}$—MePH ナノクラスター溶液をマイカや ITO 基板に滴下し、乾燥過程に強磁場(8 T）を印加して、クラスター形状と酸化還元挙動に及ぼす磁場の影響を検討した。強磁場（8 T）を印加した時の基板の AFM 像には、無磁場の場合とは異なる形状のクラスターが確認された。加えて、磁場の有無により C_{60} 由来の還元ピークが著しい変化を示した。磁場印加により C_{60} クラスターの形状に変化が起こり、加えて酸化還元特性にも変化が生じたと考えられる。

ナノスケールの SWNT/ポリマー複合体や SWNT を磁場によって配向する手法は、SWNT の異方的特性を活用した一つの方法である。また、強磁場によってナノ構造を組織化し、電気特性を変化させる技術は強磁場によるナノ材料プロセスにおいて画期的手法になると考えられる。

4. 強磁場下における反磁性および常磁性物質の精密物性測定

従来、磁気科学ではその研究対象のほとんどが強磁性体に限られており常磁性体や反磁性体はあまり研究対象とされてこなかった。近年，強磁場が比較的容易に入手できるようになり，反磁性物質などの磁場効果が研究しやすくなってきたが，10T 程度の磁場は，熱エネルギーkT と比較して依然として小さいため，磁場効果を検出するためには感度の高い検出装置を磁場下に設置する必要がある。本研究では，強磁場下において測定可能な 1mK 程度の温度分解能を持つ高感度 DSC を開発し，水，有機分子，反磁性金属，誘電体などの相転移への磁場効果の測定を行い，その機構について考察を行った。近年の磁気科学はその研究の場を機能性材料の創製などの新しい分野に拡大しつつあり，磁場下での熱量測定は材料の評価などへの基礎的データを提供することに貢献する。

まず、強磁場下測定用の示差走査熱量計を開発した。内径 100mm の 6 T ボア内に設置した高感度高分解能 DSC の概略図を図 12 に，作成した DSC の写真を図 13 に示す。試料および参照試料の温度差は多段半導体熱電素子(サーモモジュール)で測定する。半導体熱電素子を多段

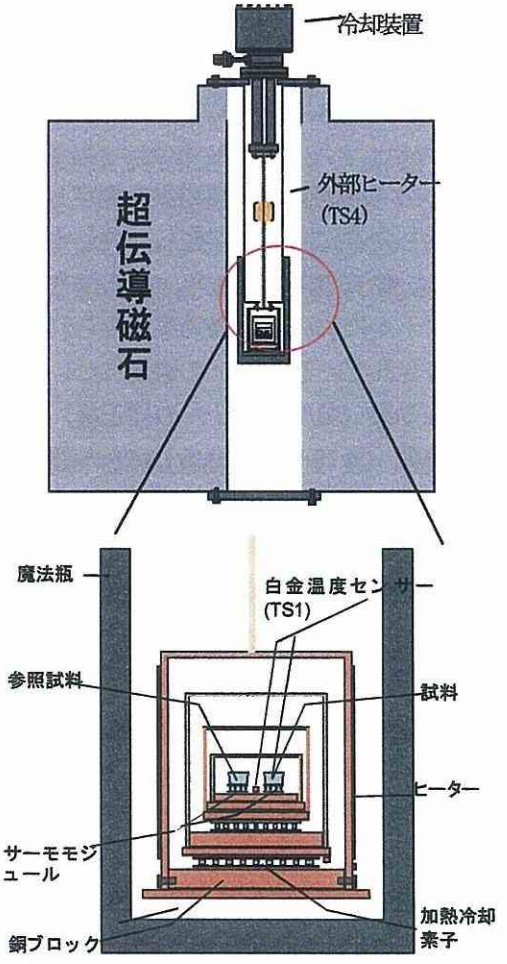

図 12. 超伝導マグネットボア中設置高感度 DSC 概略図

にしていることで DSC の感度を上げている。温度安定度は±0.2mK 程度で，ベースライン安定度は±25nW 程度であった。[10] 測定温度範囲は DSC の外部に冷却装置とヒーターを取り付けることで 120K から 420K まで可能となった。強磁場下での測定を行う前に，サーモモジュールおよび白金抵抗温度センサーTS 1 への磁場効果を調べた。図 14 に TS 1 への磁場印加効果を示す。5T 磁場の印加と除去を繰り返したところ，室温 (288.65K) において，再現性良く 18.2mK の温度上昇が見られた。このとき，外部ヒーターの温度センサーTS 4 への磁場印加効果は 0.4mK であり，TS 1 への磁場効果の 2.2%であった。半導体熱電素子への磁場効果は見られなかった。TS 1 の室温以外の温度においては，TS 4 部分で温度コントロールを行い，図 14 と同様の実験を行い，TS4 への磁場効果を補正した後，TS1 への磁場効果の温度依存性曲線を作成し，磁場印加測定における DSC の温度データの補正を行った。

次に、水の融点への磁場効果を測定した。水は私たちの身に回りに存在し，欠かすことの出来ない物質である。近年，屈折率や近赤外スペクトルにおいて磁場効果がみられることが報告されている。H_2O の融解についての磁場印加効果（温度センサーの補正後）を測定した結果，図 15 に示すように 6T の磁場印加により融点が 5.6±0.7mK 上昇した。D_2O では 6T の磁場印加により融点が 21.9 ±0.7 mK 上昇した。融点が上昇すると言うことは，磁場印加により低温相が相対的に安定化したためと考えられ，屈折率や近赤外スペクトルによる測定の傾向と一致していた。磁場印加による相転移温度の上昇について拡張した Clapeyron の式を用いて検討を行った。融点の上昇の磁場強度依存性の測定結果は，印加磁場の２乗に比例していることが分かり，この点では拡張した Clapeyron の式は成り立っていた。6 T の磁場印加においての計算値は、H_2O では 11.2μK，D_2O では 9.6μK であり，測定値は 1000 倍程度大きい。この解釈には，

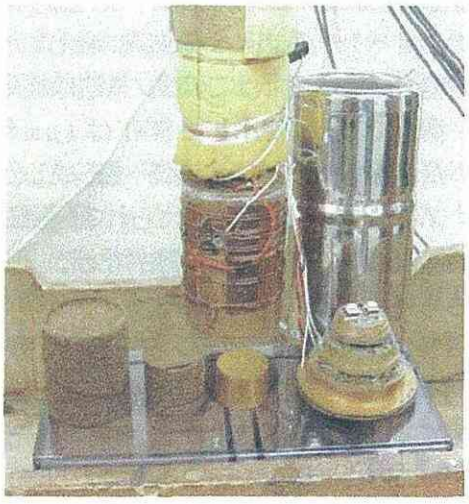

図 13. 強磁場下測定用 DSC

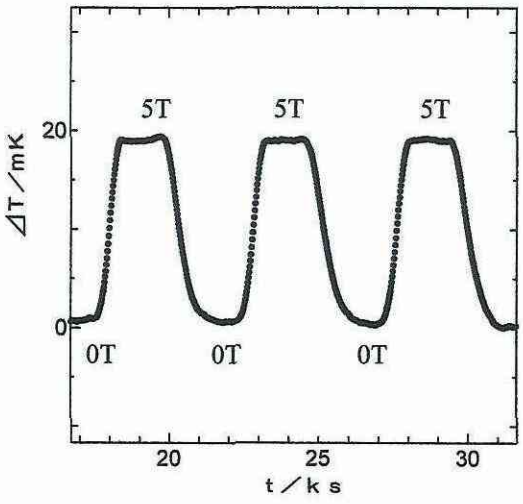

図 14. 温度センサーへの磁場印加効果

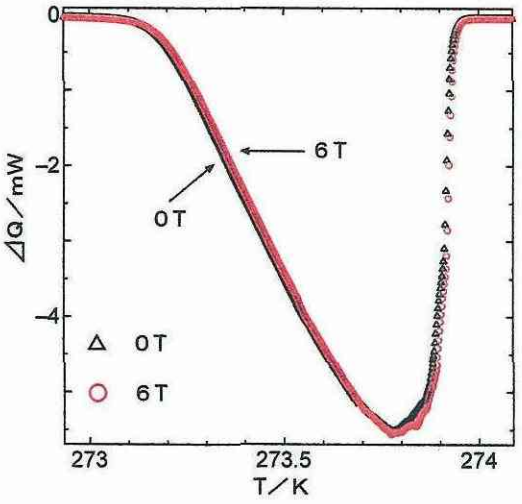

図 15. H_2O の融解に対する磁場効果

Clapeyron 式中の反磁性磁化率の項中における磁場中での分子の回転・振動による磁化率の高周波成分の寄与が考えられる。また，水の分子は極性を持つことから，その分子運動は有効電荷を持った粒子が磁場中を動くことになり，Lorentz 力を受けると考えられ，磁場は分子運動を抑制する方向に働くと考えられる。[11]

また、有機分子の融点への磁場効果では、パルミチン酸、ビフェニル，ベンゼン、クロロベンゼンなどの有機分子の融点への6T の磁場効果を測定した結果、それぞれ24.5±3.7、7.8±2.0、3.7±4.0、1.9±1.4mK上昇した。液晶物質である MBBA(N-p-methoxybenzylidene-p'-butylaniline), EBBA(N-p-ethoxy benzylidene-p'-butylaniline) の液晶-液体相転移への結果と合わせて，それぞれの相転移温度の上昇幅を比較したところ、分子の形状に異方性を持つ EBBA, MBBA, パルミチン酸のグループとビフェニル，ベンゼン、クロロベンゼンのグループに分かれることが分かった。[12]

さらに、強誘電体への磁場効果について検討した。多くの強誘電体結晶の中で、リン酸二水素カリウム（KH_2PO_4 略称 KDP）に代表される一群の結晶があり、水素結合型強誘電体と呼ばれている。KDP の重水素置換体である DKDP の強誘電相から常誘電相への固相転移について，磁場印加効果の測定を行った。結晶を c 軸を磁場に垂直になるように設置した場合、5T の磁場印加により、相転移温度は6±1mK 上昇した。DKDP の強誘電 - 常誘電相転移は、重水素位置の無秩序化を引き金として起こることが知られている。高温相において重水素が二つのサイト間に非局在化している場合には，局在化している低温相の場合より磁場中においてより大きなLorentz 力を受けると考えられ，高温相における重水素の運動の抑制において磁場印加効果が現れていると考えられる。[13]

本研究では相転移における磁場印加は，相対的に低温相を安定化させるという基礎的知見を得たが，そのメカニズムについては，まだ不明な点がある。反磁性物質の相転移に対する磁場効果の機構をさらに詳しく調べるために、従来のデータに加えて、モデル的な化合物などに対象を拡大して測定を行う必要がある。それと平行して、磁場効果の機構について理論家の寄与が望まれる。

5. おわりに

気相光化学反応を利用して超微粒子やナノ粒子を作製する際に磁場を印加すると、超微粒子の化学組成や粒子サイズが制御でき、さらに混合気体の分圧を最適化すると超微粒子が互いに結合した状態になることがわかった。これらの基礎技術を発展させると種々の化学組成をもった超微粒子やナノ粒子を自由に集積して様々な形をもった三次元機能性素子が組み立てられると期待できる。また、フラーレン誘導体と電子ドナーを連結した化合物のナノ構造体の構造と光特性が磁場で制御できた。これを発展させるとナノ素子の機能性を磁場で制御する方法が開発できると期待される。さらに、反磁性物質の相転移に対する磁場効果の研究では科学的に新規な知見が得られると期待できる。

参考文献

[1] H. Morita, Y. Takeyasu, H. Okamura, and H. Ishikawa, Magnetic field effect on gas-phase synthesis of metal-containing ultrafine particles from iron pentacarbonyl and carbon disulfide, Sci. Technol. Advanced Materials, 7 (2006), (in press).

[2] K. Abe and H. Morita, Magnetic field effect on gas-phase synthesis of metal-containing ultrafine particles from cobalt tricarbonyl nitrosyl and carbon disulfide, J. Photopolym. Sci. Technol., 19 (2006) (submitted).

[3] H. Morita and H. Ishikura, Morphological control of deposits from a gaseous mixture of allyltrimethylsilane and iron pentacarbonyl, J. Photopolym. Sci. Technol., 18 (2005) 193-198.
[4] H. Morita, Y. Okano, and H. Tonooka, Magnetic field effect on morphology of photochemical products from a gaseous mixture of trimethylsilylacetylene and iron pentacarbonyl, Proc. CD ISMS2005, 4O04 (2006).
[5] H. Yonemura, N. Kuroda, S. Moribe, and S. Yamada, Photoinduced electron-transfer and magnetic field effects on the dynamics of the radical pair in a C_{60} cluster–phenothiazine system, C.R. Chimie, 9 (2006) 254 – 260.
[6] H. Yonemura, N. Kuroda, and S. Yamada, Magnetic field effects on photoelectrochemical reactions of modified electrodes with C_{60}-phenothiazine nanoclusters, Sci. Technol. Advanced Materials (submitted).
[7] 米村弘明、有機または無機ナノ粒子を用いた薄膜の作製と光機能の磁場制御、Material Stage, 5月号(2006)（印刷中）.
[8] H. Yonemura, Y. Yomamoto, S. Yamada, Y. Fujiwara, and, Y. Tanimoto, Magnetic orientation and organization of single-walled carbon nanotubes or their composite materials using polymer wrapping, Proc. CD ISMS2005, 2O03 (2006).
[9] 米村弘明、ナノ構造と光特性に及ぼす強磁場効果、化学と教育、54, No. 1, (2006) 20-23.
[10] S. Wang, K. Tozaki, H. Hayashi, and H. Inaba,, Nano-watt stabilized DSC and its applications, J. Therm. Anal. Cal., 79 (2005) 605-613.
[11] H. Inaba, T. Saitou, K. Tozaki, and H. Hayashi, Effect of the magnetic field on the melting transition of H_2O and D_2O measured by a high resolution and supersensitive differential scanning calorimeter, J. Appl. Phys., 96 (2004) 6127-6132.
[12] 林英子, 松岡潤平, 簑原誠人, 東崎健一, 稲場秀明, ナノワット安定化DSCによる反磁性物質の相転移に及ぼす磁場効果, 第41回熱測定討論会, P09 Oct. 8-10 (2005) 九州大学.
[13] H. Hayashi, C. Nonaka, K. Tozaki, H. Inaba, and C. Uyeda, Effect of the magnetic field on the ferroelectric transition of KD_2PO_4 measured by a high resolution and super-sensitive differential scanning calorimeter, Thermochimica Acta, 431 (2005) 200-204.

強磁場が誘起する液体の構造転移と新機能の創出

中林誠一郎[1]、坂口浩司[2]
1 埼玉大学・理学部、2 静岡大学・電子工学研究所

概要

強磁場中におかれた液体、とくに水は、磁場の上昇とともに、その性質を無視できない程度に変化させる。純水を 10T 程度の強磁場におくと、磁場強度の増加とともに光学的屈折率が上昇した。10T 下では、水の屈折率は無磁場中よりも 1%増加した。とくに、水の屈折率上昇は、金属界面に補足された水で著しい。これらの実験事実を下敷きとして、固液界面およびバルクの液体物性の磁場による変化と、電気化学反応、特に、金(111)上のポリチオフェンヘテロエピタキシャル成長における新規な磁場効果を開拓・解明することを目的とした。

１．はじめに

本研究は、研究テーマ１：水および水溶液の強磁場下での物性変化、および、研究テーマ２：チオフェン分子導線成長反応の磁場制御より構成される。

研究テーマ１：水および水溶液の強磁場下での物性変化

強磁場中におかれた液体、特に水は、磁場の上昇と共に、その性質を無視できない程度に変化させる。10T 下では、水の屈折率は無磁場よりも 1%増加した。磁場効果が出現するためには、液体は、水素結合のネットワーク（過渡的なクラスター構造）を持つ事が必要である。つまり、磁場の効果は、孤立した溶媒分子に作用するのではなく、多数個の溶媒分子が構成するクラスターが磁場から影響を受けるものと推定される。本研究では、磁場誘起構造変化の分子論的実体を明らかにする事を目ざし、生体系への磁場効果や新原理による化学反応制御など、新しい磁気科学の開拓を試みる。純水の屈折率は磁束密度とともに増加し，10T において，SPR センサーを用いたときは 0.14%の増加，PSD を用いたときは 0.09%の増加を観測した。純水の屈折率の温度係数は，観測している波長域においておよそ～$1\times10^{-4}℃^{-1}$ であるので，これらの屈折率の増加は温度の変動の影響よりもかなり大きく，磁場による効果を表していると考えられる。これら２つの測定で観測される屈折率変化の差を、表面に束縛された水の効果と考え、この事を実験的に詳細に検討する。具体的には、金薄膜表面を単分子修飾して、表面と水の近距離相互作用を阻害し、表面効果の変化を調べた。

研究テーマ２：チオフェン分子導線成長反応の磁場制御

電気化学は液相中に溶解させた物質を外部電場で制御しながら基板に堆積させることが出来る有効なナノ構造構築法である．これまで電気化学的手法により金属や分子のナノワイヤの形成が報告されてきた．しかしながら単一分子レベルでの極微ワイヤ構造の作成には成功していない．本研究では単一分子ワイヤを電気化学的に任意の密度・方向・長さを制御しながら基板上に構築する新しい液相マテリアルプロセッシング技術を開発し、形成させた１本の分子ワイヤの表面構造に及ぼす強磁場効果を単一分子レベルで検討することを目的とした。

2．水および水溶液の強磁場下での物性変化[1-5]

磁場を用いて化学反応を制御する試みは，魅力的な考え方であるが，成功した例は，スピン化学とよばれる一群の研究を除いて，それほど多くなく，また劇的な効果が得られるということも少なかった．最近になって比較的手頃になった超伝導磁石を用いて，10 Tという強磁場を用いた材料プロセスの開発や新規な磁場効果の探索が行われ，成果が出つつある．筆者らは，磁場中の水の物性に注目し研究を行ってきた．Walrafenらは図１の構造に基づき，1000cm^{-1}より低振動数に現れる４つのピーク(60，175，450，~780 cm^{-1})を，それぞれ，O-H…O 水素結合骨格の変角，伸縮，および２つの秤動振動とアサインした．

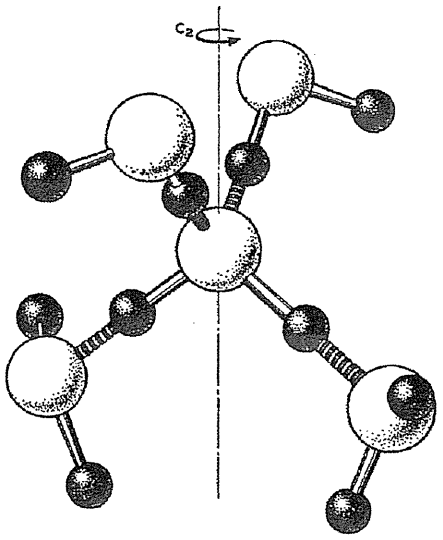

図１　水の構造

最近になって天羽および冨永らは，250cm^{-1}より低波数の偏光解消ラマンスペクトルについて，２つの振動モードおよび１つの緩和モードの重ね合わせで説明を試みた．これによると２つの振動モードはWalrafenらと同じく水素結合軸の変角と伸縮振動と考え，50cm^{-1}より低振動数にかけて急激に立ち上がるバックグラウンドを水素結合の生成・消滅による緩和モードとする．これらの重ね合わせにより低振動数のスペクトルはよく再現された．岩坂らは生体反応の磁場効果に対する興味から，14Tの磁場中に置いた水およびD-グルコース水溶液の近赤外吸収スペクトルを測定した．その結果，水の吸収スペクトルは長波長側の吸収が増大し，D-グルコース水溶液では短波長側の吸収が増大することが分かった．水のスペクトルの圧力依存性を調べた別の実験結果と比較すると，このスペクトルの変化は水１分子当たりの平均水素結合数が磁場中でわずかながら増加していることをと考えられる．磁場中で水１分子当たりの水素結合数が増加するとはどういうことであろうか．定性的には次のような議論が考えられている．水の磁化率χは次のように反磁性項χ_{dia}と常磁性項χ_{para}の和で表される．

$$\chi = \chi_{dia} + \chi_{para} \qquad (1)$$

球対称な閉殻電子構造の分子は反磁性項のみを持つが，水素結合を形成した分子は電子雲が分子間に広がって球対称な分布から大きくずれるため，常磁性項χ_{para}の増加に寄与すると考えられる．水の磁化率の温度依存性は，このモデルで説明される事が良く知られている．磁場中に置かれた水は磁化率が負であるために負の磁気エネルギーを持つ．そのため，これを打ち消すために，常磁性項が増加する方向に平衡が傾き，多くの水素結合を形成し安定化すると考えられる．

光の屈折は，媒質と電磁波の相互作用の結果起るものであり，媒質の性質の情報を含んでいる．ここで屈折率の物理的意味を簡単に述べる．電磁気学によると誘電体中を伝わる電場Eにより分極が誘起されると表される．誘電体の分極をある振動数ω_0で振動

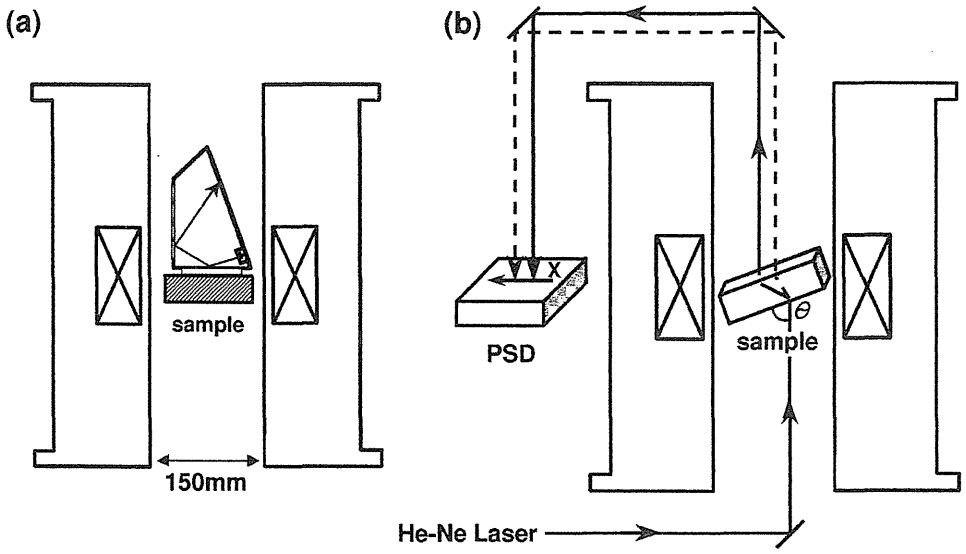

図２　測定装置

する変位電荷によるとしてこの系の電場に対する応答を考えると，感受率の表式が得られる．ここではその式を示さずに関数形の概要を説明すると，χ' および χ'' の周波数依存性はそれぞれ，ω_0 で共鳴を表すピーク，および ω_0 でゼロでその前後で大きな幅をもつ双極性のピークを持つ．屈折率 η および吸収係数 κ の振動数依存性も同様に，共鳴ピークと幅広い双極性ピークとなる．また χ' および χ''，および η と κ は，Kramers-Kronig の関係で結びつけられ，一方がすべての周波数において分かれば他方が求められる関係にある．それゆえ物質の状態変化，例えば電子状態の変化により紫外スペクトルが変化すると，それに応じて共鳴波長からはずれた可視領域においても屈折率が変化する．すなわち屈折率を測定する事は，吸収スペクトルの変化を見ていることになる．最近，表面プラズモン共鳴(SPR)を利用した屈折率センサー(SPR センサー)が市販され，対象物質の屈折率の変化を高精度に($\Delta n/n<10^{-5}$)求める事ができるようになってきた．当初，筆者らは次節で述べるように SPR センサーの感度面を化学修飾し，その化学基への磁場効果を測定することを企図した．しかし化学修飾せずに純水の磁場中での屈折率の測定を行ったところ，意図に反して水そのものの磁場効果が観測できることに気がついた．水などの反磁性物質の磁気的性質は，磁化率の絶対値の小ささ(-9.05×10^{-6})からも分かるように，それほど大きくない．それでも水が磁場に応答するのは何による

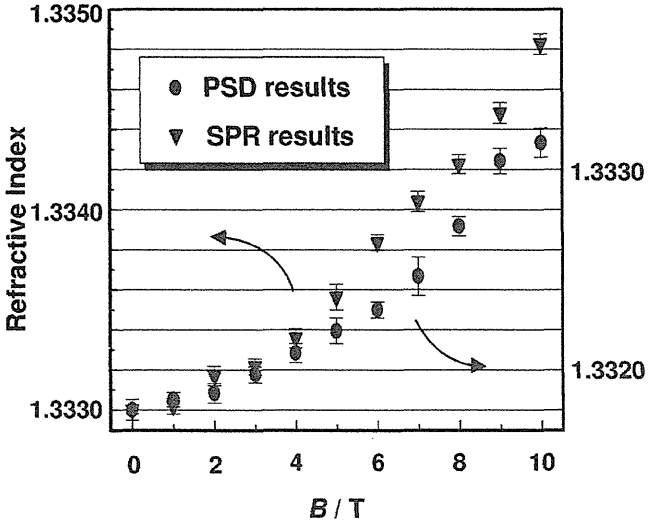

図３　水の屈折率の磁場変化

のか高感度なSPRセンサーを用いて詳しく検討を行った.

筆者らは水の屈折率の磁場依存性を，SPRセンサー以外の方法も用いて，２つの全く異なる方法で検証した．図２(a)にSPRセンサーの模式図を，図２(b)に位置敏感検出器(PSD)およびレーザーを用いた測定装置の模式図を示す．SPR センサーは市販されているもの(Spreeta, Texas Instruments, Inc.)であり，LEDから出た光(840 nm)を偏光フィルターに通し，金薄膜に入射させ，反射してきた光をフォトダイオードアレイで検出する．ある入射角で入射した光はSPRの共鳴条件を満たし反射率が小さくなることから，測定対象の屈折率を求めることができる．PSDを用いた方法は磁場中におかれた試料セルに入射・屈折した光の変位量を磁場外に置かれたPSDで測定するという保守的な手法を用いた．PSD は浜松フォトニクス製のものを，光源は He-Ne レーザー(633 nm, NEC GLG-5360)を用いた．磁場の発生には超伝導磁石(ジャパンスーパーコンダクタテクノロジー(株)，JMT-10T150)を用いた．試料は Millipore 社の超純水製造装置(Direct-Q 5, 18.2 MΩcm)で精製した水を使用した．測定室の室温は空調により 25.0±1.0℃に保った．図３に磁場中の水の屈折率の２つの測定結果を示す．SPRの測定結果(▼)とPSDによる測定結果(●)は，10T印可により，それぞれ 1.8×10^{-3} (0.14%)，1.3×10^{-3} (0.09%)の増

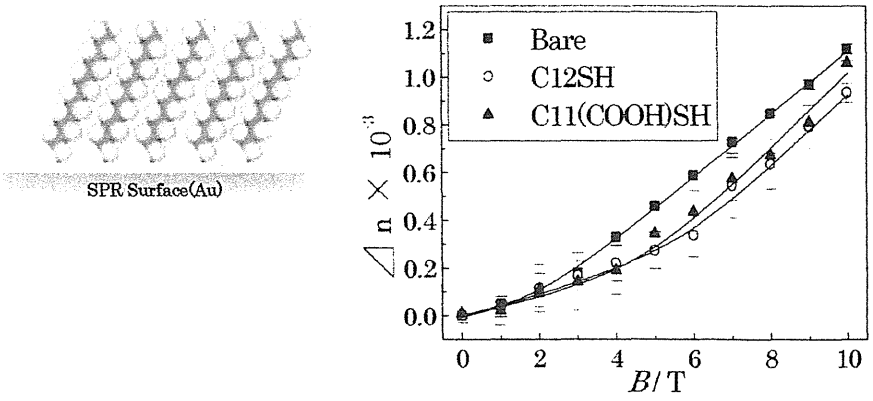

図４　　表面自己組織化単分子膜形成時の水の屈折率変化

加を示した．この波長領域の屈折率の温度係数は-1×10^{-4} ℃$^{-1}$程度であるので，この増加は温度による揺らぎよりも遥かに大きい．このため，この増加は磁場効果によるものと考えられる．SPRとPSDの結果を比べてみると，SPRの方がわずかに増加が大きかった.

一方、表面に捕獲された水については、SPR検出用の金膜の電位を規制して、電気化学的な制御下で磁場効果を測定した。電極と液体界面の構造は，イオンの統計分布を基にしたグイ・チャップマンモデルを源として，長い研究の歴史を持っている．しかし，電極表面と溶媒分子の近距離的な強い相互作用は，このモデルの範囲を超えているため，電極表面極近傍の水分子集団の構造は，未だ，充分に解明されたとは言えない．例えば，マクロな物性として，ゼロ電荷電位での金属電極の静電容量が，電極の種類によって異なる実験事実を正しく説明し得るモデルは存在しない．また，ミクロな視点では，電気化学系への表面選択的な分光の適応から，電極表面の水分子は，その並進自由度を失い，

固体表面に局在した薄い氷に近い状態となっていることが，明らかになってきた．

本節では，多結晶金電極近傍の水の磁気光学特性が，バルクの水のそれとは異なる可能性について述べる．本節の内容は，現在，研究が進みつつある領域の議論であり，確定した結論には至っていない部分があることを，初めに，お断りしたい．

図３で用いたSPR測定とPSD測定は，測定原理が異なるために，観測している水の空間位置が大きく異なる．SPRは，金薄膜から全反射状態で染みだした近接場光が屈折率をプローブするため，金薄膜表面から200nm領域までの水の屈折率を測定している．一方，PSD測定は，光の屈折に基づく光路の変位を測定しているため，ガラスセルに満たされたバルク水の屈折率を測定している．図３に現れた実験線の食い違いは，充分な追試を繰り返しても，ついに一致することはなかった．このことは，金薄膜近傍の水の磁気的性質がバルクの水のそれとは異なることを意味する．

金薄膜表面上に捕獲される水を排除するために，金上に長鎖アルカンチオールの自己組織化単分子膜を修飾し，オープンサーキット条件で水の屈折率の磁場強度依存性を測定した．図４から，アルカンチオール自己組織化単分子膜を修飾したSPRセンサーで屈折率の磁場依存性を測定すると，屈折率の変化は小さくなり，図３に示したPSD測定の結果に近づくことが判る．

金薄膜表面を電気化学的に酸化し，表面最外層が清浄金である場合と，金酸化物である場合の屈折率の磁場依存性を測定した．硫酸ナトリウム100μMを加えた超純水中で，SPRセンサーの金薄膜の電極電位を一定に保ち，磁場強度を変化させて，水の屈折率の磁場強度依存性を測定した．図５を見れば，設定電位が２重層領域内で，電極表面が金である場合の変化は，いずれの電位でもほぼ同じであると言える．しかしながら，電位を0.8Vとし，表面を酸化物へと変化させると，屈折率の磁場依存性は，顕著に減少した．さらに，電位をカソード走査し，表面の金酸化層を還元すると，屈折率の磁場依存性は，可逆的に変化することも確かめられた．

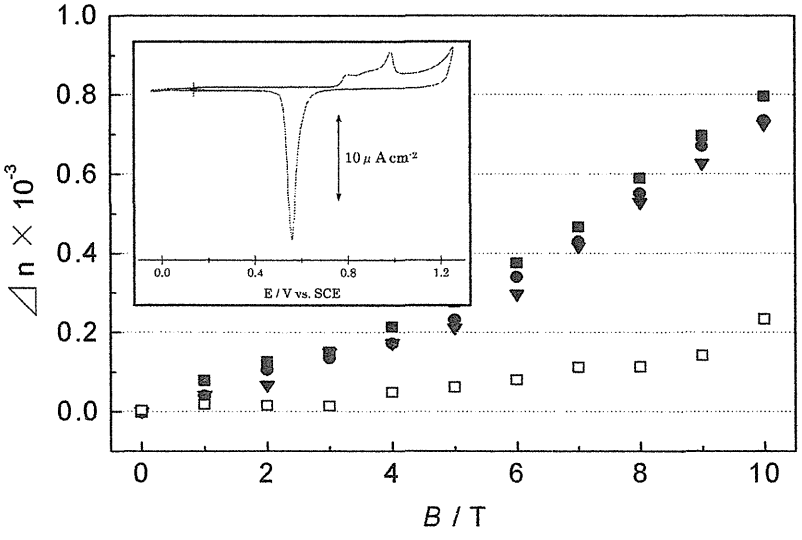

図５　電気化学的に規制したSPRセンサを用いた屈折率測定

SPRセンサーの金薄膜表面を，長鎖アルカンチオール自己組織化単分子膜で覆ったり，金酸化物へ変化させたときに観測された結果は，いずれの場合も，PSD測定によるバルク水の磁場効果へと近づいた．この事は，金表面に局在し並進運動の自由度を失った水の磁気特性は，バルクの水のそれとは大きく異なることを意味する．この磁気特性の変化は，２次元的に捕獲された水分子同士の水素結合の在り方と，バルクの水分子の水素結合の在り方に違いがあることを示唆する．

３．チオフェン分子導線成長の磁場制御[6-13]

①可溶性チオフェンモノマーと表面修飾添加剤を用いた金(111)面上への長さ 70nm に及ぶ単一ポリチオフェンワイヤの形成に成功した。②開発した単一分子ワイヤ構築法により形成した単一分子ワイヤに強磁場を印加した結果、単一分子単層構造から積層構造へ変化することが明らかになった。以下に詳細を示す。

通常の電解重合系ではポリチオフェンのバンドルからなる不規則構造が見られるのに対し、表面修飾添加物を含んだ電解重合系では最長で約 70nm ほどの直線型の単一ポリチオフェンが観測された。これはチオフェンユニット(約 3.8Å)が約２３０個程度結合した長さに相当する。また１本の長いポリチオフェンワイヤが表面上を動く過程やポーラロン（酸化種）が１本のワイヤ中を伝播すると示唆される輝点の点滅が観測された。電圧パルス印加数を変えて単一分子ワイヤの長さや密度を統計処理した結果、パルス数の増加に伴い分子ワイヤの長さが増長することが分かった。また金(111)表面の三回対称性を反映してポリチオフェンワイヤは規制された３方向に成長することが分かった。吸収スペクトルの測定から、核分子が基板表面に吸着し、これを基点として重合反応が起こり、単一分子ワイヤがｴﾋﾟﾀｷｼｬﾙに成長したものと考えられる。この方法で作成した単一分子ワイヤの配向に及ぼす強磁場効果を検討した結果、単一分子単層構造から積層構造へと変化することが明らかになった。

これまで行われてきた電界重合の研究では、１本の孤立した共役系高分子（分子ワイヤ）を絶縁基板上に形成させることが困難であった。これは生成した共役系高分子が不溶性であることや高分子の会合体を形成しやすいために基板上に１本の高分子を形成させることが困難な理由による。本研究では、重合後生成する共役系高分子が溶媒に可溶化するモノマー分子を用い、且つ特殊な表面処理を行うことによりモノマー分子が最長で２００分子ほど重合した単一分子ワイヤ（鎖長約７０nm）を任意の密度・長さで制御しながら基板水平方向に形成させ得ることを初めて明らかにすることができた。

金(111)基板を電解質中で電圧パルスを印加することにより、チオフェン誘導体の単一分子ワイヤが出現した。（図 6）単一分子ワイヤの生成機構は、重合過程で生成した分子長の短いオリゴマーが基板表面に吸着し、電解重合が単一分子レベルで起こったと考えられる。以上の結果より、“単一分子ワイヤ”を基板上に任意の密度・長さで構築する新しい液相プロセス“電気化学エピタキシャル重合”を提案し、成功することができた。単一分子ワイヤの生成に対する強磁場効果を現在検討中である。

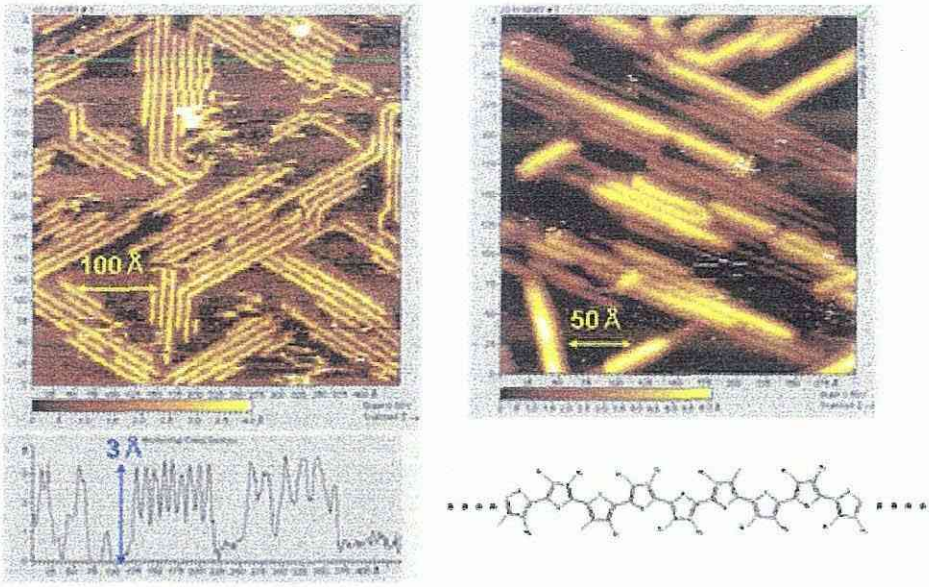

図 6.　金(111)上に成長した単一分子ワイヤの STM 像（大気中，5pA，1V）

4.おわりに

研究テーマ１に関しては、強磁場中で純水の屈折率の上昇を、２つの互いに独立な測定法を用いて測定した。測定は、①石英製のセルに純水を入れ、屈折率変化によるレーザー光線の空間的変位を測定する方法、および、②金薄膜を用いた表面プラズモン共鳴法を用いた。両者の測定は、定性的には良く一致するものの、定量的には有為な差があった。この差は、金表面に捕獲された吸着水と、バルク水の磁場効果の差と推定された。バルク水の磁場効果は、屈折率変化と同時に、近赤外領域のスペクトル変化としても観測された。吸着水の効果は、金表面の電気化学的に酸化、あるいは、金表面をアルカンチオールの自己組織化単分子膜で修飾すると消失した。この事から、金と水との近距離的な相互作用に界面での磁場効果の原因があると判った。研究テーマ２に関しては、１０Ｔの強磁場をヨウ素ー金基板上に形成させたポリチオフェンワイヤ列に印加して、配向変化を調べた。10T の磁場印加によりポリチオフェンワイヤ列は整列した構造から、分子ワイヤが表面上を動き乱れた構造を取ることがあきらかになった。以上から、研究１．２とも期待される成果に対する達成度は良好と思われる。また、研究１に関しては、表面吸着水の大きな磁場効果の発見、研究２に関しては、表面上に分子ワイヤを１分子レベルで大面積に重合する方法を見つけられたのは予想外の結果であった．今後の発展として、研究１に関しては、表面吸着分子の誘起する表面磁性の精密測定、SMOKE(Surface magneto optical Kerr effect)に着手した。研究２に関しては、電気化学エピタキシャル重合に磁場を印加することにより導電性高分子の完全結晶を形成させることを目指す。

参考文献

[1] Q.-K. Yu, Y. Miyakita, S. Nakabayashi, and R. Baba, Magnetic Field Effect on Electrochemical Oscillations during Iron Dissolution, Electrochem. Comm. 5 (2003) 321-324.

[2] A. Karantonis, M. Pagitsas, Y. Miyakita, S. Nakabayashi, From Excitatory to Inhibitory Connections in networks of Discrete Electrochemical Oscillators, J. Phys. Chem. B, 107, 14622–14630 (2003).

[3] H. Hosoda, H. Mori, N. Sogoshi, A. Nagasawa and S. Nakabayashi, Refractive Indices of Water and Aqueous Electrolyte Solutions under High Magnetic Fields, J. Phys. Chem. B 108 (2004) 1461-1464.

[4] A. Karantonis, M. Pagitsas, Y. Miyakita and S. Nakabayashi, In-phase, anti-phase and fractured synchrony in ring networks of coupled relaxation electrochemical oscillators, J. Phys. Chem. B., 108 5836 (2004).

[5] Y. Miyakita , S. Nakabayashi, A. Karantonis, Spatiotemporal Coding in an Electrochemical Oscillator Network, Phys.Rev.E, 71, 056207 1-9(2005).

[6] E. Mishina, Q.-K. Yu, T. Tamura, H. Sakaguchi, A. Karantonis, and S. Nakabayashi, Kinetic profile of adsorption and self-assembling of thiophene oligomers studied by optical second harmonic generation, Surf. Sci. 544, 269-277 (2003).

[7] E. Mishina,, T. Tamura, H. Sakaguchi, and S. Nakabayashi, Kinetics of adsorption and self-assembling of thiophene and dodecanethiol studied by optical second harmonic generation, Chemistry Letters, 32, 652-653 (2003).

[8] F. Iwata, K. Mikage, H. Sakaguchi, M. Kitao and A. Sasaki, Current-sensing scanning near-field optical microscopy using a metal probe for nanometer-scale observation of electrochromic film, J. Microscopy, 210 (2003) 241-246.

[8] T. Matsumura, H. Sakaguchi, Y. Shimoyama, Formation kinetics and structure of self-assembled poly(3-alkylthiophene) films on gold surface, Journal of Materials Science: Materials in Electronics, 14, (2003) 353-356.

[10] E. Mishina, T. Tamura, H. Sakaguchi, L.Kulyuk, S.Nakabayashi, Photoluminescence studies of oligothiophene self-assembled monolayers at low excitation energy, J. Chem. Phys., 120,9763 -9768(2004).

[11] E. Mishina, T. Tamura, H. Sakaguchi, L. Kulyuk and S. Nakabayashi, Photoluminescence Studies of Oligothiophene Self-assembled Monolayers at Low Excitation Energy, Journal of Chemical Physics, 120, pp.9763 -9768 (2004).

[12] H. Sakaguchi, H. Matsumura and H. Gong, Electrochemical Epitaxial Polymerization of Single Molecular Wires, Nature Materials, 3, pp.551-557 (2004).

[13] H. Sakaguchi, H. Matsumura, H. Gong and A. Abouelwafa, Direct visualization of the formation of single-molecule conjugated copolymers, Science, 310, (2005) 1002-1006.

7．国際シンポジウム

Proceedings of ISMS 2005

International Symposium on Magneto-Science 2005

"Fundamentals and Applications of Magnetic Field Effects on Materials Processes and Functions"

The 3rd Open Symposium on Innovative Utilization of Strong Magnetic Fields

The 9th Symposium on New Magneto-Science

November 14 (Mon) – 17 (Thu), 2005

Education and Culture Hall
Yokohama National University
79-1 Tokiwadai, Hodogaya-ku, Yokohama 240-8501, Japan

Promoted by
Scientific Research on Priority Aria "Innovative Utilization of Strong Magnetic Fields" by MEXT
New Magneto-Science Research Society of Japan

Preface

The International Symposium on Magneto-Science 2005 (ISMS 2005) -Fundamentals and Applications of Magnetic Field Effects on Materials Processes and Functions- was held in Yokohama, Japan, November 14-17, 2005. The organizers welcomed nearly 200 participants form 12 countries. High-level 114 papers were presented at ISMS 2005, which are included in these proceedings.

The term of "Magneto-Science" was invented in Japan in 1990s to make clear the essential difference between itself and the traditional magnetic science. Namely, in Magneto-science, magnetic fields are used as a dynamic and active tool to create new materials functions. The brief history of Magneto-Science is as follows: In 1970s to 1980s, the radical pair mechanism for the magnetic field effect on chemical reactions was established by Nagakura and his coworkers. This was the starter of magneto-science indeed. In 1980s to early 1990s, various magnetic field effects were discovered for chemical, biological and metallurgical systems due to the scientists in the minority. Among them, the findings of rather macroscopic phenomena such as the magnetic alignment of biological molecules, the diamagnetic levitation and the magnetic Moses effect led to the rapid progress in Magneto-Science. Especially in Japan, developing cryo-cooled superconducting magnets boosted up the studies of Magneto-Science. Then, later 1990s to now, this field is studied from fundamentals to applications systematically. We are able to know the latest results in the proceedings. Actually, the topics discussed at ISMS 2005 were diamagnetic levitation, spin chemistry, magneto-thermodynamic effects, magneto-electrochemistry, magneto-crystallization, magnetic field-induced phase transitions, novel magnetic phenomena, etc. in relation to different kinds of materials such as organic and inorganic compounds, metals and alloys, polymers and biological substances.

In Japan, the annual symposium has been promoted by the Japan Society of New Magneto-Science (President: Hitoshi Wada) since 1997. In addition to this, the open symposium has been promoted by the Scientific Research for Priority Area "Innovative Utilization of Strong Magnetic Fields" (Project chair: Masuhiro Yamaguchi), which started in 2003. The organizers joined those two domestic symposiums to ISMS 2005, welcoming scientists from abroad. The growth rate of research in this field increases world-widely and the topics diversify every year. It is considered to be very timely to have an opportunity of critical discussion and wide information exchange by active scientists from all over the world. Finally, the organizers certainly appreciate the financial support by some companies and the cooperation with many academic societies and Yokohama National University for the fruitful success of the symposium.

December 1, 2005
Masuhiro Yamaguchi
Symposium chair of ISMS 2005

1. Organization

1.1 Organizing committee

Honorary Chair

Saburo Nagakura (Tokyo)

Chair:

Masuhiro Yamaguchi (Yokohama)

Co-chair:

Hitoshi Wada (Kashiwa)

Advisors:

Hisaharu Hayashi (Tokyo)
Kazuo Kitahara (Tokyo)
Koichi Kitazawa (Tokyo)
Mitsuhiro Motokawa (Kobe)
Koshichi Noto (Iwate)
Shoogo Ueno (Tokyo)

Members:

Ryoichi Aogaki (Tokyo)
Shigeo Asai (Nagoya)
Mitsuo Ataka (Ikeda)
Giyuu Kido (Tsukuba)
Noriyuki Hirota (Tsukuba)
Hideaki Inaba (Chiba)
Tomoyuki Kakeshita (Osaka)
Tsunehisa Kimura (Hachioji)
Koji Kishio (Tokyo)
Tsukasa Kiyoshi (Tsukuba)
Jyunji Miyakoshi (Hirosaki)
Iwao Mogi (Sendai)
Hiroshi Morita (Chiba)
Seiichiro Nakabayashi (Saitama)
Hideyuki Ohtsuka (Tsukuba)
Sumio Ozeki (Matsumoto)
Yoshifumi Tanimoto (Hiroshima)
Chiaki Uyeda (Osaka)
Kazuo Watanabe (Sendai)
Tsuneo Watanabe (Hachioji)
Hitoshi Watarai (Osaka)
Isao Yamamoto (Yokohama)
Hiroaki Yonemura (Fukuoka)

1.2 International advisory board

Eric Beaugnon (Grenoble)
Peter J. Hore (Oxford)
Jan Kees Maan (Nijmegen)
Hans J. Schnneider-Muntau (Tallahassee)
Robert F. Tournier (Grenoble)

1.3 Steering committee

Masuhiro Yamaguchi (Yokohama) [Chair]
Yoshifumi Tanimoto (Hiroshima)
[Scientific program]
Sumio Ozeki (Matsumoto) [Publicity]
Tsunehisa Kimura (Hachioji) [Proceedings]
Isao Yamamoto (Yokohama) [Secretary]
Katsuhiko Fujio (Matsumoto)
Taku Iiyama (Matsumoto)
Masafumi Yamato (Hachioji)
Masao Fujiwara (Hiroshima)
Yoshihisa Fujiwara (Hiroshima)
Yoshihiro Shimazu (Yokohama)

1.4 Symposium office

M. Yamaguchi (Symposium chair) and I. Yamamoto (Symposium secretary)

Department of Physics, Yokohama National University, Tokiwadai 79-5, Hodogaya-ku, Yokohama 240-8501, Japan.
E-mail: yamaguch@ynu.ac.jp, isaoy@ynu.ac.jp
Phone and Fax: 045-339-4149 (M.Y.), 045-339-4325 (I.Y.)
Mobile phone during the symposium: 090-7733-9476 (M.Y.), 090-4457-9146 (I.Y.)

2. Sponsorship and Cooperation

The organizers of ISMS 2005 wish to acknowledge with gratitude the generous support provided by

Japan Superconductor Technology, Inc. (http://www.soc.co.jp/)
Sumitomo Osaka Cement Company, Ltd. (http://www.jastec.org/)

ISMS 2005 is held in cooperation with the following academic societies.

The Biophysical Society of Japan (http://www.biophys.jp/index.html)
The Chemical Society of Japan (http://www.chemistry.or.jp/)
Cryogenic Association of Japan (http://www.csj.or.jp/jcryo/)
The Crystallographic Society of Japan (http://wwwsoc.nii.ac.jp/crsj/)
The Electrochemical Society of Japan (http://www.electrochem.jp/index.html)
The Institute of Electrical Engineers of Japan (http://www.iee.or.jp/)
Japan Biomagnetism and Bioelectromagnetics Society (http://www.bes.d.dendai.ac.jp/JBBS/)
The Japan Institute of Metals (http://wwwsoc.nii.ac.jp/jim/)
The Japan Society for Analytical Chemistry (http://wwwsoc.nii.ac.jp/jsac/)
Japan Society for Bioscience, Biotechnology, and Agrochemistry (http://www.jsbba.or.jp/)
The Japan Society of Applied Physics (http://www.jsap.or.jp/)
Japanese Society of Clinical Neurophysiology (http://square.umin.ac.jp/JSCN/)
The Pharmaceutical Society of Japan (http://www.pharm.or.jp/)
The Physical Society of Japan (http://wwwsoc.nii.ac.jp/jps/index-j.html)
The Rare Earth Society of Japan (http://kidorui.chem.eng.osaka-u.ac.jp/)
The Society of Chemical Engineers, Japan (http://www.scej.org/)
The Society of Polymer Science, Japan (http://www.spsj.or.jp/)
The Society of Synthetic Organic Chemistry, Japan (http://wwwsoc.nii.ac.jp/ssocj/)
Yokohama National University (http://www.ynu.ac.jp/index_en.html)

6. Time table

13 Nov. (Sun)	14 Nov. (Mon)	15 Nov. (Tue)	16 Nov. (Wed)	17 Nov. (Thu)
	9:30-10:50 Registration	9:30-10:50 **Magnetic Orientation I**	9:30-10:50 **Magnetic Orientation II**	9:30-10:50 **Magnetic Orientation III**
	10:50-11:10 Opening Ceremony	10:50-11:10 Break	10:50-11:10 Break	10:50-11:10 Break
	11:10-12:30 **Morphology of Dendrites I**	11:10-12:30 **Morphology of Dendrites II**	11:10-12:30 **Magnetic Flow I**	11:10-12:30 **Magnetic Flow II**
	12:30-14:00 Lunch	12:30-14:00 Lunch	12:30-14:00 Photograph Lunch	12:30-12:40 Closing Ceremony
	14:00-15:20 **Magnetic Levitation**	14:00-15:20 **Posters I**	14:00-15:20 **Posters II**	
	15:20-15:40 Break	15:20-15:40 Break	15:20-15:40 Break	
	15:40-17:00 **Texture of Alloys I**	15:40-17:00 **Texture of Alloys II**	15:40-17:00 **Spin Chemistry**	
17:00-19:30 Registration Welcome Drink (Yokohama Kokusai Hotel)			17:30-19:30 Party (Kyaratei)	

7. Program

13 Nov. (Sun)

17:00-19:30 Registration

Welcome Drink

14 Nov. (Mon)

9:30-10:50 Registration

10:50-11:10 Opening Ceremony

11:10-12:30 **Morphology of Dendrites I** Chairs: Jean-Paul Chopart, Iwao Mogi

1O05 **Electrochemical Growths of Metal Arborescences under Magnetic Field**

Vasile Heresanu[1,2], Simona Bodea[1,3], Rafik Ballou[1], Pierre Molho[1]; [1]*Laboratoire Louis Néel, C.N.R.S.*, [2]*Aristotle University of Thessaloniki*, [3]*Institut de Recherche sur les Phénomènes Hors Equilibre*

1O06 **The role of magnetic forces during electrochemical reactions at microstructures**

Andreas Bund, Holger H. Kuehnlein; *Dresden University of Technology*

1O07 **In situ microscopic observation of magnetic field effects on the growth process of two-dimensional silver dendrites**

Noriyuki Hirota[1], Soma Hara[2], Hiromichi Uetake[2], Hiroyuki Nakamura[2], Koichi Kitazawa[2]; [1]*Tsukuba Magnet Laboratory*, [2]*University of Tokyo*

1O08 **Rotational motion of silver dendrites under magnetic field**

Akio Katsuki[1], Yoshifumi Tanimoto[2]; [1]*Shinshu University*, [2]*Hiroshima University*

12:30-14:00 Lunch

14:00-15:20 **Magnetic Levitation** Chairs: Eric Beaugnon, Tomoyuki Kakeshita

1O09 **Magnetic levitation: Experiments with cryogenic oxygen and studies of dynamics**

R. J. A. Hill, A. T. Catherall, P. J. King, P. López-Alcaraz, K. A. Benedict, L. Eaves; *University of Nottingham*

1O10 **Development of a new magnetic levitation furnace**

Kohki Takahashi, Iwao Mogi, Satoshi Awaji, Kazuo Watanabe; *Tohoku University*

1O11 **Detection of Small Magnetic Anisotropy in Micro-gravity and Diamagnetic Anisotropy Deriving From Single Chemical Bond**

Chiaki Uyeda, Ryoichi Takashima, Takaaki Abe; *Osaka University*

1O12 **Magnetic Force Enhancement Using an HTS Bulk Cylinder**

Tsukasa Kiyoshi, Toshiyuki Koizumi, Xiaojun Liu, Shinji Matsumoto; *Tsukuba Magnet Laboratory*

15:20-15:40 Break

15:40-17:00 **Texture of Alloys I** Chairs: Justin Schwartz, Chiaki Uyeda

1O13 **Presence of Intrinsic Growth Nucleï in Overheated and Undercooled Liquid Elements**

Robert F. Tournier; *Centre National de la Recherche Scientifique*

1O14 **Grain Coarsening Controlled by Magnetic Field**

Hideyuki Yasuda[1], Tomoya Nagira[1], Itsuo Ohnaka[1,2]; [1]*Osaka University*, [2]*Osaka Sangyo University*

1O15 **Effects of a High Magnetic Field on Solid/Solid Phase Transformation Behavior and Structure**

Hideyuki Ohtsuka, Xinjiang Hao; *National Institute for Materials Science*

1O16 **Crystal Orientation in Sn-Pb alloy by Imposing Electromagnetic Vibration during Solidification**

Manabu Usui, Kazuhiko Iwai, Shigeo Asai; *Nagoya University*

15 Nov. (Tue)

9:30-10:50 **Magnetic Orientation I** Chairs: Tsunehisa Kimura, Robert Tournier

2O01 **Magnetic manipulation of π-conjugated supramolecular architectures**

P. C. M. Christianen[1], I. O. Shklyarevskiy[1,2], P. Jonkheijm[2], A. P. H. J. Schenning[2], E. W. Meijer[2], J. C. Maan[1]; [1]*Radboud University Nijmegen*, [2]*Eindhoven University of Technology*

2O02 **Surprising Magnetic Properties of Organized Organic Monolayers**

Ron Naaman, Supratim G. Ray, Reit Artzi, Zeev Vager; *Weizmann Institute*

2O03 **Magnetic Orientation and Its Temperature Dependence of Carbon Nanotubes**

Masao Fujiwara, Yoshifumi Tanimoto; *Hiroshima University*

2O04 **Magnetic Orientation and Organization of Single-Walled Carbon Nanotubes or Their Composite Materials using Polymer Wrapping**

Hiroaki Yonemura[1], Yuuichi Yomamoto[1], Sunao Yamada[1], Yoshihisa Fujiwara[2], Yoshifumi Tanimoto[2]; [1]*Kyushu University*, [2]*Hiroshima University*

10:50-11:10 Break

11:10-12:30 **Morphology of Dendrites II** Chairs: Rafik Ballou, Noriyuki Hirota

2O05 **Comparison of magnetic forces acting on electrochemical systems**

Jean-Paul Chopart[1], Leila Rabah[1], Jacques Douglade[1], Jean Amblard[1], F. Debray[2], Ahmed Harrach[3]; [1]*DTI, UFR Sciences*, [2]*GHMFL, CNRS*, [3]*University of Fès Saïs*

2O06 **The effects of Magnetic fields on the Electrodeposition of Cu and Co**

M. Uhlemann, A. Krause, A. Gebert, L. Schultz; *Leibniz Institute for Solid State and Materials Research Dresden*

2O07 **3D-Morphological Chirality Induction in Membrane Tubes Prepared by Silicate Garden Reaction in Magnetic Field**

Yoshifumi Tanimoto[1], Ichiro Uechi[1], Wenyong Duan[1], Akio Katsuki[2]; [1]*Hiroshima University*, [2]*Shinshu University*

2O08 **Chiral Recognition of Ascorbic Acid by Magnetoelectropolymerized Polyaniline Electrodes**

Iwao Mogi, Kazuo Watanabe; *Tohoku University*

12:30-14:00 Lunch

14:00-15:20 **Posters I** 2P01-2P38

15:20-15:40 Break

15:40-17:00 **Texture of Alloys II** Chairs: R. B. Morgunov, Hideyuki Ohtsuka

2O13 **Application of Magnetic Fields for Grain Boundary and Grain Structure Control in Non-Ferromagnetic Metals**

Dmitri A. Molodov; *RWTH Aachen University*

2O14 **Ferrite isothermal transformation in high magnetic fields**

S. Rivoirard[1], F. Gaucherand[2], O. Bouaziz[3], E. Pinto Da Costa[3], E. Beaugnon[1,2]; [1]*CNRS-CRETA*, [2]*CNRS-Laboratoire de Cristallographie*, [3]*ARCELOR Research, voie romaine*

2O15 **Effects of Magnetic Fields on the Texturing and Properties of $Bi_2Sr_2CaCu_2O_{8+\delta}$ Wires, Tapes and Coils**

Justin Schwartz[1,2], Ulf P. Trociewitz[1], Manuel Ramos[1,2]; [1]*Florida State University*, [2]*FAMU-FSU College of Engineering*

2O16 **Selection of variants by magnetic field in some ferrous alloys**

Takashi Fukuda, Tomoyuki Kakeshita; *Osaka University*

16 Nov. (Wed)

9:30-10:50 **Magnetic Orientation II** Chairs: Masao Fujiwara, Ron Naaman

3O01 **Dynamics of Liquid Crystal Alignment near the Nematic-Isotropic Phase Boundary**

G. Tordini, P. C. M. Christianen, J. C. Maan; *Radboud University Nijmegen*

3O02 **Progress of magnetostrictive polymeric materials**

Zhan Mao-Sheng[1], Lu Yun-Hua[1], Ding Nai-Xiu[1], Tsunehisa Kimura[2,3]; [1]*Beijing*

University of Aeronautics and Astronautics, [2]*Tokyo Metropolitan University*, [3]*Tsukuba Magnet Laboratory*

3O03 **Micro-Magnetic Simulation of Magnetic Properties and Magnetic Process of SmDyCo Thin Films**

Zuo Yi Li, Fang Jin, Xiao Min Cheng, Zhen Li, Jun Bin Yan, Wei Ming Cheng; *Huazhong Univ. of Sci. & Tech.*

3O04 **Magnetic Orientation of Cast films of Pulp Cellulose Microfibrils**

Fumiko Kimura[1], Tsunehisa Kimura[1,2], Fumitaka Horii[3]; [1]*Tsukuba Magnet Laboratory*, [2]*Tokyo Metropolitan University*, [3]*Kyoto University*

10:50-11:10 Break

11:10-12:30 **Magnetic Flow I** Chairs: Jan K. Maan, Hitoshi Watarai

3O05 **Magnetic interaction of a reaction zone catalyzed over paramagnetic suspension of iron oxide nanoparticles**

Rafael M. Digilov; *Israel Institute of Technology*

3O06 **Gravitational water mist flow in an inclined bore space of a super-conducting magnet**

Xian Wang[1], Hiroyuki Hirano[1], Shu-Shen Lu[2], Toshio Tagawa[3], Hiroyuki Ozoe[4]; [1]*Okayama University of Science*, [2]*Sun Yat-Sen University*, [3]*Tokyo Metropolitan University*, [4]*AGH University of Science and Technology*

3O07 **A New Flow-Type Cell by the Application of Magnetic Micro-Fluid Chip**

Ryoichi Aogaki, Eiko Ito, Mikio Ogata; *Polytechnic University*

3O08 **Relative Change of Viscosity of Water and Several Organic Liquids under Transverse Magnetic Field of 10 T**

Kikujiro Ishii, Shunsuke Yamamoto, Hideyuki Nakayama; *Gakushuin University*

12:30-14:00 Photograph
Lunch

14:00-15:20 **Posters II** 3P01-3P38

15:20-15:40 Break

15:40-17:00 **Spin Chemistry** Chairs: Sanford Asher, Yoshihisa Fujiwara

3O13 **Static and radiofrequency magnetic field effects on photochemical reactions**

P. J. Hore; *University of Oxford*

3O14 **Dependence of Magnetic Field Effect on Solvent and Environment**

Samita Basu[1], Tamal Sengupta[2], Sharmistha Dutta Choudhury[1], Adity Chowdhury[1];

[1]*Saha Institute of Nuclear Physics*, [2]*APC Ray Polytechnic*

3O15 **Manipulation over mechanical properties of solids by control of electron spin coherency of nanoclusters in strong magnetic field**

Roman Morgunov[1], Yoshifumi Tanimoto[2]; [1]*Institute of Solid State Physics*, [2]*Hiroshima University*

3O16 **Magnetoconductivity of Poly(N-vinylcarbazole) Film as a Quasi-one Dimensional Lattice Photoconductor**

Tadaaki Ikoma, Toshinari Ogiwara, Yutaka Takahashi, Kimio Akiyama, Shozo Tero-Kubota; *Tohoku University*

17:30-19:30 Party

17 Nov. (Thu)

9:30-10:50 **Magnetic Orientation III** Chairs: P. C. M. Christianen, S. Nakabayashi

4O01 **Superparamagnetic and Ferromagnetic Monodisperse Colloidal Particles Enable Smart Photonic Crystal Materials**

S. A. Asher, X. Xu; *University of Pittsburgh*

4O02 **Molecular Assemblies under Steady Magnetic Fields: Membranes, Micelles and Vesicles**

Taisuke Takahashi, Yutaka Yaguchi, Mikako Ishii, Sumio Ozeki; *Shinshu Univesity*

4O03 **Anisotropic Properties of Magnetic Ordered Gel**

Isao Yamamoto[1], Syuji Saito[1], Testuya Makino[1], Masuhiro Yamaguchi[1], Tadashi Takamasu[2]; [1]*Yokohama National University*, [2]*National Institute for Materials Science*

4O04 **Magnetic Field Effect on Morphology of Photochemical Products from a Gaseous Mixture of Trimethylsilylacetylene and Iron Pentacarbonyl**

Hiroshi Morita, Hidetoshi Tonooka, Yoshinori Okano; *Chiba University*

10:50-11:10 Break

11:10-12:30 **Magnetic Flow II** Chairs: Peter J. Hore, Sumio Ozeki

4O05 **The Effect of Magnetic Field on the Stable and Unstable Fluid Layers in a Cubic Enclosure**

Elzbieta Fornalik[1], Tomasz Bednarz[2], Toshio Tagawa[3], Hiroyuki Ozoe[1], Janusz S. Szmyd[1]; [1]*AGH, University of Science and Technology*, [2]*Kyushu University*, [3]*Tokyo Metropolitan University*

4O06 **On-chip continuous flow separation of magnetic particles**

Nicole Pamme[1], Andreas Manz[2]; [1]*National Institute for Mateirals Science*, [2]*Institute for*

Analytical Sciences

4O07 **Convection of water in a superconducting magnet: Numerical studies at the center and various off-centered positions of a bore of the magnet**

Mitsuo Ataka, Syou Maki; *National Institute of Advanced Industrial Science and Technology*

4O08 **Damping of Solute Convection During Crystal Growth by Applying Magnetic Field Gradients**

Nobuko I. Wakayama; *Tsukuba Magnet Laboratory*

12:30-12:40 Closing Ceremony

15 Nov. (Tue)

14:00-15:20 **Posters I**

2P01 **Magnetic Oscillation of Hexagonal Ice and Origin of Diamagnetic Anisotropy**

Takaaki Abe, Ryoichi Takashima, Chiaki Uyeda; *Osaka University*

2P02 **Two-dimensional Triangle-lattice Alignments by Feeble Magnetic Particles under High Magnetic Field**

Tsutomu Ando[1], Noriyuki Hirota[2], Akira Satoh[3], Eric Beaugnon[4], Hitoshi Wada[1]; [1]*University of Tokyo*, [2]*Tsukuba Magnet Laboratory*, [3]*Akita Prefectual University*, [4]*Centre National de la Recherche Scientifique*

2P03 **Simultaneous Measurement of Mass and Magnetic Susceptibility of a Single Microparticle by Magnetophoretic Velocity Analysis in Atmosphere**

Mariko Arase, Masayori Suwa, Hitosihi Watarai; *Osaka University*

2P04 **Magnetically Aligned $Gd(OH)_3$–Polymer Composite Film**

Chengkang Chang[1], Fumiko Kimura[1], Tsunehisa Kimura[1,2], Hitoshi Wada[3]; [1]*Tsukuba Magnet Laboratory*, [2]*Tokyo Metropolitan University*, [3]*University of Tokyo*

2P05 **Magnetic Susceptibility Measurement of Solution by Interfacial Nanodisplacement Detection**

Shigeki Egami, Hitoshi Watarai; *Osaka University*

2P06 **Magnetic resonance imaging of the manipulation of a chemical wave using an inhomogeneous magnetic field**

Rob Evans[1], C. R. Timmel[1], M. Britton[2]; [1]*Oxford University*, [2]*Cambridge University*

2P07 **Nano-Carbons synthesized by Electrochemical Method under High Magnetic Field at Room Temperature**

Haruo Yokomichi[1], Fumiko Sakai[2], Masaki Ichihara[2], Shigeki Nimori[3], Naoki Kishimoto[3]; [1]*Toyama Pref. Univ.*, [2]*Univ. of Tokyo*, [3]*National Inst. for Materials Science*

2P08 **How Is Effect of Strong Static Magnetic Field on Nanorods?**

Yoshihisa Fujiwara, Naho Shibata, Yoshifumi Tanimoto; *Hiroshima University*

2P09 **Measurement of Microscopic Raman Spectra in High Magnetic Fields**

Takeyoshi Goto, Masayori Suwa, Hitoshi Watarai; *Osaka University*

2P10 **Measurement of Phase Transformation Temperature and Carbon Diffusion in Fe-C Alloys in a High Magnetic Field**

Xinjiang Hao, Hideyuki Ohtsuka; *National Institute for Materials Science*

2P11 **Electromagnetophoretic Force Measurement of Specific Cell-Protein Binding Interaction**

Yoshinori Iiguni, Hitoshi Watarai; *Osaka University*

2P12 **An EQCM Study on the Electrodeposition of Nickel-Iron Alloys in a Magnetic Field**

Adriana Ispas, Andreas Bund; *Dresden University of Technology*

2P13 **Magnetic Field Effect on Hydrogen Isotope Separation with Metal Hydrides**

Yuya Ito[1], Rui Takahashi[1], Soichiro Mizusaki[2], Isao Yamamoto[1], Tadashi Takamasu[3], Masuhiro Yamaguchi[1]; [1]*Yokohama National University*, [2]*Aoyama Gakuin University*, [3]*National Institute for Materials Science*

2P14 **Proposal of a new type of magnetic force**

Akio Katsuki[1], Yoshifumi Tanimoto[2]; [1]*Shinshu University*, [2]*Hiroshima University*

2P15 **In situ optical measurement of agarose aqueous solution**

Shinji Kittaka, Tsubasa Takeda, Isao Yamamoto, Masuhiro Yamaguchi; *Yokohama National University*

2P16 **Magnetic-Field Effect on Thermal Motions of Diamagnetic Colloidal Particles: Studies by Dynamic Light Scattering**

Yuzuru Koizumi, Hideyuki Nakayama, Kikujiro Ishii; *Gakushuin University*

2P17 **The influence of superimposed magnetic fields on the microstructure of electrodeposited Co**

A. Krause, M. Uhlemann, A. Gebert, L. Schultz; *Leibniz Institute for Solid State and Materials Research Dresden*

2P18 **Mathematical Analysis of Temperature Distribution in Hybrid Recording Film Using AFM Tip Writing**

Z. Y. Li, J. B.Yan, Z. Li, X. F. Yang, X. Sun, R. Wan, G. Q. Lin; *Huazhong Univ. of Science &Technology*

2P19 **Photoconductivity of New Molecular Complexes of Fullerene C_{60} in Magnetic Fields**

Dmitrii V. Lopatin, Vyacheslav V. Rodaev, Alexey V. Umrikhin; *Tambov State University*

2P20 **Magneto-Archimedes levitation of a number of substances: In-situ observation using pictures obtained by a CCD camera**

Syou Maki, Mitsuo Ataka; *National Institute of Advanced Industrial Science and Technology*

2P21 **Adjustable Super-strong Permanent Magnet**

Takanori Mihara[1], Yoshihisa Iwashita[1], Masayuki Kumada[2], Cherrill M. Spencer[3]; [1]*Kyoto University*, [2]*National Institute for Radiological Science*, [3]*Stanford Linear Accelerator Center*

2P22 **Morphological Change in Copper Electrodeposition under Magnetic Field Parallel to Electrode Surface**

Ryoichi Morimoto[1], Atsushi Sugiyama[2], Ryoichi Aogaki[3]; [1]*Saitama Industrial Technology Center*, [2]*Waseda University*, [3]*Polytechnic University*

2P23 **Effect of high magnetic field on Synthesis of Fe-incorporated LDH**

Hideaki Murase[1], Hideyuki Yasuda[2], Atsushi Nakahira[1]; [1]*Osaka Prefecture University*, [2]*Osaka University*

2P24 **Magnetic Field and Methylene Chain Length Effects on Photochemistry of Bichromophoric Chain Molecules Containing 7-Nitro-2-fluorenyloxy and Anilino Moieties**

Kazuya Takahashi, Yumi Satoh, Shigeru Kohtani, Ryoichi Nakagaki; *Kanazawa University*

2P25 **Therapeutical Application of Paramagnetic Liposomes for Drug Delivery System**

Hidenori Nakagawa, Masaki Sekino, Hiroko Kotani, Shoogo Ueno; *University of Tokyo*

2P26 **Removal of Aerosol by High Gradient Magnetic Separation**

Hidehiko Okada, Hideo Okuyama, Masahiro Uda, Noriyuki Hirota; *Tsukuba Magnetic Lab.*

2P27 **Quantification of Fe-C alloy isothermal ferrite transformation based on measurement of magnetic susceptibility**

Takuya Ono[1], Kensuke Sassa[1], Hideyuki Ohtsuka[2], Shigeo Asai[1]; [1]*Nagoya University*, [2]*Tsukuba Magnet laboratory*

2P28 **Magnetoadsorption of Gases on Porous Materials**

Akihito Yoshidome, Shigeo Sasahara, Taku Iiyama, Sumio Ozeki; *Shinshu University*

2P29 **The Spin Chemistry of Bird Navigation**

Christopher T. Rodgers, Christiane R. Timmel, P. J. Hore; *University of Oxford*

2P30 **Control of a switching current of a DC-SQUID with an electric current in comparison with control with magnetic field**

Yoshihiro Shimazu; *Yokohama National University*

2P31 **Magnetic Orientation of Organic Nanocrystals**

Manabu Sueda[1], Wenyong Duan[1], Yoshifumi Tanimoto[1], Yuji Kaneko[2], Tsunenobu Onodera[2], Hitoshi Kasai[2], Hidetoshi Oikawa[2], Hachiro Nakanishi[2]; [1]*Hiroshima University*, [2]*Tohoku University*

2P32 **Measurement of Interfacial Magnetic Susceptibility of Microdroplets by Magnetophoretic Velocimetry**

Masayori Suwa, Hitoshi Watarai; *Osaka University*

2P33 **The Kinetical Examination on the Magnetic Field Effect for the Autocatalytic Nonlinear Chemical Reaction**

Kazuhiro Honda[1], Kosuke Suzuki[2], Akira Sato[3], Seiichiro Nakabayashi[4]; [1]*Kanagawa Institute of Technology*, [2]*University of Tukuba*, [3]*Shonan Institute of Technology*, [4]*Saitama University*

2P34 **Magnetomigration of a Single Paramagnetic Ion**

Tsubasa Takeda, Takeru Kogawa, Isao Yamamoto, Masuhiro Yamaguchi; *Yokohama National University*

2P35 **Unusual Magnetic Properties of Water Adsorbed on Gold Surface**

Yhuhei Terui, Norihito Sogoshi, Seiichiro Nakabayashi; *Saitama University*

2P36 **Effect of the High Magnetic Field on Cylindrical Microdomains in a Block Copolymer Thin Film**

Yoshhihiro Tsuji[1], Shinichi Sakurai[1], Kazushi Yamada[1], Akira Itaya[1], Fumiko Kimura[2], Masafumi Yamato[3], Tsunehisa Kimura[2,3]; [1]*Kyoto Inst. of Tech.*, [2]*Tsukuba Magnet Laboratory*, [3]*Tokyo Metropolitan University*

2P37 **Multinuclear Radical Pairs in Low Magnetic Fields**

Nicola Wagner, P. J. Hore; *University of Oxford*

2P38 **Study of Current Source Estimation with the Use of Time Series Information in MEG**

Masuji Yamada, Gjini Klevest, Shogo Ueno; *University of Tokyo*

16 Nov. (Wed)

14:00-15:20 **Posters II**

3P01 **Fabrication of Highly Oriented Hydroxyapatite-Collagen Composite using High Magnetic Field**

Jun Akiyama[1], Masami Hashimoto[2], Hiroaki Takadama[2], Yoshiyuki Yokogawa[3], Kensuke Sassa[1], Kazuhiko Iwai[1], Shigeo Asai[1]; [1]*Nagoya University*, [2]*Japan Fine Ceramics Center*, [3]*National Institute of Advanced Industrial Science and Technology*

3P02 **Effect of variable high magnetic field on survivability of Saccharomyces cerevisiae under heat-induced oxidative stress**

Yoshimasa Ishizaki, Mutsumi Fujita, Shin-ichiro Horiuchi, Kazumasa Okuno, Takashi Ano, Susumu Kajiwara, Makoto Shoda; *Tokyo Institute of Technology*

3P03 **The Theory of Magnetic Field Dependencies of Enzymatic Reaction: Substrate Phosphorylation and Biological Electron Transfer**

Vitaly L. Berdinsky, Anatoly L. Buchachenko; *Institute of Problems of Chemical Physics RAS*

3P04 **Magnetic Field Effect on Photoinduced Electron Transfer between 4-Nitroquinoline 1-oxide and Indoles**

Sharmistha Dutta Choudhury, Samita Basu; *Saha Institute of Nuclear Physics*

3P05 **Application of Magnetic Filtration to Phosphate Elimination Using Shwertmannite**

A. Eskandarpour, K. Sassa, Y. Bando, M. Okido, S. Asai; *Nagoya University*

3P06 **Magnetic Field Effect on Single Cultured Plant Cells and Regenerating Protoplasts**

Yuu Fujimura, Daisuke Kurimoto, Masaaki Iino; *Chiba Institute of Technology*

3P07 **Effects of the Strong Static Magnetic Field on the Swimming Behavior of Some Protists**

Yoshihisa Fujiwara, Masahiko Tomishige, Yasuhiro Itoh, Naho Shibata, Yoshifumi Tanimoto, Toshikazu Kosaka, Hiroshi Hosoya; *Hiroshima University*

3P08 **Bubble behavior in an electrically conductive liquid under static magnetic field**

Ippei Furuhashi, Kazuhiko Iwai, Shigeo Asai; *Nagoya University*

3P09 **Magnetic Field Effects on the Photochemical Reactions Interpreted by the Relaxation Mechanism**

Atom Hamasaki[1], Kiyoshi Nishizawa[2], Yoshio Sakaguchi[2], Kido Giyuu[3], Masanobu Wakasa[1]; [1]*Saitama University*, [2]*RIKEN*, [3]*NIMS*

3P10 **Effect of static high magnetic field on the growth of Caenorhabditis elegans and its aging**

Shin-ichiro Horiuchi, Yoshimasa Ishizaki, Kazumasa Okuno, Takashi Ano, Makoto Shoda; *Tokyo Institute of Technology*

3P11 **Analysis of high magnetic field effects on yeast Saccharomyces cerevisiae using DNA microarray technology**

Yoshimasa Ishizaki, Mutsumi Fujita, Shin-ichiro Horiuchi, Kazumasa Okuno, Takashi Ano, Katsuhiko Shirahige, Makoto Shoda; *Tokyo Institute of Technology*

3P12 **Simultaneous measurements of Hall and magnetoresistance effects in liquid metals and amorphous metal foils**

Takanori Ito[1], Tadashi Ooi[1], Masami Ogita[1], Iwao Mogi[2], Satoshi Awaji[2], Kuniyoshi Yokoo[3]; [1]*Shizuoka University*, [2]*Tohoku University*, [3]*Research Institute of Electrical Communication*

3P13 **Growth of PbBr2 using the magneto-influenced gel**

Takamasa Kaito[1], Shin-ichiro Yanagiya[1], Atsushi Mori[1], Mami Kurumada[2], Chihiro Kaito[2], Tetsuo Inoue[1]; [1]*University of Tokushima*, [2]*Ritsumeikan University*

3P14 **The application of a magnetic field for the control of the colloidal crystal structure**

Kazutoshi Kitajima, Kazushi Kobayashi, Toma Fujita, Norihito Sogoshi, Seiichiro Nakabayashi; *Saitama University*

3P15 **Faraday Effect of Magnetic Opal Films**

Kazushi Kobayashi, Kazutoshi Kitajima, Norihito Sogoshi, Seiichiro Nakabayashi; *Saitama University*

3P16 **Photoinduced Convection of Organic Solution in Magnetic Field**

Fumi Koyama, Yoshifumi Tanimoto; *Hiroshima University*

3P17 **Fabrication of crystal oriented Bi_2Te_3 by use of slip casting in a high magnetic field**

Toshiyuki Kuribayashi, Mun-Gyu Sung, Kensuke Sassa, Shigeo Asai; *Nagoya University*

3P18 **Optimization on Solenoid Coils for Magnetic Force Enhancement**

Xiaojun Liu and Tsukasa Kiyoshi; *Tsukuba Magnet Laboratory*

3P19 **Study on the Application of Magnetic Field and Magnetic Field Induced Materials in China**

Zhan Mao-Sheng[1], Yin Shu-Gung[1], Lu Yun-Hua[1], Tsunehisa Kimura[2,3]; [1]*Beijing University of Aeronautics and Astronautics*, [2]*Tokyo Metropolitan University*, [3]*Tsukuba Magnet Laboratory*

3P20 **Magnetic field effects on viscoelasticity of agarose gels**

Tetsuya Makino, Kyohei Ogawa, Isao Yamamoto, Masuhiro Yamaguchi; *Yokohama National University*

3P21 **Effects of Magnetic Annealing on Growth of Pentacene Thin Film**

Junta Miyamoto[1], Takamasa Kaito[1], Shin-ichiro Yanagiya[1], Atsushi Mori[1], Hitoshi Suzuki[2], Chihiro Kaito[2], Tetsuo Inoue[1]; [1]*University of Tokushima*, [2]*Ritsumeikan University*

3P22 **Functionalization of supramolecular biosystems in magnetic fields**

Toru Oba[1], Takero Nagai[1], Yoshifumi Tanimoto[2]; [1]*Utsunomiya University*, [2]*Hiroshima University*

3P23 **The Interaction of Carotenoids with Model Membranes Studied by ^{13}C and ^{31}P Nuclear Magnetic Resonance**

Hidenori Nakagawa, Shigeru Okada, Hiroki Abe; *University of Tokyo*

3P24 **Static magnetic field has little effect on gene expression in in vitro: Microarray analysis**

Takehisa Nakahara, Tomonori Sakurai, Junji Miyakoshi; *Hirosaki University*

3P25 **Analysis of protein expression in Escherichia coli under high magnetic field by the two-dimensional gel electrophoresis**

Shin-ichiro Horiuchi, Yoshimasa Ishizaki, Kazumasa Okuno, Takashi Ano, Makoto Shoda; *Tokyo Institute of Technology*

3P26 **Magnetic-Field-Induced Structures and Functions of Hydro gels**

Ichiro Otsuka, Sumio Ozeki; *Shinshu University*

3P27 **Magnetic Alignment and Patterning of CNTs in Conducting Polymer**

Guangzhe Piao[1], Fumiko Kimura[1], Tsunehisa Kimura[1,2], Kaoru Tsuda[3]; [1]*Tsukuba Magnet Laboratory*, [2]*Tokyo Metropolitan University*, [3]*Nano Frontier Co.*

3P28 **Grazing Incidence Small-Angle X-Ray Scattering Studies on Influence of High Magnetic Fields on a Single Nano-cylinder in a Block Copolymer Thin Film**

Shinichi Sakurai[1], Yoshhihiro Tsuji[1], Sono Sasaki[2], Hiroshi Okuda[3], Fumiko Kimura[4], Masafumi Yamato[5], Tsunehisa Kimura[4,5]; [1]*Kyoto Inst. of Tech.*, [2]*JASRI/SPring-8*, [3]*Kyoto Univ.*, [4]*Tsukuba Magnet Laboratory*, [5]*Tokyo Metropolitan University*

3P29 **In situ Observation of Laser-induced Convection of Water in Magnetic Field**

Kazutaka Sueda[1], Fumi Koyama[1], Masahiro Irie[2], Akio Katsuki[3], Yoshifumi Tanimoto[1]; [1]*Hiroshima University*, [2]*Kyushu University*, [3]*Shinshu University*

3P30 **Examination of Spin Electrode with Carbon Micro-Electrode**

Atsushi Sugiyama[1], Tetsuya Osaka[1], Ryoichi Aogaki[2]; [1]*Waseda University*, [2]*Polytechnic University*

3P31 **DNA Electrophoresis under Strong Magnetic Fields**

Kohei Suzuki[1], Kohei Yoshida[1], Isao Yamamoto[1], Masuhiro Yamaguchi[1], Tadashi Takamasu[2]; [1]*Yokohama National University*, [2]*National Institute for Materials Science*

3P32 **Magnetic Alignment of Paramagnetic and Diamagnetic Silicate Crystals Achieved at Low Field Intensity below 1 mT in Planetary Formation Regions**

Ryoichi Takashima, Takaaki Abe, Chiaki Uyeda; *Osaka University*

3P33 **Magnetic Levitation of Plastic Chips: Applications for Magnetic Susceptibility Measurements and Magnetic Separation**

Yoshifumi Tanimoto, Masao Fujiwara, Manabu Sueda; *Hiroshima University*

3P34 **Molecular alignment control of liquid crystalline polymers containing photo-crosslinkable side groups**

Hisashi Tetsutani[1], Hiroshi Awano[1], Takahashi Tatsuhiro[1], Koichiro Yonetake[1], Yoshiyuki Oishi[2]; [1]*Yamagata University*, [2]*Iwate University*

3P35 **Uniaxially Oriented Collagen Fibrils Mineralized with Calcium Phosphate by Using of a High Magnetic Field**

Cunyou Wu, Kensuke Sassa, Kazuhiko Iwai, Shigeo Asai; *Nagoya University*

3P36 **Structural Control of Mesoporous Silicas by Magnetic Fields**

Yasuyuki Yamane, Sumio Ozeki; *Shinshu University*

3P37 **Electro-magnetic inspection for aged power plants**

Yoshihiro Yamashita; *Hitachi, Ltd.*

3P38 **Combined effect of strong static magnetic fields and radiation on cell viability and mutagenisity**

Ryoichi Yamauchi[1], Shingo Terashima[1], Saori Ito[2], Takashi Matsudate[3], Keito Hamada[1], Takehisa Nakahara[1], Junji Miyakoshi[1]; [1]*Hirosaki University*, [2]*Aomori General Examination Center*, [3]*Iwate Medical University*

In situ microscopic observation of magnetic field effects on the growth process of two-dimensional silver dendrites

Noriyuki Hirota[1], Soma Hara[2], Hiromichi Uetake[2], Hiroyuki Nakamura[2]
[1]*Tsukuba Magnet Laboratory, National Institute for Materials Science*
Sakura, Tsukuba 305-0003, Japan
[2]*Department of Advanced Materials Science, University of Tokyo*
Kashiwanoha, Kashiwa 277-8561, Japan
(HIROTA.Noriyuki@nims.go.jp)

Abstract
The mechanism of the morphological effect of magnetic fields on electroless silver deposition was investigated through *in situ* microscopic observation by using a periscope system that was developed on the basis of a confocal scanning laser microscope. At the growth front of a silver dendrite, under a 12 T magnetic field applied perpendicularly to the sample plane, a silver branch was grown straightly for a while; then, a certain length of the branch at the neighbor of the tip started moving rapidly and was bent in an integrated manner. As a result of the process, a dense silver dendrite in the shape of a vortex was formed. When the sample space was narrowed, the branch did not bend due to the increase in the static friction between the branch and the glass plates. Judging from these observations, the mechanism of the formation of a dense vortex dendrite was thought to be the effect of a Lorentz force acting on the branch due to the electric current flowing through the branch itself accompanied by the silver deposition and the copper dissolution reactions.

Keywords
electroless silver deposition, confocal microscope, periscope, high magnetic fields, Lorentz force

1. Introduction

The recent remarkable diffusion of a cryo-cooler operated superconducting magnet is making it possible to easily use high magnetic fields in large-scale room-temperature spaces. With these new developments, it has become popular to study magnetic field effects on dia- and para-magnetic materials, i.e., feeble magnetic materials, or the processes consisted by feeble magnetic materials. There have been many reports on the effects of magnetic fields on some crystal growth processes or material processing. In some studies, high magnetic fields are used in an attempt to control the morphology or structure of the materials. For example, it has been reported that the orientation of some ceramics, due to their magnetic anisotropy, was controlled by adopting a slip-casting method under high magnetic fields [1, 2]. In the solidification process of some alloys or metals, inclusions can be isolated by utilizing the Lorentz force due to their difference in conductivity with the main matrix [3]. By utilizing magnetic dipole interactions in many-particle systems, some ordered alignments such as chain-like alignments and triangle-lattice alignments were obtained under high magnetic fields [4].

One of the remarkable magnetic field effects in the field of material processing is that the morphology of silver dendrite changes drastically in the electroless silver deposition process [5]. When electroless silver deposition occurs in a very thin sample space, the shape of the silver dendrite becomes similar to that of a diffusion-limited aggregation (DLA) cluster. Branches of the dendrite are scattered and vary in length. Under high magnetic fields of several Teslas applied perpendicularly to the sample plane, the morphology of the silver dendrite changes into a dense vortex shape. The lengths of the branches in this case are almost uniform.

From a macroscopic observation, the formation of the dense morphology was attributed to the change in the rate-determining process from a diffusion-limited process to a reaction-limited one, and the vortex shape was thought to be the result of the Lorentz force acting on the silver ions in the

solution.

However, the magnetic energy induced in feeble magnetic materials seems too small to change the rate-determining process of a deposition reaction even under high magnetic fields. Even though the effect of the Lorentz force on the silver ion is considered, it seems unlikely that a winding branch would grow as reported. According to the result of the Monte Carlo simulation that evaluated the morphological change in the DLA pattern under a rotating flow [6], even if the flow of the solution is induced by the Lorentz force acting on the silver ions, the branch winding should be in the opposite direction of the one observed.

While the observations are interesting from the viewpoint of engineering, the mechanism remains unclear. An understanding of the mechanism of the magnetic field effect on the morphology of a silver dendrite would provide important information that could be used to design how to control some processes, such as material processing by magnetic fields, or to evaluate the effects of magnetic fields on chemical and biological reactions. More details may be obtained from microscopic observations of this phenomenon, which have not been conducted yet.

Therefore, in this study, *in situ* microscopic observations of electroless silver deposition were conducted under a 12 T magnetic field using a periscope system that was developed for use under high magnetic fields on the basis of the commercially available confocal scanning laser microscope.

2. Experimental

The electroless silver deposition reaction is expressed in the following chemical equation:

$$2Ag^{+} + Cu \rightarrow 2Ag\downarrow + Cu^{2+}.$$

This reaction occurs when a piece of copper is introduced into a silver nitrate aqueous solution due to the difference in the oxidation-reduction potential. In the experiment here, this chemical reaction was carried out in a space sandwiched between two glass plates, and the behavior of the silver deposition was then observed *in situ* under a high magnetic field of 12 T.

The size of the sample space was fixed to 18 mm square, and the thickness was adjusted to 100 μm or 3 μm by using Teflon spacer between the two glass plates.

The size of the copper metal sheets was 2 mm square, and their thickness was 50 μm or 2 μm depending on the thickness of the sample space, 100 μm or 3 μm, respectively. The concentration of the silver nitrate aqueous solution was 0.1 and 0.25 mol/dm^3.

At first, a piece of copper was put in the sample space. After a few drops of the silver nitrate aqueous solution were placed into this space, the upper glass plate was set in place to form a closed system. The deposition reaction started immediately after the drop of the solution was placed. The sample was quickly introduced into the superconducting magnet. The magnet used in this study was a cryocooler operated type of superconducting magnet, model HF12-100VHT, manufactured by Sumitomo Heavy Industry Co., Ltd. This magnet has a room-temperature bore with a diameter of 100 mm and can produce 12 T magnetic fields at a maximum on the bore axis.

It took about 60 minutes to grow enough of the silver dendrite crystal in the experimental condition here. During this period, *in situ* observations of the silver dendrite growth were carried out under a magnetic field of 12 T. To observe the dendrite, the CCD camera, model QN42 of ELMO Co., Ltd., was used. For the *in situ* microscopic observation of the growth front, the periscope system was used. This system was specially developed for utilization under high magnetic fields based on the confocal scanning laser microscope, model VL-2000, of Lasertec Co., Ltd. A gallium nitride light-emitting diode was used

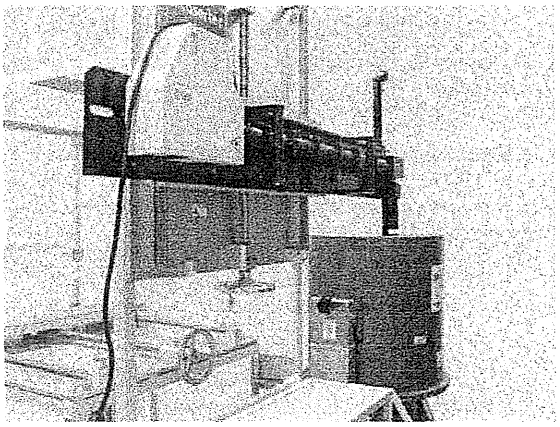

Fig. 1 Photograph of the periscope system and the superconducting magnet

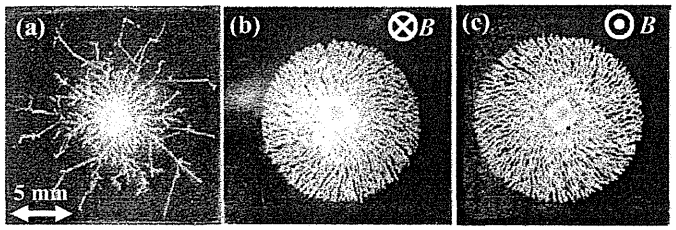

Fig. 2 Macroscopic observation of the morphology of silver dendrites by CCD camera

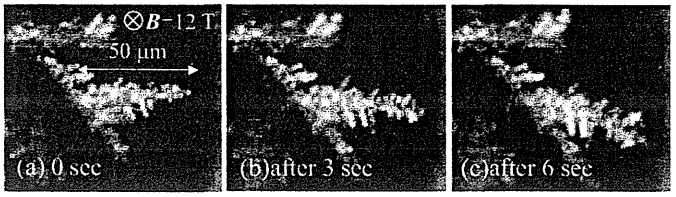

Fig. 3 *In situ* microscopic observation of the silver branch growth at the tip

as a light source, and its wavelength was 410 nm. The full resolution of the image was 0.15 μm. Figure 1 shows the photograph of the entire system.

Control experiments under a zero field were also carried out in the superconducting magnet without applying magnetic fields.

3. Results and Discussion

The results of a macroscopic observation of the morphology of the silver dendrite obtained using a CCD camera are shown in Fig. 2. The thickness of the sample space was always 100 μm, and the concentration of the silver nitrate aqueous solution was 0.25 mol/dm^3. These photographs were taken 60 minutes after the start of the reaction. Without a magnetic field, the morphology of the silver dendrite becomes a typical DLA pattern, as shown in Fig. 2 (a). Under a magnetic field of 12 T applied perpendicularly to the sample plane, it was confirmed, as reported [5], that the morphology of the silver dendrite became a dense vortex shape and the direction of the branch winding was reversed depending on the direction of the magnetic field, as shown in Figs. 2 (b) and (c).

Then, *in situ* microscopic observations of the growth front of the dendrite were carried out by using the periscope system. In this experiment, a silver nitrate aqueous solution of 0.10 mol/dm^3 was used. The thickness of the sample space was 100 μm, and the applied magnetic field was 12 T. Typical results of the observation are shown in Fig. 3 as a series of photographs of a growth front, taken every 3 seconds from a certain time. At the growth front, first, a silver branch was grown straightly for a while, then, a certain length of the branch at the neighbor of the tip started moving rapidly and was bent in an integrated manner. This rapid bending of the silver branch was observed everywhere.

It is obvious that the Lorentz force plays an important role in this phenomenon because the direction of branch winding depends on the direction of the applied magnetic field. If, however, the vortex shape were formed due to the Lorentz force acting on the silver ion in the solution, a spirally winding branch should be formed from the beginning. Judging from the observation here, this mechanism seems unlikely.

The points where silver deposition and copper dissolution occur are apart from each other and are connected electrically by silver branches. Therefore, the electric current flows in silver branches due to the transfer of electrons accompanied by the progress of the reaction. Because the direction of this current flow is perpendicular to the applied magnetic field, the Lorentz force acts on branches as a conductor. The direction of branch winding agrees with the direction of the Lorentz force. The mechanism of the rapid bending of branches is thought to be the effect of the Lorentz force acting on the branch due to the flow of the electric current.

The intensity of the Lorentz force acting on a silver branch observed in the case of Fig. 3 was estimated. Assuming that the density of silver cylinder is ρ kg/m^3 in consideration of the filling factor, the intensity of the Lorentz force acting on the bent silver branch was estimated to be as $2.6\times10^{-15}\times\rho$ [N]. On the other hand, the intensity of gravity acting on the bent branch was $1.7\times10^{-14}\times\rho$ [N]. The intensity of the Lorentz force was 15 % of the gravity force acting on the branch. Considering that the bent silver branch had several tips and silver deposition occurred at

various sites simultaneously, it is possible that a fairly large Lorentz force was acting on this branch.

The silver branch appeared to be at the bottom of the silver nitrate aqueous solution, touching with the glass surface, because it was much heavier than the solution. When the Lorentz force acting on the branch was smaller than the static friction between the branch and the glass surface, the branch did not move. As the growth front increased, the Lorentz force became gradually larger because of the increase in the number of deposition sites. When the Lorentz force exceeded the static friction, the branch appeared to start moving and bend rapidly.

According to this hypothesis, the bending of silver branches should be suppressed due to the increase of the static friction when the space between the two glass plates containing the sample is narrow and the silver branches touch glass on both sides. From the result of the experiments, the approximate diameter of a silver branch seems to be several micrometers; therefore, the distance between the two glass plates was 3 μm. In this condition, the silver branches grew straight, unlike those shown in Fig. 3. Even though the Lorentz force was acting on the branches, their movement was assumed to be impeded by the anticipated increments of static friction.

4. Conclusions

In this study, to understand the mechanism of the magnetic field effect on the morphology of silver dendrite reported so far, an *in situ* microscopic observation of the electroless silver deposition process under a 12 T magnetic field was carried out by using a periscope system. Observations under a 12 T magnetic field showed that the branch grew straight for a while on the growth front; then, a certain length of the branch at the neighbor of the tip started moving rapidly and was bent in an integrated manner. As a result, a dense vortex shape of silver dendrite was formed. Then, in an experiment in which the sample space was narrowed to increase the static friction between branches and the glass plates, straight silver branches grew. Based on these observations, it was concluded that the mechanism of the formation of a vortex morphology under a magnetic field was the effect of the Lorentz force acting on the silver branch due to the electric current flowing through the branch itself accompanied by the silver deposition and the copper dissolution reactions.

The observations here suggest that the morphology or structure of materials may be controlled in some material processing that contains electrolysis or electro-crystallization as an element process by the utilization of high magnetic fields. The use of magnetic fields is characteristic for its non-contact manner, i.e., magnetic fields can have an effect on material processing without any direct contact with the matter. Therefore, the information obtained in this study is useful to design novel way of control for material processing by utilizing magnetic fields.

Acknowledgements

This work was partially supported by Grant-In-Aid of Scientific Research for Priority Area (Area 767, No.15085204) from MEXT of Japan.

References

[1] T. S. Suzuki, Y. Sakka, K. Kitazawa, Advanced Engineering Materials, **3** (2001) 490.
[2] S. Horii, I. Matsubara, M. Sano, K. Fujie, M. Suzuki, R. Funahashi, M. Shikano, W. Shin, N. Murayama, J. Shimoyama, K. Kishio, Jpn. J. Appl. Phys., **42** (2003) 7018.
[3] J. P. Park, K. Sassa, S. Asai, J. Jpn. Inst. Metals, **59** (1995) 733.
[4] T. Takayama, Y. Ikezoe, T. Kaihatsu, H. Uetake, N. Hirota, K. Kitazawa, Trans. Mater. Res. Soc. Jpn., **27** (2002) 43.
[5] I. Mogi, S. Okubo, Y. Nakagawa, J. Phys. Soc. Jpn., **60** (1991) 3200.
[6] T. Nagatani, F. Sagues, J. Phys. Soc. Jpn., **59** (1990) 3447.

Rotational motion of silver dendrites under magnetic field

Akio Katsuki[1] and Yoshifumi Tanimoto[2]
[1]*Department of Chemistry, Faculty of Education, Shinshu University, 6-Ro, Nishi-Nagano, Nagano 380-8544, Japan*
[2]*Graduate School of Science, Hiroshima University, Higashi-Hiroshima 739-8526, Japan*
(akatuki@shinshu-u.ac.jp)

Abstract
The "*in situ*" observation of the growth of dendrites was carried out in the superconducting magnet. The small dendrites showed the precession in the magnetic field. A period of the precession depended on the magnetic field intensity and the concentration of silver ions. The precession was caused by Lorentz force on silver ions, and the boundary condition promoted the motion. The boundary-assisted MHD is main mechanism of the precession.

Keywords
precession, boundary-assisted MHD mechanism, silver dendrite

1. Introduction

Magnetic field effects on chemical reactions are a very interesting topic and useful technique. Our group has observed interesting results from the use of a superconducting magnet for some years: magnetic orientation of diamagnetic crystals,[1–4] drastic changes of metal dendrites because of magnetic force,[5–9] chirality induction of zinc silicate membrane tube by boundary-assisted MHD,[10,11] and so on. Our previous studies have investigated magnetic field effects on the growth of silver dendrites that was produced by the reaction between silver ion and zinc metal. We observed particular magnetic orientation.[12] To elucidate that orientation, we investigated magnetic field effects on the reaction between silver ion and zinc metal and the growth of silver metal two-dimensional (2D) dendrites. We have also undertaken *in situ* observation of dendrite growth using a CCD camera, which revealed the unique motion of dendrites.

2. Experimental

A superconducting magnet (Spectromag-1000; Oxford Instruments PLC) was used in our experiment. This magnet had a room temperature horizontal bore tube of 50 mm diameter. Its maximum field and gradient field were 8 T and ± 410 T^2/m, respectively. Figure 1 shows a distribution of the magnetic field, where z is the distance from the centre of the bore tube along the bore. Silver nitrate (GR grade; Nacalai Tesque Inc.) was used as received. Distilled water was used. A zinc metal sheet (thickness: 1.0 mm, 99.5%; Nilaco Corp.) was polished just before the experiment. A silver nitrate solution (0.01 - 0.05 mol/dm^3) was filled into a cylindrical vessel (volume: ca. 30 mL). A reaction system was constructed using a metal sheet sandwiched between two acrylic plates, as described in a previous paper.[12] Dendrites grew two-dimensionally from the upper and lower surfaces of the sheet; the dendrites grew parallel to the magnetic field. The vessel was capped with a rubber stopper. It was placed at the position in the horizontal bore tube, of which magnetic conditions are 2.0 - 8.0 T and 0 T^2/m (see Fig. 1). All experiments were carried out at room temperature. *In situ* observation was carried out using a CCD camera (OH-411; Olympus Optical Co. Ltd.) installed in a fiber scope (R100-095-090-50; Olympus Optical Co. Ltd.), and pictures were recorded in a digital video cassette recorder.

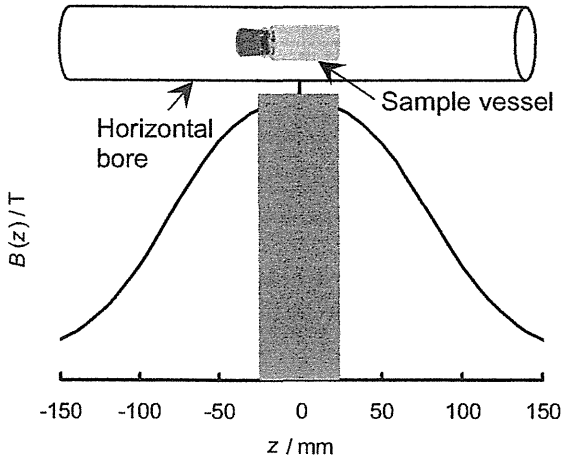

Fig. 1. The distribution of the *horizontal* magnetic field $B(z)$. z is the distance from the center of the magnetic field (max. 8 T) along the magnetic axis. The gray part shows the area of the magnetic fields where the sample vessel was placed. The magnetic conditions of the position were 8.0 T and 0 T^2/m. The upper *horizontal* bore's picture corresponds to the plot of distribution of the magnetic field.

3. Results and Discussion

We observed the following redox reaction.

$$Zn + 2Ag^+ \rightarrow Zn^{2+} + 2Ag$$

The silver metal appears on zinc metal sheet as dendrites. This reaction involves only diamagnetic species.

Figure 2 shows results of *in situ* observation at 8 T and 0 T^2/m. Here, magnetic forces can be neglected. The magnetic field was applied in a longitudinal direction on these images. During the reaction, which proceeded for 5 min, some small dendrites (ca. 0.5 mm high) grew and began to rotate along the magnetic field. The precession occurred counterclockwise in view from the zinc metal plate. Precession stopped suddenly and started again. The precession occurs intermittently until the dendrites are too large to rotate without contact with the wall. The dendrites, however, continue growing without the precession.

The reciprocal of periods of the precession showed linear relationship for the magnetic field, as shown in Fig. 3. Additionally, it depended on the concentration of silver ions. Moreover the direction of the precession was determined by the surrounding condition.

According to SEM pictures, the dendrites comprised many nano-size dendrites.[12] For that reason, the dendrites were very flexible for a perturbation such as that of a magnetic field.

Because the phenomena were observed at no magnetic field gradient, magnetic forces did not operate on the reaction system. One possible mechanism is the Lorentz force on silver ions, as shown in Fig. 4. The silver ion in the solution undergoes a Lorentz force in the left side for traveling

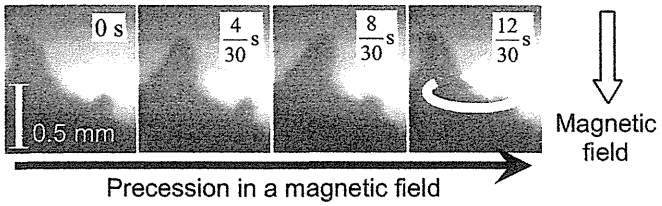

Fig. 2. Image sequence of the precession of silver dendrites produced at the $Zn–Ag^+$ system in a horizontal magnetic field (8 T).

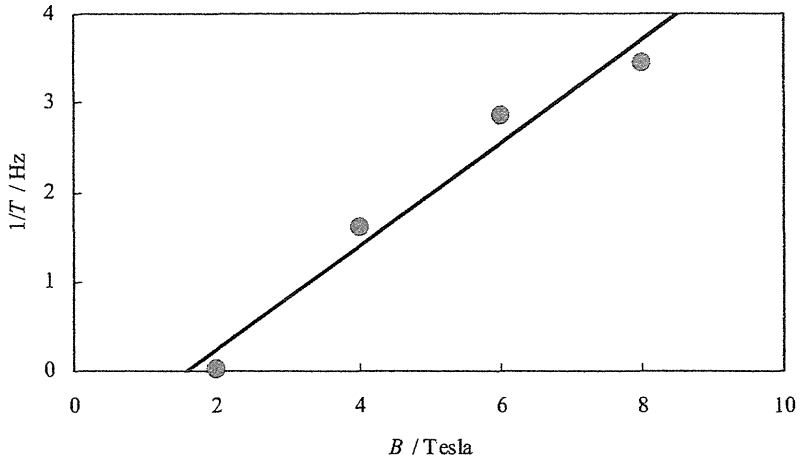

Fig. 3. Magnetic field strength dependence of rotational period $1/T$.
$1/T$ was proportional to the magnetic field strength.

direction. Subsequently, counterclockwise convection occurred; finally, the dendrites rotate along the magnetic field. The mechanism is similar to a micro-MHD mechanism.[13] Ion motions are reflected in the dendrites' behavior. When the silver ions' concentration around the dendrite decreases by a local redox reaction, the precession stops until the concentration is recovered. Therefore, the period of the precession will depend on the magnetic field and the concentration of the silver ions.

Moreover, boundary-assisted MHD mechanism promotes precession. Uechi et al. reported that a zinc silicate membrane tube grew spirally by Lorentz force.[10,11] Usually, because ions in bulk solution move in all directions, the Lorentz forces on them are averaged and thereby become inconsequential. However, at the boundary, such as a wall of a vessel, the ions move anisotropically. The Lorentz forces are not averaged and a certain component of the Lorentz force remains effective. Therefore, the boundary-assisted MHD causes one-way convection, thereby promoting the spiral structure. In our system, one-way convection will occur by the boundary-assisted MHD mechanism. In the moving components of the silver ions, some small perpendicular components to the magnetic field triggers the generation of the Lorentz force. Furthermore, the boundary, such as the wall,

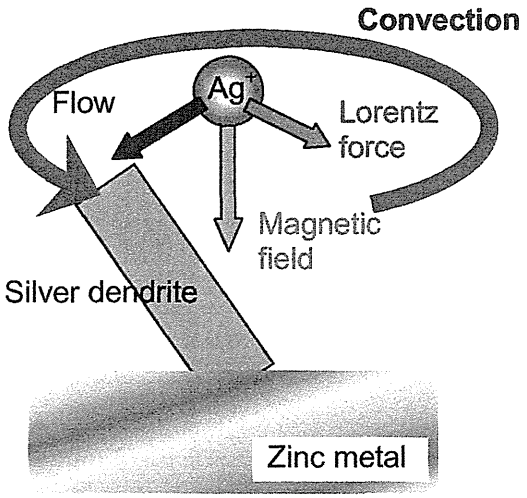

Fig. 4. Possible mechanism of precession.
A silver ion receives the Lorentz force in the right hand for traveling direction. A silver dendrite rotates by convection caused by the Lorentz force.

emphasizes the anisotropy of the Lorentz force, which causes the one-way convection. The mechanism implies that the surrounding condition will determine the direction of the precession. The silver dendrites are tethered to the zinc sheet surface. Therefore, they rotate by the convection. It is important that the phenomenon shows the transformation from chemical potential to mechanical energy by the magnetic field.

4. Conclusions

The magnetic field causes a unique motion similar to that created by a micromotor. Boundary-assisted MHD is the main mechanism of the precession. The phenomenon implies that the magnetic field has the potential of the transformation from chemical potential to mechanical energy in microscale condition. Moreover, this suggests that the magnetic field still offers the potential to control general redox reactions.

Acknowledgements

This research was partially supported by the Joint Studies Program (2003) of IMS, Grant-in-Aid for Encouragement of Young Scientists, 14740396, 2002, Grant-in-Aid for Scientific Research on Priority Area "Innovative utilization of strong magnetic fields" (Area 767, Nos. 15085208 and 15085205) from MEXT of Japan, and a Grant-in-Aid for Scientific Research (B), 16350007, 2004.

References

[1] A. Katsuki, R. Tokunaga, S. Watanabe, and Y. Tanimoto, Chem. Lett., 1996, 607.
[2] M. Fujiwara, R. Tokunaga, and Y. Tanimoto, J. Phys. Chem. B, 102, 5996 (1998).
[3] M. Fujiwara, M. Fukui, and Y. Tanimoto, J. Phys. Chem. B, 103, 2627 (1999).
[4] Y. Tanimoto, R. Yamaguchi, Y. Kanazawa, and M. Fujiwara, Bull. Chem. Soc. Jpn., 75, 1133 (2002).
[5] A. Katsuki, S. Watanabe, R. Tokunaga, and Y. Tanimoto, Chem. Lett., 1996, 219.
[6] Y. Tanimoto, A. Katsuki, H. Yano, and S. Watanabe, J. Phys. Chem. A, 101, 7359 (1997).
[7] W. Duan, M. Fujiwara, and Y. Tanimoto, Bull. Chem. Soc. Jpn., 73, 2461 (2000).
[8] A. Katsuki, I. Uechi, M. Fujiwara, and Y. Tanimoto, Chem. Lett., 2002, 1186.
[9] A. Katsuki, I. Uechi, and Y. Tanimoto, Bull. Chem. Soc. Jpn., 77, 275 (2004).
[10] I. Uechi, A. Katsuki, L. Dunin-Barkovsky, Y. Tanimoto, J. Phys. Chem. B, 108(8), 2527-2530 (2004).
[11] W. Duan, S. Kitamura, I. Uechi, A. Katsuki, Y. Tanimoto, J. Phys. Chem. B, 109(28), 13445-13450 (2005).
[12] A. Katsuki, I. Uechi, and Y. Tanimoto, Bull. Chem. Soc. Jpn., 78(7), 1251-1255 (2005).
[13] R. Aogaki and A. Sugiyama, Proc. 6th Symp. New Magneto-Science 2002, Nov. 6-8, 2002, Tsukuba, Jpn., (2002) pp. 136 – 141.

Development of a new magnetic levitation furnace

Kohki Takahashi, Iwao Mogi, Satoshi Awaji and Kazuo Watanabe
HFLSM, Institute for Materials Research, Tohoku University
Katahira, Aoba-ku, Sendai 980-8577, Japan
(kohki@imr.tohoku.ac.jp)

Abstract
The magnetic levitation for diamagnetic materials is a quasi-microgravity condition and enables containerless melting for materials synthesis. In order to perform a homogeneous heating of a levitating sample, a new magnetic levitation furnace has been developed using an electric furnace. Spherical samples of a cycloolefin polymer were obtained by using this furnace under the magnetic levitation condition.

Keywords
magnetic levitation, microgravity, magnetic levitation furnace

1. Introduction

Diamagnetic materials receive a repulsive force in a magnetic field gradient. When this magnetic force balances with the gravitational force, the materials can be levitated [1-5]. The magnetic levitation is considered to be a quasi-microgravity condition because the counterbalance between the magnetic force and the gravity holds for each molecule constituting the material. Therefore, the magnetic levitation enables containerless melting for materials synthesis. A containerless technique provides a clean environment free from contamination caused by a container, leading to easy supercooling and easy supersaturation. In the case of the magnetic levitation, magnetic orientation effect is expected additionally for materials with an anisotropic susceptibility. Therefore processing of materials under the magnetic levitation condition is considered to be a new technique for synthesis of novel materials.

In order to perform containerless melting, it is necessary to heat-treat materials under the magnetic levitation condition. We call such an apparatus a magnetic levitation furnace. The design of a magnetic levitation furnace requires several specific features. The first is to heat samples in high magnetic field. Because the furnace is placed in a hybrid magnet generating fields up to 30 T, it is necessary to operate it satisfactorily in such an environment. The second is to install the furnace in a confined narrow space in a hybrid magnet, which usually has a 52 or 32 mm bore. The third is to observe the behavior of a levitating sample in the furnace. It is indispensable to check whether the sample actually levitates or not in heating and cooling processes. If the magnetic susceptibility of the sample changes at melting or solidification, the sample falls down or flies away. We have developed various magnetic levitation furnaces for containerless melting experiment under the magnetic levitation condition and have performed the experiments by using them so far.

2. Magnetic levitation furnace

2.1 Laser furnace

Laser furnaces have advantages when they are used for containerless melting under the magnetic levitation condition. A laser beam is not affected by magnetic fields, and the local irradiation just on a sample allows the use of observation systems including a CCD camera near the sample. Laser furnaces, however, have also disadvantages in heating a levitating sample. When a sample does not absorb the laser light, the sample cannot be heated. If a sample is heated inhomogeneously and thermal conductivity of the sample is very small, the sample is partially heated just on the area irradiated by the laser light. In such case, the temperature of the irradiated part of the sample rises

rapidly and only thermal decomposition occurs before the whole sample melts. Such a behavior was observed when a piece of PMMA, one of clear plastics, was heated by the CO_2 laser furnace. If the absolute value of the magnetic susceptibility of a sample increases with increasing temperature by the laser irradiation, the sample moves upward and because the upward magnetic force acting on the sample become larger. When the change of the magnetic susceptibility is very large, the sample loses the horizontal stable position and moves to the wall of a magnet bore. Then the sample moves to the outside of the irradiated area, the sample cannot be heated any more.

2.2 Electric furnace

Electric furnaces for a cryogen-free superconducting magnet or a hybrid magnet [8] have been used for high field heat-treatment for high-T_c superconducting materials and various magnetic materials [9-11] or DTA analysis in magnetic fields [12]. An electric furnace with an outer diameter of 50 mm produces high temperature up to 1200°C in magnetic fields. A heater is made of platinum wires of 1 mm diameter. The outer furnace wall is cooled by water so as to eliminate thermal inputs to the magnets. The temperature of a sample is monitored and controlled using a thermocouple of Pt-Rh. If an electric furnace is used, homogeneous heating becomes possible. Figure 1 illustrates the outline of an electric furnace for a hybrid magnet. The difference between an electric furnace for a cryogen-free superconducting magnet and for a hybrid magnet is the access length to a heater center from a top flange.

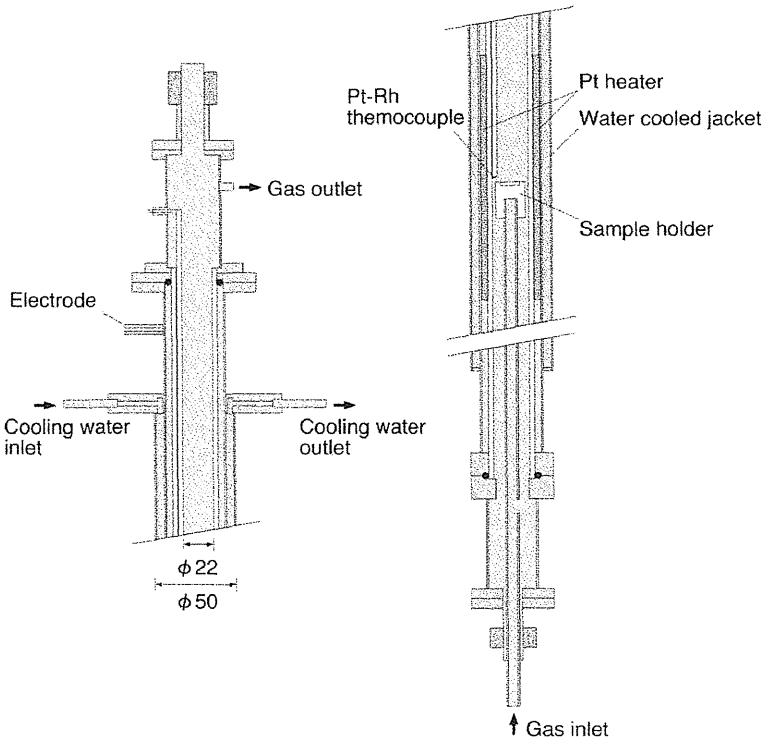

Fig. 1. Schematic drawing of an electric furnace for a hybrid magnet.

For the use of an electric furnace as a magnetic levitation furnace, however, there was a problem how to observe the levitating sample in heating process. We solved this problem by using a heatproof bore scope (Schölly Fiberoptic GmbH). The bore scope with optical relay lenses cooled by a water jacket can be used up to 800°C. Figure 2 shows the schematic illustration of the heatproof bore scope. It is possible to observe a containerless melting process in the electric furnace by inserting the bore scope into the furnace from a Wilson seal port on the top end.

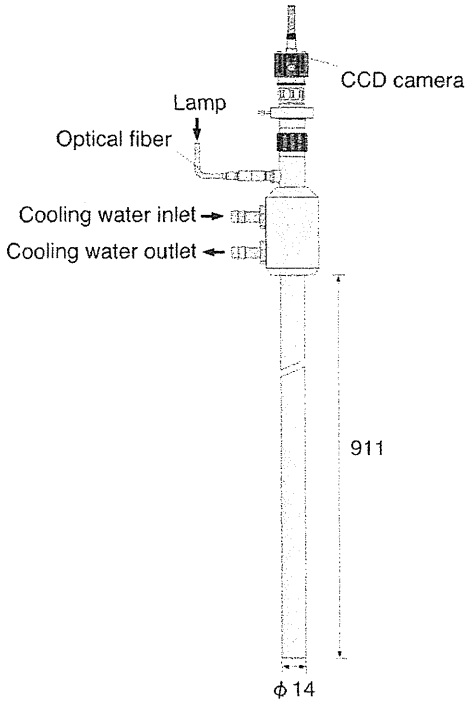

Fig. 2. Schematic illustration of a heatproof bore scope.

3. Application of a magnetic levitation electric furnace

We performed containerless melting experiments with a magnetic levitation electric-furnace. The sample was a clear plastic, a cycloolefin polymer; ZEONEX® (ZEON Corp.). The sample was an elliptic cylinder with the major axis, the minor axis and the height of 3 mm, 2 mm and 3 mm, respectively. The magnetic susceptibility, χ_g, was -10.63×10^{-9} m^3/kg estimated by a SQUID magnetometer. The melting point of the sample is not clear but the glass transition temperature is 138°C. In order to achieve the magnetic levitation of ZEONEX, we used a cryogen-free hybrid magnet (27.5T-CHM) with a room temperature bore of 52 mm [13].

A piece of ZEONEX sample almost levitated at z = 91 mm, when the center filed became 17.3 T. The temperature was increased up to 268°C at a rate of 7.5°C/min. The sample was heated in a N_2 gas atmosphere. It was observed that the sample levitated and moved upward with increasing temperature below 188°C. This means that $|\chi_g|$ of the sample increases with increasing temperature. This behavior of the sample was often observed for other samples. Then, falling down of the sample was observed above the temperature around 188°C, at which the sample began to melt. This implies that $|\chi_g|$ of the sample decreases with melting. The sample did not moved after it came to contact with the sample holder. This is because the viscosity of the sample prevented from moving on the sample holder.

In other run, we changed the condition of the heating process. The temperature was raised to 225°C at a rate of 15°C/min at a central field of 17.0 T. After the sample began to melt, the magnetic filed was adjusted to 18.0 T. The sample melted in the condition that its bottom contacted a sample holder. Figure 3 shows the top view of the heating process. The sample solidified in almost sphere shape in spite of the contact as is shown in Fig. 4(a). This means that the melt of the sample was under the microgravity condition. Figure 4(b) shows a sample melted and solidified in zero magnetic filed under the same heat-treatment condition and its shape was not spherical but ellipsoidal.

Small bubbles were observed in the solidified sample. It is not good for optical application. It is thought that this problem can be solved, if the heating process is reexamined.

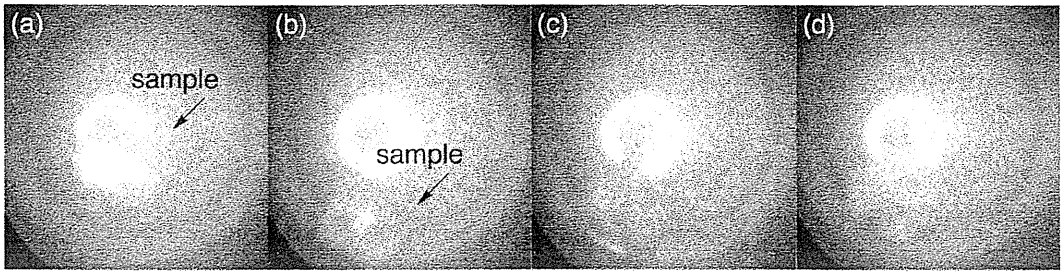

Fig. 3. Melting process of a piece of a ZEONEX. The temperature and the magnetic filed are; (a) 18°C, 17.0 T, (b) 147°C, 17.0 T, (c) 213°C, 18.0 T and (d) 226°C, 18.0 T, respectively.

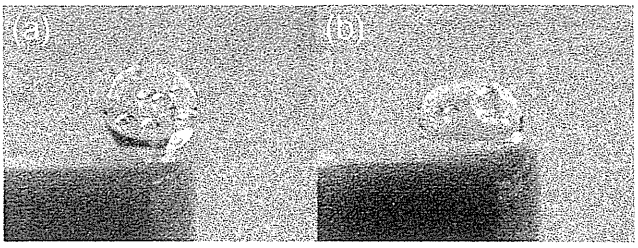

Fig. 4. Samples solidified (a) under the magnetic levitation condition and (b) in zero field.

4. Conclusions

We developed a new magnetic levitation furnace that consists of an electric furnace and a heatproof bore scope with a hybrid magnet. Homogeneous heating of a levitating sample in this furnace allows containerless melting of polymers. We have succeeded in preparing a spherical sample of cycloolefin polymer.

Acknowledgements

This work was supported by Grant-in-Aid for Scientific Research on Priority Area (Area 767, No. 15085201) from MEXT of Japan.

References

[1] E. Beaugnon and R. Tournier, Nature 349 (1991) 749.
[2] M. A. Weilert, D. L. Whitaker, H. J. Maris and G. M. Seidel, Phys. Rev. Lett. 77 (1996) 4840-4843.
[3] J. M. Valles Jr., K. Lin, J. M. Denegre and K. L. Mowry, Biophys. J. 73 (1997) 1130-1133.
[4] M. V. Berry and A. K. Geim, Eur. J. Phys. 18 (1997) 307-313.
[5] M. Motokawa, I. Mogi, M. Tagami, M. Hamai, K. Watanabe and S. Awaji, Physica B 256-258 (1998) 618-620.
[6] N. Kitamura, M. Makihara, M. Hamai, T. Sato, I. Mogi, S. Awaji, K. Watanabe and M. Motokawa, Jpn. J. Appl. Phys. 42 (2003) L715-L717.
[7] K. Takahashi, C. Umeki, I. Mogi, K. Koyama, S. Awaji, M. Motokawa and K. Watanabe, Physica B 346-347 (2004) 277-281.
[8] K. Watanabe, S. Awaji and K. Kimura, Jpn. J. Appl. Phys. 36 (1997) L673-L675.
[9] W. P. Chen, H. Maeda, K. Kakimoto, P. X. Zhang, K. Watanabe, M. Motokawa, H. Kumakura and K. Itoh, J. Cryst. Growth 204 (1999) 69-77.
[10] S. Awaji, K. Watanabe, M. Motokawa, A. Kuramochi, T. Fukase and K. Kimura, IEEE Trans.

Appl. Supercond. 9 (1999) 2014-2017.
[11] H. Kato, T. Miyazaki, M. Sagawa and K. Koyama, Appl. Phys. Lett. 84 (2004) 4230-4232.
[12] S. Awaji, K. Watanabe and M. Motokawa, J. Cryst. Growth 226 (2001) 83-87.
[13] K. Watanabe, G. Nishijima, S. Awaji, K. Takahashi, K. Koyama, N. Kobayashi, Proc. of 19th Int. Conf. on Magnet Technology (MT-19), Sep. 18-23 (2005) Genova, Italy.

Detection of Small Magnetic Anisotropy using Micro-gravity and Diamagnetic Anisotropy Deriving From a Single Chemical Bond in Inorganic Oxides

Chiaki Uyeda[1], Mikito Mamiya[2], Ryoichi Takashima[1],
Takaaki Abe[1], Hideaki Nagai[2] and Takeshi Okutani[2]
1 Institute of Earth and Space Science, Graduate School of Science, Osaka University
Machikaneyama 1-1, Toyonaka, Osaka, 560-0043, Japan
2 National Institute of Advanced Industrial Science and Technology (AIST)
Tsukuba Central 5, 1-1-1 Higashi, Tsukuba, Ibaraki, 305-8565, Japan
(uyeda@ess.sci.osaka-u.ac.jp)

Abstract

A new principle is introduced to detect magnetic anisotropy which is based on the observation of a field-induced rotational-oscillation of a stable-axis of a solid body floated in microgravity. Sensitivity was improved by excluding the fiber which suspended the sample in a magnetic field in conventional methods; the restoration force of the fiber was previously the standard to measure anisotropy. The measured values of diamagnetic anisotropy $(\Delta\chi)_{DIA}$ were explained consistently by assigning a constant $(\Delta\chi)_{DIA}$ tensor on individual bonds, namely on a T-O bond of a tetrahedral $[TO_4]$ unit, on a hydrogen bond and on a M-O bond of a octahedral $[MO_6]$ unit. Accordingly, most of the unmeasured oxides are expected to posses a finite amount of $(\Delta\chi)_{DIA}$. Many of the magnetic effects caused by $(\Delta\chi)_{DIA}$ are expected to occur at the level of 1Tesla according to the above analysis.

Keywords

Magnetic alignment, magnetic orientation, magnetic oscillation, diamagnetic anisotropy, torque method, microgravity

1. Introduction

Magnetic alignment has been reported on various sold materials containing no spontaneous magnetic moments[1,2]; the alignment is caused by the anisotropy of diamagnetic susceptibility $(\Delta\chi)_{DIA}$. Alignments of various materials such as DNA, blood cells, agarose, lysozime or ceramic crystals are usually observed in strong magnetic fields of the level of 5 to 10 Tesla. Various magnetic effects have been reported for diamagnetic materials at similar field intensity, which are considered to derive from diamagnetic anisotropy. The minimum field intensity to achieve the effects is not discussed intensively at present. The $(\Delta\chi)_{DIA}$ values are essential in investigating the effects quantitatively; however the values are too small to be detected by the conventional torque methods in many cases[3]. The effects are hence recognized only for limited number of materials at present.

The conventional methods to measure magnetic anisotropy were based on a principle first proposed by Krishnan Guha and Banergee[4]; Magnetic anisotropy-energy induced in the sample is measured by restoration force of the fiber suspending the sample in a horizontal field B. Hence the sensitivity of $\Delta\chi$ value is limited by the physical conditions of the fiber. The effect of the fiber was controlled to be negligible compared to the anisotropy energy by the present authors for the purpose of improving sensitivity. Direction of magnetically stable-axis showed rotational oscillation with respect to $\boldsymbol{B}$ in the improved method, and $\Delta\chi$ was obtained from the period of oscillation with high sensitivity[5].

The number of small $(\Delta\chi)_{DIA}$ values increased considerably for inorganic materials using this method The origin of diamagnetic anisotropy was analyzed successfully based on the accumulated data[6-10]. However, the sensitivity achieved in the above method is not high enough to accumulate the $(\Delta\chi)_{DIA}$ values for many other diamagnetic materials. Accumulation was essential to clarify the overall characteristics of diamagnetic anisotropy of solid materials in general. It was proposed that

the fiber itself should be deleted from the system in order to achieve higher sensitivity.

Results of preliminary observations to examine the above proposal are described in the present report[11]. The significance of detecting small $(\Delta\chi)_{DIA}$ in proceeding investigations on new magnetic effects caused by diamagnetic anisotropy is discussed in connection with the origin of anisotropy.

2. Experimental methods

Equation for a rotational motion of a solid body having a magnetic anisotropy $\Delta\chi$ [emu/g] suspended with a fiber in a horizontal field B is described as,

$$I(d^2\theta/dt^2) = -(1/2)B^2N\Delta\chi \sin 2\theta - (D/\ell)\theta. \quad (1)$$

Here θ is the angle between $\boldsymbol{B}$ and the direction of stable-axis of the body. I and N are the moment of inertia and the weight of the sample, respectively[4]. D and ℓ denote the tensional rigidity and the length of the fiber, respectively. A pair of magnetically stable and unstable axes rotated in the horizontal plane. Sensitivity of $\Delta\chi$ was limited by D and ℓ in the conventional method.

Direction of magnetically stable-axis showed rotational harmonic oscillation with respect to $\boldsymbol{B}$ in the improved method as mentioned above; the second term was controlled to be negligibly small compared to the first term in eq.(1). Accordingly, $\Delta\chi$ was obtained with high sensitivity from the gradient of the proportional relationship between τ and B^{-1} as $\Delta\chi = 4\pi^2 IN^{-1}(B\tau)^{-2}$; $\Delta\chi$ was determined without D and ℓ . A $\Delta\chi$ value as small as 10^{-12}emu/sample was detected in the field intensity of 5T using a sub-millimeter sized single crystal of α-quartz having the weigh of 8×10^{-4}g.[7]

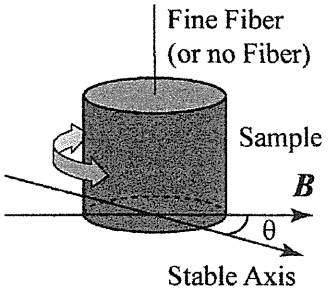

Fig.1 Principle to measure magnetic anisotropy using field-induced rotational-oscillation of a solid body.

The fiber itself was deleted from the method described above in order to realize further improvement of sensitivity[11]. An observation to examine this principle was performed at two different drop-shaft facilities; namely at the National Institute of Advanced Industrial Science and Technology AIST (Sapporo, Hokkaido, Japan) and at MGLAB. At AIST, the duration of microgravity was 1.3sec, and gravitational acceleration was 5.0×10^{-2}G, respectively. At MGLAB, these conditions were 4.5 sec and 5.0×10^{-5}G. A Helmholz-coil system was loaded on a drop capsule; the coil could produce homogeneous field up to 0.05T in a large spherical region of 0.20m in diameter. The large area was prepared because considerable amount of transferring was expected for the samples floated in microgravity conditions.

3. Results

Periods of oscillation τ' of the samples were measured from visual images taken by two CCD cameras. A typical example of a visual image of a graphite crystal floated in micro-gravity is shown in Fig.1. The measured τ' values were shorter than 0.75seconds. Theoretical τ' is calculated by deleting the second term of eq.(1) as

$$\tau = 2\pi(I/N\Delta\chi)^{-1/2}B^{-1}(1 + \theta_0^2/4 + \text{---}), \quad (2)$$

where θ_0 denote the angle of amplitude which was 45° in the present experiment. The $\Delta\chi$ value of graphite was obtained by inserting the measured values of τ, B, N, θ_0 and I in eq.(2). The obtained

value was consistent with the published value; accordingly, factors other than magnetic torque can be neglected as the cause of the oscillation. The principle of $\Delta\chi$ measurement in microgravity was verified in condition that the sample had $\Delta\chi$ values above the level of 10^{-5}emu/g.[7] Rotational-oscillation was observed for mm-sized single crystal of graphite floated in microgravity in a low magnetic field of 0.015T. Small magnetic torque of 0.004dyn cm was detected in the experiment.

The sensitivity can be improved by increasing the length of the measurable τ' values up to several seconds, this length is comparable to the duration of microgravity at ground based facilities. The enhancement of B is effective in improving sensitivity as well. This can be done by introducing a permanent magnetic circuit which produces homogeneous field above 1 Tesla in a small spatial region of about 1cm. The replacement can be done since the use of a mobile sample stage can stabilize a sample in a small region according to the results of the experiment described in Fig.2.[7]

The sensitivity measured in microgravity was improved recently to the level of 10^{-9}emu/g by increasing the field intensity to 1.3T[12]. The efficiency of the system was confirmed by measuring various popular materials with different published $(\Delta\chi)_{DIA}$ of the level of 10^{-8}emu/g to 10^{-9}emu/g.; measurement were performed on apophylite, calcite, gypsum, KDP, ,urea and Rochelle salt.

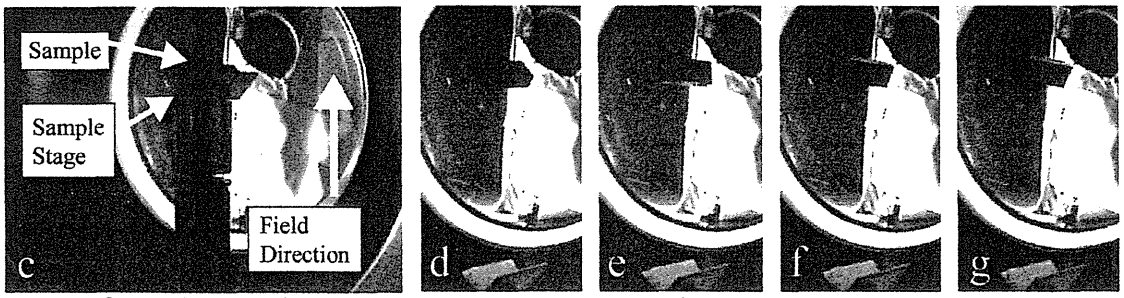

Fig.2. Visual images of field-induced rotational-oscillation of graphite crystal floated in microgravity
Image on the left end was taken just before micro-gravity was applied. Graphite crystal was initially placed on a sample stage with inclination of 45 degrees; c-planes of graphite (magnetically stable planes) were placed parallel to the inclined slope. The stage was removed from its initial position with high velocity immediately after achievement of micro-gravity, which was effective to minimize the amount of kinetic energy transferred from the stage to the sample. The c-plane showed rotational oscillation with respect to $\boldsymbol{B}$ in microgravity. Images were taken every 0.07sec, placed in the order of time from left to right.

4. Discussion

The development of system to measure $\Delta\chi$ with sensitivity has increased the number of published $(\Delta\chi)_{DIA}$ data considerably for popular inorganic materials as mentioned before[13,14]. The $(\Delta\chi)_{DIA}$ values of α-quartz, orthoclase, KDP, ADP, apophylite, hexagonal-ice, gypsum, MgO, $Mg(OH)_2$, $Al(OH)_3$ AlOOH and corundum were analyzed consistently by assigning a constant amount of $(\Delta\chi)_{DIA}$ on individual chemical bonds. Diamagnetic susceptibility of a no-metallic material is approximately equivalent to the summation of susceptibility assigned to the individual electron orbital consisting the material according to a Pascal's law [3]. The summation is described by a χ-tensor of a material, assuming that each orbital posses an constant uniaxial anisotropy $\Delta\chi_{BO} = \chi_{BO\parallel} - \chi_{BO\perp}$, $\chi_{BO\parallel}$ and $\chi_{BO\perp}$ denote the susceptibilities parallel and perpendicular to the bond direction, respectively. The direction of the bond is parallel to the principle axis. $\Delta\chi$ value of a bond is obtained from a field-induced energy ,which is expressed by a direction cosine of B and that of bond direction, which are defined as (a,b,c) and (α,β,γ), respectively .The x-, y- and z- coordinate of the vector components are identical to the three magnetic principle-axes of the crystal. The field-induced energy of a bond is described as $U(B)= -(1/2)B^2\{\chi_{BO\perp}+\Delta\chi_{BO}(a^2\alpha^2+ b^2\beta^2+c^2\gamma^2)\}$. The measured $(\Delta\chi)_{DIA}$ values of the crystal between x-y, y-z and z-x axes should be proportional to $\Sigma\alpha^2-\Sigma\beta^2$, $\Sigma\beta^2$

$\Sigma\gamma^2$ and $\Sigma\gamma^2$ -$\Sigma\alpha^2$, respectively; the proportionality was expected from the model. $\Sigma\alpha^2$,$\Sigma\beta^2$ and $\Sigma\gamma^2$ are calculated for all the bonds included in a unit cell of the material; the calculations can be performed for any crystal by using the published data of atomic positions. A $(\Delta\chi)_{DIA}$ value of a single bond has been assumed previously to analyze the diamagnetic anisotropy of organic molecules[1,3]. The positive correlations expected in the model were clearly seen for 3 types of bonds, namely for the T-O bonds composing the tetrahedral [TO_4] units, for the hydrogen bonds [9] and for the M-O bonds of the [MO_6] units. The $(\Delta\chi)_{DIA}$ values assigned to the bonds were[13,14],

T-O bond composing the tetrahedral [TO_4] units: 1.1×10^{-30}emu
M-O bond of the octahedral [MO_6] units: 0.32×10^{-30} emu
Hydrogen bond: 3.7×10^{-30} emu

these bonds are the major types of chemical bonds composing the inorganic oxides. Accordingly, $(\Delta\chi)_{DIA}$ values are expected to exceed 1×10^{-10}emu/g for many of the unmeasured oxides which are composed of the above mentioned bonds. Accordingly, these materials can cause magnetic alignment at low field intensities below several Tesla [14], according to the Langevin process mentioned before, which may not require a superconducting magnet. The possibility of producing new magnetic devises may increase considerably when the potential of choosing magnetically active materials are expanded to diamagnetic materials in general.

As mentioned above, the sensitivity to measure $\Delta\chi$ in terrestrial gravity is not high enough to detect the small$(\Delta\chi)_{DIA}$ values expected for the unmeasured materials. $\Delta\chi$ measurements in microgravity can be a breakthrough to improve the sensitivity[12]. Very small $\Delta\chi$ may be detected in an orbital laboratory where a long τ of range of 1 minute can be measured. Development of the measuring system is now carried out to achieve the expected sensitivity.

5. Conclusions

1. A new principle to detect magnetic anisotropy $\Delta\chi$ of a solid body with high sensitivity was established which was based on the observation of a period of rotational-oscillation of the stable-axis with respect to the field. Sensitivity is improved by excluding the restoration force of the fiber suspending the crystal in a horizontal field by floating the sample in microgravity; the restoration force had been the standard in the conventional methods. Number of $(\Delta\chi)_{DIA}$ data is expected to increase considerably by this method. Very small $\Delta\chi$ can be detected in an orbital laboratory where a long period of oscillation having the length of 1 minute can be measured.
2. Measured $(\Delta\chi)_{DIA}$ values of popular inorganic oxides were explained quantitatively by assuming a constant $(\Delta\chi)_{DIA}$ tensor on individual bonding orbital. The $(\Delta\chi)_{DIA}$ values determined for the bonds were 3.7×10^{-30} emu for a hydrogen bond, 1.1×10^{-30}emu for a T-O bond composing the tetrahedral [TO_4] units and 0.32×10^{-30} emu for a M-O bond of the octahedral [MO_6] units. These bonds are the major types of chemical bonds composing the inorganic oxides.. Hence, most of the unmeasured inorganic oxides are expected to possess a finite amount of $(\Delta\chi)_{DIA}$ to cause magnetic alignment as well as other magnetic effects due to magnetic anisotropy

Acknowledgements

This work was supported by Grant-in-Aid for Scientific Research (B) (No23958433) and Grant-in-Aid for Scientific Research for Priority Areas (No.15085204, Area 767) from MEXT of Japan.

References

[1]. G.Malet & K.Dransfeld: Topics in App. Phys., 57, 144 (1985).
[2]. for example, various paper appearing in, Proc.Intern.Symp. New Magneto-Sci (Jpn.Sci. Tec.Corp., NIMS 1999)
[3]. for example, R.Guputa, in, Diamagnetism"Landort Bornstein"(Springer-Verlag, Berlin), (1983)
[4]. K.S.Krishnann &S.Banerjee:Philos.Trans.R.Soc.London A231 (1933) 235.
[5]. C.Uyeda: Jpn.J.App.Phys., 32, (1993) L268.
[6]. C.Uyeda et al, Phys. Chem. Minerals, 20 (1993) 82.
[7]. C.Uyeda H.Chihara and K.Okita, Physica B,246- 247,171 (1998)
[8]. C.Uyeda, K.Ohtawa and K.Okita, Jpn. J. Appl. Phys., 39, (2000) L514.
[9]. C.Uyeda, K.Ohtawa, K.Okita and N.Uyeda, Jpn.J.App.Phys.39,(2000) L890
[10]. C.Uyeda, K.Ohtawa, K.Okita, *J.Phys.Soc.Jpn.*,69,1019 (2000).
[11]. C.Uyeda, K.Tanaka and R.Takashima, Jpn.J. Appl. Phys., 42, L1226(2003).
[12]. C.Uyeda, R.Takashima and T.Abe, Appl. Phys. Lett. submitted.
[13]. C.Uyeda and K.Tanaka, J. Phys. Soc. Jpn.,72 (2003) 2334.
[14]. C.Uyeda, K.Tanaka and R.Takashima, Appl.Phys.Lett 86 (2005) 094103.

Magnetic Force Enhancement Using an HTS Bulk Cylinder

Tsukasa Kiyoshi[1], Toshiyuki Koizumi[1], Xiaojun Liu[1], and Shinji Matsumoto[1]
1 Tsukuba Magnet Laboratory, National Institute for Materials Science,
3-13 Sakura, Tsukuba, Ibaraki 305-0003, Japan
(kiyoshi.tsukasa@nims.go.jp)

Abstract
In order to obtain a large magnetic force environment using a commercially available superconducting magnet, a high-temperature superconductor (HTS) bulk cylinder with a G-M cryocooler down to approximately 20 K was developed. The cryostat was inserted so that the bulk cylinder might be located at the mid-plane of a 12-T magnet. From 5 and 11.5 T, field-cooling experiments were performed. Experimental data of magnetic field profiles along the *Z*-axis exhibited good accordance with calculation results. As a force field of about -1000 T^2/m was obtained, the enhancement of the magnetic force with the HTS bulk cylinder was confirmed.

Keywords
field cooling, high-temperature superconductor, HTS bulk, magnetic force

1. Introduction

Magnetic levitation has the potential to open a new frontier of magnetic processing because it has some advantages, such as the no-wall effect or emulation of a microgravity environment. Several studies in this respect have already been performed.[1-3]

In the case of pure water, a magnetic force field defined by grad $B^2/2$ of about 1400 T^2/m is required for levitating against gravity. The value is two or three times larger than those obtained using conventional superconducting magnets. Several methods have been employed to increase the magnetic force fields.[4-6]

For magnetic force enhancement, the distortion of magnetic fields is very important. The high current densities of HTS bulks in high magnetic fields [7, 8] can be used for this purpose. Here, we report on magnetic force enhancement using an HTS bulk cylinder.

2. Experimental

In the experiment, the hollow cylinder of a Gd-based superconductor produced by Nippon Steel was used. Its inner diameter, outer diameter, and height were 25, 60, and 20 mm, respectively. The outer side was reinforced with a SUS316L.

The cryostat to install the HTS bulk cylinder was newly developed. Its schematic cross section is shown in Fig. 1. It was designed to be inserted in the 100-mm diameter room-temperature bore of a conventional superconducting magnet. The cylinder was placed so that it might be located at the mid-plane of the backup magnet. It was cooled with a G-M cryocooler (54 W at 40 K) through a thermal path made of copper. The cryostat had a room-temperature bore of 20 mm in diameter.

The cryostat was inserted in a 12-T cryocooler-cooled superconducting magnet with a room-temperature bore of 100 mm in diameter. Its minimum value of the magnetic force field along the *Z*-axis was calculated to be -564 T^2/m at 12 T. This magnet has a persistent current switch (PCS). During the excitations, the switch was turned off with a heater.

We measured the magnetic field profiles along the *Z*-axis by moving a Hall probe. The backup field was decreased with a sweep rate of 2.05×10^{-3} T/s. We held the backup field with an interval of a few T and measured the magnetic field profiles.

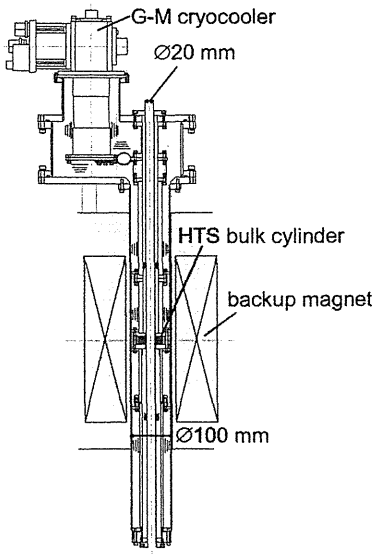

Fig. 1. Schematic cross-sectional view of the newly developed cryostat.

3. Results

The first experiment was performed at a backup field of 5.0 T. The cylinder was cooled down to 20.5 K. It took about 2.3 hours to cool it down below 30 K. After the cooling of the cylinder, the backup field was decreased to 0 T step by step. The measured magnetic field profiles are compiled in Fig. 2. As shown in Fig. 2, the bulk cylinder maintained the magnetic flux during the backup field decrease of 5 T, although a slight decrease was observed (1.7 % at the mid-plane).

In the next excitation, the backup field was increased up to 11.5 T, and the cylinder was cooled. After it was cooled down to 21.5 K, the backup field was decreased step by step. In this operation, at a field of 7.6 T, the cylinder was quenched. The power supply continued to decrease, and the current was held at 7.22 T. As discussed later, this value displayed in the power supply did not agree with the current in the backup magnet after the cylinder was quenched. However we use the value displayed in the power supply for the sake of convenience. During its decrease from 7.22 T to 4 T, the cylinder was quenched again at 5.1 T. The field (current) value indicated in the power supply was held at 5.17 T. After this quench, the magnet was decreased to 0 T with a magnetic field profile measurement at 3

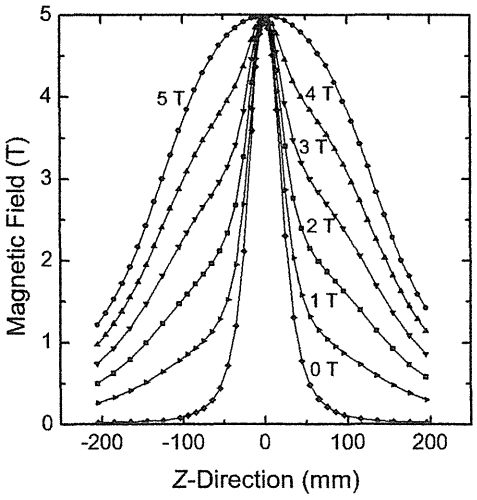

Fig. 2. Magnetic field profiles during the field cooling experiment from 5 to 0 T.

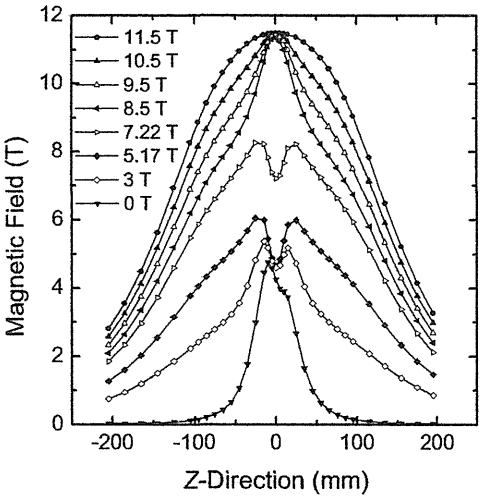

Fig. 3. Magnetic field profiles during the field cooling experiment from 11.5 to 0 T. The magnetic field values were those displayed in the power supply and do not agree with the actual backup fields after the first quench of the HTS bulk cylinder.

T. The magnetic field profiles in the series experiment are shown in Fig. 3.

4. Discussion

By assuming the HTS bulk cylinder as a conductor of low resistivity (10^{-20} Ωm), transient analyses were performed using FEM on software ANSYS. As shown in Fig. 4, good accordance was observed between the experimental results and calculations before the cylinder was quenched.

In the calculation, a minimum BdB/dz of -1029 T^2/m was estimated to be generated along the Z-axis by field cooling from 11.5 T to 8.5 T. As the minimum BdB/dz of the backup magnet is -564 T^2/m even at 12 T, the enhancement of the magnetic force with the HTS bulk cylinder was confirmed.

After the quench at 7.6 T, the magnetic field profiles changed remarkably. The HTS cylinder seemed to generate magnetic fields in the opposite direction. We concluded that the following events occurred in a short period.

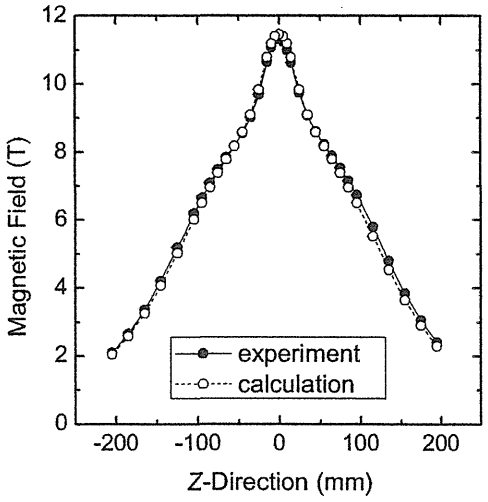

Fig. 4. Calculation results at 8.5 T in the field cooling experiment from 11.5 to 0 T.

(1) The HTS bulk cylinder was quenched and could not maintain the magnetic flux.
(2) The current of the backup magnet increased the compensation of the magnetic flux maintained in the HTS cylinder (the energy in the cylinder was partially transferred to the backup magnet).
(3) The HTS bulk cylinder returned to the superconducting state.
(4) As the backup magnet increased the magnetic field, the current in the HTS cylinder flowed in the reverse direction so as not to increase the magnetic flux inside cylinder.

Although further analyses are required, calculation results exhibiting good accordance to the experimental results were obtained by assuming that the current directions in the cylinder were different.

5. Conclusions

Magnetic force enhancement using an HTS bulk cylinder was experimentally confirmed. A force field that was about twice as large was obtained by using the 12-T superconducting magnet. The value may be improved by decreasing the backup field more slowly, by starting higher fields, or by improving the critical currents, mechanical strength, and thermal conductivity of an HTS bulk cylinder. In order to obtain a higher magnetic force field, the combination of HTS bulk cylinders and ferromagnetic materials is planned.

Acknowledgements

This work was partially supported by a Grant-in-Aid for Scientific Research for Priority Area (Area 767, No.15085204) from MEXT of Japan.

References

[1] D. C.Yin, N. I. Wakayama, K. Harata, M. Fujiwara, T. Kiyoshi, H. Wada, N. Niimura, S. Arai, W. D. Huang, and Y. Tanimoto, J. Crystal Growth 270 (2004) 184-191.
[2] N. Hirota, H. Uetake, T. Takayama, H. Nakamura, M. Kurashige, S. Hara, Y. Saito, Y. Ikezoe, T. Ando, H. Wada, and K. Kitazawa, *Materials Processing In Magnetic Fields*, H. Wada and H. J. Schneider-Muntau eds., pp. 269-277, World Scientific Publishing, Singapore (2005).
[3] I. Mogi, K. Takahashi, A. Awaji, K. Watanabe, and M. Motokawa, *Materials Processing In Magnetic Fields*, H. Wada and H. J. Schneider-Muntau eds., pp. 278-284, World Scientific Publishing, Singapore (2005).
[4] R. Hirose, K. Saito, Y. Watanabe, and Y. Tanimoto, IEEE Trans. Appl. Supercond. 14 (2004) 1693-1695.
[5] M. Kyoto, S. Hanai, H. Takano, K. Takahashi, G. Nishijima, S. Awaji, K. Watanabe, and M. Motokawa, IEEE Trans. Appl. Supercond. 14 (2004) 384-387.
[6] O. Ozaki, T. Kiyoshi, S. Matsumoto, J. Fujihira, and H. Wada, IEEE Trans. Appl. Supercond. 14 (2004) 1663-1665.
[7] M. Tomita and M. Murakami, Nature 421 (2003) 517-520.
[8] S. Matsumoto, T. Asano, T. Kiyoshi, and H. Wada, IEEE Trans. Appl. Supercond. 14 (2004) 1666-1669.

Magnetic Orientation and Its Temperature Dependence of Carbon Nanotubes

Masao Fujiwara and Yoshifumi Tanimoto
Graduate School of Science, Hiroshima University
Kagamiyama, Higashi-Hiroshima 739-8526, Japan
(fujiwara@sci.hiroshima-u.ac.jp)

Abstract

The suspension of carbon nanotubes has been placed in magnetic fields of 0.0–80.0 kOe. The SEM observation shows that the nanotubes are oriented with the tube axis parallel to the magnetic field. The magnetic field intensity dependence of the orientation is analyzed by the Boltzmann law, and the anisotropy of the susceptibilities parallel ($\chi_{\parallel}$) and perpendicular ($\chi_{\perp}$) to the tube axis is estimated to be $\chi_{\parallel} - \chi_{\perp} = 12.9 \times 10^{-6}$ cm^3 mol^{-1} ($\chi_{\perp} < \chi_{\parallel} < 0$) at 313 K.

Keywords

Magnetic Orientation, Carbon Nanotubes, Carbon Fibers

Introduction

The molecular aggregates with ordered structure are oriented in magnetic fields. The phenomenon is called magnetic orientation. The following points have been clarified up to now: (1) The magnetic orientation results from the susceptibility anisotropy of the molecular aggregates; (2) When the molecular aggregates have a large size (>1 μm), the magnetic orientation occurs against the thermal disordering; (3) The distribution of the orientation follows the Boltzmann law for variation of the magnetic field intensity at a fixed temperature.

Here, we study the temperature dependence of the magnetic orientation for carbon nanotubes and carbon fibers, discussing the relationship between the magnetic energy and thermal energy for these molecular aggregates.

Experiment

Carbon nanotubes (20 nm diameter, 1–2 μm length) and carbon fibers (6 μm diameter, 0.5 mm length) were suspended in dichloromethane solvent by ultrasonication. Liquid N_2 was also used as solvent. The suspension was placed in the horizontal bore of a superconducting magnet at a fixed temperature. After the medium was vaporized, the orientation was observed with a scanning electron microscope (for nanotubes) and an optical microscope (for fibers).

Result and Discussion

Carbon nanotubes and carbon fibers can be regarded as magnetically symmetric about their long axis Z. The susceptibility $\chi_{\parallel}$ parallel to the symmetric axis Z is larger than the susceptibility $\chi_{\perp}$ perpendicular to it ($\chi_{\perp} < \chi_{\parallel} < 0$). When these molecular aggregates are placed in a magnetic field H, the magnetic energy is expressed by

$$E(\theta, H) = -(nH^2/2)\,[\chi_{\perp} + (\chi_{\parallel} - \chi_{\perp})\cos^2\theta]$$

where θ is the angle between the symmetric axis Z and magnetic field H ($-\pi/2 \leq \theta < \pi/2$), and n is the mole number of carbon atoms contained in the molecular aggregates. If the symmetric axis Z is directed parallel to the magnetic field H ($\theta = 0$), the magnetic energy is minimum and the molecular aggregates are stabilized.

In the present experiment, the following approximation is made: The symmetric axis Z and magnetic field H both lie in the horizontal plane, i.e., the symmetric axis Z moves in the two-dimensional space. In this condition, the probability that the molecular aggregates are directed between the angles θ and $\theta + d\theta$ at thermal equilibrium is given by the Boltzmann law as

$$P(\theta, H)\, d\theta = \exp[-E(\theta, H)/kT]\, d\theta \,/\, \int_{-\pi/2}^{\pi/2} \exp[-E(\theta, H)/kT]\, d\theta$$

with T being the temperature and k being the Boltzmann constant.

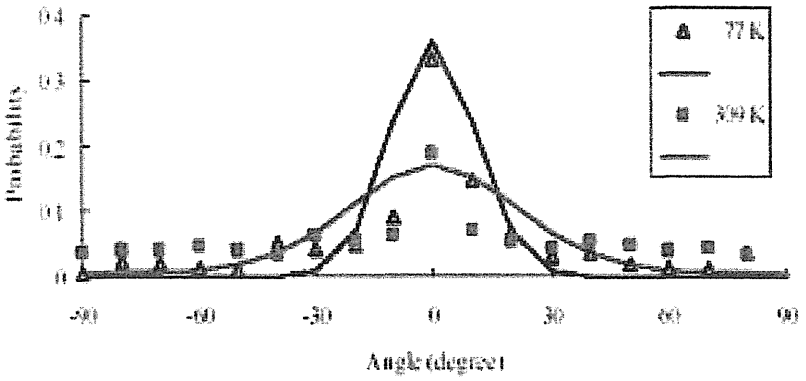

Fig. 1. The observed (points) and calculated (lines) distributions for the directions of carbon fibers in the 80.0 kOe horizontal magnetic field.

First, the results on carbon fibers are discussed (Fig. 1). At high temperature, the thermal energy is supplied into the rotational motion. The molecular aggregates are not directed in the stable direction parallel to the magnetic field ($\theta = 0$), and are rotated to any direction where the magnetic energy is not minimum (θ), i.e., they are not oriented, and are rotated to random direction by the thermal motion. At low temperature, the thermal energy is not sufficient in the rotational motion. The molecular aggregates are restricted to the stable direction ($\theta = 0$), and are not inclined to any direction (θ). In this way, the magnetic orientation of carbon fibers follows the Boltzmann law, and the susceptibility anisotropy is estimated to be $\chi_{\parallel} - \chi_{\perp} = 6.1 \times 10^{-12}$ cm^3 mol^{-1}, which is independent of the temperature.

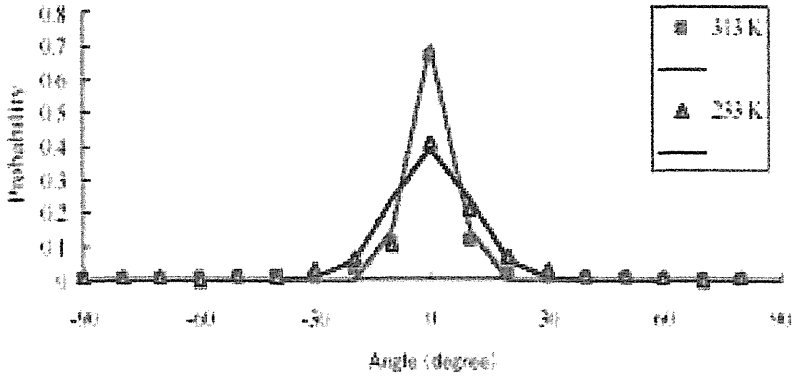

Fig. 2. The observed (points) and calculated (lines) distributions for the directions of carbon nanotubes in the 80.0 kOe horizontal magnetic field.

Next, the results on multi-walled carbon nanotubes are discussed (Fig. 2). As the temperature is raised, the probability that the carbon nanotubes are oriented to the parallel direction to the magnetic field increases. The higher orientation at higher temperature cannot be explained by the Boltzmann law. Instead, the susceptibility anisotropy must be considered to increase at higher temperature. Thus, the susceptibility anisotropy is estimated to be $\chi_{\parallel} - \chi_{\perp} = 12.9 \times 10^{-6}$ cm^3 mol^{-1} at 313 K, and its temperature dependence is calculated to be 0.2×10^{-6} cm^3 mol^{-1} K^{-1}. It is shown that, unlike general diamagnetics, the magnetic anisotropy of multi-walled carbon nanotubes depends on the temperature.

C_{60} crystals are reported to undergo a first-order phase transition at 259 K. Similarly, multi-walled carbon nanotubes might change into a structure in which the intershell overlap is stabilized below room temperature. Because carbon nanotubes involve tubules with different diameters and thicknesses, the transition temperature would be broad, not sharp.

Conclusion

Carbon nanotubes are oriented in magnetic fields. The magnetic properties of nanotubes can be investigated from the magnetic orientation. The orientation experiments have the advantage of observing the magnetic susceptibilities of a single nanotube that is free and isolated from the others in a suspension, whereas the SQUID experiments measure the magnetic properties of aggregated nanotube bundles. It is shown that the anisotropic susceptibilities of nanotubes depend on the temperature.

Acknowledgment

The work was partly supported by a Grant-in-Aid for Scientific Research on Priority Areas (Area 767, No. 15085208) from the Ministry of Education, Culture, Sports, Science, and Technology (MEXT) of Japan.

References

(1) M. Fujiwara, E. Oki, M. Hamada, Y. Tanimoto, I. Mukouda, Y. Shimomura, *J. Phys. Chem. A 105*, 4383-4386 (2001).
(2) M. Fujiwara, K. Kawakami, Y. Tanimoto, *Mol. Phys. 100*, 1085-1088 (2002).

Magnetic Orientation and Organization of Single-Walled Carbon Nanotubes or Their Composite Materials using Polymer Wrapping

Hiroaki Yonemura[1], Yuuichi Yomamoto[1], Sunao Yamada[1], Yoshihisa Fujiwara[2], and Yoshifumi Tanimoto[2]

1 Department of Applied Chemistry, Faculty of Engineering, Kyushu University, Hakozaki, Higashi-ku, Fukuoka 812-8581, Japan

2 Department of Mathematical and Life Science, Graduate School of Science, Hiroshima University, Higashi-Hiroshima 739-8526, Japan

(yonetcm@mbox.nc.kyushu-u.ac.jp)

Abstract

Magnetic orientation and organization of single-walled carbon nanotubes (SWNTs) or the polymer wrapping SWNTs using poly[2-methoxy-5-(2'-ethylhexyloxy) -1,4-phenylene vinylene] (MEHPPV) were examined. Shortened SWNTs were added to the DMF solution of MEHPPV, and then sonicated. The formation of SWNT/MEHPPV composites was confirmed by absorption and fluorescence spectra. The aqueous solution of the shortened SWNTs or the DMF solution of SWNT/MEHPPV composite was dropped on mica or glass plate. The magnetic field was applied by using two superconducting magnets (horizontal and vertical direction of magnetic field). In the horizontal direction (8 T), the AFM images indicated that the SWNT/MEHPPV composites or the SWNTs were oriented randomly in the absence of magnetic field, while they placed in the magnetic field (8 T) were oriented with the axis of the composites parallel to the magnetic field. The results of polarized absorption spectra supported the magnetic orientation of the SWNT/MEHPPV composites or the SWNTs. In the vertical direction, the AFM images indicated that the interesting nanostructures, that there are the networks of organization of bundles consisting a certain amount of nanofibers with several nanometer in width, were observed at the top position. At the top position, the magnetic orientation occurred and the magnetic force acted on the materials as counterbalance with the gravitation. In the addition of these interactions, the nanostructures are probably interpreted by the contribution of the interaction of induced magnetic moment of SWNTs due to the strong magnetic fields to the formation of the nanostructures.

Keywords

magnetic orientation, single-walled carbon nanotube (SWNT), magnetic organization, composite material, polymer wrapping

1. Introduction

Since the discovery of single-walled carbon nanotubes (SWNTs), they have been expected to become building blocks of next generation functional nano-materials. However, their strong cohesive property and poor solubility have been restricting SWNTs for fundamental and applied research fields. One of the methods to overcome these problems is that one should make soluble the SWNTs in solvents by wrapping them with polymers.[1] At the same time, the fabrication of high-performance carbon nanotube-based composites is driven by the ability to create anisotropy at the molecular level to obtain appropriate functions. Several groups have reported magnetic orientation of carbon nanotubes by using strong magnetic fields.[2,3] In this study, we have examined magnetic orientation and organization of the SWNTs or the polymer-wrapped SWNTs using poly[2-methoxy-5-(2'- ethylhexyloxy)-1,4-phenylene vinylene] (MEHPPV) by measurements of AFM images and polarized absorption spectra.

2. Experimental methods

2.1 Magnet apparatus (horizontal direction of magnetic field) [2]

A superconducting magnet (Oxford Instrument, Spectromag-1000) was used in the experiments of horizontal direction of magnetic field as reported in the previous papers.[2] In the superconducting magnet a bore tube (50 mm ϕ) was installed horizontally. Distribution of the magnetic field was approximated with a Gaussian distribution. The maximum strength of the magnetic field is 8.0 T at center position.[2]

2.2 Magnet apparatus (vertical direction of magnetic field) [4]

A superconducting magnet (Japan Superconductor Technology, JMTD-LH15T40) was used in the present study as reported in the previous papers.[4] It has a room temperature bore tube with of 40 mm. The distribution of the magnetic field is reported in the previous papers [4]. The maximum field (B_{max}(vertical)) and field (B) ×gradient field (dB/dz) were 15 T and 1500 T^2/m, respectively, where z is the distance from the center of the bore tube along the tube. Three samples were placed at the positions in the bore tube, of which B and BdB/dz were 5.6 T and -940 T^2/m for the top position, 15 T and 0 T^2/m for the middle position, and 9.8 T and +1070 T^2/m for the bottom position, and one was placed outside of the tube as a control.

2.3 Preparation of sample

Single-Walled Carbon Nanotubes (SWNTs) (Carbon Nanotechnologies Incorporated) were shortened by ultrasonication with a probe-type sonicator (Branson model 250) in the mixed acids (H_2SO_4 and HNO_3) for 10 min under ice-cooling. After diluting mixture with water (MiliQ), the shortened SWNTs were filtered though PTEE membrane filter (pore size: 1 μm). The shortened SWNTs were added to the DMF solution (1.4 μM) of MEHPPV (Aldrich). Then, the suspension was sonicated with a bath-type sonicator (Branson model 1510). Centrifugation (6000 rpm) of the suspension for 15 min gave the DMF solution of the SWNT/MEHPPV composite.

2.4 Measurements of applying magnetic fields.

The DMF solution of the SWNT/MEHPPV composite was dropped on freshly cleaved mica or a glass plate. The aqueous solution of the shortened SWNTs was also dropped on the mica or the glass plate.

The magnetic field (vertical direction (three positions: top, middle, and bottom) and horizontal direction (center position)) was applied during the evaporation of solvents by using the above two superconducting magnets. Samples were placed in the absence of magnetic field (outside of the bore tube) and used as the control.

2.5 Measurements of AFM images and polarized absorption spectra

After drying at 283 K (horizontal direction) or ambient temperature (vertical direction), the AFM images of the SWNTs or the SWNT/MEHPPV composites on mica were recorded in contact mode using a Nanoscope IIIa (Digital Instrument).

Steady-state and polarized absorption spectra were recorded on a UV-VIS-NIR scanning spectrometer (Shimadzu UV-3150) using a polarizer (Assy III; 260-2500 nm) and a sample immobilization set of glass plates.

3. Results and discussion

3.1 Absorption and fluorescence spectra of SWNT/MEHPPV composites

Absorption spectra of MEHPPV and MEHPPV in the addition of SWNT (ca. 0.1 mg) in DMF were measured to examine the formation of SWNT/MEHPPV composite (Fig. 1(A)). In the addition of SWNT, after the procedure in the experimental methods, the absorption spectrum (Fig. 1(A)(a)) of SWNT-MEHPPV system is different from that (Fig. 1(A)(b)) of MEHPPV because of the solvation of SWNTs. The characteristic absorption bands in NIR region (Fig. 1(B)) due to the interband transition between the mirror image spikes in the density of states of SWNTs [5], in other words, due to the semiconducting SWNT. Therefore, Fig. 1 strongly shows that MEHPPV made soluble the SWNTs in DMF by wrapping them with polymers, and the formation of SWNT/MEHPPV

composite occurred.

Fluorescence spectra of MEHPPV and MEHPPV in the addition of SWNT in DMF were also measured to examine the formation of SWNT/MEHPPV composite (Fig. 2). The fluorescence peak due to MEHPPV was observed at 550 nm in DMF solution of MEHPPV. In the addition of SWNT, the fluorescence intensity decreased drastically as comparison with that of only MEHPPV. Three peaks were observed and are different from that of MEHPPV. These results indicate that there are strong interactions between MEHPPV and SWNT. Thus, the results of fluorescence spectra supported the formation of SWNT/MEHPPV composite as suggested in the absorption spectra.

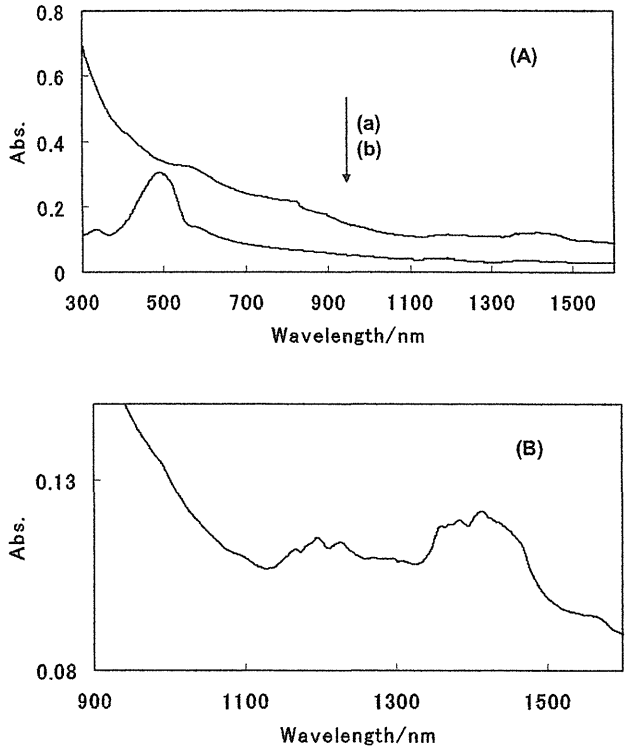

Fig. 1. Absorption spectra of (A) (a) MEHPPV (1.4 μM) in the addition of SWNT and (b) MEHPPV (1.4 μM) and (B) absorption spectrum of (a) in NIR region (900-1600 nm) in DMF.

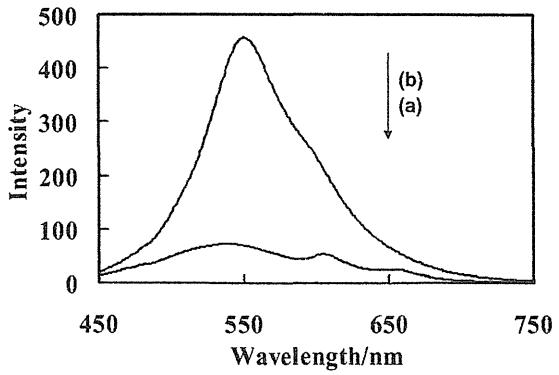

Fig. 2. Fluorescence spectra of (a) MEHPPV(1.4 μM) in the addition of SWNT and (b) MEHPPV (1.4 μM) in DMF.

3.2 AFM images using the horizontal direction of magnetic field

3.2.1 AFM images of SWNT/MEHPPV composites

In the case of horizontal direction of magnetic field, after drying at 283 K under the magnetic field at 8 or 0 T (control), the AFM images of the SWNT/MEHPPV composites on the mica were measured (Fig. 3). The heights of the top of SWNT/MEHPPV composites the along line were 6-15 nm (Fig. 4). The results indicate that SWNT/MEHPPV composites consist of bundles of 4-21 SWNTs, since the diameter of the SWNTs is 0.7-1.5 nm.

The AFM images strongly indicate that the SWNT/MEHPPV composites are oriented randomly at 0 T (Fig. 3(a)), while oriented with the tube axis of the composites parallel to the direction of magnetic field at 8 T (Fig. 3(b)).

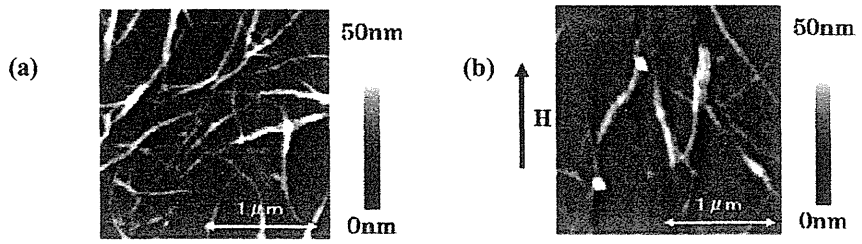

Fig. 3. AFM images of SWNT/MEHPPV composites on mica placed at (a) 0 and (b) 8 T using magnet apparatus (horizontal direction of magnetic field).

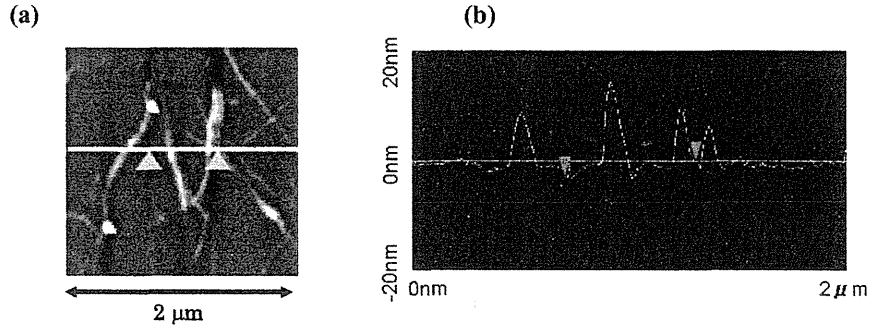

Fig. 4. (a) AFM images of SWNT/MEHPPV composites on mica placed at 8 T and (b) cross-section profile indicated line in (a).

3.2.1 AFM images of SWNTs

In the case of horizontal direction of magnetic field, after drying at 283 K under the magnetic field of 8 or 0 T (control), the AFM images of the SWNTs on the mica were measured (Fig. 5). The AFM images strongly indicate that the SWNTs are oriented randomly at 0 T (Fig. 5(a)), while oriented with the tube axis of the composites parallel to the direction of magnetic field at 8 T (Fig. 5(b)).

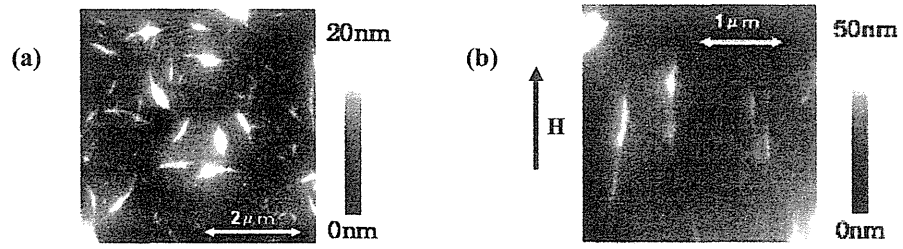

Fig. 5. AFM images of SWNTs on mica placed at (a) 0 and (b) 8 T using magnet apparatus (horizontal direction of magnetic field).

On the basis of the AFM images (Figs 3 and 5), the magnetic orientation of SWNT/MEHPPV

composites is most likely ascribed to the anisotropy in susceptibilities of SWNTs.

3.3 AFM images using the vertical direction of magnetic field

In the case of vertical direction of magnetic field, after drying at ambient temperature under the magnetic field at three positions (top, middle, and bottom positions) and in the absence of magnetic field (outside of the bore tube) as the control, the AFM images of the SWNTs on the mica were measured (Fig. 6). The AFM image (Fig. 6(e)) outside of the bore tube (at 0 T) is similar to that in Fig.4(a).

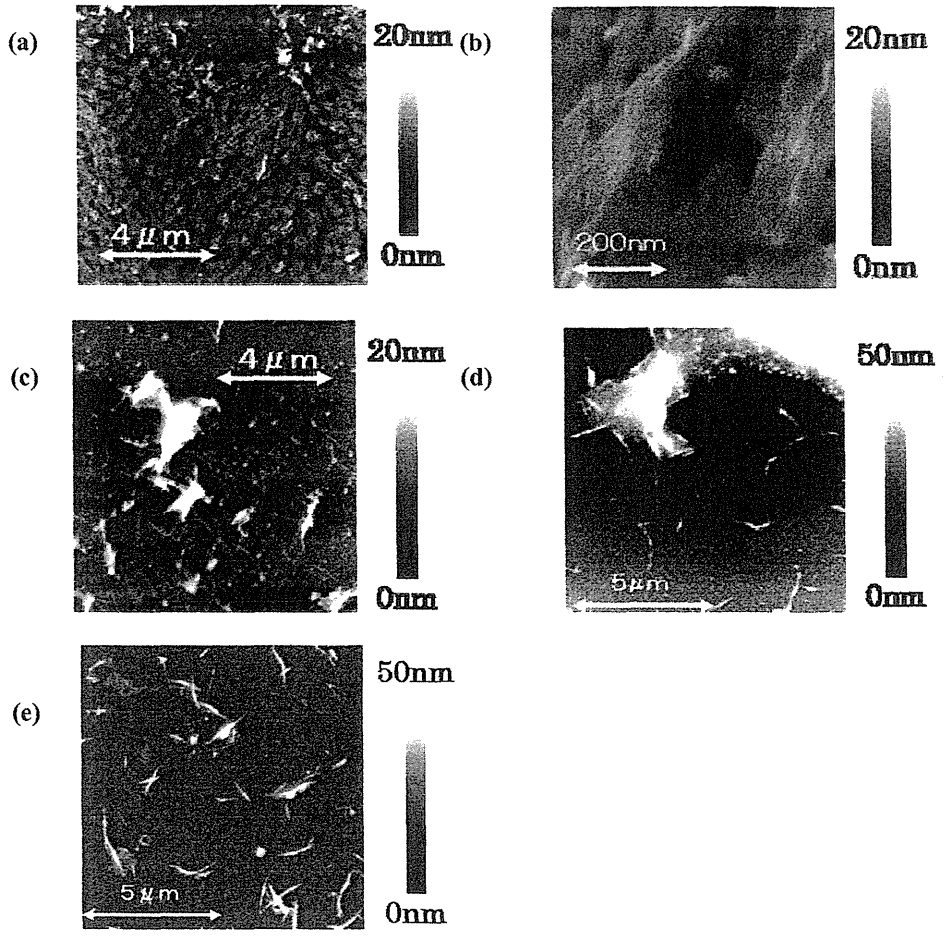

Fig. 6. AFM images of SWNTs on mica placed at the top ((a) and (b)), the middle (c), and the bottom (d) positions using magnet apparatus (vertical direction of magnetic field) and outside position (e) of the bore tube (0 T).

Network of organization of bundles consisting of a certain amount of nanofibers with several nanometers in width was observed at the top position as shown in Figs. 6(a) and 6(b). Interesting nanostrutures was not observed in other positions (middle and bottom positions, and outside of the bore tube). The heights of the top of nanofibers the along line were 2-3 nm (Fig.7). The results indicate that the nanofibers consist of individual SWNT or bundles of some SWNTs, since the diameter of the SWNTs is 0.7-1.5 nm.

On the basis of these observations, the interesting formation of nanostrutures consisting of SWNTs was probably achieved by magnetic force, magnetic orientation, interaction of induced magnetic

moment of SWNTs due to strong magnetic fields, and self-assembly and organization of SWNTs due to hydrophobic interaction in aqueous solution and so on.

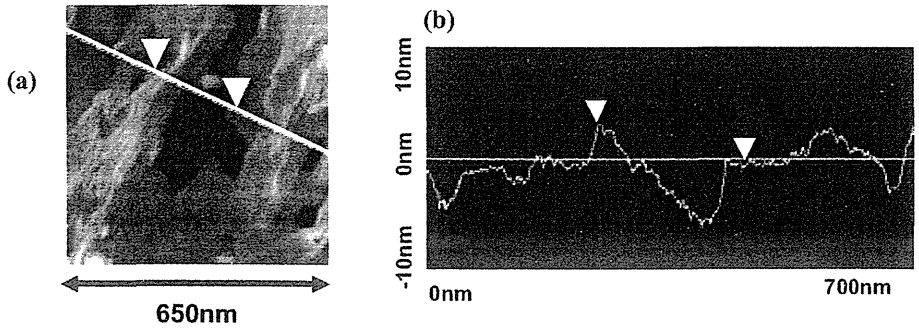

Fig. 7. (a) AFM images of SWNTs on mica placed at the top position and (b) cross-section profiles indicated line in (a).

3.4 Polarized absorption spectra

3.4.1 Polarized absorption spectra of SWNT/MEHPPV composites on glass plates

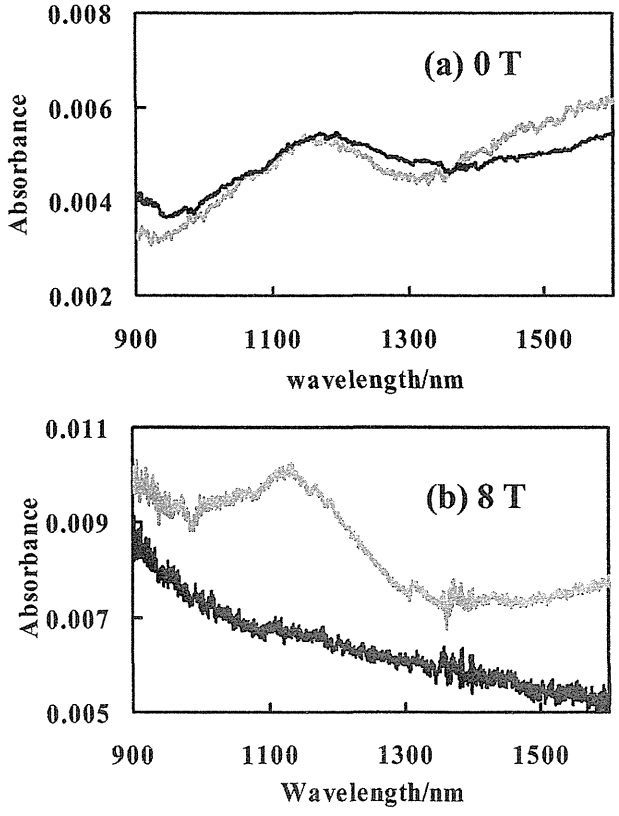

Fig. 7. Polarized absorption spectra of SWNT/MEHPPV composites on glass plates at (a) 0 and (b) 8 T. In the case of 0 T, The polarization direction of the light against the longitudinal direction of glass plates is horizontal (0°;) or vertical (90°;). In the case of 8 T, the polarization direction of the light against the direction of magnetic field is horizontal H(//)(0°;) or vertical H(⊥) (90°;) .

Polarized absorption spectra of SWNT/MEHPPV composites on glass plates were measured in NIR region (900-1600 nm) by an UV-VIS-NIR spectrometer. In the absence of magnetic field (0 T), the absorption bands (at 1150 nm and 1300~1600 nm) due to semiconducting SWNT were observed in both polarization directions (horizontal and vertical) (Fig. 7(a)). The absorption bands on the glass plate are similar to that in DMF solution (Fig. 1(B)). On the other hand, in the presence of magnetic field (8 T), the absorption band was observed in the horizontal polarization direction against the direction of magnetic field (H(//); 0°), while not in the vertical polarization direction (H(⊥); 90°) (Fig. 7(b)).

The results of polarized absorption spectra supported the magnetic orientation of SWNT/ MEHPPV composites which the SWNT/MEHPPV composites were oriented with the tube axis of the composites parallel to the direction of magnetic field at 8 T as suggested from the results of the AFM images (Fig. 3).

3.4.2 Polarized absorption spectra of SWNTs on glass plates

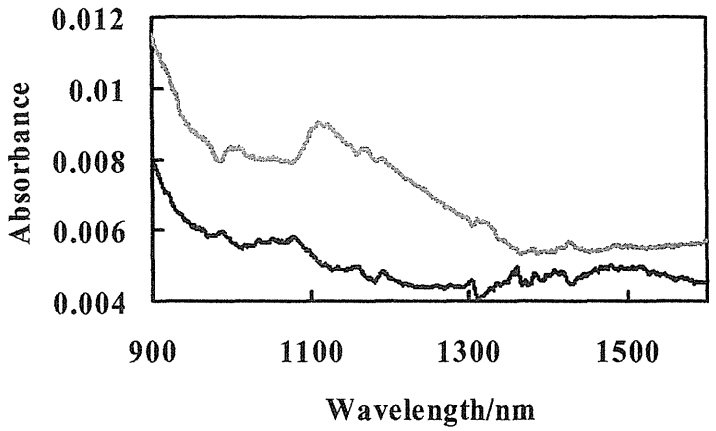

Fig. 8. Polarized absorption spectra of SWNTs on glass plates at 8 T. The polarization direction of the light against the direction of magnetic field is horizontal H(//)(0°; ═) or vertical H(⊥) (90°; ═).

Polarized absorption spectra of SWNTs on glass plates were measured in NIR region (900-1600 nm) by an UV-VIS-NIR spectrometer. In the absence of magnetic field, the absorption bands (at 1150 nm and 1300~1600 nm) due to semiconducting SWNT were observed in both polarization directions (horizontal and vertical) (not shown). In contrast, in the presence magnetic field (8 T), the absorption band was observed in the horizontal polarization direction against the direction of magnetic field (H(//); 0°), while not in the vertical polarization direction (H(⊥); 90°) (Fig. 7(b)).

The results of polarized absorption spectra supported the magnetic orientation of SWNTs, which the SWNTs were oriented with the tube axis of the composites parallel to the direction of magnetic field (8 T), achieved as suggested from the results of the AFM images (Fig. 3).

On the basis of the polarized absorption spectra (Figs 6 and 7), the magnetic orientation of SWNT/MEHPPV composites is most likely ascribed to the anisotropy in susceptibilities of SWNTs, similar to the comparison of AFM images (Figs 3 and 5) as described above.

5. Conclusions

On the basis of observations of the AFM images and the polarized absorption spectra of SWNT/MEHPPV composites or SWNTs on substrates (mica or glass plate), the magnetic orientation of SWNTs/MEHPPV composites or SWNTs on substrates (mica or glass plate) could be achieved by use of strong magnetic field (8T; horizontal direction). The SWNT/MEHPPV composites or the SWNTs were oriented with the tube axis of the composites parallel to the direction of magnetic field.

From the comparison between SWNT/MEHPPV composites and SWNTs, the magnetic orientation of SWNT/MEHPPV composites is most likely ascribed to the anisotropy in susceptibilities of SWNTs.

From of the AFM images of SWNTs on mica, network of organization of bundles consisting of a certain amount of nanofibers with several nanometers in width was observed at the top position (B and BdB/dz were 5.6 T and -940 T^2/m, respectively; vertical direction). Further investigations on the mechanism of the formation of nanostrutures at the top position at vertical magnetic field and quantitative analysis of the magnetic orientation of the SWNT/MEHPPV composites or the SWNTs at horizontal magnetic field (8 T) are now in progress.

Acknowledgements

The present study was financially supported by the grants of the Inamori Foundation and the society for the support of Kyushu University, and by the Grant-in-Aids for Scientific Research: Priority Area of "Innovative Utilization of Strong Magnetic Fields" (Area 767, No. 15085203) and "Molecular Nano Dynamics" (Area 432, No. 17034051), Scientific Research (C) (No. 17550131), and 21st Century COE Program "Function Innovation of Molecular Informatics" from MEXT of the Japan.

References

[1] D. A. Walters, M. J. Casavant, X. C. Qin, C. B. Huffman, P. J. Boul, L. M. Ericson, E. H. Haroz, M. J. O'Connell, K. Smith, D. T. Colbert, R. E. Smalley, Chem. Phys. Lett. 338, 14-20 (2001).

[2] M. Fujiwara, E. Oki, M. Hamada, Y. Tanimoto, I. Mukouda, Y. Shimomura, J. Phys. Chem. A, 105, 4383-4386 (2001).

[3] J. E. Fischer, W. Zhou, J. Vavro, M. C. Llaguno, C. Guthy, R. Haggenmueller, M. J. Casavant, D. E. Walters, R. E. Smalley, J. Appl. Phys., 93, 2157- 2164 (2003).

[4] A. Katsuki, I. Uechi, Y. Tanimoto, Bull. Chem. Soc. Jpn., 77, 275-279 (2004).

[5] H. Kataura, Y. Kumazawa, Y. Maniwa, I. Umezu, S. Suzuki, Y. Ohtsuka, Y. Achiba, Synth. Met., 103, 2555-2558 (1999).

3D-Morphological Chirality Induction in Membrane Tubes Prepared by Silicate Garden Reaction in Magnetic Field

Yoshifumi Tanimoto,[1] Ichiro Uechi,[1] Wenyong Duan,[1] and Akio Katsuki[2]
[1]*Graduate School of Science, Hiroshima University, Higashi-Hiroshima 739-8526, Japan*
[2]*Faculty of Education, Shinshu University, Nagano 380-8544, Japan*
(tanimoto@sci.hiroshima-u.ac.jp)

Abstract

We studied the effects of magnetic field (≤15 T) on the membrane tube morphology prepared by a silicate garden reaction. At zero field, membrane tubes prepared by the reaction of sodium silicate aqueous solution and zinc sulfate, magnesium chloride, and copper sulfate crystals grow straight upward. In the presence of *vertical* magnetic fields (5-15 T), they grow helically with the right-handedness along the inner surface of a vessel. The tubes grow helically with the lift-handedness along the outer surface of the rod, when they grow near a glass rod placed in the vessel. In the presence of a *horizontal* magnetic field of 8 T, tubes grow circularly along the inner surface of the vessel. All the observation is interpreted in terms of a boundary-assisted MHD mechanism.

Keywords

magnetic field effect, Lorentz force, handedness, chirality, silicate garden reaction

1. Introduction

It is known that magnetic field is a very interesting tool to control various chemical and physical processes. Especially, high magnetic field of 10 T or so could affect even the processes associated with non-magnetic (diamagnetic) materials. Silicate garden reaction is a well-known reaction in which sodium silicate aqueous solution and solid metal salt form water-insoluble semi-permeable membrane tubes. We have studied effects of magnetic field on 3D-morphology of the membrane tubes prepared by the reactions using a *vertical* and *horizontal* magnetic fields.[1-3]

2. Experimental methods

Vertical and horizontal magnetic fields were applied using a superconducting magnet (JASTEC, JMTD-LH15T40, 15 T) and a superconducting magnet (Oxford, Spectromag-1000, 8 T), respectively.

Sodium silicate (WAKO), magnesium chloride (WAKO), zinc sulfate (WAKO), and copper sulfate (WAKO) were used as supplied. Distilled and deionized water was used.

Circular glass vessels (typically, 8 mm diameter × 30 mm length) containing sodium silicate aqueous solution and a small amount of metal salt were placed in the bore tube of the magnet and outside of the magnet (leak field, ca. 2 mT). After the reaction proceeded for 30–60 min in the bore tube, the vessels were removed from the bore tube and the membrane tubes' respective morphologies were recorded using a conventional digital camera. Hereafter, metal ion's name is used as membrane tube's name. All experiments were carried out at room temperature.

In situ observation of the motion of the solution during the reaction in a magnetic field was also carried out with a CCD camera and a digital video recorder. Plastic micro-particles (polyethylene, ca. 180 μm; Aldrich) were added to the solution as tracer.

3. Results

3.1 Tubes formed in *vertical* magnetic field

Figure 1 shows Zn(II) membrane tubes grown in *vertical* magnetic fields. Tubes grow straight upward at zero field. In the presence of magnetic fields, they grow helically in the right-handed direction. Even varying the vessel diameter from 3 to 20 mm, the tubes grow helically in the vertical magnetic field.

Analogous magnetic field effects are observed for the tubes when magnesium chloride and copper sulfate crystals are used. In the case of the Cu(II) tube formation, elongated helical tubes are formed when they grow in a magnetic field of +1200 T^2/m (11 T). No tube is formed when it grows to in a magnetic field of -379 T^2/m (15 T). These facts indicate a magnetic force is not a cause of helical growth of the membrane tube.

When a glass rod is placed in a reaction vessel, Zn(II) and Mg(II) tubes grow helically on the outer surface of the rod in the left-handed direction.

Furthermore, the tubes apart from the vessel's wall, grow in twisted shape in the left-handed direction as shown in Fig. 2.

In situ observation of the solution during the reaction is carried out in magnetic field. At zero field no convection of the solution is observed. In the presence of a magnetic field, rapid convection of the solution is observed, indicating that a magnetic field induces the solution convection during the ionic reaction.

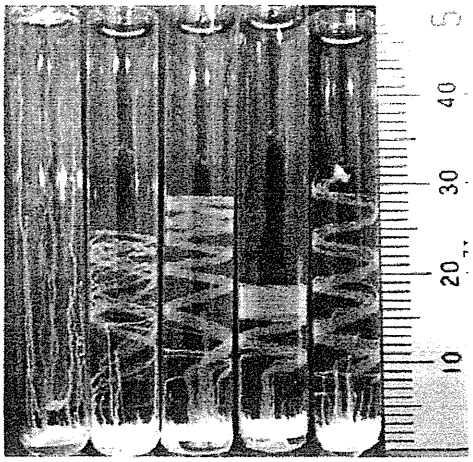

Fig. 1 Zn(II) membrane tubes grown in magnetic fields.

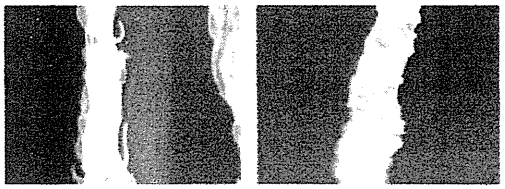

Fig. 2 Zn(II) membrane tubes apart form a vessel wall. (a) 0 T (b) 15 T.

3.2 Tubes formed in *horizontal* magnetic field

Figure 3 shows Zn(II) tubes prepared in a *horizontal* magnetic field of 8 T. The tubes do not grow helically but grow circularly along the inner surface of the vessel. The tubes grow upward up to the ceiling of the vessel and then grow downward along the surface in the magnetic field.

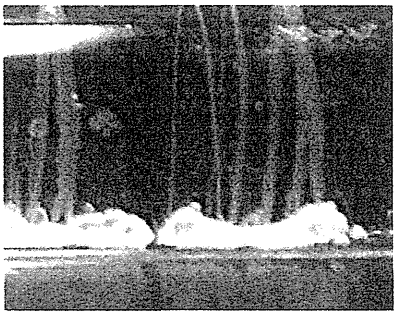

Fig. 3 Zn(II) membrane tubes grown in a horizontal field of 8 T.

4. Discussion

Mechanism of membrane tube growth is complicated. Aqueous solution dissolves metal salt and water-insoluble and semi-permeable membrane deposits on the surface of the salt. The water penetrates into the interface between the membrane and the salt surface. Because of osmotic pressure, the membrane is disrupted and the metal ion-rich solution flows out from the disrupted exit. The outflow then reacts with the solution surrounding it to form a membrane tube. Therefore, it is reasonable to consider that the magnetic field affects transportation of ions to the reaction zone. Furthermore, as presented in Section **3**, magnetic field induces membrane tube growth in the plane perpendicular to the magnetic field axis. This type of effects can be explained solely by the Lorentz force, though there are several mechanisms of magnetic field effects. An ion, whose electric charge is q, receives the Lorentz force, $\boldsymbol{F}_L$, when it moves with the velocity of $\boldsymbol{v}$ in a magnetic field, $\boldsymbol{H}$,

$$F_L = q\, v \times H \qquad (1)$$

The force induces convection of the solution containing ions.

Figure 4 shows the mechanism of helical growth of membrane tubes in a magnetic field. The outflow from the tube exit, which is rich with negative ions, spread out not only upward but also in the plane perpendicular to the magnetic field axis. Negative ions in the outflow moving in the plane perpendicular to the field axis receive the Lorentz force. This force results in the convection of the solution near the tube exit, since the force on the ions are transferred to the bulk solution due to collision. Because of this convection, the tube apart from the vessel wall grows in twisted shape.

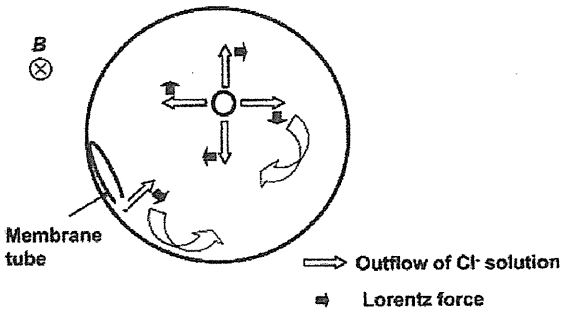

Fig. 4 Mechanism of 3D-morphological chirality induction (top view).

In the case of the tube growing near the vessel surface, the motion of ions becomes asymmetric because of the bound of the ions on the surface. This asymmetric motion of ions results in the asymmetric convection of the solution near the tube exit. Therefore, the role of a vessel wall or a glass rod surface takes an important role in determining the direction of the solution.

Acknowledgements

This work was supported partly by Grants-in-Aid for Scientific Research (Nos. 15350016, 15085208) from the Ministry of Education, Culture, Sports, Science, and Technology of Japan.

References

[1] I. Uechi, A. Katsuki, L. Dunin-Barkovskiy, and Y. Tanimoto, *J. Phys. Chem. B*, **108**, 2527 (2004).
[2] W. Duan, S. Kitamura, I. Uechi, A. Katsuki, and Y. Tanimoto, *J. Phys. Chem. B*, **109**, 13445 (2005).
[3] Y. Tanimoto, in "Magneto-Science", M. Yamaguchi and Y. Tanimoto (eds.), Kodansha, Tokyo, in press.

Chiral Recognition of Ascorbic Acid by Magnetoelectropolymerized Polyaniline Electrodes

Iwao Mogi and Kazuo Watanabe
Institute for Materials Research, Tohoku University, Katahira, Sendai 980-8577, Japan
(mogi@imr.tohoku.ac.jp)

Abstract

Polyaniline film electrodes were prepared by a magnetoelectropolymerization (MEP; electropolymerization under magnetic fields) method, and their chiral electrode properties were examined for L- and D-ascorbic acids by cyclic voltammetry. The MEP film electrodes showed different oxidation currents between enantiomers, and those prepared under reverse magnetic fields showed opposite chirality. These results indicate that the MEP method introduces chirality to the polyaniline films through the Lorentz force and such film electrodes possess the ability of chiral recognition for ascorbic acid.

Keywords

chirality, enantioselective recognition, magnetic field, electropolymerization, polyaniline

1. Introduction

Enantioselective recognition of chiral molecules is one of the most important goals in biochemistry. Chiral surfaces of heterogeneous catalysts have the enantioselective properties, and thus considerable effort has been devoted in preparing chiral surfaces by adsorbing chiral molecules [1,2] or slicing single crystals.[3] Chirality was also introduced into conducting polymers by doping chiral molecules,[4-6] and chiral polyaniline films exhibited enantioselective recognition for several amino acids.[5]

Magnetic fields induce chiral structures through the Lorentz force acting on currents in solutions. Two-dimensional spiral structures were found in the electrodeposition of metals [7,8] and conducting polymers,[9] and three-dimensional helical structures in silicate membrane growth,[10] though both structures were on the millimeter scale. If chiral structures on the molecular scale were induced on the surface of the films formed under magnetic fields, such film surfaces would serve as enantioselective catalysts.

We attempted to prepare conducting polymer films with a chiral surface by magnetoelectropolymerization (MEP), which is electropolymerization under magnetic fields.[11] Polyaniline is one of the most promising materials for electronic devices, and its films are easily prepared by the oxidative electropolymerization of aniline in acidic aqueous solutions. Aniline monomers are stoichiometrically oxidized in front of the polymer chain, and then electrons are transported from the front to the substrate electrode within the chain. Under magnetic fields, the Lorentz force is expected to act on currents within the polymer chain and induce helical growth. Otherwise, if the racemic helical chains were formed spontaneously, the Lorentz force would induce a one-handed structure. Thus, it is interesting to examine whether the MEP films exhibit chiral electrode properties. Here, we show the voltammetric responses of the MEP polyaniline films to L-ascorbic acid and its

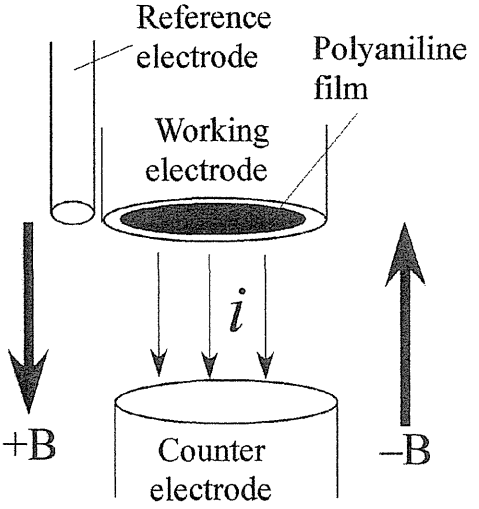

Fig.1 Electrode configuration in the magnetoelectropolymerization process. Magnetic fields ***B*** are applied parallel (+) or antiparallel (–) to faradaic currents, and they are perpendicular to the electrode surface.

enantiomer, erythorbic acid (D-ascorbic acid).

2. Experimental methods

For electrochemical experiments, a conventional system with the following three electrodes was employed: a platinum disc working electrode with a diameter of 3 mm, a platinum plate counter electrode, and a Ag/AgCl/sat.NaCl) reference electrode. Polyaniline films were prepared on the working electrode by potentiostatic electropolymerization at 0.9 V by a passing charge of 0.1 C cm^{-2} in a 0.5 M (mol dm^{-3}) sulfuric acid aqueous solution containing 50 mM aniline. The obtained films are the oxidized form of SO_4^{2-}-doped polyaniline. The MEP experiments were conducted at 25°C under a magnetic field of 5 T in a cryocooled superconducting magnet (Sumitomo Heavy Industries Ltd.), the schematic illustration is shown in Fig. 1. The applied magnetic fields were parallel or antiparallel to faradaic currents, and the MEP films prepared under these fields are called the +5T-film or the −5T-film, respectively. The MEP films were used as modified electrodes, and their chiral properties were examined by measuring the cyclic voltammograms (CVs) of L-ascorbic acid (L-AA) and erythorbic acid. The latter is the enatiomer of L-AA, and thereby, it is called D-ascorbic acid (D-AA) in this paper. The CVs of 20 mM L- or D-AA were measured in a 0.5 M H_2SO_4 aqueous solution with a potential sweep rate of 50 mV s^{-1} in the absence of a magnetic field. To obtain reproducible CVs, the polyaniline films were pretreated with a five-cycle potential sweep in the range of −0.1 to 1.1 V in a 0.5 M H_2SO_4 aqueous solution.

3. Results and discussion

The current-time curves during the electropolymerization of aniline at 0 and +5T are shown in Fig. 2. The curves at −5 T was nearly the same as that at +5 T. The magnetic fields do not affect the polymerization rate of polyaniline under the present condition. This is partly because the magnetic fields were applied parallel to the faradaic currents to minimize the MHD effect, and partly because the electrode potential of 0.9 V is under kinetic-controlled conditions. Figure 3 shows CVs for the redox response of the polyaniline films themselves in a 0.5 M H_2SO_4

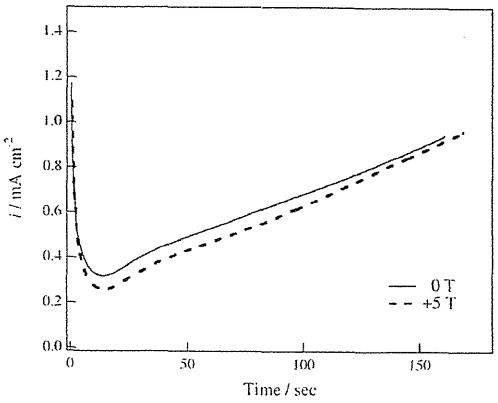

Fig. 2 Current-time curves during the electropolymerization of aniline at 0 and +5 T in a 0.5 M H_2SO_4 aqueous solution.

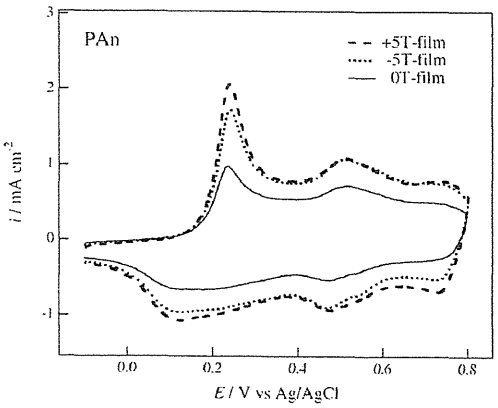

Fig. 3 Cyclic voltammograms of 0, +5 and −5T-films of polyaniline in a 0.5 M H_2SO_4 aqueous solution.

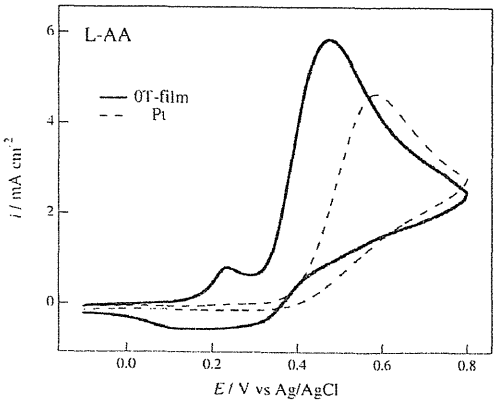

Fig. 4 Cyclic voltammograms of 20 mM L-ascorbic acid (L-AA) in a 0.5M H_2SO_4 aqueous solution on the polyaniline 0T-film electrode and a bare Pt electrode.

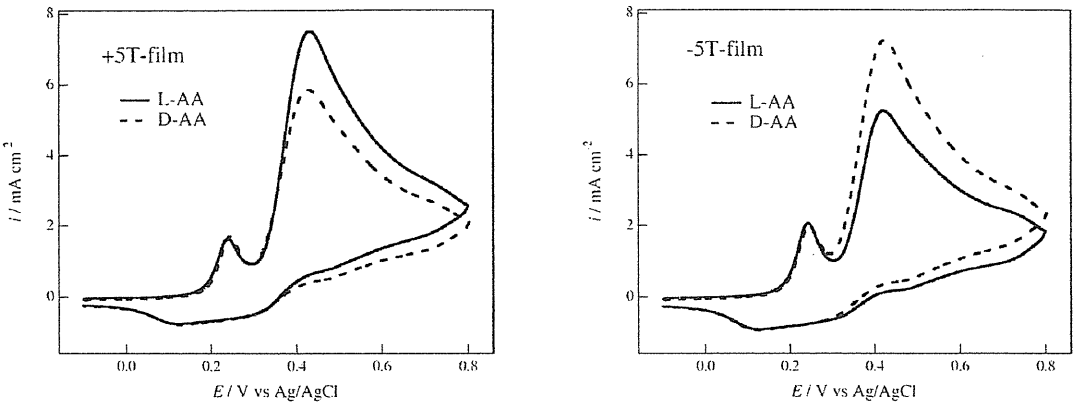

Fig. 5 Cyclic voltammograms of L- and D-ascorbic acids in a 0.5 M H_2SO_4 aqueous solution on (a) the +5T-film and (b) the –5T-film electrodes.

aqueous solution. The CV peak potentials of the MEP films were coincident with those for the redox response of the 0T-film.

A polyaniline film electrode shows electrocatalytic properties for several organic molecules such as L-AA [12-14] and hydroquinone.[15] Figure 4 shows the CVs of L-AA on the 0T-film electrode and a bare Pt electrode. A small peak at 0.2 V in the CV on the 0T-film electrode, which is not seen in the CV on the Pt electrode, represents the oxidation of polyaniline.[16] L-AA is irreversively oxidized to dehydroascorbic acid on the electrodes. This reaction occurs at 0.4 V on the polyaniline electrode, while it occurs at a more positive potential of 0.6 V on the Pt electrode. In addition, the peak current on the polyaniline electrode is much larger than that on the Pt electrode. These observations indicate that the polyaniline film plays a catalytic role in the oxidation reaction of L-AA.

Generally, electrocatalytic reactions are sensitive to the surface structure of the electrode through specific adsorption. If the MEP process induces changes in the surface structure of the polyaniline films, such changes would be reflected in the voltammetric response to ascorbic acid. Figure 5 shows the CVs of L-AA (solid line) and D-AA (broken line) on (a) the +5T-film and (b) –5T-film electrodes. In both figs. 5(a) and 5(b), the CV curves of the solid and broken lines are coincident for the oxidation peaks of polyaniline at 0.2 V. The difference between the enantiomers is clear on the oxidation peak at 0.4 V. The peak current for L-AA is larger than that for D-AA on the +5T-film electrode (Fig. 5(a)). In contrast, the result is opposite on the –5T-film electrode; the peak current for D-AA is larger than that for L-AA (Fig. 5(b)). This result indicates that the MEP induces the ability of enantioselective recognition for the polyaniline film and that the reverse magnetic field during the MEP process produces the opposite chirality.

The electrocatalytic properties of polyaniline depend on dopant anions. We thus examined chirality for the MEP films with other dopants. Figure 6 shows CVs of L-AA (solid line) and D-AA (broken line) on the +5T-film of Cl^--doped polyaniline in a 1 M HCl aqueous solution. The oxidation peak appears at 0.5 V, being more positive than that of SO_4^{2-}-doped polyaniline. The CVs exhibit the chiral properties of the +5T-film, but the peak current difference is quite smaller than that in Fig. 5(a). This result implies that the ability of chiral recognition depends on the electrocatalytic properties of polyaniline.

In the two-dimensional electrodeposition of metals under magnetic fields, the spiral growth direction was reversed by the reversal of the

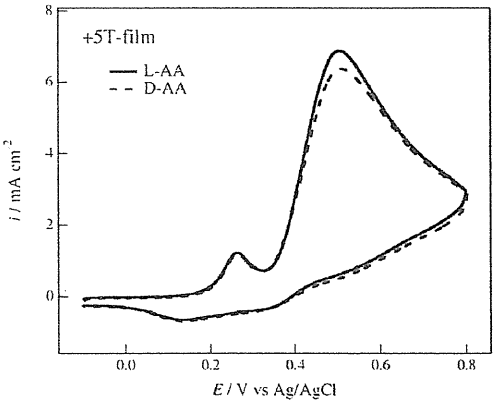

Fig. 6 Cyclic voltammograms of L- and D-ascorbic acids on the +5T-film of Cl^--doped polyaniline in a 1 M HCl aqueous solution.

applied magnetic fields because the spiral growth comes from the Lorentz force acting on currents in electrolytic solutions.[17] Similarly, the opposite chirality of the polyaniline film electrode for the reverse magnetic field indicates that the origin of the chirality is the Lorentz force. Shinohara et al. showed that the Lorentz force couples with small currents around humps on fluctuated surfaces and produces the vortex structures of electrodeposits.[18] The sizes of the vortices, however, are of the order of micrometers, being much larger than the molecular size. The enantioselective recognition for L- and D-AA implies that the MEP films possess a molecular-level chiral structure.

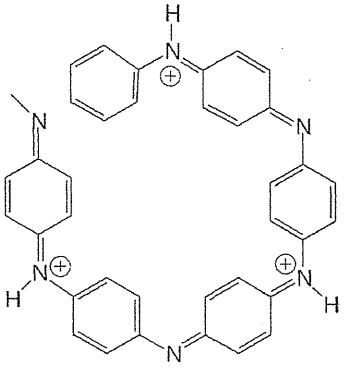

Fig. 7 Proposed helical structure of polyaniline.

Ashraf et al. reported that chiral dopants such as (+)- or (–)-camphorsulfonate induces a helical structure of polyaniline.[19] This means that there exists a possible helical structure in polyaniline. A molecular model study indicates a helical molecular structure, as shown in Fig. 7. The probabilities for right- and left-handed helical structures are equal in the absence of a chiral dopant and a magnetic field. It is, hence, most feasible that the Lorentz force acting on the currents within the polymer chains changes the probability for the right- and left-handed helical structures.

4. Conclusions

We showed that the polyaniline film electrodes prepared by the MEP method exhibit the ability of enantioselective recognition for L- and D-ascorbic acids. The films electropolymerized under the reverse magnetic fields showed an opposite chirality. This result indicates that the origin of the chirality is the Lorentz force, which could change the probability for the right- and left-handed helical structures in the polymer chains.

Acknowledgements

The MEP experiments with a cryocooled superconducting magnet were performed in the High Field Laboratory for Superconducting Materials, IMR Tohoku University. This work was partly supported by a Grant-In-Aid of Scientific Research for Priority Area (Area 767) from MEXT of Japan.

References

[1] J. A. Switzer, H. M. Kothari, P. Polzot, S. Nakanishi and E. W. Bohannan: Nature **425** (2003) 490.
[2] M. O. Lorenzo, C. J. Baddeley, C. Muryn and R. Raval: Nature **404** (2000) 376.
[3] C. F. McFadden, P. S. Cremer and A. J. Gellman: Langmuir **12** (1996) 2483.
[4] M. R. Majidi, L. A. P. Kane-Maguir and G. G. Wallace: Aust. J. Chem. **51** (1998) 23.
[5] H. Guo, C.M. Knobler and R. B. Kaner: Synth. Met. **101** (1999) 44.
[6] G. L. Yuan and N. Kuramoto: Polymer **44** (2003) 5501.
[7] I. Mogi, S. Okubo and Y. Nakagawa: J. Phys. Soc. Jpn. **60** (1991) 3200.
[8] I. Mogi, M. Kamiko and S. Okubo: Physica B **211** (1995) 319.
[9] I. Mogi and M. Kamiko: Denki Kagaku **64** (1996) 842.
[10] I. Uechi, A. Katsuki, L. Dunin-Barkovskiy and Y. Tanimoto: J. Phys. Chem. B **108** (2004) 2527.
[11] I. Mogi, K. Watanabe and M. Motokawa: Electrochemistry **67** (1999) 1051.
[12] I. G. Casella and M. R. Guascito: Electroanalysis **9** (1997) 1381.
[13] S. L. Mu and J. Q. Kan: Synth. Met. **132** (2002) 29.
[14] L. Zhang and S. J. Dong: J. Electroanal. Chem. **568** (2004) 189.

[15] G. Erdogdu and A. E. Karagozler: Talanta **44** (1997) 2011.
[16] T. Ohsaka , Y. Ohnuki, N. Oyama, G. Katagiri and K. Kamisako: J. Electroanal. Chem. **161** (1984) 399.
[17] I. Mogi, S. Okubo and M. Kamiko: Current Topics in Cryst. Growth Res. **3** (1997) 105.
[18] K. Shinohara, K. Hashimoto and R. Aogaki: Electrochemistry **70** (2002) 772.
[19] S.A. Ashraf, L.A.P. Kane-Magire, M.R. Majidi, S.G. Pyne and G.G. Wallace, Polymer, **38** (1997) 2627.

Selection of variants by magnetic field in some ferromagnetic alloys

Takashi Fukuda, Tomoyuki Terai and Tomoyuki Kakeshita
Department of Materials Science and Engineering,
Graduate School of Engineering, Osaka University
2-1, Yamadaoka, Suita, Osaka 565-0871, Japan
(fukuda@mat.eng.osaka-u.ac.jp)

Abstract

We have investigated the influence of magnetic field on rearrangement of crystallographic domains (variants) formed by diffusionless and/or diffusion solid-solid phase transformations. Following results are obtained: the rearrangement of martensite variants formed by diffusionless (martensitic) transformation occurs in Fe-31.2mol%Pd, Fe_3Pt and Ni_2MnGa; and the variant with the lowest magnetic energy (mainly magnetocrystalline anisotropy energy) is selected to grow in each alloy. The same selected growth of the variant formed by diffusion transformation is observed in CoPt showing a disorder-order transformation. The condition for the rearrangement of martensite variant driven by magnetic field is discussed quantitatively.

keywords

magnetocrystalline anisotropy, preferential arrangement

1. Introduction

In accordance with recent progress on magnet technology, the effect of magnetic field on solid-solid phase transformation has been extensively studied. One important effect of magnetic field is the change in free energy between different phases. For example, magnetic field will decrease the free energy of a ferromagnetic phase compared with that of paramagnetic phase, promoting the formation of ferromagnetic phase under a magnetic field. Such behavior is observed in some ferrous alloys in which a ferromagnetic martensite phase is induced from a paramagnetic and/or ferromagnetic parent phase by magnetic field. Another important effect is the change in free energy between different crystallographic domains (variants), which arises from magnetic anisotropy. In the following, we focus on the latter effect on the microstructure formed by solid-solid transformations.

An alloy exhibiting a solid-solid phase transformation usually forms variants in its low symmetry phase. Every variant has the same free energy unless external fields, such as stress and magnetic field, are applied. Under a magnetic field, however, there arises difference in magnetic energy among them especially when the low temperature phase is ferromagnetic with large magnetocrystalline anisotropy. In such a case, the variant with the lowest magnetic energy is expected to be selected to grow under a magnetic field.

In the present study, we confirmed that such a selected growth is actually realized in two cases: one is the rearrangement of martensite variants (RMV) by magnetic field in some ferromagnetic shape memory alloys (Fe-31.2Pd, Fe_3Pt and Ni_2MnGa), and the other is the selected growth of a specific variant during a disorder-order (A1-$L1_0$) transformation in CoPt. The former is a typical example of diffusionless process (atoms do not move more than one atomic distances), and the other is a typical example of diffusion process. For both cases, magnetocrystalline anisotropy is essentially important for the microstructure formed under a magnetic field.

2. Experimental Procedures

Ingots of Fe-31.2Pd, Fe_3Pt, Ni_2MnGa and CoPt are prepared by arc melting. Single crystal of each alloy is prepared by floating zone method or Bridgeman method and then heat treated for homoginization. Lattice parameters of the alloys were determined by x-ray analysis, magnetic field-induced strain was measured by three terminal capacitance method, magnetization was measured by SQUID magnetometer and stress-strain curves are obtained by Instron-type machine.

Details of the procedure are given elsewhere [1-3]. Ordering heat treatments of CoPt under a magnetic field were made by using a furnace inserted in a superconducting magnet. The position of the specimen is located at the center of the hot zone which is also the center of the magnetic field.

3. Results and Discussion

3.1 Magnetic field-induced strain associated with RMV in ferromagnetic shape memory alloys

Figure 1 shows the temperature dependence of lattice parameter of Fe-31.2mol%Pd (a), Fe_3Pt with degree of order about 0.8 (b) and stoichiometric Ni_2MnGa (c). Every alloy exhibits a thermoelastic martensitic transformation from a ferromagnetic parent phase to a ferromagnetic martensite phase. The transformation temperature T_M is 230 K for Fe-31.2Pd, 85 K for Fe_3Pt and 202 K for Ni_2MnGa. In the martensite phase, the lattice parameters change gradually for Fe-31.2Pd and Fe_3Pt while they are nearly constant for Ni_2MnGa as temperature decreases below each T_M. Since the martensite phase is tetragonal or psudotetragonal for all the alloys, there are three corresponding variants because a and c axes correspond to $<001>_P$ (P stands for the parent phase) of the parent phase.

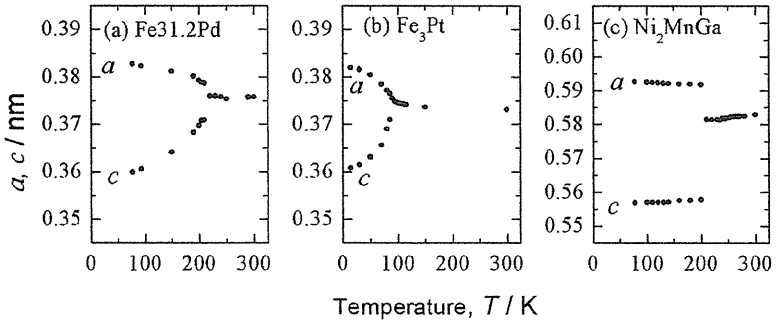

Fig. 1 Temperature dependence of lattice parameters of ferromagnetic shape memory alloys.

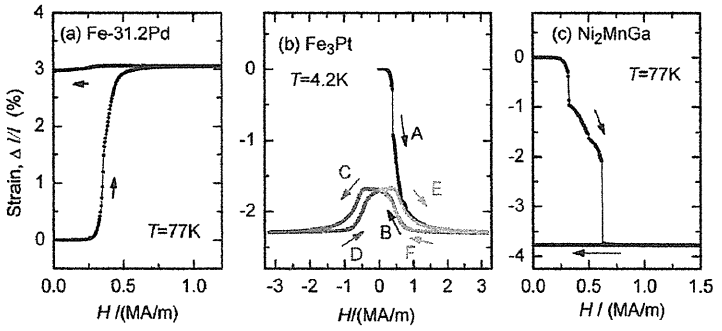

Fig. 2 Magnetic field-induced strain of ferromagnetic shape memory alloys.

Figure 2 shows magnetic field-induced strain (MFIS) of the three alloys associated with the rearrangement of martensite variants (RMV). The shape of each specimen used is rectangular with about 3 mm^3 in dimension and the measurement was made by a capacitance method after cooling down below the martensitic transformation temperature without applying magnetic field. So, the starting point of the specimen is multi-variant state (three variants exist). Then, we applied magnetic field along the $[001]_P$ direction and measured the strain along the field direction. As a result, the Fe-31.2Pd expands along the field direction, and Ni_2MnGa and Fe_3Pt contract along the field direction. The difference of the sign of the strain is due to the difference in easy axis; that is, the easy axis is the a axis for the Fe-31.2Pd, but the c axis for the Ni_2MnGa and Fe_3Pt. For all the alloys, the fraction of the variant whose easy axis lies along the field direction (the variant whose magnetic energy is lowest among the three variants) increases by the field application; it reaches 100% for

Fe-31.2Pd and Ni_2MnGa, but does not for the Fe_3Pt. It should be also noted in Fig. 2 that a part of strain (0.6%) recovers for the Fe_3Pt while does not for Fe-31.2Pd and Ni_2MnGa; the reason of the recovery is not known yet but possibly related to accumulation of elastic energy or demagnetization effect.

3-2 Condition for RMV by magnetic field

In order to understand the condition for RMV by magnetic field, we introduce magnetic shear stress τ_{mag} acting across the twinning plane. The reason for introducing τ_{mag} is that we usually evaluate a shear stress for analyzing a twinning plane movement. Using the value of τ_{mag}, the condition for RMV by magnetic field will be explained as: the value of τ_{mag} is larger than the shear stress required for the RMV, τ_{req}. In the following we will show that this condition is certainly satisfied when RMV occurs by magnetic field.

The value of τ_{mag} is expressed as $\Delta U_{mag}/s$, where ΔU_{mag} is the magnetic energy difference per unit volume between the two variants separated by the twinning plane considered, and s is the corresponding twinning shear. Assuming that the magnetic energy is mainly composed of magnetocrystalline anisotropy energy and Zeeman energy, the maximum of ΔU_{mag} is equal to the uniaxial magnetocrystalline anisotropy constant $|K_u|$ under the $[001]_P$ field. Then the maximum value of magnetic shear stress, τ_{mag}^{m}, will be $|K_u|/s$ under the $[001]_P$ field.

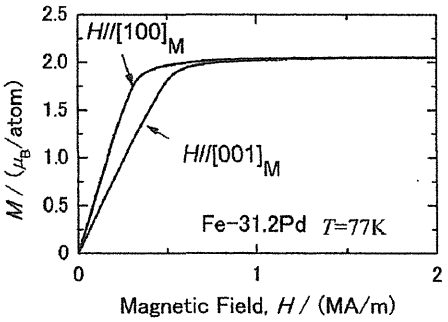

Fig. 3 Magnetization curve along a axis ($[100]_M$) and c axis ($[001]_M$) of Fe-31.2Pd at 77K.

The value of $|K_u|$ is obtained from the area enclosed by the two magnetization curves: along hard magnetization axis and along easy magnetization axis. In order to obtain these curves, we must make magnetization experiments of a single variant state in martensite phase, which is realized by applying a compressive stress along one of $<001>_P$ directions. The magnetization curves along the a axis and along the c axis thus obtained for the Fe-31.2Pd alloy at 77 K is shown in Fig. 3. It is clearly seen that the a axis is the easy axis and the c axis is the hard axis; the value of $|K_u|$ obtained from the enclosed area is 180 kJ/m^3. Similar measurements were made for various temperatures and the result of $|K_u|$ is shown in Fig. 4. The values shown in the figure are one order in magnitude larger than those of Fe-30Pd alloy around room temperatures reported by Cui et al. [4], but are the same order as that of off-stoichiometric Ni-Mn-Ga alloys reported previously [5].

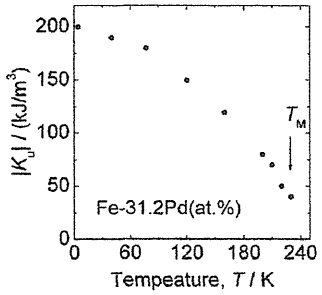

Fig. 4 Magnetocrystalline anisotropy constant K_u of Fe-31.2Pd.

The amount of twinning shear for the present alloys is express as $s=\{ 1-(c/a)^2 \}/(c/a)$, because the twinning plane is $\{101\}_M$. Then we can easily calculate s from the lattice parameters shown in Fig. 1. The calculated value of s decreases monotonically with increasing temperature.

Using the value of $|K_u|$ and s thus obtained, we calculated the maximum of magnetic shear stress τ_{mag}^m, which is shown in Fig. 5. The value of τ_{mag}^m does not change significantly below the transformation temperature.

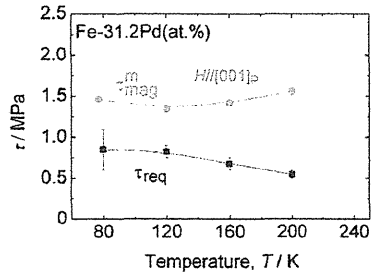

Fig. 5 Temperature dependence of the maximum of τ_{mag} and τ_{req}.

In evaluating τ_{req}, we made tensile tests. Figure 6 is a stress-strain curve obtained at 80 K by a tensile test along $[001]_P$ direction. The stage around uniaxial tensile stress of 2 MPa is due to the twinning plane movement. The corresponding τ_{req} is obtained to be 1 MPa (Schmidt factor is 0.5). By making the same experiments at some different temperatures, we obtained temperature dependence of τ_{req} as shown in Fig. 5.

Comparing τ_{mag}^m and τ_{req} shown in Fig. 5, it is obvious that the value of τ_{mag}^m is larger than τ_{req} at any temperature below T_M. In this way, we have confirmed that the condition for the RMV by magnetic field mentioned before is quantitatively satisfied below T_M in the Fe-31.2 Pd alloy. This condition is also confirmed to be satisfied in stoichiometric Ni_2MnGa. Concerning the Fe_3Pt, the comparison is not made because compressive tests at cryogenic temperatures have not been made yet.

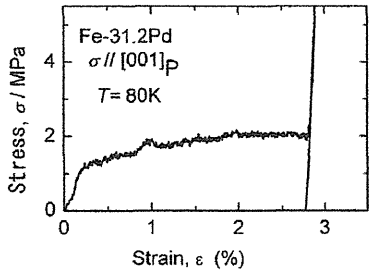

Fig. 6 Stress strain curve of single-crystalline Fe-31.2Pd.

3.3 Growth of a specific variant in CoPt during the ordering heat treatment under a magnetic field

Co-50mol%Pt transforms from a disordered A1-type (cubic) structure to an ordered $L1_0$-type (tetragonal) structure at 1100K, and the tetragonal phase has three variants. The ordered phase has a Curie temperature of 760 K, and has a high magnetocrystalline anisotropy of 4.1 MJ/m^3 [6] at room temperature, where the easy axis is the c axis and the hard axis is the a axis. Therefore, there arises a significant energy difference between variants under a magnetic field below the Curie temperature, and the variant with the lowest magnetic energy is expected to form preferentially compared with other variants.

In order to confirm the above expectation, we made ordering treatment of CoPt with and without applying magnetic field. The specimens used in the study are cube ones with each edge parallel to <100>; the three edges are termed as X, Y, Z directions. The specimens were first solution treated at 1273 K followed by quenching into iced water to obtain the disordered state. The specimen was then

subjected to the following ordering heat treatment: heating up to 1023K with a heating rate of about 150 K/min and keeping at 1023 K for 3 h. This heat treatment was made under a magnetic field of 10 T applied along the Z direction. The same heat treatment without applying magnetic field was also made for comparison.

After the ordering heat treatment, magnetization curves were measured along the X, Y, Z directions, which are shown in Fig. 7. When the ordering were made without applying the magnetic field, the magnetization curves measured along the three directions are almost the same with one another as seen in Fig. 7(a). This means that three variants are almost equivalently formed by this heat treatment. On the other hand, when the ordering was made under the magnetic field of 10 T applied along Z direction, the magnetization measured along the Z axis saturates easily compared with X and Y directions. This means that almost single variant, whose easy axis (*c* axis) lies along the Z direction, was formed by the ordering under the magnetic field. The same selection of specific variant was reported in FePd by Tanaka et al.[7] At the present stage the mechanism of the selected growth of the preferable variant under a magnetic field is not clear, and it is a subject in the future.

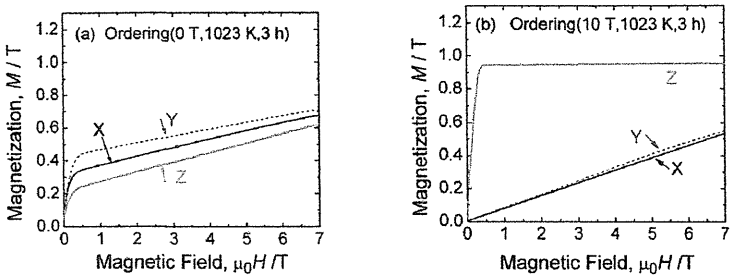

Fig. 7 Magnetization curves of CoPt ordered under without magnetic filed (a) and under a magnetic field of 10T applied along Z direction (b).

4. Conclusions

Magnetic field is effective for the arrangement of variants formed by martensitic transformation and ordering process. For both cases, the variant with the lowest magnetocrystalline anisotropy energy is selected to grow consuming others under a magnetic field. We demonstrated such behavior in three shape memory alloys (Fe-31.2Pd, Ni_2MnGa and Fe_3Pt) and a hard magnetic material of CoPt.

Acknowledgements

This work is supported by Grant-in-Aid for Scientific Research on Priority Area "Innovative utilization of strong magnetic fields" (Area 767, No.15085206).

References

[1] T. Fukuda, T. Sakamoto, T. Kakeshita, T. Takeuchi and K. Kishio, Mater. Trans., **45** (2004) 188-192.

[2] T. Sakamoto, T. Fukuda, T. Kakeshita, T. Takeuchi and K. Kishio, Science and Technology of Advanced Materials **5** (2004) 35-40

[3] N. Okamoto, T. Fukuda, T. Kakeshita, T. Takeuchi and K. Kishio, Science and Technology of Advanced Materials **5** (2004) 29-34

[4] J. Cui, T.W. Shield, R.D. James, Acta Mater. **52**, (2004) 35-47.

[5] L. Straka and Oleg Heczko, J. Appl. Phys., **93** (2003) 8636-8638.

[6]H. Shima, K. Oikawa, A. Fujita, K. Fukamichi, K. Ishida, S. Nakamura, T. Nojima, J. Mag. Mag. Mater., **290-291**(2005) 566-569.

[7] K. Tanaka, T. Ichitsubo, M. Koiwa, Materials Sci. Eng., **A312** (2001) 118-127.

Magnetic Orientation of Cast films of Pulp Cellulose Microfibrils

Fumiko Kimura[1], Tsunehisa Kimura[1,2] and Fumitaka Horii[3]
1 Tsukuba Magnet Laboratory, National Institute for Materials Science,
3-13 Sakura, Tsukuba, Ibaraki 305-0003, Japan
2 Department of Applied Chemistry, Tokyo Metropolitan University,
1-1 Minami-ohsawa, Hachioji, Tokyo, 192-0397, Japan
3 Institute for Chemical Research, Kyoto University,
Uji, Kyoto 611-0011, Japan
(KIMURA.Fumiko@nims.go.jp)

Abstract

Suspensions of wood cellulose microfibrils were prepared by acid hydrolysis of the wood cellulose. They formed a chiral nematic phase above a critical concentration. External magnetic fields were applied to the suspensions in two different manners to control the structure of cast films. (i) A 12 T static magnetic field was used to align the chiral nematic axis (helical axis) in the field direction. (ii) A rotating magnetic field (0.5 T, 6 rpm and 30 rpm) was applied to unwind the helices. The obtained alignments were interpreted in terms of the anisotropic diamagnetic susceptibility of the cellulose microfibril. The diamagnetic susceptibility of the microfibril is smaller in the direction parallel ($\chi_\parallel$) to the fiber axis than in the direction perpendicular ($\chi_\perp$) to the fiber axis, that is, $\chi_\parallel < \chi_\perp < 0$. Because the helical axis coincides with the direction normal ($\perp$) to the fiber axis, the helical axis aligned parallel to the applied field. On the other hand, the rotating magnetic field induced the uniaxial alignment of the smallest susceptibility axis, that is, $\chi_\perp$ in the present case, and brought about unwinding of the helices.

Keywords

Cellulose microfibril, Magnetic alignment, Cast film, Chiral nematic phase, Nematic phase

1. Introduction

The alignment manner of fibers under static magnetic field depends on the anisotropic nature of the fibers. For example, fibers with positive diamagnetic anisotropy ($\chi_a = \chi_\parallel - \chi_\perp > 0$) undergo uniaxial alignment, that is, they align with their fiber axes parallel to the applied field, while those with negative diamagnetic anisotropy ($\chi_a < 0$) undergo planar alignment. Here $\chi_\parallel$ and $\chi_\perp$ are the diamagnetic susceptibilities in the directions parallel and perpendicular to the fiber axis, respectively. Carbon fibers and carbon nanotubes belong to the former, while polyethylene and cellulose fibers belong to the latter.

Recently, one of the authors (T.K.) reported uniaxial alignment of the smallest diamagnetic susceptibility axis using a rotating magnetic field.[1] It was shown experimentally and theoretically that a nylon fiber ($\chi_a < 0$) underwent uniaxial alignment under a rotating magnetic field. This technique is applied not only to fiber suspensions but also to many other systems possessing negative anisotropic diamagnetic susceptibilities.

Cellulose microfibrils align perpendicular to the magnetic field, because the anisotropic diamagnetic susceptibility is negative.[2] Suspensions of the cellulose microfibrils form a chiral nematic phase above a critical concentration. It was reported that a film of the chiral nematic phase cast under a vertical magnetic field showed an orientation with the texture characteristic to chiral nematic phase being maintained, which was confirmed by the induced circular dichroism of the dye molecules in the film.[3] The texture observed, however, did not exhibit high order. In this study, we show that the chiral nematic suspension cast under a statistic magnetic field exhibit an alignment with the finger print texture being nicely maintained. Also, the alignment under a rotating

magnetic field is reported.

2. Experimental methods

2.1 Preparation of cellulose microfibril suspension

Cellulose microfibril suspensions were prepared by hydrolysis of Whatman CF11 cellulose powder with 64 wt % sulfuric acid at 45° for 1 h. The acid was removed by centrifugation and prolonged dialysis with pure water.

2.2 Cast film.

Cast films were prepared under static and rotating magnetic fields. 75 or 200μl suspension was poured onto a cover glass or a home-made cell which had rim wall to prevent flow of the suspension. Water was evaporated under the magnetic fields until the suspension was solidified.

2.3 Magnetic field

Static Magnetic Field. A cryogen-free superconducting magnet of Japan Superconductor Technology was used to generate a horizontal static magnetic field of 12 T.

Rotating Magnetic Field. A pair of electromagnets were used to generate rotating magnetic field (6 or 30 rpm, magnetic field 0.3T). Axis of rotating magnetic field was horizontal.

3. Results and Discussion

Photographs of a film prepared under 12T are shown in Fig. 1. Photographs at magnification of x40 show blue or orange color indicating that the film is almost uniform. Moreover, finger print texture was observed in the photographs at magnification of x400, proving the preservation of high regularity of finger print texture. The orientation of the chiral nematic axis parallel to the applied static magnetic field is realized in suspension.[4,5] On the other hand, in cast films it seems to be very difficult to preserve the uniform chiral texture, because the texture could be distorted during evaporation of water. However, we observed the alignment of the chiral nematic axis parallel to the static magnetic field in the cast film.

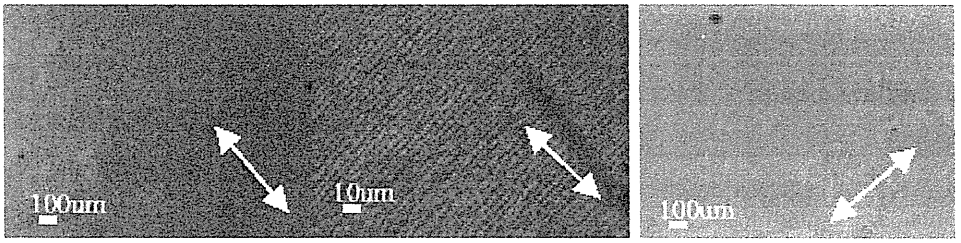

Fig. 1. Photomicrographs of a cellulose film aligned in a 12T horizontal magnetic field observed between crossed polars. White arrows indicate the direction of magnetic field. Magnifications are x40, x400, and x40, from left to right.

Photographs of a film prepared under a rotating magnetic field and 0 T magnetic field are shown in Fig. 2. The applied rotating magnetic field is 0.3T at 6 rpm. Photographs of the sample prepared under the rotating magnetic field shows almost orange or blue colors, indicating the film is aligned. Because of the negative diamagnetic anisotropy of the individual cellulosic microfibrils composing the suspension, they tend to align uniaxially under a rotating magnetic field, with the fiber axis parallel to the rotating axis of the magnetic field. Cellulose microfibrils have a birefringence with $n_{\parallel} > n_{\perp}$, where $n_{\parallel}$ and $n_{\perp}$ are the refractive indices parallel and perpendicular to the fiber axes, respectively. If the fiber axes of the microfibrils are aligned in the direction parallel

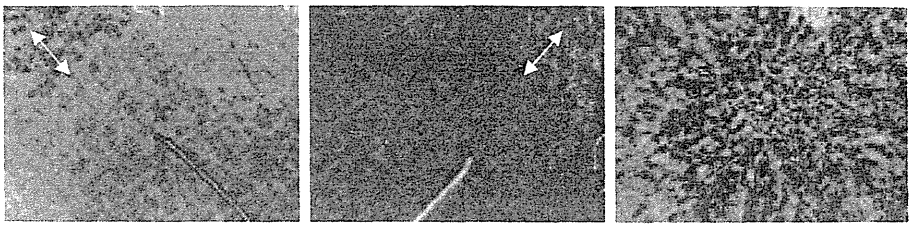

Fig. 2. Photomicrographs of cellulose films observed between crossed polars. Left and middle: the sample aligned in a rotating magnetic field (0.3T, 6rpm). The blue and orange lines resulted from a scratch. White arrows indicate the direction of rotating axis. Right: the sample prepared under 0 T. Magnifications are x40.

to the rotating axis, we should observe the positive birefringence. The result shown in Fig. 2 indicates that the cast film has positive birefringence. On the contrary, the cast film prepared under the 12T static magnetic field shows the negative birefringence, because the microfibrils are aligned perpendicular to the static magnetic fields.

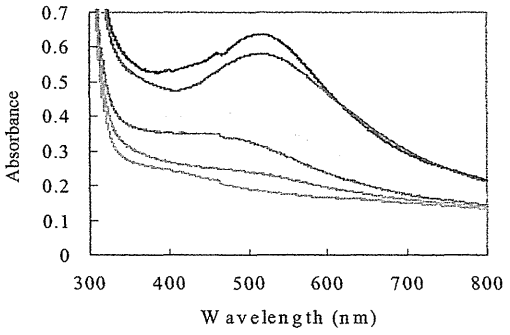

Fig. 3. Polarized transmission UV/Vis spectra. (i) – and – indicate 0 and 90° (parallel and perpendicular to the magentci field) polarization of the sample prepared under 12 T horizontal magnetic field. (ii) – and – indicate 0 and 90° (parallel and perpendicular to axis of rotating magnetic field) polarization of the sample prepared under 0.3 T rotating (30rpm) magnetic field. (iii) – and – indicate 0 and 90° polarization of the sample under 0 T magnetic filed.

Figure 3 shows the polarized transmission spectra of the samples prepared under 0 T and 12 T static magnetic fields, and the rotating magnetic field (30 rpm, 0.3T). A band at 550 nm was observed for the film prepared under 0T magnetic field. This band presumably corresponds to the pitch of the chiral nematic phase (actual pitch is about 3000 nm), because the light is reflected between layers of chiral nematic phase. The bands disappear for the sample prepared under the static magnetic field, indicating that the layers perpendicular to the direction of the impinging light do not exist because the layers align parallel to the UV/Vis light incident direction. For the sample prepared under the rotating magnetic field, the band intensity is weak compared to the sample prepared under 0 T magnetic field, and large polarization are observed between 320 nm and 800 nm, indicating that the unwinding of the helix occurs. However, there remains some amount of chiral nematic phase, because we observed a trace of band at 550 nm.

5. Conclusions

Magnetic alignment of the cast films from the suspension of cellulose microfibrils prepared by acid hydrolysis of the wood pulp was reported. The helical axis of the chiral nematic phase aligned in the direction of the applied static field, resulting in highly regular mono domain. Exposure to the rotating magnetic field caused unwinding of the helical axes to form nematic-like alignment.

Acknowledgements

Acknowledgments: This work was partially supported by a Grant-in-Aid for Scientific Research on Priority Area "Innovative utilization of strong magnetic fields" (Area 767, No. 15085207) from MEXT of Japan.

References

[1] Kimura, T.; Yoshino, M.; Yamane, T.; Yamato, M.; Tobita, M. *Langmuir 20(*2004, 5669-5672.
[2] J. Sugiyama, H. Chanzy, and G. Maret, Macromolecules 25 (1992) 4232-4234.
[3] C. D. Edgar, and D. G. Gray, Cellulose 8 (2001) 5-12.
[4] J.-F. Revol, L. Godbout, X.-M. Dong, D. G. Gray, H. Chanzy, and G. Maret, Liquid Crystals 16 (1994) 127-134.
[5] F. Kimura, T. Kimura, M. Tamura, A. Hirai, M. Ikuno, and F. Horii, *Langmuir* 21(2005) 2034-2037.

Molecular Assemblies under Steady Magnetic Fields: Membranes, Micelles and Vesicles

Taisuke Takahashi, Yutaka Yaguchi, Mikako Ishii and Sumio Ozeki
Department of Chemistry, Faculty of Science, Shinshu Univesity,
3-1-1 Asahi, Matsumoto, Nagano 390-8621, Japan
(sozeki@shinshu-u.ac.jp)

Abstract

Steady magnetic fields extended wormlike micelles and deformed entangled threadlike micelles. The radius of gyration R_G of micelles of hexadecyltrimethylammonium bromide (CTAB) in aqueous NaBr or sodium salicilate (NaSal) solutions, estimated by the angular dependence of light scattering intensity, increased at more than 5T. In the both systems, the wormlike and threadlike micelles having R_G of more than 120 nm grew by magnetic fields; i.e., R_G of micelles in 50 mM CTAB and 100mM NaSal solution changed from145 nm to 168 nm by the application of 10 T. The molecular orientation in a membrane and deformation of vesicles was observed by changes in membrane potential and resistance of black lipid membranes and in scattering intensities of light and neutron from vesicles, respectively. Much higher magnetic fields induced magnetofusion and magnetodivision of vesicles according to the following condition: $6(1 - n) - c_0 r_0 (n^{1/2} - n) \geq 0$ when n vesicles of initial radius r_0 having the local curvature of a vesicle c_0 associate with a vesicle of radius r under a magnetic field.

Keywords
magnetic field effects, micelles, vesicles, liposomes, black lipid membranes, light scattering

1. Introduction

A magnetic field is one of potential methods to align and orient molecular domains. It is well established that diamagnetic domains having magnetic anisotropy will become oriented or rotate in a steady magnetic field so as to obtain the minimum-energy state [1-5]. The magnetic orientational energy (E_r) of a diamagnetic lipid domain containing N molecules (volume Nv), whose long molecular axis is at an angle φ to H and which have the diamagnetic anisotropy, $\Delta\chi$, and the magnetic susceptibility perpendicular to H, $\chi_\perp$, is given by the following equation [6]:

$$E_r = -(H^2/2)(\chi_\perp + \Delta\chi\cos^2\varphi)Nv \qquad (1)$$

When H and/or N is as large as E_r overcomes the thermal energy, the long molecular axis of hydrocarbon chains in a domain can be cooperatively aligned in the direction of averaged φ. Lipid molecules in a lipid membrane will tend to tilt against membrane surface when a magnetic field is applied in perpendicular to the surface. In the case of micelles and vesicles (liposomes), high magnetic fields may make them deform to lead to ellipsoidal shape and surface undulation because of balance of elastic energy from deformation and magnetic energy. Helfrich [7] predicted theoretically the magnetic deformation of phospholipid liposomes from a sphere to an ellipsoid, which was shown experimentally by Tenforde and Liburdy [8].

In this paper, function regulation of black lipid membranes and structural control of micelles and vesicles due to steady magnetic fields [9-13] are reported.

2. Membrane potential of black lipid membranes under magnetic fields

Biological cells contain many components and elementary processes for molecular syntheses,

mass transport and metabolism. To elucidate the magnetic effects on biosystems, those on each elementary process should be examined. An artificial lipid bimolecular membrane, the so-called black lipid membrane (BLM), is useful for a model for biomembranes, although such thermodynamical lipid membranes must be too simple.

The membrane potential (Ψ) and resistance (R) of BLMs, comprising didodecyl phosphite (DP), dipalmitoylphosphatidylcholin (DPPC) and of dioctadecyldimethylammonium chloride (DODAC), changed remarkably under low, steady magnetic fields [9-11]. The magnetic field effects on the electrical properties seem to occur not via the Lorentz force on the ion flux but via a cooperative orientation of lipid molecules. The BLMs in aqueous solutions was formed at 316 K in the hole (ca. 0.8 mm diameter) of a thin Teflon sheet that divided the Teflon cell into two compartments. The Ψ arising across a BLM by maintaining a 10-fold difference in the NaCl concentration was measured with a couple of Ag-AgCl electrodes. BLM-forming solutions were prepared by mixing 20 ppm of lipid with (3+2) octane-dodecane. Figure 1 shows that the magnetic response in membrane potential of BLM of DP was very reproducible and reversible even at low magnetic fields (<0.5 T). Membrane resistance also responded very sensitively in the same manner to magnetic fields. The features in the experimental magnetic responses of Ψ and R seem to be consistent with the theory [10] that both values were determined by an effective fixed charge density of a membrane. Therefore, magnetic fields should change the density of lipid molecules in the membrane, which depends on a tilt angle of the molecular axis against the membrane surface. Under high magnetic fields, the membrane potential increased markedly at around 12 T, suggesting increase in effective fixed charge density due to membrane undulation, as prediced by Helfrich [8].

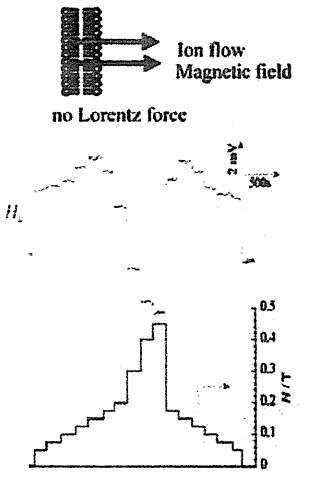

Figure 1. Changes in membrane potential of a black DP membrane with magnetic field of up to 0.45 T at 298 K. The magnetic field was applied in perpendicular to the membrane surface, thus there was no Lorentz force.

3. Magnetofusion and magnetodivision of vesicles

High steady magnetic fields should induce membrane deformation, as suggested above. The bilayer membrane is not a homogeneously curved surface in the case that it has different elastic properties. The Helfrich theory for the magnetodeformation, s_2/r_0, of a spherical bilayer vesicle of radius r_0, in which the domains in the bilayer have a local curvature c_0, gives the equation

$$s_2/r_0 = r_0^2 \Delta\chi b H^2/3k_c(6 - c_0 r_0) \qquad (2)$$

where b is a measure for the thickness of the bilayer and k_c is the curvature-elastic modulus [23]. Figure 2 shows the average size of vesicles comprising mixture of sodium dodecylsulphate (SDS) and hexadecyltrimethylammonium bromide (CTAB) as a function of magnetic field intensity. The radius of gyration calculated from scattering angle dependence of scattered light intensity may give schematic images for the size change of sphere to ellipsoid.

When much higher magnetic fields were applied to vesicles, whether or not may fusion among vesicles and division of a vesicle occur? The total energy ($E^H(r_0)$) of a liposome which has initially radius r_0 comprises the curvature-elastic (E_c) and magnetic energies (E_H),

$$E^H(r_0) = E_c + E_H \qquad (3)$$

Liposome growth from radius r_0 to r with the association of n vesicles under a magnetic field may be possible when the following relation is satisfied:

$$E^H(r_0) \geq (1/n)E^H(r)$$

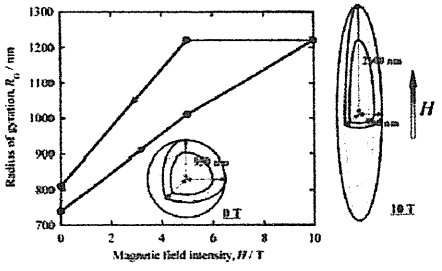

Figure 2. Magnetic field dependence of the radius of gyration of vesicles prepared by mixing 50 mM SDS and 10 mM CTAB at 298 K. Concentration of SDS: 50 mM. Concentration of CTAB: 10 mM.

(4)

When association occurs without changes in the liposome surface area, r is simply given by

$$r = n^{1/2} r_0 \qquad (5)$$

When H is large enough (~10T) (case 1) or the shape of a liposome is exactly an ellipsoid of revolution (case 2), the following relation is obtained if c_0 is unchanged during the size change [26]:

$$6(1 - n) - c_0 r_0 (n^{1/2} - n) \geq 0 \qquad (6)$$

This relation was derived from eqs.(2), (3),and (4) using the two equations (E_c and E_H) in ref.23 for case 1 or the following two equations for case 2:

$$E_c = (8\pi/5) k_c (6 - c_0 r_0)(s_2/r_0)^2 \qquad (7)$$

$$E_H = -(16\pi/15)\, \Delta\chi b H^2 r_0 s_2 \qquad (8)$$

Solving Eq.6 and adding the condition $(6 - c_0 r_0) > 0$, possible association in vesicles having radius r_0 may be estimated for a given radius of curvature ρ ($=1/c_0$), as shown in Figure 3. The shadowing in the figure illustrates the regions of magnetofusion ($n>1$) and magnetodivision ($n<1$) for $\rho = 10$ nm. When $n = 1$, a liposome of size r_0 is stable against or insensitive to a certain magnetic field; that is, the apparent $\Delta\chi$ of a whole liposome should be zero.

DPPC and DODAC vesicles were prepared from chloroform solutions of DPPC with the Bangham method. The average vesicle size was determined as a sphere from the Einstein-Stokes equation by dynamic light scattering at 298 K under no magnetic fields. Vesicles of both DPPC and DODAC grew when they were exposed to high magnetic fields more than 12 T at 318 K for 1 h. Figure 4 shows a typical example of changes in size of DODAC vesicles under a 10 T magnetic field. In smaller size than 500 nm in radius the vesicles grew and over 500 nm in radius the vesicles became small. The optical microscopic observation indicated that the size change of vesicles due to magnetic fields may occur by fusion and division. Therefore, we refer the size change to magnetofusion and magnetodivision of vesicles. The addition of magnetic-field sensitive molecules such as anthracene and pyrene induced such size change at much lower magnetic fields. Figure 3 summarizes experimental n values as a function of r_0, along with the theoretically possible region. Comparison of the theoretical to the experimental vesicle size under magnetic fields shows that almost all experimental points drop in the theoretical region for 10 or 20 nm for ρ_0.

The dynamical process in the magnetofusion and magnetodivision seems to be very fast, because just a 2 ms-pulse of a 10T magnetic field promoted significant fusion of liposomes to change from a monomodal size distribution to a typical bimodal one.

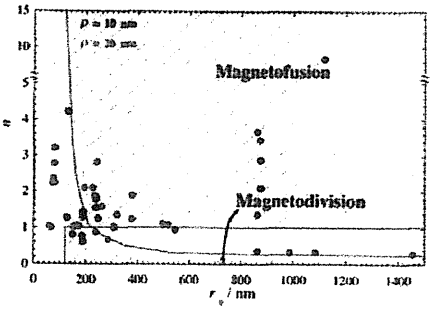

Figure 3. Comparison between experimental and theoretical association number of DPPC vesicles under magnetic fields. Theoretically possible regions are shown by shadowing for $\rho = 10$ nm and oblique line for $\rho = 20$ nm. Vesicle size changed from $r0$ to r ($n \sim r^2/r_0^2$) by application of magnetic fields of 10 – 30 T at 418 K.

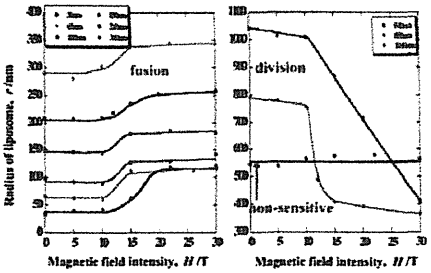

Figure 4. Magnetic field dependence of size of DODAC vesicles having different initial size at 318 K.

4. Structural changes of flexible micelles due to magnetic fields

Persistence length of rodlike micelles of hexadecyltrimethylammonium bromide (CTAB) increases by addition of NaBr and sodium salicilate (NaSal), which refer to wormlike and threadlike micelles. Since magnetic ordering of surfactant micelles will be reversible, we measured micelle deformation with static light scattering apparatus under magnetic fields. When the radius of gyration (R_G) of CTAB micelles in aqueous NaBr or NaSal solutions was less than 120 nm, no magnetic field changed their sizes, suggesting that rodlike or short wormlike micelles are non-sensitive to magnetic fields. Increasing NaSal concentration, magnetic fields decreased light

scattering intensity from aqueous CTAB/NaSal solutions (Figure 5). Figure 6 shows that the R_G values estimated from the intensity increased by magnetic fields when R_G >120 nm. It suggests that long wormlike micelles should be extended, and that entangled threadlike micelles (or random coil) should be deformed to be extended coil. The deformation arises from magnetic anisotropy of CTA^+ and Sal^-, especially distribution and orientation of Sal^- in micelles.

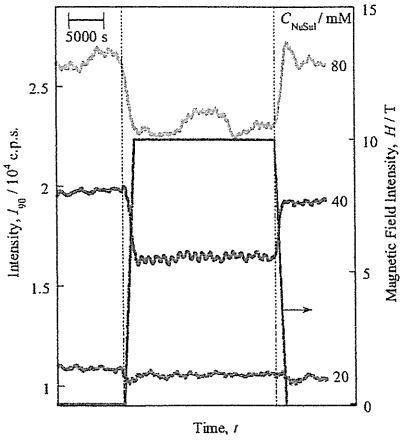

Figure 5. Changes of scattering light intensity of 20 mM aqueous CTAB solutions containing NaSal (20, 40, and 80 mM) with application of magnetic fields at 298 K.

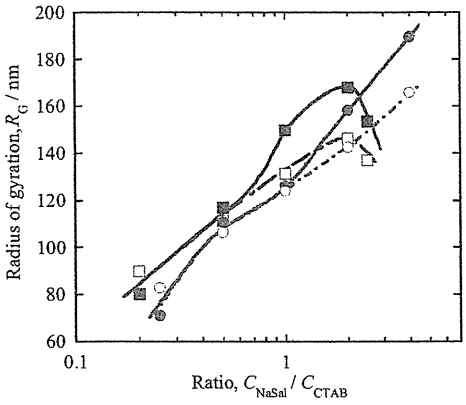

Figure 6. Magnetic field effects on the radius of gyration of micelles in aqueous CTAB solutions containing NaSal of different concentrations. Concentration of CTAB, C/mM: circle, 20; square, 50. Magnetic field intensity, H / T: open, 0 ; solid, 10.

5. Conclution

Deformation in lipid membranes due to steady magnetic fields led to the fusion and division of its vesicle and large changes in the electrical properties of their black membranes. In the BLM, very low, steady magnetic fields less than 0.1 T brought about significant responses in membrane potential and resistance. The time scale of such processes should be less than msec-order. Rodlike or threadlike micelles may be extended or grown up by magnetic fields. In these systems, magnetically anisotropic molecules can effectively control the magnetic responses in structures and functions of molecular assembly systems. These examples demonstrate the potentiality of various magnetic fields that can regulate functions, structures, and sizes of artificial organized molecular assemblies.

Acknowledgment

This work was supported by Grant-in-Aid for Scientific Research on Priority Area "Innovative utilization of strong magnetic fields" (Area 767, No.15085205) from MEXT of Japan.

References

1. Gaffney, B. J.; McConnell, H. M., *Chem. Phys. Lett.*, **1974**, *24*, 310-313.
2. Maret, G.; Dransfeld, K., *Phisica* **1977**, *86-88B*, 1077-1083.
3. Meirovitch, E.; Freed, J. H., *J. Phys. Chem.* **1980**, *84*, 3295-3303.
4. Speyer, J. B.; Sripada, P. K.; Das Gupta, S. K.; Shipley, G. G.; Griffin, R. G., *Biophys. J. Biophys. Soc.* **1987**, *51*, 687-691.
5. Seeling, J.; Borle, F.; Cross, T. A., *Biochim. Biophys. Acta* **1985**, *814*, 195-198.
6. Bragonza, L. F.; Blott, B. H.; Coe, T. J.; Melville, D., *Biochim. Biophys. Acta* **1984**, *801*, 66-75.
7. Helfrich, W., *Phys. Lett.* **1773**, *43A*, 409-410; *Zeit. Naturforsch.*, **1973**, *28C*, 693-703.
8. Tenforde, T. S.; Liburdy, R. P., *J. Theor. Biol.* **1988**, *133*, 385-396.
9. Khan, H. R.; Ozeki, S., *J. Colloid Interface Sci.* **1996**, *177*, 628-632.

10. Ozeki, S.; Kurashima, H.; Miyanaga, M.; Nozawa, C., *Langmuir*, **2000**, *16*, 1478-1480.
11. Ozeki, S.; Kurashima, H.; Abe, H., *J. Phys. Chem. B*, **2000**, *104*, 5657-5660.
12. Kurashima, H.; Abe, H.; Ozeki, S. Molecular Physics, 100, 1445-1450 (2002).
13. Ozeki, S.: Kurashima, H. Encyclopedia of Surfaces and Colloid Science, ed. Arthor Hubbard, Marcel Dekker, Vol.3, 3109-3119, 2002.

Anisotropic Properties of Magnetic Ordered Gel

Isao Yamamoto[1], Syuji Saito[1],Tetsuya Makino[1],
Masuhiro Yamaguchi[1] and Tadashi Takamasu[2]
1 Department of Physics, Yokohama National University,
Tokiwadai, Hodogaya-ku, Yokohama 240-8501, Japan
2 National Institute for Material Science
Sengen, Tsukuba, Ibaraki 305-0047, Japan
(isaoy@ynu.ac.jp)

Abstract

The magnetic ordering, magnetic field effects on the phase transition and some applications are investigated for high polymer gels. Agarose gel formed in strong magnetic fields shows the birefringence which is optical anisotropy as an evidence of magnetic ordering. The melting temperature of the ordered gel has high melting temperature which is correlated to the birefringence. Other isotropic structure of the ordered gel is measured by velocities of DNA electrophoresis and ultrasonic propagation, and a shrinkage in the acetone-water system. The magnetic field induced effects are discussed with anisotropic network structure.

Keywords

magnetic field effect, magnetic ordering, agarose gel, DNA, electrophoresis

1. Introduction

A well known natural gel is agar, whose main component is polysaccharide agarose. The agarose consist many sequence of β-*D*-galactose and 3,6-anhydoro-α-*L*-galactose. The aqueous solution shows a thermo-reversible sol-gel phase transition with a thermal hysteresis. The agarose gel melts to form a solution at elevated temperatures and gelation occurs at room temperature. Agarose is classified into several types according as the melting temperature and the elasticy. A gelation model in the cooling process has been suggested[1)]: a random coil shape of the chains at elevated temperatures changes to α-helix at moderate temperatures. Then, the two helices intertwine to form the double helix. Many double helices are aligned and assembled to form high concentration regions, called domains. Linkages between the domains are generated and progressed to form the gel at the gelation temperature. The transition temperature is about T_g=310K for gelation, and T_m=350K for melting for the typical agarose solution. In addition, the agarose gel indicates the gel-gel volume transition in an acetone-water system: the gel shrinks in high concentration solution. The sieve effect of the agarose gel is used for the supporting medium of the DNA electrophoresis in the field of medicine. In the present paper, physical properties are investigated for the magnetically ordered agarose gel.

2. Experimental

Superconducting magnets (Type SM-5, Sumitomo Heavy Industries Ltd. and Type JMTD-10T100NC-mkII and JMTD-13T100EF3, JASTEC) and a hybrid magnet (NIMS, Tsukuba) were used to apply the magnetic fields. Homogeneity of the field was less than 3% in a space of ±25mm at the center of the magnets. The raw materials used were Agarose type II with a gel strength of 6000-8000kg/m^2 and type L with 4500kg/m^2 supplied by Wako Chemicals. They are a special grade for electrophoresis. The molecular weight was 55×10^3g. The mixture of the agarose powder and distilled water was prepared at various concentrations of up to 4.0wt.% and stirred at room

temperature. Five thermal cycles, heating and cooling, were repeated for homogenization before measurement. The temperature was controlled to form the gel by temperature-controlled water through the water jacket set in the bore of the magnet. The physical properties, melting temperature, birefringence, electrophoretic velocity, elasticity and shrinkage, were measured for the gels formed in strong magnetic fields and zero field.

3. Birefringence

The birefringence was measured optically to investigate the magnetically induced ordering of agarose molecules.[15, 16] The sample gel was prepared in an optical cell with a 10mm path. The birefringence Δn, which was calculated from the extinction angle measured with an accuracy of 0.1deg by the Senarmont method, was observed for 4.0wt.% Agarose-L gel formed in the magnetic fields up to 5T. The averaged value at ten points for each gel was plotted in Fig. 1(a) as a function of the magnetic field exposed. The birefringence was very small but increased lineally with increasing magnetic field exposed below 2T. However, it tended to saturate toward $\Delta n=3\times10^{-7}$ in high magnetic fields above 3T. It is considered that the value of the birefringence is proportional to the amount of the ordered region called domain in the gel. Therefore, the ratio of the magnetic ordered region was increased with increasing the exposed magnetic field. The saturation of the birefringence means that the ordering of the domains were saturated at around 3T. Meanwhile, the concentration dependence of the birefringence was also measured for the gel formed at 5T. In the measurement up to 4.0wt.%, the birefringence was increased linearly with increasing gel concentration up to 2.0wt.% and its gradient was decreased above 3T.[2]

These results were the direct evidence of the magnetic ordering of agarose molecules. The magnetic ordering depended on the strength of the field exposed and the concentration of the gel. According to another optical experiment, the direction of the magnetic ordering of the agarose molecules was determined to be perpendicular to the magnetic fields.

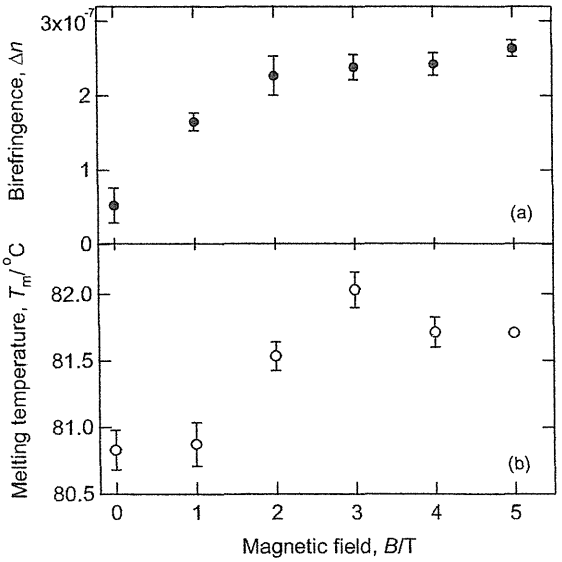

Fig. 1. (a) Birefringence of the 4.0wt.% Agarose II gel formed under the influence of magnetic field up to 5T, and (b) Melting temperature of 0.5wt.% Agarose L gel. Both the magnetic field effects saturated at around 3T.

3. Melting temperature

A hot solution of agarose II was poured into a Pyrex-glass tube with a diameter of 3mm and a length of 50mm. Each sample tube enclosed a stainless-steel made micro-ball with a diameter of 2mm to determine the melting temperature by the ball-dropping method. Then the inlet of the tube was sealed by burner to avoid the change in the concentration and to repeat the measurement. The sample tubes containing the hot solution were set in a water jacket in the bore of the vertical type magnet to control the temperature. Ten samples were placed at the center of the magnet and the other ten 600mm below the center of the magnet, the bottom of the water jacket. When the applied magnetic field was 5T at the center, the field was less than 10mT at the bottom position with no magnetic field. The samples were cooled to form the gel at a rate of –0.3K/min. The twenty samples were taken out of the magnet at zero field at room temperature after gelation. Then the tubes were turned and set into a temperature controllable water bath at room temperature. The increasing rate of the bath temperature was kept at +0.03K When the gel changed to the sol at melting temperature, then the micro-ball dropped, taking about 0.5s. The melting temperature was determined at the moment the micro-ball dropped 20mm from the original position.

Figure 1(b) shows the magnetic field dependence of the melting temperature T_m of the 0.5wt.% agarose gel. The averaged temperature was T_m=80.8C for the reference gel.[3-6] The magnetic-exposed gel melted at T_m=81.8C. An increase in the melting temperature by ΔT_m=+1.0K was observed as the magnetic field effect of B=5T. The melting temperature increased with increasing exposed fields but saturated at around a magnetic field of 3T. The same saturation tendency was observed for the 0.3wt.% agarose gel.[7] The magnetic field effect on the melting temperature was not detected for the 1.4wt.% gel but became large for dilute gels.[3, 10] The results suggest that the gel was stabilized thermally when it was formed in strong magnetic fields.

In comparison with Figs. 1(a) and (b), the same saturation tendencies were recognized in spite of different concentration and different type of the agarose. The correlation coefficient between the birefringence and the melting temperature against the magnetic field was calculated to be 0.85 for 0.5wt.% agarose gel. The highest coefficient of 0.95 was observed for 0.3wt.% gel, but it decreased for high concentrated gels because the change in the melting temperature was not observed above 1.0wt.% by this boll-dropping method.

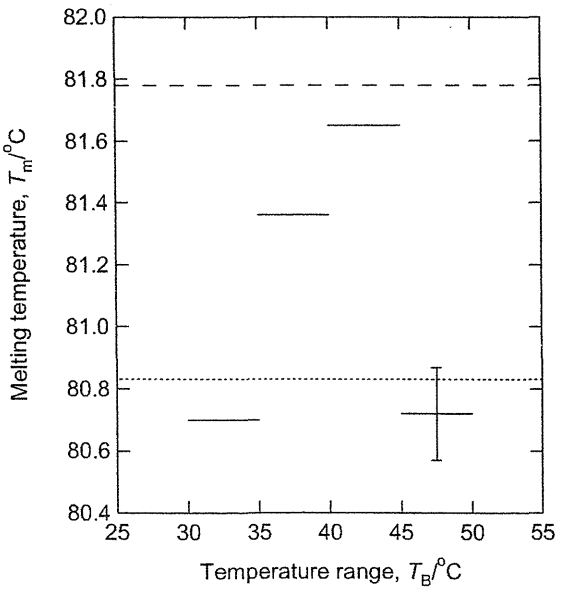

Fig. 2. Melting temperature of 0.5wt.% agarose gel formed in a magnetic field of 5T. The broken and dotted lines denote the melting temperature of the gel formed in constant magnetic fields of 5T and 0T, respectively.

As the next experiment, magnetic fields were applied to investigate which gelation process was influenced to change the melting temperature by the fields. The agarose solution was exposed to a magnetic field of 5T in a limited temperature range in the cooling process, for example, between 45C and 40C. The higher broken line and the lower dotted line in Fig. 2 indicated the melting temperature of the gel formed under the influence of magnetic fields of 5T and 0T, respectively. In the case of the magnetic exposure above 45C, the effect was not observed because of the small $\Delta\chi$ of each random coil. When the solution was exposed to a magnetic field of 5T below 35C, the effect was also not obtained because of strong network interdomains of the gel. The magnetic field effect on the melting temperature of the gel was found for the temperature range between 45C and 35C, especially 45C and 40C. This melting temperature was close to that for 5T as shown by the broken line in Fig. 2 [8,9] At a temperature around 40C, the structure of the solution is considered to be such that the self-oriented domains have a large anisotropic susceptibility but the interdomain linkage has not progressed. Therefore, the domains were easy to rotate by a magnetic field of 5T. The same tendency was observed for 0.3wt.% gel; the most effective zone also appeared at around 40C.[10,11]

Previous papers reported that the phase transition temperature depended on the cooling rate, and the quenched agarose gel indicates low melting temperature.[1] The domain growth process is necessary to give the high melting temperature. Accordingly, it is considered the strong magnetic field helped to generate the crystalline core and/or to grow the crystalline domains.

4. DNA electrophoresis

The network structure of the agarose gel has been applied to DNA electrophoresis. According to the electrophoretic velocity depended on the size, DNAs were separated in the gel as the sieve. The reason is that the submicron size of DNA is almost equal to the vacant size of the gel sieve. If the network structure changes by the exposure to the magnetic field, the velocity of the DNA must be changed because of the change in the sieve size of the gel. The crystalline region was expected to become large due to the results of the increase in the melting temperature. On the other hand, the non-crystalline region has to be decreased to the contrary. Therefore, the increase in the DNA velocity is expected.

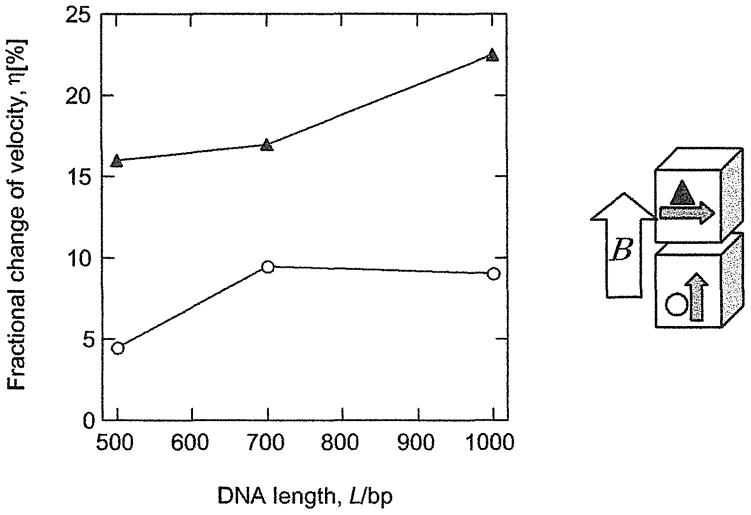

Fig. 3. Change in the electrophoretic velocity of DNA in 2.5wt.% gels along the direction perpendicular (closed triangle) and parallel (open circle) to the exposed field of 10T. The electrophoresis was performed with the voltage of 70V for 60min under zero magnetic field in 2.5wt% Agarose-L gels at 5^0C.

The gels of 2.5wt.% of Agarose-L were formed under the magnetic fields of 10T for the ordered gel and in 0T for the random gel. The ordered gel was cut to two peaces as shown in Fig. 3. The electrophoresis of DNAs (500, 700 and 1000bp) was performed for the three gels in zero magnetic field at the electrophoretic voltage of E=70V for t=60min at T=5C. The electrophoretic velocities along the two directions were compared with that in the random gel.

The change in velocity was observed as shown in Fig. 3. The increase in the velocity by 5-20% was found in the gels formed in the magnetic field of 10T. This magnetic field induced effect along the direction perpendicular to the exposed field was twice compared with that along the other. Both the effects were increased with increasing size of DNA. As a result of the electrophoretic experiment, the vacant of the network in the gel was expanded anisoropically by exposure to magnetic fields.

5. Elasticity

The anisotropic hardness of the gel was expected if the network structure, namely sieve changed anisotropically and/or if the crystalline regions, namely domains ordered each other. The hardness was investigated by measurement of the velocity of one cycle signal of 3.2MHz ultrasonic wave. As our expectation, the ultrasonic wave propagated fast in the ordered gel with different velocity depended on the direction. Fig. 4 explains the gel concentration dependence of the elasticy. Where the storage modulus m' means the elasticy, that is, hardness. The elasticy was proportional to the gel concentration below 3.0wt.%, however, tended to saturate in high concentration regions for all the gels. This results suggest that the linkage density was proportional to the gel concentration below 3.0wt.% and at the high concentration the linkage among the agarose molecules is controlled. It seems the important information that the elasticity of the random gel took the medium value between the anisotropic ones of the ordered gel. The linkage density was not influenced on the whole by exposure to strong magnetic field but changed to anisotropic linkage structure.

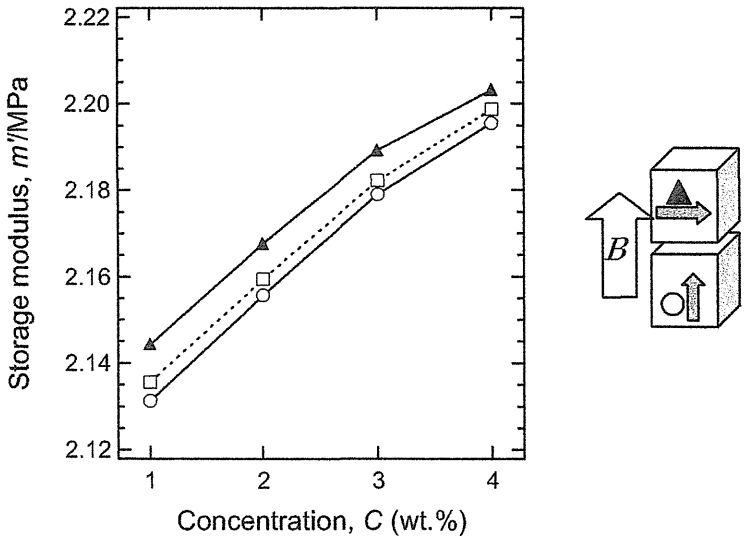

Fig. 4. Storage modulus m' as a function of the gel concentration up to 4wt.% Agarose-L gels at 12^{0}C. The broken and solid curves denote the m' for the random gel (open square) formed in 0T and ordered gel formed in 13T, respectively. The m' were measured along perpendicular (closed triangle) and vertical (open circle) directions to the field exposed.

6. Shrinkage

The agarose gel shows a volume transition in the acetone-water system. In the present experiment, the volume transition was measured for 4.0wt.% Agarose-L gel formed in the magnetic fields of 10T to get another evidence of the anisotropic change in the network structure. The gel was prepared in capillary tubes with diameter of 1.0mm and length of 50mm, and the tubes were situated parallel or perpendicular to the magnetic field of 10T. The length of gel was measured along the two axes as a function of acetone concentration at zero field at room temperature.

The length decreased with increasing acetone concentration for both gels, and remarkable shrink was observed at a concentration of 70wt.%-acetone, as shown in Fig. 5. Both shrink ratios were saturated at around 80wt.%. The length of the gels after the shrinking was differed from each other: the lengths parallel and perpendicular to the magnetic field were observed to be 92% and 94%, respectively. It is considered that this anisotropic shrinkage occurs in the structure of the anisotropic network rather than in the anisotropic structure of the domain region of the gel. The elastic measurements using an ultrasonic wave indicated anisotropic increase in the elasticy in the gel and the hard direction was perpendicular to the magnetic field exposed. The high elastic direction agreed with the shrinkable axis from the point of view of the hardness.

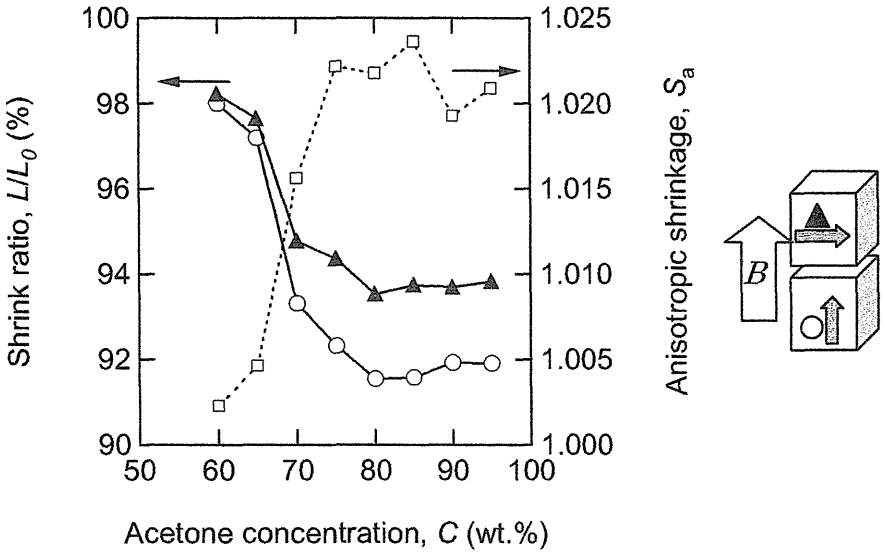

Fig. 5. Anisotropic shrinkage of 4.0wt.% agarose-L gel in acetone-water system at 293K. Open and closed symbols on the solid curves denote the normalized lengths parallel and perpendicular to the exposed magnetic field of 10T, respectively. The broken curve corresponds the ratio of the two directions defined as $S_a=L_{//}/L_{\perp}$.

6. Conclusions

The magnetic field induced changes in the structure of the agarose gel were measured. The increase in the melting temperature indicated the growth of the crystalline region. The optical measurement showed the molecular ordering occurred under the magnetic field in particular temperature range. The evidences of the anisotropic structure of the magnetically ordered gel were observed. The increase in the electrophoretic velocity of DNA indicated the roughen sieve structure. The elastic propagation measurement shows the anisotropic storage modulus. Both the anisotropic velocity of DNA and ultrasonic exhibited the anisotropic change in the linkage structure. The shrinkage measured in acetone-water system also showed the anisotropic linkage structure. The agarose molecules were ordered perpendicular to the magnetic field and its direction agreed with the roughen sieve, harden linkage, and less-shrinkable direction.

Acknowledgements

This work was supported by Grant-in-Aid for Scientific Research for Priority Areas (No.15085204, Area 767) from MEXT of Japan.

References

[1] A. Hayashi, K. Kinishita and A. Yasueda, Polymer J., 12, 447 (1980).
[2] T. Usui, T. Fushimi, K. Nomoto, I. Yamamoto and M. Yamaguchi, TML Annual Rept.2002 Suppl. II, 167 (2003).
[3] I. Yamamoto, Y. Matsumoto, M. Yamaguchi, Y. Shimazu and F. Ishikawa, Physica B, 246-247, 408 (1998).
[4] M. Yamaguchi and I. Yamamoto, in Jikikagaku (S. Ozeki, Y. Tanimoto and M. Yamaguch, eds.), Ipc Inc., Tokyo (2002), Chapt. 5 (in Japanese).
[5] Y. Matsumoto, I. Yamamoto and M. Yamaguchi, The Papers of Technical Meeting on Magnetics, IEE Japan, MAG-97-35 (1997) (in Japanese).
[6] I. Yamamoto, Y. Matsumoto, M. Yamaguchi, F. Ishikawa and Y. Shimazu, J. Jpn. Biomagnetism and Bioelectromagnetics Soc., 18, 130 (1997) (in Japanese).
[7] Y. Matsumoto, I. Yamamoto, M. Yamaguchi, Jpn. J. Appl. Phys. 36/10B, L1397 (1997).
[8] T. Kato, M. Yokoyama and A. Takahashi, Colloid and Polymer Sci., 256, 15 (1978).
[9] I. Yamamoto, O. Tsubouchi, M. Yamaguchi, F. Ishikawa and Y. Shimazu, J. Jpn. Biomagnetism and Bioelectromagnetics Soc., 11, 158 (1998) (in Japanese).
[10] M. Yamaguchi, O. Tsubouti and I. Yamamoto, Proc. 2nd Symp. New Magneto-science '98, 121 (1999) (in Japanese).
[11] I. Yamamoto, O. Tsubouchi, M. Yamaguchi, Y. Shimazu and F. Ishikawa J. Jpn. Biomagnetism and Bioelectromagnetics Soc., 11, 196 (1999) (in Japanese).

Magnetic Field Effect on Morphology of Photochemical Products from a Gaseous Mixture of Trimethylsilylacetylene and Iron Pentacarbonyl

Hiroshi Morita[1,2], Yoshinori Okano[1], and Hidetoshi Tonooka[2]
1 Department of Information and Image Sciences, Faculty of Engineering
Chiba University, Yayoi-cho, Inage-ku, Chiba 263-8522, Japan
2 Graduate School of Science and Technology, Chiba University
Yayoi-cho, Inage-ku, Chiba 263-8522, Japan
(hmorita@faculty.chiba-u.jp)

Abstract

Under UV light irradiation with a medium pressure mercury lamp, a gaseous mixture of iron pentacarbonyl and trimethylsilylacetylene produced a film and/or sedimentary aerosol particles depending on the strength of applied magnetic field. In the absence of a magnetic field, a thin film was formed as a photochemical product of the gaseous mixture, but the morphology of the deposit has changed into sedimentary aerosol particles in the presence of a magnetic field of 3 T. This is the first observation of magnetic field effect on morphological change of the photochemical product deposited from gaseous mixtures.

Key words

magnetic field effect, morphology, photochemical product, trimethylsilylacetylene, iron pentacarbonyl

1. Introduction

Ultrafine and nanometer-size metal particles can be used as a building block of nano-wires and nanometer-size devices in nano-fabrication. Synthesis of metal nanoparticles in the vapor phase has been done successfully by irradiating IR laser light on gaseous iron pentacarbonyl ($Fe(CO)_5$) sensitized by SF_6, resulting in the production of nanoparticles of metal iron with a size of ~10 nm.[1] Under light irradiation with a medium pressure mercury lamp at 313 nm, pure $Fe(CO)_5$ vapor did not produce aerosol particles but produced crystalline ragged deposits with sizes of 20 and 4 μm.[2] Ultrafine and nanoparticles can be produced from gaseous mixtures using photochemical reactions of organic molecules such as acrolein[3] and carbon disulfide (CS_2).[4] Actually, a gaseous mixture of $Fe(CO)_5$ and CS_2 produced spherical aerosol particles with a mean diameter of 0.6 μm under UV light irradiation at 313 nm.[2]

$Fe(CO)_5$ molecules, when excited by UV light, can also react with some organosilicon compounds such as allyltrimethylsilane (ATMeSi). A gaseous mixture of $Fe(CO)_5$ and ATMeSi produced a small amount of sedimentary aerosol particles (with a mean diameter of 0.5 μm) in addition to crystalline-like deposits with a size of ~5 μm.[5] In the present paper, photochemical reaction between $Fe(CO)_5$ and trimethylsilylacetylene (TMeSiA) was studied. The gaseous mixture of $Fe(CO)_5$ and TMeSiA produced a film and/or sedimentary aerosol particles depending on the strength of the external magnetic field. Magnetic field effect on morphology of the deposits from gaseous mixtures has been studied in a helium-free superconducting magnet.

2. Experimental

$Fe(CO)_5$ (Kanto, 95%) and TMeSiA (Tokyo Kasei, G. R. grade) were degassed by freeze-pump-thaw cycles and purified by vacuum distillation immediately before use. Each vapor was introduced successively into a cross-shaped Pyrex cell having a long (length 160 mm, inner diameter (ID) 35 mm) and short (length 80 mm, ID 20 mm) arms equipped with a couple of quartz and KBr windows or into a cylindrical Pyrex cell (length 160 mm, ID 35 mm, volume 154 cm^3; or length 160 mm, ID 20 mm, volume 50 cm^3) through a vacuum line equipped with a capacitance manometer (Edwards Barocel Type 600). The background pressure of the irradiation cell was 8×10^{-5} Torr (1 Torr = 133.3 Pa). Gaseous samples were irradiated with a medium pressure mercury lamp (Ushio UM-452, 450 W) through a UV29 (or UV31) and a UVD33S filters. The exposure light at 313 nm can excite only $Fe(CO)_5$ molecules.

Monitor (He-Ne laser) light intensity scattered by the aerosol particles formed in the cell under UV light irradiation was measured through a Y-52 filter with a combination of a photomultiplier tube (EMI 6256S) and a lock-in amplifier (SRS SR-530). FT-IR spectra of a gaseous mixture of TMeSiA and $Fe(CO)_5$ and of pure gaseous $Fe(CO)_5$ before and after UV light irradiation were measured with a Nicolet NEXAS 470 FT-IR spectrometer. The depletion of TMeSiA and $Fe(CO)_5$ was followed using diagnostic bands at 1259 cm^{-1} for TMeSiA, and 2038 and 645 cm^{-1} for $Fe(CO)_5$. FT-IR spectra of deposits in KBr pellets were also measured with a Nicolet NEXAS 470 FT-IR spectrometer. SEM images of deposits were taken with a JEOL JSM 6060 scanning electron microscope. Thin films were also produced from the gaseous mixture in a helium-free superconducting magnet (Toshiba TM-5SP) to study the magnetic field effect on the chemical processes.

3. Results and Discussion

Under UV light irradiation at 313 nm with a mercury lamp for 1 h, pure $Fe(CO)_5$ vapor (1 Torr) produced crystalline-like ragged deposits with sizes of ca. 20 and 4 μm,[2] whereas a gaseous mixture of $Fe(CO)_5$ (2.5 Torr) and TMeSiA (19 Torr) produced a thin film of brownish yellow color. To investigate film formation processes, monitor (He-Ne laser) light intensity scattered by the aerosol

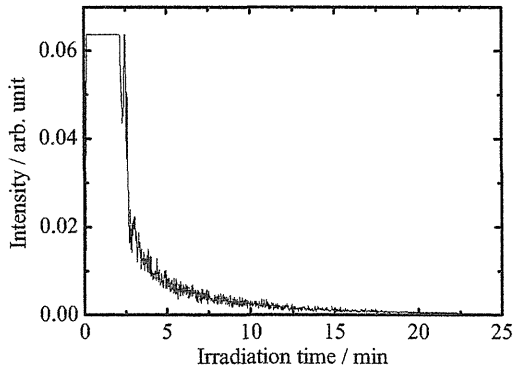

Fig. 1. He-Ne laser light intensity scattered by the aerosol particles produced from a gaseous mixture of $Fe(CO)_5$ (2.5 Torr) and TMeSiA (19 Torr) under light irradiation at 313 nm.

particles as formed under light irradiation at 313 nm was measured. The result is shown in Fig. 1. Scattered light was detected during the first 20 min, indicating that sedimentary aerosol particles contributed to the initial phase of film formation and after prolonged light irradiation, chemical reaction of molecules adsorbed on the substrate became dominant. To study irradiation time dependence of morphology of the deposited product, SEM images were taken on the deposits produced under light irradiation for 1 and 5 min. The results are shown in Fig. 2. The product deposited under light irradiation only for 1 min has already formed a thin film from deposited particles. Under light irradiation for 5 min, the film surface became more dense and uniform.

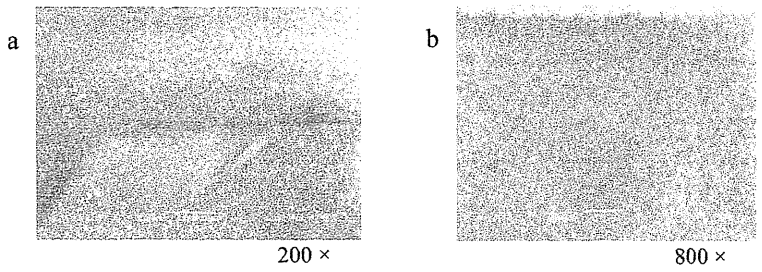

Fig. 2. SEM images of photochemical product from a gaseous mixture of $Fe(CO)_5$ (2.5 Torr) and TMeSiA (19 Torr) under light irradiation at 313 nm for (a) 1 and (b) 5 min.

The depletion of gaseous molecules due to photochemical reactions was evaluated from the intensity change of FT-IR bands. The spectra of a gaseous mixture of $Fe(CO)_5$ (2.5 Torr) and TMeSiA (19 Torr) are shown in Fig. 3. For the gaseous mixture, depletion of TMeSiA after 2 min light irradiation was evaluated to be 0.69 Torr from the intensity change of $\delta(Si\text{-}CH_3)$ band at 1259 cm^{-1}, and the one of $Fe(CO)_5$, to be 0.71 Torr from that of $\nu(C\equiv O)$ band at 2038 cm^{-1}. The molar ratio of depleted molecules was nearly 1:1 during 2 min light irradiation, suggesting that equal numbers of $Fe(CO)_5$ and TMeSiA molecules were incorporated into the photochemical processes.

Chemical structure of the deposited film was investigated from FT-IR spectrum. FT-IR spectrum of the film deposited from a gaseous mixture of $Fe(CO)_5$ (2.5 Torr) and TMeSiA (19 Torr) under

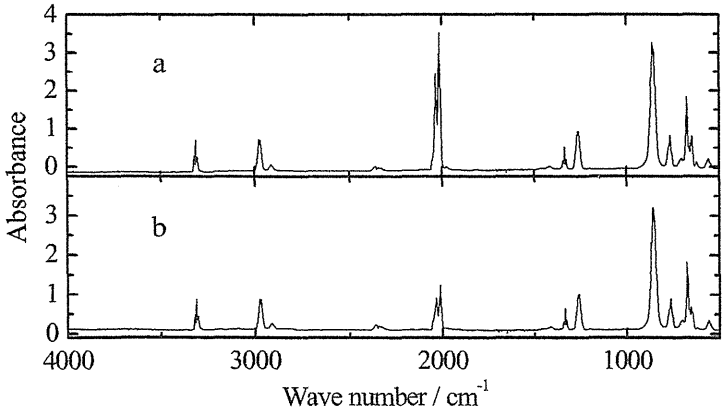

Fig. 3. FT-IR spectra of a gaseous mixture of $Fe(CO)_5$ (2.5 Torr) and TMeSiA (19 Torr) under light irradiation at 313 nm for (a) 0 and (b) 12.5 min.

light irradiation for 5 min is shown in Fig. 4, compared with the spectrum of the product deposited from pure $Fe(CO)_5$ vapor. In contrast to the spectrum of deposits from pure $Fe(CO)_5$, 1829 cm^{-1} band ascribed to ν (>C=O) band bridging two Fe atoms disappeared, although ν(-C≡O) band of $Fe(CO)_5$ in ~2000 cm^{-1} region still strongly appeared. The characteristic band assigned to C≡C bond of TMeSiA also disappeared, although strong bands characteristic of trimethylsilyl group was observed at 1250 and 837 cm^{-1}. Besides these bands, a medium band assignable to ν(C=C) band was observed at 1604 cm^{-1}. These results indicated that excited $Fe(CO)_5$ molecule evolved one CO group and resulting $Fe(CO)_4$ interacted with C≡C bond of TMeSiA to initiate polymerization reaction of TMeSiA.

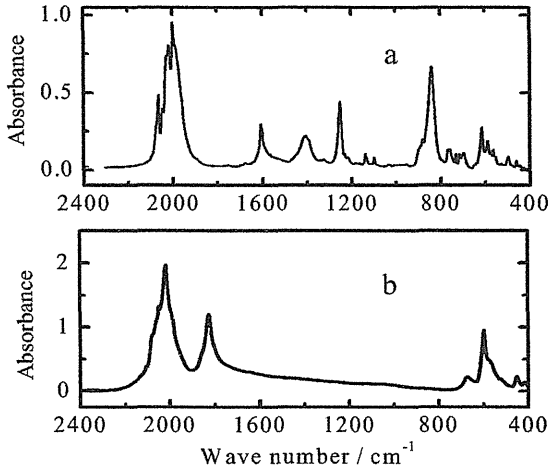

Fig. 4. FT-IR spectra of deposits from (a) a gaseous mixture of $Fe(CO)_5$ (2.5 Torr) and TMeSiA (19 Torr) and (b) pure $Fe(CO)_5$ vapor (1 Torr) under light irradiation at 313 nm.

To investigate magnetic field effect on film formation process, photochemical reactions between $Fe(CO)_5$ and TMeSiA took place in the presence of a magnetic field of up to 5 T in a helium free superconducting magnet. In the presence of a magnetic field of 3 T, a gaseous mixture of $Fe(CO)_5$ (2.5 Torr) and TMeSiA (19 Torr) produced only sedimentary aerosol particles under light irradiation for 5 min (Fig. 5a). Under light irradiation for 15 min and for longer time, we could not detect any particles but a film as the final product. Under a magnetic field of 5 T, the gaseous mixture produced a non-uniform film-like deposit under light irradiation for 5 min (Fig. 5b). The deposited film had many small holes inside the entire deposited material. The morphological change of the photochem-

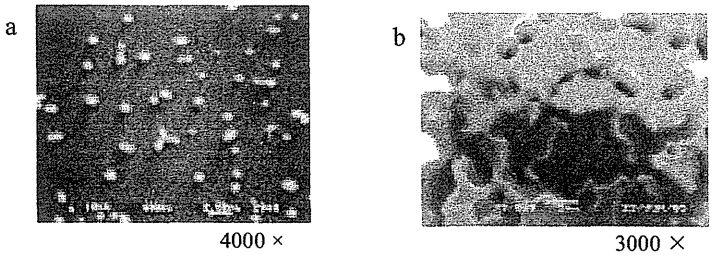

Fig. 5. SEM images of photochemical products deposited from a gaseous mixture of $Fe(CO)_5$ (2.5 Torr) and TMeSiA (19 Torr) under light irradiation at 313 nm for 5 min in the presence of a magnetic field of (a) 3 and (b) 5 T.

ical products under the magnetic field clearly shows that the photochemical reactions in the gas phase and on the surface of the substrate were influenced by the application of a magnetic field.

4. Conclusions

The magnetic field influenced the chemical reaction between $Fe(CO)_5$ and TMeSiA and resulted in the change in morphology of the photochemical products. This is the first observation of the magnetic field effect on morphological change of photochemical products from gaseous mixtures.

Acknowledgements

This work was supported by Grant-in-Aid for Scientific Research on Priority Area "Innovative utilization of strong magnetic fields" (Area 767, No. 15085203) from MEXT of Japan.

References

[1] R. Fajgar, Z. Bastl, J. Šubrt, K. Vacek, and J. Pola, Phys. Chem. Chem. Phys. 5 (2003) 3789.
[2] H. Morita, H. Okamura, and H. Ishikawa, Proceedings of the 7th Meeting on New Maneto-science (2003) pp.263-266.
[3] H. Morita and M. Shimizu, J. Phys. Chem. 99 (1995) 7621.
[4] H. Morita and K. Kanazawa, J. Photochem. Photobiol. A:Chem. 112 (1998) 81.
[5] H. Morita and H. Ishikura, J. Photopolym. Sci. Technol. 18 (2005) 193.

The Role of Water Molecules and Hydrogen Bonds on Magnetic Alignments Observed for Popular Diamagnetic Crystals Including Hexagonal Ice

Takaaki Abe[1], Ryoichi Takashima[1] and Chiaki Uyeda[1]
1 Department of Earth and Space Science, Osaka University, Machikaneyama-cho, Toyonaka-shi, Osaka, 560-0043, Japan
(taka@ess.sci.osaka-u.ac.jp)

Abstract

The relationship between diamagnetic anisotropy $(\Delta\chi)_{DIA}$ and the directions of water molecules or hydrogen bond in the crystal structures are discussed based on the published $(\Delta\chi)_{DIA}$ data of KDP, ADP, gypsum, free water molecule and hexagonal ice (I_h). Anisotropy is attributed to the direction of individual hydrogen bond in the crystal; the bond direction is the magnetically unstable axis. $(\Delta\chi)_{DIA}$ of ice I_h was 2.9×10^{-10} emu/g according to $(\Delta\chi)_{DIA}$ - T relationship observed between T = 190 K and 250 K. Theoretical $(\Delta\chi)_{DIA}$ is zero for ice I_h, since the directions of the O-H bonds are distributed symmetrically in its crystal structure.

Keywords

diamagnetic anisotropy, hydrogen bond, magnetic alignment, hexagonal ice, KDP, gypsum

1. Introduction

Water molecules and hydrogen bonds are often included in both organic and inorganic materials. The configurations of hydrogen bonds in the material are essential in considering the origin of magnetic alignment; the alignment is observed recently in various diamagnetic materials. [1] This is because the anisotropy of spatial distribution of localized electrons in the material is the major origin of diamagnetic anisotropy $(\Delta\chi)_{DIA}$, which is the cause of the alignment.

$(\Delta\chi)_{DIA}$ data were obtained recently for KDP, ADP and gypsum. [2] The origin of $(\Delta\chi)_{DIA}$ was analyzed consistently by assigning a constant uniaxial $(\Delta\chi)_{DIA}$ tensor to the individual hydrogen bond. Similar analysis was successfully performed on a T-O bond of tetrahedral [TO_4] units and a M-O bond of octahedral [MO_6] units. [3] Many of the inorganic oxides are expected to possess a $(\Delta\chi)_{DIA}$ value that is larger than 10^{-9} emu/g, since these bonds are the major types of chemical bonds which compose inorganic oxides.

Quantitative analysis on the magnetic alignment observed for small particles due to the

magnetic anisotropy $\Delta\chi$ are not popularly done at present. It is deduced from a well known theory proposed by Langevin and Curie that the minimum field intensity required to achieve alignment of the particles is determined by 3 parameters, namely $\Delta\chi$ and weight of the particle M, and the temperature of the dispersing medium T. Hence, alignments of micron-sized particles, including materials composed of the hydrogen bonds, are expected to occur below 1 Tesla at room temperature for various diamagnetic materials, since published values of their diamagnetic anisotropy $(\Delta\chi)_{DIA}$ usually exceed 10^{-9} emu/g.

$(\Delta\chi)_{DIA}$ value reported previously for hexagonal ice (I_h) was 3.3×10^{-9} emu/g [4], which was small compared to typical inorganic materials. It was concluded then that the small $(\Delta\chi)_{DIA}$ value derived from the high crystal symmetry of ice I_h. Indeed, no diamagnetic anisotropy is exist for ice I_h according to the above mentioned model, since the tetrahedral units in the crystals structure hold regular symmetry and the $\Delta\chi_{OH}$ tensors in a unit cell are expected to cancel out. The $(\Delta\chi)_{DIA}$ value of hexagonal ice is examined in the present work using a high-sensitivity method, which is based on a field-induced harmonic oscillation of the crystal. [5]

2. Experimental

Temperature dependence of $\Delta\chi$ was measured for ice I_h in the range of T = 190 K and 250 K to clarify the contribution of paramagnetic anisotropy $(\Delta\chi)_{PARA}$. The published $(\Delta\chi)_{DIA}$ value of ice I_h was considerably small, which can be easily disturbed by $(\Delta\chi)_{PARA}$ caused by a small amount of impurity ions. A sectional view of the apparatus used in the $\Delta\chi$ - T measurement is shown in Fig. 1.

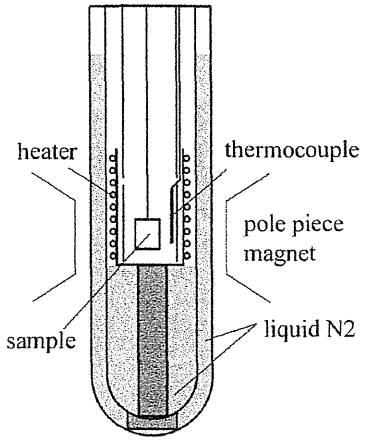

Fig. 1. Apparatus for $\Delta\chi$ - T measurement in the low temperature region

Single crystal of ice I_h was produced from high-purity water in the laboratory. The growth rate of the sample ice I_h was about 1 cm a day in the direction of c-axis at 263 K. The concentration of impurity including paramagnetic ions was below the detection limit. The sample (0.9 cm × 1.19 cm × 1.04 cm) was suspended inside a copper sample cell filled with N_2 gas. The temperature of the sample was reduced using liquid N_2 as freezing medium, which was filled in Dewar vessels surrounding the sample cell. A temperature controller adjusted the current intensity supplied to the heater coil placed around the sample cell, in order that the setting temperature coincided with the temperature measured by a thermocouple set near the sample. $\Delta\chi$ could be measured in a temperature range of $T = 340$ K to $T = 80$ K with the accuracy of ±0.2 K.

A thin fiber suspended the ice single-crystals in a horizontal magnetic field; the direction of magnetically stable and unstable axes may rotate in the horizontal plane. The unstable axis is identical to the c-axis and the stable axis took an arbitrary direction in the c-plane in the case of ice I_h. The direction of stable axis of the crystal show rotational harmonic oscillation with respect to $\boldsymbol{B}$ which follows the equation described as

$$I\,(d^2\Theta/\,dt^2) = -B^2 M\Delta\chi\Theta, \qquad (1)$$

provided that the restoration torque of the fiber suspending the sample is negligible compared to the field induced anisotropy energy; Θ denote the angle of the stable axis with respect to $\boldsymbol{B}$. A PET string of 13.5 μm in diameter was used as the fiber in order to fulfill the above mentioned condition. It is deduced from eq. (1) that $\Delta\chi$ is obtained from the gradient of the proportional τ^{-1} - B relationship, $\tau^{-1} = 2\pi(I/M\Delta\chi)^{1/2} B$, without the effect of the restoration force of the fiber. $\Delta\chi$ values of the level of 1×10^{-9} emu/g were obtained from mm-sized samples in terms of this method.

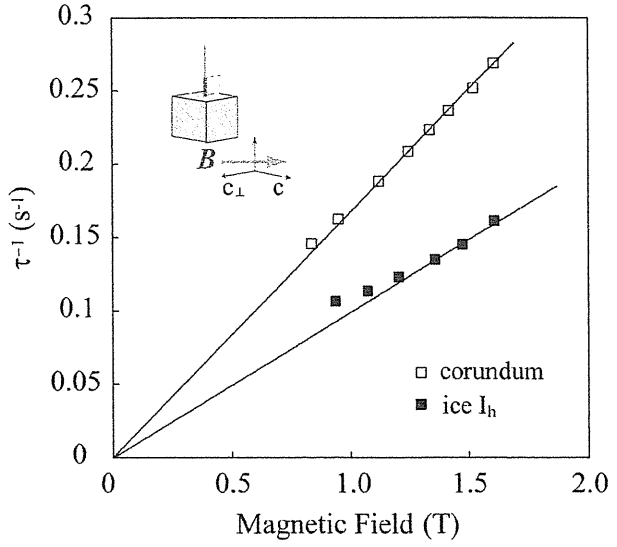

Fig. 2. $\tau^{-1} - B$ relationship measured for ice I_h at $T = 196$ K. I/M of ice I_h was 0.10 cm^2

3. Results

A example of $\tau^{-1} - B$ relationship measured for ice I_h at $T = 196$ K is shown in Fig. 2. It is seen that the period of rotational oscillation τ^{-1} is proportional to B in the high field conditions. The $\Delta\chi$ value obtained from the gradient of the proportional $\tau^{-1} - B$ relationship is 3.9×10^{-10} emu/g; a small $\Delta\chi$ value of the level of 10^{-10} emu/g was detected for the first time using the method of the above mentioned harmonic oscillation. It is noted that the data point of measured $\tau^{-1} - B$ relationship deviate from the proportional line below 1.2T; which is caused by the restoration torque of the fiber mentioned before. The deviation occurs at lower field intensity for a corundum sample which has a similar weight but a larger $(\Delta\chi)_{DIA}$ value of 1.0×10^{-10} emu/g. Accordingly, the data shown in Fig. 2 indicate that $\Delta\chi$ values smaller than that of ice I_h may not be detected by the present method.

Measured $\Delta\chi$ - T relationship of ice I_h is shown in Fig. 3. No evidence of temperature dependence due to paramagnetic anisotropy, following the Curie's law, was detected from the data; $\Delta\chi$ value was almost constant with respect to temperature. $(\Delta\chi)_{DIA}$ value of ice I_h was distributed from 2.7×10^{-10} emu/g to 3.9×10^{-10} emu/g in the range of $T = 190$ K to 250 K (the average of the $\Delta\chi$ values was 2.9×10^{-10} emu/g). This value was about 12 % of the above mentioned published value.

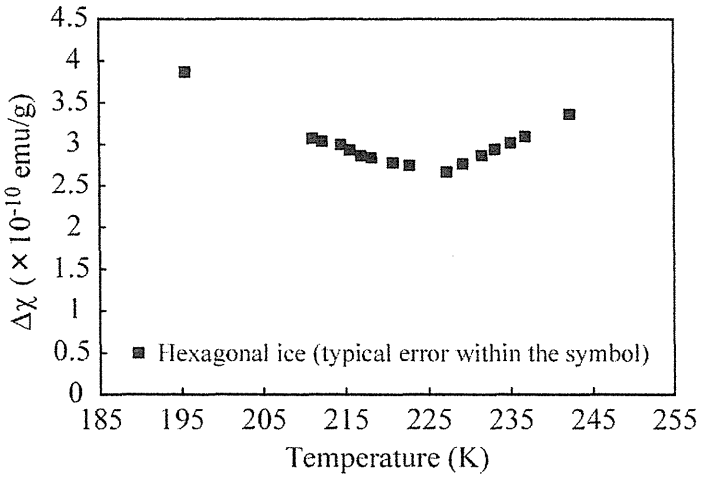

Fig. 3. Measured $\Delta\chi$ - T relationship of ice I_h

$\Delta\chi$ - T relationship of Fig. 3 had a minimum value at about $T = 230$ K. This pattern of $(\Delta\chi)_{DIA}$ variation with respect to temperature is similar to that of the c/a ratio of the lattice constant reported previously. [6] $\Delta\chi$ values at lower temperature regions are required since the temperature dependence of c/a ratios are measured down to $T = 10$ K

4. Discussions

As mentioned before, the origin of measured $(\Delta\chi)_{DIA}$ values was discussed recently for various inorganic oxides, α-quartz, apophylite, orthoclase, gypsum, KDP, ADP, hexagonal ice, free water molecule, corundum and $Mg(OH)_2$, $Al(OH)_3$ and AlOOH. [3] The published $(\Delta\chi)_{DIA}$ values were explained quantitatively by assigning a constant amount of uniaxial $(\Delta\chi)_{DIA}$ tensor to the individual bonds. Proportional relations ships between measured and calculated $(\Delta\chi)_{DIA}$ values were examined separately as shown in Fig. 4 for 3 types of chemical bonds, namely the hydrogen bond, a T-O bond of tetrahedral $[TO_4]$ units and a M-O bond of octahedral $[MO_6]$ units. The linear correlations seen in the figure indicate that the measured $(\Delta\chi)_{DIA}$ derive mainly from the anisotropy of individual chemical bond. The $(\Delta\chi)_{DIA}$ value of a single bond is determined from the gradient of each proportional line. It is also concluded from the relationship that the bond direction is the magnetically unstable axis.

The numerical data listed in Table 1 were used in the analysis of hydrogen bond. The origin of $(\Delta\chi)_{DIA}$ assigned to a single hydrogen bond, namely $\Delta\chi_{OH} = -3.7\times10^{-30}$ emu, is understood qualitatively by assuming that the spatial electron distribution is spread preferentially in the direction perpendicular to the bond direction. This situation is compatible with the covalent characteristics frequently discussed for the hydrogen bonds. [2] Quantitative evaluation of the $(\Delta\chi)_{DIA}$ value of a O-H bond should be carried out on basis of the spatial distribution determined from the molecular orbital of a hydrogen bond. It was deduced from Fig. 4 that the effective spatial anisotropy of the O-H bonds are similar among the measure materials although the nature of the hydrogen bonds are different in each. The position of the proton is localized in the case of gypsum, while the proton sites are in a resonant site between two potential minima in the case of KDP and ADP.

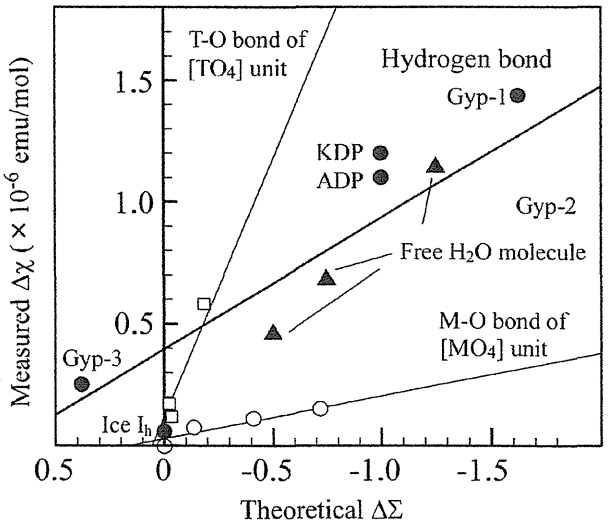

Fig. 4. Comparison between measured and calculated values of diamagnetic anisotropy. Configurations of the principle axes are listed in Table 1 for each data points. [2]

Table 1. Diamagnetic anisotropy of inorganic oxides composed of hydrogen bonds.

Material	Principle axis	$(\Delta\chi)_{DIA}$ [$\times 10^{-9}$ emu/g]	Magnetically stable axis
ADP	[a-c]	11±0.5	a-axis
Gypsum	[χ_1-χ_2]	9.6±0.2	
	[χ_1-χ_3]	7.0±0.1	$\chi_1 > \chi_2 > \chi_3$
	[χ_3-χ_2]	2.2±0.1	
KDP	[a-c]	8.3±0.3	a-axis
Ice I_h	[c-a]	0.29	$c_\perp$-axis

It is deduced from Fig. 4 and 5 that the geometrical configurations of water molecules or hydrogen bonds in a solid material are related directly to the potential of magnetic alignment expected for the material. Magnetic alignment of solid materials composed of hydrogen bonds has been reported recently on various materials; from biological textures to ceramic materials such as clay mineral grains. In the case of KDP(KH_2PO_4) and ADP($NH_4H_2PO_4$), for example, the O-H bonds lie in the c-plane of the tetrahedral crystal structure; the crystal tend to rotate so as to align the c-axis in a direction parallel to the field. As for gypsum, the H_2O molecular planes are nearly parallel to the (001) plane; accordingly the c-plane of the crystal tend to align perpendicular to the field. The anisotropy of spatial electron distribution other than the O-H bonds were negligibly small for these crystals. [2] It is hence effective to choose a solid material which has a high degree of preferential alignment of hydrogen bonds in the material, in order to obtain high efficiency of magnetic alignment in the course of a material processing.

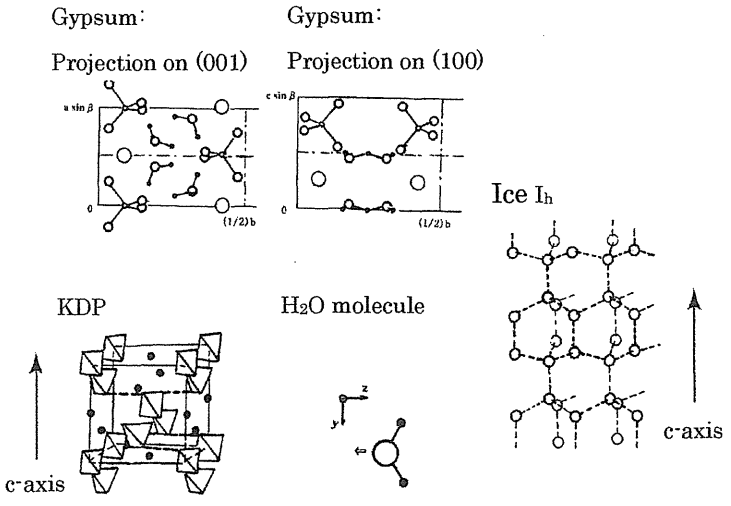

Fig. 5. Crystal structures of oxide crystals composed of hydrogen bond.
O-H bonds are shown by broken lines. (from Ref. [2])

$(\Delta\chi)_{DIA}$ should be zero for hexagonal ice according to the above mentioned model, since the tetrahedral units in the crystal hold regular symmetry and the direction cosines of the bond direction are in an isotropic configuration. Accordingly the $\Delta\chi_{OH}$ tensors in a unit cell cancel out. The variation of the above mentioned c/a ratios of the lattice constant due to temperature may cause a slight deviation of the configuration of the four $\Delta\chi_{OH}$ in the tetrahedral unit from regular symmetry (see Fig. 5). The summation of the $\Delta\chi_{OH}$ tensors over the unit cell may not cancel out due to this deviation, which may be the cause of the measured $(\Delta\chi)_{DIA}$ of ice I_h $(\Delta\chi)_{DIA}$ - T data down to 10 K is required as mentioned before, in order to evaluate the correlation between the temperature dependence of c/a ratios show a intrinsic temperature dependence down to 10 K; the $(\Delta\chi)_{DIA}$ - T measurement is necessary to confirm whether the temperature dependence of $\Delta\chi$ has definite correlation with that of the a/c ratio.

In conclusion, water molecules as well as hydrogen bonds contained in a solid material originate the potential to cause anisotropy energy in the presence of magnetic field, which may be the cause of various magnetic effects of the bulk material. The origin of various magnetic effects presently discussed on liquid water may be reconsidered in this sense; a very small deviation of the isotropic configuration of the molecules in the material, as discussed for hexagonal ice, can the origin of field-induced anisotropy energy.

References

[1] for example, Proc. Intern. *Symp New Magneto-Sic.* (Jpn. Sci. Tec. Corp., NIMS 1999)

[2] C. Uyeda, K. Ohtawa, K. Okita and N. Uyeda, Jpn. J. Appl. Phys. **39** (2000) L890-893

[3] C. Uyeda, R. Takashima, and K. Tanaka, Appl. Phys. Lett. **86**, 094103 (2005)

[4] K. Lonsdale, Nature **164**, 101 (1949)

[5] C. Uyeda, Jpn. J. Appl. Phys. **32** (1993) L268-270

[6] K. Röttger, A. Endriss and J Ihringer, Acta Cryst. (1994) **B50**, 644-648

Two-dimensional Triangle-lattice Alignments by Feeble Magnetic Particles under High Magnetic Field

Tsutomu Ando[1], Noriyuki Hirota[2], Akira Satoh[3], Eric Beaugnon[4], Hitoshi Wada[1]
1 *Department of Advanced Materials Science, The University of Tokyo, Kashiwanoha, Kashiwa, Chiba 277-8561, Japan*
2 *Tsukuba Magnet Laboratory, National Institute for Materials Science, Sakura, Tsukuba, Ibaraki 305-0003, Japan*
3 *Department of Machine Intelligence and Systems Engineering, Akita Prefectural University, Tsuchiya-aza, Honjyo, Akita 015-0055, Japan*
4 *Consortium de Recherches pour L'Émergence de Technologies Avancées (CRETA), Centre National de la Recherche Scientifique, Grenoble 38042, France*
(tando@k.u-tokyo.ac.jp)

Abstract
Using a two-dimensional closed vessel filled with an aqueous solution, we present triangle-lattice alignments with some spacing formed by interactions among magnetic dipoles induced in feeble magnetic substances under high magnetic fields. We conducted an experiment and a numerical simulation using Au particles with a 1 mm diameter dispersed in a $MnCl_2$ aqueous solution and compared their configurations quantitatively. We verified that the interaction among induced magnetic dipoles is a significant force that governs the structure formed by feeble magnetic substances under high magnetic fields.

Keywords
feeble magnetic materials, induced magnetic dipoles, triangle-lattice alignment, molecular dynamics simulation

1. Introduction

In recent years, a high magnetic field with several Tesla can be generated using superconducting magnets, so that significant effects on para- and diamagnetic substances, namely, feeble magnetic substances caused by such magnetic field are recognized [1-4]. These effects are mainly based on interactions between fields and feeble magnetic substances. In a series of studies using high magnetic fields, however, Takayama *et al.* [5] observed interactions acting among magnetic dipoles induced in feeble substances and triangle-lattice alignments with some spacing formed by them in the air-liquid surface without friction. Since almost all the materials on the earth are feeble magnetic substances, these results suggest that high magnetic fields make it possible to arrange substances and to control the internal structure of a substance. Therefore, the application of the interaction among the induced magnetic dipoles under high fields is expected to contribute to various aspects of material processing, for example, a structural control of colloidal and photonic crystals, and so forth.

In the present study, we investigate the two-dimensional triangle-lattice alignments with some spacing by means of an experiment and a numerical simulation. First, in order to eliminate the influence of air-liquid surface on gold particles, we carried out an experiment in which the gold particles were dispersed in the closed vessel filled with the medium. Next, we developed a simulation model based on the molecular dynamics (MD) method and investigated the motion of particles in aqueous solution. The results between experiment and numerical simulation are quantitatively compared.

2. Experiment

2.1 Experimental conditions

The experimental setup is shown in Fig. 1 and also the physical conditions in the experiment and numerical simulation are indicated in Table 1. The triangle-lattice structure of gold particles on the air-liquid interface with a petri dish was observed by Takayama *et al.* [5]. When the air-liquid interface exists, it is difficult to evaluate accurately the magnetic dipole moment because the particle is levitated and its head is exposed to the air. In addition, the air-liquid interface also exerts the surface tension on particles. Therefore, in order to eliminate these unknown factors, we used the closed vessel and observed the formed structure in it, as shown in Fig. 1.

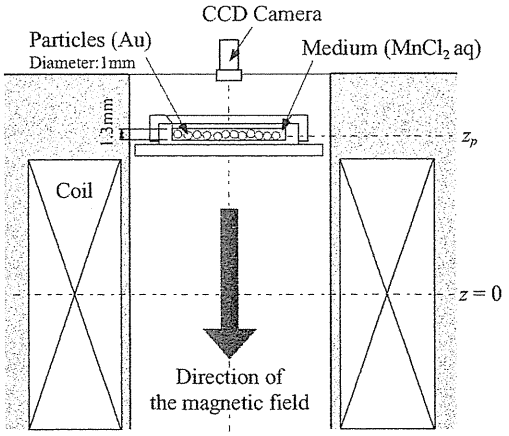

Fig. 1: Experimental setup.

Table 1: Physical conditions of experiment and numerical simulation.

	Nomenclature		Value
Particle (Au)	Diameter	d_p [mm]	1.0
	Volume magnetic susceptibility	χ_p [-(SI)]	-3.45 $\times 10^{-5}$
	Density	ρ_p [kg/m^3]	1.93 $\times 10^4$
Medium ($MnCl_2$ aq)	Concentration	C [wt%]	40
	Volume magnetic susceptibility	χ_f [-(SI)]	7.99 $\times 10^{-4}$
	Density	ρ_f [kg/m^3]	1.39 $\times 10^3$
	Viscosity	η_f [mPa·s]	8.32±1
Imposed magnetic field	Position of particle	z_p [mm]	148±1
	Direction	—	z
	Amplitude at z_p	B_0 [T]	(4.9)

2.2 Experimental results

The experiment for the number of particle, $N = 100$, has been performed. Figure 2(a) shows a typical configuration of $N = 100$. On this photo, it is confirmed that gold particles with a 1 mm diameter form the triangle-lattice alignments with some spacing and that the particle-particle distance in the center is relatively narrow, and this distance increases gradually with apart from the center.

3. Numerical simulation

3.1 Numerical model for simulation

We have used the notation $U_i^{(H)}$ for the total potential energy of gravitation and the interaction between particle i and applied magnetic field $\boldsymbol{H}$ and also $U_{ij}^{(m)}$ for the magnetic dipole interaction energy among particles i and j. Then, the expressions for these quantities are written as

$$U_i^{(H)} = \frac{\pi {d_p}^3}{6}\left[-\frac{1}{2\mu_0}(\chi_p - \chi_f){\boldsymbol{B}_i}^2 + (\rho_p - \rho_f)gz_i\right] , \tag{1}$$

$$U_{ij}^{(m)} = \frac{\mu_f}{4\pi {r_{ij}}^3}\left[(\boldsymbol{m}_i \cdot \boldsymbol{m}_j) - \frac{3}{r_{ij}}(\boldsymbol{m}_i \cdot \boldsymbol{r}_{ij})(\boldsymbol{m}_j \cdot \boldsymbol{r}_{ij})\right] , \tag{2}$$

where $\boldsymbol{r}_{ij} = \boldsymbol{r}_i - \boldsymbol{r}_j$, $r_{ij} = \mid \boldsymbol{r}_{ij} \mid$, $r_i(= \mid \boldsymbol{r}_i \mid)$ and z_i is the position of particle i for r and z-direction, respectively, and g is the acceleration of gravity. Since χ_p and $\chi_f \ll 1$, we regard $\boldsymbol{H}$ as $\boldsymbol{H} \simeq (1/\mu_0)\boldsymbol{B}$. The effective dipole moment $\boldsymbol{m}_i$ in Eq.(2) denotes the induced magnetic dipole moment of diamagnetic particle i in medium, and it is represented by the following equation [6]:

$$\boldsymbol{m}_i = \frac{\pi {d_p}^3}{2}\frac{\mu_p - \mu_f}{\mu_p + 2\mu_f}\boldsymbol{H}_i . \tag{3}$$

At $z = 148$ mm, the ratio of B_r/B_z is very small. Therefore, we ignore r-component of $\boldsymbol{H}$ and carry out the two-dimensional simulation, that is, all magnetic dipole moments turn to z direction.

3.2 Equations of motion

The motion of an arbitrary particle i in the model system is governed by the following equation, which is expressed in a non-dimensional form:

$$\frac{d\boldsymbol{v}^*{}_i}{dt} = \sum_{i \neq j}^{N} \boldsymbol{F}_{ij}^{(m)*} + \boldsymbol{F}_i^{(H)*} - \boldsymbol{F}_i^{(v)*} . \tag{4}$$

Each force in the above equation denotes

$$\boldsymbol{F}_{ij}^{(m)*} = R_{ij}^{(m)}\frac{1}{{r_{ij}}^{*4}}\boldsymbol{t}_{ij} , \quad \boldsymbol{F}_i^{(H)*} = R_i^{(H)}\boldsymbol{t}_i , \quad \boldsymbol{F}_i^{(v)*} = R^{(v)}{\boldsymbol{v}_i}^* . \tag{5}$$

where $\boldsymbol{F}_{ij}^{(m)*}$,$\boldsymbol{F}_i^{(H)*}$ and $\boldsymbol{F}_i^{(v)*}$ are the magnetic interaction force between particles i and j, the magnetic force that the applied magnetic field exerts on particle i and the viscous drag by medium, respectively. The unit vectors $\boldsymbol{t}_{ij}$ and $\boldsymbol{t}_i$ are given by $\boldsymbol{t}_{ij} = \boldsymbol{r}_{ij}/r_{ij}$ and $\boldsymbol{t}_i = \boldsymbol{r}_i/r_i$. ${\boldsymbol{v}_i}^*$ is the velocity of particle i. The dimensionless parameters $R_{ij}^{(m)}$, $R_i^{(H)}$ and $R^{(v)}$ are normalized by the representative force $F_{r0}^{(m)}$. The representative length and time are d_p and $T = (md_p/F_{r0}^{(m)})^{1/2}$, respectively, where m is the mass of a particle.

4. Results and discussion

4.1 Final particle position at a steady state

Here, we discuss the final configuration formed by particles at a steady state. The final configurations for the particle number $N = 100$ are shown in Fig. 2(b). The maximum number of time steps is 4.5×10^5 steps. The result of the final configurations show that

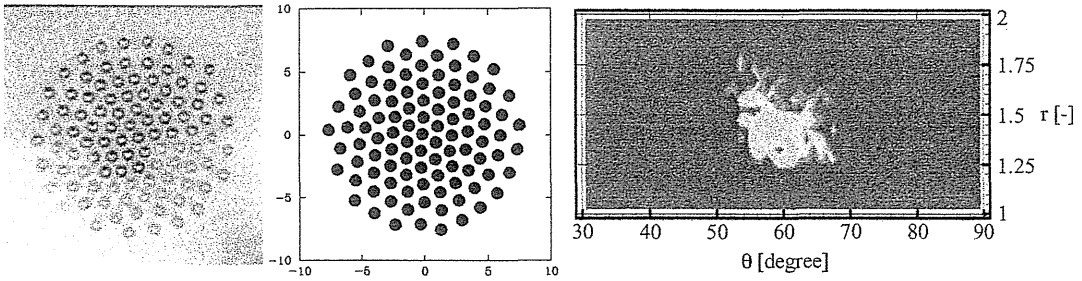

(a) Experiment (b) Numerical analysis (c) Three-body distribution function $f_3(r,\theta)$ of numerical analysis

Fig. 2: Results of experiment and numerical analysis for $N = 100$.

the particle density is relatively high in the central part and becomes relatively lower in the outer part, as in the experiments.

4.2 Three-body distribution function

In order to analyze quantitatively the final configuration of particles in the numerical simulation, we defined the three-body distribution function $f_3(r,\theta)$. The three-body distribution function $f_3(r,\theta)$ represents the probability density function with respect to the two variables of r-θ. That is, $f_3(r,\theta)\Delta r\Delta\theta$ means the probability of $(r-\Delta r/2) \sim (r+\Delta r/2)$ and $(\theta - \Delta\theta/2) \sim (\theta + \Delta\theta/2)$. The result of the three-body distribution function $f_3(r,\theta)$ for $N = 100$ is shown in Fig. 2(c). $f_3(r,\theta)$ is calculated by taking account of all particles. It is seen that both results have a peak near 60° at a certain r range and the gathering particles forms the triangle-lattice alignments.

5. Conclusion

The following results could be confirmed in the present study.

1. Two forces arising due to high magnetic fields acted on the Au particles with a 1 mm diameter used in the experiment. A numerical model to demonstrate the motion of feeble magnetic particles in high magnetic fields was developed.
2. The numerical simulation demonstrates the formation of triangle-lattice alignments in a two-dimensional plane, as obtained in the experiment, and the results of numerical simulation agree well with those of the experiment. The obtained results verified that the interaction among induced magnetic dipoles is a significant force and governs the structural formation of feeble magnetic substances under high magnetic fields.

References

[1] E. Beaugnon and R. Tournier, *Nature* **349** (1991) 470.

[2] S. Ueno and M. Iwasaka, *J. Appl. Phys.* **75** (1994) 7177.

[3] M.A. Weilert, D.L. Whitaker, H.J. Maris and G.M. Seidel, *Phys. Rev. Lett.* **77** (1996) 4840.

[4] M.V. Berry and A.K. Geim, *Eur. J. Phys.* **18** (1997) 307.

[5] T. Takayama, Y. Ikezoe, H. Uetake, N. Hirota and K. Kitazawa, *Material Transactions* **44** (2003) 2563–2566.

[6] T. B. Jones, *Electromechanics of Particles*, Cambridge University Press, New York (1995).

Magnetically Aligned $Gd(OH)_3$–Polymer Composite Film

Chengkang Chang[1], Fumiko Kimura[1] Tsunehisa Kimura[1,2] and Hitoshi Wada[3]
1 Tsukuba Magnet Laboratory, National Institute for Materials Science
3-13 Sakura, Tsukuba, Ibaraki 305-0003, Japan
2 Department of Applied Chemistry, Tokyo Metropolitan University
1-1Minami-ohsawa, Hachioji, Tokyo 192-0397, Japan
3 Department of Advanced Materials Science, Graduate School of Frontier Sciences, The University of Tokyo
Kashiwanioha 5-1-5, Kashiwa 277-8561, Japan
(chang.chengkang@nims.go.jp)

Abstract
This paper reports the preparation and optical behavior of a $Gd(OH)_3$–PVA nano composite. Nano scaled $Gd(OH)_3$ crystallites were prepared by hydrothermal method, with a rod like morphology. The $Gd(OH)_3$-PVA nano composite obtained by casting the composite solution under 5T showed a preferred orientation, with the *c* axis aligned along the applied field direction. This aligned nano composite showed birefringence when observed under optical microscope with a pair of crossed polars, implying a potential application in optical area. The birefringence value was determined as 0.013 using a computer simulation method.

Keywords
Hydrothermal, $Gd(OH)_3$, Nanorod, Magnetic alignment, Birefringence

1. Introduction

Feeble magnetic particles are affected when they are subjected to magnetic fields. Various behaviors will be observed if the magnetic energy exceeds the thermal energy. Recently, research attentions have been paid to the use of magnetic field for materials processing since the use of high magnetic fields has become possible at laboratory level at a relatively low cost owing to the development in the superconducting technology. Up to now, many research works have been reported, including crystal growth in magnetic field[1-4], magnetic levitation [5-8], magnetic alignment [9-12] and so on.

Concerning the magnetic alignment, both organic and inorganic particles with anisotropy in magnetic susceptibility show preferred orientation under a magnetic field. The alignment causes a texture structure and results in anisotropy in optical, mechanical, thermal, and electrical properties. The magnetic alignment technique therefore seems to be a useful method for the researchers to investigate the anisotropic properties by simply using the textured materials, which shows notable advantage over the method that employs single crystals, since single crystal samples are relatively hard to obtain for most of the materials. A number of papers on magnetic alignment of organic and polymeric materials have been so far reported, but there are few reports on inorganic materials[13-15], since the processing at high temperatures in a superconducting magnet to prepare a bulk inorganic compact with anisotropic property requires a specially designed furnace operating safely in a narrow space of the magnet.

An alternative way of taking maximum advantage of the anisotropic properties provided by the inorganic crystallites is attained through the composite with polymeric materials. Fine inorganic crystallites suspended in a polymer melt or a polymer solution are subjected to the magnetic field, and then the alignment is fixed by solidification of the matrix polymer by cooling down the polymer melt or evaporating the solvent from the solution. To do so, the preparation of mono dispersive crystallites with fine crystal size is a key step that determines the quality of the obtained composite. In this paper, nanorods $Gd(OH)_3$, prepared by a hydrothermal method, were suspended in 20%PVA solution and subjected to a 5T magnetic field. This magnetically aligned $Gd(OH)_3$ –PVA nano

composite readily showed optical anisotropy under a polarized microscope, suggesting a potential application in optical area.

2. Experimental methods

2.1 Nanorod $Gd(OH)_3$ preparation and characterization

The rod like $Gd(OH)_3$ nano crystallites was prepared through a hydrothermal method. In a typical routine, 0.005 mole $Gd(NO_3)_3 \cdot 5H_2O$ was dissolved in 20 ml distilled water to form a clear Gd^{3+} solution of 0.25M in a 100ml glass beaker. 20ml of 0.75M KOH solution was added to the solution dropwisely with continuous stirring to generate a colloidal solution. The obtained solution was supersonically treated for 10 min. before it was transferred to a 50 ml Teflon linked autoclave. The autoclave was sealed and kept in an electric oven at 200°C for 18 h. When the autoclave was cooled down to the room temperature, a white precipitate was obtained. The precipitate was collected and washed with distilled water several times, centrifuged and dried at 60°C for 24 h.

The obtained powder was then subjected to various characterizations. A JEOL-JDX3500 X-ray diffractometer was employed to investigate the phase composition, using Cu Kα radiation(1.5418A), with a scanning rate of 0.02°/ s in the 2 θ range from 10° to 70°. The morphologies of the crystals were observed by a field emission scanning electron microscopy (FE-SEM), performed on a JEOL-JSM-6700F scanning electron microanalyzer.

2.2 Magnetic alignment of nanorods and optical characterization

The as-prepared nanorods were subjected to 5T magnetic field in a 20% PVA suspension. 0.08 grams of $Gd(OH)_3$ nanorods were dispersed in 40ml distilled water supersonically until a mono dispersive suspension was obtained. Then 8 grams of PVA (MW=22000) were added to the above suspension with continuous stirring until a transparent "solution" was formed. 2 ml of such solution was casted into a glass container with diameter around 40mm. The container then was held in 5T magnetic field until a transparent film was formed. Two kinds of alignment method were employed in the experiment, i.e., horizontal and vertical alignments, as shown in Fig.1. For the horizontal alignment, the film obtained served as a top view sample from a bulk material. For the vertically aligned sample, it served as the edge view sample in the experiment. These two samples are hereafter referred to as top and edge views.

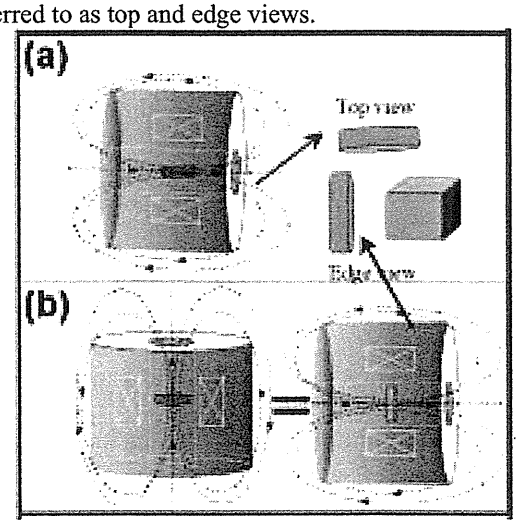

Fig. 1: Sample preparation method in the experiment. (a), horizontal alignment for a top view sample and (b) vertical alignment for an edge view sample.

To make sure that a textured structure is formed, the ordinary X ray diffraction was conducted with the same diffractometer mentioned before. A Laue X ray diffractometer was used to determine the alignment direction.

For the investigation of the anisotropy in optical property, the aligned nano composite was

observed under an optical microscope with crossed polars. Obvious birefringence was readily observed. To determine the value of the birefringence, He-Ne laser source was employed. The experimental setup is shown schematically in Fig. 2. The sample was put between a pair of crossed polars. The nano composite film was rotated. The output light intensity is expressed by

$$I^2 = I_0^2 \sin^2 2\theta \sin^2 \frac{\pi\delta}{\lambda}, \quad \delta = \Delta n \times d \qquad (1)$$

where I_0 is the impinging laser light intensity, θ is the rotation angle with respect to the polarizer direction, δ is the retardation caused by the difference in reflective indices, and λ is the wavelength of the impinging laser light, 632.8nm. The retardation, δ, was determined using a software, Biref Analyzer.

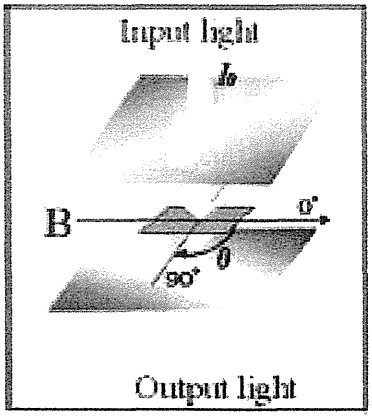

Fig. 2: Method for birefringence measurement. Laser light with wavelength of 628nm was employed. The observed sample was put between a pair of crossed polars. The alignment direction is indicated by B.

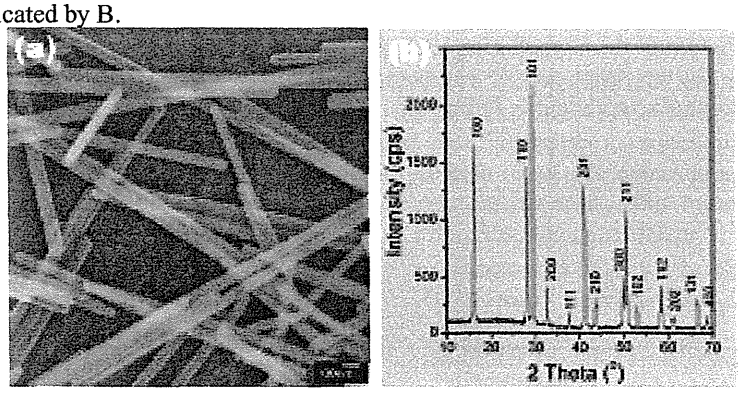

Fig. 3, Characterization of $Gd(OH)_3$ nanorods. (a), SEM morphology of the $Gd(OH)_3$ precursor, revealing a rod shape. (b) XRD pattern of the precursor, a pure phase was indicated.

3. Results and discussion

3.1 Characterization of $Gd(OH)_3$ nanorods

Nano scaled $Gd(OH)_3$ was obtained through the hydrothermal routine. SEM observation of the nanorods is shown in Fig. 3a. It can be seen from the micrograph that the $Gd(OH)_3$ nanorods have a very uniform shape, with diameter around 50 nm. XRD pattern shown in Fig.3b revealed a pure phase. All the peaks in the pattern can be indexed into a hexagonal structure, which is in good agreement with the PDF 83-2037. No other phases were found from the pattern, suggesting that a

pure phased nanorod $Gd(OH)_3$ was obtained by the hydrothermal routine.

3.2 Alignment of $Gd(OH)_3$ under magnetic field

The hydrothermally prepared $Gd(OH)_3$ nanorods showed preferred orientation under 5T magnetic field. XRD patterns for the magnetically treated sample (the top view and side view) are shown in Fig. 4. It is very clear that the reflections from the same lattice plane change greatly according to the observation direction. For the XRD pattern3, which corresponds to the top view, the increase in the reflection from (100) (110) lattice plane is obvious. However, in the XRD pattern2, which represents the edge view sample, the reflection from above mentioned lattice plane is suppressed, while those from (101), (201) and (211) plane are increased significantly. Such significant change in the diffraction intensity really suggested that those tiny nano sized crystallites were actually aligned.

A SEM observation was conducted for the aligned sample prepared just with the $Gd(OH)_3$ nanorods themselves (no PVA was added to the $Gd(OH)_3$ suspension). The result is shown in Fig. 4b. It can be seen clearly from the micrograph that the nanorods formed wire like structure and most of them run along the applied field direction, which shows a direct evidence of the nanorods alignment.

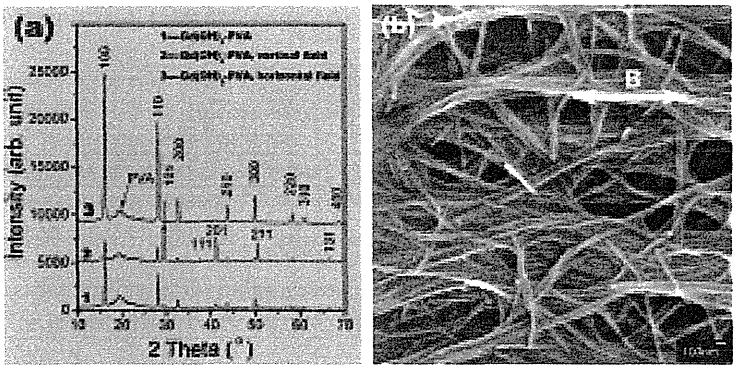

Fig. 4: (a), XRD Pattern of the aligned sample. 1, 2 and 3 represent the not aligned sample, the edge view sample and the top view sample respectively, and (b), SEM micrograph for the aligned nanorods, showing the alignment along field direction. B represents the direction of the applied field.

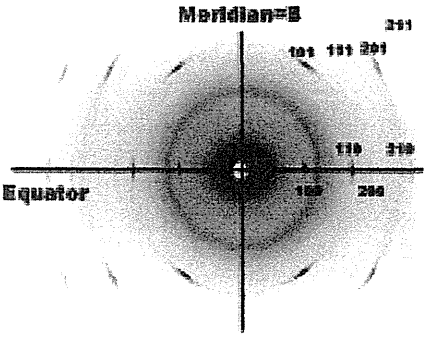

Fig.5: XRD Laue photograph of the magnetically aligned sample, indicating that the c axis was aligned along the applied field direction.

To determine the orientation direction of the crystallographic axis, the aligned samples were further examined using X Ray image method, as shown in Fig. 5. The Laue photograph of the top view sample shown in Fig. 3 shows clearly diffraction spots. These spots in the photograph show another proof that the alignment did take places, otherwise the Debye rings rather than the spots will be observed. Those spots represent the diffractions from the related lattice planes, as marked on the photograph. It is obvious in the figure that the diffraction spots for (100) and (110) planes run in a line, indicating that the incoming X ray beam runs parallel to the ab plane, otherwise the projections

of the two vectors will shown a certain angle between each other. This is clearly an indicator that the ab plane of all the individual nanorods were aligned parallel to the incoming x ray beam. Because the rod direction lies in the meridian direction, the above result implies that the c axis of the nanorod, which is also the rod direction, was aligned along the applied magnetic field.

3.3 observation of birefringence under microscope and the measurement using 628 nm laser light

The obtained c axis aligned composite shows birefringence readily under the optical microscope with a pair of crossed polars. Fig. 6 shows the observation result of the top view sample with a color plate inserted. It can be seen from Fig.6 that the images change colors when the sample was rotated, showing the birefringence nature of the nano composite film. If the sample was turned around for 360° degree, 2 times of such color change will be observed, which is very similar to the behavior of single crystals under crossed polars. However, It should be noted here that no color change was observed for the edge view sample, due to the hexagonal structure of the $Gd(OH)_3$ nanorods.

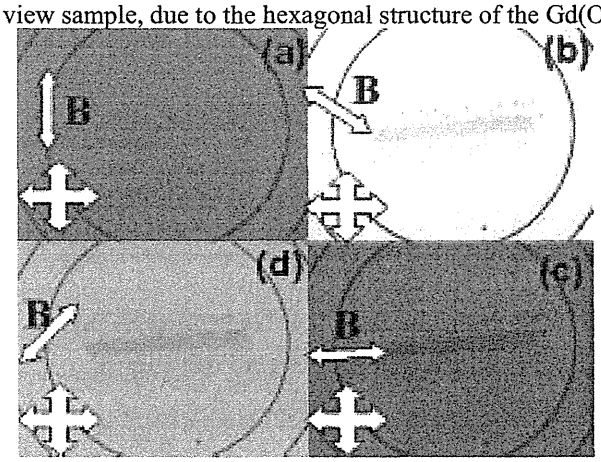

Fig.6: Optical micrograph of the top view sample observed under crossed polars, with a color plate inserted. The crossed lines indicate the direction of the polarized light. The arrows indicate the alignment direction, which parallel to the magnetic field direction.

This birefringence behavior from the magnetically alignment sample suggested a potential application of magnetic field for the measuring of the birefringence of crystalline materials even in nano scale, by simply simulating the experimental data according to equation 1 and carefully measure the thickness of the film. The using of crystals in small size shows great advantage over the traditional methods where large size of single crystals was required. Fig. 7 shows the change of output light against the film rotation degree, together with the simulated result. The retardation δ obtained by the simulation is 37.42nm. By a careful measurement from the SEM micrograph, the thickness of the nano composite film was determined as 125μm. Therefore, the Δn was calculated as 0.013.

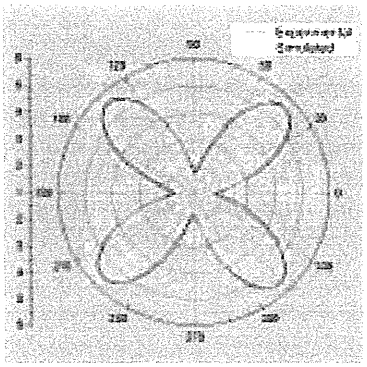

Fig. 7: experimental and simulated results for the Δn measurement

4. Conclusions

We presented in this paper the hydrothermal preparation and optical behavior of a $Gd(OH)_3$–PVA nano composite.. The obtained Gd(OH)3 crystallites showed a rod like morphology with diameter around 50nm. These single crystalline nanorods aligned under 5T magnetic field with their c axes parallel to the field direction. Such alignment caused birefringence for the PVA-$Gd(OH)_3$ nano composite, which indicates the potential application in optical area. The birefringence value was further determined using the sample with high alignment degree, and the calculated Δn is 0.013.

Acknowledgements

This work was supported by Grant-in-Aid for Scientific Research on Priority Area "Innovative utilization of strong magnetic fields" (Area 767, No.15085207) from MEXT of Japan.

References

1. J. W. Qi and N. I. Wakayama, Phys. Fluids, 16 (9), 3450, (2004)
2. H. Adachi, H. Matsumura, A. Niino, K. Takano, T. Kinoshita, M. Warizaya, T. Inoue and Y. Mori, Japan. J. Appl. Phys. Part2, 43 (4B), L522, (2004)
3. C. W. Zhong, L. B. Wang and N. I. Wakayama, J. Cryst. Growth, 233 (3), 561, (2001)
4. A. Katsuki, R. Tokunaga, S. Watanabe and Y. Tanimoto, Chem. Lett. 8, 607, (1996
5. M. Motokawa, M. Hamai, T. Sato, I. Mogi, S. Awaji, K. Watanabe, N. Kimura and M. Makihara, Physica B, 294, 729, (2001)
6. N. Kimura, M. Makihara, M. Hamai, T. Sato, I. Mogi, S. Awaji, K. Watanabe and M. Motokawa, Japan. J. Appl. Phys. Part2, 39 (4A), L324, (200)
7. T. Kimura, M. Yamato and A. Nara, Langmuir, 20 (3), 572, (2004)
8. T. Kimura, S. Mamada and M. Yamato, Chem. Lett. 11, 1294, (2000)
9. Y. Sakka, T. S. Suzuki, N. Tanabe, S. Asai and K. Kitazawa, Japan. J. Appl. Phys. Part 2, 41 (12A), L1416, (2002)
10. H. Garmestani, M. S. Al-Haik, K. Dahmen, R. Tannenbaum, D. S. Li, S. S. Sablin and M. Y. Hussaini, Adv. Mater. 15 (22), 1918 (2003)
11. T. Kimura, Mater. Trans. 44 (12), 2520, (2003)
12. T. Kimura, Polymer J., 35(11), 823-843 (2003).
13. C. Uyeda, R. Takashima, K. Hiraoka, Japan. J. Appl. Phys. Part 2, 44 (12-15), L371-L374 (2005).
14. C. Uyeda, M. Sakakibara, K. Tanaka, Phys. Chem. Miner. 30 (7), 425-429, (2003).
15. C. Uyeda, R. Takashima, K. Tanaka, Appl. Phys. Lett. 86 (9), Art. No. 094103, (2005).

How Is Effect of Strong Static Magnetic Field on Nanorods ?

Yoshihisa Fujiwara[1], Naho Shibata[2] and Yoshifumi Tanimoto[1]
1 Department of Mathematical and Life Sciences,
Graduate School of Science, Hiroshima University,
Kagamiyama 1-3-1, Higashi-Hiroshima, Hiroshima 739-8526, Japan
2 Department of Chemistry, Faculty of Science, Hiroshima University,
Kagamiyama 1-3-1, Higashi-Hiroshima, Hiroshima 739-8526, Japan
(fuji0710@sci.hiroshima-u.ac.jp)

Abstract
For the purpose of seeking the minimal size necessary for the magnetic orientation due to anisotropic magnetic susceptibility, dependence of the magnetic orientation on length of diamagnetic nanorods was investigated by using a vertical strong magnetic field. Furthermore, effects of hypergravity and microgravity, which are features of the vertical strong magnetic field with a large magnetic field gradient, on orientation of the nanorods were compared with the magnetic orientation under the normal gravity. As a result, advantage of the hypergravity was demonstrated for alignment of diamagnetic substances to which the magnetic orientation due to anisotropic magnetic susceptibility was inapplicable. The mechanism was explained by hydrodynamics of the non-spherical nanorod of which precipitation was accelerated by the downward magnetic force.

Keywords
strong magnetic field; tetrakis(4-sulfonatophenyl)porphine, nanorod, diamagnetic, magnetic orientation, hypergravity, microgravity, hydrodynamics

1. Introduction

One of charms brought by a strong magnetic field lies in both the magnetic orientation of diamagnetic substances due to their magnetic susceptibility anisotropies and the strong magnetic force toward them. Our group has investigated the magnetic orientation of some substances by using strong static magnetic fields up to 15 T. For instance, it was demonstrated that benzophenone crystal was aligned by the strong horizontal magnetic field of 8 T,[1] in which the magnetic orientation was explained by the anisotropic magnetic susceptibility of benzophenone. Furthermore, through the simulation of experimentally-obtained temperature dependence of the magnetic orientation, the minimal number of the molecule, which was necessary for the magnetic orientation of the crystal, was evaluated to be about 3×10^8 molecules at least. However, since actual size of the crystal aligned in the experiment was several millimeters in length at least, the number of the molecule packed in the crystal apparently exceeded the minimal value by far. Therefore, in order to seek the smallest size of a substance necessary for the magnetic orientation, we used aggregates made of tetrakis(4-sulfonatophenyl)porphine.[2] The aggregates are called nanorods, of which typical size is w100×h4×*l*1000 nm. Whereas the width and height are respectively almost constant among rods, only the length varies in a range from nanometer to micrometer. Thus, for the purpose, we examine rod-length dependence of the magnetic orientation. Furthermore, as a new method to align nanometer-sized diamagnetic substances, we insist on advantage of hypergravity created by combined use of the gravity and downward magnetic force in a vertical large magnetic field gradient.

2. Experimental methods

2.1 Preparation of nanorods

The nanorods were prepared by aging an acidic solution of tetrakis(4-sulfonatophenyl)porphine

according to the literature.[2] Thereafter, a substrate, mica, for a scanning probe microscope was sunk in the acidic colloidal solution including the nanorod, and then, let alone during about two days in the absence and presence of the vertical strong static magnetic field.

2.2 Vertical strong static magnetic fields with large magnetic field gradients

A superconducting magnet (Japan Superconductor Technology, JASTEC LH15T40, ϕ 40 mm bore diameter) capable of providing the vertical strong magnetic fields of up to 15 T was employed for the experiment. The magnetic field intensities used were 10.7, 12, and 15T. The field of 10.7 T, in which the magnetic field gradient exists, provides the microgravity created by counterbalance between the gravity and the upward strong magnetic force in the case of diamagnetic substances. On the contrary, the field of 12 T affords the hypergravity corresponding to about twice of the normal gravity on the earth. The field of 15 T is obtained at a center of the magnet and thereby no magnetic force is present there. A geomagnetic field, which is normally about 0.05 mT, was treated as 0 T in this study.

2.3 Measurement of atomic force microscope images of nanorods on mica and analyses of distributions in length and angle

After the immersion, the mica was taken out from the colloidal solution of nanorods and the excess solution on the mica surface was sucked away. To probe the surface of mica, atomic force microscope (AFM) images were measured by a scanning probe microscope (SII, SPI 3800N & SPA-400). Analyses of distributions in length and angle of the nanorods were carried out with commercially obtainable software (Library, Cosmos32).

3. Results

Figure 1a shows an AFM image of the nanorods adsorbed on the mica surface immersed at 0 T. A single whitish line corresponds to a piece of the nanorod which remain one on top of the other at several places. The distribution in length and direction were measured by using only alone nanorods.

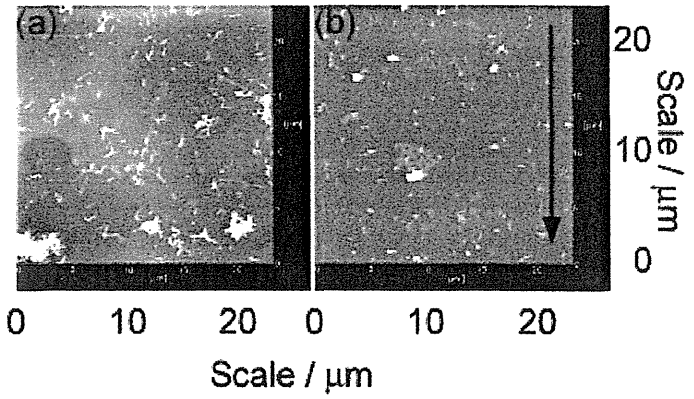

Fig. 1. The AFM images of the mica surfaces where the nanorods were adsorbed at (a) 0 and (b) 12 T, respectively. The whitish lines show the nanorods. The black arrow at 12 T indicates a direction of the vertical magnetic field.

The length varied in a range from nanometer to micrometer. Figure 2 demonstrates the distribution in length in which the most populated length is around 600 nm. There seemed no appreciable difference in the distribution among 0, 10.7, 12, and 15 T. Interestingly, on the other hand, the direction of the nanorod looks to orient to around -45 and 45 degrees even at 0 T, as shown in Figure 3a, where all the range in length were used to make the graph. The standard of the angle showing a direction of alignment is based on the direction of the vertical magnetic field, and the zero degree means a direction coincident with the vertical magnetic field and thereby gravity. When the

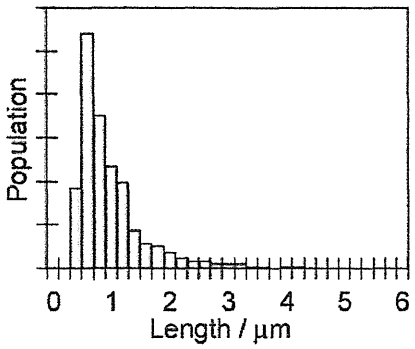

Fig. 2. The distribution in length of the nanorod on mica immersed at 0 T.

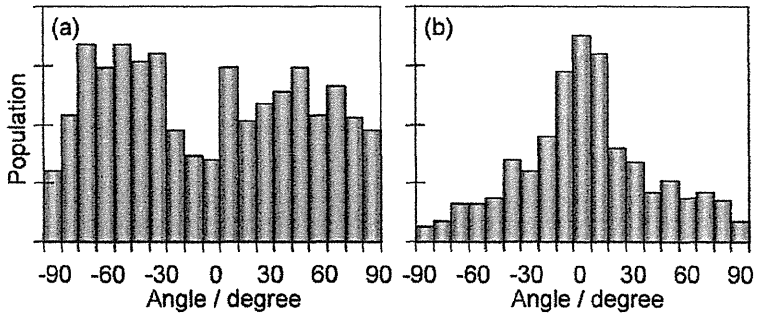

Fig. 3. The distributions in angle of the nanorod on mica immersed at (a) 0 and (b) 12 T, respectively.

distributions in angle were redrawn in the two cases classified into less than and more than 600 nm in length, no appreciable difference was detected between them. Further, the directions even in 10.7 and 15 T showed almost the same distribution in angle in spite of the presence of the vertical magnetic field. However, the orientation and distribution in angle obtained at 12 T were distinct from those of 0, 10.7 and 15 T. Figure 1b depicts the AFM image at 12 T, showing that the nanorod orients parallel to the vertical magnetic field of 12 T, namely, the gravity at several places. Figure 3b also displays the distribution in which the most populated angle shifts to 0 degree. However, no substantial distinction was observed between the distributions in angle of the two cases classified into less than and more than 800 nm in length which was the most populated length at 12 T.

4. Discussion

It was found that the nanorods made by a self-assembly of tetrakis(4-sulfonatophenyl)porphine had a wide range of length from 200 nm to 4000 nm, as shown in Figure 1. Even at 15 T, however,, we obtain no evidence for the magnetic orientation of the nanorod. We did not observe the orientation even if we paid attention to the length longer than 800 nm. Unfortunately, this result indicates that the magnitude of the field of 15 T and/or anisotropic magnetic susceptibility is insufficient for aligning the nanorod at room temperature. Since there is a certain extent of the orientation even at 0 T, as shown in Figure 3a, there might be interaction between the nanorod and mica surface. However, it is surprising that the nanorod was aligned to some extent at 12 T smaller than 15 T. This apparently points out that the magnetic orientation seen at 12 T does not result from the magnetic susceptibility anisotropy of the nanorod. We now tentatively consider the mechanism as the following. The rod is non-spherical and diamagnetic. Hence, if the precipitation of the diamagnetic

nanorod is accelerated by acquiring the downward magnetic force in the hypergravity at 12 T, the non-spherical nanorod seems to orient in such a way that the long axis is aligned parallel to the downward stream, that is, the vertical magnetic field and gravity as a result of hydrodynamics. If this interpretation is right, then this interesting phenomenon is available as a new technique to align tiny nanometer-sized substances whose magnetic orientation due to the anisotropic magnetic susceptibility fails. We name this new technique the hypergravity-induced magnetic orientation (HiMO). This phenomenon is governed by not only shape and size of the nanorod but also balances in diamagnetic susceptibilities and densities, respectively, of the nanorod and the solvent. Therefore, even if a diamagnetic substance is magnetically isotropic, it can be arranged in principle when the shape is non-spherical. Moreover, paramagnetic and ferromagnetic substances are also considered to be aligned by using the magnetic force toward a center of a magnet.

5. Conclusions

We presented the possibility and thereby a new technique that nanometer-sized and/or probably magnetically isotropic substances showing no magnetic orientation due to the anisotropic diamagnetic susceptibility can be aligned by hydrodynamic stream enhanced by the magnetic force in the hypergravity. This technique is considered to be applicable to alignment of paramagnetic and/or ferromagnetic substances by utilizing a stream toward the magnet center enhanced by the magnetic force.[3]

Acknowledgements

This work was supported by Grant-in-Aid for Scientific Research on Priority Area "Innovative utilization of strong magnetic fields" (Area 767, No. 15085208) from MEXT of Japan.

References

[1] M. Fujiwara, M. Fukui and Y. Tanimoto, J. Phys. Chem. B, 103 (1999) 2627.
[2] A. D. Schwab, D. E. Smith, C. S. Rich, E. R. Young, W. F. Smith and J. C. de Paula, J. Phys. Chem. B, 107 (2003) 11339.
[3] Y. Fujiwara, N. Shibata and Y. Tanimoto, to be submitted.

Magnetic Field Effects on Hydrogen Isotope Separation with Metal Hydrides

Yuya Ito[1], Rui Takahashi[1], Soichiro Mizusaki[2], Isao Yamamoto[1],
Tadashi Takamasu[3] and Masuhiro Yamaguchi[1]
1 Department of Physics, Yokohama National University,
79-5 Tokiwadai, Hodogaya-ku, Yokohama 240-8501, Japan
2 Department of Electrical Engineering and Electronics, Aoyama Gakuin University,
5-10-1 Fuchinobe, Sagamihara, Kanagawa 229-8558, Japan
3 Tsukuba Magnet Laboratory, National Institute for Material Science,
Sengen, Tsukuba, Ibaraki 305-0047, Japan
(d04gd203@ynu.ac.jp)

Abstract
The influence of magnetic fields was investigated on the ability of hydrogen isotope separation with metal hydrides. The deuterium concentration in the gas phase after hydrogen-absorbing reactions was increased with increasing applied magnetic fields for ferromagnetic $LaCo_5$, but not for paramagnetic $LaNi_5$. The isotope separation factor $\alpha=(D/H)_{gas}/(D/H)_{solid}$ was enhanced from 1.54 in zero field to 2.25 at 13T in the β+γ region for the system $LaCo_5$-(H_2+D_2). The enhancement in α is related to the magnetic field effect on the equilibrium pressure in ferromagnetic metal hydrides.

Keywords
hydrogen isotope separation, metal hydride, $LaCo_5$, $LaNi_5$, isotope separation factor, protium, deuterium, high magnetic field

1. Introduction

Metal hydrides have potential applications to energy technology and materials processes. One of them is the hydrogen isotope separation between the protium H, deuterium D and tritium T.[1] This method is based on the hydrogen isotope effect of the equilibrium pressure between the protide MH_x, deuteride MD_x and tritide MT_x. If, for instance, the equilibrium pressure of the deuteride P^D is larger than that of the protide P^H, deuterium is concentrated in the gas phase, and vice versa. Below, the terms "hydrogen" and "hydride" represent all of the elements of H, D and T and the compounds of MH_x, MD_x and MT_x, respectively.

The systems $LaCo_5$-H_2(D_2) and $LaNi_5$-H_2(D_2) indicate such an isotope effect with excellent rates of hydrogen-absorbing and desorbing reactions. The system $LaCo_5$-H_2(D_2) has two plateaus of the α+β region ($0.3<x<3.4$) and the β+γ region ($3.4<x<4.3$) at room temperature.[2] The equilibrium pressure of the deuteride P^D is higher than that of the protide P^H in both regions and this isotope effect is more appreciable in the β+γ region ($P^D/P^H=1.70$) than the α+β region ($P^D/P^H=1.40$). On the other hand, the system $LaNi_5$-H_2(D_2) has one plateau of the α+β region ($0.3<x<7$). The deuterium pressure P^D is smaller than the protide one P^H at 303K ($P^D/P^H= 0.915$), but P^D is larger than P^H at 313K ($P^D/P^H= 1.10$).[3]

Meanwhile, the system $LaCo_5$-H_2(D_2) exhibits the magnetic field effect that the equilibrium hydrogen pressure is changed with increasing applied magnetic fields B according as

$$P_B = P_0 \exp\left(\frac{2B\Delta M_s}{RT}\right) \tag{1}$$

where P_B is the equilibrium pressure in the magnetic field and P_0 is that in zero field. This magnetic field effect originates from the ferromagnetic property of this hydride which is expressed by the change in the saturation magnetization per mole of desorbed hydrogen, ΔM_s.[4] For the system $LaCo_5$-H_2, as a matter of fact, P_0=232kPa in zero field and P_B=281kPa in 15T in the $\beta+\gamma$ region with ΔM_s=15.7JT^{-1}(molH)$^{-1}$ at 303K.[5, 6] The same magnetic effect occurs for the corresponding deuterium system $LaCo_5$-D_2 because the magnetic properties of the deuteride $LaCo_5D_x$ is the same as those of the corresponding protide $LaCo_5H_x$ in the magnetic fields below 35T which are currently available as steady magnetic fields.[7] Consequently, the value of ΔM_s is common to both the protide and deuteride systems. Even so, Eq. (1) suggests that the pressure difference P^D–P^H is increased with increasing applied magnetic fields.

Assuming that the isotope separation ability is related to the pressure difference P^D–P^H, we can enhance it by applying magnetic fields. In this work, we investigate the magnetic field effect on the isotope separation ability with the ferromagnetic $LaCo_5$. In addition, we examined the paramagnetic $LaNi_5$ compounds for comparison: The system $LaNi_5$-$H_2(D_2)$ also shows the isotope effect on the equilibrium pressure, but not the magnetic field effect on the equilibrium pressure because of non-ferromagnetic property. We presume that the latter system does not show such a magnetic field-induced enhancement of the isotope separation ability.

2. Experimental

$LaCo_5$ and $LaNi_5$ compounds were prepared by arc melting cobalt or nickel and lanthanum in an argon atmosphere. The purity of the raw materials is 99.99% for Co and Ni and 99.9% for La. The ingots were annealed at 1223K for 48h for homogenization. The samples were pulverized in an argon atmosphere in sizes under 10μm. X-ray powder diffraction showed that they were single phase with the $CaCu_5$ structure.

Isotope separation experiment was performed under the influence of magnetic fields by using the apparatus shown in Fig. 1, by which the deuterium/protium concentration in the gas phase was measured before and after the hydrogen-absorbing reaction of the compounds. First, the 1:1 mixed gas of H_2 and D_2 was prepared in a tank with the volume of 500cm^3 at the pressure of 1.2MPa. The purity of the gas was 99.99999% for protium and 99.5 D/(D+H)% for deuterium. This mixed gas was stored for 24 hours for homogenization at room temperature. Then, the mixed gas was introduced to a reservoir with the volume of 59.3cm^3 at an initial pressure $P_{initial}$. Next, we introduced this initial gas into a reactor to react with $LaCo_5$ or $LaNi_5$ compound of about 2g. Here, the reactor was situated in the center of a cryo-cooled superconducting magnet with the maximum field of 13T and the inner bore of 100mm (JMTD-13T100EF3, Japan Superconducting Technology Co. Ltd.). The temperature of the reactor was controlled at 303.0±0.1K or 313.0±0.1K by circulating temperature-controlled water in a water jacket.

The process of the hydrogen absorption was monitored by the pressure in the reservoir with a strain-gauge type transducer. Within 1 min. from the start of reaction, the pressure attained a constant value when the hydrogen absorption was completed at the final pressure P_{final}. Eventually, the hydride $LaCo_5(H,D)_x$ or $LaNi_5(H,D)_x$ was formed with the final hydrogen composition of x. The deuterium/protium concentration in the initial or final gas was measured by a mass spectrometer (Quadstar TM 421 QMS200, Balzers Co. Ltd.). The experimental error of the concentration was less than ±1.5%. Because the gas included a small amount of HD molecules, we divided them into the H and D concentration equally.

Before the main experiment of isotope separation, we operated this experimental apparatus without samples in the reactor. As a result, the deuterium concentration was measured to be 55.0 % in the initial gas and 54.6 % in the final gas, which agree with each other within the experimental error. This confirmed that the deuterium concentration in the reservoir is not affected by the gas handling itself.

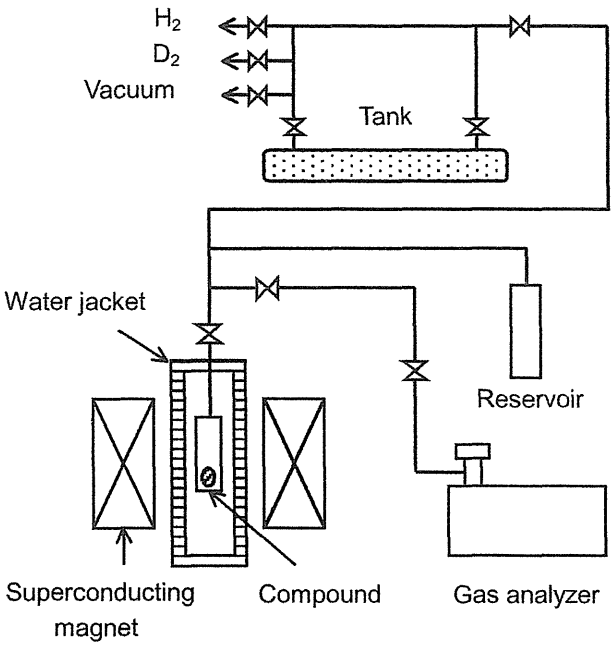

Fig. 1. Hydrogen isotope separation equipment with a superconducting magnet.

Figure 2 exemplifies the time-variation of the pressure in the gas phase during the isotope separation experiment where the $LaCo_5$ compound was applied to a magnetic field of 13T at 303K. The pressure was $P_{initial}$=0.564kPa and P_{final}=0.137kPa. The deuterium concentration was 54.4% in the initial gas and 68.7% in the final gas. The final hydrogen composition in the solid phase was x=3.8 in the β+γ region. As a consequence, the ratio between hydrogen isotopes was estimated to be D/H=2.19 in the gas phase and D/H=0.975 in the solid phase after the completion of hydrogen absorption.

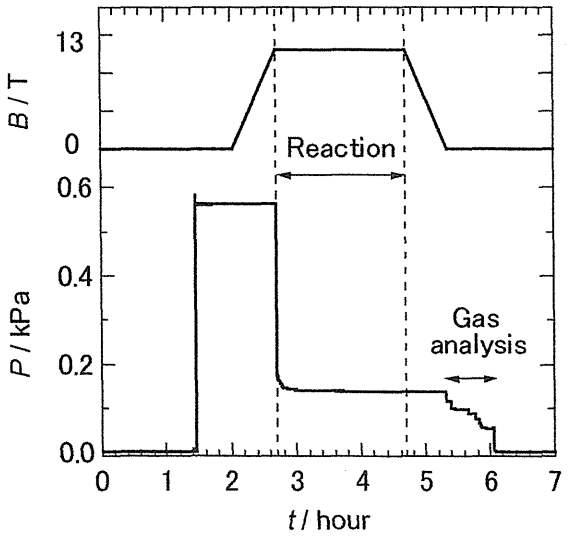

Fig. 2. Time-variations in the hydrogen pressure and magnetic field during a run of the isotope separation experiment when the $LaCo_5$ compound absorbed (H_2+D_2) gas at 303K

3. Results and Discussion

Figure 3 illustrates the deuterium concentration in the gas phase before and after the reaction for the isotope separation experiment. In both the α+β and the β+γ regions for the Co-system, deuterium is concentrated in the gas phase after the reaction. Moreover, the deuterium concentration is increased with increasing magnetic fields and this magnetic field effect is more appreciable in the β+γ region than the α+β region. The Ni-system shows, on the other hand, that the deuterium concentration is little changed at 303K in 0T and 13T. At 313K, the deuterium is concentrated in the gas phase at 313K, but it hardly depends on applied magnetic fields.

One of measures for the isotope separation ability of metal hydrides is the isotope separation factor defined by

$$\alpha = \frac{(\mathrm{D/H})_{\mathrm{gas}}}{(\mathrm{D/H})_{\mathrm{solid}}} \tag{2}$$

where the isotope separation ability is increased with leaving α from 1. For instance, we estimated to be α=2.25 in the separation experiment shown in Fig. 2. The observed values of the separation factor are summarized in Table I, which indicates the following features with some considerations.

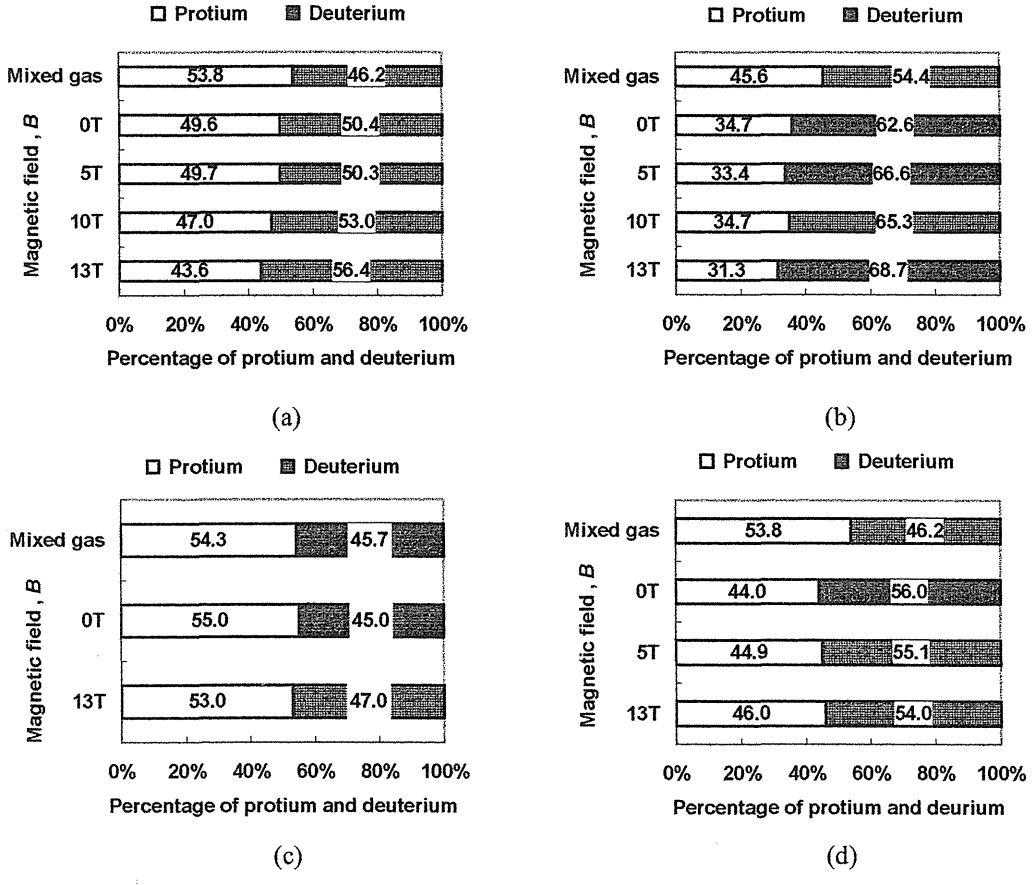

Fig. 3. Magnetic field dependence of the deuterium concentration in the gas phase for the isotope separation experiment with metal hydrides. (a) $LaCo_5(H,D)_x$ in the α+β region at 303K, (b) $LaCo_5(H,D)_x$ in the β+γ region at 303K, (c) $LaNi_5(H,D)_x$ in the α+β region at 303K and (d) $LaNi_5(H,D)_x$ in the α+β region at 313K.

Table I. Collected data of the hydrogen isotope separation with metal hydrides under the influence of magnetic fields.

System	Region	Temp. (K)	Pressure ratio [a] P^D/P^H	Magnetic field (T)	Separation factor α	ΔM_s (JT^{-1} $(molH)^{-1}$)	Pressure difference [b] P^D-P^H (kPa)
$LaNi_5$ -(H_2+D_2)	α+β	303	0.915	0	0.954	~0	-17.8
				13	1.05		
	α+β	313	1.10[c]	0	1.90	~0	44.6 [c]
				5	1.78		
				13	1.70		
$LaCo_5$ -(H_2+D_2)	α+β	303	1.40	0	1.19	8.7	0.931
				5	1.19		0.964
				10	1.45		0.998
				13	1.53		1.019
	β+γ	303	1.70	0	1.54	15.7	85.3
				5	1.95		91.0
				10	2.00		97.1
				13	2.25		101.0

a) Pressure ratio in zero field.
b) The values in 0T are observed and those in 5~13T are calculated.
c) After Biris et al. [3]

(1) Deuterium is concentrated in the gas phase after the reaction under zero field in the α+β and β+γ regions for the Co-system at 303K and in the α+β region for the Ni-system at 313K. On contrary, protium is concentrated in the gas phase in the α+β region for the Ni-system at 303K. This satisfies the basic principle of the hydrogen isotope separation: The gas with the higher equilibrium pressure is concentrated in the gas phase.
(2) In zero field, the separation factor is increased with increasing the pressure ratio P^D/P^H for both the La- and Ni-systems. This is simply explained by the thermodynamic model that the separation factor is related to the pressure ratio, that is, $\alpha=P^D/P^H$. This model assumes the equilibrium state between H_2, D_2, MH_x and MD_x. [1]
(3) The magnetic field effect on the isotope separation factor is exhibited by the Co-system, but not by the Ni-system. This is ascribed to the magnetic properties of the hydrides that the $LaNi_5(H,D)_x$ is paramagnetic and the $LaCo_5(H,D)_x$ is ferromagnetic. Consequently, the former system has no magnetic field effect on the equilibrium pressure but the latter system has a remarkable magnetic effect.
(4) For the Co-system, the magnetic field effect on the separation factor in the β+γ region is greater than that in the α+β region. This can be connected to the value of ΔM_s, which is 15.7 and 8.7 $JT^{-1}(molH)^{-1}$ for the β+γ and the α+β regions, respectively.

Obviously, the consideration of (3) contradicts to that to (2). The pressure ratio P^D/P^H maintains constant with increasing magnetic fields because Eq. (1) stands on the protide $LaCo_5H_x$ and the deuteride $LaCo_5D_x$ with the same value of ΔM_s. This suggests that the separation factor depends not only on but also, to an extent, on another factor, which is considered to be the pressure difference P^D-P^H. The pressure difference P^D-P^H is increased even if the value of ΔM_s is the same for the protide and deuteride, according as

$$P_B^D - P_B^H = \left(P_0^D - P_0^H\right)\exp\left(\frac{2B\Delta M_s}{RT}\right) \tag{3}$$

The calculated values of the pressure difference are listed in Table I. It is observed that the separation factor is increased with increasing magnetic field, associated with the increase in the pressure

difference. It is speculated that the separation factor is also dominated by the reaction kinetics which depends on the pressure difference $P^D - P^H$ while the equilibrium separation factor is given by the pressure ratio P^D/P^H.

In conclusion, the isotope separation ability is enhanced with increasing magnetic fields with the ferromagnetic metal hydride. This enhancement can be explained by the magnetic field effect on the equilibrium hydrogen pressure in ferromagnetic metal hydrides. The isotope separation factor α was increased from 1.54 at zero field to 2.25 at 13T in the $\beta+\gamma$ region for the $LaCo_5$-$H_2(D_2)$ system.

Acknowledgements

This work was supported by Grant-in-Aid for Scientific Research (No.14350041) and Grant-in-Aid for Scientific Research on Priority Area (Area 767, No. 15085204) from MEXT of Japan.

References

[1] B. M. Andreev, E. P. Magomedbekov and G. H. Sicking, Interaction of hydrogen isotopes with transition metals and intermetallic compounds, Springer (1996).
[2] F. A. Kuijpers, Philips Res. Rep. Suppl. No.2 (1973) 1.
[3] A. Biris, R. V. Bucur, P. Ghete, E. Indrea and D. Lupu, J. Less-Common Met. 49 (1976) 477.
[4] I. Yamamoto, N. Deguchi, M. Yamaguchi, Y. Shimazu, F. Ishikawa and S. Miura, Physica B 246-247 (1995) 404.
[5] M. Yamaguchi and I. Yamamoto, Chap. 5, pp.131-151 in Dynamic spin chemistry, S. Nagakura, H. Hayashi and T. Azumi eds., Kodansha-Wiley, Tokyo (1998)
[6] I. Yamamoto, K. Ishikawa, S. Mizusaki, Y. Shimazu, M. Yamaguchi, F. Ishikawa, T. Goto and T. Takamasu, Jpn. J. Appl. Phys. 41 (2002) 416.
[7] F. Ishikawa, I. Yamamoto, M. Yamaguchi, Y. Shimazu, T. Goto and H. Mitamura, J. Alloys Comp. 293-295 (1999) 243.

Proposal of a new type of magnetic force

Akio Katsuki[1] and Yoshifumi Tanimoto[2]
[1]*Department of Chemistry, Faculty of Education, Shinshu University, Nishi-Nagano, Nagano 380-8544, Japan*
[2]*Graduate School of Science, Hiroshima University, Higashi-Hiroshima 739-8526, Japan*
(akatuki@shinshu-u.ac.jp)

Abstract
We propose another type of magnetic force, magnetic susceptibility gradient force, which works at interfaces under homogeneous magnetic field.

Keywords
magnetic force, magnetic field gradient force, magnetic susceptibility gradient force

1. Introduction

Generally, it is well known that the magnetic force works effectively only under existence of a magnetic gradient. However, it is reported that some magnetic forces work under a homogeneous magnetic field at certain conditions.[1,2] Especially, these forces appear to work at interfaces, such as those between solid and liquid. We propose a new type of magnetic force, which works at interfaces, that is, a magnetic susceptibility gradient force.[3]

2. Theory

The usual magnetic energy E is given by the following equation,

$$E = -\frac{1}{2}\mu_0 \chi_V V H^2 \tag{1}$$

where μ_0 is a magnetic permeability of vacuum, χ_V is a volume magnetic susceptibility, V is a sample volume, H is a magnetic field. The general magnetic force F is given by a gradient of the magnetic energy as follows,

$$F = -\mathrm{grad}E \tag{2}$$

Substituting eq. (1) into eq. (2) gives the following equation.

$$F = -\mathrm{grad}E = \mu_0 \chi_V V H \frac{dH}{dz} + \frac{1}{2}\mu_0 \frac{d\chi_V}{dz} V H^2 \tag{3}$$

The first term shows a usual magnetic force. Because this term contains a magnetic field gradient at a position z, dH/dz, the degree of the magnetic field gradient determines the magnitude and direction of this force. The second term is a new type force, that is, this term is governed by a magnetic susceptibility gradient. We shall call the first term magnetic field gradient force F_{MFG}, and the second term magnetic susceptibility gradient force force F_{MSG}. Namely,

$$F_{MFG} = \mu_0 \chi_V V H \frac{dH}{dz} \tag{4}$$

$$F_{MSG} = \frac{1}{2}\mu_0 \frac{d\chi_V}{dz} V H^2 \tag{5}$$

The character of this force is described as follows,

1. This force is effective under a homogeneous magnetic field.

2. The direction of this force is determined by the sign of a magnetic susceptibility gradient $d\chi_V/dz$, not that of the magnetic susceptibility χ_V.
3. The magnitude of this force is very sensitive to the magnetic susceptibility gradient $d\chi_V/dz$ at interfaces, and depends on the square of a magnetic field H.

We should consider the third character here. When S is a cross section of a region where the magnetic susceptibility gradient force F_{MSG} works, the sample volume V is described as follows,

$$V = Sdz \tag{6}$$

Substituting eq. (6) into eq. (5) gives the following equation.

$$F_{MSG} = \frac{1}{2}\mu_0 d\chi_V SH^2 \tag{7}$$

The force per unit area, that is, a magnetic susceptibility gradient pressure P_{MSG}, is described as follows,

$$P_{MSG} = \frac{1}{2}\mu_0 d\chi_V H^2 \tag{8}$$

These equations indicate that the magnetic susceptibility gradient force depend on the difference of susceptibilities at an interface between two phases, $d\chi_V$ and the cross section, S.

3. Conclusions

The magnetic susceptibility gradient force F_{MSG} will be effective at interfaces between different phases or materials. These show the possibility of a new type of magnetic force.

Acknowledgements

This work was partially supported by Grant-In-Aid of Scientific Research for Priority Area (Area 767, No. 15085208 and 15085205) from MEXT of Japan, and Grant-in-Aid for Scientific Research (B), 16350007, 2004.

References

[1] W. Duan, M. Fujiwara, Y. Tanimoto, Jpn. J. Appl. Phys., 43(12), 8213-8216 (2004).
[2] F. Tang, A. Katsuki, Y. Tanimoto, *submitted.*
[3] Y. Tanimoto, "Magneto-science: -Magnetic Fundamentals and Applications of Field Effects on Materials-," ed. by M. Yamaguchi and Y. Tanimoto, Kodansha/Springer, Tokyo (2005), Chap. 2-4.

In situ optical measurement of agarose aqueous solution

Shinji Kittaka[1], Shuji Saitou[1], IsaoYamamoto[1],
Masuhiro Yamaguchi[1] and Tadashi Takamasu[2]
1 Department of Physics, Yokohama National University,
Tokiwadai, Hodogaya-ku, Yokohama 240-8501, Japan
2 Tukuba Magnet Laboratory, National Institute for Material Science,
Sengen, Tukuba, Ibaraki, 305-0047, Japan
(d04gd215@ynu.ac.jp)

Abstract
The magnetic field induced changes in the optical properties are measured *in situ* for agarose solution. The birefringence is measured *in situ* by Senarmont method under the influence of the magnetic field of 5T as a function of temperature. The gradually increase in the birefringence is observed in a limited temperature range. The experimental results of the orientation behavior are discussed with the crystal growth in the solution during gelation.

Keywords
magnetic field effect, magnetic alignment, agarose gel, birefringence

1. Introduction

The agarose aqueous solution shows the thermo reversible sol-gel phase transition. Polymer chains consisting of *β-D*-galactose and 3, 6-anhydro *α-L*-galactose form random coils in the solution phase at high temperature. They transform to the double helix structure during gelation process. A gelation model is suggested as follows;[1] many double helices are assembled and aligned to form high concentration regions, called domains. The networks inter the domains develop in gelation process.

The agarose gel formed in the strong magnetic field during gelation process is magnetic aligned because of anisotropic diamagnetic susceptibility of the domain.[2, 3] The birefringence is observed for aligned gel by optical measurement. In the previous studies, we reported that the birefringence of agarose gel formed in magnetic field depends on the magnetic field strength exposed, the magnetic field direction and the concentration of agarose.[3-5] Information of the alignment of the agarose molecules as a function of the temperature is important to understand the sol-gel phase transition and its mechanism under the influence of the magnetic field. In present work, we measured the birefringence of the agarose solution under the strong magnetic field *in situ* to investigate the alignment behavior of the agarose molecules.

2. Experimental methods

2.1 Preparation of agarose gel

The raw material was Agarose type L with the gel strength of 450g/cm^2 supplied from Wako Chemicals. The mixture of agarose powder and distilled water was prepared at the concentration of 2.0wt.% and stirred at room temperature. The agarose solution was heated up to 95℃ and cooled down to 5℃ to form the gel. The gel was heated up again and the hot solution was poured into optical cells with path length of 10mm.

2.2 *In situ* optical measurement

The birefringence was measured *in situ* with the apparatus illustrated schematically in Fig 1. Light from a He-Ne laser passed through a prism, a polarizer with the azimuthal angle of 45deg with respect to horizon, a sample cell, a half wave plate with 22.5deg, a prism, a quarter wave plate with

0deg, a polarizer with (90+ϕ)deg as an analyzer, and an avalanche photodiode as a detector. The analyzer was rotated automatically by using stepping motor, and its angle was controlled with 0.1deg step between $\pm$1.5deg. In our optical system, detected light intensity I is expressed as Eq. (1).

$$I \propto \cos^2(\phi \pm \frac{\delta}{2}), \tag{1}$$

where δ is the retardation by the sample. The minimize angle was estimated to determine the extiction angle by the curve fitting. The retardation δ was obtained from the difference between extinction angles with and without the sample. The birefringence Δn in the sample is calculated according as Eq. (2).

$$\Delta n = \frac{\delta\lambda}{360d}, \tag{2}$$

where λ(=632.8nm) is the wavelength of the laser and d(=10mm) is the pass length of sample.

For *in situ* measurement, the optical cell was set in a horizontal superconducting magnet and exposed to the magnetic fields of 0T and 5T. The optical cell was put between two peltiert devices to control the temperature. The birefringence of agarose solution was measured *in situ* during cooling process from 60℃ to 30℃.

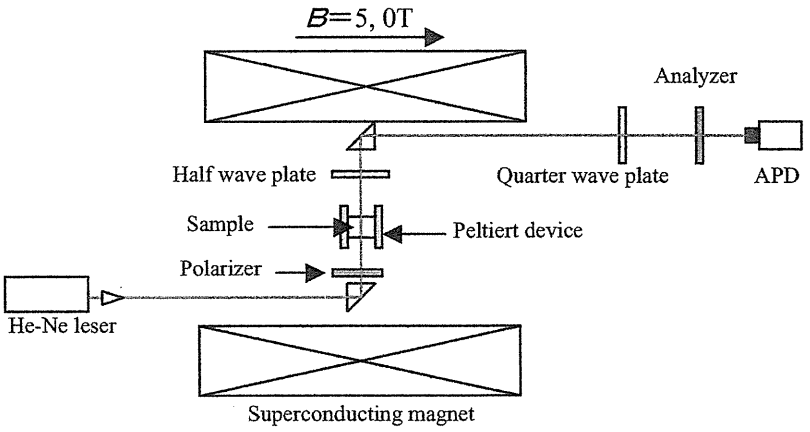

Fig. 1. *In situ* Optical measurement system under magnetic field (top view).

3. Results and discussion

3.1 Concentration dependency

Figure 2 shows the concentration dependence of the birefringence for agarose gels formed in the magnetic field of 5T. The marks and errors bar were calculated from the measurements at the five different points of the same sample. The birefringence was increased with increasing concentration. The birefringence was increased lineally for low concentration gels. However, it tended to saturate toward Δn=1.6$\times 10^{-7}$ for high concentrated gels. The ratio of the magnetic aligned region was not constant but decreased with increasing the concentration of agarose. The magnetic aligned region, namely crystal region was not increased The results show that the domains are difficult to align in high concentration solution with high viscosity.

3.2 Temperature dependency

As shown in Fig. 3, the temperature dependences of the birefringence were measured for agarose solution with the concentration of 2.0wt.% and distilled water in the magnetic fields of 5T and 0T. Here, the birefringence in Fig. 3 was normalized to be Δn=1.35$\times 10^{-7}$ in low temperature region, assuming both the 2.0wt.% gels have the same birefringence of Δn=1.35$\times 10^{-7}$ because of the same

gelation condition of the cooling rate and the influence under the magnetic field of 5T. According to the measurement of distilled water with no birefringence, the experimental accuracy was estimated to be $\Delta n=2\times10^{-8}$.

In the absence of field, the two dates of agarose solution and distilled water agreed well. Accordingly, the orientation did not occur as same as water. On the other hand, the birefringence of agarose solution was increased with decreasing temperature from 54℃ to 40℃ in the magnetic field of 5T. The increase in the birefringence of agarose solution under the magnetic field of 5T was discussed based on gelation model.(ref) Many double helices of agarose polymer chains are aligned and assembled to form the domains in the gelation process. The domains grow gradually with decreasing temperature, and the anisotropic diamagnetic susceptibility of the domains is increased simultaneously. Therefore, under the influence of strong magnetic fields, the domains are oriented because they have large magnetic free energy compared with thermal disturbance. The results shown in Fig. 3 suggest that the growth of domains occurred in the temperature range from 54℃ to 40℃.

The constant birefringence was observed in low temperature region. The growth of domains are thought to be stopped below 40℃. Meanwhile, the birefringence was not observed in elevated temperature region. The large orderable domains do not exist below 54℃.

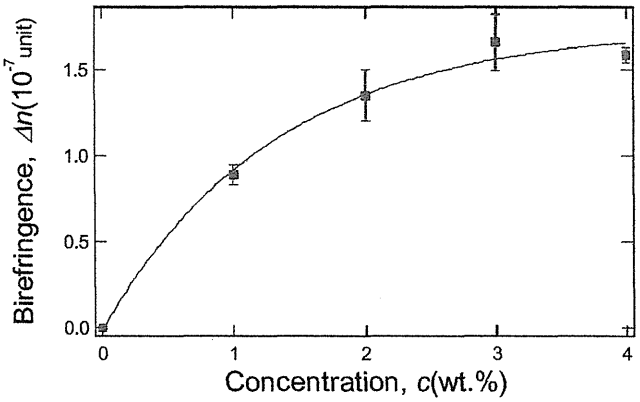

Fig. 2. The concentration dependence of birefringence of agarose gel formed in the magnetic field of 5T.

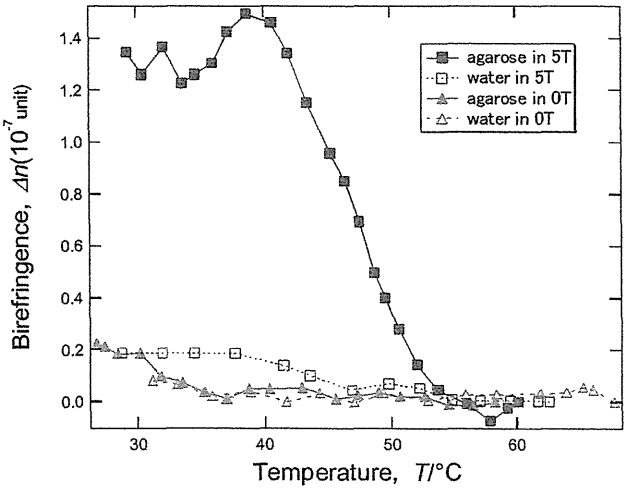

Fig. 3. The temperature dependence of birefringence of agarose solution of 2.0wt.% and distilled water in the magnetic fields of 5T and 0T in cooling process.

5. Conclusions

The birefringence of the agarose solution was measured to investigate the orientation behavior of agarose domains by Senarmont method under the strong magnetic field *in situ*. No magnetic field effect was observed in the absent of magnetic field as same as water. However, the birefringence of agarose solution of 2.0wt.% increased gradually with decreasing temperature from 54℃ to 40℃ in the magnetic field of 5T. As a result of the discussion with the gelation model, the growth of domains was started at 54℃ and finished at 40℃. The region of the domains was increased gradually.

Acknowledgements

This work was supported by Grant-in-Aid for Scientific Research for Priority Areas (No.15085204, Area 767) from MEXT of Japan.

References

[1] A. Hayashi and K. Kinoshita, Polymer J. 12 (1980) 447.
[2] D. W. Kalkwarf and C. Langford, DOS Symp. Ser. 50 (1978) 408.
[3] T. Usui, T. Fushimi, K. Nomoto, I. Yamamoto and M. Yamaguchi, TML Annual Rept. 2002 Suppl. II (2003) 173.
[4] I. Yamamoto, M. Yamaguchi, T. Fushimi, T. Takamasu, TML Annual Rept. 2002 (2003) 99.
[5] T. Usui, Y. Nagano, I. Yamamoto and M. Yamaguchi, Proc. 5th Symp. New Magneto-Science 2002 (2003) 227.

Magnetic Field and Methylene Chain Length Effects on Photochemistry of Bichromophoric Chain Molecules Containing 7-Nitro-2-fluorenyloxy and Anilino Moieties

Kazuya Takahashi[1], Yumi Satoh[2], Shigeru Kohtani[1] and Ryoichi Nakagaki[1]
1 Graduate School of Natural Science and Technology, Kanazawa University, Kakumamachi, Kanazawa 920-1192, Japan
2 Faculty of Pharmaceutical Sciences, Kanazawa University Kakumamachi, Kanazawa 920-1192, Japan
(nakagaki@p.kanazawa-u.ac.jp)

Abstract
Photoredox reaction yields for bifunctional long-chain species consisting of hydrogen-donating and hydrogen-accepting moieties, e.g. 7-nitro-2-fluorenyloxy and alkylanilino chromophores, are critically dependent upon the magnetic field strength. A biradical intermediate with long methylene chain produced by intramolecular hydrogen abstraction may undergo intramolecular cage and intermolecular escape processes. Spin conversion processes between the singlet and triplet biradicals are influenced on application of external magnetic fields. The bichromophoric species with three methylene groups undergoes intermolecular photoredox reactions instead of photo-Smiles rearrangement.

Keywords
Magnetic field effects, Photoredox reactions, Biradical intermediate, Hydrogen abstraction, Cage and escape processes, Chain-length effects

1. Introduction

The intermolecular photoredox reaction for nitro-aromatic species is rather complicated in comparison with intramolecular photoredox processes involving nitro-to-nitroso deoxygenation. The complicated nature comes from the secondary reactions of primary photoproduct, nitroso-aromatic species with reducing reagents. It is, therefore, advantageous to investigate intramolecular photoreaction for bichromophoric chain molecules containing hydrogen-donating anilino-alkyl and hydrogen-accepting nitro-aromatic functionalities.

2. Experimental

2.1 Preparation of Chain-linked Species

2-Amino-7-nitrofluorene was obtained by reduction of 2, 7-dinitrofluorene [1]. This amine was converted into 2-Hydroxy-7-nitrofluorene [2], which was coupled with α, ω-dibromoalkane. The resultant 2-(ω-bromoalkoxy)-7-nitrofluorene was treated with aniline to form the title compounds [3]. In the present study, bichromophoric species with 3 and 12 methylene groups were synthesized and photolyzed in the absence and presence of magnetic fields. An authentic sample for oxidation product with ω-formylalkoxy side chain was obtained by oxidation of 2-(ω-hydroxyalkoxy)-7-nitrofluorene. The structures of starting species and photoproduct were confirmed by means of NMR spectroscopy and mass spectrometry.

2.2 Irradiation

The degassed sample solution was irradiated with UV light from a high-pressure mercury arc (Ushio USH-500D). The spectral line at 365nm was chiefly used for selective excitation of nitro-aromatic chromophore.

2.3 Analysis and Identification of Photoproducts

The sample solutions photolyzed in the absence and presence of magnetic fields were analyzed by means of high-performance liquid chromatography (HPLC). A Waters model 515 was used as a pump for HPLC analysis.

2.4 Magnetic Field Effects on Photoredox Reactions

A conventional electromagnet was used for generation of magnetic fields lower than 1 T. Photoinduced changes in absorption spectra were recorded in the absence and presence of magnetic fields. Spectral changes were measured on a Hitachi U-3210 spectrophotometer.

3. Results and Discussion

3.1 Methylene Chain-length Effects

Bichromophoric chain species consisting of nitro-aryloxy and anilino chromophores undergo photo-Smiles rearrangement when the number of methylene groups is smaller than 6 (see Scheme 1) [4]. However, what we have found in the present study is photoredox reaction for the nitrofluorenyl derivative with three methylene chain instead of photochemical rearrangement (Scheme 2). Table 1 summarizes the photoreaction type of compounds containing nitroaryloxy and anilino-propyl groups. The efficiency of photoredox process may be related with the radical scavenging ability of the starting nitro-aromatic species in the ground state. Scheme 2 implies that the 2-formylethoxy side chain is formed on an intermolecular photoredox reaction, since the intramolecular hydrogen abstraction is impossible for short-chain species. This photoredox process is to be studied in full detail.

Table 1. Chain-length Effects on Photochemistry of Three-methylene-linked compounds

Nitro-aromatic Chromophore	Type of Photoreaction
4-nitro-1-naphthoxy	Photo-Smiles Rearrangement
7-nitro-2-fluorenyloxy	Intermolecular Photoredox Reaction

3.2 External Magnetic Field Effects on Reaction Yields

Scheme 3 describes the inter- and intramolecular photoredox reactions for the bifunctional species consisting of 7-nitro-2-fluorenyloxy and anilino moieties with twelve methylene groups. The magnetic field effects on cage and escape product formation were determined from the intensity ratio of chromatographic peaks. Namely, the relative intensity I(H)/I(0) was calculated and listed in Table 2, where I(H) and I(0) were peak intensity of the products obtained by photolysis in the presence and absence of 1 T. In this study, larger external magnetic field effects were observed on the reaction yields for the intramolecular cage and bimolecular escape processes of 7-nitro-2-fluorenyloxy species with twelve methylene groups than the corresponding 4-nitro-1-naphthoxy derivative [5].

Since oxidative dealkylation of anilino-alkyl side chain may take place through both the cage and escape processes, no magnetic field effects were observed on the formation yield of aniline.

Table 2. Magnetic Field Effects on Reaction Yield Ratios I(H)/I(0)

Nitro-aromatic Chromophore	Cage Product (Nitroso-1)	Escape Product (Nitro)
4-nitro-1-naphthoxy	0.59 ± 0.09	1.99 ± 0.63
7-nitro-2-fluorenyloxy	0.52 ± 0.05	2.44 ± 0.98

The escape products (aniline, nitro and nitroso-2) are formed via triplet biradical intermediates formed by intramolecular hydrogen abstraction by nitro-aromatic moiety in the excited triplet state. The cage compounds (aniline and nitroso-1) are produced through intersystem crossing (ISC) and/or spin-lattice relaxation (SLR) from the triplet to singlet biradicals. A ratio of cage to escape product yields is critically dependent on the magnetic field strength. The major product in the zero-field (nitroso-1) becomes a minor product on application of 1T, while the minor product in the zero-field (nitro) becomes a major product in the presence of 1T. In other words, magnetic fields can give rise to switching of reaction pathways.

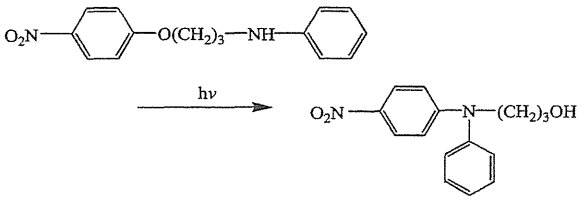

Scheme 1. Photo-Smiles rearrangement of N-[3-(4-nitrophenoxy)propyl]aniline

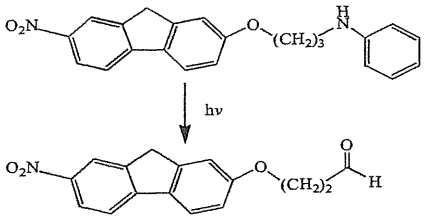

Scheme 2. Photo-induced oxidative dealkylation of N-[3-(7-nitro-2-fluorenyloxy)propyl]aniline

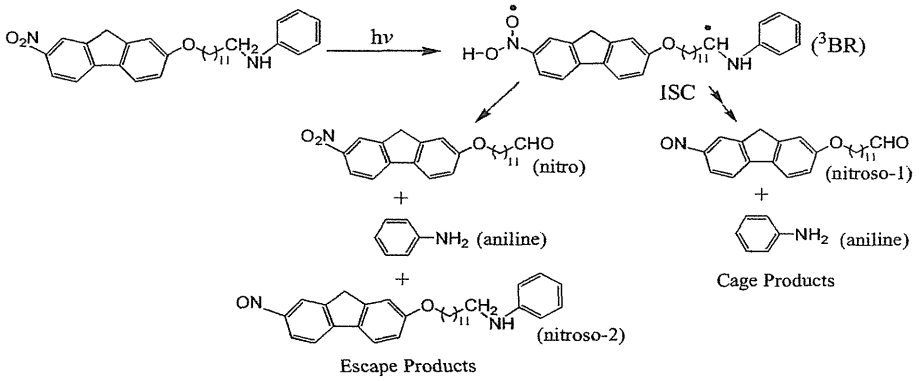

Scheme 3. Photoredox reactions of 2-(12-anilinododecyloxy)-7-nitrofluorene

Acknowledgement

This work was partly supported by a Grant-in-Aid for Scientific Research on Priority Area "Innovative Utilization of Strong Magnetic Fields" (Area767, No.15085208) and "Fundamental Science and Technology of Photofunctional Interface" (Area 417) from MEXT of Japan. One of the authors (K. T.) thanks the Japan Science Society for Research Grant for the financial support of Sasakawa Scientific Research Grant.

References

[1] G. Saroja, Z. Pingzhu, N. Ernsting, and J. Liebshcer, J. Org. Chem., 69 (2004) 987-990.
[2] M. Hayashi and N. Ishikawa, J. Synth. Org. Chem., 13 (1955) 171-174.
[3] R. Nakagaki, M. Yamaoka, and K. Mutai, Bull. Chem. Soc. Jpn., 72 (1999) 347-355 and references cited therein.
[4] R. Nakagaki and K. Mutai, Bull. Chem. Soc. Jpn., 69 (1996) 261-274 and references cited therein.
[5] R. Nakagaki, Riken Review, No. 44, (2002) 63-65.

Magnetoadsorption of Gases on Porous Materials

Akihito Yoshidome, Shigeo Sasahara, Taku Iiyama and Sumio Ozeki
Department of Chemistry, Faculty of Science, Shinshu University
3-1-1 Asahi, Matsumoto, Nagano 390-8621, Japan
(sozeki@shinshu-u.ac.jp)

The magnetic-field-induced adsorption and desorption (MAD) of paramagnetic NO and diamagnetic H_2O and organics was found under external, steady magnetic fields less than 10 T. In microporous materials, such as zeolites and activated carbons, MAD depended strongly on solids and magnetic field intensity. Such MAD of physisorbed molecules in multilayers and pores, i.e., the magnetic effect on the adsorption equilibrium, should be accompanied by changes in the magnetic moment of the adsorptives and/or solids while adsorbing under a steady magnetic field, as given by the following equation:

$$\Delta p / p_0 = -\Delta M H / RT,$$

where H is the external magnetic field, p_0 the initial pressure at $H = 0$, Δp the pressure change by applying a magnetic field H, ΔM the magnetization change of the system due to the adsorption of 1 mol of an adsorptive under H, R the gas constant, and T the absolute temperature. On the other hand, even when the magnetic moment of an adsorption system remains unchanged, a magnetic effect on the adsorption may kinetically occur if a local magnetic field is produced around the solids by applying a steady magnetic field.

In this study, magnetic field effects on adsorption of various gases, especially hydrogen adsorption near the critical temperature, on activated carbons and carbon nanotubes will be reported. The hydrogen pressure decrease due to a 10 T magnetic field was found at all temperature range examined (Fig.1). There is a slight slippage from the curve in the critical temperature region. They suggest that adsorbed hydrogen should be magnetic and the adsorption state (structure and magnetism) of hydrogen should be change at the critical temperature.

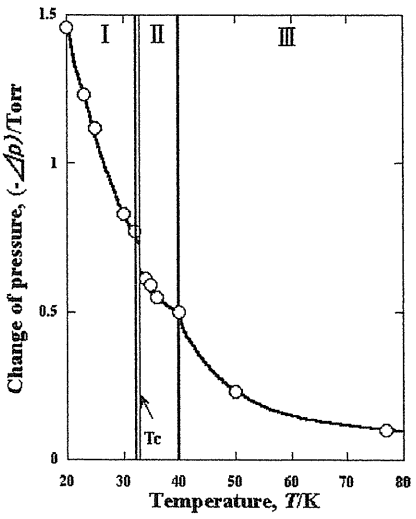

Fig1. Temperature dependence of pressure change due to a 10T magnetic field.(11.6Torr)

Acknowledgment: This work was supported by Grant-in-Aid for Scientific Research on Priority Area "Innovative utilization of strong magnetic fields" (Area 767, No.15085205) from MEXT of Japan.

Magnetic Orientation of Organic Nanocrystals

Manabu Sueda[1], Wenyong Duan[1], Yoshifumi Tanimoto[1], Yuji Kaneko[2], Tsunenobu Onodera[2], Hitoshi Kasai[2], Hidetoshi Oikawa[2], and Hachiro Nakanishi[2]

[1] *Graduate School of Science, Hiroshima University, Higashi-Hiroshima 739-8526, Japan*

[2] *Institute of Multidisciplinary Research for Advanced Materials, Tohoku University, Sendai 980-8577, Japan*

(paku@hiroshima-u.ac.jp)

Abstract

We examined the orientation of organic nanocrystals (perylene and poly-DCHD) in a horizontal magnetic field (8T). Nanocrystals in water suspension were deposited on a glass plate by solvent evaporation and their orientation was observed by AFM. The perylene rectangular and fiber nanocrystals are likeky oriented in a magnetic field of 8 T, whereas the poly-DCHD nanocrystals are not.

Keywords

magnetic field effect, magnetic orientation, nanocrystal, AFM, poly-DCHD, perylene

1. Introduction

In a high magnet field, many inorganic and organic materials are oriented because of their anisotropic magnetic susceptibility.[1] In a previous paper,[2] we have shown that carbon nanofibers are oriented in a magnetic field of 8 T, indicating that magnetic orientation of nano-scale crystals is capable. It is considered that magnetic alignment of nano-scale aggregates is very important technique in nano-technology for improving the quality of nano-materials, because functional nano-materials are expected to have many new characteristics with a magnetic alignment.[3,4,5]

In this paper, we examined magnetic orientation of organic nanocrystals using a horizontal magnetic field (8 T). It is suggested that magnetic orientation of perylene rectangular and fiber nanocrystals is capable, whereas that of poly-DCHD nanocrystals is not.

2. Experimental methods

The nanocrystals used for this experiment were obtained by the re-precipitation method.[3,4] An acetone solution saturated with perylene was prepared, and this acetone solution (ca. 0.2ml) was injected into distilled hot water (ca. 343K and 10ml) while stirring. After two hours' retention time, water suspension of rectangular perylene nanocrystals was obtained. Perylene fiber nanocrystal suspension was obtained similarly. Poly-DCHD fiber nanocrystal suspension was obtained as follows. An acetone solution (0.6ml) of DCHD (1,6-di (N-carbazolyl)-2,4-hexadiyen) (1mM) was injected into distilled water (30ml) while stirring and DCHD nanocrystals were solid-state polymerized.[5]

A glass vessel (φ = 3.1cm), in which two alkali-solution-treated glass plates (1.2×1.2×0.2 mm) were placed, was filled with the suspension of nanocrystals (ca, 2.0ml) and was placed in a bore of a superconducting magnet (Oxford, Spectromag-1000). As a control, another vessel was placed outside the magnet. Temperature of the solution was kept at ~343K by circulating hot water. Nanocrystals were deposited on the glass plates by solvent evaporation. Orientation of nanocrystals on the glass plate was observed by using a scanning probe microscope (SII, SPI 3800N/SPA 400) with AFM tapping mode.

3. Results

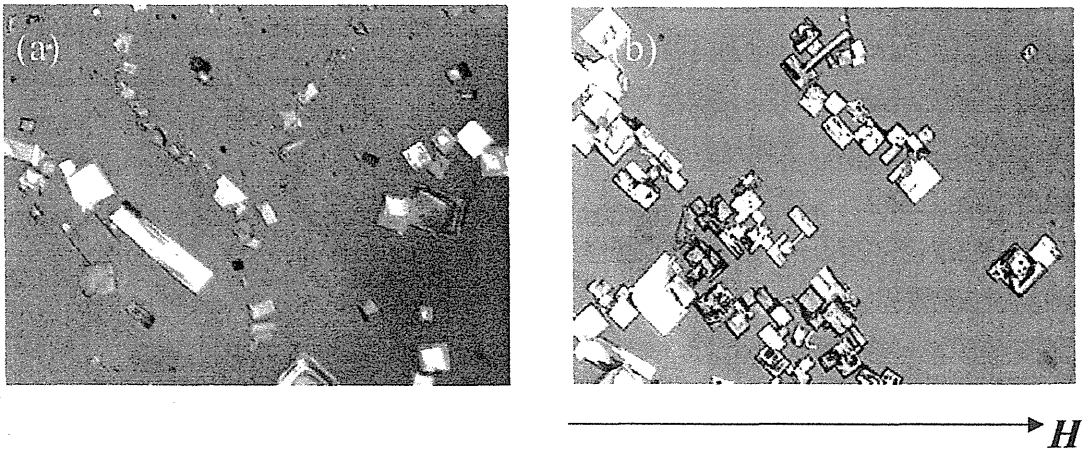

Figure 1. The typical photo-images of perylene micorocrystals (a) 0 T, (b) 8 T. The arrow indicates the direction of magnetic field. The size of the image is 0.76 mm×1.06 mm.

As a preliminary experiment, the magnetic orientation of perylene microcrystals, obtained from solvent evaporation of its acetone saturated solution, was examined. Figure 1 shows the typical photo-image (×300) of perylene microcrystals in the absence and presence of a magnetic field of 8 T. At zero field, the rectangular crystals are randomly oriented. At 8T, the crystals are oriented in such away that the angle between the crystal's long axis and the direction of magnetic field is about 50°. This confirms that magnetic orientation of perylene crystals with micrometer size is experimentally capable. Taking this result into account, the magnetic orientation of perylene rectangular nanocrystals was carried out.

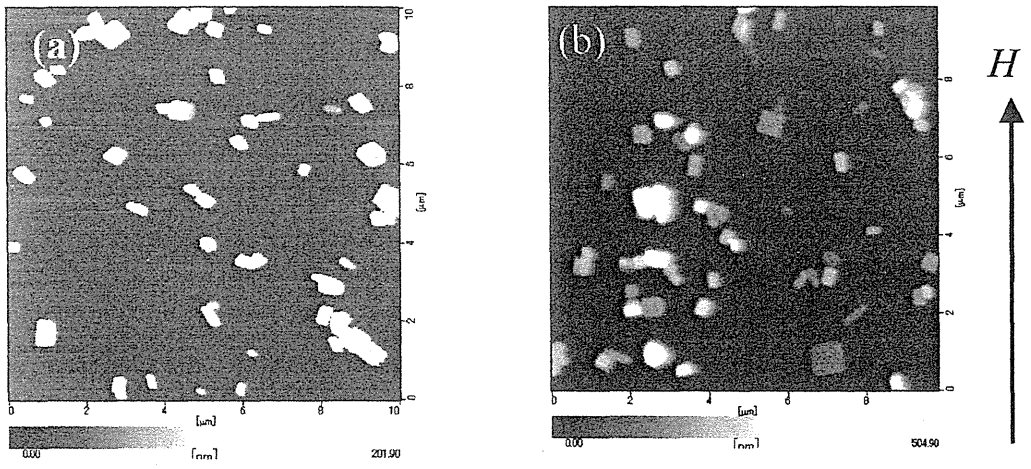

Figure 2. AFM images of perylene nanocrystals (a) 0 T, (b) 8 T. The arrow indicates the direction of magnetic field. The size of image is 10μm×10μm.

Figure 2 shows the AFM images of perylene rectanglar nanocrystals in the absence and presence of a magnetic field of 8 T. At zero field, the nanocrystals are oriented randomly. At 8T, the nanocrystals seem to be oriented in such away that the rectangular crystal's long axis is almost parallel to the direction of magnetic field. Rectangular crystals are not convenient for orientation determination. So we examined nanocrystals with fiber-shape.

Figure 3 shows the AFM images of perylene fiber-nanocrystals in the absence and presence of magnetic field. Both fiber-nanocrystals with about 2μm length and rectangular ones with about 1μm are observed in these images. From comparison of (a) and (b), it is suggested that perylene fiber-nanocrystals seem to be oriented at 8 T in such away that its long axis is perpendicular to the direction of magnetic field.

As another example of fiber-shape nanocrystal, magnetic orientation of poly-DCHD fiber nanocrystals was examined. Figure 4 shows the AFM images of poly-DCHD nanocrystals deposited (a) at 0T and (b) at 8T. Poly-DCHD fiber nanocrystals whose length is about 5μm are certainly deposited on a glass plate. However, from the comparison of (a) and (b), it is concluded that the nanocrystals seem to be randomly oriented regardless of magnetic field.

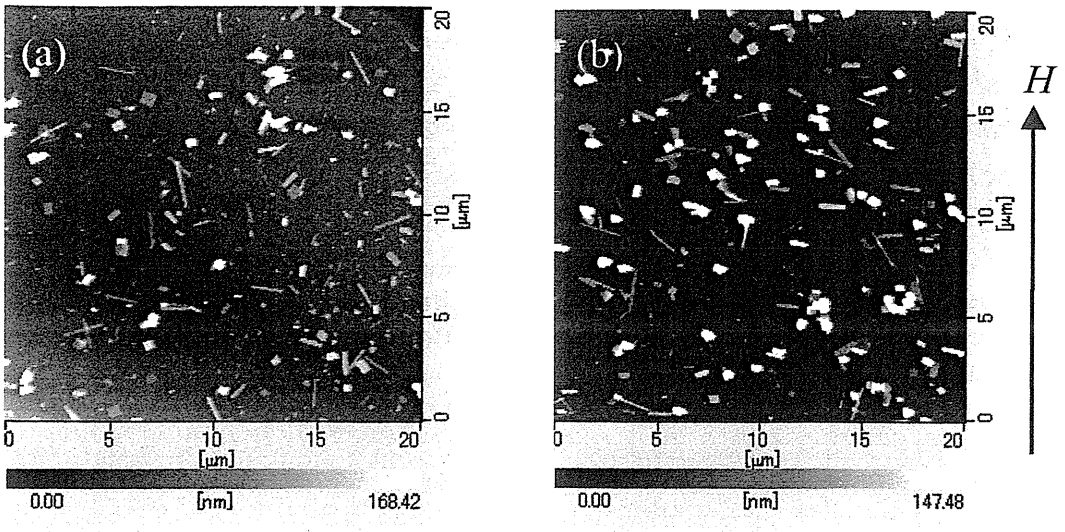

Figure 3 The typical images of perylene fiber-nanocrystal at (a) 0T, (b) 8T. The arrow indicates the direction of magnetic field, (↑*H*). The size of image is 20μm×20μm.

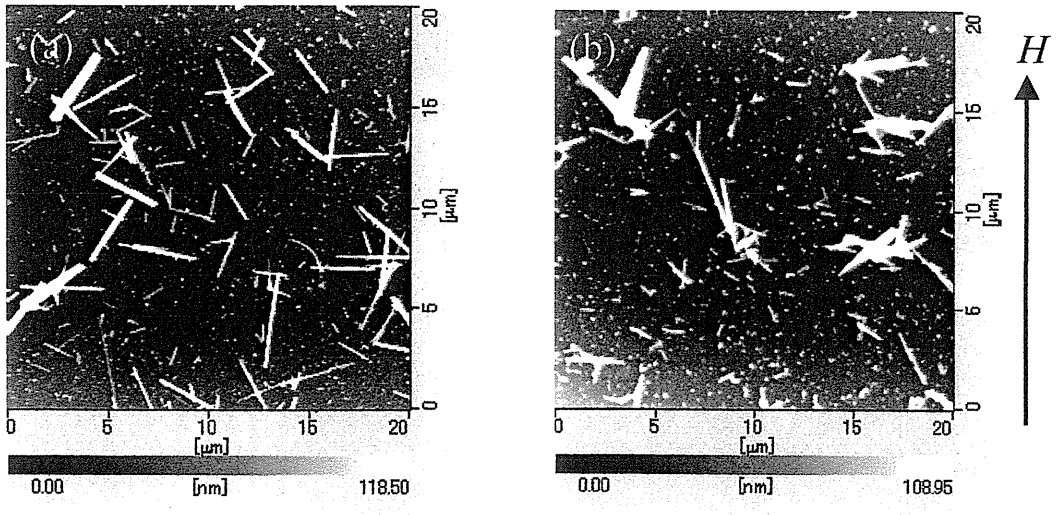

Figure 4 Typical images of poly-DCHD nanocrystals at (a) 0T and (b) 8T magnetic field. The direction of magnet field is expressed as the arrow (↑*H*). The size of image is 20μm×20μm.

4. Discussion

When materials having anisotropic magnetic susceptibilities are placed in magnetic field, its orientation energy (E) can be expressed as below. [1,2,4]

$$E = - N \Delta\chi B^2 / 2\mu_0 \qquad (1)$$

where N is the number of molecules, $\Delta\chi$ is the anisotropy of magnetic susceptibility, B is the magnetic flux density, and μ_0 is the magnetic permeability of vacuum. When E is sufficiently larger than the thermal energy, materials placed in a magnetic field are oriented at a certain angle from the direction of magnetic field.

In a previous paper,[6] one of the authors has studied the magnetic field dependence of angular distribution of benzophenone rod-like crystals ($\Delta\chi = 88.3 \times 10^{-6}$ cm^3 mol^{-1}) with 2-3 cm in length. It is estimated that their magnetic orientation occurs at 8 T when they grow to the critical crystal size of $1.9 \times 0.2 \times 0.2\mu$m. Crystal sizes of nanocrystals studied here are more or less similar to the critical size for magnetic orientation estimated. Therefore, it seems that magnetic orientation of perylene nanocrystals is experimentally capable at 8 T, though poly-DCHD nanocrystals are not. Furthermore, in the case of perylene fiber nanocrystals the orientation direction is different by 90° from that estimated by the optical polarization measurements.[4] These facts means that there exist several experimental factors influencing magnetic orientation of nanocrystals. The first is the orientation energy. As estimated from the previous work, [6] the magnetic flux density of 8 T is not sufficiently strong to overcome the disturbance induced by the thermal energy, indicating the utilization of higher field for the magnetic orientation is preterable. The second is that the magnetic orientation of nanocrystals achieved in the solution might be disturbed by evaporation. Because of the turbulent motion of solution during evaporation might disturbes orientation of nanocrystals might be disturbed significantly. The third is the evaporation process for preparation of oriented nanocrystals. Evaporation of solvent is complex. On the glass plate nanocrystals do no deposit uniformly but deposit in stripe-shape, as well-known by the name of non-linear phenomena. Formation of stripes might influence somewhat the hydrodynamics of the solution near the stripe, though the images shown in Figs. 2-4 are taken at the glass surface where no stripe exists. In order to overcome these difficulties, it is better to use a higher magnetic field, since orientation energy can exceed the thermal energy of nanocrystals and fix their orientation strictly. In order to solve the stripe formation on the glass, it might be better to use some other plate in place of glass plate. Research based on the above consideration is in progress.

Acknowledgements

This work was supported partly by a Grant-in-Aid for Scientific Research on Prioirty Area (Area 767, No. 15085208) from the Ministry of Education, Culture, Sports, Science, and Technology of Japan.

References

1) M. Fujiwara, T. Chidiwa and Y. Tanimoto, *J. Phys. Chem. B,* **104** (2000) 8075.

2) M. Fujiwara, E. Oki, M. Hamada, Y. Tanimoto, I. Mukouda and Y. Shiomura, *J. Phys. Chem. A,* **105** (2001) 4383.

3) T. Onodera, H. Kasai, S. Okada, H. Oikawa, K. Mizuno, M. Fujitsuka, O. Ito and H. Nakanishi, Optical Materials **21** (2002) 595.

4)Y. Kaneko, T. Onodera, H. Kasai, S. Okada, H. Oikawa, H. Nakanishi, T. Fukuda and H. Matuda, *J. Mater. Chem.* **15** (2005) 253.

5)T. Onodera, T. Oshikiri, H. Kasai, S. Okada, H. Oikawa, M, Terauchi, M. Tanaka, H. Nakanishi, *J. Cryst. Growth* **229** (2001) 586

6) M. Fujiwara, M. Fukui and Y. Tanimoto, *J. Phys. Chem. B,* **103** (1999) 2626

Magnetic Field-induced Migration of a Paramagnetic Ion in the Aqueous Solution

Tsubasa Takeda, Takeru Kogawa, Isao Yamamoto and Masuhiro Yamaguchi
Department of Physics, Yokohama National University,
Tokiwadai, Hodogaya-ku, Yokohama 240-8501, Japan
(d05gd228@ynu.ac.jp)

The magnetic force-induced migration (magnetomigration) of a single paramagnetic ion was observed in the aqueous solution for the first time. 1N Dy^{3+} aqueous solution was situated in a gradient magnetic field ($0<B<12.6$T) at 293.2±0.2 K for 336 hours, followed by the optical measurement of ion concentration. The concentration difference was Δc=0.67±0.42% between the solutions at high field side ($9.1<B<12.3$T) and that at low field side ($3.5\text{T}<B<9.1\text{T}$). This is consistent to the calculated value of Δc=0.87% on the basis of the diffusion equation including the drifting term by the magnetic force. The dependence of the concentration difference on the duration of magnetic field exposure indicated that the magnetomigration was saturated at 168 hours.

KEYWORDS: magnetomigration, magnetic force, dysprosium ion, ion migration, high magnetic field

1. Introduction

The magnetic force (Faraday force) acting on a single ion is much weaker compared with thermal disturbance. Therefore, it is difficult to separate or concentrate ions in the aqueous solution without other influences such as electric field, chemical reactions, droplets, absorbents, etc. For instance, transition metal ions were separated with the aid of a liquid-solid redox reaction and the absorption on silica gels.[1,2] In this paper, we intend to observe the magnetic force-induced migration (called magnetomigration) of a single paramagnetic ion in the aqueous solution without any other influences. Basically, the magnetic force is proportional to the square of the effective moment for an ion and a magnetic field. We select the Dy^{3+} ion because it has the largest effective moment ($\mu_{eff}=10.63\mu_B$) of all metallic ions and high magnetic fields up to 13T.

2. Prediction

Let us suppose the one-dimensional system in which the ion concentration $n(x,t)$ depends on only the x coordinate under the influence of the magnetic field $B(x)$. The time and spatial variation in $n(x,t)$ obeys the diffusion equation, assumed that the temperature T is constant throughout time and position since the phenomenon proceeds very slowly.

$$\frac{\partial n(x,t)}{\partial t} = D\frac{\partial^2 n(x,t)}{\partial x^2} - \mu\frac{\partial}{\partial x}\{f(x)n(x,t)\} \tag{1}$$

where D and μ are the diffusion constant and the mobility of the ion in the solution, respectively and the Einstein's relation $D/\mu=k_BT$ is satidfied. The drift is caused by the magnetic force $f(x)$.

$$f(x) = \kappa_{ion}B(x)\frac{dB(x)}{dx} \tag{2}$$

where κ_{ion} is the magnetic susceptibility per ion.

$$\kappa_{ion} = \frac{\mu_{eff}^2}{3k_B T}, \qquad (M_{ion} = \kappa_{ion}(\mu_0 H)) \tag{3}$$

When the steady state is attained, the left-hand side of Eq.(1) becomes zero and the ion flow disappears, then, the spatial distribution of ion concentration is expressed by

$$n(x) = C\exp\left(\frac{\kappa_{ion}}{2k_B T}B(x)^2\right) \tag{4}$$

where C is the constant which is determined by the total number of ions in the solution.

If the Dy^{3+} ion (κ_{ion}=8.007×$10^{-25}$$JT^{-2}ion^{-1}$) is exposed by a magnetic field of 13T at 300K, the ratio of ion concentration at 13T to that at 0T is $n(B$=13T)/$n(B$=0T)=1.009. This is possibly observed in a sever experiment. In contrast to this, if the Cu^{2+} ion (κ_{ion}=0.212×$10^{-25}$$JT^{-2}ion^{-1}$) is examined, that ratio is $n(B$=13T)/n(B=0T)=1.0004, actually resulting in an impossible observation.

3. Experimental methods

3.1 Requirements

We must set careful experimental conditions in order to detect the concentration difference of less than 1% for Dy^{3+} ion. The temperature gradient of 1K in a solution at 300K possibly causes the concentration difference of 0.3% on the assumption of an ideal solution. Accordingly, the temperature is desired to be controlled within the deviation of 0.2K throughout the sample. Judging from the mobility of a metallic ion in the aqueous solution by an electric field, it may take several hundred hours for Dy^{3+} ions to migrate a distance of a few mm by the magnetic force produced by a 13T magnet.

3.2 Samples and equipment

The sample was 0.9N-$Dy(NO_3)_3 6H_2O$ aqueous solution. Nitrogen gas was bubbled into the solution for removing oxygen and stirring it for 30 min. This solution was fully contained in sample tubes with the inside bore of 6mm and the total length of 200mm. Each sample tube consisted of two 90mm-long glass tubes (A-R and R-A') connected by a 20mm-long rubber joint R as shown by the inset in Fig.1. We use a cryo-cooled superconducting magnet (JMTD-13T100EF3, Japan Superconducting Technology Co. Ltd.) with the maximum field of 13T and 100mm bore at room temperature. The magnet was horizontally situated. The temperature of samples was controlled at 293.2±0.2K during magnetic field exposure by the temperature-controlled water which was circulated through a double wall jacket inside of the magnet's bore. The temperature gradient was less than 0.1K along the sample tubes. This was measured by a thermister (YSI44004, TDK) which output scarcely depended on magnetic fields.

3.3 Magnetic field exposure

We made two kinds of experiments for magnetic field exposure. In Experiment 1, we prepared 32 sample tubes and classified them into two assemblies with 16 tubes each. The two assemblies were located in different positions in the magnet' bore as shown in Fig. 1. One assembly was located in Position A-R-A' with high fields between 12.3T at A, 9.1T at R and 3.5T at A' and the other assembly was in Position B-R-B' with law fields between 0.2T at B, 0.13T at R and 0.1T at B' when the magnetic field was 12.6T at the magnet's center. The magnetic field was exposed for 336 hours. Immediately after the field exposure, each sample tube was separated into two parts at the central

rubber joint R. Then, outside of the magnet, the Dy^{3+} concentration in the solution was measured by the intensity I of absorption line at 806.9nm with a spectrometer (UV-1700, Shimadzu Co.). The concentration difference was obtained from $\Delta c=(I_A-I_{A'})/I_A$ or $(I_B-I_{B'})/I_B$ where I_A, $I_{A'}$, I_B and $I_{B'}$ were the line intensities of the solution at Parts A, A', B and B' respectively. The experimental error of the concentration difference was ±0.1% for each sample tube.

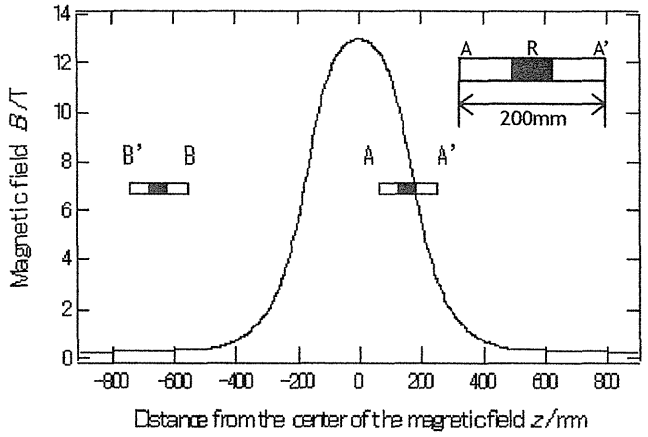

Fig.1. Spatial distribution of magnetic fields and Positions A-A' and B-B' of the sample tubes for magnetic field exposure. The inset shows a sample tube.

In Experiment 2, we prepared 7assemblies with 8 sample tubes each. The assemblies were located in the same position of A-R-A' and exposed by the same magnetic field as in Experiment 1. But the exposed duration was varied between 24 and 672 hours.

3. Results and Discussion

Figure 2 shows the result of Experiment 1 by the distribution of the measured values for the concentration difference Δc. Obviously, the samples in Position A-R-A' has non-zero value of Δc=0.67±0.42%; in contrast to this, the samples in Position B-R-B' has nearly zero value of Δc=0.07±0.42%.

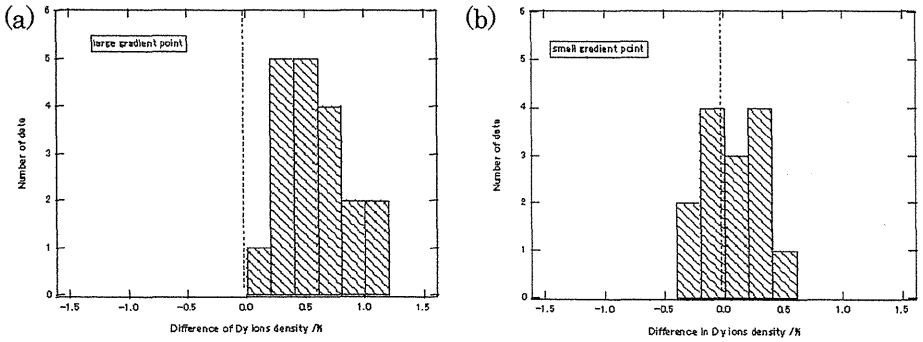

Fig. 2. Distribution of the measured values for the concentration difference Δc. (a) Position A-R-A' and (b) Position B-R-B'.

We compare these values with the calculation based on Eq.(4). For the solution of Position A-R-A', for instance,

$$\Delta c = \left(\int_{A}^{R} n(x)dx - \int_{R}^{A'} n(x)dx \right) \Big/ \int_{A}^{R} n(x)dx \qquad (5)$$

The calculation gave Δc=0.87% for Position A-R-A' and Δc~0.00% for Position B-R-B'. These values agree with the observed ones. We have confirmed that Dy^{3+} ions were migrated in the aqueous solution by the magnetic force.

Figure 3 illustrates the result of Experiment 2 by the dependence of the ion concentration difference Δc on the duration of magnetic field exposure. It is observed that the ion migration gets saturated in about 168 hours. The time dependence obtained can be fitted by the exponential type relation.

$$\Delta c(t) = A(1 - \exp(-t/\tau)) \qquad (6)$$

where A is the calculated steady value of Δc=0.87% and τ is the effective time constant of 96 hours. In the present 0.9N solution, the ions migrate in a larger velocity than that we predicted. It is speculated that the ions in a concentrated solution are much more forced by magnetic fields compared with ones in a dilute solution.

In conclusion, we have observed the magnetomigration of a single paramagnetic ion in the aqueous solution using by the Dy^{3+} ion solution in high magnetic fields up to 13T.

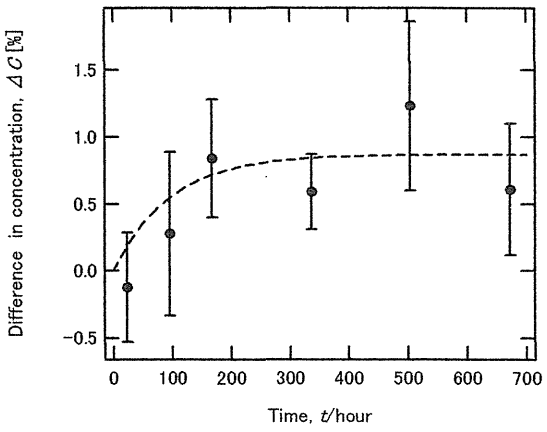

Fig.3. Ion concentration difference Δc vs. the duration of magnetic field exposure. The broken line is the fitting curve according to Eq.(6).

Acknowledgement

This work was supported by Grant-in-Aid for Scientific Research on Priority Area "Innovative utilization of strong magnetic fields" (Area 767, No.15085204) from MEXT of Japan.

References

[1] Y. Tanimoto, H. Yano, S. Watanabe, A. Katsuki, W. Duan and M. Fujiwara, Bull. Chem. Soc. Jpn. 73 (2000) 867.
[2] M. Fujiwara, K. Chie, J. Sawai, D. Shimizu and Y. Tanimoto, J. Phys. Chem. B 108 (2004) 3531.

Unusual Magnetic Properties of Water Adsorbed on Gold Surface

Yhuhei Terui, Norihito Sogoshi and Seiichiro Nakabayashi
Department of Chemistry, Faculty of Science Saitama University,
Shimookubo 255, Sakura- ku, Saitama 338-8570, Japan
(moonhill_1@chem.saitama-u.ac.jp)

Various investigations have been carried out on the adsorption of water on metal surfaces. Ito *et al.*[1] showed that the structure of adsorption of water on metal surfaces including Pt(111) and Ru(001). From IR spectra and STM, a water molecule is bound to a surface metal atom strongly, and H atoms of the water molecule are oriented upward. The water molecules forms a triangulear lattice in the first layer. In the second layer, a water molecule is bound to three water molecules in the first layer to form a tetrahedral-like structure. This structure is called a bilayer ice structure.

Harigaya *et al.* [2] showed that stacked nano-graphite has paramagnetism by π-π interaction between the sheets using the Hubbard type model theory. Furthermore, they suggested that the paramagnetism decreases dramatically on adsorption of water on the sheets.

Recently, we are interested in hydrogen bonds of water on the metal and its magnetism. Magnetism of hydrogen bonds was investigated by measuring refractive index of water under a strong magnet field.[3] Although the refractive index changes only by ~0.1% at 10T, it is attributed to the magnetic response of hydrogen bonds. This means hydrogen bonds are stabilized under a magnetic field. Results of deuterium substitution and other organic solvent support this hypothesis. Furthermore, it was found that the magnetism of water adsorbed on a gold surface is different from that of bulk water.

In order to study the interfacial magnetism of water on a gold surface, self-assembled monolayers (SAM) of alkanethiol were used, changing the length of the alkyl chain and the terminal group between hydrophilic and hydrophobic ones. We used a surface plasmon resonance sensor that measures the refractive index of liquid on the gold film very sensitively. In Fig. 1, the change of refractive index of water was plotted against the magnetic field. The increase of the refractive index for SAM surfaces is similar to each other and to the one of bulk water (not shown). The substitution between ionic (-COOH) and nonionic ($-CH_3$) terminal groups have no remarkable effect on the behavior under the magnetic field. This suggests that water in the electric double layer does not respond to the magnetic field. Therefore, we can conclude that water in the inner Helmholz layer, that is, water adsorbed on the surface contributes the interfacial magnetism significantly.

Currently, the direct investigation of the interface magnetism is under progress using a surface sensitive magnetic measurement like Surface Magneto-Optical Kerr Effect (SMOKE).

Reference:
1) M. Nakamura, Y. Shingaya and M. Ito, Surf. Sci., 502-503 (2002) 474
2) K. Harigaya, Hyoumenkagaku, 26 (2005) 47
3) H. Hosoda, N. Sogoshi and S. Nakabayashi, J. Phys. Chem. A, 108 (2004) 1461

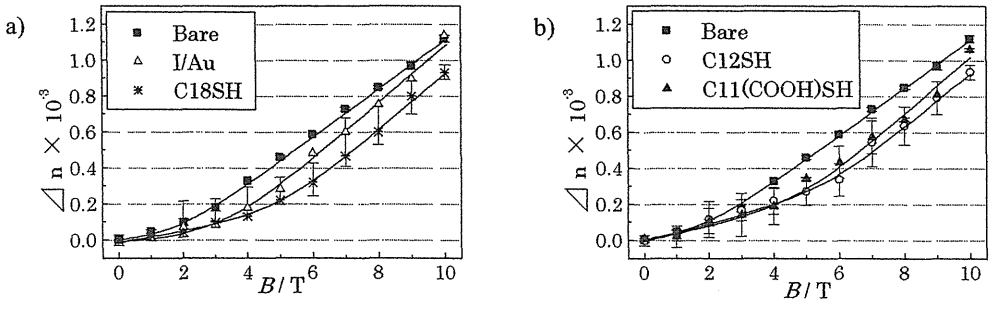

Fig.1 Refractive index of water measured by SPR sensor. The Au surface of the SPR sensor was clean (squares, Bare) and a) modified by iodine atoms (open triangles, I/Au) and 1-octadecanethiol (stars, C18SH), b) undecanethiol (circles, C12SH) and mercapt undecanoic acid (close triangles, C11(COOH)SH).

Effect of the High Magnetic Field on Cylindrical Microdomains in a Block Copolymer Thin Film

Yoshhihiro Tsuji[1], Shinichi Sakurai[1] , Kazushi Yamada[2] , Akira Itaya[1] ,
Fumiko Kimura[3] , Masafumi Yamato[4] and Tsunehisa Kimura[3,4]
1 Department of Polymer Science and Engineering, Kyoto Inst. of Tech.
Matsugasaki, Sakyo-ku, Kyoto 606-8585, Japan ,
2 Venture Laboratory, Kyoto Inst. of Tech.
3 Tsukuba Magnet Laboratory, National Institute of Material Science
4 Graduate School of Engineering, Tokyo Metropolitan University
(Tsuji04@kit.jp)

Magnetic-field induced orientation of microdomain structures was examined for block copolymers comprising non-crystalline block chains. We consider that microdomains may be oriented by applying the magnetic field, bearing in mind that the microdomain interface possibly possesses a diamagnetic susceptibility. To experimentally confirm this idea, we used thin film of a polystyrene-*block*-poly(ethylene-*co*-but-1-ene)-*block*-polystyrene triblock copolymer (SEBS), which forms PS cylinders in PEB matrix. The SEBS sample was spin-cast on Si wafer. High magnetic fields with 30 Tesla were imposed on the thin film at 180 ℃ and the orientation of the PS cylinders was examined by atomic force microscope (AFM) at room temperature.

The SEBS sample was spin-cast on Si wafer. The film thickness is about 20 nm. The sample was further annealed at 180 ℃ for 12 hours to induce the in-plane orientation of the PS cylinders (Figure 1) and then the sample was annealed in the presence of the magnetic field of 30 Tesla at 180 ℃ for 3 hours. Figure 2 shows that the PS cylinders were destroyed by the magnetic field applied perpendicular to the cylinder axis. On the contrary, the cylinders almost align parallel to the magnetic field applied parallel to the thin film, as shown in Figure 3.

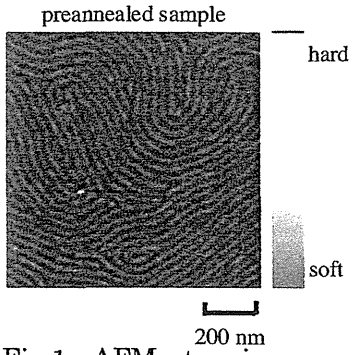

Fig.1 AFM tapping mode phase images for pre-annealed samples (180℃, 12h).

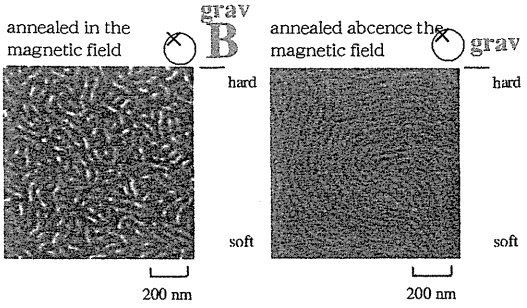

Fig.2 AFM tapping mode phase images for annealed samples (thin films) in the presence of perpendicular magnetic field and in the absence of the magnetic field

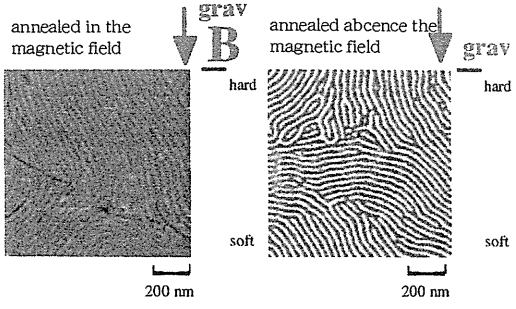

Fig.3 AFM tapping mode phase images for annealed samples (thin films) in the presence of parallel magnetic field and in the absence of the magnetic field

Effects of the Strong Static Magnetic Field on the Swimming Behavior of Some Protists

Yoshihisa Fujiwara[1], Masahiko Tomishige[1], Yasuhiro Itoh[2], Naho Shibata[2], Yoshifumi Tanimoto[1], Toshikazu Kosaka[1] and Hiroshi Hosoya[1]
1 Graduate School of Science, Hiroshima University, Kagamiyama 1-3-1, Higashi-Hiroshima, Hiroshima 739-8526, Japan
2 Department of Chemistry, Faculty of Science, Hiroshima University, Kagamiyama 1-3-1, Higashi-Hiroshima, Hiroshima 739-8526, Japan
(fuji0710@sci.hiroshima-u.ac.jp)

Abstract
Effects of strong static magnetic field on swimming behaviors of *Paramecium caudatum* (*P. caudatum*), *Blepharisma japonicum* (*B. japonicum*), and *Euplotes woodruffi* (*E. woodruffi*) were studied by using a superconducting magnet. In the case of *P. caudatum*, random swimming at 0 T and aligned swimming parallel to the magnetic field (MF) of 8 T were observed around a center of a round vessel. In the other two protists of *B. japonicum* and *E. woodruffi*, no appreciable effect was observed. It was experimentally revealed that the MF-induced parallel swimming of *P. caudatum* was caused physicochemically by the parallel magnetic orientation of the cell itself. The orientation of the cell was considered to result from the magnetic orientation of the cell membrane.

Keywords
strong magnetic field; swimming behavior; *Paramecium caudatum*; *Blepharisma japonicum*, *Euplotes woodruffi*; magnetic orientation

1. Introduction

Effect of a magnetic field in biological research fields has long attracted much attention of scientists. One of the reasons might lie in a point of view whether the effect occurs physicochemically or biologically. The studies of the magnetic field effects (MFEs) on organisms carried out till the beginning of 1990s had been already reviewed,[1] some of which were imagined to remain uncertain owing to experimentally and instrumentally yielded inaccuracy, and insufficient intensity of the magnetic field used. However, recently developed technique and apparatus enable the scientists to measure even the effect of an extremely small geomagnetic field. Very recently, two groups independently demonstrated the appreciable effects of the geomagnetic field on the movement of a migratory bird,[2] a lobster,[3] and a sea-turtle.[4] The spin chemistry is now taken notice as a mechanism of the effect on the migratory bird. As the opposite side, on the other hand, the effect of strong magnetic fields of several tesla on organisms is an important subject to be explored since, for instance, a nuclear magnetic resonance imaging (MRI) using such a strong magnetic field is nowadays employed frequently as the technique essential for accurate and right medical inspection. Our group has contributed to the construction of a field of studies, the spin chemistry, through numerous studies of the MFEs on photochemical reactions in the strong magnetic fields of up to 14 T.([5-7] and references therein) Regardless of the magnetic field intensity, the spin chemistry is now recognized to be one of the core mechanisms for the MFEs. Besides it, the strong magnetic force and the enhanced magnetic orientation are important features in the strong magnetic field, and thereby other MFEs not explained by the spin chemistry can be expected even in organisms at the strong magnetic field. Thus, we initiated to explore the effects of horizontal strong magnetic fields on organisms by using some protists which are well-known to be sensitive to some environmental stimuli such as gravity. The horizontal magnetic fields were utilized for the purpose of removing the influence of gravity. First of all, our group detected two intriguing MFEs in *Euglena gracilis* (*E. gracilis*) which contains several tens of chloroplasts inside the cell.[8] One of them was the swimming aligned perpendicularly to the magnetic field (the MF-induced perpendicular

swimming). This means that a long axis of the cell is aligned perpendicularly to the field (the perpendicular magnetic orientation). Another MFE was that, although each cell kept the perpendicular swimming, the cell distribution in a vessel altered so as to become higher at the side closer to the magnet center at about two hours after the vessel was set in the magnetic gradient generating the strong magnetic force (the positive magnetotaxis). The MF-induced perpendicular swimming was explained by the magnetic orientation of the chloroplasts tightly packed inside *E. gracilis*. Further, the positive magnetotaxis was interpreted by the combination mechanism of the perpendicular magnetic orientation of the cell itself and the inhomogeneous distribution of the diamagnetic chloroplasts inside the cell. As a result, the MFEs of *E. gracilis* were interpreted physicochemically. In this paper, we present the MFE on *P. caudatum* in the horizontal strong static magnetic fields. Since *P. caudatum* has no chloroplasts responsible for the magnetic orientation like *E. gracilis* and further the magnetic field used is horizontal, the MFE is considered to give a chance to understand the magnetic orientation of the protist in detail without the influence of gravity. Independently, two groups already reported the MFE on the swimming of a paramecium at the vertical magnetic field where the MFE should be estimated by taking the influence of gravity into account.[9, 10] However, there was inconsistency between their results that the paramecium swam perpendicularly to the field of 0.68 T [9] in contrast with parallel to the field of 18 T.[10] We had the impression of the necessity of removing the influence of gravity to simplify the interpretation of the MFE because *P. caudatum* is known to have the geotaxis.[11] In this work, it is reported that *P. caudatum* actually orients and swims parallel to the horizontal magnetic field of 8 T.[12]

2. Experimental methods

Ciliated protozoa of *P. caudatum*, *B. japonicum*, and *E. woodruffi* in the steady state growth period were employed for the experiment. The cultivation was performed according to the literature.[13, 14] Figure 1 shows pictures of the protists. All of them consist of a single cell which includes a cell membrane, cilia, etc. Especially, *P. caudatum* has a specific organ, trichocyst, buried beneath the membrane which is released toward a predator and stimuli such as chemicals.

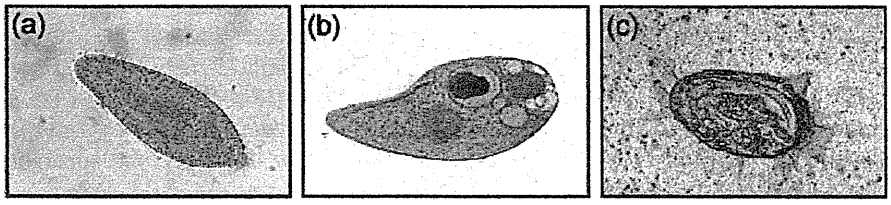

Fig. 1. Snapshots of (a) *P. caudatum*, (b) *B. japonicum*, and (c) *E. woodruffi*.

The horizontal strong static magnetic fields of up to 8 T were afforded by a superconducting magnet (Oxford Instruments, SM-1000-11, ϕ 50 mm bore diameter). The vertical strong magnetic fields of 10.7, 12 and 15 T used for comparison were provided with a superconducting magnet (Japan Superconductor Technology, JASTEC LH15T40, ϕ 40 mm bore diameter). A geomagnetic field, which was normally about 0.05 mT, was treated as 0 T in this study.

A round glass vessel (ϕ = 30 mm) containing each of the protists was set inside the horizontal magnetic field equipped with a thermostat maintained at 298 K. The swimming behaviors of them were measured from an upside of the vessel with a CCD camera (OLYMPUS, OH-411) – light source (OLYMPUS, ILK-5) – light guide (OLYMPUS, R100-095-090-50) – display monitor (SONY, EVM-9010R) – digital video cassette recorder (SONY, GV-D1000 NTSC) system. In the case of the vertical magnetic field, the swimming was monitored from a side of the vessel. Every experiment of the measurement was initiated at the same early time in the afternoon to avoid the influence of the circadian rhythm of the protists. In seeking the magnetic orientation of the cell as an assembly of simple chemical substances, immobilized *P. caudatum* was prepared by adding

ethylenediamine-N,N,N',N'-tetraacetic acid, disodium salt (EDTA) (0.003 – 0.02 mol/dm^3) into the solution containing the living cells in advance. No organic disruption of the cell was detected in the EDTA treatment.

3. Results

3.1 Effect of horizontal strong magnetic field on swimming of *P. caudatum* and its magnetic field dependence

Figure 2 shows snapshots of videos recording the behavior of *P. caudatum* swimming around a center of the vessel in the absence and presence of the horizontal strong magnetic field of 8 T. A dark gray ellipse and an arrow in front of it show a single cell of *P. caudatum* and the swimming direction, respectively. It is clear that the arrows are in disorder at 0 T (Figure 2a) whereas they are almost restricted to orient parallel to the magnetic field of 8 T (Figure 2b).

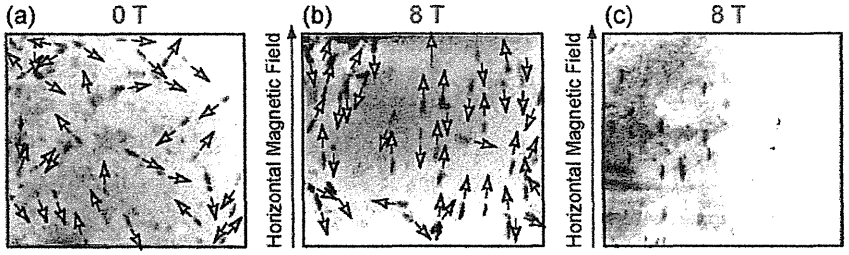

Fig. 2. Snapshots of videos recording the behavior of *P. caudatum* around a center of the round vessel in the case of (a) living cells at 0 T; (b) living cells at 8 T; and (c) immobilized cells at 8 T, respectively. All snapshots are taken from an upside of the round vessel (i.e. top view). Original magnification is ×20 in all cases. One dark gray spot corresponds to one single cell. Arrows drawn in (a) and (b) indicate the swimming direction of each living cell.

This MF-induced parallel swimming appeared immediately after being exposed to the magnetic field, and disappeared without delay when removed from the field. From these results, we recognized that *P. caudatum* was definitely affected by the strong magnetic field so as to swim parallel to the strong magnetic field. In other words, the cell of *P. caudatum* can be said to show the magnetic orientation parallel to the field (the parallel magnetic orientation). In fact, the parallel magnetic orientation of the cell as an assembly of simple chemical substances is confirmed by using the immobilized *P. caudatum* (vide infra). Furthermore, it was revealed that the MF-induced parallel swimming speed reduced when the exposure to the strong magnetic field lasted for more than several ten minutes. However, no recovery in the speed was detected even if the cell was removed

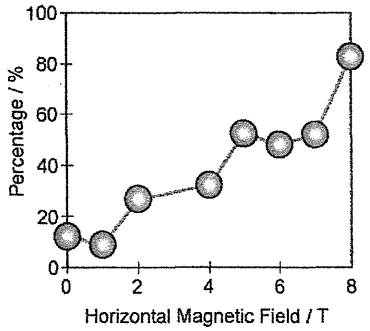

Fig. 3. MFDs of the percentages of *P. caudatum* showing the MF-induced parallel swimming around a center of the round vessel.

from the field although the direction of the swimming became in disorder promptly.

Plots of closed circles in Figure 3 display magnetic field dependence (MFD) of a percentage of the cells showing the MF-induced parallel swimming. The percentage was calculated in terms of dividing the number of cells swimming parallel to the field by the whole number of cells coming into the field of view of the microscope during a constant time. In the graph, it appears that the percentage increases together with increasing the magnetic field. The percentage at 8 T was approximately seven times larger than that at 0 T. Incidentally speaking, no magnetotaxis, which was seen in the case of *E. gracilis*,[8] was observed in the magnetic gradient.

For comparison, the swimming behaviors of the cell in the vertical strong magnetic fields of 10.7, 12, and 15 T besides 0 T were shown in Figure 4. The apparent MF-induced parallel swimming was confirmed even in the three vertical strong magnetic fields. This result was consistent with that of 18 T by Valles's group.[10] The decrease in the swimming speed was also detected during and after the exposure to the vertical magnetic field as well as the horizontal magnetic field.

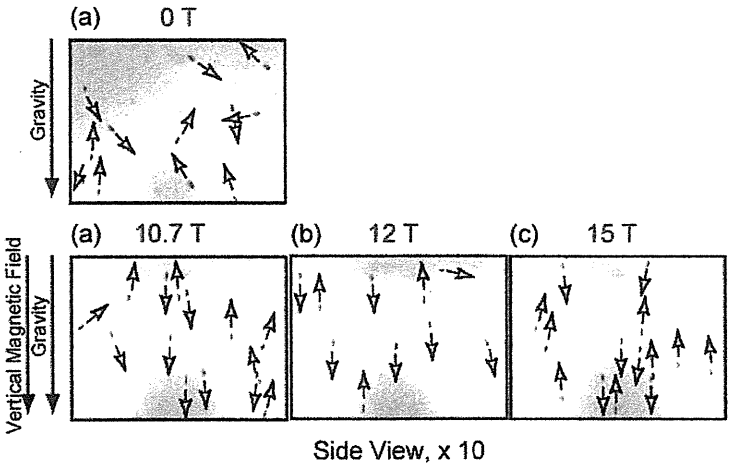

Fig. 4. Snapshots of videos recording the swimming behavior of *P. caudatum* in the vertical magnetic fields of 10.7, 12, and 15 T besides 0 T. All snapshots are taken from a side of the vessel (i.e. side view). Original magnification is ×10 in all cases. One gray spot corresponds to one single cell. Arrows indicate the swimming direction of each living cell.

3.2 Magnetic orientation of immobilized *P. caudatum* cells

In order to elucidate a mechanism of the MF-induced parallel swimming, we investigated the magnetic orientation of the cell immobilized with EDTA. This is an important experiment because the result leads to reply a question that the MF-induced parallel swimming occurs physicochemically or biologically. Figure 2c exhibits a snapshot obtained from the video recording the orientation of the immobilized *P. caudatum* at 8 T. After the solution containing the immobilized cells was stirred by inclining the vessel compulsorily, the video was recorded continuously until the cells came to a standstill and oriented in the presence of the field of 8 T. Figure 2c is the snapshot at the standstill demonstrating that the immobilized cell as an assembly of simple chemical substances is arranged parallel to the field. In Figure 2c it is found that most of the cells align their long axes of the ellipse body parallel to the magnetic field.

3.3 Swimming behaviors and no MFE of *B. japonicum* and *E. woodruffi*

The swimming behaviors of the other protists, *B. japonicum* and *E. woodruffi*, were monitored at a horizontal magnetic field of 8 T. However, none of them shows appreciable MFE on the swimming. *B. japonicum* swam turning around and around during observation, which probably resulted from phototaxis induced by the light for monitoring. *E. woodruffi* also showed no MF-induced aligned swimming as well as at 0 T.

4. Discussion

4.1. MF-induced parallel swimming as a consequence of parallel magnetic orientation of *P. caudatum*

The experiment of the immobilized *P. caudatum* indicates that the MF-induced parallel swimming (Figure 2b) observed around a center of the vessel is simply attributed to the magnetic orientation of the cell itself since the cell is regarded as an assembly of chemical substances and organs, as well as the interpretation of Nakaoka's and Valles's groups.[9, 10] That is, it is found that the MF-induced parallel swimming is interpreted physicochemically not biologically. If this interpretation is right, the orientation is explained by the magnetic susceptibility anisotropy of the cell.

Assuming that the *P. caudatum* is magnetically symmetric along its long axis like a cylinder and possess susceptibilities parallel ($\chi_{//}$) and perpendicular ($\chi_{\perp}$) to the axis, the magnetic energy $E(\theta, H)$ per cell at a magnetic field H is expressed as

$$E(\theta,H) = -(H^2/2)[\chi_{\perp} + (\chi_{//} - \chi_{\perp})\cos^2\theta] \quad (1)$$

where θ is an angle between the long axis and the magnetic field H.[15] In the case of the MF-induced parallel swimming, the angle θ is equal to zero. The magnetic orientation occurs so that the magnetic energy $E(\theta, H)$ becomes minimum. However, the magnetic orientation of the cell holding the magnetic energy $E(\theta, H)$ at temperature T is disordered by thermal energy of T. According to the Boltzmann statistics, therefore, the probability $P(\theta, H, T)d\theta$ of the cell existing between the angles θ and $\theta+d\theta$ is written as

$$P(\theta,H,T)d\theta = \frac{\exp[-E(\theta,H)/kT]d\theta}{\int_0^{\pi}\exp[-E(\theta,H)/kT]d\theta} \quad (2)$$

where k is the Boltzmann constant.[16] Here, since the denominator in Equation 2 is considered common to all the magnetic fields used, a ratio $R(\theta = 0)$ at $\theta = 0$ of the probability at a magnetic field H toward that at 0 T is simplified as

$$R(\theta=0) = \frac{P(0,H,T)}{P(0,0,T)} = \exp\left[\frac{H^2}{2kT}(\chi_{//} - \chi_{\perp})\right] \quad (3)$$

Thus, the logarithmic transformation of both hand sides in Equation 3 gives

$$\ln(R(\theta=0)) = \frac{1}{2kT}(\chi_{//} - \chi_{\perp})H^2 = \frac{1}{2kT}\Delta\chi H^2 \quad (4)$$

with $\Delta\chi = (\chi_{//} - \chi_{\perp})$. If the experimental result in this work obeys this relation, it reveals that the MF-induced parallel swimming is ascribed to physicochemical phenomenon of the parallel magnetic orientation due to the magnetic susceptibility anisotropy of the cell as an assembly of chemical substances.

Figure 5 is a graph plotted according to Equation 4. The plots satisfy the relation within an experimental error, which verifies the parallel magnetic orientation of the cell induced physicochemically , as described above. A straight line superimposed on the plots is the best fitted line acquired by the least-squares method. The anisotropy $\Delta\chi$ of the susceptibility per cell was obtained from the slope to be 3.4×10^{-23} emu cell^{-1} at the experimental temperature of 298 K. To the best of our knowledge, this is the first evaluation of the anisotropic value per cell of the living *P. caudatum*. This value was smaller than values of some substances (benzophenone: 3.0×10^{-20} emu crystal^{-1}; single multiwall carbon nanotube: 6.5×10^{-22} emu nanotube^{-1}; erythrocyte: 8.2×10^{-22} emu

cell^{-1}; blood platelet 1.2×10^{-21} emu cell^{-1}) experimentally so far obtained.[15-17]

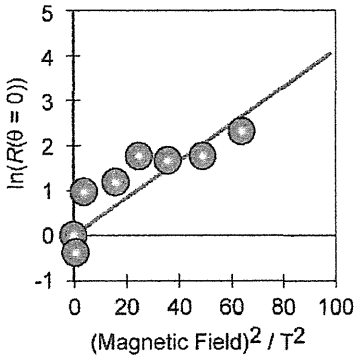

Fig. 5. A ratio of $\ln(R(\theta = 0))$ against a square of the horizontal magnetic field of H plotted according to Equation 4. The straight line superimposed is the best fitted line toward the observed plots estimated by a least squares method.

4.2. Origin of parallel magnetic orientation of *P. caudatum*

We sought an origin of the magnetic orientation of *P. caudatum*. We observed the swimming of *P. caudatum* parallel to the horizontal magnetic field at 8 T from an upside of the round vessel while Nakaoka et al. observed the horizontal swimming of *P. multimicronucleatum* perpendicular to the vertical magnetic field of 0.68 T from a side of the rectangular vessel.[9] The relationship between the MF-induced alignment and the magnetic field was distinct from each other in these cases. Further, Nakaoka et al. also measured parallel magnetic orientations of two principal organs of cilia and trichocysts, of which respective long axes were both parallel to the vertical low field used. Since the cilia grow perpendicularly from the cell surface and the trichocysts are buried maintaining the long axis at right angles to the surface, they led to the conclusion that the perpendicular magnetic orientation of the cell results from the magnetic orientation of the two organs. Since a side of the cell surface is by far wide in area, the magnetic orientation caused by the two organs at the side is more remarkable than in the head and tail. However, this interpretation is inapplicable to our case of the parallel magnetic orientation of *P. caudatum*. Thus, we examined a cell membrane as a candidate of the origin. It is well-known that the membrane consists of a bi-layer of upright phospholipids which have long chains of hydrocarbons. Since such a long hydrocarbonaceous chain is found to have a certain magnitude of magnetic susceptibility anisotropy,[18] the membrane as an assembly of the upright hydrocarbons should be aligned to the magnetic field. For instance, stearic acid ($CH_3(CH_2)_{16}COOH$) possesses $\chi_{//} = -235.7\times10^{-6}$ emu mol^{-1} and $\chi_{\perp} = -208.2\times10^{-6}$ emu mol^{-1}).[18] The relationship of $\chi_{//} < \chi_{\perp}$ indicates that the membrane comprising many upright stearic acids is arranged parallel to the magnetic field. Therefore, this arrangement of the membrane is proper to explain our observed magnetic orientation of the cell itself parallel to the magnetic field since a side of the non-spherical cell is wider in area than a head and a tail. If we roughly calculate the magnetic susceptibility anisotropy of the membrane based on assumptions that (i) the membrane consists of only stearic acid which has a cylindrical structure and (ii) the cell is also symmetric like a cylinder of 200 μm in length and 60 μm in diameter, then it is approximately estimated to be $\Delta\chi = 1.5\times10^{-17}$ emu cell^{-1} by taking account of a diameter of cylindrical stearic acid. This value is considerably larger than that ($\Delta\chi = 3.4\times10^{-23}$ emu cell^{-1}) obtained for the cell in this study. However, the difference in the two values seems to be compensated with the anisotropy of cilia and trichocysts. Judging from the direction of the magnetic orientation of cilia and trichocysts measured by Nakaoka et al., the relationship between $\chi_{//}$ and $\chi_{\perp}$ of the two organs is certainly $\chi_{//} > \chi_{\perp}$ as opposed to $\chi_{//} < \chi_{\perp}$ of stearic acid. Therefore, adding the magnetic orientation of the two organs leads to reduce a value of the susceptibility anisotropy ($\Delta\chi$), that is, the obtained small value ($\Delta\chi = 3.4\times10^{-23}$ emu cell^{-1}) means an apparent value which results from a total effect due to several

substances having independently different susceptibility anisotropies. The smallness of the apparent $\Delta\chi$ value of *P. caudatum* might imply that $\Delta\chi$ for the membrane is merely different in the absolute value from that of a total $\Delta\chi$ for the two organs, though the sign is opposite to each other. In other words, the smallness might suggest that *P. caudatum* has a tendency of easy alteration of the magnetic orientation (the MF-induced swimming) of the cell by the scanty difference and sign in $\Delta\chi$ of the cell membrane and the combination of cilia and trichocysts. Hence, it might first be said that the difference in the magnetic orientations between Nakaoka et al. and us arises from a difference in a species of paramecium though there still remain influences of gravity and vessel shape.

5. Conclusions

In this study we revealed the MF-induced parallel swimming results from the magnetic orientation of the cell itself as an assembly of chemical substances by using horizontal strong magnetic fields unnecessary to take the gravity into account. We proposed the possibility of the cell membrane as the origin of the magnetic orientation by evaluating the susceptibility anisotropy value $\Delta\chi$ of the cell.

Acknowledgements

This work was partly supported by Grant-in-Aid for Scientific Research on Priority Area "Innovative utilization of strong magnetic fields" (Area 767, No. 15085208) from MEXT of Japan.

References

[1] C. B. Grissom, Chem. Rev., 95 (1995) 3-24.
[2] W. Wlltschko, J. Traudt, O. Güntürkün, H. Prior and R. Wlltschko, Nature, 419 (2002) 467-470.
[3] L. C. Boles and K. J. Lohmann, Nature, 421 (2003) 60-63.
[4] K. J. Lohmann, C. M. F. Lohmann, L.M. Ehrhart, D.A.Bagley and T. Swing, Nature, 428 (2004) 909-910.
[5] Y. Tanimoto and Y. Fujiwara, J. Synth. Org. Chem. Jpn., 53 (1995) 413-422.
[6] Y. Fujiwara, R. Nakagaki and Y. Tanimoto. *Dynamic Spin Chemistry*, S. Nagakura, H. Hayashi and T. Azumi eds., pp. 49-81, Kodansya, Tokyo and JohnWiley & Sons, New York (1998).
[7] Y. Tanimoto and Y. Fujiwara, *Handbook of Photochemistry and Photobiology, Volume I: Inorganic Chemistry*, H. S. Nalwa ed., pp. 413-446, American Scientific Publishers, USA (2003).
[8] Y. Tanimoto, S. Izumi, K. Furuta, T. Suzuki, Y. Fujiwara, M. Fujiwara, T. Hirata and S. Yamada, Int. J. Appl. Electromagn. Mech., 14 (2001/2002) 311-316.
[9] Y. Nakaoka, R. Takeda and K. Shimizu, Bioelectromagnetics, 23 (2002) 607-613.
[10] J. M. Valles, JR. and K. Guevorkian, *Materials Prpcessing In Magnetic Fields*, H. Wada and H. J. Schneider-Muntau eds., pp. 257-265, World Scientific, Singapore (2005).
[11] R. Wichteman, *The Biology of Paramecium*, Plenum Press, New York (1986).
[12] Y. Fujiwara, M. Tomishige, Y. Itoh, M. Fujiwara, N. Shibata, T. Kosaka, H. Hosoya and Y. Tanimoto, Mol. Phys., submitted.
[13] T. Kosaka, J. Protozool., 38 (1991) 140-148.
[14] T. Takahashi, M. Okubo and H. Hosoya, J. Euk. Microbiol., 45 (1998) 369-380.
[15] M. Fujiwara, M. Fukui and Y. Tanimoto, J. Phys. Chem. B, 103 (1999) 2627-2630.
[16] M. Fujiwara, E. Oki, M. Hamada, Y. Tanimoto, I. Mukouda and Y. Shimomura, J. Phys. Chem. A, 105 (2001) 4383-4386.
[17] A. Yamagishi, T. Takeuchi, T. Higashi and M. Date, Physica B, 177 (1992) 523-526.
[18] K. Lonsdale, Proc. Roy. Soc. London, A171 (1939) 541-567.

Application of magnetic fields for the control of the colloidal crystal structure

Kazutoshi Kitajima, Toma Fujita, Norihito Sogoshi, and Seiichiro Nakabayashi
Department of Chemistry, Faculty of Science, Saitama University,
Shimo-Ohkubo 255, Sakura-Ku, Saitama, 338-8570
(k-kazutoshi@chem.saitama-u.ac.jp)

Abstract

Monodisperse silica spheres with a diameter of ca. 140 nm containing magnetic cores of γ-Fe_2O_3 were synthesized following a similar method by Stöber[1] and Philipse.[2] Rendering a structural color was successfully achieved by thorough deionization of the aqueous suspension of the spheres. The magnetic tunability of the structural color of the colloidal crystal was demonstrated. The optical property was characterized by UV-Vis. reflection spectra.

Keywords
Magnetic composite particle, colloidal crystal, structural color

1. Introduction

Recently, colloidal crystals attract much attention of researchers aiming the realization of three-dimensional photonic crystals.[3,4] Bragg diffraction by the periodic structure of dielectric materials is the basis of photonic properties.[5] Dilute charged colloidal crystals are interesting since the crystal structure is sustained by the electrically repulsive interaction and is affected by ionic atmosphere of the solvent.[6,7] They are useful to the study of photonic crystals owing to the flexible structure. Colloidal crystals composed of magnetic particles are particularly promising in this respect for its in-situ tunabily using external magnetic fields. Wagner et al. reported synthesis of magnetic composite particles ($CoFe_2O_4$@SiO_2) and the control of the structural color of the suspension by magnetic fields.[8] Philipse et al. reported the synthesis of magnetic particle of γ-Fe_2O_3@SiO_2.[2] However, they did not present the formation of the colloidal crystal, possibly because of relatively poor uniformity of the particles. The aim of this work is the improvement for the synthesis of γ-Fe_2O_3@SiO_2 particles and the realization of the colloidal crystallization. Moreover, spectroscopic characterization of the crystal is presented.

2. Experimental methods

All reagents were purchased from Wako Pure Chemical Industries, LTD. Fine γ-Fe_2O_3 particles were prepared by co-precipitation.[9] $FeCl_2$ of 2.08 g and $FeCl_3$ of 5.22 g were dissolved in 380 mL ultrapure water, and 20 mL of 25% NH_3 was added to the solution with acute agitation for one hour. After ultrafine γ-Fe_2O_3 particles were flocculated, the supernatant liquid was removed by decantation. 40 mL 2 M HNO_3 was added to the sediment with stirring for five minutes. 60 mL 0.35 M $Fe(NO_3)_3$ was slowly added to the solution boiling for one hour. After standing for a while, the supernatant was again removed by decantation. The dark reddish-brown sedimentation was washed with 2 M HNO_3, and precipitated using a permanent magnet. The dark reddish-brown precipitate was dissolved in 1 L of distilled water. The point of zero charge of γ-Fe_2O_3 particles was lowered by adding a 0.01 M citric acid solution until precipitation was visible.[9] The precipitation was separated by filtration, and dissolved in 40 mL 20% tetraethylammoniumhydroxide (TEAH).

Controling the number density of the core particles is very important to synthesize monodisperse

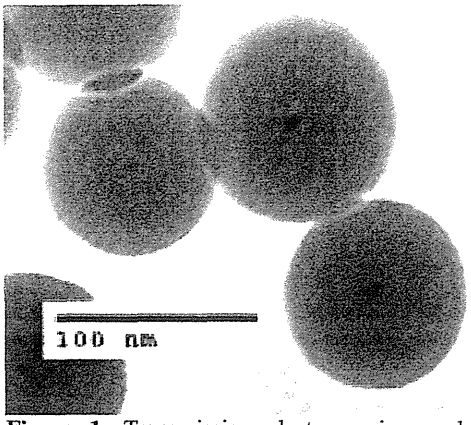

Figure 1. Transmission electron micrograph of colloidal core-shell particles. Ferromagnetic core can be seen as a dark spot at the center of particles.

composite particles.[10] The target number is 4.5×10^{10} particles/mL. In order to synthesize composite particles (Fe_2O_3@SiO_2), the TEAH solution of 0.5 mL is mixed with ultrapure water and added to 720 mL 2-propanol and 240 mL ethanol. Tetraethylorthosilicate and 25% NH_3 were added with sonication. After one hour of agitation, yellow ocher particles were synthesized. To remove stray ions from the suspension, the particles were separated using a centrifuge and diluted in ultrapure water. The last procedure was repeated several times to complete deionization.

3. Results and discussion

Figure 1 shows a transmission electron micrograph of the particles synthesized. A magnetic core was found at the center of each particle, which is visible as a dark spot in a gray sphere in Figure 1. The average diameter of particles is 144 nm, which is estimated using a particle analyzer (UPA-150; Microtrac, Inc). The standard deviation of diameter was 43 nm, which was relatively large possibly due to the partial aggregation of particles.

Colloidal crystals are known to have a face-center-cubic (fcc) crystal structure typically.[11] The (111) facet is parallel with the wall of the container. The distance between the nearest (111) faces of the colloidal crystal was determined from reflection spectra. The reflection spectra were measured with an UV-Vis. spectrometer (UV-570, JASCO Corp.) equipped with a rotatable stage and an integrating sphere. A rectangular quartz cell filled with the colloidal crystal was placed on

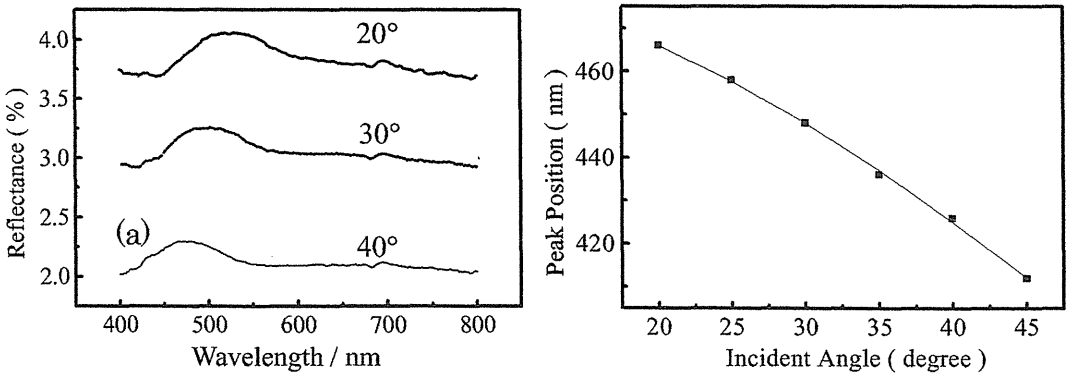

Figure 2. (a) Reflection spectra of the colloidal crystal of composite magnetic particles with incident and reflected angle angles of 20°, 30° and 40°. The baseline of each spectrum is vertically shifted for clarity. (b) Incident angle dependence of the peak wavelength of Bragg diffraction.

the rotatable stage. The incident and reflective angles were set to be identical. Figure 2(a) shows reflective spectra with altering incident angles. The peak of the reflective spectra shifted to longer wavelengths with increasing incident angles. The reason for rather large peak width is not clear. However, the shapes of the peak for different incident angles are quite similar, which may mean the (111) faces near the cell wall were well defined. In Figure 2(b), the wavelength of the reflection peak is plotted against the incident angle. The distance between (111) faces (α) was obtained as 240 nm using the relation of $\alpha = (\lambda/2)[1-(\sin\theta/n)^2]^{1/2}$ (λ: the peak wavelength of reflection spectra, θ: incident angle, n: the volume average of the refractive index of the suspension).[12] The volume average of the refractive index (n) was decided from the relation to be 1.37. This value is reasonable since it is close to the refractive index of pure water (1.33).

In Figure 3, pictures showing the change of the structural color by magnetic fields are presented. In Fig.3(a), the colloidal crystal with a structural color (violet) is seen at the middle of the container. The apparent sedimentation of the crystal phase and the disordered phase above it may indicate the critical concentration for the crystallization. In order to perturb the interaction between particles, a permanent magnet (SmCo, 0.3 T) was attached at the top of the container. The structural color changed gradually from violet to green as shown in Fig.3(b) and became stationary after about eight hours. This change of the structural color means the expansion of the lattice. Since magnetic particles are attracted toward the magnet at the top and this cancels the gravity acting on the particles. Therefore, the particle density decreases and lattice spacing increases. After removing the magnet, the color was reverted to violet within half an hour. Figure 3(c) shows reflective spectra with and without magnetic fields. The peak wavelength was 504 nm (without magnetic field) and 520 nm (with magnetic field). A rather irregular deformation of the shape of the peak was observed upon magnetization. This is possibly due to imperfect colloidal crystallization, since the probe beam was rather wide (100 μm × 10 mm), which incidented both of the ordered and disordered phases. The rate of the change of the structural color is rather slow. It is reported that the phase transition of the colloidal crystal is quite slow.[13] Further characterization of reflective spectra is under progress.

4. Conclusions

In summary, we have succeeded in rendering the structural color of the γ-Fe_2O_3@SiO_2 magnetic colloid. The crystal constant was obtained from UV-Vis. reflective spectra. Magnetic tuning of the structural color was demonstrated.

Acknowledgements

This manuscript is reproduced from Kitajima et al. Chem. Lett. **33**(9), 1106-1107 (2004). This work was supported by Grant-in-Aid for Scientific Research for Priority Areas (No.15085202, Area 767) from MEXT of Japan.

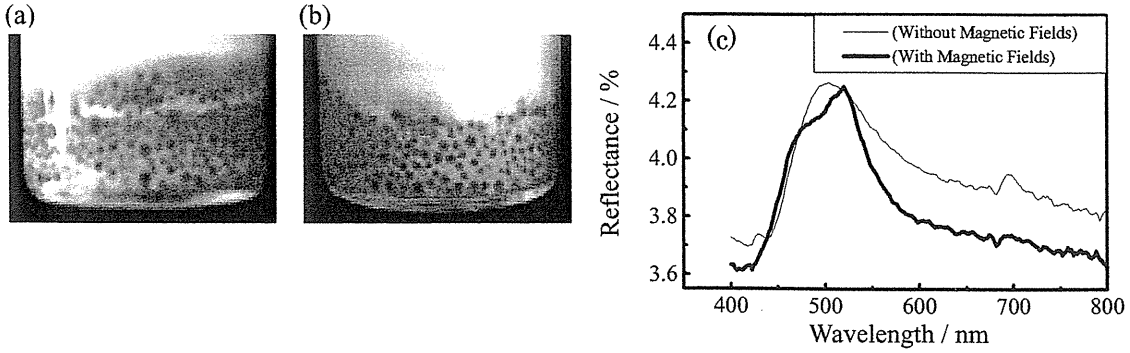

Figure 3. Color photographs of a composite magnetic colloidal crystal. Red spheres are ion-exchange resin beads. The structural color is seen in the middle of photographs and it changed from violet (a) to green (b) when magnetic fields were applied. (c) Difference of reflective spectra without and with magnetic fields. The peak of the reflective spectra is 508 nm in absence of magnetic fields and shifted to 520 nm in presence of magnetic fields.

References

[1] W. Stöber, A. Fink, and E. Bohn, *J. Coll. Interface Sci.*, **26**, 62 (1968).
[2] A. P. Philipse, M. P. B. van Bruggen, and C. Pathmamanoharan, *Langmuir*, **10**, 92 (1994).
[3] H. Míguez, C. López, F. Meseguer, A. Blanco, L. Vázquez, R. Mayoral, M. Ocaña, V.
[4] Fornés, and A. Mifsud, *Appl. Phys. Lett.*, **71**, 1148 (1997).
[5] A. D. Dinsmore, J. C. Crocker, and A. G. Yodh, *Curr. Opin. Coll. Interface Sci.*, **3**, 5 (1998).
[6] J. D. Joannopoulos, P. R. Villeneuve, and S. Fan, *Nature*, **386**, 143 (1997).
[7] K. Yoshinaga, M. Chiyoda, H. Ishiki, and T. Okubo, *Coll. Surf. A*, **204**, 285 (2002).
[8] H. Yoshida, J. Yamanaka, T. Koga, T. Koga, N. Ise, and T. Hashimoto, *Langmuir*, **15**, 2684 (1999).
[9] J. Wagner, T. Autenrieth, and R. Hempelmann, *J. Magn. Magn. Mater*, **252**, 4 (2002).
[10] G. A. van Ewijk, G. J. Vroege, and A. P. Philipse, *J. Magn. Magn. Mater*, **201**, 31 (1999).
[11] Y. Lu, Y. Yin, Z.-Y. Li, and Y. Xia, *Nano Lett.*, **2**, 785 (2002).
[12] I. I. Tarhan and G. H. Watson, *Phys. Rev. Lett.*, **76**, 315 (1996).
[13] T. Kanai, T. Sawada, and K. Kitamura, *Langmuir*, **19**, 1984 (2003).
[14] S. Dosho, N. Ise, K. Ito, S. Iwai, H. Kitano, H. Matsuoka, H. Nakamura, H. Okumura, T. Ono, I. S. Sogami, Y. Ueno, H. Yoshida, and T. Yoshiyama, *Langmuir*, **9**, 394 (1993).

Faraday Effect of Magnetic Opal Films

Kazushi Kobayashi ,Kazutoshi Kitajima ,Norihito Sogoshi and Seiichiro Nakabayashi
Department of Chemistry, Faculty of Science, Saitama University,
Shimo-Okubo 255, Sakura-ku, Saitama, 338-8570
(kobakazu@chem.saitama-u.ac.jp)

Opal is known to be one of the photonic crystals found in nature. It is composed of spherical silica particles. We reported synthesis of spherical silica particles containing the magnetic core of γ -Fe_2O_3.[1] As shown in Figure 1, the magnetic core can be seen as a dark spot at the center of particles. The opal film made from this magnetic particles is expected to be a new optical material which can respond to a magnetic field. The Faraday effect is one of the magneto-optical properties of materials. The direction of polarization of light propagating parallel to a magnetic field is rotated when light pass through magnetized material. We fabricated magnetic opal films and measured the Faraday effect of the films.

Artificial opal films were fabricated from ethanol suspensions by a vertical deposition method. Composite particles with a diameter of ca.200nm were dispersed in ethanol. A glass substrate was cleaned by concentrated sulfuric acid, and immersed approximately vertically into the suspension. After the evaporation of the solvent, silica spheres were self-assembled onto the substrate. Uniform colored film was obtained. Figure 2 shows an atomic force micrograph of this film. From this picture, it was found that this film has a relatively well-ordered structure. The reflection spectra were measured with a UV-VIS.spectrometer. We observed the sharp peaks due to the Bragg diffraction of visible light from the periodic structure.

Next, we set up the apparatus for the Faraday effect measurement using a superconductive magnet. We measured the Faraday effect of silica opal films with and without magnetic cores, respectively. Figure 3 shows the dependence of the Faraday rotation on the magnetic field. Compared to the film without magnetic cores, it was found that light intensity of the film with magnetic core increased dramatically. In general, the relation between the Faraday effect and magnetization is proportional. In this case, the intensity increased linearly to the magnetic field, and therefore magnetization of the cores is not saturated. Thus, we suppose that the composite particle is not ferromagnetic but superparamagnetic due to the small volume of the cores.

1)Kitajima et al.,Chem.Lett.33(2004),1006

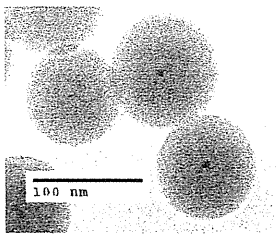

Fig.1. TEM image of γ -Fe_2O_3@SiO_2 particles.

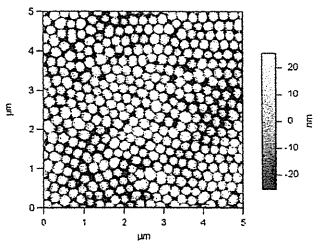

Fig.2. AFM image of magnetic opal film.

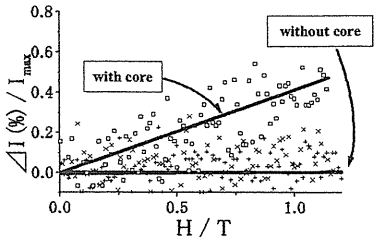

Fig.3. The dependence of the Faraday rotation on the magnetic field.

Photoinduced Convection of Organic Solution in Magnetic Field

Fumi Koyama and Yoshifumi Tanimoto
Graduate school of Science, Hiroshima University
1-3-1, Kagamiyama, Higashi-Hiroshima 739-8526, Japan
(m052892@hiroshima-u.ac.jp)

Abstract

We studied the rising pattern of a colored benzene solution photochemically generated by the reaction of diphenylamine and carbon tetrabromide in high magnetic field. At zero field the colored solution stayed on the bottom after 10 s laser irradiation. At $-1400T^2\ m^{-1}$ the solution rose fast with forming a pipe-like shape, at $-54T^2\ m^{-1}$ it rose straight from the center of the vessel, and at $+1155T^2\ m^{-1}$ it rose slowly after 1 minute from irradiation, These results can be understood, to some extent, by the magnetic force applied to the colored solution.

Keywords

carbon tetrabromide, diphenylamine, photochemical reaction, thermal convection, magnetic force, magnetic susceptibility, magnetic field effect

1. Introduction

Recently, because of development of superconducting magnet technology, high magnetic field has been available, and many kinds of research on magnetic phenomena have been reported. To know the convection of liquid solution caused by magnetic field leads to a new viewpoint of heterogeneous solution's convection. But few experiments were held to observe convection, and further studies are required about it. Therefore we studied the rising pattern of colored benzene solution photochemically generated by the reaction of diphenylamine and carbon tetrabromide in magnetic field.

2. Experimental

Diphenylamine (DPA: WAKO, special grade), CBr_4 (WAKO, special grade) and benzene (WAKO, spectrosol) were used as received. In this experiment equimolar benzene solution of DPA

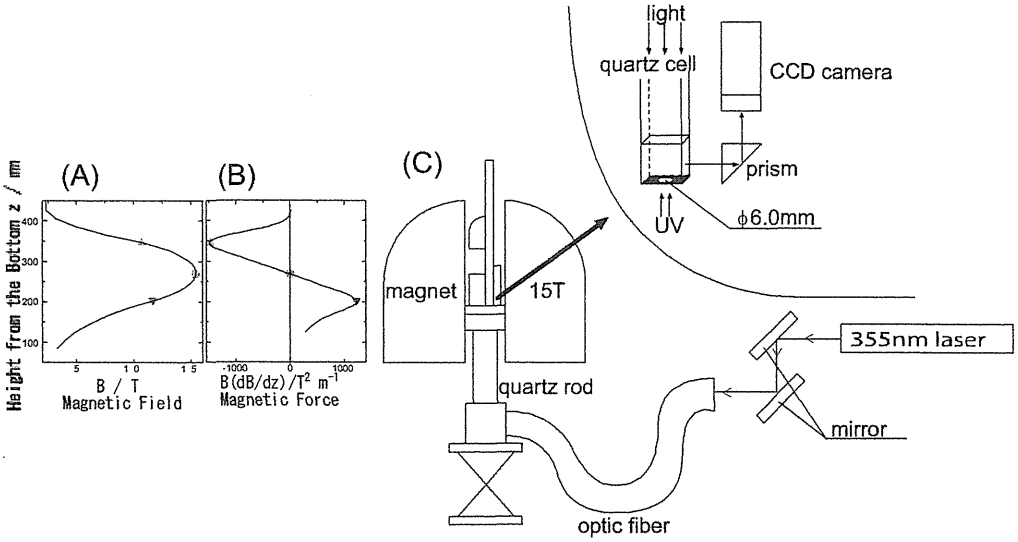

Fig.1. (A)Distributions of magnetic field and (B)magnetic force of the magnet. (C)Experimental setup for *in situ* observation.

and CBr_4 were used. A 1ml sample solution in a 1cm x 1cm x 4cm quartz cell was degassed by passing through argon gas for 10 minutes. The cell was still standing in the magnetic field for 3 minutes.

Figure 1 shows the experimental setup for *in situ* observation of convection in a magnet. Magnetic field was generated by a superconducting magnet (JASTEC, JMTD-LH15T40). A solution in the quartz cell, placed in the bore, was irradiated by a 355-nm light from a pulsed Nd:YAG laser (Spectra-Physics, Quanta-Ray INDI) from the bottom of the cell through a 6-mm hole for 10 s. Rising pattern of the photogenerated colored solution was recorded by CCD camera (TELI, CSU9000B) and video recorder (SONY, GV-D1000). *In situ* observation was carried out at 3 positions in the magnet bore, i.e., "Upper" ($-1400T^2\ m^{-1}$), "Middle" ($-54T^2\ m^{-1}$), and "Lower" positions ($+1155T^2\ m^{-1}$) and outside the magnet ($0T^2\ m^{-1}$) as control experiment. The product of magnetic field and its gradient in the radial direction was 50-100 T^2m^{-1} at three positions.

3. Results and Discussion

10-Second laser irradiation of the benzene solution of DPA and CBr_4 immediately generates a colored solution on the bottom of the cell. Figure 2 shows the rising patterns of the colored solution.

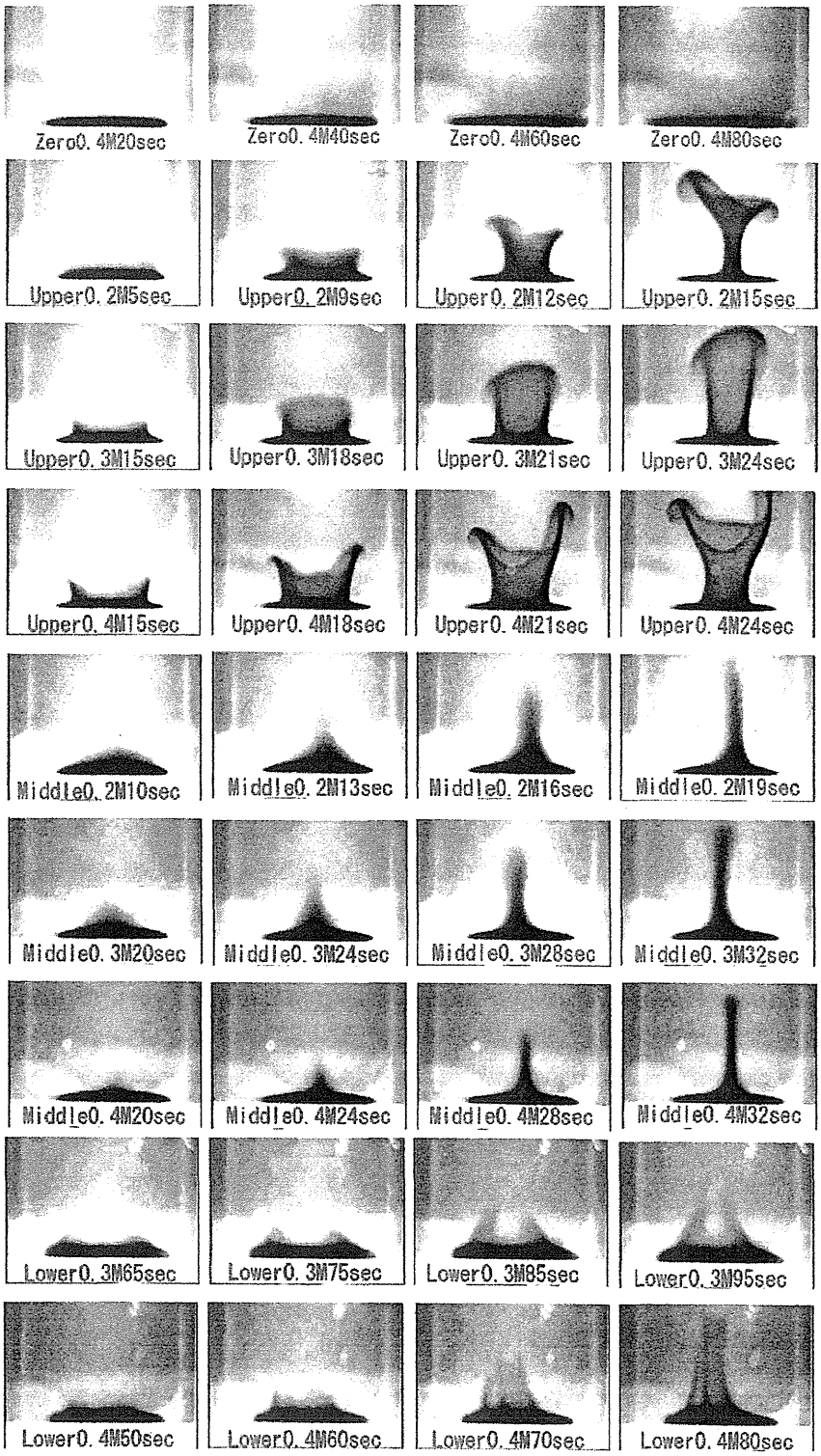

Fig.2. Rising patterns of colored solution (side view). Upper: $-1400T^2m^{-1}$, Middle: $-54T^2m^{-1}$, Lower: $+1155T^2m^{-1}$, Zero: $0T^2m^{-1}$.

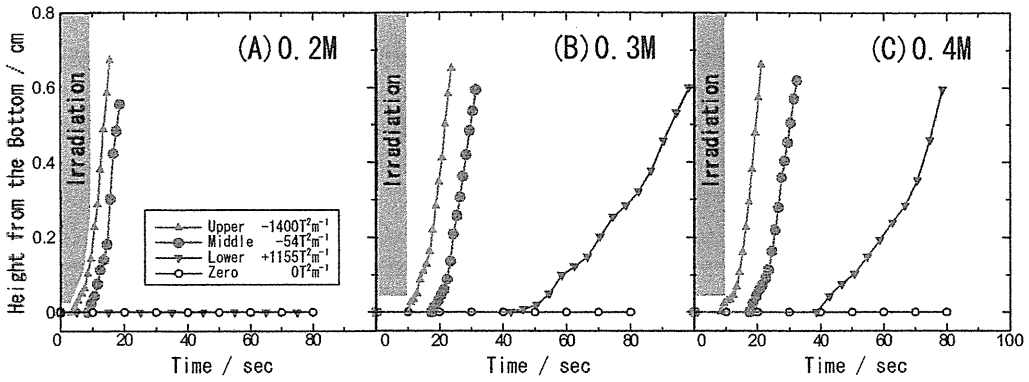

Fig.3. The distance between the bottom of the cell and the top of the colored solution with time from start of irradiation. (A)[CBr_4]=[DPA]=0.2M, (B)0.3M, (C)0.4M

It is obvious from the figure that the patterns are strongly affected by the magnetic fields. The movement of the colored solution's frontier was analyzed manually and the results are given in Fig. 3. When the concentration of solutes was 0.4 M, for example, the retention time and rising speed of the colored solution are: >150 s and 0 mm s^{-1} ($0T^2$ m^{-1}), 6.1 s and 1.1 mm s^{-1} ($-1400T^2$ m^{-1}), 13.1 s and 0.8 mm s^{-1} ($-54T^2$ m^{-1}), 29 s and 0.4 mm s^{-1} ($+1155T^2$ m^{-1}). For all cases, the strength and direction of the magnetic force influenced the rising patterns of the colored solution.

If diamagnetism of the colored solution is stronger than the surrounding bulk solution, the magnetic force against magnetic center is applied to the colored solution for z direction, and the force to the bore center axis is applied to the colored solution for r direction (fig.4). These forces were very dominant.

Magnetic force (F_{mag}) to z direction which acts the colored solution can be written as a follow.

$$F_{mag} = \frac{\chi_B - \chi_A}{\mu_0} V_B B \frac{\partial B}{\partial z}$$

Where χ_A is the magnetic susceptibility of around colorless solution, χ_B is the magnetic susceptibility of the colored solution, μ_0 is the magnetic permeability of vacuum. V_B is the volume of colored solution, **B** is the magnetic field, and $\partial \mathbf{B}/\partial z$ is the magnetic gradient for z axis.
The value of (χ_B-χ_A) depends on the concentration of the solution, and the product of the flux density and its gradient, ($\mathbf{B}\,\partial \mathbf{B}/\partial z$), depends on the position in the magnet bore.

At zero field ($0T^2m^{-1}$), the colored solution did not move since the density of the colored solution is too large to thermal convection under the circumstances.

At Upper position ($-1400T^2$ m^{-1}), the colored solution rose very fast by the strong upward magnetic force with shrinking rapidly in shape from the bottom due to the radial magnetic force (50-100 T^2m^{-1}). The reason why the colored solution began to rise from circumference of the

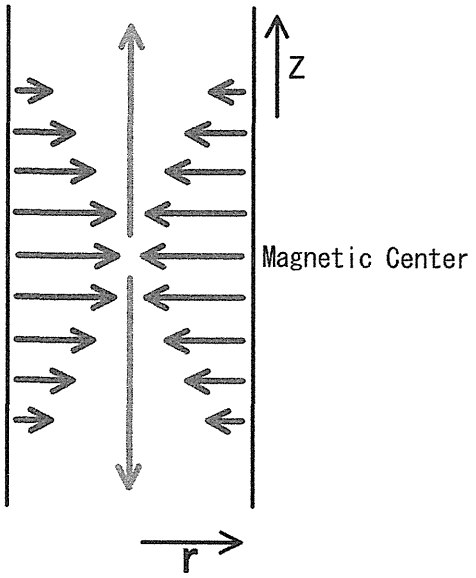

Fig.4. Magnetic force in the bore tube.

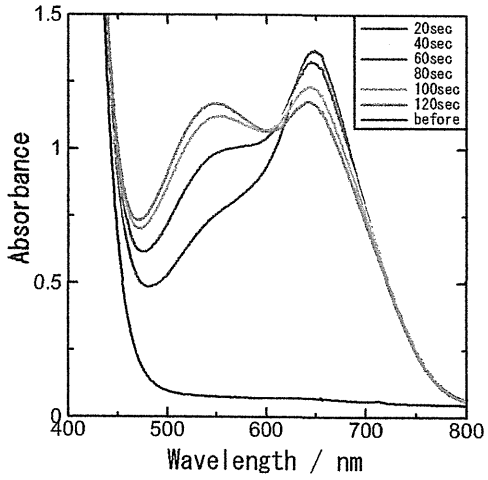

Fig.5. Absorption spectra of benzene solution of CBr_4 and DPA after UV-irradiation.[CBr4]=[DPA]=0.4M. Solution was degassed by 10min Ar-bubbling and irradiated for 1-sec by a high pressure Hg lamp.

colored solution can't be explained well.

At Middle position ($-54T^2$ m^{-1}), the colored solution gathered to the center and rise slowly, because the radial magnetic force (50-100 T^2m^{-1}) might be stronger than the vertical one.

At Lower position ($+1155T^2$ m^{-1}), because of strong magnetic force to downward, the colored solution could not rise. But in fact the colored solution rose slowly at a 1 minute delay after irradiation. The reason was tentatively speculated as follows: At first, a green compound, whose absorption peak was 650nm, was produced by UV irradiation. Since it was not stable, it changed into a red compound whose absorption peak was 540nm, as shown in Fig. 5. If the magnetic susceptibility of the red compound was different from that of green compound and if the red compound had larger magnetic susceptibility than that of the bulk solution, the colored solution may rise because of the upward magnetic force. It was found from SQUID measurement that magnetic susceptibility of the red compound ($-0.51 \times 10^{-6} cm^3 g^{-1}$) is larger than that of benzene ($-0.702 \times 10^{-6} cm^3 g^{-1}$). Thus the assumption seems reasonable. Then the rising colored solution was gathered by the radial magnetic force. As concentration of solutes increase, more green compound and, therefore, more red compound was produced. As a result upward magnetic force applied to the colored solution, contained red compound, became stronger, and colored solution rose faster.

4. Conclusions

We studied the rising pattern of the colored benzene solution photochemically generated by the reaction of DPA and CBr_4 in high magnetic fields. *In situ* observation of the motion of the solution showed that the direction and strength of the magnetic force influenced significantly the rising pattern and speed of the colored solution. In addition the concentration of the solutes also influenced the rising speed.

Acknowledgements

We thank Professor Katsuya Inoue for the use of a SQUID apparatus. This work was supported partly by a Grant-in-Aid for Scientific Research on Priority Area (Area 767, No. 15085208) from the Ministry of Education, Culture, Sports, Science, and Technology of Japan.

Reference

[1]R. H. Sprague, H. L. Fichter, and E. Wainer, *Photogr. Sci. Eng.*, **5**, 98 (1961)

[2]F. Koyama, W. Duan, and Y. Tanimoto, Joint Symposium on Magneto-Science 2004, Yokohama December 2004, 1Bb2

[3]T. Miwa and T. Ishikawa, *Nippon Shashin Gakkaishi*, **38**, 360 (1975)

Optimization on Solenoid Coils for Magnetic Force Enhancement

Xiaojun Liu and Tsukasa Kiyoshi
Tsukuba Magnet Laboratory, National Institute for Materials Science
3-13 Sakura, Tsukuba, Ibaraki 305-0003, Japan
(LIU.Xiaojun@nims.go.jp)

Abstract

High magnetic force plays an important role in many applications of magnetic processing, such as the magnetic separation of ferromagnetic materials and the magnetic levitation of diamagnetic materials. To enhance a magnetic force, a new numerical optimization method using only solenoid coils was developed. With this method, the magnetic flux density B, the magnetic field gradient *grad* B, and the magnetic force field *grad* $(B^2/2)$ in the z-axis, as objective functions, were maximized with the total volumes of the coils and the B-J characteristics of superconductors. As a result, the optimal shapes for a single coil and double coils were exhibited.

Key words

magnetic force, solenoid coils, optimization, FEM

1. Introduction

High magnetic fields can be used in various disciplines, such as physics, biology, chemistry, materials science, and geology, for research and development in science and technology. They can facilitate understanding of microscopic states and the control of movement in materials. The interest in the research of magnetic force enhancement is growing. Experimental methods in recent years, including a high-temperature superconductor (HTS) bulk cylinder, were used to enhance the magnetic force [1], and a magnetic force booster was also developed to create stronger magnetic force [2]. In addition, as the technology for calculation has developed, many numerical methods have also become widely used in the optimal design of magnet or magnetic force enhancement. A solution to the problem of reducing the cost of coils for magnets was sought [3], and the optimization of an HTS bulk cylinder was studied for determining its optimal shape and arrangement [4]. Several numerical methods have been proposed; however, their range of application is limited to high magnetic fields and their homogeneity and excludes magnetic force.

A new method of numerical optimization using only solenoid coils to enhance a magnetic force was developed. In this method, not only the magnetic flux density B but also the magnetic field

gradient *grad B* and the magnetic force *grad* $(B^2/2)$ in the z-axis, as objective functions, were maximized with the total volumes of the coils and the *B-J* characteristics of superconductors. The method is a combination of the Finite Element Method (FEM) and the global optimization method. It was carried out on software ANSYS (version 8.1). As a result, the optimal shapes for a single coil and double coils were exhibited.

2. Physical conditions

We assumed that solenoid coils were made of superconducting wires, which were rectangular in this case. Their specifications are given in Table 1. Equations ① and ② are the B-J characteristic curves of Nb_3Sn and NbTi, respectively.

Table 1. Specifications of the superconducting wire materials

Coil number	coil1	coil2	coil3
Superconductor	Nb_3Sn	NbTi	NbTi
Acu/Asc	0.75	2.80	4.78

Nb_3Sn : $J = -80B+1500$ $[A/mm^2]$ ①

NbTi : $J = -400B+4200$ $[A/mm^2]$ ②

3. Mathematical problem

To solve the physical problem, finding max *B*, max *grad B*, and max *grad* $(B^2/2)$ in the z-axis by using the total volumes of coils, the following equivalent mathematical problem is proposed:

$$\textbf{Problem (P):} \quad \begin{cases} \underset{z \in z\_axis}{Maximum} \left\{ f(z) \mid f(z) := B,\ grad\ B,\ and\ grad(B^2/2) \right\} \\ subject\ to \begin{cases} \sum_i V_i = const. \\ J_i \le g_{ij}(B) \qquad (j \le i = 1\ or\ 2) \end{cases} \end{cases}$$

where V_i is the volume of the ith coil, J_i is the current density in the coil, and $g_{ij}(B)$ is the constraint function for the jth coil, which is similar to Equation ① or ②. When i=1, g_{1j} (j=1) is for a single coil, and, when i=2, g_{2j} (j=1,2) is for double coils. In this case, g_{21} is defined for the inner coil and g_{22} for the outer coil, and $J_1=J_2$. ***Problem (P)*** is a nonlinear optimization problem, which was solved

by using a combination of the FEM and global nonlinear programming method. Figure 1 shows a flow chart of the optimization method.

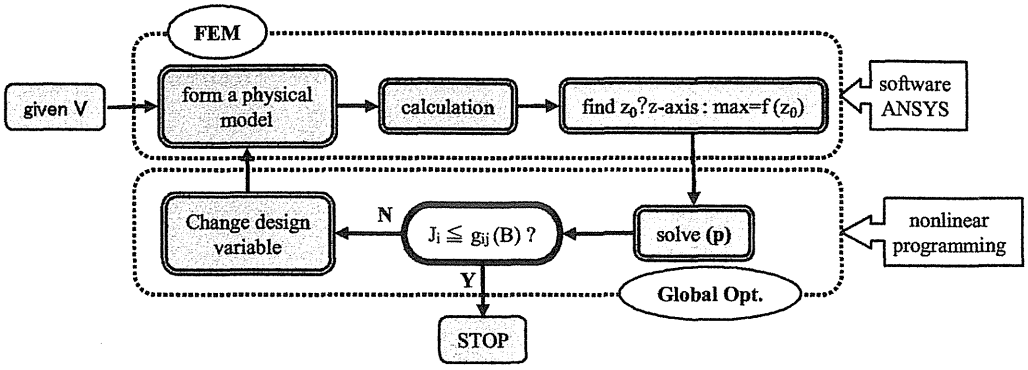

Fig. 1 Flow chart of the optimization method.

4. Calculation examples

4.1 A single coil

First, we carried out an optimization method on a single coil. In this case, coil 3 in Table 1 was used for the calculation; here, the constraint function $g_{11}(B) = -400B+4200$ [A/mm^2]. Its model is shown in Fig. 2, and the specifications are given in Table 2.

Table 2. Specifications of a single coil

volume (m^3)	inside radius (mm)	constraint at A point (A/mm^2)	design / dependent variable
V	R=50	$J_A = g_{11}(B_A) \leqq J$	T / B

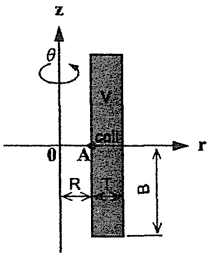

Fig.2 Model for optimization.

As an example, we gave V=0.33×10^{-2} (m^3). By solving ***problem (P)*** for the volume, max *B*, max *grad B*, and max *grad* ($B^2/2$) in the z-axis were found. Figures 3, 4, and 5 show the optimal critical current density in a superconducting wire for obtaining the maximum values for *B*, *grad B*, and *grad* ($B^2/2$), respectively.

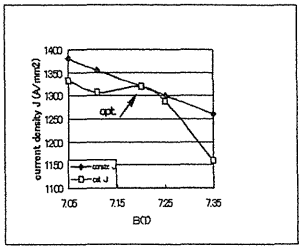

Fig.3 Optimal current density at Max *B*.

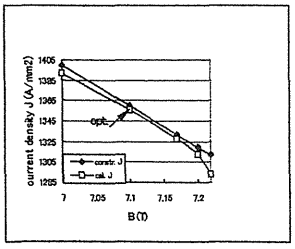

Fig.4 Optimal current density at Max *grad B*.

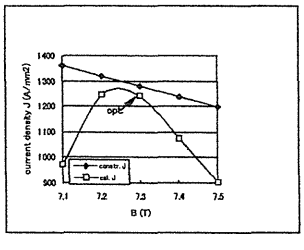

Fig.5 Optimal current density at Max *grad* ($B^2/2$).

Figures 6, 7, and 8 show the optimal shapes (models) for max B, max *grad B*, and max *grad* $(B^2/2)$.

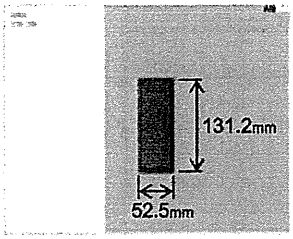

Fig.6 Optimal model at Max B, J=1320A/mm^2.

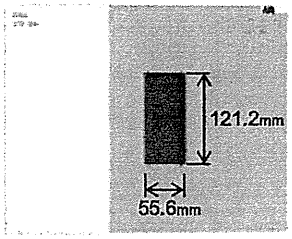

Fig.7 Optimal model at Max *grad B*, J=1356.6A/mm^2.

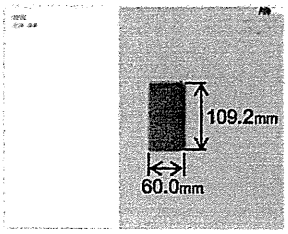

Fig.8 Optimal model at Max *grad* $(B^2/2)$, J=1243.3A/mm^2.

Figures 9, 10, and 11 show the values of B, *grad B*, and *grad* $(B^2/2)$ along the z-axis for the optimal models above.

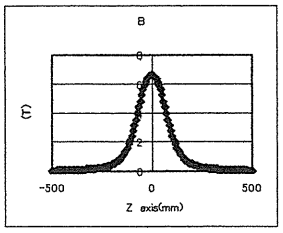

Fig.9 B distribution along the z-axis.

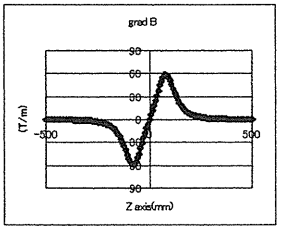

Fig.10 *Grad B* distribution along the z-axis.

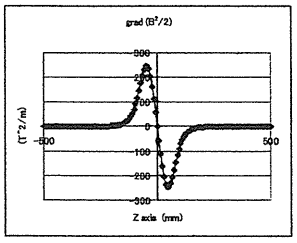

Fig.11 *Grad*$(B^2/2)$ distribution along the z-axis.

4.2 Double coils

Secondly, we carried out an optimization method on double coils. In this case, coils 1 and 2 in Table 1 were used for the calculation; here, the constraint function $g_{21}(B)$= -80B+1500 [A/mm^2] and $g_{22}(B)$= -400B+4200 [A/mm^2]. Their model is shown in Fig. 12, and specifications are given in Table 3. In Fig. 12, the constraint point P is selected between P1 and P2 for coil 2.

Table 3. Specifications of the double coils

coils	volume (m^3)	interval (mm)	inside radius (mm)	constraint at A & P points (A/mm^2)	design/ dependent variable
coil1	V_1	No	R=50	$J_A=_{21}(B_A) \leqq J_1$	b_1, b_2, t_1 / t_2
coil2	V_2	D=1	R+D+t_1	$J_P=g_{22}(B_P) \leqq J_2$	

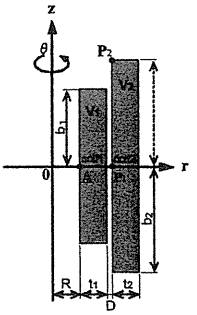

Fig.12 Model for optimization.

For the double coils, we also obtained the optimal shapes (models) for the max B, max *grad B*, and max *grad* $(B^2/2)$. Figures 13, 14, and 15 show three cases of the

optimal shapes for max *B*. In one case, we obtained b1> b2 ($V=0.5\times10^{-2}$ m^3), but, in others, we had b1=b2 ($V=1.02\times10^{-2}$ m^3) and b1<b2 ($V=1.3\times10^{-2}$ m^3).

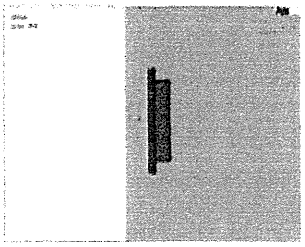

Fig.13 Optimal model at Max *B* ($V=0.5\times10^{-2}$ m^3).

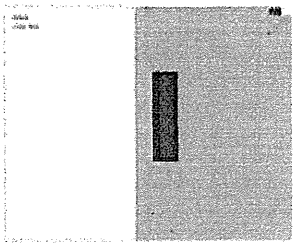

Fig.14 Optimal model at Max *B* ($V=1.02\times10^{-2}$ m^3).

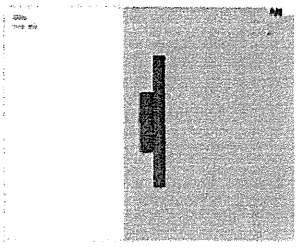

Fig.15 Optimal model at Max *B* ($V=1.3\times10^{-2}$ m^3).

Figures 16, 17, and 18 show the *B* values along the z-axis for the optimal models above.

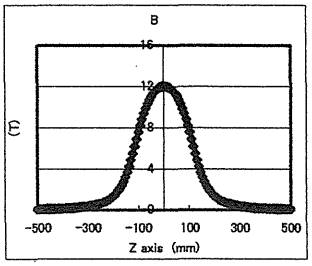

Fig.16 *B* distribution along the z-axis ($V=0.5\times10^{-2}$ m^3).

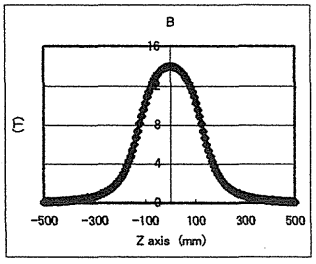

Fig.17 *B* distribution along the z-axis ($V=1.02\times10^{-2}$ m^3).

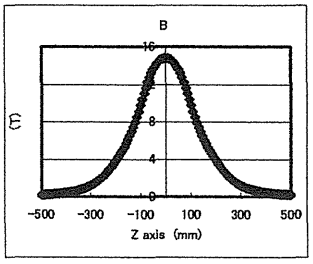

Fig.18 *B* distribution along the z-axis ($V=1.3\times10^{-2}$ m^3).

Figures 19, 20, and 21 show three optimal shapes for the Max *grad B* in volumes $V=0.5\times10^{-2}$ m^3, 0.95×10^{-2} m^3, and $V=1.3\times10^{-2}$ m^3.

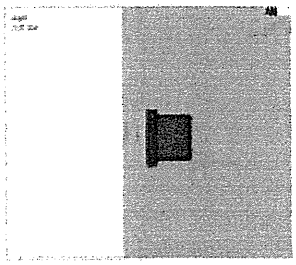

Fig.19 Optimal model at Max *grad B* ($V=0.5\times10^{-2}$ m^3).

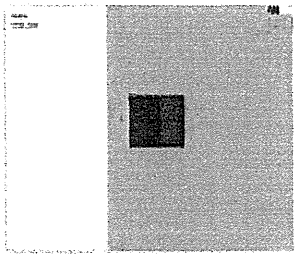

Fig.20 Optimal model at Max *grad B* ($V=0.95\times10^{-2}$ m^3).

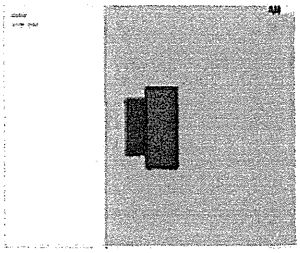

Fig.21 Optimal model at Max *grad B* ($V=1.3\times10^{-2}$ m^3).

Figures 22, 23, and 24 show the *grad B* values along the z-axis about their optimal models above.

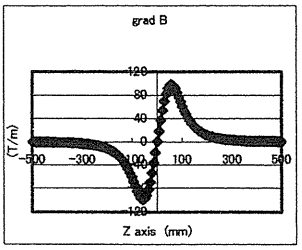

Fig.22 *Grad B* distribution along the z-axis ($V=0.5\times10^{-2}$ m^3).

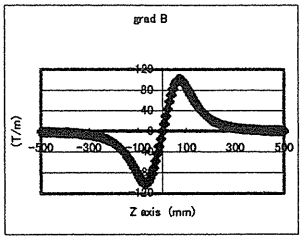

Fig.23 *Grad B* distribution along the z-axis ($V=0.95\times10^{-2}$ m^3).

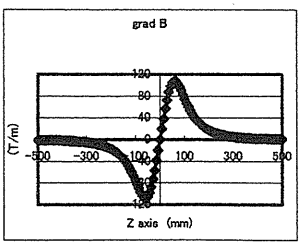

Fig.24 *Grad B* distribution along the z-axis ($V=1.3\times10^{-2}$ m^3).

Figures 25, 26, and 27 show three optimal shapes for the Max *grad* $(B^2/2)$ in volumes $V=0.5\times10^{-2}$ m^3, 0.6×10^{-2} m^3, and $V=1.3\times10^{-2}$ m^3 respectively.

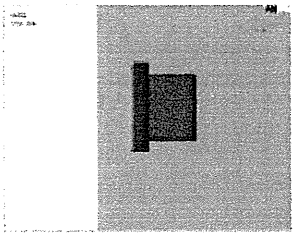

Fig.25 Optimal model at Max *grad*$(B^2/2)$ ($V=0.5\times10^{-2}$ m^3).

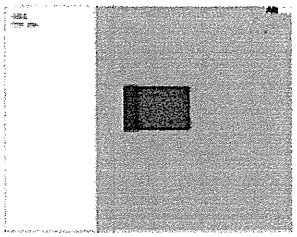

Fig.26 Optimal model at Max *grad*$(B^2/2)$ ($V=0.6\times10^{-2}$ m^3).

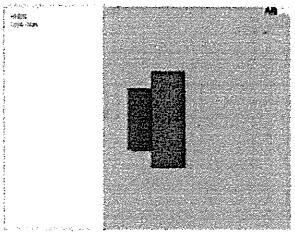

Fig.27 Optimal model at Max *grad*$(B^2/2)$ ($V=1.3\times10^{-2}$ m^3).

Figures 28, 29, and 30 show the Max *grad* $(B^2/2)$ values along the z-axis for the optimal models above.

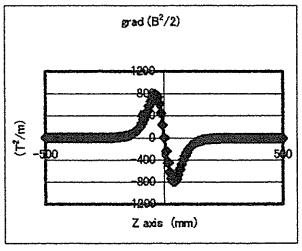

Fig.28 *Grad* $(B^2/2)$ distribution along the z-axis ($V=0.5\times10^{-2}$ m^3).

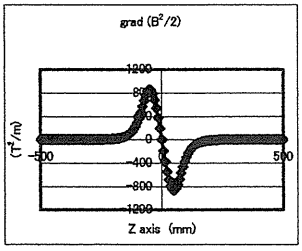

Fig.29 *Grad* $(B^2/2)$ distribution along the z-axis ($V=0.6\times10^{-2}$ m^3).

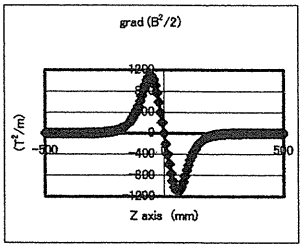

Fig.30 *Grad* $(B^2/2)$ distribution along the z-axis ($V=1.3\times10^{-2}$ m^3).

5. Discussion

The total volumes (V1+V2) were only assumed to be constant in double coils; however, the cost of two coils was not considered. That may account for the variety of optimal shapes in calculating the max B, max *grad B,* and max *grad* $(B^2/2)$. To further research magnetic force enhancement, it will be necessary to consider the cost of coils and minimize them.

6. Conclusions

In this paper, a new numerical optimization method using only solenoid coils was developed to enhance a magnetic force. In this method, once the total volume of coils is given, max B, max *grad* B, and max *grad* $(B^2/2)$ in the z-axis and their optimal shapes can be obtained under the constraint condition on the B-J characteristic curve of superconducting wire materials. From the results obtained with this method, it is evident that, when the volume of coils increases, the increase of B and *grad* $(B^2/2)$ is remarkable, but the change in *grad* B is little. Therefore, when superconducting magnets are designed, it would be best to maximize *grad* $(B^2/2)$ only.

References:

[1] S. Matsumoto, T. Kiyoshi, T. Asano, O. Ozaki, K. Koyanagi, J. Fujihira, and H. Wada, IEEE Trans. Appl. Supercond. 13 (2003) 1652-1655.

[2] O. Ozaki, et al., IEEE Trans. Applied Supercond. 14 (2004) 1663-1665.

[3] A. Ishiyama and K. Shimizu, An Optimal Design Method for Multi-Section Superconducting Magnets, IEEE Trans. Magn. 28 (1992) 919-922.

[4] X. J. Liu, S. Matsumoto, and T. Kiyoshi, Program and Abstracts of the 8th Symposium on New Magneto-Science. Dec. (2004).

Magnetic field effects on viscoelasticity of agarose gels

Tetsuya Makino, Kyohei Ogawa, Isao Yamamoto and Masuhiro Yamaguchi
Department of Physics, Yokohama National University,
Tokiwadai, Hodogaya-ku, Yokohama 240-8501, Japan
(d05gd238@ynu.ac.jp)

Abstract

A mechanical property of agarose gel aligned in strong magnetic fields is investigated by acoustic measurement. The propagation of ultrasonic wave pulse through magnetic treated gels indicates anisotropic elasticity. The perpendicular direction in the gel is harder than the parallel one to the magnetic field exposed. The anisotropy of elasticity decreases with increasing concentration of agarose. These results are discussed with the structure of the gel and under the influence of the strong magnetic field.

Keywords

magnetic field effect, magnetic order, agarose gel, viscoelasticity, ultrasonic wave

1. Introduction

Agarose is a natural high polymer extracted from seaweeds and the main component of agar. The agarose molecule is chain-like structure which consists of β-D-galactose and 3, 6-anhydro-α-L-galactose. The molecule orients perpendicularly to the magnetic field due to its diamagnetic anisotropy. The agarose solution shows thermo reversible sol-gel phase transition: the gel melts above temperature of 338K and gelates again below 300K. Once it is formed in the magnetic field, macromolecular aggregates (called "domain") in the gel order perpendicularly to the field.

Our previous studies reported the order of agarose molecules and the changes in the properties of the gel formed in magnetic field, as follows. The network structure of the gel changes anisotropically by measurements of the velocity of DNA electrophoresis and the volumetric shrinkage in acetone-water system [1, 2]. Accordingly, the anisotropic changes in the cross-linking structure and/or the bridging density are expected for the magnetic ordered gel. In this paper, the change in mechanical property of the magnetic ordered gel is investigated by using ultrasonic wave.

2. Experimental methods

2.1 Gel preparation

Hot aqueous solution of agarose (Agarose-L, JUNSEI CHEMICAL CO. LTD.) was poured into an acryl-made sample holder with w10×d10×h30mm^3 in capacity. The concentration of the solutions was prepared to be 1.0, 2.0, 3.0, and 4.0wt. %. The solutions within the holders were set up in the bore of a superconducting magnet. The setting positions were the center of magnetic field and 450mm distance from there. The magnetic flux densities were 13T at the center and 0.5T at 450mm position, respectively. No magnetic effects of the gel formed below 0.5T were observed by optical measurement [3]. Temperature of the sample space in the bore was controlled by flowing water. The samples were cooled-down from 70 °C to 15 °C for 3 hours under the influence of the constant magnetic field. Thus, the magnetic ordered gels and the disordered (random) gels were prepared simultaneously in the same cooling rate.

2.2 Ultrasonic measurements

Ultrasonic waves were chosen to measure the mechanical properties of the gels. The measurement device could be miniaturized by using ultrasonic wave. The same sample can be measured many times because the ultrasonic wave does not destroy the ordered structure of the gel.

The ultrasonic wave transducer and the hydrophone were fixed on the acryl-made holder and sunk into a water bath at 12°C as shown in Fig. 1. Two large wave pulses with the time difference were observed on the monitor of the oscilloscope. The first wave passed directly through the holder and the sample. On the other hand, the second wave was reflected twice on the inside walls of the holder. The ultrasonic wave transmitted the ordered gels perpendicularly and parallel to the magnetic field exposed.

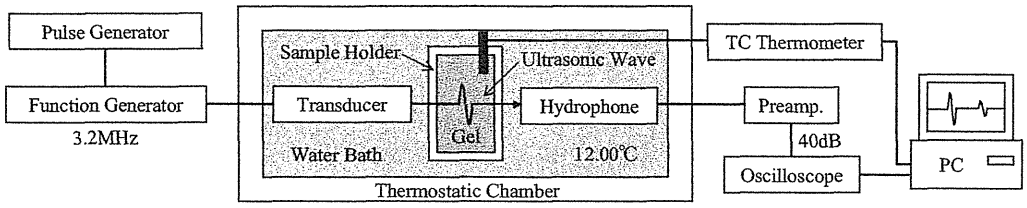

Fig. 1. The ultrasonic wave measurement system was constructed of a function generator to control the frequency and the shape of the wave pulse, a transducer (PRECISION ACOUSTICS LTD., Pa075) to make the ultrasonic wave of one cycle, a needle hydrophone (NTR SYSTEMS INC., TNU001) as a detector, a pre-amplifier to 40dB amplify the detected signal, and an oscilloscope.

3. Results and Discussion

As the preliminary experiment, the sonic velocity in distilled water was measured to confirm the accuracy of our system. The sonic velocity c in the sample is expressed by Eq. (1).

$$c = \frac{2d}{\Delta t}, \tag{1}$$

where d is thickness of the sample and Δt is the time difference between the first and the second waves. Figure 2 shows the temperature dependence of the sonic velocity which was calculated according as Eq. (1). For example, the sonic velocity was 1454 m/sec at 12.0 °C. The solid curve shows a value of empirical formula by Greenspan-Tschiegg [4]. The measured values agreed with this empirical formula within ±0.1 %.

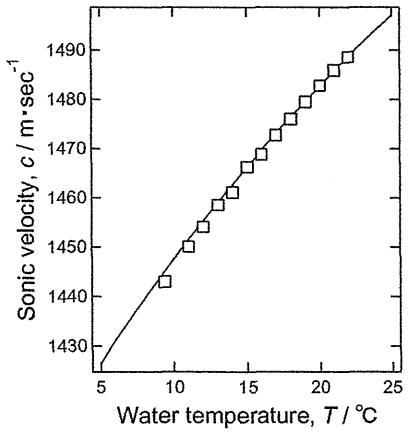

Fig. 2. Temperature dependence of sonic velocity c in distilled water. The symbols and curve denote the measured values and the empirical value after Greenspan and Tschiegg, respectively.

In the same way, the sonic velocities were measured for the magnetic ordered gels and random gels. Fig. 3 illustrates the sonic velocities in the gels as a function of the agarose concentration. All the sonic velocities were increased with increasing the concentration. The liner relation was observed for dilute gels but tended to be saturated at 4wt. %. It is considered that this saturation phenomenon relates with the limit of solubility of 5wt. %. The anisotropic sonic velocity was found for the magnetic ordered gels as shown in Fig. 3: the velocities were faster along the perpendicular direction than the parallel one of the magnetic field exposed.

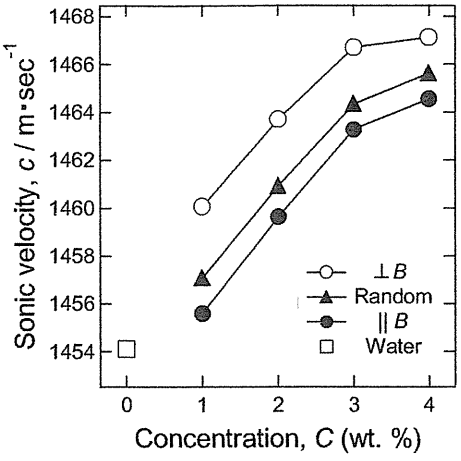

Fig. 3. Sonic velocity in the magnetic ordered gels formed in the magnetic field of 13T.

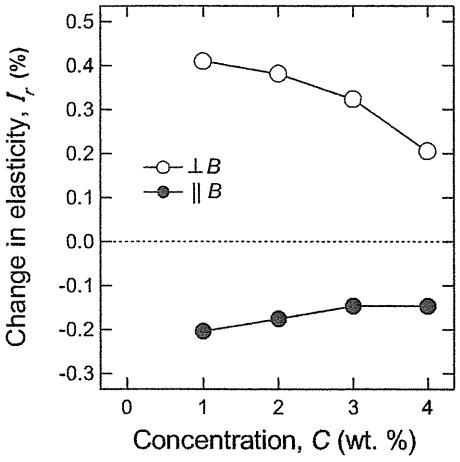

Fig. 4. Concentration dependency of change in elasticity of magnetic ordered gel

The elastic modulus m' of gel is expressed by Eq. (2).

$$m' = \rho c^2, \tag{2}$$

where ρ is density of the gel. Equation (2) means that the increase in the sonic velocity corresponds to the increase in hardness of the gel. Figure 4 indicates the change in the ratio of elasticity defined by Eq. (3).

$$I_r = \frac{m'_{ordered} - m'_{random}}{m'_{random}} \times 100, \tag{3}$$

where $m'_{ordered}$ and m'_{random} are elastic modulus of the ordered and random gels, respectively. In Fig. 4, the ordered gels had the anisotropic elasticity: the perpendicular direction in the ordered gel was harder than the random gel at all concentrations. On the other hand, the parallel directions in the ordered were softer than the random. This magnetic field effect in the perpendicular direction was twice compared to the parallel one. Furthermore, the anisotropy was decreased with increasing concentration.

It was reported that the magnetic ordered gel shrunk anisotropically in acetone-water system [2]. The perpendicular direction was less shrinkable to the magnetic field exposed than the parallel direction. This unshrinkable direction of the anisotropic gel was agreed with the hard direction in the present results. The elasticity and shrinkage of the agarose gel depend on the cross-linking structure and the bridging density. These results reflect the change in the structure among "domains" in the gel. It is considered that the ordered gels have the anisotropic elasticity because the magnetic field has controlled anisotropically the gelation process.

4. Conclusions

The mechanical properties have been investigated for agarose gels formed in the strong magnetic field of 13T by using ultrasonic wave. The magnetic ordered gels had anisotropic elasticity, which was decreased as the concentration increase. The high elasticity direction was agreed with that of the poor shrinkage in acetone-water system. It is considered that the agarose gel has anisotropic structure and elasticity because the gelation process is controlled anisotropically with the magnetic field.

References

[1] T. Fushimi, T. Usui, S. Irita, I. Yamamoto and M. Yamaguchi, *The Papers of Technical Meeting on Magnetics, IEE Japan,* MAG-03-33 (2002) (in Japanese).
[2] I. Yamamoto, *Kobunshi,* 54/7, 482 (2005) (in Japanese).
[3] T. Usui, T. Fushimi, K. Nomoto, I. Yamamoto and M. Yamaguchi, *TML Annual Rept.2002 Suppl. II,* 167 (2003).
[4] C. E. Tschiegg and M. Greenspan, *Jour. Acous. Soc. Am.,* 28, 158 (1956).

Functionalization of supramolecular biosystems in magnetic fields

Toru Oba[1], Takero Nagai[1] and Yoshifumi Tanimoto[2]
1 Faculty of Engineering, Utsunomiya University,
7-1-2 Yoto, Utsunomiya, Tochigi 321-8585, Japan.
2 Graduate School of Science, Hiroshima University,
1-3-1 Kagamiyama, Higashi-hiroshima, Hiroshima 739-8526, Japan.
(tob_p206@cc.utsunomiya-u.ac.jp)

Abstract
This study aims at functionalization of supramolecular biosystems in high magnetic fields. We integrated molecular devices on cytoskeletal nano-tubules, and operated them as on-demand nano-devices. We developed new tools that enable application of diamagnetic orientation to the device system, which can provide higher functionalizations of the nano-devices.

Keywords
high magnetic field, tubulin, microtubule, nano-device, photosynthesis

1. Introduction

Nano-integrated circuits, which have been extensively studied for downsizing and energy-saving in the field of electronics and photonics, may be afforded by elaborate arrangements of various molecular- and nano-devices. Development of methods to integrate functional molecules into well-defined nano structures is crucial for fabrication of future materials and novel supramolecular systems. We fabricated a unique nano-device by utilizing cytoskeleton 'microtubule (MT)' [1,2]. MT is a hollow cylinder whose outer and inner diameters are 25 and 13 nm, respectively, and is formed by assembly of cytoskeletal protein 'tubulin' heterodimer (Tub; *ca.* 5×5×4 nm and 55 kDa for both α and β-subunits). MTs can be decomposed into the building-blocks (Tubs) by *e.g.* lowering temperature to 0 °C, and the Tubs can reassemble to form MTs at 37 °C in the presence of nucleotide. We conjugated various molecular devices with Tub, and integrated them in the nano-ordered structure by self-assembly of the protein. The 'functionalized MT' is characteristic for its on-demand function, reusability, repairability, and modifiability.

Arrangement of the functionalized MTs into ordered nano structures, as well as further integration of various functional elements, including another functionalized MTs, are advantageous for fabrication of elaborate nano devices. It was reported that, in spite of extremely low diamagnetic anisotropy of Tub, the assembly of Tub into MT in strong magnetic fields showed diamagnetic orientation of MTs [4,5]. Diamagnetic orientation may be a powerful method to afford ordered arrangements of the MT nano-devices. Here we report on our attempts to functionalize the MTs in strong magnetic fields.

2. Experimental methods

Unlabeled tubulin, fluorescein-labeled tubulin (labeling stoichiometry, Flu/Tub = 1), tetramethylrhodamine-labeled tubulin (TMR/Tub = 1), and biotinylated tubulin (biotin/Tub = 1) were all obtained from Cytoskeleton Inc. Avidin ('Avidin D') and biotinylation reagent 'biotin (Long Arm) NHS' were from Vector Laboratories Inc. Bovine serum albumin was obtained from Nacalai tesque. Visible absorption spectra were recorded on a JASCO spectrophotometer V-550 at 25 °C. The corrected fluorescence spectra were obtained using by a JASCO fluorescence spectrophotometer FP-777 at 25 °C.

Conjugation of a fluorophore and a photosensitizer-labeled hemoprotein to Tubs, and fabrication of the photofunctional MTs were described previously [1,2]. Flow-cells we used to apply magnetic

fields to the MTs and to fix the MTs on substrates consists of a substrate plates (ITO, quartz, silicon *etc.*) pretreated with 3-aminopropyltriethoxysilane (or poly-L-lysine), spacers and a glass cover slip. Biotinylated albumin, avidin, and diluted, paclitaxel stabilized MT were loaded into this flow-cell, in this order, and incubated to fix them on the surface of the substrate. The flow-cell was then subjected to magnetic field and to visible absorption, fluorescence and microscopic measurements.

Fluorescence anisotropy measurements (excited at 470 nm) for oriented MT was carried out for an aqueous solution of relatively condensed, fluorescein-labeled Tub (10mg/mL, 5 μL). The MT was prepared by incubation of the Tub solution in a thin quartz cuvette in magnetic field (6 T) at 37 °C for 15 min [3,4].

For integration of various functional elements on the surface of MT, we designed a peptide referring to the MT-associated proteins [5,6]: biotin – Ahex – Cys – Ahex – Lys– Asn – Val – Arg – Ser – Lys-Val – Gly – Ser – Thr – Glu – Asu – Ile – Lys – His – Gln – Pro – Gly – Gly – Arg – Ala – Lys (Ahex, 6-aminohexanoic acid). The peptide was synthesized by NIBB Center for Analytical Instruments (National Institute for Basic Biology, Okazaki, Japan), and was purified by using a reversed-phase HPLC. The peptide was labeled with tetramethylrhodamine (Morecular Probes, Inc.) and purified by conventional way (in what follows the labeled peptide is denoted as 'TMR-MAP').

3. Results and Discussion

3.1 Development of a setup that allows magnetic field application to the functionalized MTs

For higher device function, and for observation of orientation of MTs, it is necessary that the MTs are fixed onto appropriate substrates without disruption of the orientation by, say, diffusion and washing. We designed and fabricated flow-cells that facilitate functionalization of the MTs including application of magnetic fields. The flow-cell was constructed on the ITO glass plate, or other substrates, pretreated with 3-aminopropyltriethoxysilane. Biotinylated albumin, avidin, and diluted MT solutions were loaded into this flow-cell. The sample was subjected to fluorescence measurements after washing inside of the flow-cell with buffer. Fluorescence spectra show emission bands both from avidin and MT (Figure 1A), suggesting formation of the ternary complex of albumin – avidin – MT (Figure 1B) in the flow-cell. Essentially the same results were obtained for ploy-L-lysine treated substrates. Adsorption of MTs in the flow-cells was also revealed by AFM measurements (Figure 2). The flow-cell will also be advantageous for facile integration and facile exchange of the functional elements and blocks that facilitate dynamic manipulation and function of the nano-device.

3.2 Diamagnetic orientation of MT

The fluorescein-labeled MT prepared in the magnetic field (6 T) showed fluorescence anisotropy of 0.22 (detected at 530 nm). When the fluorescein-labeled MT formed in 6 T was disassemble out of the field, the fluorescence anisotropy value of the sample increased to be 0.26. Fluorescein-labeled MTs prepared out of the magnetic field (0 T) gave the value of 0.25. Fluorescence anisotropy value in general can decrease by arranging the orientation of filamentous aggregates of proteins. The observed difference between the values of the MTs prepared in and out of the magnetic field is attributable to diamagnetic orientation of the MTs. We now examine evaluation of degree of orientation by using SEM and AFM, as well as functionalization of diamagnetically oriented MTs.

3.3 Development of a new method of integration

We had so far utilized the specific interaction between avidin and biotin to conjugate functional elements with MT [1,2]. Alternative ways should be developed for further integration of various functional elements, wiring of the devices, and connection of the nano-device to the macro world. We examined utility of a specific peptide, MAP peptide, as a tool for this purpose. TMR-MAP was mixed with a solution of fluorescein-labeled MT. Fluorescence from fluorescein decreased with increase of the coexisting TMR-MAP, due to excitation energy transfer from fluorescein to

tetramethylrhodamine. This indicates association of TMR-MAP with the surface of the MT. The dissociation constant of TMR-MAP and MT was calculated to be $5 \times 10^3 \sim 1.5 \times 10^4$ M^{-1} (Figure 3). Because MAP can be conjugated with various functional elements, it enables further functionalization and wide extension of MT nano-device in and out of the magnetic fields.

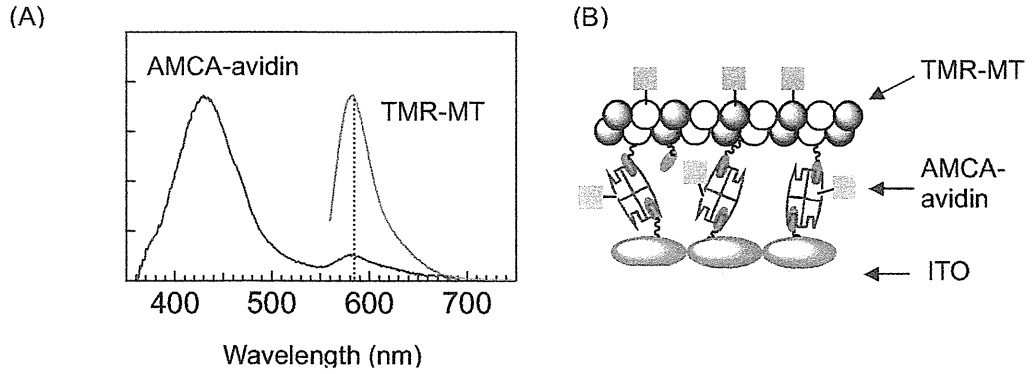

Fig. 1. (A) Fluorescence emission spectra of the ternary complex of albumin – avidin – MT in the flowcell fabricated on an ITO glass plate. MT and avidin were labeled with TMR and AMCA (aminomethylcoumarin), respectively. Fluorescence from AMCA and TMR were measured by excitations at 350 and 550 nm, respectively, at room temperature. (B) Schematic representation of the ternary complex of albumin – avidin – MT formed in the flowcell.

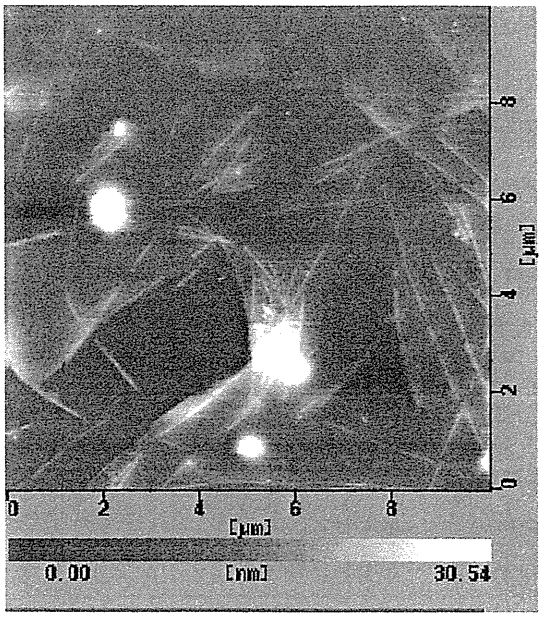

Fig. 2. An AFM image of MTs deposited on a silicon surface by using the flow-cell (in zero field).

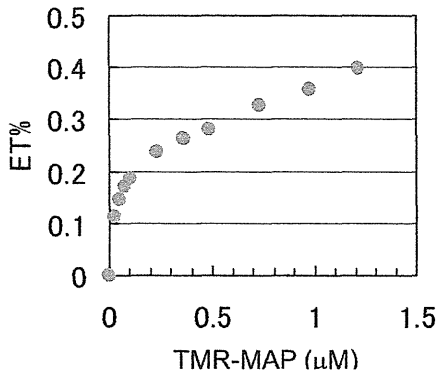

Fig. 3. Efficiency of excitation energy transfer between fluorescein fixed on the MT surface and TMR of the TMR-MAP (fluorescein-labeled tubulin, 36 nM; measured at room temperature).

5. Conclusions

We developed new tools that facilitate further development of the MT nano-devices. The flow-cell, magnetic orientation, and the 'MAP peptide' will enable a variety of manipulations and functionalizations of the MT nano-devices. Further investigations for evaluation of degree of orientation and functionalization of oriented MTs in the magnetic field are now underway.

Acknowledgements

This work was supported by Grant-in-Aid for Scientific Research on Priority Areas "Innovative utilization of strong magnetic fields" (Area 767, No.15085204) from MEXT of Japan. We thank to Prof. K. Iimura (Utsunomiya University, Japan) for AFM measurements, NIBB Center for Analytical Instruments (National Institute for Basic Biology, Japan) for their help in peptide synthesis and analyses, and Collaboration Center for Research and Development of Utsunomiya University for their technical assistance. We also thank to Prof. M. Karikomi, Prof. M. Minabe, Dr. S. Ito, and Prof. K. Hiratani (Utsunomiya University, Japan) and Dr. Y. Saga and Prof. H. Tamiaki (Ritsumeikan University, Japan) for their assistance.

References

[1] T. Oba, M. Hanasaki, M. Minabe, H. Tamiaki., Chem. Lett., 34 (2005) 150-151.
[2] M. Hanasaki, M. Sato, M. Minabe, H. Tamiaki, T. Oba, *Photosynthesis: fundamental aspects to global perspectives*, A. van der Est, and D. Bruce eds., pp.1079-1080, Allen Press, Lawrence (2005).
[3] W. Bras, G. P. Diakun, J. F. Diaz, G. Maret, H. Kramer, J. Bordas, F. J. Medrano, Biophys. J., 74 (1998) 1509-1521.
[4] T. Higashi, *Jiki-kagaku*, S. Ozeki, Y. Tanimoto, and M. Yamaguchi eds., IPC, Tokyo (2002).
[5] H. Aizawa, H. Kawasaki, H. Murofushi, S. Kotani, K. Suzuki, H. Sakai, J. Biol. Chem., 264 (1989) 5885-5890.
[6] Y. Okada, N. Hirokawa, Proc. Natl. Acad. Soc. USA, 97 (2000) 640-645.

Magnetic-Field-Induced Structures and Functions of Hydrogels

Ichiro Otsuka and Sumio Ozeki

Department of Chemistry, Faculty of Science, Shinshu University, 3-1-1 Asahi, Matsumoto 390-8621, Japan

(sozeki@shinshu-u.ac.jp)

Abstract

Magnetic field induced structures and functions were examined using hydrogeks of acrylamide (AAm), *N*,*N*-diethylacrylamide (DEAA), and *N*-isopropylacrylamide (NIPA) gels. The diameter of those gels prepared under high magnetic field became larger than that of each zero-field gel at 298K, e.g., 40% larger in a NIPA gel prepared at 30T. Volume phase transition temperature did not change by magnetic fields in preparing gels, but the heat of volume phase transition was increased. When magnetic fields were applied to reactant solutions in the preparation conditions for continuous volume change gels, the prepared gels showed the discontinuous volume change. The effective degree of cross-linkage of gels prepared under magnetic fields decreased steeply with increasing magnetic field. Magnetic fields induced formation of dangling chains and orientation of polymer chains to make gels soft and anisotropic. The anisotropic gels controlled molecular diffusion in them. Furthermore, when magnetic fields were applied to prepared gels, the gels swelled, e.g., in NIPA gels, about 9% larger in a 30T magnetic field than zero fields.

Kyewords

hydrogel, magnetic field, magneto-orientation, hydration, volume phase transition

1. Introduction

Hydrogels have been investigated from the view point of scientific and technological aspects. It is very important to investigate the methodology for control structures and physical properties of gels. Although magnetic energy is much less than thermal energy, macromolecules would orient under high magnetic fields because of molecular magnetic anisotropy. Therefore, magnetic fields may be one of useful energies for structural control of gels. Magnetic anisotropy of monomer itself is not enough to response to magnetic fields, but polymer chains produced in the polymerization processes may orient cooperatively even to relatively low magnetic fields. When oriented polymer chains are cross-linked, the structured gel would be taken out from magnetic fields. Moreover, application of magnetic field to gels would bring about chains in orientation and hydration of

polymer chains. In this work, magnetic field-induced structures and functions were examined using various hydrogels including thermo-responsive gels.

2. Experimental methods

NIPA gels were prepared by radical polymerization with monomers (acrylamide (AAm), *N*,*N*-diethylacrylamide (DEAA), and *N*-isopropylacrylamide (NIPA)), *N*, *N*"-methylenebis-acrylamide (BIS) as a cross-linker, potassium peroxodisulfate (KPS) as an initiator, and *N*,*N*,*N*',*N*'-tetramethylethylenediamine (TEMED) as an accelerator[1,2]. NIPA concentration was fixed 700mM and BIS concentration varied from 4.3mM to 34.4mM (usual condition was 8.6mM) to investigate the effect of cross-link density. The polymerization was allowed to proceed for 1h at 278K in 0.4mm (i.d.) glass capillary to make cylindrical gels. Magnetic fields were applied perpendicular ($H_{\perp}$) and parallel ($H_{//}$) to the capillary for 1h using superconducting magnet ($H \leq 10$T) and hybrid magnet ($H \leq 30$T; National Institute for Materials Science). Then, the capillary remained silently under zero-field at 278K for 24h. Gel prepared were taken out of the capillaries, washed repeatedly by temperature swing in large amount of distilled water to remove residual chemicals, and then dried at room temperature in an air.

The gels with diameter of 0.4mm was cut into 20mm rods and immersed into distilled water for 24h to reach swelling equilibrium. The swelling behavior of gels were observed by an optical microscope coupled with CCD camera as temperature was increased from 278K to 318K under zero field. Equilibrium time was 2h for each temperature.

Swelling experiments under magnetic field was carried out in hybrid magnet. Temperature was kept 298K and diameter change due to magnetic field was observed with the CCD camera.

The molecular diffusion in gels was examined at 298K using both $H_{\perp}$ and $H_{//}$ gels and a zero-field gel in 2.0mm (i.d.) glass capillaries. One side of a gel containing 1% starch was vertically immersed into an aqueous KI/I_2 solution, and the velocity of color changing head in the gel was observed at zero-field.

3. Results and Discussion

The gel diameter prepared under magnetic fields increased in swelling state. The gel diameter increased linearly with increase in magnetic field below 10T to become 40% larger than that of zero-field gel[3]. On the other hand, it is well known that decrease of BIS concentration in preparation makes gel swell. This suggests that the increase of gel diameter due to magnetic fields would be ascribed to reduction of cross-link density in polymer network. Magnetic field dependence of the effective degree of cross-linkage (q^{eff}) was estimated by comparison of the

diameter of gels prepared at different degree of cross-linkage q^{pre} ($\equiv C_{BIS}/C_M$; C_M = 700mM, monomer concentration) with that of gels prepared under various magnetic fields, as shown in Fig. 1. It shows that magnetic field reduced the effective cross-linkage from $q^{pre} = 0.0123$ to $q^{eff} \approx 1/3\ q^{pre}$ at 15T. The q^{eff} reduction means that gels were softened by magnetic fields which was supported by decrease in Young's modulus. The Young's modulus of the gel prepared under 10T magnetic field was about 1/3 of zero-field gel. Considering that no change in an averaged q^{eff} value estimated from C/N ratios in NIPA gels with the elemental analysis was detected by magnetic field, dangling chains, whose one side is not cross-linked, would be increased by magnetic fields. The increase in dangling chain due to magnetic fields was confirmed by the results that the elastic relaxation time of magnetic field gels was much longer than that of zero-field gels.

When a magnetic field was applied to a gel in preparing at preparation conditions for no volume phase transition gels, discontinuous volume change (i.e. volume phase transition) appeared (Fig. 2 upper). The discontinuity in the volume phase transition of NIPA gel was enlarged with increasing magnetic field intensity, and not saturated even at 30T yet. The swelling and shrinking lines of gels prepared at various q crossed at a critical magnetic field intensity, H_v, where volume phase transitions induced as shown in Fig. 2. The same phenomenon was observed in AAm gels, although AAm gels are well known as a non-volume phase transition gel.

The diameter changes of $H_\perp$ gels were much larger than those of $H_{//}$ gels, suggesting that magnetic orientation of polymer chains in gels

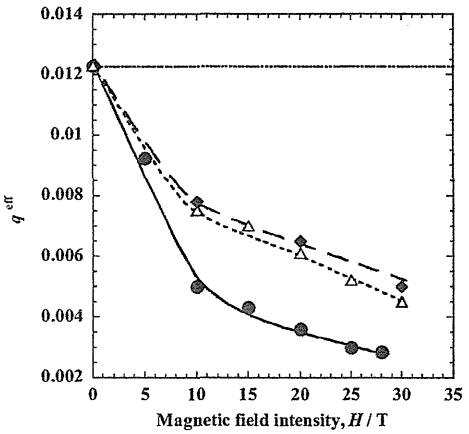

Fig. 1 Effective cross-linkage (q^{eff}) as a function of magnetic fields. ●, NIPA; △, DEAA; ◆, AAm. Dotted line shows an averaged q value estimated from elemental analysis.

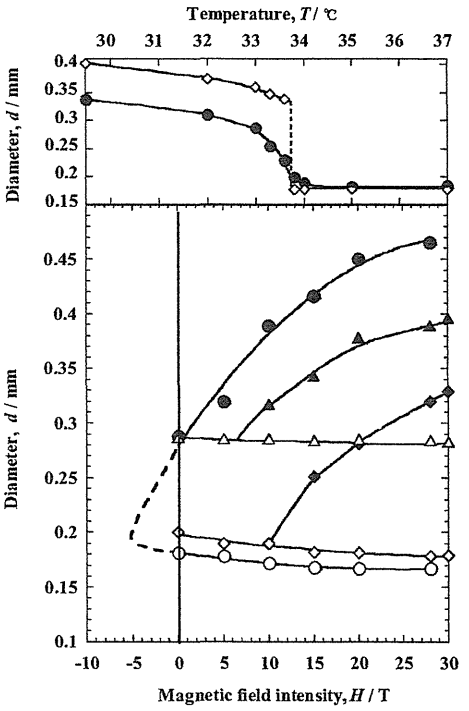

Fig.2 upper: Continuous and discontinuous diameter change of NIPA gel. Magnetic field, H / T: ●, 0; ◇, 30. lower: Magnetic field dependence of gel diameter before and after volume phase transition at 33.8℃. ●, NIPA, q^{pre} =0.0123; ◆, NIPA, q^{pre} =0.0492; ▲, AAm, q^{pre} =0.0123. Closed and open symbols show swelling and shrinking state, respectively.

made gels anisotropoic. The structural anisotropy brought about changes in the iodine diffusion rate in $H_{\perp}$ and $H_{//}$ gels, about 10% faster and 20% slower than that of a zero-field gel, respectively, as shown in Fig. 3. Magnetic fields can control molecular diffusion in gels.

Time course of gel diameter with changing magnetic field intensity is shown in Fig. 4. Gel volume increased with magnetic field intensity, suggesting that polymer chains should be cooperatively oriented by water-assist under magnetic fields. DSC measurement supported this by increase in the heat of volume change under magnetic fields. The magnetic field-induced volume change in NIPA gels was a very fast process, different from the thermal volume change. This process might be affected by hydration change due to magnetic field.

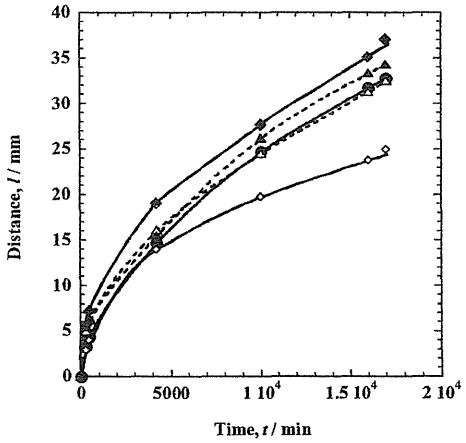

Fig. 3 Time course of diffusion distance of I_2. Magnetic field, H / T: ●, 0; ▲, 5; ◆, 10 . Open and closed symbols are $H_{//}$ and $H_{\perp}$, respectively.

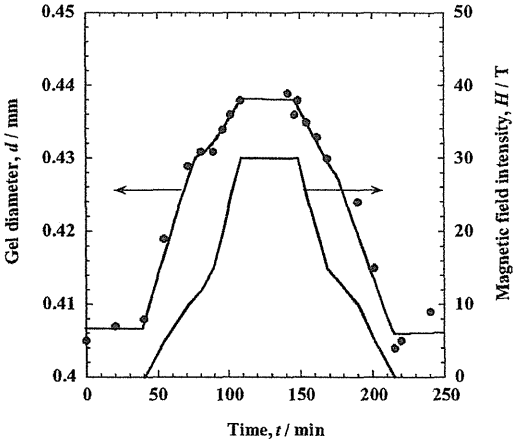

Fig. 4 Change of gel diameter with application of magnetic field.

Acknowledgement

This work was supported by Grant-in-Aid for Scientific Research on Priority Area (Area 767, No. 15085205) from MEXT Japan. The experiment of high magnetic fields up to 30T was performed at Tsukuba Magnet Laboratory

Reference

1) Y. Hirose, T. Amiya, Y. Hirokawa, and T. Tanaka, *Macromolecules*, **1987**, *20*, 1342.

2) H. Kawasaki, S. Sasaki, and H. Maeda, *Langmuir*, **1998**, *14*, 773.

3) I. Otsuka and S. Ozeki, Magnetoscience (Jikikagaku), Industrial Publishing & Consulting Inc., **2002**, 184.

Magnetic Alignment and Patterning of CNTs in Conducting Polymer

Guangzhe Piao[1], Fumiko Kimura[1], Tsunehisa Kimura[1,2] and Kaoru Tsuda[3]
1 Tsukuba Magnet Laboratory, National Institute for Materials Science, 3-13 Sakura, Tsukuba, Ibaraki, 305-0003 Japan
2 Department of Applied Chemistry, Tokyo Metropolitan University, Minamiohsawa, Hachioji, Tokyo192-0397
3 Nano Frontier Co., 3-10-105 Shinagawaku, Oozaki, Tokyo, 141-0032 Japan
(piao.guangzhe@nims.go.jp)

Abstract
In this paper, we demonstrate a simple and general strategy, namely, simultaneous alignment and line patterning of disordered multi-walled carbon nanotubes (CNTs) in conducting polymer/CNT composite films. The CNTs were first dispersed in an aqueous solution containing SDS (sodium dodecyl sulfate). Then, the dispersed CNTs were mixed with a conducting polymer, poly(3,4-ethylenedioxythiophene)-poly(styrene sulfonate) (PEDT-PSS), aqueous solution to form a conducting polymer/CNTs composite solution. The PEDT-PSS/CNT composite solution was dropped onto the surface of a substrate put on the top surface of a field modulator placed in the magnet generating a horizontal field of 10 T. Due to the modulated field, diamagnetic CNTs are trapped to the place where the field strength is weak. At the same time, the CNTs are aligned due to their diamagnetic anisotropy

Keywords
magnetic alignment, conducting polymer, carbon nanotube, pattern, diamagnetic anisotropy

1. Introduction

In recent years, a number of works have been reported on CNTs due to their excellent optoelectric properties and resultant applications to electronic devices such as field effect transistor (FET). There is also an increasing interest in polymer/CNT composites because of their superior mechanical/electromechanical properties [1,2]. For example, addition of only 1% multi-walled CNTs to polystyrene results in a significant increase in the mechanical properties of the polymer because the external load is effectively transferred to the nanotubes [3]. The presence of single-walled CNTs in poly (*m*-phenylene vinylene-co-2, 5-dioctoxy-*p*- phenylene) (PmPV), a conducting polymer, induces the shift of the radiative recombination region in the double-emitting organic light-emitting diodes (OLEDs) without changing the PmPV emission energy [4]. The introduction of multi-walled CNTs to polyaniline, another conducting polymer, enhances the electrical properties because their presence facilitates the process of the charge-transfer between the two components [5]. The polymer composites with carbon nanotubes have potential to the applications in optoelectronic devices such as OLEDs and photovoltaic devices.

However, a simple mixing of CNTs with a polymeric matrix just results in random dispersion of CNTs. If they are aligned, they can exhibit their higher performance due to their intrinsic anisotropic physical properties. Aligned CNTs offer many advantages compared to the random tangles of bundled tubes [6-7] and in developing optoelectronic devices based on the conducting polymer/CNT composite layer, it is necessary to pattern the CNTs within the composite one. A number of approaches on alignment and patterning of CNTs have been reported [8-13]. However, there is little report on simultaneous alignment and patterning of CNTs within the polymer/CNT composite system [14-15]. The need to develop special patterning techniques for the polymer/CNT composite is important, and here the use of modulated magnetic field offers alternatives [16]. The substrate surface is exposed to a microscopically modulated magnetic field that traps diamagnetic particles to the place where the field strength is weak. Due to its diamagnetic anisotropy, CNT is also expected to align at the same time. Combining these two magnetic effects together, it is

possible to obtain patterning of CNTs with alignment within the polymer/CNT matrix. Poly(3,4-ethylenedioxythiophene)-poly(styrene sulfonate) (PEDT-PSS, see Figure 1), a particular conducting polymer with a high application potential[17], is a promising candidate for the formation of such aligning and patterning conducting polymer/CNT composites suitable for improved structural or functional applications.

The present paper describes a novel, facile method for simultaneous orientation and line patterning of CNTs within the conducting polymer/CNT matrix on a glass substrate using a microscopically modulated magnetic field. This method is superior to other methods in that it does not require a pretreatment of the substrate needed for the patterning and alignment.

2. Experimental methods

2.1 Preparation of PEDT-PSS /CNT composite solution

The multi-walled CNT aqueous dispersion assisted by SDS was prepared according to the method reported by Zhang et al [18]. Multi-walled CNTs (from Showa Denko Co., diam.×length: 100 nm×10 μm) were dispersed in SDS aqueous (1wt%) solution followed by homogenization, ultrasonication, and ultra-centrifugation. Then, to the decanted supernatant 200μl, 2.8 wt% concentration PEDT-PSS 2ml was added to prepare PEDT-PSS /CNT composite solution.

2.2 Magnet field modulator and patterning procedure

The field modulator used was similar to that used in the previous work [16]. They are composed of alternating aluminum and iron sheets 300 μm thick, forming a layer structure of periodicity of 600 μm. The PEDT-PSS /CNT composite solution 50 μl was poured into a plastic vessel whose bottom is covered with a cover glass (ϕ22 mm, 120μm thickness). Then, the above vessel was put on the top surface of the modulator placed in the center of a JASTEC cryogen-free superconducting magnet generating a horizontal field of 10 T, allowed the evaporation of the solvent overnight at room temperature.

2.3 Optical system

Observation of alignment and patterning of the PEDT-PSS/CNT was carried out by using a polarized optical microscope (Olympus) connected to a digital camera.

3. Results and dicussion

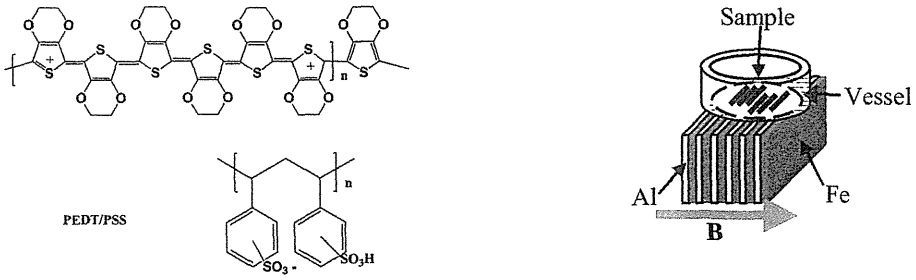

Figure 1 Molecular structure of PEDT-PSS(left) and experimental setup (right)

Figure 1 shows the molecular structure of PEDT-PSS and the experimental setup. A field modulator composed of alternating aluminum and iron layers (300 μm thickness) was placed in a homogeneous horizontal magnetic field (10 T) to generate a field gradient over a glass substrate that was in touch with the modulator. At this experimental setup, the magnetic flux density is lower over the iron layers than the aluminum layers because of the flux is selectively absorbed by the iron

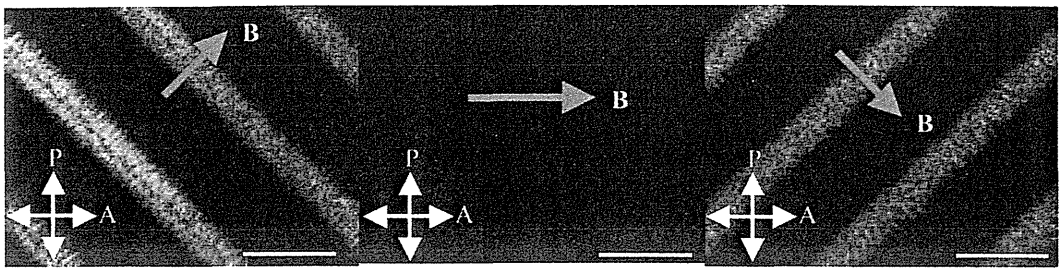

Figure 2 Polarizing optical micrographs of the aligned and patterned CNTs in a PEDT-PSS/CNT composite. Scale bar is 600μm.

layers (ferromagnetic). If the applied external field is higher than that necessary to saturate the magnetic moment induced in the iron layers, the horizontal component of the magnetic flux remains over the modulator surface, enabling the magnetic alignment of particles. The strength of 10 T used in the present study is high enough for this purpose. The field modulation over the modulator surface persists approximately only over the distance of the thickness of the alternating layer (300μm). The thickness (120 μm) of the glass substrate used in the present study is thin enough to meet this requirement. The modulated field produces two effects [16]. One is the micro-Moses effect. A thin liquid layer on a substrate exposed to the modulated field exhibits undulation of its surface. If the liquid is diamagnetic, the tops of the undulation are formed over the iron layers where the field strength is weak, while if the liquid is paramagnetic, they are formed over the aluminum layers. The other effect is the trapping of particles. If particles (magnetic susceptibility of χ_p) suspended in a liquid medium (magnetic susceptibility of χ_m) are exposed to a modulated field B, they receive a force $\Delta\chi V\nabla B^2$, where $\Delta\chi = \chi_p - \chi_m$ and V is the volume of the particle. Depending on the sign of $\Delta\chi$, the particles are trapped at the location with a high field strength ($\Delta\chi > 0$) or a low field strength ($\Delta\chi < 0$). Because the trapping force is proportional to $\Delta\chi V$, the trapping efficiency is low for smaller particles and/or for particles whose magnetic susceptibility is close to that of the surrounding medium. In such cases, the micro-Moses effect could become dominant over the trapping. CNTs were trapped over the iron layers. Figure 2 shows the polarizing optical microscope (POM) observation of the obtained line pattern of the PEDT-PSS/CNT composite. The change in colors under different rotation angles (45 and 135°) clearly demonstrates the orientation of CNTs within the PEDT-PSS/CNT matrix. The observation shows that the magnetic susceptibility $\Delta\chi = \chi_p - \chi_m < 0$, and the trapping mechanism are dominant. In the meantime, they were aligned parallel to a 10 T magnetic field. The result can be explained by the susceptibility anisotropy. They are magnetically symmetric along the tube axis and possess molar susceptibilities parallel ($\chi_{//}$) and perpendicular ($\chi_{\perp}$) to it. Due to a large magnetic anisotropy of CNTs, the magnetic energy is largely reduced when the long axes align parallel to the applied magnetic field.

4. Conclusions

Here we have demonstrated a simple and general strategy, namely, simultaneous alignment and line patterning of disordered multi-walled CNTs in conducting polymer/CNT composite films.

Acknowledgements

This work was partially supported by Grant-in-Aid for Scientific Research on Priority Area "Innovative utilization of strong magnetic fields" (Area 767, no. 15085207) from MEXT of Japan.

References

[1] S. Iijima, Nature 354 (1991) 56.
[2] A. B. Kaiser, G. Dűsberg, and S. Roth, Phys. Rev. B 57 (1998) 1418.
[3] D. Qian, E. C. Dickey, R. Andrews, T. Rantell, Appl .Phys. Lett. 76(2000) 2868.
[4] H. S. Woo, R. Czerw, S. Webster, D. L. Carroll, J. Ballato, A. E. Strevens, D. O'Brien, and W. J.Blau, Appl Phys Lett.77(2000) 1393.
[5] M. Cochet, W. K. Maser, A.M. Benito, M. A. Callejas, M. T. Martinez, J. M. Benoit, J. Schreiber*b* and O. Chauvet, Chem Commun. (2001) 1450.
[6] B.W. Smith, Z. Benes, D. E. Luzzi, J. E. Fischer, D. A. Walters, M. J. Casavant, J. Schmidt, R. E. Smalley, Appl. Phys. Lett. 77 (2000) 663.
[7] P. M. Ajayan, O. Stephan, C. Colliex, D. Trauth, Science 265 (1994) 1212.
[8] W. A. de Heer, W. S. Bacsa, A. Chatelain, T. Gerfin, R. Humphrey-Baker, L. Forro, D. Ugarte, Science 268 (1995) 845.
[9] W. Z. Li, S. S. Xie, L. X. Qian, B. H. Chang, B. S. Zou, W. Y. Zhou, R. A. Zhao, G. Wang, Science 274 (1996) 1701.
[10] T. Kyotani, L. Tsai, A. Tomita, Chem. Mater. 8 (1996) 2109.
[11] G. Che, B. B. Lakshmi, E. R. Fisher, C. R. Martin, Nature 393 (1998) 346.
[12] S. Fan, M. G. Chapline, N. R. Franklin, T. W. Tombler, A. M. Cassell, H. Dai, Science 283 (1999) 512.
[13] M. Fujiwara, E. Oki, M. Hamada, and Y. Tanimoto, I. Mukouda, Y. Shimomura, J. Phys. Chem. A 105 (2001) 4383.
[14] Y. Moritani, H. Awano, T. Takahashi, K. Yonetake, T. Kimura, "8th Symposium on New Magneto-Science2004 Preprints", 2004, p78.
[15] G. Piao, F. Kimura, T. Kimura, K. Tsuda, Polymer preprints, Japan, 45 (2005) 3722.
[16] T.Kimura, M Yamato, A Nara, Langmuir 20 (2004) 572.
[17] H. W. Heuer, R. Wehrmann, S. Kirchmeyer, Adv. Funct. Mater. 12(2002) 89.
[18] X. Zhang, T.Liu, T. V. Sreekumar, S. Kumar, V. C. Moore, R. H. Hauge, R. E. Smalley,Nano Lett. 3(2003) 1285.

Grazing Incidence Small-Angle X-Ray Scattering Studies on Influence of High Magnetic Fields on a Single Nano-cylinder in a Block Copolymer Thin Film

Shinichi Sakurai[1], Yoshhihiro Tsuji[1], Sono Sasaki[2], Hiroshi Okuda[3], Fumiko Kimura[4] , Masafumi Yamato[5] and Tsunehisa Kimura[4,5]

[1]*Department of Polymer Science and Engineering, Kyoto Inst. of Tech. Matsugasaki, Sakyo-ku, Kyoto 606-8585, Japan.*

[2]*JASRI/SPring-8, 1-1-1, Kouto, Mikazuki, Sayo, Hyogo 679-5198, Japan.*

[3]*International Innovation Center, Kyoto Univ. Sakyo-ku, Kyoto 606-8501 Japan*

[4]*Tsukuba Magnet Laboratory, National Institute of Material Science, Tsukuba, Japan.*

[5]*Graduate School of Engineering, Tokyo Metropolitan University, Hachioji, Japan.*

(shin@kit.jp)

Magnetic-field induced orientation of microdomain structures was examined for block copolymers comprising non-crystalline block chains. Especially, influences of high magnetic fields (as high as 30T) on a single nano-cylinder of a polystyrene (PS) microdomain in a thin film were examined by grazing incidence small-angle X-ray scattering (GISAXS). We have found by atomic force microscopy (AFM) that the PS nano-cylinders almost align parallel to the magnetic field applied parallel to the thin film of a polystyrene-*block*-poly(ethylene-*co*-but-1-ene)-*block*-polystyrene triblock copolymer (SEBS), which forms PS nano-cylinders in the PEB matrix. In the present study, we intend to further confirm this fact and more rigorously examine orientation angle of a PS nano-cylinder with respect to the applied magnetic fields by conducting GISAXS on the thin film.

The SEBS sample was spin-cast on Si wafer (the film thickness ~ 20 nm). The thin film was further annealed at 180℃ for 12 h to induce the in-plane orientation of the PS cylinders (Fig. 1) and then the thin film was annealed in the presence of the magnetic field of 30T at 180 ℃ for 3 h. Fig. 2 shows that the PS cylinders were destroyed by the magnetic field applied perpendicular to the cylinder axis (to the thin film). On the contrary, the cylinders almost align parallel to the magnetic field applied parallel to the thin film, as shown in Fig. 3. The corresponding GISAXS results are presented together in these figures. The appearance of the GISAXS peaks (in Figs. 1 & 3 but no peak in Fig. 2 in the regions specified by white circles) indicates existence of oriented cylinders parallel to the incident X-ray beam. In principle, the GISAXS results are consistent with the AFM results. Furthermore, the GISAXS results rigorously indicate that the most PS cylinders in the thin film are almost perfectly aligned parallel to the magnetic field. Especially, the results shown in Fig. 2 suggest that the 30T magnetic field can orient a single PS nano-cylinder (ca. 13 nm diameter) existing in the 20nm-thick film. Thus, although the sample is non-crystalline, such a small size of the single PS cylinder can possess a magnetic torque against the thermal random force.

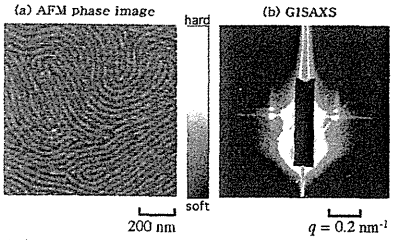

Fig. 1 AFM phase image and corresponding GISAXS result for the thin film before applying magnetic field.

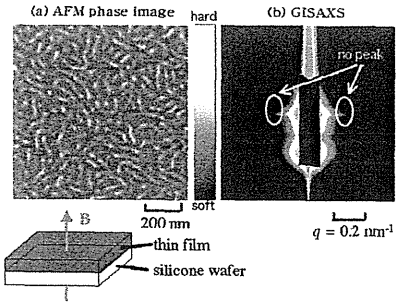

Fig. 2 AFM phase image and corresponding GISAXS result for the thin film annealed at 180℃ for 3 h in the presence of the 30T magnetic field perpendicular to the thin film.

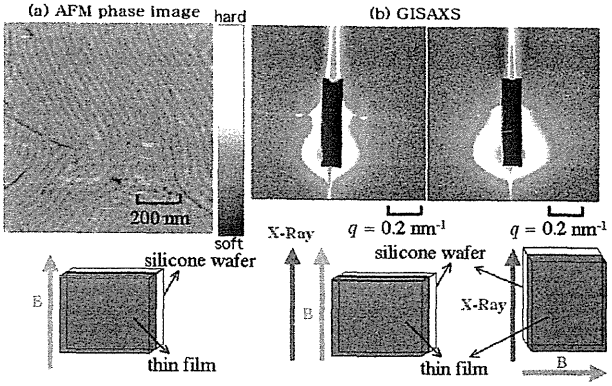

Fig. 3 AFM phase image and corresponding GISAXS result for the thin film annealed at 180℃ for 3 h in the presence of the 30T magnetic field parallel to the thin film.

In situ Observation of Laser-induced Convection of Water in Magnetic Field

Kazutaka Sueda[1], Fumi Koyama[1], Masahiro Irie[2], Akio Katsuki,[3] and Yoshifumi Tanimoto[1]

[1]*Graduate School of Science, Hiroshima University, Higashi-Hiroshima 739-8526, Japan*

[2]*Graduate School of Engineering, Kyushu University, Fukuoka 812-8581, Japan*

[3]*Faculty of Education, Shinshu University, Nagano 380-8544, Japan*

(kazu.42427481.sue@r4.dion.ne.jp)

Abstract

We studied the effects of vertical magnetic field on the laser-induced convection of water by using water-soluble diaryethene (WDAE). When a WDAE solution is irradiated by a 355-nm light from Nd:YAG laser from the bottom of a vessel, WDAE undergoes photo-isomerization to its photoisomer (PI) and the color of the solution changes to blue. At zero field, it is 1.0 mm/min. In the presence of magnetic fields the speeds are 1.2 (11T, -1500 T^2/m), 1.6 (15T, -100 T^2/m), and 2.5 mm/min (11T, +1200 T^2/m), respectively.

Keywords

magnetic field effect, magnetic force, thermal convection, diarylethene

1. Introduction

Gravity due to earth induces convection of liquid solution and, therefore, it is very important to control convection of solution in chemistry and physics. In a previous paper,[1] we reported the control of thermal convection of benzene using a magnetic field. In this paper, we studied the effects of vertical magnetic field on the laser-induced convection of water, as it is the most important solvent in life sciences. Here a photochromic reaction of water-soluble diaryethene (WDAE) is used for visualize thermal convection, since photon energy absorbed by WDAE is used partly to undergo isomerization raction to its isomer (PI) and partly to heat the PI solution.

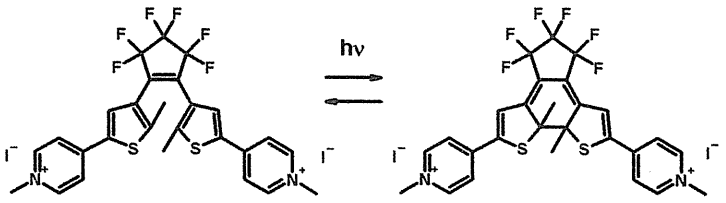

WDAE PI

2. Experimental methods

WDAE was synthesized and H_2O were used as received. The concentration of WDAE in H_2O was about 3.1×10^{-3}M.

In situ observation of photoinduced convection was carried out by using an experimental setup shown in Fig. 1. A quartz cell (1×1×4 cm) containing a WDEA aqueous solution was placed in a bore tube of a superconducting magnet (JASTEC, LH15T40). The solution was irradiated by a 355 nm laser (Spectra Physics, INDI-40-TBH-W) through a 6-mm hole from its bottom. The movement of the blue PI solution was observed by a CCD camera and recorded by a video recorder.

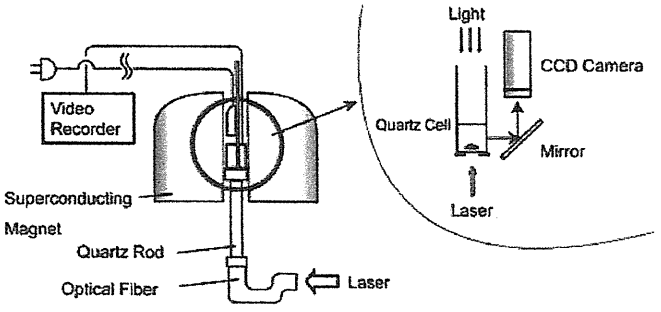

Fig. 1 Experimental setup

The experiments were carried out at three different positions in the bore tube of the magnet, i.e., Upper (11T, -1500 T^2/m), Middle (15T, -100 T^2/m), and Lower (11T, +1200 T^2/m) and outside the magnet, i.e., Outside (0T, $0T^2/m$) at room temperature.

3. Results

Figure 2 shows sequential photos of the laser-irradiated WDAE aqueous solution. After the laser shot, a thin layer of aqueous solution of WDAE at the bottom of the vessel changes its color to blue due to its photoisomer (PI) and the PI solution starts to move upward. The movement of the PI solution in magnetic fields is different from that at zero field. The movement of the frontier of the PI solution was analyzed manually.

Figure 3 shows the movement of the frontier of the PI solution in magnetic fields. From the slope of the plots shown in Fig. 3, the lift speeds of the solution are calculated. At zero field, it is 1.0 mm/min. In the presence of magnetic fields the speeds are 1.2 (11T, -1500 T^2/m), 1.6 (15T, -100 T^2/m), and 2.5 mm/min (11T, +1200 T^2/m), respectively. Photoinduced thermal convection is enhanced by application of +1200 T^2/m by 2.5 times in a magnetic field of +1200 T^2/m.

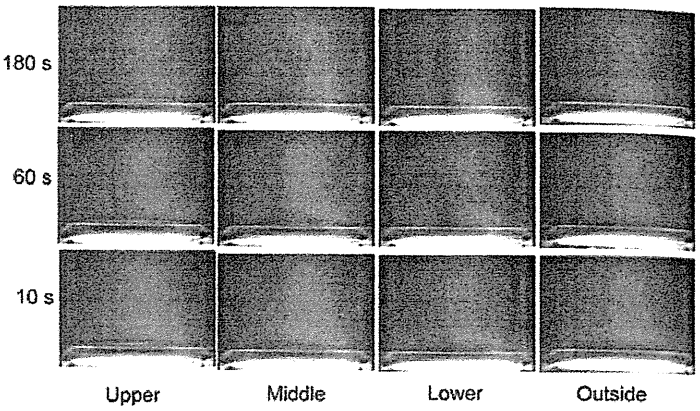

Fig. 2 Sequential photos of the WDAE aqueous solution taken after laser irradiation (Side-view).

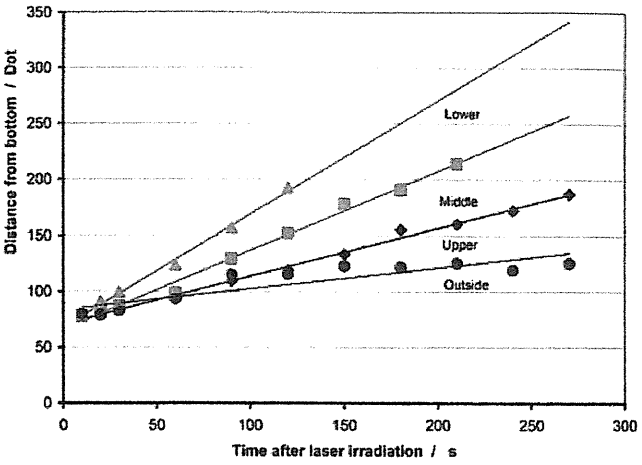

Fig. 3 Movement of the frontier of PI solution after laser irradiation

4. Discussion

The movements of the blue PI solution shown in Fig. 3 can be explained by the force difference, ΔF, of the bulk WDAE solution and the PI solution, calculated using the following equation.

$$\Delta F = (\Delta\rho_{solution})gV + (\Delta\chi_{H2O})(1/\mu_0)VB\partial B/\partial z + (\chi_{PI} - \chi_{WDAE})c(1/\mu_0)VB\partial B/\partial z \quad (1)$$

Where, $\Delta\rho_{solution}$ is the density change of the solution, $\Delta\chi_{H2O}$ is the magnetic susceptibility change of water induced by the temperature jump, V is the volume of the PI solution, g is gravity, μ_0 is the magnetic permeability in vacuum, B is the magnetic flux density, $VB\partial B/\partial z$ is the gradient of B in the vertical z direction, χ_{PI} and χ_{WDAE} are the magnetic susceptibilities of PI and WDAE, and c is the concentration of the solute.
The first term of the right-hand side of eq. 1 is the buoyancy due to earth gravity, the second term is the magnetic force due to the magnetic susceptibility change of water and the last term is the magnetic force due to the magnetic susceptibility change of the solute.

Since $\Delta\rho_{solution} < 0$ and $\Delta\chi_{H2O} > 0$ by thermal expansion of the water, the magnetic field effect on the water convection shown in Fig. 3 can be explained only when $\chi_{PI} < \chi_{WDAE} < 0$. This consideration is consistent with a simple calculation that $(\chi_{PI} - \chi_{WDAE}) < 0$.

Acknowledgements

This work was supported partly by a Grant-in-Aid for Scientific Research on Prioirty Area (Area 767, No.

15085208) from the Ministry of Education, Culture, Sports, Science, and Technology of Japan.

References

[1] W. Duan *et al.*, *Jpn. J. Appl. Phys.*, **43**, 8213 (2004).

DNA Electrophoresis under Strong Magnetic Fields

Kohei Suzuki[1], Kohei Yoshida[1], Shuji Saito[1], Isao Yamamoto[1], Masuhiro Yamaguchi[1] and Tadashi Takamasu[2]
1 Department of Physics, Yokohama National University
Tokiwadai, Hodogaya-ku, Yokohama 240-8501, Japan
2 National Institute for Materials Science
Sengen, Tsukuba, Ibaraki 305-0047, Japan
(d04gd225@ynu.ac.jp)

Abstract

A new magnetic field effect on the electrophoresis is discovered. The electrophoresis of DNA is performed in magnetic fields up to 12T. The velocities of DNAs are decreased with increasing magnetic field. The magnetic field effect also depends on the shapes and lengths of DNAs. Electrophoresis under magnetic field can be used for a new separation method of DNAs.

Keywords

magnetic field effect, magnetic orientation, DNA, electrophoresis

1. Introduction

DNAs carry genetic informations and it is essential for the biological studies to analyze the structures and the sequences of bases of DNAs. Phosphates, component parts of DNA, are charged negatively, so DNAs move from a cathode to an anode by an electric field. For such an electrophoresis, a gel is used as the support media. The mobility of DNA in gel depends on their molecular weight and shape because the gel behaves as a molecular sieve. Therefore, the gel electrophoresis is often used for the separation method of various DNAs.

On the other hand, it has been reported that DNAs are oriented perpendicularly to the magnetic field as a result of the anisotropy of diamagnetic susceptibility.[1] In the present study, the electrophoresis of DNA is performed in magnetic fields up to 12T, then the magnetic field effect on the electrophoretic velocity of DNAs are observed. In previous experiments, the velocities of double stranded DNAs were decreased with increasing magnetic field.[2] The structure dependence of the magnetic field effect is examined in this experiment. Possibilities of a new separation method of DNAs are investigated utilizing the magnetic field effect.

2. Experimental methods

First, we made two small electrophoresis systems (w70xd96xh34mm^3) to place in the water jacket set on the superconducting magnet. The surface of buffer used in the present experiment is affected by strong magnetic fields due to its diamagnetic property. The cover was attached to the top of the electrophoresis system to prevent the change of the buffer surface and current. Platinum wires were used for the electrodes at both ends.

Two types of DNA were prepared for electrophoresis. "M13 mp18 single stranded DNA" supplied from TAKARA Bio Corporation is single stranded DNA with cyclic shape (7249bp round). "Molecular Ruler 2.5kb" supplied from Bio-Rad Laboratories included various sizes of double stranded DNA with linear shape. We

observed only the 5kbp-long DNA among them. It was verified experimentally that this cyclic DNA and 5kbp linear DNA have the same velocities in zero magnetic fields.

Agarose gels (2.0wt.%) were prepared as the support media for the electrophoresis. The plate-like gel (w40xd40xh7mm^3) formed in zero fields was put in the electrophoresis system. Cyclic DNA of 1 μ l, linear DNA of 1.5 μ l, and the mixed DNA of them were injected into different three wells of the gel. Then, the two system filled with TAE buffer were prepared in this way.

These two systems were placed at the center of the magnetic field and 750mm distance from the center (Fig. 1.) Where, the magnetic field below 0.2T at 750mm distance from the center was weak enough, so that no magnetic field effect occurs for DNAs there. Hence, the electrophoresis at this position was regarded as the control experiment. The temperature of the sample space was kept at 5℃ by circulating water of the thermostatic bath. Then the same voltage of 50V was applied parallel to the direction of the magnetic field to the systems for three hours.

After the electrophoresis, the gels were dyed by ethidium bromide solution and DNA bands were observed by irradiating UV rays. The velocities of DNAs were calculated by measuring patterns of DNA bands.

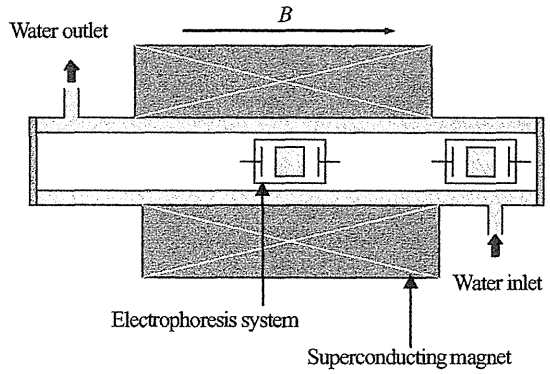

Fig. 1. Electrophoresis system of DNA under magnetic field (Top-view).

3. Results and Discussion

Fig. 2. shows magnetic field dependence of fractional change in electrophoretic velocity of DNA. The fractional change in velocity is defined by $(v\text{-}v_0)/v_0$, where v is the velocity in the magnetic fields and v_0 is that in the zero fields. The velocity of the double stranded DNA with linear shape was decreased down to –25% with increasing magnetic fields and the decrease was saturated at 4T. If DNA is oriented perpendicularly to the magnetic field or the electrophoretic direction, then the velocity of DNA must be decreased due to the increase of the cross-section to the sieve of the gel. These results suggest (1) the electrophoretic velocity was decreased because of the orientation of DNA and (2) the orientation of linear DNA was saturated at 4T. On the other hand, the velocity of the single stranded DNA with cyclic shape was not decreased below 8T. The single stranded DNA tends to form complicated shape by intramolecular bonding. Consequently, the magnetic anisotropy of the single stranded DNA is considered to become weak in comparison with that of the double stranded DNA. Thus, it is considered that the double stranded DNA with linear shape is easier to orient than the single stranded DNA with cyclic shape.

The mixed DNA cannot be separated with usual electrophoresis because of the same velocity. According to the above results, the velocity of linear DNA is less than that of cyclic DNA under the influence of the magnetic field. The separation was expected to become possible with the electrophoresis under the magnetic field

because the difference in the velocity enhances under the magnetic field between 4T and 8T in particular. The electrophoresis was examined for the linear, cyclic and mixed DNA under the influence of magnetic field of 6T.

Fig. 3(a) shows the electrophoretic patterns of DNAs after the electrophoresis in the absent of magnetic field. The 5kbp linear DNA moved at the same velocity as cyclic DNA in the zero fields. As a result, mixed DNA was not separated. On the other hand, the velocities of DNAs were decreased as a whole in the magnetic field of 6T as shown in Fig. 3(b). Moreover, the change in velocity of the linear DNA was larger than that of cyclic DNA. Then the mixed DNA was separated successfully into two bands as our expectation.

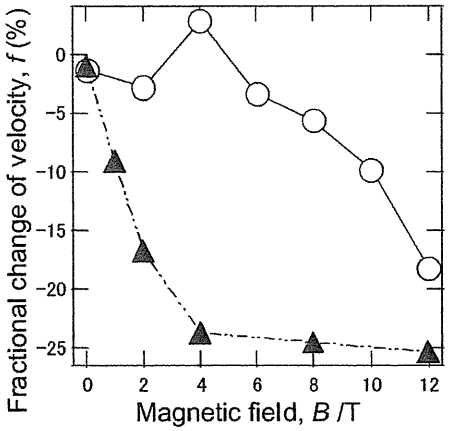

Fig. 2. Magnetic field dependence of change in electrophoretic velocity under magnetic fields.
The circles and triangles denote cyclic and linear DNA, respectively.

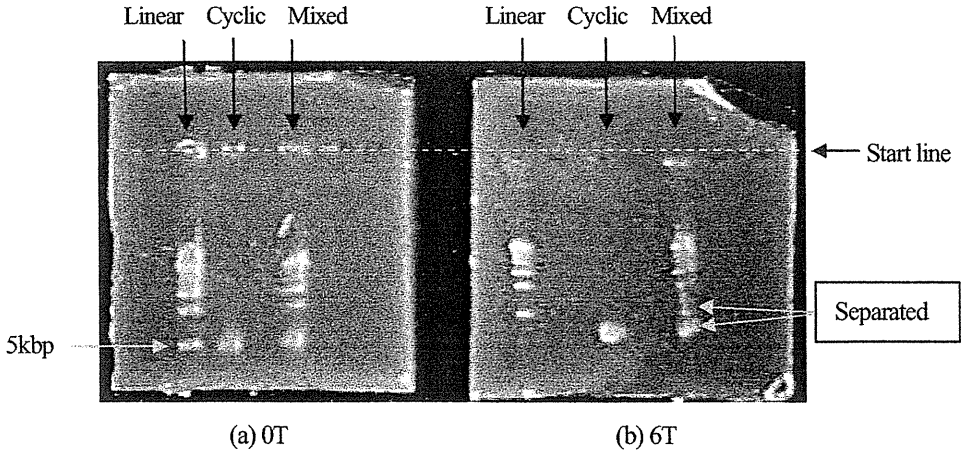

Fig. 3. Electrophoretic patterns of DNAs (Cyclic, Linear and Mixed).
Broken line denotes the start position of DNAs.
E=50V, t=3h, T_0=5℃.

4. Conclusion

The electrophoresis of DNA was performed under strong magnetic fields. The electrophoretic velocities of DNAs decreased under magnetic field. The structure dependence of magnetic field effect was discovered and expected to be applied to the separation method of DNAs. The separation of double stranded DNA and single stranded DNA was accomplished. These results demonstrated that the electrophoresis under magnetic field can be used for a new separation method of DNAs.

Acknowledgements

This work was supported by Grant-in-Aid for Scientific Research on Priority Area (Area 767, No. 15085204) from MEXT of Japan.

References

[1] N. Morii, H. Suzuki, Y. Kido, S. Nimori and N. Morii: Summary of 7th symposium on new magneto-science (2003)1.
[2] K. Suzuki, K. Yoshida, S. Saito, I. Yamamoto, M. Yamaguchi: Abstract of this symposium (3P31).
[3] T. Fushimi: "Electrophoresis of DNA under the influence of high magnetic fields", Master's thesis, Yokohama National University (2004).

Magnetic Alignment of Magnetic Silicate Crystals Achieved at Low Field Intensities below 1 mT in Star Formation Regions Caused by Paramagnetic Impurity Ions

Ryoichi Takashima, Takaaki Abe and Chiaki Uyeda
Department of Earth and Space Science, Graduate School of Science, Osaka University
1-1 Machikaneyama, Toyonaka, Osaka 560-0043, Japan
(ryoichi@ess.sci.osaka-u.ac.jp)

Abstract
Magnetic alignment of micro-sized particles was achieved at low fields below B = 1 mT for major rock forming minerals such as forsterite, enstatite, and biotite; the crystals contain paramagnetic ions. The alignment was detected in low temperature condition of T = 90 K using He gas as a dispersing medium. Field intensity to achieve alignment was reduced at low temperatures considerably due to the decrease of thermal agitation energy that randomizes directions of crystal axes; the increase of paramagnetic anisotropy deriving from the impurity ions was the cause of the reduction of the field intensity as well. The results serve as a basis to solve the origin of alignment of dust particles which is commonly observed in star formation regions.

Keywords
magnetic alignment, forsterite, enstatite, magnetic anisotropy

1. Introduction

Magnetically stable-axes of micron-sized non-ferromagnetic crystals dispersed in a fluid medium are known to align parallel to magnetic field at infinite intensity [1,2]. The magnetic alignment proceeds by field induced anisotropy energy $N\Delta\chi B^2/2$ originated from the anisotropy of magnetic susceptibility $\Delta\chi$ of material at magnetic field intensity B. The anisotropy of magnetic susceptibility of a crystal is defined as $\Delta\chi = \chi_{\parallel} - \chi_{\perp}$ where $\chi_{\parallel}$ and $\chi_{\perp}$ are the susceptibility per unit mass parallel and perpendicular to the stable axis, respectively. The weight of a particle is denoted as N. The alignment is achieved when the magnetic energy is comparable to the energy of Brownian motion $k_B T/2$ at temperature T; the motion randomizes directions of a magnetic stable axes. The $\Delta\chi$ value of a non-ferromagnetic material is the sum of intrinsic diamagnetic anisotropy $(\Delta\chi)_{DIA}$ and paramagnetic anisotropy $(\Delta\chi)_{PARA}$ originating from paramagnetic impurity ions [3]. The effective magnetic anisotropy $\Delta\chi$ of a non-ferromagnetic material is hence expressed as $\Delta\chi = (\Delta\chi)_{DIA} + (\Delta\chi)_{PARA}$. The amount of $(\Delta\chi)_{PARA}$ is known to be proportional to the reciprocal of T in accordance with Curie law.

The application of magnetic alignment due to paramagnetic anisotropy in terrestrial and cosmic conditions has been discussed previously [4,5]. One of the applications is concerned with the alignment of cosmic dust particles. The circumstellar field in a star formation region that may cause dust alignment is one of the essential factors to understand stellar and planetary formation. Magnetic alignment of major rock forming minerals, namely forsterite, enstatite, kaolinite, muscovite, talc and biotite are reported in the present work [6,7]. These samples have paramagnetic Fe impurity ions. Forsterite and enstatite are considered to be the major components of circumstellar disks [8]. The origin of dust alignment, which is observed in star formation regions, can be discussed on the basis of the measured results.

2. Experiment

2.1 Definition of the field of magnetic alignment B_s

Quantitative analysis on the magnetic alignment process is not popularly done at present. The alignment is achieved only at infinite field intensity. The field of magnetic alignment B_s was therefore introduced tentatively, which was used as an indicator to compare the field intensity causing the alignment [6].

Relationship between degree of the magnetic alignment and field intensity, observed for micron-sized particles, was analyzed successfully by the theory first proposed by Langevin and Curie [9]. Degree of alignment is generally defined by an order parameter, which is a Boltzmann average of a function described as

$$\langle m \rangle = \langle (3\cos^2\theta - 1)/2 \rangle. \quad (1)$$

An angle between a magnetically stable axis and a field direction is denoted as θ. Completely random state and completely ordered state of the crystals correspond to $\langle m \rangle = 0$ and 1, respectively. A Boltzmann average is calculated by using the free energy U of a particle, $U = -(NB^2/2)\{\chi_\perp + \Delta\chi\cos^2\theta\}$.

The field intensity, where $\langle m \rangle$ amounts to $\langle m \rangle = 0.78$ in eq. (1), is defined as the field of magnetic alignment B_s as shown in fig. 2 (a),

$$B_s = (15k_BT / N\Delta\chi)^{1/2}. \quad (2)$$

It is seen explicitly that the value of B_s depends on N, $\Delta\chi$ and T; accordingly alignments of micron-sized particles are expected to occur below B = 1 T at room temperature for various diamagnetic materials, since published values of $\Delta\chi$ usually exceed 10^{-9} emu/g [10]. However; the study of the magnetic alignment due to magnetic anisotropy $\Delta\chi$ is not popularly done at present. Hence the limited number of materials is recognizedto align by magnetic field.

2.2 Apparatus to measure the alignment of particles dispersed in gas medium

The measurement of the magnetic alignment was allowed only above T = 160 K previously, when liquid was used as a dispersing medium [6]. A new method was developed to measure the value of B_s at low temperatures [11]. The alignment was performed for micron-sized crystals dispersed in cold He gas. He gas is a unique medium that can disperse micron-sized particles and remains as fluid below T = 160 K. Temperature dependence of the magnetic alignment process was examined in the range of T = 340 K and T = 90 K.

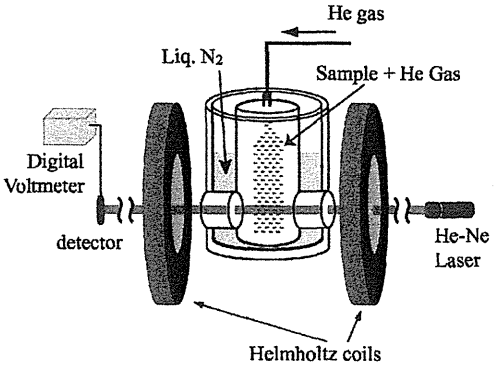

Fig. 1. A schematic view of apparatus developed to observe magnetic alignment below T = 100 K.

3. Results

3.1 Effects of concentration of paramagnetic ions

Magnetic alignment was achieved at low field intensities when concentrations of paramagnetic ions were high (see Fig.2 (b), (c), (d)) [7]. The B_s value observed for biotite micro-crystals having paramagnetic susceptibility of $\chi_{PARA} = 4.4\times10^{-5}$ emu/g was B_s = 0.021 T. B_s was 0.060 T for

muscovite micro-crystals with $\chi_{PARA} = 4.8\times10^{-6}$ emu/g. The alignment has not been reported at such low field intensities for non-ferromagnetic oxide particles. B_s of synthetic phlogopite free of paramagnetic ions was measured to be $B_s = 3.6$ T in previous studies [7]. The crystal structures of biotite and phlogopite are nearly equivalent, and are considered to posses similar $(\Delta\chi)_{DIA}$ values. The small B_s value of biotite is hence attributed to $(\Delta\chi)_{PARA}$. Indeed the measured B_s value of biotite was consistent with the calculated B_s value based on $\Delta\chi$ obtained from bulk crystal measurement; the observed $\Delta\chi$-T relationships on bulk crystals showed explicitly that $(\Delta\chi)_{PARA}$ was considerably large compared to $(\Delta\chi)_{DIA}$. The paramagnetic origin of alignment was examined simultaneously for grains of muscovite, kaolinite and talc as well [3,12]. $\Delta\chi$ values generally showed Curie temperature dependences for most of the measured oxides such as for talc, brucite [13], orthoclase, petalite, scapolite [14] and kaolinite [15]. Hence the effect of $(\Delta\chi)_{PARA}$ in reducing B_s as observed is likely to occur for inorganic oxides in general.

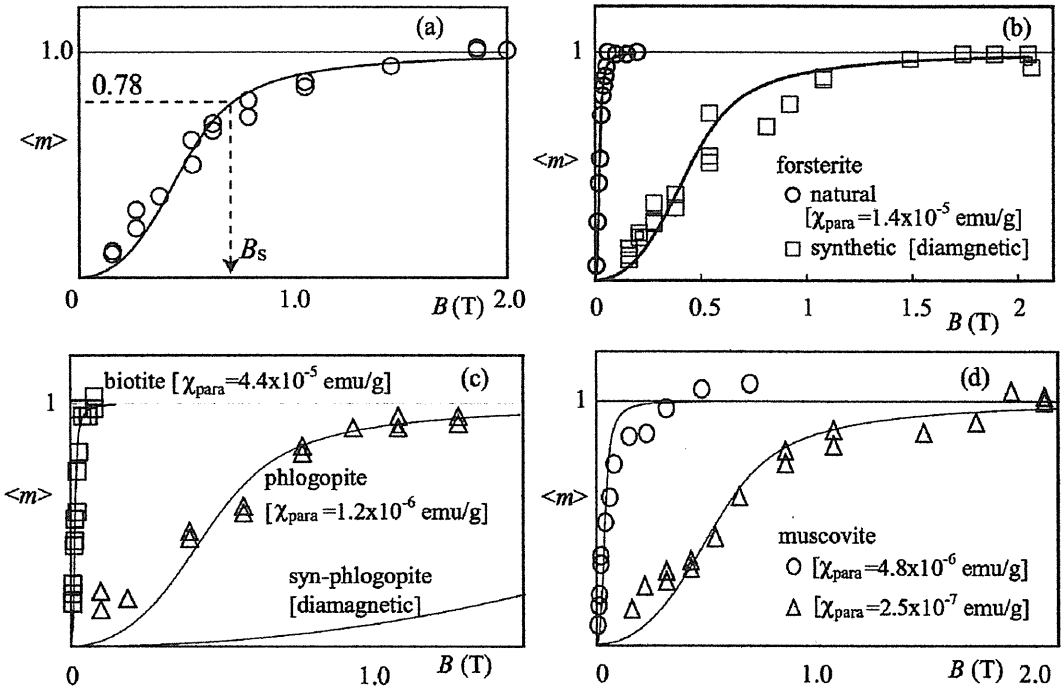

Fig. 2 (a) The process of magnetic alignment. The field intensity at $\langle m\rangle$=0.78 is denoted as B_s. (b), (c), (d) The magnetic alignment measured for forsterite, biotite, phlogopite and muscovite.

3.2 Effect of Reduction of Temperature

The obtained B_s-T' relationship for grains dispersed in He gas is shown in Fig. 3. The measured data of enstatite and forsterite are shown in red-opened square and green-opened circle respectively. The solid line of B_s is calculated from eq. (2) using the $\Delta\chi$ values measured for bulk single crystals of each mineral. The remarkably small B_s values of enstatite and forsterite in the low temperature region derive from the large $(\Delta\chi)_{PARA}$ caused by the paramagnetic ions. B_s was proportional to T for forsterite and enstatite according to Fig.3. This is because the energy of Brownian motion $k_BT/2$ that randomizes the particles decreases with the temperature, and also because the amount of $(\Delta\chi)_{PARA}$ is known to be proportional to the reciprocal of T following the Curie law. This relationship is observed for micro-crystals of kaolinite [15] and talc [3] as well; these materials contained paramagnetic ions. The effect may be expected for other inorganic materials. The $\Delta\chi$-T' relationships shown in the Fig. 3 indicate that B_s becomes smaller than 1 mT below $T' = 10$ K for these materials; partial alignment by terrestrial field may be detected at this condition.

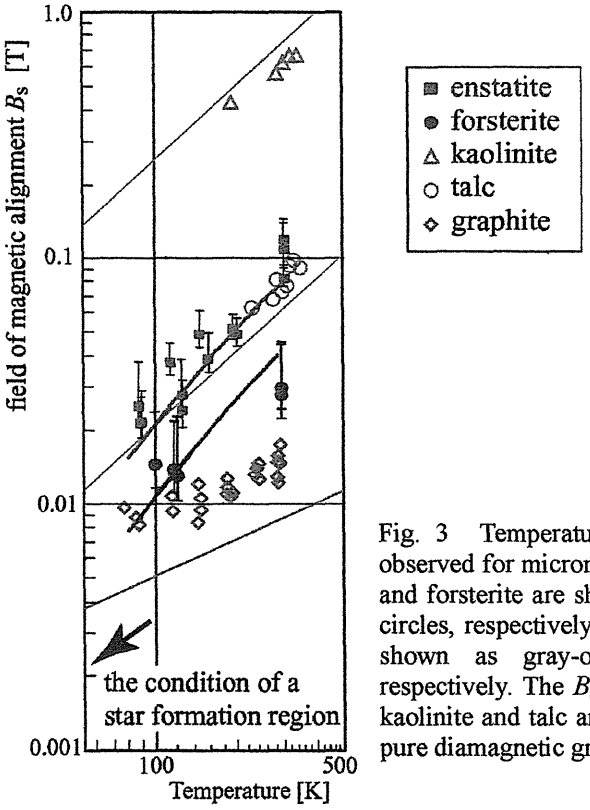

Fig. 3 Temperature dependence of the magnetic alignment observed for micron-sized grains. The measured data of enstatite and forsterite are shown as red-closed squares and green-closed circles, respectively. The data of kaolinite, talc and graphite are shown as gray-opened triangles, circles and diamonds, respectively. The B_s values of paramagnetic enstatite, forsterite, kaolinite and talc are proportional to T whereas the B_s values of pure diamagnetic graphite are proportional to $T^{1/2}$.

4. Discussion

This study can be applied to the discussion of the structure of the circumstellar field in star formation regions as mentioned above. Observation of starlight polarization caused by aligned dust particles is one of the standard techniques to determine interstellar magnetic field (see Fig. 4). Information on cosmic field is a base to understand stellar and planetary evolution. For example, recombination of magnetic field, assumed in the planetary formation region, is considered to be the heat source of producing planetary materials; however the alignment mechanism of dust particles is less well understood.

It is necessary to know the approximate values of N, $\Delta\chi$, and T of eq.(2), in the region in order to discuss the possibility of the dust alignment. The temperature is considered to range between $T = 10$ and 100 K. The enstatite grains are assumed to have a size of 3 μm ($N \sim 5\times10^{-11}$ g). The $\Delta\chi$ value is 2×10^{-5} emu/g at $T = 50$ K according to $\Delta\chi$-T measurements of bulk crystals. Accordingly, the B_s value is 9×10^{-4} T. The actual field intensity has not been determined yet; however, the circumstellar magnetic field of about $B = 0.3\sim3\times10^{-4}$ T was proposed. Therefore, it is possible that partial alignment of silicate grains may cause polarization in star formation regions.

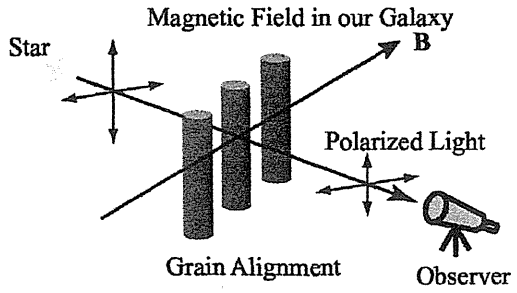

Fig. 4 The mechanism of polarization caused by the elongated grains.

5. Conclusion

1. Field intensity where an order parameter $\langle m \rangle = \langle (3\cos^2\theta - 1)/2 \rangle$ reaches $\langle m \rangle = 0.78$ is defined as the field of magnetic alignment B_s; θ is the angle between the stable axis of the solid body and the field. B_s is calculated as $B_s = (15k_BT/N\Delta\chi)^{1/2}$. It is important to define a indicator such as B_s in order to clarity the origin of magnetic alignment quantitatively.
2. B_s was proportional to $T^{1/2}$ for diamagnetic crystals free of paramagnetic ions, while B_s was proportional to T for particles including paramagnetic ions since $\Delta\chi$ was proportional to T following the Curie law; the effect is expected to occur for many of the non-ferromagnetic materials since their $\Delta\chi$-T relationship on bulk crystals followed the Curie law. The particles are dispersed in the He gas medium in order to realize alignment at low temperatures.
3. The doping of paramagnetic ions is effective in reducing B_s, since the paramagnetic anisotropy increases the effective $\Delta\chi$ value considerably. The alignment has not been reported at such low fields for non-ferromagnetic oxide particles previously. Practical efficiency of magnetic alignment can be enhanced considerably in the course of material processing.
4. Silicate grains have a possibility to align partially in star formation regions, according to the estimate using the measured results. The data of the magnetic alignment measured at low temperatures comparable to that of the condition of a star formation region would be a basis to discuss the magnetic structure of this region, which is considered to control the stellar and planetary evolution.

References

[1] G.Maret and K.Dansfeld:Topics in App. Phys. (1985) 57 144.
[2] Proc.Intern Symp.New Magneto-Sci., (Jpn. Sci. & Tec. Corp., NIMS, 1999).
[3] Uyeda C, Tanaka K, Takashima R, Sakakibara M (2004) Jpn J Appl Phys 43:980-984
[4] Uyeda C, Takeuchi T, Yamagishi A, Yamanaka T, Tsuchiyama A, Date M (1993) Phys Chem Minerals 20:369-374
[5] Chihara H, Uyeda C, Tsuchiyama A, Yamanaka T (1998) Publ Astron Soc Jpn 50:149-154
[6] Uyeda C, Takeuchi T, Yamagishi A, Date M (1991) J Phys Soc Jpn 60:3234-3237
[7] Uyeda C, Takashima R, Hiraoka K (2005) Jpn J Appl Phys 44:L371-L374
[8] e.g. Molster FJ and Waters LBFM (2002) Henning Th ed., Astromineralogy, Springer, 121-170
[9] Langevin P, Curie P (1910) CP Acad Sci Paris 151:331-368
[10] Uyeda C, Tanaka K, Takashima R (2005a) Appl Phys Lett 86: 094103
[11] Uyeda C, Komatsu T, Sakakibara A, Tanaka K (2003) Astron Astrophys 400:805-810
[12] C. Uyeda, K. Tanaka, R. Takashima and M. Sakakibara: Mater. Trans. (2004) 44 2594-2598
[13] Uyeda C, Ohtawa K, Okita K (2000) Jpn J Appl Phys 39:L514-L517
[14] Uyeda C, Ohtawa K, Okita K (2000) J Phys Soc Jpn 69:1019-1022
[15] Uyeda C, Sakakibara M, Tanaka K (2003) Phys Chem Minerals 30:425-429

Magnetic Levitation of Plastic Chips – Applications for Magnetic Susceptibility Measurements and Magnetic Separation

Yoshifumi Tanimoto, Masao Fujiwara, and Manabu Sueda

Graduate School of Science, Hiroshima University, Higashi-Hiroshima 749-8526, Japan

(tanimoto@sci.hiroshima-u.ac.jp)

In this paper, we report straightforward applications of magnetic levitation to diamagnetic susceptibility measurement and magnetic separation of diamagnetic plastic chips.[1)]

A diamagnetic particle can be levitated magnetically when a magnetic force is applied to it in the opposite direction to gravity with equal intensity:

$$(m\chi/\mu_0)B(z)\mathrm{d}B(z)/\mathrm{d}z = mg. \quad (1)$$

Here, χ is the magnetic susceptibility per unit mass of a particle, μ_0 is the magnetic permeability of vacuum, $B(z)$ is the magnetic flux density at z in the vertical position, $\mathrm{d}B(z)/\mathrm{d}z$ is the density gradient, m is the particle mass, and g is the gravitational acceleration. Levitated positions of different chips in the tube are different, when their magnetic susceptibilities are different. So, diamagnetic susceptibilities of plastic chips were calculated from their levitated positions, z, in the tube.

Magnetic levitation of diamagnetic plastic chips was carried out by using a compact superconducting magnet, producing a horizontal magnetic force of 1500 T^2m^{-1}. Table 1 shows the results of magnetic levitation of plastic chips. They were in agreement with those obtained by SQUID, indicating that one can determine magnetic susceptibility of plastic chips from levitated position, z.

Next, magnetic separation of plastic chips was examined. In the bore tube, a home-made separator is installed by which levitated and non-levitated chips are removed and collected separately. When polypropylene and poly(ethylene terephthalate) chips are randomly introduced to the separator one by one, they are separated into two groups.

In conclusion, it is shown that magnetic levitation is a convenient and useful technique for both diamagnetic susceptibility measurement and magnetic separation of diamagnetic substances.

Table 1 Magnetic levitation and magnetic susceptibility of plastic chips

Name	z[a)] / mm	$B(z)\mathrm{d}B(z)/\mathrm{d}z$ / T^2m^{-1}	χ(Levitation)[b)] / 10^{-9} m^3kg^{-1}	χ(SQUID)[c)] / 10^{-9} m^3kg^{-1}
Polypropylene	367.5	-1070	-11.51	-9.63
Polyethylene	367.0	-1081	-11.34	-8.87
Polystyrene	361	-1270	-9.70	-7.85
Polyamide	357.5	-1358	-9.07	-7.78
Polycarbonate	351	-1481	-8.29	-7.08
Poly(methyl methacrylate)	348.5	---	---	---
Poly(ethylene terephthalate)[d)]	---	---	----	-6.28

[a)] Distance from the magnet bottom. [b)] Diamagnetic susceptibility obtained from magnetic levitation. [c)] Diamagnetic susceptibility obtained from SQUID. [d)] Not levitated.

References:

1) Y. Tanimoto *et al.*, *Jpn. J. Appl. Phys.*, **44**, 0000 (2005).

Structural Control of Mesoporous Silicas by Magnetic Fields

Yasuyuki Yamane and Sumio Ozeki
Department of Chemistry, Faculty of Science, Shinshu Univesity,
3-1-1 Asahi, Matsumoto, Nagano 390-8621, Japan
sozeki@dione.shinshu-u.ac.jp

Abstract

Mesoporous silica films were prepared a by dip coating method using Pluronic P123 ($EO_{20}PO_{70}EO_{20}$) and hexadecyltrimethylammonium bromide (CTAB) as templates under steady magnetic fields. Synthesized mesoporous silicas were characterized by X-ray diffraction, scanning electron microscopy, transmission electron microscopy. Hexagonal packed silicate/P123 (or CTAB) hybrids were oriented with long axes parallel to the direction of applied magnetic fields because of negative diamagnetic anisotropy of template molecules. We have synthesized successfully SBA-15 and MCM-41 films with very long straight and lying pores and standing pores against the substrate when parallel and perpendicular magnetic fields, respectively.

Keywords
magnetic orientation, mesoporous silica, SBA-15, MCM-41,

1. Introduction

Steady magnetic field was applied to surfactant/silicate hybrids having hexagonal structure in order to prepare the highly ordered structural mesoporous silicas, which were prepared by calcination of amphiphiles in the hybrids. This method made it possible to align a silica skeleton through magnetic orientation of CTAB and Pluronic P123 molecules as templates. The mesoporous silicas having a honeycomb structure have homogeneous mesopores with a narrow size distribution. Therefore, mesoporous silicas as a potential material have been paid attention from the viewpoint of both fundamentals and application. In this study, application of magnetic fields to film formation of mesoporous silica is reported. Oriented domain of honeycomb structure of mesoporous silicas prepared under magnetic fields was much larger than that of conventionally synthesized mesoporous silicas.

2. Experimental Section

2.1 Materials

Silica films were synthesized by a dip coating method using a blockcopolymer of poly ethylene oxide and poly propylene oxide ($EO_{20}PO_{70}EO_{20}$, Pluronic P123) and hexadecyltrimethylammonium bromide (CTAB) as templates under steady magnetic fields. The precursor was prepared from P123, ethanol (EtOH) and silicate solution which was a supplied by mixture of tetraethyl orthosilicate (TEOS), EtOH, water, and hydrochloric acid. The molar ratio of the precursor solutions for SBA-15 and MCM-41 films was TEOS : P123 : H_2O : HCl : EtOH = 1 : 0.014 : 15 : 0.16 : 39 and TEOS : CTAB : H_2O : HCl : EtOH = 1 : 0.1 : 5 : 0.04 : 3.8, respectively. The solutions were stirred for about 30 min at 308 K and employed to coat a film on a pyrex glass as substrate under steady magnetic fields ($H \leq 6$ T). Magnetic fields were applied in parallel and perpendicular to the film (substrate) surface for 4h at 308 K. The films were calcined in air by increasing slowly temperature from room temperature to 773 K and kept the temprature for 6h.

2.2 Characterization.

X-ray diffraction (XRD) experiments were conducted on a Rigaku MultiFlex diffractometer

3.2 X-ray diffraction

XRD patterns of SBA-15 and MCM-41 films are shown in Figure 2. Three diffraction peaks observed in as-synthesized sample, which have a *d* spacing ratio of 1: 1/2: 1/3, could be indexed as the (100), (200) and (300) reflections of a two-dimensional hexagonal structure (Figure 2A). The (110) reflections of hexagonal structure disappeared by formation of the pore channels parallel to the substrate surface. The intensity of (100) peak of $H_{\parallel}$ and $H_{\perp}$ films were higher than that of zero field film. This suggests increasing crystallinity and uniformity.

In order to examine the angle dependence of diffraction intensity, the films were rotated horizontally at various angles (-90°to 90°) and X-ray was irradiated at different angles. If pores stand on the substrate or are not oriented, the diffraction intensity must not depend on the angle. The $H_{//}$ film depended on the angle, but the film prepared under zero fields and $H_{\perp}$ film didn't. These results indicate that the pores of the $H_{\perp}$ film are ordered in perpendicular to the film surface and $H_{\parallel}$ film are lying in parallel to it. Furthermore, when the film prepared under perpendicular magnetic fields was rotated at 45°, the (110) reflection was observed, as shown in Figure 2B. These results are agreed with the electron microscopic images.

In the case of MCM-41 films, three diffraction peaks observed could be indexed as the (100), (110) and (200) reflections of a two-dimensional hexagonal structure (Figure 2C). This suggests that the pores stand in part on the substrate. Also, is considered that the pores of MCM-41 are shorter than pores of SBA-15.

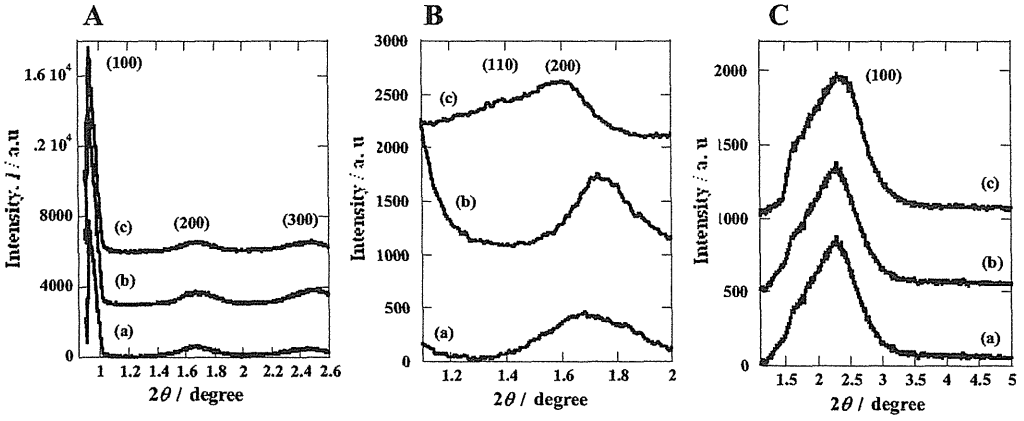

Figure. 2. XRD patterns

A and B: XRD patterns of as-synthesized SBA-15 films prepared under zero fields (a), parallel (b) and perpendicular (c) by 6T to film surface. Film was not rotated when X-ray was irradiated to films. B: Film was rotated at 45°.

C: XRD patterns of as-synthesized MCM-41 films prepared under zero fields (a), parallel (b) and perpendicular (c) by 6T to film surface.

4. Conclusion

We successfully accomplished the synthesis of SBA-15 and MCM-41 films with very long straight, standing nanopores. The nanopores oriented with their long axes parallel to the applied magnetic fields due to negative diamagnetic anisotropy of templates. Therefore, the structures of mesoporous silica films can be controlled bystanding magnetic fields.

Acknowledgments

This work was supported by Grant-in-Aid for Scientific Research on Priority Area "Innovative utilization of strong magnetic fields" (Area 767, No.15085205) from MEXT of Japan.

(BD2548N) using CuKα radiation operated at 40 kV and 20 mA. The samples were scanned from 0.9° to 5° (2θ) with a step of 0.02° and counting time of 0.25 s. Sample morphology and microstructure were examined by a JEOL scanning electron microscope JSM-6000F; SEM) and a JEOL transmission electron microscope JEM-3500EX; TEM with acceleration voltage of 300 kV.

3. Results and Discussion

3.1 Electron microscopy

SEM images of SBA-15 reveal that the film prepared under zero field was worm-like having about 300 nm in outer diameter, as shown Figure 1A (a). However, when the hybrid was prepared at same conditions under magnetic fields applied parallel to film surface ($H_{\parallel}$ film), the morphology changed to be rod-like, (straight cylinder), as shown in Figure 1A (b). On the other hand, films prepared under magnetic fields perpendicular to film surface ($H_{\perp}$ film) showed vague short worm–like cylinder (Figure 1A c). The cylinder in a hybrid domain under zero and parallel magnetic fields were laid on the substrate. On the contrary, the cylinders seem standing in the film, when magnetic fields were applied in parallel to the film substrate.

TEM image of SBA-15 films prepared under zero, parallel, and perpendicular magnetic fields are shown in Figure 1B. Hexagonally arranged mesopores were observed in all cases. The curved pores having 5-6 nm diameter were observed in the zero field film. The $H_{\parallel}$ film had very long straight pores oriented in the same direction as, magnetic field. The pores of film prepared under zero field also are locally oriented, but their domain was not so large. The cross-section of the cylinder or pore diameter seems to be observed in the $H_{\perp}$ film, but not to be in zero field and $H_{\parallel}$ films.

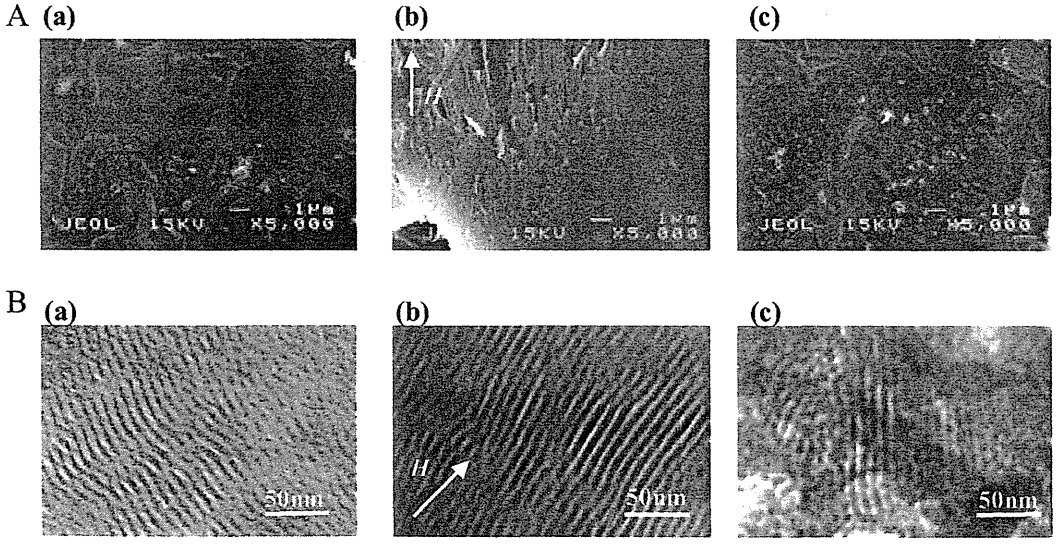

Figure 1. Electron microscopic images of SBA-15 films. The arrow shows the direction of applied magnetic fields.
A: SEM images of as-synthesized SBA-15 films prepared under zero fields (a), 6 T fields applied parallel (b) and perpendicular (c) to film surface.
B: TEM images of calcined SBA-15 films prepared under zero fields (a), 6 T fields applied parallel (b) and perpendicular (c) to film surface.

８．研究発表

９．特許

１０．主催した学術会合

8．研究発表

(1) 研究課題ア

雑誌論文

2003

1) I. Mogi, C. Umeki, K. Takahashi, S. Awaji, K. Watanabe and M. Motokawa, Control of Thermal Convection in Water by Strong Gradient Magnetic Fields. Jpn. J. Appl. Phys. 42 (2003) L715 - L717.
2) 高橋弘紀，梅木千巧，茂木巖，淡路智，小山佳一，本河光博，渡辺和雄，日本応用磁気学会誌，27 (2003) 1125-1129.
3) I. Mogi, M. Hamai, T. Sato, K. Takahashi, S. Awaji, K. Watanabe and M. Motokawa, Application of Magnetic Levitation to Materials Processing, Magnetohydrodynamics, 39 (2003) 403-410.
4) I. Mogi and K. Watanabe, Magnetoelectropolymerization Effects on Redox Behavior of Ferricyanide Incorporated in Polypyrrole Films, Jpn. J. Appl. Phys. 42 (2003) L1397-L1399.

2004

1) K. Takahashi, C. Umeki, I. Mogi, K. Koyama, S. Awaji, M. Motokawa, and K. Watanabe, Magnetic Orientation of Paraffin in a Magnetic Levitation Furnace, Physica B, 346-347 (2004) 277-281.
2) N. Kitamura, K. Fukumi, J. Nishi, K. Takahashi, I. Mogi, S. Awaji and, K. Watanabe, Effect of Magnetic Field on Thermal Convection of Glass Melt, J. Ceram. Soc. Jpn., 112 (2004) S1210-S1213.
3) I. Mogi, C. Umeki, K. Takahashi, S. Awaji, K. Watanabe and M. Motokawa, Heat Transfer in Water under Strong Gradient Magnetic Fields, IEEE Trans. On Applied Superconductivity, 14 (2004) 1682-1684.
4) M. Ogita, M. Nakao, C.D. Singh, I. Mogi and S. Awaji, A Novel Approach for Simultaneous Measurements of Hall Effect and Magnetoresistance Effect in Solid and Liquid State of Gallium and Mercury Metals, Physica B, 346-347 (2004) 306-309.
5) H. Matsushima, T. Nohira, I. Mogi and Y. Ito, Effects of Magnetic Fields on Iron Electrodeposition, Surface and Coating Technology, 179 (2004) 245-251.
6) T. Hasebe, S. Okada, M. Ishizuka, T. Tsurudome, T. Ito, H. Ookubo, J. Sakuraba, K. Watanabe, S. Awaji, K. Koyama, G. Nishijima and K. Takahashi, Desigun of a cryocooler-cooled large bore superconducting magnet for a 30 T hybrid magnet, IEEE Trans. on Appl. Supercond. 14 (2004) 368-371.
7) M. Kyoto, S. Hanai, T. Takano, K. Takahashi, G. Nishijima, S. Awaji, K. Watanabe and M. Motokawa, Development of a cryo-cooled superconducting magnet with a large magnetic-force field, IEEE Trans. on Appl. Supercond. 14 (2004) 384-387.
8) K. Watanabe, G. Nishijima, S. Awaji, K. Takahashi, K. Koyama, M. Motokawa, M. Ishizuka, T. Hasebe and J. Sakuraba, Advances in the first cryogen-free hybrid magnet, IEEE Trans. on Appl. Supercond. 14 (2004) 388-392.

2005

1) I. Mogi and K. Watanabe, Chirality of Magnetoelectropolymerized Polyaniline Electrodes, Jpn. J. Appl. Phys., 44 (2005) L199-L201.
2) N. Kitamura, M. Makihara, I. Mogi, S. Awaji, K. Watanabe and M. Motokawa, Microspheres of Tellurite Glass Formed by Evaporation-Condensation Process under High Magnetic Field, Jpn. J. Appl. Phys., 44 (2005) 7546-7549.
3) Hasanudin, N. Kuroda, T. Sugimoto, I. Mogi, K. Watanabe, High-pressure infrared absorption in Cs_2TCNQ_3 crystals grown under magnetic field, Synth. Met., 148 (2005) 307-312.
4) M. Ogita, T. Ito, M. Isai, I. Mogi, S. Awaji, K. Yokoo, Dynamics of simultaneous measurements of hall and magnetoresistance effects in liquid metals and semiconductors, J. Optoelect. Adv. Mat., 7 (2005) 677-685.

2006

1) I. Mogi and K. Watanabe, Chiral Recognition of Magnetoelectropolymerized Polyaniline Film Electrodes, Sci. Tech. Adv. Matt. (2006) (in print).
2) I. Mogi and K. Watanabe, Chiral Electrodes of Magneto-Electropolymerized Polyaniline Films, Magnetohydrodynamics (2006) (in print).

3) I. Mogi and K. Watanabe, Chirality of Polyaniline Induced by Magneto-Electropolymerization, Electrochimica Acta (2006) (in print).
4) K. Takahashi, S. Awaji, Y. Sasaki, K. Koyama, and K. Watanabe, Design of an 8 MW water-cooled magnet for a 35 T hybrid magnet at the HFLSM, IEEE Trans. Appl. Supercond (2006) (in print).
5) K. Takahashi, I. Mogi, T. Onogi, S. Awaji, M. Motokawa and K. Watanabe, Materials processing in magnetic levitation furnaces, Sci. Tech. Adv. Mat.(2006) (in print).
6) K. Watanabe, G. Nishijima, S. Awaji, K. Takahashi, K. Koyama and N. Kobayashi, Performance of a cryogen-free 30 T hybrid magnet, IEEE Trans. Appl. Supercond. (2006) (in print).

国際会議

2003

1) I. Mogi, C. Umeki, K. Takahashi, S. Awaji, K. Watanabe and M. Motokawa, Control of Thermal Convections in Water by Strong Gradient Magnetic Fields, 3rd Int. Conf. on Electromagnetic Processing of Materials, October 13-17 (2003)Lyon, France.
2) I. Mogi, C. Umeki, K. Takahashi, S. Awaji, K. Watanabe and M. Motokawa, Heat Transfer in Water under Strong Gradient Magnetic Fields, The 18th Int. Conf. on Magnet Technology, October 20-24 (2003) Morioka, Japan.
3) I. Mogi and K. Watanabe, Magnetoelectropolymerized Polypyrrole Film Electrodes, The Electrochemical Society 203rd Meeting, April 27-May 2 (2003) Paris, France.
4) K. Takahashi, C. Umeki, I. Mogi, K. Koyama, S. Awaji, M. Motokawa and K. Watanabe, Magnetic orientation of paraffin in a magnetic levitation furnace, 7th Int. Symp. on Research on High Magnetic Fields, July 20-23 (2003) Toulouse, France.

2004

1) I. Mogi, K. Takahashi, S. Awaji, K. Watanabe and M. Motokawa, Application of Magnetic Levitation to Processing of Diamagnetic Materials, Int. Workshop on Materials Analysis and Processing in Magnetic Field, March 17-19 (2004) Tallahassee, USA.
2) I. Mogi, C. Umeki, K. Takahashi, S. Awaji, K. Watanabe and M. Motokawa, Thermal Convection in Water under Strong Gradient Magnetic Fields, 2004 Joint Int. Meeting of Electrochemical Society, October 3-8 (2004) Honolulu, Hawaii, USA.

2005

1) I. Mogi, K. Watanabe, Chiral Electrodes of Magneto-Electropolymerized Polyaniline Films, 6th Riga and pamir Conference on Fundamental and Applied MHD, June 26-July 1 (2005) Riga-Jurmala, Latvia.
2) I. Mogi, K. Watanabe, Chirality of Magnetoelectropolymerized Polyaniline Electrodes, 56th Annual Meeting of the International Society of Electrochemistry, September 25-30 (2005) Busan, Korea.
3) I. Mogi, K. Watanabe, Chirality of Polyaniline Induced by Magneto-Electropolymerization, 4th Int. Symp. on Electrochemical Processing on Tailored Materials, October 3-5 (2005) Kyoto, Japan.
4) I. Mogi, K. Watanabe, Chiral Recognition of Ascorbic Acid by Magnetoelectropolymerized Polyaniline Electrodes, Int. Symp. on Magneto-Science 2005 November 14-17 (2005) Yokohama, Japan.
5) I. Mogi, K. Watanabe, Enantioselective Recognition of Magnetoelectropolymerized Polyaniline Film Electrodes, PACIFICHEM 2005, December 15-21 (2005) Honolulu, Hawaii, USA (invited).
6) K. Takahashi, S. Awaji, Y. Sasaki, K. Koyama, and K. Watanabe, Design of an 8 MW water-cooled magnet for a 35 T hybrid magnet at the HFLSM, 19th Int. Conf. on Magnet Technology, Sep. 18-23 (2005) Genova, Italy.
7) K. Takahashi, I. Mogi, S. Awaji and K. Watanabe, Development of a new magnetic levitation furnace, Int. Symp. on Magneto-Science, Nov. 14-17 (2005) Yokohama, Japan.
8) K. Takahashi, I. Mogi, T. Onogi, S. Awaji, M. Motokawa and K. Watanabe, Materials processing in magnetic levitation furnaces, Pacifichem2005, Dec. 15-20 (2005) Honolulu, USA.

2006

1) I. Mogi, K. Watanabe, Chiral Electrochemical Reactions on Magnetoelectropolymerized Polyaniline Electrodes, 2nd Int. Workshop on Materials Analysis and Processing in Magnetic Fields, March 19-22 (2006) Grenoble, France.
2) K. Takahashi, I. Mogi, S. Awaji and K. Watanabe, Thermal behavior of diamagnetic materials in magnetic levitation furnace, 2nd Int. Workshop on Materials Analysis and Processing in Magnetic Fields, Mar. 19-22 (2006) Grenoble, France.

解説・書籍等

2005

1) I. Mogi, K. Takahashi, S. Awaji, K. Watanabe and M. Motokawa, Application of Magnetic Levitation to Processing of Diamagnetic Materials, Materials Processing in Magnetic Fields, Eds. H.J. Schneider-Muntau and H. Wada, World Scientific, Singapore (2005) pp.278-284.

2) 茂木巖，高橋弘紀，淡路智，渡辺和雄，本河光博，磁気浮上と材料プロセス，Electrochemistry, 73 (2005) 440-445.

2006

1) 茂木巖，磁気浮上–強磁場がつくる擬似無重力状態–，化学と教育，54 (2006) 12-15.

2) I. Mogi and K. Takahashi, Magnetic levitation of diamagnetic materials, Magneto-Science, Springer, (in print).

(2) 研究課題イ

雑誌論文

2003

1) R. B. Morgunov, S. Z. Shmurak, A. A. Baskakov, and Y. Tanimoto, Magnetosensitive Defects Generated during Plastic Straining of NaCl:Eu Crystals, J. Experimental and Theoretical Physics, 97, 754-762 (2003).

2) K. Chie, M. Fujiwara, Y. Fujiwara, and Y. Tanimoto, Magnetic Separation of Metal Ions, J. Phys. Chem. B, 107, 14374-14377 (2003).

3) S. Kohtani, M. Koshiko, A. Kudo, K. Tokumura, Y. Ishigaki, A. Toriba, K. Hayakawa, and R. Nakagaki, Photodegradation of 4-alkylphenols using $BiVO_4$ photocatalyst under irradiation with visible light from a solar simulator, Appl. Catal. B: Environ., 46 (2003) 573-586.

4) H. Saigusa, N. Miyakoshi, C. Mukai, T. Fukagawa, S. Kohtani, R. Nakagaki, and R. Gordon, Twisted S_1 excited state geometries in 4-dimethylaminobenzonitrile and dimethylaniline: New $-d_6$ origin bands, J. Chem. Phys. 119 (2003) 5414-5422.

5) K. Toriyama, M. Okazaki, ESR Detection of the Isotopic-site-preference in the Jahn-Teller Distorted Benzene Cation Radicals Produced in MCM-41, Silica Gel, and Halocarbons, Chem. Lett., l32, 1020-21 (2003).

2004

1) Yu. A. Ossipyan, R. B. Morgunov, A. A. Baskakov, S. Z. Shmurak, and Y. Tanimoto, New Luminescence Bands Induced by Plastic Deformation of NaCl:Eu Phosphors, Phys. Stat. Sol.(a), 201, 148-156 (2004).

2) A. Katsuki, I. Uechi, and Y. Tanimoto, Effects of a High Magnetic Field on the Growth of 3-Dimensional Silver Dendrites, Bull. Chem. Soc. Jpn., 77, 275-279 (2004).

3) I. Uechi, A. Katsuki, L. Dunin-Barkovskiy, and Y. Tanimoto, 3D-Morphological Chirality Induction in Zinc Silicate Membrane Tube Using a High Magnetic Field, J. Phys. Chem. B, 108, 2527-2530 (2004).

4) H. Yonemura, H. Nobukuni, S. Moribe, S. Yamada, Y. Fujiwara, and Y. Tanimoto, Magnetic Field Effects on the Decay Rates of Triplet Biradical Photogenerated from Intramolecular Electron-Transfer in a Zinc-Tetraphenylporphyrin-Fullerrene Linked Compound, Chem. Phys. Lett., 385 (2004) 417-422.

5) M. Okazaki, K. Toriyama, N. Sawaguchi and K. Oda, Spin-Probe Study on the Dynamics and Distortion of Solution Molecules in the Nano-Channel of MCM-41, Bulletin of the Chemical Society of Japan, 77, 87-93 (2004).

6) M. Fujiwara, K. Chie, J. Sawai, D. Shimizu, and Y. Tanimoto, On the Movement of Paramagnetic Ions in an Inhomogeneous Magnetic Field, J. Phys. Chem. B 108, 3531-3534 (2004).

7) R. B. Morgunov, A. A. Baskakov, L. R. Dunin-Barkovskiy, S. S. Khasnov, R. P. Shibaeva, T. G. Prokhorova, E. B. Yagubskiy, T. Kato, and Y. Tanimoto, Localization of Conduction-band electrons in β''-(BEDT-TTF)$_4$NH$_4$[Cr(C_2O_4)$_3$] · DMF Single Crystals, J. Phys. IV France 114, 335-337 (2004).

8) D. C. Yin, N. I. Wakayama, K. Harata, M. Fujiwara, T. Kiyoshi, H. Wada, N. Niimura, S. Arai, W. D. Huang and Y. Tanimoto, Formation of Protein Crystals (Orthorhombic Lysozyme) in Quasi-microgravity

Environment Obtained by Superconducting Magnet, J. Cryst. Growth, 279, 184-191 (2004).
9) W. Duan, M. Fujiwara, and Y. Tanimoto, In situ Observation of Laser-Induced Convection of Benzene Solution of Photochromic Compound in High Magnetic Fields, Jpn. J. Appl. Phys., 43, 8213-8216 (2004).
10) S. Kohtani, N. Yamamoto, K. Kitajima, A. Kudo, H. Kato, K. Tokumura, K. Hayakawa, and R. Nakagaki, Photodegradation of 4-n-nonylphenol and natural estrogens using heterogeneous visible-light-driven $AgNbO_3$ or $BiVO_4$ photocatalyst, Photo/Electrochemistry and Photobiology in Environment, Energy and Fuel, (2004) 173-184.
11) K. Toriyama, M. Okazaki, M. Jansson, A. Lund, and S. Lunell, Isotope effect on the J-T distortion of partially deuteriated benzene cation radicals: an experimental EPR and theoretical DFT study, Phys. Chem. Chem. Phys., 6 (2004) 1658-1665.
12) K. Toriyama and M. Okazaki, Molecular packing of long-chain n-alkanes in the MCM-41 nanochannel as probed by the free radicals produced by γ-irradiation, J. Phys. Chem. B, 108 (2004) 12917-12920.
13) M. Okazaki, K. Toriyama, and S. Anandan, Dynamics and packing mode of long-chained n-alkane molecules in the nano-channel of MCM-41, Chem. Phys. Lett., 401 (2005) 363-367
14) T. Oba, M. Hanasaki, M. Minabe, and H. Tamiaki, Fabrication of a novel nano-device that functions on demand, Chem. Lett. 34 (2005) 150-151.

2005
1) A. A. Baskakov, L. R. Dunin-Barkovskii, R. B. Morgunov, Y. Tanimoto, and S. Z. Shmurak, The Magnetic Properties of Eu Nanoclusters Formed in NaCl Crystals during Plastic Deformation and Aggregation, J. Experimental and Theoretical Physics, 100, 66-76 (2005).
2) Y. Tanimoto, S. Ogawa, K. Fujitani, Y. Fujiwara, S. Izumi, and T. Hirata, Effects of a High Magnetic Field on E. Coli Movement, Environ. Sci., 18, 53-56 (2005).
3) M. Fujiwara, Y. Mouri, K. Araki, and Y. Tanimoto, Photodissociation of p-Xylene in Polar and Nonpolar Solutions, J. Phys. Chem. A, 109, 36-39 (2005).
4) S. Kohtani, J. Hiro, N. Yamamoto, A. Kudo, K. Tokumura, and R. Nakagaki, Adsorptive and photocatalytic properties of Ag-loaded $BiVO_4$ on the degradation of 4-n-alkylphenol under visible light irradiation, Catal. Commun. 6 (2005) 185-189.
5) W. Duan, S. Kitamura, I. Uechi, A. Katsuki, and Y. Tanimoto, Three-Dimensional Morphological Chirality Induction Using High Magnetic Fields in Membrane Tubes Prepared by a Silicate Garden Reaction, J. Phys. Chem. B, 109, 13445-13450 (2005).
6) Y. Tanimoto, M. Fujiwara, M. Sueda, K. Inoue, and M. Akita, Magnetic Levitation of Plastic Chips: Application for Magnetic Susceptibility Measurement and Magnetic Separation, Jpn. J. Appl. Phys. 44, 6801-6803 (2005).
7) A. Katsuki, I. Uechi, and Y. Tanimoto, The Magnetic Orientation of 2-Dimensional Silver Dendrites, Bull. Chem. Soc. Jpn., 78, 1251-1255 (2005).
8) R. Morgunov, S. Gudoshnikov, Yu. Ossypian, V. Ovcharenko, R. Sagdeev, V. Skomarovskii and Y. Tanimoto, Imprinting magnetic memory cells in molecular based $NiL_2(C_2H_5OH)_2$ heterospin crystals, phys. stat. sol. (a) 202, R47-R49 (2005).
9) R. Morgunov, A. Baskakov, S. Shmurak, L. Dunin-Barkovskii, Y. Tanimoto, Magnetic properties of Eu nano-clusters forming during plastic deformation and aggregation of NaCl crystals, J. Exper. Theor. Phys., 100, 66-76 (2005).
10) L. Dunin-Barkovskii, R. Morgunov, Y.Tanimoto, Influence of static magnetic field up to 15 T on Portevein – Le- Shatelie effect in NaCl:Eu single crystals, Phys. Solid State, 47, 1282-1288 (2005).
11) V. Blokhin, A. S. Markosyan, R. B. Morgunov, K. Inoue, Y. Tanimoto, and Y. Yoshida, Magnetic Resonance in a $[\{Cr(CN)_6\}\{Mn(S)\text{-}pnH\text{-}(H_2O)\}] \cdot H_2O$Single-Crystal Molecular Ferrimagnet, Phys. Solid State, 47, 2106–2113 (2005).
12) Y. Mouri, Y. Fujiwara, T. Aoki, H. Yoshida, K. Naka, Y. Aoki, H. Yonemura, S. Yamada, T. Haino, Y. Fukazawa, and Y. Tanimoto, High Magnetic Field Effects on Biradical Lifetimes - Evaluation of Magnetic Field Dependence and Chain Length Dependence Using Calculated g and Hyperfine Tensors, Bull. Chem. Soc. Jpn., 78 (2005) 804-813.
13) T. Yamaguchi, Y. Yamamoto, Y. Fujiwara, and Y. Tanimoto, Evidence for a Transition State Model Compound of In-Plane Vinylic SN_2 Reaction, Org. Lett., 7 (2005) 2739-2742.
14) M. Fujiwara, Y. Mouri, K. Ariki, and Y. Tanimoto, Photodissociation of p-Xylene in Polar and Non-Polar Solutions, J. Phys. Chem. A 109 (2005) 36-39.
15) S. Kohtani, M. Tomohiro, K. Tokumura, and R. Nakagaki, Photooxidation reactions of polycyclic

aromatic hydrocarbons over pure and Ag-loaded $BiVO_4$ photocatalysts, Appl. Catal. B: Environ. 58 (2005) 265-272.
16) S. Kohtani, Y. Ohama, Y. Ohno, I. Tsuji, A. Kudo, and R. Nakagaki, Photoreductive defluorination of hexafluorobenzene on metal-doped ZnS photocatalysts under visible light irradiation, Chem. Lett. 34 (2005) 1056-1057.
17) N. Kitamura, Y. Toriumi, S. Kohtani, and R. Nakagaki, Crystal structure of a coumarin-indoline hybrid dye, Anal. Sci. 21 (2005) X101-X102.
18) N. Kitamura, S. Kohtani, and R. Nakagaki, Molecular aspects of furocoumarin reactions: Photophysics, photochemistry, photobiology, and structural analysis, J. Photochem. Photobiol. C: Rev. 6 (2005) 168-185.
19) M. Okazaki and K. Toriyama, Spin-probe ESR Study on the Dynamics of Liquid Molecules in the MCM-41 Nano-channel: Temperature dependence on 2-propanol and water, J. Phys. Chem. B, 109, 13180-13185 (2005).
20) M. Okazaki and K. Toriyama, Entrappment of organic solutes by the water cage in the nanochannel of MCM-41, J. Phys. Chem., B, 109, 20068-20071 (2005).
21) T. Oba, M. Hanasaki, M. Minabe, and H. Tamiaki, Fabrication of a novel nano-device that functions on demand , Chem. Lett. 34 (2005) 150-151.
22) J. Yamamoto, T. Kimura, Y. Takabayashi, T. Oba, M. Karikomi, M. Minabe, Liquid crystallinity of 2-fluorenyl 4-alkylbenzoates, Bull. Chem. Soc. Jpn., 78 (3), 523-528 (2005).
23) T. Oba, H. Tamiaki, Stereochemical effects of peripheral substituents on the fifth ligand binding in chlorophylls, and nomenclature of the asymmetric coordination complexes, Bioorg. Med. Chem., 13 (20), 5733-5739 (2005).

2006
1) R. B. Morgunov, R. P. Shibaeva, É. B. Yagubski, T. Kato, Y. Tanimoto, Localization of Conduction Electrons and the Magnetic Properties of the Molecular Metals b"–(BEDT–TTF) $_4NH_4[M(C_2O_4)_3]$ · DMF($M = Cr^{3+}$, Fe^{3+}), J. Exper. Theor. Phys., 102, 121–130 (2006).
2) F. Koyama and Y. Tanimoto, Photo-induced Convection of Benzene Solution of Diphenylamine and Carbon Tetrabromide, Mol. Phys., (in press).
3) F. Tang, A. Katsuki, and Y. Tanimoto, Effect of High Magnetic Field on a Quasi-3D Silver Dendrite Growing System, Mol. Phys., (in press).
4) M. Sueda, A. Katsuki, Y. Fujiwara, and Y. Tanimoto, Influence of High Magnetic Field on Glycine Crysal Growth, Science and Technology of Advanced Materials, (in press).
5) A. Katsuki, S. Aibara, and Y. Tanimoto, Crystal Morphology Change by Magnetic Susceptibility Force, Science and Technology of Advanced Materials, (in press).
6) Y. Fujiwara, M. Tomishige, Y. Itoh, M. Fujiwara, N. Shibata, T. Kosaka, H. Hosoya, and Y. Tanimoto, Effect of horizontal strong static magnetic field on swimming behavior of Paramecium caudatum, Mol. Phys., (in press).

国際会議
2003
1) E. B. Yagubskii, T. G. Prokhorova, A. A. Baskakov, R. B. Morgunov, L. R. Dunin-Bakowskii, T. Kato, and Y. Tanimoto, ESR Studies of Molecular Metals Based on BEDT-TTF Radical Cation Salts β"-(BEDT-TTF)4NH4[Cr(C2O4)3] · DMF, NATO Advance Study Institute Organic Conductors, Superconductors, and Magnets: From Synthesis to Molecular Electronics, Corfu, Greece, April, 2003, F6.
2) M. Fujiwara, Y. Tanimoto, N. I. Wakayama and R. Hirose, Crystal Growth under Microgravity Environment in a Superconducting Magnet, International Symposium on Diffraction Structural Biology 2003, Tsukuba, May 2003, P-084.
3) Y. Fujiwara, J. Hamada, Y. Tanimoto, H. Yonemura, S. Moribe, H. Nobukuni, and S. Yamada, High Magnetic Field Effect on Lifetimes of Biradicals Generated by Photo-induced Intramolecular Electron Transfer in Electron Donor-Acceptor (C60) Linked Compounds, XXIth International Conference on Photochemistry, Nara July 2003, 2P63.
4) M. Kamochi, Y. Fujiwara, and Y. Tanimoto, Magnetic Field Effects on TiO_2 Photocatalytic Reaction, XXIth International Conference on Photochemistry, Nara July 2003, 5P63.
5) A. Katsuki and I. Uechi, and Y. Tanimoto, Effects of a High Magnetic Field on the Growth of Silver Dendrites, 8th International Symposium on Spin and Magnetic Field Effects in Chemistry and Related

Phenomena, Chapel Hill, USA, September 2003.
6) Y. Fujiwara, J. Hamada, Y. Tanimoto, H. Yonemura, S. Moribe, H. Nobukuni, M. Noda, and S. Yamada, High Magnetic Field Effects on Lifetimes of Biradicals Generated by Photo-Induced Intramolecular Electron Transfer in Electron Donor-Acceptor (C60) Linked Compounds, 8th International Symposium on Spin and Magnetic Field Effects in Chemistry and Related Phenomena, Chapel Hill, USA, September 2003.
7) I. Uechi, A. Katsuki, L. Dunin-Barkovskiy, and Y. Tanimoto, Magnetic Chirality Induction in Zinc Silicate Membrane Tube Morphology, 8th International Symposium on Spin and Magnetic Field Effects in Chemistry and Related Phenomena, Chapel Hill, North Carolina, September 21-26, 3003. （招待講演）
8) R. B. Morgunov, A. A. Baskakov, E. B. Yagubskii, T. G. Prokhorova, L. R. Dunin-Barkovskii, T. Kato and Y. Tanimoto, Localization of Conduction-Band Electrons in β"-(BEDT-TTF)$_4$NH$_4$[Cr(C_2O_4)$_3$]· DMF Crystals, Vth International Symposium of Crystalline Organic Metals, Superconductors and Magnets, Port-Bourgenay (France), September 2003.
9) N. I. Wakayama, D. C. Yin, M. Fujiwara, Y. Tanimoto, D.C. Yin and K. Hirata, Protein Crystal Growth in Micro G, 1G and 1.8 G in a New Type of Superconducting Magnet, Microgravity Transport Processes in Fluid, Thermal, Biological and Materials Sciences III, Davos (Switzerland), September 2003, Paper No. 100.
10) Y. Tanimoto, Magneto-Science – Chemistry in a High Magnetic Field, Singapore International Chemical Conference III: Frontiers in Physical and Analytical Chemistry, Singapore, December15-17 2003 (invited).
11) A. A. Baskakov, L. R. Dunin-Barkovskii, M. Fujiwara, R. B. Morgunov, Y. Tanimoto, Magnetic Field Control over Luminescence of Eu^{2+} Nanoclusters Incorporated in Crystal Lattice, International Symposium on Functional Clusters and Cluster-Based Nano-Materials, Dec. 15-18 (2003), Okazaki, Japan.
12) M. Fujiwara and Y. Tanimoto, Magnetic Orientation of Carbon Clusters, International Symposium on Functional Clusters and Cluster-Based Nano-Materials, Dec. 15-18 (2003), Okazaki, Japan.
13) N. I. Wakayama, D.C. Yin, Y. Tanimoto, M. Fujiwara, K. Harata, and H. Wada, Protein Crystal Growth in 0G, 1G and 1.8G Provided by a New Type of Superconducting Magnet, International Workshop on Materials Analysis and Processing in Magnetic Fields, Tallahassee, USA, March 2004.
14) Y. Tanimoto, Application of High Magnetic Field to Chemical and Physical Processes, International Workshop on Materials Analysis and Processing in Magnetic Fields, Tallahassee, USA, March 17-19, 2004 (invited).
15) T. Oba, Toward the fabrication of the self-healing nanodevice, 21st ICP Satellite Symposium on Photochemistry and Photobiology of Complexes Including Supramolecular Systems and Coordinated Compounds, Aug 1-3 (2003) Kusatsu, Japan.
16) T. Oba, H. Tamiaki, Asymmetry of molecular structure of chlorophylls and its possible functions, International Workshop on Green and Heliobacteria, Aug 22-24 (2003) Kisarazu, Japan.
17) T. Oba, H. Tamiaki, Origin and roles of the planar chirality of chlorophylls, International Conference on Tetrapyrrole Photoreceptors in Photosynthetic Organisms, Oct 6-10 (2003) Passau, Germany.
18) K. Takahashi, S. Kohtani, and R. Nakagaki; Asymmetric photolysis of large ring 2-phenylcycloalkanones with circularly polarized light in static magnetic fields, 21st Int. Conf. on Photochemistry, July 26-31 (2003) Nara.
19) S. Kohtani, N. Yamamoto, A. Kudo, K. Tokumura, K. Hayakawa, and R. Nakagaki, Photocatalytic degradation of endocrine disrupting chemicals using Ag- or CuO-loaded $BiVO_4$ under visible light, 21st Int. Conf. on Photochemistry, July 26-31 (2003) Nara.
20) H. Saigusa, N. Miyakoshi, C. Mukai, T. Fukagawa, S. Kohtani, R. Nakagaki, and R. Gordon, Twisted S1 excited state geometries in 4-dimethyaminobenzonitrile and dimethylaniline, 21st Int. Conf. on Photochemistry, July 26-31 (2003) Nara.

2004

1) S. Kohtani, M. Tomohiro, J. Hiro, A. Kudo, K. Tokumura, and R. Nakagaki, Photooxidation reactions of aromatic compounds using Ag-loaded $BiVO_4$ photocatalyst under visible light irradiation, 15th Int. Conf. on Photochemical Conversion and Storage of Solar Energy, July 4-9 (2004) Paris, France.
2) Y. Tanimoto, Magneto-Science. Application of High Magnetic Field to Chemical and Physical Processes, II All-Russian Conference on High-spin Molecules and Molecular Magnets, Novosibirsk (Russia), May 2004 (invited).

3) F. Koyama, W. Duan and Y. Tanimoto, Photochemical Reaction of Diphenylamine and Carbon Tetrebromide in Benzene under Pseudo-Microgravity and Hypergravity Produced by High Magnetic Fields, 2004 Korea-Japan Symposium on Frontier Photoscience "Photochemistry and Nanotechnology", Daejeon, Korea, November 2004.
4) A. Baskakov, L. Dunin-Barkovskii, R. Morgunov, T. Prohorova, L. Zorina, S. Hasanov, R. Shibaeva, E. Yagubskii, Y. Tanimoto, Magnetic properties of molecular metals based on BEDT-TTF salt containing paramagnetic ions: $(BEDT\text{-}TTF)_4NH_4\{M(C_2O_4)_3\}DMF$, M = Cr, Fe, II All Russian Conference on High-spin Molecules and Molecular Magnets, Nobosibirsk (Russia), May 2004.
5) A. Baskakov, S. Gudoshnikov, R. Morgunov, Yu. Ossipyan, V. Ovcharenko, R. Sagdeev, V. Skomarovskii, Y. Tanimoto, S. Fokin, Creation of magnetic memory cells during deformation of molecular magnets $NiL_2(C_2H_5OH)$, II All-Russian Conference on High-spin Molecules and Molecular Magnets, Novosibirsk (Russia), May 2004.
6) A. Baskakov, L. Dunin-Barkovskii, R. Morgunov, S. V. Simonov, S. Hasanov, R. Shibaeva, A. Dubrovskii, N. Spitsina, L. Buravov, E. Yagubskii, Y. Tanimoto, Interrelation between magnetic and electrical properties of cation-radical salt BEDO-TTF containing paramagnetic ions $[CrNO(CN)_5]^{3-}$, II All-Russian Conference on High-spin Molecules and Molecular Magnets, Novosibirsk (Russia), May 2004.
7) L. Dunin-Barkovskii, A. Baskakov, R. Morgunov, Y. Tanimoto, Magnetic field effects upon macroscopic plastic deformation of diamagnetic single crystals containing paramagnetic impurity, XXI International Conference "Relaxation phenomena in solids," Voronezn (Russia) October 2004.
8) R. Morgunov, L. Dunin-Barkovskii, A. Baskakov, Y. Tanimoto, Magnetic field control over relaxation of excited system of paramagnetic impurity in NaCl:Eu single crystals, XXI International Conference "Relaxation phenomena in solids," Voronezn (Russia) October 2004.
9) R. Morgunov, Y. Tanimoto, Spin micromechanics in phisics of plasticity, The International Conference "Plasticity of solids," Chernogolovka (Russia) September 2004.
10) A. Baskakov, R. Morgunov, R. Shibaeva, G. Prokhorova, E. Yagubskii, and Y. Tanimoto, CW-ESR Line Shape as a Precision Indicator of Conduction-band Electrons Localization, International School on EPR/ESR Spectroscopy and Free Radical Research, Mumbai (India), Nov. 2004.
11) S. Kohtani, M. Tomohiro, J. Hiro, A. Kudo, K. Tokumura, and R. Nakagaki, Photooxidation reactions of aromatic compounds using Ag-loaded $BiVO_4$ photocatalyst under visible light irradiation, 15th Int. Conf. on Photochemical Conversion and Storage of Solar Energy, July 4-9 (2004) Paris, France.
12) S. Kohtani and R. Nakagaki, Photooxidation Reactions of Polycyclic Aromatic Hydrocarbons on Pure and Ag-loaded $BiVO_4$ photocatalysts, 2004 Korea-Japan Symposium on Frontier Photoscience "Photochemsitry and Nanotechnology", Nov. 20-23, (2004) Daejeon, Korea.
13) T. Oba, Functionalized Cytoskeleton as a Possible Nano-device, International Workshop on Supramolecular Nanoscience of Chemically Programmed Pigments, Jun 16–18 (2004), Kusatsu (invited).
14) T. Oba, H. Tamiaki, Chirality at the central metal atoms of chlorophylls, The 13th International Congress on Photosynthesis, Aug. 29 - Sep. 3 (2004) Montreal, Canada.
15) H.Takatoya, A. Ugajin, H. Tobita, K. Ogura, M. Minabe, T. Oba, Syntheses and properties of novel cationic chlorophyll derivatives, The 13th International Congress on Photosynthesis, Aug. 29 - Sep. 3 (2004) Montreal, Canada.
16) M. Hanasaki, M. Sato, M. Minabe, H. Tamiaki, T. Oba, Fabrication of an artificial nano-device on a design principle of photosynthetic systems, The 13th International Congress on Photosynthesis, Aug. 29 - Sep. 3 (2004) Montreal, Canada.
17) K. Takahashi, Y. Itoh, M. Akiyama, T. Watanabe, K. Inoue, T. Oba, M. Umetsu, M. Kobayashi, Delicate distinction between absorption spectra of 'normal' and 'prime' bacteriochlorophylls, The 13th International Congress on Photosynthesis, Aug. 29 - Sep. 3 (2004) Montreal, Canada.

2005

1) T. Oba, M. Hanasaki, M. Minabe, Development of a new intelligent supramolecular systems: Toward self-healing artificial systems, International symposium on molecular smart system, Mar. 16-17 (2005) Tsukuba.
2) 藤原好恒, 谷本能文, ポリ 9-ビニルカルバゾールフィルム上の自己組織化による微視的パターンに対する強磁場の効果, 広島大学・首都師範大学学術・技術交流会 2005 北京, Mar. 25-26 (2005) 北京, 中国.
3) S. Kohtani, Y. Ohama, Y. Ohno, I. Tsuji, A. Kudo, and R. Nakagaki, Photoreductive defluorination of

hexafluorobenzene on metal-doped ZnS photocatalysts under visible light irradiation, 22nd International Conference on Photochemistry, July 24-29 (2005) Cairns, Australia.
4) S. Kohtani, J. Hiro, and R. Nakagaki, Active oxygen species formed on pure and Ag-loaded $BiVO_4$ photocatalyst: Comparison with TiO_2, 22nd International Conference on Photochemistry, July 24-29 (2005) Cairns, Australia.
5) F. Koyama, W. Duan, and Y. Tanimoto, Control of Thermal Convection Using High Magnetic Field, 9th International Symposium on Spin and Magnetic Field Effects in Chemistry and Related Phenomena (Spin Chemistry Meeting 2005), Sep. 11-17 (2005) Oxford, UK (invited).
6) A. Katsuki and Y. Tanimoto, Precession of Silver Dendrites under a High Magnetic Field, 9th International Symposium on Spin and Magnetic Field Effects in Chemistry and Related Phenomena (Spin Chemistry Meeting 2005), Sep. 11-17 (2005) Oxford, UK.
7) W. Duan, S. Kitamura, I. Uechi, A. Katsuki, and Y. Tanimoto, Three-dimensional Morphological Chirality Induction Using High Magnetic Field in Membrane Tubes Prepared by Silicate Garden Reaction, 9th International Symposium on Spin and Magnetic Field Effects in Chemistry and Related Phenomena (Spin Chemistry Meeting 2005), Sep. 11-17 (2005) Oxford, UK.
8) N. I. Wakayama, D. C. Yin, K. Harata, T. Kiyoshi, M. Fujiwara, and Y. Tanimoto, Protein Crystallization in Microgravity Generated by a Superconducting Magnet, 9th International Symposium on Spin and Magnetic Field Effects in Chemistry and Related Phenomena (Spin Chemistry Meeting 2005), Sep. 11-17 (2005) Oxford, UK.
9) Y. Fujiwara, M. Tomishige, Y. Itoh, Y. Tanimoto, T. Kosaka, and H. Hosoya, Effects of the Strong Static Magnetic Field on the Swimming Behaviour of Some Protists, 9th International Symposium on Spin and Magnetic Field Effects in Chemistry and Related Phenomena (Spin Chemistry Meeting 2005), Sep. 11-17 (2005) Oxford, UK.
10) H. Yonemura, S. Moribe, S. Harada, S. Yamada, Y. Fujiwara, Y. Mouri, J. Hamada, Y. Tanimoto, Magnetic Field Effects on the Decay Rates of Photogenerated Biradical in Donor-C_{60} Linked Compounds: Contribution of Spin-Spin Relaxation Mechanism, 9th International Symposium on Spin and Magnetic Field Effects in Chemistry and Related Phenomena (Spin Chemistry Meeting 2005), Sep. 11-17 (2005) Oxford, UK.
11) Y. Yomamoto, H. Yonemura, S. Yamada, Y. Fujiwara, and Y. Tanimoto, Magnetic Orientation and Photoelectrochemical Reactions of Composite Materials Consisting of Conjugated Polymers and Single-Walled Carbon Nanotubes, 2005 Korea-Japan Symposium on Frontier Photoscience, Oct. 7-11 (2005) Busan, Korea.
12) Y. Tanimoto, I. Uechi, W. Duan, and A. Katsuki, 3D-Morphological Chirality Induction in Membrane Tubes Prepared by Silicate Garden Reaction in Magnetic Field, International Symposium on Magneto-Science 2005 (ISMS2005), Nov. 14-17 (2005) Yokohama.
13) A. Katsuki and Y. Tanimoto, Rotational Motion of Silver Dendrites under Magnetic Field, International Symposium on Magneto-Science 2005 (ISMS2005), Nov. 14-17 (2005) Yokohama.
14) F. Koyama and Y. Tanimoto, Photoinduced Convection of Organic Solution in Magnetic Field, International Symposium on Magneto-Science 2005 (ISMS2005), Nov. 14-17 (2005) Yokohama.
15) K. Sueda, F. Koyama, M. Irie, A. Katsuki, and Y. Tanimoto, In situ Observation of Laser-induced Convection of Water in Magnetic Field, International Symposium on Magneto-Science 2005 (ISMS2005), Nov. 14-17 (2005) Yokohama.
16) M. Sueda, W. Duan, Y. Tanimoto, Y. Kaneko, T. Onodera, H. Kasai, H. Oikawa, and H. Nakanishi, Magnetic Orientation of Organic Crystals, International Symposium on Magneto-Science 2005 (ISMS2005), Nov. 14-17 (2005) Yokohama.
17) Y. Tanimoto, M. Fujiwara, and M. Sueda, Magnetic Levitation of Plastic Chips – Applications for Magnetic Susceptibiity Measurements and Magnetic Separation, International Symposium on Magneto-Science 2005 (ISMS2005), Nov. 14-17 (2005) Yokohama.
18) Y. Fujiwara, M. Tomishige, Y. Itoh, N. Shibata, Y. Tanimoto, T. Kosaka, and H. Hosoya, Effects of the Strong Static Magnetic Field on the Swimming Behavior of Some Protists, International Symposium on Magneto-Science 2005 (ISMS2005), Nov. 14-17 (2005) Yokohama.
19) Y. Fujiwara, N. Shibata, and Y. Tanimoto, How Is Effect of Strong Static Magnetic Field on Nanorods?, International Symposium on Magneto-Science 2005 (ISMS2005), Nov. 14-17 (2005) Yokohama.
20) H. Yonemura, Y. Yomamoto, S. Yamada, Y. Fujiwara, and Y. Tanimoto, Magnetic Orientation and Organization of Single-Walled Carbon Nanotubes or Their Composite Materials using Polymer Wrapping, International Symposium on Magneto-Science 2005 (ISMS2005), Nov. 14-17 (2005) Yokohama.

21) M. Fujiwara and Y. Tanimoto, Magnetic Orientation and Its Temperature Dependence of Carbon Nanotubes, Int. Symp. Magneto-Science 2005, Nov. (2005) Yokohama, Japan.
22) R. Morgunov and Y. Tanimoto, Manipulation over Mechanical Properies of Solids by Control of electron Spin Coherency of Nanoclusters in Strong Magnetic Field, International Symposium on Magneto-Science 2005 (ISMS2005), Nov. 14-17 (2005) Yokohama.
23) Y. Tanimoto, N. Matsumura, W. Duan, M. Sakai, and H. Segawa, Magnetic Orientation of Porphine Crystals, 2005 Int. Chemical Congr. Pacific Basin Societies, Dec. (2005) Honolulu, USA.
24) Y. Tanimoto, W. Duan, S. Kitamura, I. Uechi, and A. Katsuki, Magnetic Induction of 3D-Morphological Chirality of Membrane Tubes Prepared by Silicate Garden Reaction, 2005 Int. Chemical Congr. Pacific Basin Societies, Dec. (2005) Honolulu, USA.
25) Y. Tanimoto, F. Koyama, and W. Duan, Control of Thermal Convection of Benzene Solution Using Vertical Magnetic Field, 2005 Int. Chemical Congr. Pacific Basin Societies, Dec. (2005) Honolulu, USA.
26) M. Fujiwara and Y. Tanimoto, Magnetic Separation of Transition Metal Ions, 2005 Int. Chemical Congr. Pacific Basin Societies, Dec. (2005) Honolulu, USA.
27) Y. Fujiwara, M. Tomishige, Y. Itoh, Y. Tanimoto, T. Kosaka, and H. Hosoya, Effects of the Strong Static Magnetic Field on the Swimming Behavior of Some Protists, The 2005 International Chemical Congress of Pacific Basin Societies (PACIFICHEM2005), Dec. 15-20 (2005) Honolulu, U.S.A.
28) Y. Fujiwara and Y. Tanimoto, Effects of the Strong Static Magnetic Field on Microscopic Patterns of Self-Organized Poly(9-vinylcarbazole) Films, The 2005 International Chemical Congress of Pacific Basin Societies (PACIFICHEM2005), Dec. 15-20 (2005) Honolulu, U.S.A.
29) H. Yonemura, Y. Yomamoto, S. Yamada, Y. Fujiwara, Y. Tanimoto, Orientation and Organization of Composite Materials Based on Single-walled Carbon Nanotubes by Use of Strong Magnetic Fields as a New Tool, The 2005 International Chemical Congress of Pacific Basin Societies (PACIFICHEM2005), Dec. 15-20 (2005) Honolulu, U.S.A.
30) S. Kohtani, Y. Ohama, Y. Ohno, I. Tsuji, A. Kudo, and R. Nakagaki, Photoreductive defluorination of hexafluorobenzene on metal-doped ZnS photocatalysts under visible light irradiation, 22nd International Conference on Photochemistry, July 24-29 (2005) Cairns, Australia.
31) S. Kohtani, J. Hiro, and R. Nakagaki, Active oxygen species formed on pure and Ag-loaded $BiVO_4$ photocatalyst: Comparison with TiO_2, 22nd International Conference on Photochemistry, July 24-29 (2005) Cairns, Australia.
32) K. Takahashi, Y. Satoh, S. Kohtani, and R. Nakagaki, Magnetic Field Effects on Photochemistry of Chain-linked Nitro-aromatic Compounds, 9th International Symposium on Spin and Magnetic Field Effects in Chemistry and Related Phenomena (SCM2005), September 11-17, Oxford, UK.
33) K. Takahashi, Y. Satoh, S. Kohtani, and R. Nakagaki, Magnetic Field and Methylene Chain Length Effects on Photochemistry of Bichromophoric Chain Molecules Containing 7-Nitro-2-fluorenyloxy and Anilino Moieties, International Symposium on Magneto-Science 2005 (ISMS2005), November. 14-17, Yokohama, Japan.
34) T. Oba, M. Hanasaki, M. Minabe, Development of a new intelligent supramolecular systems: Toward self-healing artificial systems, International symposium on molecular smart system, Tsukuba, Mar. 16-17, 2005.
35) T. Oba, M. Hanasaki, M. Minabe, "Development of an on-demand nano-device and a concept for self-healing material systems", The 6th International Conference on Intelligent Materials and Systems (ICIM'05), Tokyo, Jul. 4-6, 2005. (「高木賞」受賞)
36) M. Karikomi, M. Sudo, M. Shibuya, T. Oba, M. Minabe, Synthesis of chiral helical quinines by oxidative coupling of 2-hydroxy[n]helicenes, ISCD-17, Palma, Italy , Sept. 11-14, 2005.
37) T. Oba, Aya Ugajin, K. Ogura, M. Karikomi, M. Minabe, Synthesis and Properties of Novel Photosensitizers for Photodynamic Therapy (P-059), The 42nd Japanese Peptide Symposium, Osaka, Oct. 27-29, 2005.
38) T. Oba, T. Nagai, Y. Tanimoto, Functionalization of supramolecular biosystems in magnetic fields, International Symposium on Magneto-Science 2005 (ISMS2005), Yokohama, Nov. 14-17, 2005.
39) T. Oba, M. Hanasaki, M. Sato, T. Nagai, M. Karikomi, M. Minabe, S. Ito and K. Hiratani, Integration and Function of Molecular Devices on a Dynamic Supramolecular System, International Symposium on Molecular Scale Electronics (in conjugation with 6th Molecular Scale Electronics Workshop in Japan), Tsukuba, Dec. 5-6, 2005.

2006

1) Y. Fujiwara, N. Shibata, and Y. Tanimoto, Magnetic orientation of porphyrin nano-rods in the presence and absence of strong magnetic force, 2nd International Workshop on Materials Analysis and Processing in Magnetic Fields, Mar. 19-22 (2006) Grenoble, France.
2) K. Takahashi, S. Kohtani, and R. Nakagaki, Magnetic Field and Methylene Chain Length Effects on Photochemistry of Bichromophoric Chain Species Containing 7-Nitro-2-fluorenyloxy and Anilino Chromophore, XXIst IUPAC Symposium on Photochemistry, April 2-7, Kyoto, Japan. (発表予定).
3) Y. Tanimoto, F. Koyama, K. Sueda, and M. Irie, *In situ* Observation of Laser-induced Convection in Magnetic Field Using Photochromic Reaction, XXIst IUPAC Symposium on Photochemistry, April 2-7, Kyoto, Japan. (発表予定).

解説・書籍等

2003

1) 大庭　亨, 民秋　均, 「裏表のなし裏表の話 ～平面分子の非平面性とキラリティ～」, 化学, 58 (11), 12-18 (2003).
2) Y. Tanimoto and Y. Fujiwara, Effects of High Magnetic Fields on Photochemical Reactions, in Handbook of Photochemistry and Photobiology 1, H.S. Nalwa (ed.), American Scientific Publishers, Stevenson Ranch, California, 2003, pp.413-446.

2004

1) 藤原好恒, シンクロトロン放射光を用いた円二色性スペクトルの測定, 分光研究, 52(5), 288-289 (2003)
2) 谷本能文, 高磁気力用超伝導磁石による磁場効果の研究, 信学技報 EMJC-2003-138, 73-76 (2004).
3) 若狭雅信, 谷本能文, "磁場による触媒反応の制御, 触媒, 46, 224-229 (2004).

2005

1) T. Oba, H. Tamiaki, Chirality at the central metal atoms of chlorophylls, In Photosynthesis: fundamental aspects to global perspectives (A. van der Est, and D. Bruce. eds.), pp.886-888 , Allen Press, Lawrence, KS, USA (2005).
2) H. Takatoya, A. Ugajin, H. Tobita, K. Ogura, M. Minabe, T. Oba, Syntheses and properties of novel cationic chlorophyll derivatives, In Photosynthesis: fundamental aspects to global perspectives (A. van der Est, and D. Bruce. eds.), pp.1080-1082, Allen Press, Lawrence, KS, USA (2005).
3) M. Hanasaki, M. Sato, M. Minabe, H. Tamiaki, T. Oba, Fabrication of an artificial nano-device on a design principle of photosynthetic systems, In Photosynthesis: fundamental aspects to global perspectives (A. van der Est, and D. Bruce. eds.), pp.1079-1080, Allen Press, Lawrence, KS, USA (2005).
4) K. Takahashi, Y. Itoh, M. Akiyama, T. Watanabe, K. Inoue, T. Oba, M. Umetsu, M. Kobayashi, Delicate distinction between absorption spectra of 'normal' and 'prime' bacteriochlorophylls, In Photosynthesis: fundamental aspects to global perspectives (A. van der Est, and D. Bruce. eds.), pp.46-48, Allen Press, Lawrence, KS, USA (2005).
5) Y. Tanimoto and W. Duan, Application of High Magnetic Field to Chemical and Physical Processes, in "Materials Processing in Magnetic Fields," H. Wada and H. J. Schneider-Muntau (eds.), World Scientific Publishing, Singapore, 141-146 (2005).
6) S. Anandan and M. Okazaki, Dynamics, flow motion and nanopore effect of molecules present in the MCM-41 nanopores-An overview, *Microporous and Mesoporous Materials,* **87,** 77-92, 2005.

2006

1) 谷本能文, 光化学と磁場効果, 「光科学研究の最前線」, 「光科学研究の最前線」編集委員会編, 強光子科学研究懇談会, 東京, 292-293 (2005).
2) Y. Fujiwara, in Magneto-Science, M. Yamaguchi and Y. Tanimoto (eds.), Kodansha-Springer, Tokyo, (in press).
3) R. Nakagaki and S. Kohtani, (Eds) Yamguchi, M; Tanimoto, Y., Magneto-Science, Kodansha-Springer, (in press).
4) M. Okazaki and K. Toriyama, Spin probe and spin-trapping study on the magnetic field effect on chemical reactions in the nanospace of MCM-41, in Magneto-Science, Chapter 6, Sect.3, Kodansha-Springer, (in press).

7) 谷本能文，シリケートガーデン反応の磁場効果—磁場で形態的キラリティーを誘導する—，化学と教育，54, 4-7 (2006).

(3) 研究課題ウ

雑誌論文

2003

1) Thi T. Nge, N. Hori, A. Takemura, H. Ono, and T. Kimura, Phase Behavior of Liquid Crystalline Chitin/Acrylic Acid Liquid Mixture, Langmuir 19 (2003) 1390-1395.
2) K. Tozaki, H. Inaba, H. Hayashi, C. Quan, N. Nemoto, and T. Kimura, Phase transitions of n-C32H66 measured by means of high resolution and super-sensitive DSC, Thermochimica Acta 397 (2003) 155-161.
3) Thi T. Nge, N. Hori, A. Takemura, H. Ono, and T. Kimura, Synthesis and Orientation Study of a Magnetically Aligned Liquid-Crystalline Chitin/Poly(acrylic acid) Composite, Journal of Polymer Science Part B Polymer Letters 41 (2003) 711-714.
4) T. Kimura. Study on the Effect of Magnetic Fields on Polymeric Materials and Its Application, Polymer J 35 (2003) 823-843.
5) S. Sato, H. Sakamoto, K. Mizoguchi, H. Morioka, and T. Kimura, Orientational distribution of PPy rings analyzed with g-shift anisotropy of ESR, Synth. Metals (2003) 135-136 421-422.
6) T. Kimura. Phase Transformation of Polymeric Materials in High Magnetic Field, Materials Transactions 44 (2003) 2595-2598.

2004

1) T. Kimura, M. Yamamoto and A. Nara. Particle Trapping and Undulation of Liquid Surface using Microscopically Modulated Magnetic Field, Langmuir 20 (2004) 572-574.
2) M. Tsuburaya and H. Saito, Crystallization of polycarbonate induced by spinodal decomposition in polymer blends, Polymer 45 (2004) 1027-1032.
3) S. Takahashi and H. Saito, Conformational Change of Phenyl Ring Side Group during Stress Relaxation in Glassy Poly(styrene-co-acrylonitrile), Macromolecules, 37 (2004), 1062-1066.
4) T. Oda and H. Saito, Exclusion Effect of Carbon Dioxide on the Crystallization of Polypropylene, J. Polym. Sci., Pt. B, Polym. Phys., 42 (2004) 1565-1572.
5) T. Kimura, M. Yamato, A. Nara, Particle Trapping and Undulation of a Liquid Surface Using a Microscopically Modulated Magnetic Field, Langmuir, 20 (2004) 572-574.
6) T. Kimura, M. Yoshino, T. Yamane, M. Yamato, M. Tobita, "Uniaxial Alignment of the Smallest Diamagnetic Susceptibility Axis Using Time-Dependent Magnetic Fields, Langmuir, 20 (2004) 5669-5672.
7) 山登正文，高分子プロセッシングへの磁場応用，高分子論文集，61 (2004) 433-441.
8) G. Teramoto, T. Oda, H. Saito, H. Sano, Y. Fujita, Morphology Control of Polypropylene by Crystallization under Carbon Dioxide, J. Polym. Sci., Polym. Phys. Ed., 42, (2004) 2738-2746.
9) M. Hatanaka, H. Saito, In-situ Investigation of Liquid-liquid Phase Separation in Polycarbonate/Carbon Dioxide System, Macromolecules, 37 (2004) 7358-7363.
10) Y. Miwa, K. Tanida, K. Yamamoto, S. Okamoto, M. Sakaguchi, M. Sakai, S. Makita, S. Sakurai, S. Shimada, Dynamic Heterogeneity in Interfacial Region of Microphase-Separated Polystyrene-block-poly(methyl acrylate) Studied by the ESR Spin-Label Technique, Macromolecules, 37, (2004) 3707-3716.
11) K. Sasaki, H. Nakagawa, X. Zhang, S. Sakurai, K. Kano, Y. Kuroda, Construction of porphyrin-cyclodextrin self-assembly with molecular wedge, Chem. Commun., (2004) 408-409.
12) S. Okamoto, K. Yamamoto, K. Nomura, S. Hara, I. Akiba, K. Sakurai, A. Koyama, M. Nomura, S. Sakurai, Crystallization in Microdomains of a Block Copolymer Comprising Semi-crystalline Block Observed by Simultaneous Measurement of SAXS and WAXS with Hv-SALS or DSC, J. Macromol. Sci., Physics, B43 (2004) 279-296.
13) S. Sakurai, T. Kota, D. Isobe, S. Okamoto, K. Sakurai, T. Ono, K. Imaizumi, S. Nomura, Synchrotron Small-Angle X-ray Scattering Studies on Flow-Induced Gyroid to Cylinder Transition in an Elastomeric SBS Triblock Copolymer, J. Macromol. Sci., Physics, B43 (2004) 1-11.

14) 舩井栄志、櫻井伸一、原滋郎、山本勝宏、岡本茂、小島潤一、鞠谷雄士，高速紡糸ポリエチレンテレフタレート繊維のシンクロトロンX線散乱法による精密構造解析，繊維学会誌，59 (2004) 322-330.
15) 林 京子・江島 靖和・清水 武史・木崎 寿美子・原 滋郎・山本 勝宏・岡本 茂・櫻井 伸一，小角・広角 X 線散乱／Hv 光散乱同時測定による直鎖状低密度ポリエチレン／ゴムブレンド中での結晶化挙動の解析，日本レオロジー学会誌、32, (2004) 179-187.

2005
1) T. Kimura, Y. Sato, F. Kimura, M. Iwasaka, and S. Ueno, Micropatterning of Cells Using Modulated Magnetic Fields, Langmuir 21 (2005) 2034-2037.
2) T. Kimura and M. Yoshino, Three-Dimensional Crystal Alignment Using Time-Dependent Elliptic Magnetic Field, Langmuir 21 (2005) 4805-4808.
3) N. Intawong, T. Kimura, M. Tamura, L. Xiaojun, and Sombatsompop, Magnetic Effects on Extrudate Swell of a Polystyrene Melt in Capillary Extrusion Dies, Polym. J. 37 (2005) 541-544.
4) C-K. Chang, F. Kimura, T. Kimura, H. Wada, Preparation and characterization of rod-like Eu:Gd2O3 phosphor through a hydrothermal routine, Materials Letters 59 (8-9) (2005) 1037-1041.
5) F. Kimura, T. Kimura, M. Tamura, A. Hirai, M. Ikuno, F. Horii, Magnetic Alignment of the Chiral Nematic Phase of a Cellulose Microfibril Suspension, Langmuir 21 (2005) 2034-2037.
6) Y. Jeong, K. Hanabusa, H. Masunaga, I. Akiba, K. Miyoshi, S. Sakurai, and K. Sakurai, Solvent/Gelator Interactions and Supra molecular Structure of Gel Fibers in Cyclic Bis-Urea/Primary Alcohol Organogels, 2005, Langmuir, 21 (2005) 586-594.
7) Y. Jeong, A. Friggeri, I. Akiba, H. Masunaga, K. Sakurai, S. Sakurai, S. Okamoto, K. Inoue, S. Shinkai, "Small-angle X-ray scattering from a dual-component organogel to exhibit a charge transfer interaction.", J. Colloid. Int. Sci., 283 (2005) 113-122.
8) T. Nambu, Y. Yamauchi, T. Kushiro, S. Sakurai, Micro-convection, Dissipative Structure and Pattern Formation in Polymer Blend Solutions under Temperature Gradients, Faraday Discussions, 128 (2005) 285-298.
9) 綾哲也、松田明祐、鈴木五大、福岡麻里、斎藤拓、市原祥次、石油樹脂のブレンドによるポリオレフィンの非晶構造制御と力学物性，高分子論文集、62 (2005) 579-584.
10) K. Suzuki, H. Saito, M. Tokita, and J. Watanabe, Development of co-continuous structure in liquid crystalline polyester, Polymer, 46 (2005) 8313-8320.
11) K. Maeyama, I. Hikiji, K. Ogura, A. Okamoto, K. Ogino, H. Saito, and, N.Yonezawa, Synthesis of Optically Active Aromatic Poly(ether ketone)s via Nucleophilic Aromatic Substitution Polymerization, Polym. J., 37 (2005) 707-710.
12) K. Maeyama, I. Hikiji, K. Ogura, A. Okamoto, K. Ogino, H. Saito, and N.Yonezawa, Nickel Complex-mediated Synthesis of Optically Active Wholly Aromatic Polyketones Bearing 2,2'-Dimethoxy-1,1'-binaphthy-6,6'-ene Units, Polym. J., 37 (2005) 736-741.
13) K. Maeyama, S. Maeda, K. Ogino, H. Saito, and N. Yonezawa, Synthesis of Optically Active Aromatic Poly(ether ketone)s containing 2,2'-bis(4-benzoylphnoxy)- 1,1'-binaphthyl- 6,6'-ene backbones, Reactive & Functional Polymers, 65 (2005) 229-237.

2006
1) M. Fukuoka, T. Aya, H. Saito, S. Ichihara, and H. Sano, Role of amorphous region on the deformation behavior of crystalline polymers, Polym. J. 38 (in print).
2) T. Kimura, F. Kimura, and M. Yoshino, Magnetic Alteration of Crystallite Alignment Converting Powder to a Pseudo Single Crystal, Langmuri (in print).
3) G. Piao, F. Kimura, and T. Kimura, Simultaneous Alignment and Micropatterning of Organic Crystallites Under a Modulated Magnetic Field, Langmuir (in print).
4) T. Uemura, T. Kimura, M. Sugitani, and M. Kumakura, Formation of contact holes on bumps on semiconductor chip by micro-Moses effect, Adv. Mater. (in print).
5) M. Yamato and T. Kimura, Relationship between magnetic alignment and the crystallization condition of isotactic polystyrene, Science and Technology of Advanced Materials (in print).

国際会議
2003
1) T. Oda, H. Saito, Crystallization Kinetics of Polypropylene under CO2, International Workshop on

Foam Processing & Supercritical Fluid Aided Polymer Processing, 147-148, 2003/12/5.
2) M. Hatanaka, H. Saito, Development of Modulated Structure in CO2/polycarbonate System, International Workshop on Foam Processing & Supercritical Fluid Aided Polymer Processing, 149-150, 2003/12/5.
3) T. Yabuhara, H. Saito, Molecular Motion of PMMA under Supercritical CO2, International Workshop on Foam Processing & Supercritical Fluid Aided Polymer Processing, 151-152, 2003/12/5.
4) T. Kimura, Polymer Processing under High Magnetic Fields, Pacific Polymer Conference 8 (PPC8) Nov. 24-27, (2003) Bangkok, Thailand (invited).

2004
1) M. Yamato and T. Kimura. Magnetic alignment and crystallization behavior of istactic polystyrene, International Workshop on Materials Analysis and Processing in Magnetic Fields, March 16-19 (2004) Tallahassee, USA.
2) T. Kimura and M. Yamato. Processing of polymer materials in magnetic fields, International Workshop on Materials Analysis and Processing in Magnetic Fields, March16-19, (2004) Tallahassee, USA.
3) T. Kimura, M. Yamato, Magnetic Processing of Feeble Magnetic Materials, Japan-France Cooperative Science Program Seminar on Evolving New Fields in Electromagnetic Processing of Materials, Oct. 25-27 (2004) Nara, Japan (invited).
4) S. Sakurai, E. Funai, S. Munakata, S. Okamoto, M. Yamato, and T. Kimura, Orientation of Cylindrical Microdomains of Block Copolymers under the Magnetic Fields, International Micro-symposium on Generation and Manipulation of Hierarchical Structures in Soft Materials, February 6-7 (2004) Nagoya, Japan, Abstract Book, p.1.
5) T. Kimura, Orientation of Cylindrical Microdomains of Block Copolymers under the Magnetic Field, S. Sakurai, Faraday Discussion 128, Self-Organizing Polymers, July 19-21 (2004) Leeds, UK.
6) S. Sakurai, S. Okamoto , E. Funai, M. Yamato, and T. Kimura, Effects of the Magnetic Field on Cylindrical Microdomain Structures in Polystyrene-block-poly(ethylene-co-but-1-ene)-block- polystyrene Triblock Copolymers, 日英ワークシップ, 京都大学化学研究所、April 1-24 (2004).
7) M. Shioya, T. Kawazoe, J. Kojima, S. Sakurai, Time-resolved SAXS measurements during tensile deformation of poly(ethylene terephthalate) films, PPS 2004 Polymer Processing Society Asia/Australia Meeting, Abstracts, 31-O-G6-03.

2005
1) T. Kimura, Magnetic Alignment and Patterning, EuroMagNET Workshop, June 27-28 (2005) Nijmegen, The Netherlands (invited).
2) H. Saito, Morphology Control of Polymers by Supercritical Carbon Dioxide, Harima International Forum – Smart Polymer and Smart Surface in Medicine and Industry, Center for Advanced Science and Technology, Jan. 31-Feb. 1 (2005) Hyogo, Japan.
3) S. Sakurai, E. Funai, S. Okamoto, K. Yamamoto, Effects of magnetic field on hexagonally-ordered cylindrical microdomains in triblock copolymers, 8th European Symposium on Polymer Blends and Eurofillers 2005, May 9-12, (2005) Bruge, Belgium.
4) M. Yamato, T. Kimura, Processing of crystalline polymers in a magnetic field, the 8th SPSJ International Polymer Conference, 258 (July 26-29, 2005), Fukuoka, Japan.
5) M. Iwasaka, S. Ueno, T. Kimura, F. Kimura, Cellular assembly formation under strong magnetic fields , PACIFICHEM 2005 , Prog. No. 220 (Dec. 2005), Honolulu, USA.
6) K. Uematsu, S. Tanaka, A. Makiya, Y. Hattori, N. Uchida, T. Kimura, K. Kitazawa, Y. Doshida, Crystal orientated ferroelectrics ceramics fabricated by high magnetic field , PACIFICHEM 2005 , Prog. No. 295 (Dec. 2005), Honolulu, USA.
7) T. Kimura, Magnetic field to align and pattern feeble magnetic materials, PACIFICHEM 2005, Prog. No. 510 (Dec. 2005), Honolulu, USA.
8) S. Okamoto, A. Mizutani, H. Yoshimizu, Y. Tsujita, Y. Sugino, S. Hara, K. Yamamoto, S. Sakurai, F. Kimura, M. Yamamto, T. Kimura, Orientation control of syndiotactic polystyrene containing form under the rotating magnetic field , PACIFICHEM 2005, Prog. No. 511 (Dec. 2005), Honolulu, USA.
9) M. Ichikawa, T. Kimura, Magnetic effect on the surface tension of cellulose microfibril suspension, PACIFICHEM 2005, Prog. No. 706 (Dec. 2005), Honolulu, USA.
10) T. Suzuki, T. Kimura, Viscoelastic properties of concentrated polymer solutions under magnetic field, PACIFICHEM 2005, Prog. No. 708 (Dec. 2005), Honolulu, USA.
11) T. Uemura, M. Sugitani, M. Kumakura, T. Kimura, Formation of contact holes on semiconductor

chips using micro Moses effect , PACIFICHEM 2005, Prog. No. 712 (Dec. 2005), Honolulu, USA.
12) Y. Sato, M. Iwasaka, F. Kimura, T. Kimura, S. Ueno, Micropatterning of cells using modulated magnetic field , PACIFICHEM 2005, Prog. No. 713 (Dec. 2005), Honolulu, USA.
13) T. Kamioka, T. Kimura, Micropatterning of bacterial cellulose using magnetic trapping, PACIFICHEM 2005, Prog. No. 714 (Dec. 2005), Honolulu, USA.
14) G. Piao, F. Kimura, K. Tsuda, T. Kimura, Micro - patterning and alignment of CNTs in water - soluble conducting polymers, PACIFICHEM 2005, Prog. No. 716 (Dec. 2005), Honolulu, USA.
15) M. Yamato, T. Kimura, Relationship between magnetic alignment and crystallization condition of isotactic polystyrene, PACIFICHEM 2005, Prog. No. 717 (Dec. 2005), Honolulu, USA.
16) C. Chang, F. Kimura, T. Kimura, H. Wada, Polarized photoluminescence from magnetically aligned Eu:GdPO4 - PVA composite film, PACIFICHEM 2005, Prog. No. 718 (Dec. 2005), Honolulu, USA.
17) M. Yoshino, T. Kimura, Rotating magnetic field to align the smallest magnetization axis, PACIFICHEM 2005, Prog. No. 720 (Dec. 2005), Honolulu, USA.
18) F. Kimura, T. Kimura, A. Hirai, M. Ikuno, F. Horii, Magnetic phase transition from chiral nematic phase to nematic phase for cellulose microfibril suspension, PACIFICHEM 2005, Prog. No. 722 (Dec. 2005), Honolulu, USA.
19) Y. Take, S. Nomura, M. Yamato, T. Kimura, Induced magnetic alignment of isotactic poly propylene, PACIFICHEM 2005, Prog. No. 725 (Dec. 2005), Honolulu, USA.
20) S. Sakurai, E. Funai, S. Okamoto, K. Yamamoto, Effects of magnetic field on hexagonally-ordered cylindrical microdomains in triblock copolymers, 8th European Symposium on Polymer Blends and Eurofillers 2005, May 9-12, (2005) Bruge, Belgium.
21) Y. Tsuji, S. Sakurai, K. Yamada, A. Itaya, F. Kimura, M. Yamato and T. Kimura, Effect of the High Magnetic Field on Cylindrical Microdomains in a Block Copolymer Thin Film, ISMS 2005, p. 104, Nov. 14-17 (2005) Yokohama.
22) S. Sakurai, Y. Tsuji, S. Sasaki, H. Okuda, F. Kimura, M. Yamato and T. Kimura, Grazing Incidence Small-Angle X-Ray Scattering Studies on Influence of High Magnetic Fields on a Single Nano-cylinder in a Block Copolymer Thin Film, ISMS 2005, p. 134, Yokohama, Nov. 14-17 (2005) Yokohama.
23) Y. Tsuji, E. Funai, F. Kimura, Y. Sugino, K. Yamamoto, S. Okamoto, M. Yamato, T. Kimura and S. Sakurai, Effects of strong magnetic fields on regularity and orientation of microdomains in block copolymers, The International Chemical Congress of Pacific Basin Societies (Pacifichem2005), Dec. 15-20 (2005) Honolulu.
24) Y. Sawada, H. Saito, M. Yamato, T. Kimura, Morphology control of polypropylene by magnetic field under supercritical carbon dioxide, PACIFICHEM2005, Dec. 14-18 (2005) Hawaii, USA.
25) Y. Koga, H. Saito, Porous structure of crystalline polymers by exclusion effect of carbon dioxide, PACIFICHEM2005, Dec. 14-18 (2005) Hawaii, USA.
26) K. Kawagishi, H. Saito, H. Furukawa, K. Horie, Phase separated and porous structure of polyimide gels by using supercritical carbon dioxide in drying process, PACIFICHEM2005, Dec. 14-18 (2005) Hawaii, USA.
27) A, Nishijima, H. Saito, S. Ichihara, Nano-phase structure formed by reaction induced phase separation of phenolic resin blends, PACIFICHEM2005, Dec. 14-18 (2005) Hawaii, USA.

2006
1) T. Kimura, Magnetic alignment of crystallites, 2nd International Workshop on Materials Analysis and Processing in Magnetic Fields, March 19-22 (2006) Grenoble, France (invited).
2) T. Kimura, Magnetic Alignment of Semicrystalline Polymers, Polychar14, April 17-20 (2006) Nara, Japan, Organizing member (発表予定).
3) T. Kimura, Materials Processing Under Magnetic Fields (Keynote Speaker), The 5th International Symposium on Electromagnetic Processing of Materials EPM2006, Oct. 2-6 (2006) Sendai, Japan (invited) (発表予定).

(4) 研究課題エ

雑誌論文
2004
1) T. Iiyama, Y. Kobayashi, K. Kaneko, and S. Ozeki, In Situ Small-Angle X-ray Scattering Study of

Cluster Formation in Carbon Micropores , Colloids and Surfaces A, 241, 207-213 (2004).
2) F. Ito, N. Tanaka, A. Katsuki, A. Kakehi, and T. Fujii, Synthesis and characterization of flavylium salts having three types color depending on recrystallization conditions, Research on Chemical Intermediates, 30(3), 331-336 (2004).
3) F. Ito, N. Tanaka, A. Katsuki, T. Fujii, Modulation of color changing paths for flavylium salts by solvent and concentration, J. Photochem. Photobiol. A: Chem., 161, 111-118 (2004).
4) A. Katsuki, I. Uechi, Y. Tanimoto, Effects of a high magnetic field on the growth of 3-dimensional silver dendrites, Bull. Chem. Soc. Jpn., 77(2), 275-279 (2004).
5) I. Uechi, A. Katsuki, L. Dunin-Barkovsky, Y. Tanimoto, 3D-Morphological Chirality Induction in Zinc Silicate Membrane Tube Using a High Magnetic Field, J. Phys. Chem. B, 108(8), 2527-2530 (2004).

2005
1) A. Katsuki, Y. Tanimoto, Precession of Silver Dendrites in a Magnetic Field Due to MHD Induced Convection, Chem. Lett. 34(5), (2005) 726-727.
2) A. Katsuki, I. Uechi, Y. Tanimoto, The Magnetic Orientation of 2-Dimensional Silver Dendrites, Bull. Chem. Soc. Jpn. 78(7), (2005) 1251-1255.
3) W. Duan, S. Kitamura, I. Uechi, A. Katsuki, Y. Tanimoto, Three-Dimensional Morphological Chirality Induction Using High Magnetic Fields in Membrane Tubes Prepared by a Silicate Garden Reaction, J. Phys. Chem. B 109(28), (2005) 13445-13450.
4) 大塚伊知郎，福井克彦，中川和典，尾関寿美男，中山武典，細木哲郎，佐伯主税，りん脱酸銅の水ぬれ性におよぼす磁気処理の影響，銅と銅合金，44, 196-200 (2005).
5) T. Iiyama, Y. Kobayashi, A. Matsumoto, Y. Nakahigashi, S. Ozeki, Structural Study of $CHCl_3$ Molecular Assemblies in Micropores Using X-ray Techniques, Adsorption, 11, 169-172 (2005).

2006
1) I. Otsuka and S. Ozeki, Does magnetic treatment of water change its properties?, J. Phys. Chem. B, 1509-1512 (2006).
2) F. Tang, A. Katsuki, Y. Tanimoto, Effect of High Magnetic Field on a Quasi-3D Silver Dendrite Growing System, Mol. Phys. in press.
3) A. Katsuki, S. Aibara, Y. Tanimoto, Crystal morphology change by magnetic susceptibility force, Science Technology of Advanced Materials, (in press).
4) I. Otsuka, H. Abe, and S. Ozeki, Magnetic field control of Structure and Function of poly(N-isopropylacrylamide) gels, Sci. and Technol. Adv. Mater., (in press).

国際会議
2003
1) S. Ozeki, I. Ohtsuka, H. Kawasaki, H. Maeda, Induced Volume Phase Transition of Hydrogels prepared under Steady Magnetic Fields, ISSP International Workshop 5th Gel Symposiumu Polymer Gels; Fundamentals and Nano-Fabrications, November 17-21 (2003), Kashiwa, Japan.
2) I. Otsuka, T. Takahashi, Y. Yaguchi, S. Ozeki, Magnetic field control of structures and properties of diamagnetic molecular assemblies, International Workshop on Materials Analysis & Processing in Magnetic Fields, March 16-19 (2004) Tallahassee, USA
3) A. Katsuki, N. Matsumoto, H. Nishikiori, N. Tanaka, T. Fujii, Study of the electron transfer reaction in gel thin layers prepared by a dip-coating method, XXIst International Conference on Photochemistry (ICP21), July 26-31 (2003) Nara.
4) A. Katsuki, I. Uechi, Y. Tanimoto, Effects of a high magnetic field on the growth of silver dendrites", The 8th International Symposium on Spin and Magnetic Field Effects in Chemistry and Related Phenomena, Sep. 21-26, (2003) USA.
5) I. Uechi, A. Katsuki, L. Dunin-Barkovskiy, Y. Tanimoto, Magnetic chirality induction in zinc silicate membrane tube morphology, The 8th International Symposium on Spin and Magnetic Field Effects in Chemistry and Related Phenomena, Sep. 21-26, (2003) USA.

2004
1) S. Ozeki, T. Takahashi, Y. Yaguchi, and K. Fukui, Deformation and Transformation of Molecular Organized Structures due to Magnetic Fields, The 2004 Japan-Australia International Symposium, September 9-11 (2004), Yamaguchi, Japan.

2) I. Otsuka, and S. Ozeki, Control of Structure and Physical Properties of Hydrogels due to Steady Magnetic Fields, The 2004 Japan-Australia International Symposium, September 9-11 (2004), Yamaguchi, Japan.
3) A. Katsuki, T. Komatsu, Y. Takeda, M. Okamoto, T. Joh, H. Nishikiori, N. Tanaka, T. Fujii, Photolysis of dimethylphthalate and cyclohexane by xenon light, XX IUPAC Symposium on photochemistry, July 17-22 (2004) Granada, SPAIN.
4) A. Katsuki, Y. Tanimoto, H. Nishikiori, N. Tanaka, Morinobu Endo, and Tsuneo Fujii, Trial of control on the orientation of carbon nanofibres by high magnetic field, International symposium on nanocarbons, November 15-18 (2004) Nagano.

2005
1) T. Iiyama, T. Urushibara, Y. Nakahigashi, S. Ozeki, The direct determination of intermolecular structure of adsorbed phase using in situ XRD and reverse Monte-Carlo method, 7th International Symposium on the Characteris of Porous Solids, May 26-28 (2005) Aix en Provence, France.
2) A. Katsuki, Y. Tanimoto, Precession of silver dendrites under a high magnetic field, 9th Int. Symp. on Spin and Magnetic Field Effects in Chemistry and Related Phenomena, Sep. 11-17 (2005) St. John's College and Physical & Theoretical Chemistry Laboratory, University of Oxford, United Kingdom.
3) W. Duan, S. Kitamura, I. Uechi, A. Katsuki, Y. Tanimoto, Three-dimensional morphological chirality induction using high magnetic field in membrane tubes prepared by silicate garden reaction, 9th Int. Symp. on Spin and Magnetic Field Effects in Chemistry and Related Phenomena, Sep. 11-17 (2005) St. John's College and Physical & Theoretical Chemistry Laboratory, University of Oxford, United Kingdom.
4) A. Katsuki, Y. Tanimoto, Rotational motion of silver dendrites under magnetic field, Int. Symp. on magnetic field effects on materials, Nov. 11-12 (2005) Tokyo.
5) A. Katsuki, Y. Tanimoto, Proposal of a new type of magnetic force, Int. Symp. on magnetic field effects on materials, Nov. 11-12 (2005) Tokyo.
6) Y. Tanimoto, I. Uechi, W. Duan, A. Katsuki, 3D-morphological chirality induction in membrane tubes prepared by silicate garden reaction in magnetic field, Int. Symp. on magnetic field effects on materials, Nov. 11-12 (2005) Tokyo.
7) K. Sueda, F. Koyama, M. Irie, A. Katsuki, Y. Tanimoto, In situ observation of laser-induced convection of water in magnetic field, Int. Symp. on magnetic field effects on materials, Nov. 11-12 (2005) Tokyo.
8) T. Takahashi, Y. Yaguchi, M. Ishii and S. Ozeki, Molecular Assemblies under Steady Magnetic Fields: Membranes, Micelles and Vesicles, International Symposium on Magneto-Science 2005, Nov. 14-17 (2005) Yokohama.
9) A.Yoshidome, S. Sasahara, T. Iiyama and S. Ozeki, Magnetoadsorption of Gases on Porous Materials, International Symposium on Magneto-Science 2005, Nov. 14-17 (2005) Yokohama.
10) I. Otsuka and S. Ozeki, Magnetic-Field-Induced Structures and Functions of Hydro gels, International Symposium on Magneto-Science 2005, Nov. 14-17 (2005) Yokohama.
11) Y. Yamane and S. Ozeki, Structural Control of Mesoporous Silicas by Magnetic Fields, International Symposium on Magneto-Science 2005, Nov. 14-17 (2005) Yokohama.
12) T. Iiyama, T. Urushibara, S. Ozeki, The Direct Determination of Intermolecular Structure of Molecular Assemblies in a Nanospace Using in situ XRD and Reverse Monte Carlo Method, 8th Japan-Australia Colloid and Interface Science Gakkai, Nov. 27-30 (2005) Terrigal, Australia.
13) I. Otsuka, S. Ozeki, Hydrogels Deformed by Steady Magnetic Fields, 8th Japan-Australia Colloid and Interface Science Gakkai, Nov. 27-30 (2005) Terrigal, Australia.
14) S. Ozeki, Magnetic field control of structures and functions of organized molecular systems, Pacifichem 2005, Dec. 15-20, (2005) Honolulu, USA.
15) K. Fujio, T. Miyazawa, K. Kobayashi, S. Ozeki, Effects of added salts on adsorbed films and aggregates of crown-ether surfactant, Pacifichem 2005, Dec. 15-20, (2005) Honolulu, USA.
16) I. Otsuka, S. Ozeki, Novel structures and functions of organic gels induced by steady magnetic fields, Pacifichem 2005, Dec. 15-20, (2005) Honolulu, USA.
17) I. Otsuka, K. Fukui, K. Nakagawa, T. Nakayama, T. Hosogi, C. Saeki, S. Ozeki, Is there a magnetized water? Examination from a viewpoint of surface chemistry, Pacifichem 2005, Dec. 15-20, (2005) Honolulu, USA.
18) S. Sasahara, A. Yoshidome, T. Iiyama, K. Tange, S. Ozeki, Magnetic field effect on hydrogen adsorption near critical point, Pacifichem 2005, Dec. 15-20, (2005) Honolulu, USA.
19) G Saravanan, K. Fujio, S. Ozeki, Electron-transfer reaction of redox ion-pairs on gold electrode surfaces: Tunneling process and its magnetic-field control, Pacifichem 2005, Dec. 15-20, (2005) Honolulu,

USA.
20) A. Katsuki, Y. Tanimoto, Unique motion of silver dendrites in a magnetic field, Pacifichem 2005, Dec. 15-20, (2005) Honolulu, USA.
21) Y. Tanimoto, W. Duan, S. Kitamura, I. Uechi, A. Katsuki, Magnetic induction of 3D-morphological chirality of membrane tubes prepared by silicate garden reaction, Pacifichem 2005, Dec. 15-20, (2005) Honolulu, USA.

2006
1) S. Ozeki (invited), Structural Control of Organized Molecular Assemblies due to Magnetic Fields, the 16th symposiums on Surfactants in Solutions, June 4-9, 2006, Seoul, Korea.(発表予定)
2) T. Iiyama, T. Urushihara, K. Hagi, Y. Nakahigashi, S. Ozeki, Direct determination of intermolecular structure of adsorbed phase in micropore by using X-ray diffraction and reverse Monte Carlo method , Characterization of Porous Materials: From Angstroms to Millimeters, June 21-23,2006, Princeton, USA. (発表予定)
3) T. Iiyama, T. Urushihara, N. Katsu, Y. Nakahigashi, S. Ozeki, The study of intermolecular structure of binary adsorbed molecules by XRD, Characterization of Porous Materials: From Angstroms to Millimeters, June 21-23,2006, Princeton, USA. (発表予定)
4) T. Iiyama, K. Hagi, Y. Nakahigashi, S. Ozeki, Intermolecular structure of adsorbed ethanol in a micropore at low temperature, Characterization of Porous Materials: From Angstroms to Millimeters, June 21-23,2006, Princeton, USA. (発表予定)
5) Y. Matsumura, T. Iiyama, S. Ozeki, Determination of heat of adsorption and kinetic constant by temperature stimulation pressure response method, Characterization of Porous Materials: From Angstroms to Millimeters, June 21-23,2006, Princeton, USA. (発表予定)
6) Akio Katsuki, Mari Miyata, Eri Komagome, Hiromasa Nishikiori, Nobuaki Tanaka, Tsuneo Fujii, Hiroaki Horiuchi, Hiroshi Hiratsuka and Shozo Tero-Kubota, Photolysis of cyclohexane by xenon light, XXIst IUPAC Symposium on Photochemistry, April 2-7 (2006) Kyoto.

解説・書籍等
2004
1) 尾関寿美男，磁気科学と材料，未来材料，4 (11)，42-49 (2004).

2005
1) I. Otsuka, T. Takahashi, Y. Yaguchi, H. Abe, S. Ozeki, Magnetic Field Control of Structures and Properties of Diamagnetic Molecular Assemlies, Materials Processing in Magnetic Fields, 330-336 (2005).

2006
1) S. Ozeki and K. Fujio, Magnetic field controls of molecular assemblies and gels, in Magneto-Science, Kodansha-Springer, 2005, (in press).
2) S. Ozeki and T. Iiyama, Magnetic field effects on adsorption of gas, in Magneto-Science, Kodansha-Springer, 2005, (in press).

(5) 研究課題オ

雑誌論文
2003
1) T. Takayama, Y. Ikezoe, H. Uetake, N. Hirota, and K. Kitazawa, , Control of alignment of feeble magnetic particles utilizing induced magnetic dipole interactions Trans. Mater. Res. Soc. Jpn. 28 (2003) 231-233
2) T. Takayama, Y. Ikezoe, H. Uetake, N. Hirota, and K. Kitazawa, Interactions among magnetic dipoles induced in feeble magnetic substances under high magnetic fields, J. Mag. Soc. Jpn. 27 (2003) 299-302

2004
1) N. Hirota, M. Kurashige, M. Iwasaka, M. Ikehata, H. Uetake, T. Takayama, H. Nakamura, Y. Ikezoe, S.

Ueno, H. Wada, and K. Kitazawa, Magneto-Archimedes separation and its application to the separation of biological materials, Physica B 346-347, (2004) 267-271.
2) T. Takayama, Y. Ikezoe, H. Uetake, N. Hirota, and K. Kitazawa, Interactions among magnetic dipoles induced in feeble magnetic substances under high magnetic fields, Physica B 346-347, (2004) 272-276.
3) O. Ozaki, T. Kiyoshi, S. Matsumoto, J. Fujihira and H. Wada, Development of a magnetic force booster, IEEE Trans. Appl. Supercond. 14 (2004) 1663-1665.
4) S. Matsumoto, T. Asano, T. Kiyoshi and H. Wada, Magnetic flux concentration using YBCO hollow and solid cylinders, IEEE Trans. Appl. Supercond. 14 (2004) 1666-1669.
5) S. Matsumoto, T. Kiyoshi, T. Asano, A, Sato and H. Wada, Comprehensive applications of high magnetic fields at TML, Physica B 346-347 (2004) 633-637.
6) Y. Shimazu and T. Yokoyama, Measurement of kinetic inductance of superconductingting wires and application for measuring flux state of Josephson-junction loops, Physica C, 412-414 (2004) 1451-1454.

2005
1) S. Mizusaki, T. Miyatake, N. Sato, I. Yamamoto, M. Itou, Y. Sakurai and M. Yamaguchi, Magnetic Compton scattering studies of the electrochemically hydrogenated nickel, Jpn. J. Appl. Phys.44 (2005) 3939-3944.
2) S. Mizusaki, T. Miyatake, N. Sato, M. Itou, I. Yamamoto, Y. Sakurai and M. Yamaguchi, Experimental determination of the $PdH_{0.84}$ Fermi surface, J. Alloys Compd. 404-406 (2005) 169-171.
3) N. Hirota, T. Takayama, E. Beaugnon, Y. Saito, T. Ando, H. Nakamura, S. Hara, Y. Ikezoe, H. Wada, K. Kitazawa, Control of structures of feeble magnetic particles by utilizing induced magnetic dipoles, Journal of Magnetism and Magnetic Materials, 293 (2005) 87-92.
4) T. Takayama, Y. Ikezoe, H. Uetake, N. Hirota, K. Kitazawa, Self-Organization of nonmagnetic spheres by magnetic field, Applied Physics Letters, 86 (2005) 234103.
5) H. Nakamura, T. Takayama, H. Uetake, N. Hirota, K. Kitazawa, Magnetically Controlled Convection in a Diamagnetic Fluid, Physical Review Letters, 94 (2005) 144501.
6) M. Takeda, Y. Okuji, T. Akazawa, X. Liu and T. Kiyoshi, Fundamental studies of helical-type seawater MHD generation system , IEEE Trans. Appl. Superconduct. 15 (2005) 2170-2173.
7) T. Asano, K. Itoh, S. Matsumoto, T. Kiyoshi, H. Wada and G. Kido, Enhanced concentration of the magnetic flux in a superconducting cylinder, IEEE Trans. Appl. Superconduct. 15 (2005) 3157-3160.
8) Y. Shimazu, Y. Wada, T. Niizeki, Y. Yamamoto, T. Yoshida, Z. Wada and T. Yokoyama, Observation of excitation in asymmetric flux qubits coupled inductively, Physica E, 29/3-4 (2005) 679-683.

2006
1) N. Hirota, S. Hara, H. Uetake, H. Nakamura, K. Kitazawa, In situ microscopic observations of an electroless silver deposition process under high magnetic fields, Journal of Crystal Growth, 286 (2006) 465-469.
2) N. Hirota, T. Ode, Development of a periscopic confocal microscope for in situ observation under high magnetic fields, Review of Scientific Instruments, 77 (2006) 036107.
3) S. Mizusaki, T. Miyatake, N. Sato, I. Yamamoto, M. Yamaguchi, M. Itou and Y. Sakurai, Electron momentum density and the Fermi surface of palladium hydride by Compton scattering, Phys. Rev. B 73 (2006) 113101
4) I. Yamamoto, T. Makino and M. Yamaguchi, The anisotropic properties of magnetically ordered gel, Science and Technology of Advanced Materials (in print).
5) Y. Ito, R. Takahashi, S. Mizusaki, I. Yamamoto and M. Yamaguchi, Magnetic field effects on the hydrogen isotope separation with metal hydrides, Science and Technology of Advanced Materials (in print).
6) T. Ando, N. Hirota, A. Sato, E. Beaugnon, Experiment and numerical simulation of interactions among magnetic dipoles induced in feeble magnetic substances under high magnetic field, Journal of Magnetism and Magnetic Materials, (in print).
7) Y. Shimazu, T. Niizeki, Y. Wada, Fabrication and characterization of a switchable flux transformer using a DC-SQUID, Physica C (2006) (in print).

国際会議
2003
1) N. Hirota, M. Kurashige, M. Iwasaka, M. Ikehata, H. Uetake, T. Takayama, H. Nakamura, Y. Ikezoe, S. Ueno, H. Wada, and K. Kitazawa, Magneto-Archimedes separation and its application to the separation of

biological materials, 7th International Symposium of Research in High Magnetic Fields, Jul. 20-23 (2003) Toulouse, France.
2) T. Takayama, Y. Ikezoe, H. Uetake, N. Hirota, and K. Kitazawa, Interactions among magnetic dipoles induced in feeble magnetic substances under high magnetic fields, 7th International Symposium of Research in High Magnetic Fields, Jul. 20-23 (2003) Toulouse, France.
3) N. Hirota, H. Uetake, T. Takayama, H. Nakamura, M. Kurashige, Y. Ikezoe, H. Wada, and K. Kitazawa, Magneto-Archimedes separation as a novel way of materials recycling, 4th International conference on Electromagnetic Processing of Materials, Oct. 13-17 (2003) Lyon, France.
4) N. Hirota, H. Uetake, T. Takayama, Y. Ikezoe, H. Wada, and K. Kitazawa, Magnetic field effects on feeble magnetic materials and their applications, 4th International conference on Electromagnetic Processing of Materials, Oct. 13-17 (2003) Lyon, France (Invited).
5) T. Takayama, Y. Ikezoe, H. Uetake, N. Hirota, and K. Kitazawa, A novel way of controlling materials structures by magnetic fields, 4th International conference on Electromagnetic Processing of Materials, Oct. 13-17 (2003) Lyon, France.
6) S. Matsumoto, T. Asano, T. Kiyoshi, and H. Wada, Magnetic flux concentration using YBCO hollow and solid cylinders, 18th International Conference on Magnet Technology, Oct 20-24 (2003) Morioka.
7) O. Ozaki, T. Kiyoshi, S. Matsumoto, J. Fujihira, and H. Wada, Development of a magnetic force booster, 18th International Conference on Magnet Technology, Oct. 20-24 (2003) Morioka.
8) Y. Shimazu, T. Yokoyama, Estimate of kinetic inductance of superconductcting wires and application for measuring flux State of Josephson-junction loops, The 16th International Symposium on Superconductivity, Oct.28 (2003), Tsukuba.

2004

1) M. Yamaguchi and I. Yamamoto, Magneto-Chemical Systems under Strong Magnetic Fields: Fundamentals and Applications, International workshop on materials analysis and processing in magnetic fields, Mar. 17-19 (2004) Tallahassee, USA.
2) N. Hirota, H. Uetake, T. Takayama, H. Nakamura, M. Kurashige, S. Hara, Y. Saito, Y. Ikezoe, T. Ando, H. Wada, and K. Kitazawa, Effects of magnetic fields on feeble magnetic materials, International workshop on materials analysis & processing in magnetic fields, Mar. 17-19 (2004) Tallahassee, USA.
3) M. Ogura, S. Iwai, Y. Zhang, J. Otomo, H. Takahashi, N. Hirota, T. Okubo, Toward the preparation of aligned mesopores perpendicular to the substrate using magnetic field, 4th International Mesostructured Materials Symposium May 1-4 Cape town, South Africa.
4) M. Yamaguchi, S. Mizusaki, T. Miyatake, N. Sato, I. Yamamoto, M. Itou and Y. Sakurai, Electronic states in palladium hydrides studied by Compton scattering, HTM2004, 2005 May 17-21, Donetsk, Ukraine.
5) N. Hirota, T. Takayama, Y. Saito, T. Ando, H. Uetake, H. Nakamura, S. Hara, Y. Ikezoe, H. Wada, K. Kitazawa, Control of the Structure of Feeble Magnetic Particles by Using Induced Magnetic Dipole Interactions, 5th International Conference on the Scientific and Clinical Applications of Magnetic Carriers, May 20-22 (2004) Lyon, France.
6) I. Yamamoto, S. Mizusaki, Y. Itoh and M. Yamaguchi, Isotope Effects on the Equilibrium Pressure of the RCo5-Based Hydrides and Deuterides, 15th WHEC, 30B-07, June 27-July 2, Yokohama, Japan.
7) S. Mizusaki, N. Sato, I. Yamamoto, M. Itou, M. Sakurai, M. Yamaguchi, Electronic States of Hydrogen in Metal hydrides Studied by Compton Scattering, 15th WHEC, 29B-08, June 27-July 2, Yokohama, Japan.
8) S. Mizusaki, T. Miyatake, N. Sato, M. Itou, I. Yamamoto, Y. Sakurai, M. Yamaguchi, Experimental determination of the PdH Fermi surface, Int. Symp. Metal-hydrogen Systems, Abs. Th-082, pp. 152, Sept. 5-10, Cracow, Poland.
9) N. Sato, S. Mizusaki, M. Itou, I. Yamamoto, Y. Sakurai, M. Yamaguchi, Compton scattering studies of the electronic structure for vanadium deuteride, Int. Symp. Metal-hydrogen Systems, Abs. Th-100, pp. 157, Sept. 5-10, Cracow, Poland.
10) N. Hirota, H. Uetake, T. Takayama, H. Nakamura, S. Hara, Y. Saito, T. Ando, Y. Ikezoe, H. Wada, K. Kitazawa, Effects of Magnetic Force on Feeble Magnetic Materials and their Applications -Levitation, Materials Separation, control of physicochemical processes and self organization of particles-, Workshop on Magnetic Forces in Bio- and Nanotechnologies, Sept. 16-18 (2004) Riga, Latvia.
11) T. Asano, K. Itoh, S. Matsumoto, T. Kiyoshi and H. Wada, Enhanced concentration of the magnetic flux in a superconducting cylinder, ASC 2004, Oct. 3-8 (2004) Jacksonville, U.S.A.
12) M. Takeda, Y. Okuji, T. Akazawa, X. Liu and T. Kiyoshi, Fundamental studies on helical-type

seawater MHD generation system, ASC 2004, Oct. 3-8 (2004) Jacksonville, U.S.A.
13) N. Hirota, H. Uetake, T. Takayama, H. Nakamura, M. Kurashige, S. Hara, Y. Saito, Y. Ikezoe, T. Ando, K. Kitazawa, Effects of Magnetic fields on feeble magnetic substances, Japan-France cooperative science program seminar on Evolving New Fields in Electromagnetic Processing of Materials, Oct. 4-7 (2004) Kyoto, Japan (Invited).
14) X. Liu, T. Kiyoshi and M. Takeda, A simulation on a seawater MHD power generation system, Asian Conference 2004 on Applied Superconductivity and Cryogenics, Dec. 13-14 (2004) Miyazaki, Japan.

2005

1) T. Ando, N. Hirota, A. Sato, E.Beaugnon, Experiment and Numerical Analysis of Magnetic Dipole Interactions among Magnetic Substances under High Magnetic Field, the Joint 15th Riga and 6th pamir International Conference on Fundamental and Applied MHD, June 27-July 1 (2005), Riga, Latvia.
2) H. Okada, H. Okuyama, M. Uda, N. Hirota, Removal of aerosol by magnetic separation, 19th International Conference on Magnet Technology, Instito Nazionale di Fisica Nucleare, Sept.18-23 (2005) Genova, Italy.
3) Y. Ito, R. Takahashi, S. Mizusaki, I. Yamamoto, T. Takamasu and M. Yamaguchi, Magnetic Field Effect on Hydrogen Isotope Separation with Metal Hydrides, ISMS2005, Nov. 15 (2005), Abs. 2P13, p. 81, Yokohama, Japan.
4) S. Kittaka, T. Takeda, I. Yamamoto and M. Yamaguchi, In situ optical measurement of agarose aqueous solution, ISMS2005, Nov. 15 (2005), Abs. 2P15, p. 83, Yokohama, Japan.
5) T. Takeda,T. Kogawa, I. Yamamoto and M. Yamaguchi, Magnetimigration of a Single Paramagnetic Ion, ISMS2005, Nov. 15 (2005), Abs. 2P34, p. 102, Yokohama, Japan.
6) T. Makino,K. Ogawa, I. Yamamoto and M. Yamaguchi, Magnetic Field Effect on viscoelasticity of agarose gels, ISMS2005, Nov. 16 (2005), Abs. 3P20, p. 126, Yokohama, Japan.
7) K. Suzuki, K. Yoshida, I. Yamamoto, M. Yamaguchi and T. Takamasu, DNA Electrophoresis under Strong Magnetic Fields, ISMS2005, Nov. 16 (2005), Abs. 3P31, p. 137, Yokohama, Japan.
8) I. Yamamoto and M. Yamaguchi, Anisotropic Properties of Magnetic Ordered Gel, ISMS2005, Nov. 17 (2005), Abs. 4O03, p. 63, Yokohama, Japan.
9) N. Hirota, S. Hara, H. Uetake, H. Nakamura, In situ microscopic observation of magnetic field effects on the growth process of two-dimensional silver dendrites, International Symposium on Magneto-Science 2005,Nov. 14-17 (2005), Yokohama, Japan.
10) T. Kiyoshi, T. Koizumi, X. Liu and S. Matsumoto, Magnetic force enhancement using an HTS bulk cylinder, ISMS 2005, 1O12, Nov. 14-17 (2005) Yokohama.
11) X. Liu and T. Kiyoshi, Optimization on solenoid coils for magnetic force enhancement, ISMS 2005, 3P18, Yokohama, Nov. 14-17 (2005) Yokohama.
12) Y. Shimazu, Control of a switching current of a DC-SQUID with an electric current in comparison with control with magnetic field, ISMS, 2P 30, Nov. 14-17 (2005), Yokohama.
13) I. Yamamoto, T. Makino and M. Yamaguchi, Anisotropic properties of magnetically ordered gel, Pacifichem2005, Dec. 16 (2005), Hawaii, USA.
14) M. Yamaguchi and I. Yamamoto, Magnetic field effect on hydrogen isotope separation with metal hydrides, Pacifichem2005, Dec. 18 (2005), Hawaii, USA.
15) N. Hirota, T. Takayama, T. Ando, E. Beaugnon, Y. Saito, H. Nakamura, S. Hara, Y. Ikezoe, Structure control of feeble magnetic materials by magnetic fields, Pacifichem 2005, 2005.12.15-2005.12.20, Honolulu, Hawaii, USA (Invited).
16) Y. Shimazu, T. Niizeki, Y. Wada, Fabrication and characterization of a switchable flux transformer using a DC-SQUID, 18th International Symposium on Superconductivity, Oct. 26 (2005), Tsukuba.

2006

1) M. Yamaguchi, T. Takeda, T. Kogawa and I. Yamamoto, Magnetomigtration of paramagnetic ions, 2nd I. Workshop on Materials Analysis and Processing in Magnetic Fields, March 19-22 (2006) Grenoble, France.
2) I. Yamamoto, K. Suzuki, K. Yoshida, T. Fushimi and M. Yamaguchi, Electrophoresis of DNA in Magnetic Fields, 2nd I. Workshop on Materials Analysis and Processing in Magnetic Fields, March 19-22 (2006) Grenoble, France.
3) N. Hirota, K. Yokoyama, Magneto-Archimedes separation of biological materials and its application, March 19-22, (2006) Grenoble, France.
4) T. Okano, H. Nakamura, N. Hirota, Control of the convection of diamagnetic fluid by static high

magnetic fields, March 19-22, (2006) Grenoble, France.
5) S. Matsumoto, T. Kiyoshi, T. Asano, T. Koizumi, X. Liu and H. Okada, Magnet developments for Magneto-Science at Tsukuba Magnet Laboratory, IWMAP2, March 19-22 (2006) Grenoble, France.
6) T. Kiyoshi, T. Koizumi, X. Liu and S. Matsumoto, Magnetic force field enhancement by field cooling of HTS bulk cylinder, ASC 2006, Aug. 27-Sep. 1 (2006) Seattle, USA (発表予定).
7) S. Matsumoto, J. Fujihira, T. Kiyoshi and H. Okada, Development of workbench magnet, ASC 2006, Aug. 27-Sep. 1 (2006) Seattle, USA (発表予定).
8) Y. Shimazu, T. Niizeki, Characteristics of a switchable superconducting flux transformer using a DC-SQUID, International Symposium on Mesoscopic Superconductivity and Spintronics MS+S 2006, Oct. 28 (2006), Atsugi (発表予定).

解説・書籍等

2004

1) 廣田憲之、反応場制御による新しい材料プロセッシング —協奏増幅を利用した材料創製—, アイピーシー、Jan. 20 (2004) (部分執筆).

2005

1) 山本勲、磁場配向ゲル、高分, 54(7), July 1 (2005) pp. 482.
2) N. Hirota, H.Uetake, T. Takayama, H. Nakamura, M. Kurashige, S.Hara, Y. Saito, Y. Ikezoe, T. Ando, H.Wada, K. Kitazawa, Effects of magnetic fields on feeble magnetic materials, pp.269-277 in Materials Processing in Magnetic Fields, , H. Wada and H. J. Schneider-Muntau Eds., World Scientific, Singapore (2005).
3) O. Ozaki, S. Matsumoto, T. Kiyoshi and H. Wada, Generation of Uniform Magnetic Force Field, pp.352-359 in Materials Processing in Magnetic Fields, , H. Wada and H. J. Schneider-Muntau Eds., World Scientific, Singapore (2005).
4) M. Yamaguchi and I. Yamamoto, Magneto-chemical systems under strong magnetic fields, pp.147-154, in Materials Processing in Magnetic Fields, , H. Wada and H. J. Schneider-Muntau Eds., World Scientific, Singapore (2005).

2006

1) 山本勲, 山口益弘, 有機高分子ゲルの磁場効果—寒天ゲルを強磁場でそろえる, 変える, 探る、化学と教育、54, 16-19 (2006).
2) 廣田憲之、木吉 司、横山和哉、物質の磁気的性質を視覚的に理解するためのデモンストレーションに関する検討, 化学と教育, 54, 166-169 (2006).
3) N. Hirota, Magneto-Archimedes effect and related phenomena, in Magneto-Science, Kodansha-Springer, (in press).
4) T. Kiyoshi, High field generation for magnetic processing, in Magneto-Science, Kodansha-Springer, (in press).
5) I. Yamamoto, Magnetic alignment of polymer gels, in Magneto-Science, Kodansha-Springer, (in print).
6) M. Yamaguchi and Y. Tanimoto, eds. Magneto-Science, Kodansha-Springer, (in press).

(6) 研究課題カ

雑誌論文

2003

1) T. Sakamoto, T. Fukuda, T. Kakeshita, T. Takeuchi and K. Kishio, Magnetic field-induced strain in iron-based ferromagnetic shape memory alloys, J. Appl. Phys. 93 (2003), 8647-8649.
2) T. Terai, H. Fujita, T. Murata, T. Kakeshita, T. Fukuda and K. Kishio, Magnetoresistance of La0.7Ca0.3MnO3 single crystal and polycrystalline, Transactions of the Materials Research Society of Japan, 28[2] (2003), 243-244.
3) T. Fukuda, T. Inoue, T. Kakeshita, T. Takeuchi K. Kishio, Temperature dependence of magnetic field-induced strain of Fe3Pt, Transactions of the Materials Research Society of Japan, 28[2] (2003), 249-250.
4) T. Sakamoto, T. Fukuda, T. Kakeshita, T. Takeuchi and K. Kishio, Crystallographic orientation

dependence of magnetic field-induced strain in an Fe-31.2Pd alloy, Transactions of the Materials Research Society of Japan, 28[2] (2003), 247-248.
5) N. Okamoto, Y. Nakamura, T. Fukuda, T. Kakeshita, T. Inoue and K. Kishio, Magnetic field-induced strain of ferromagnetic shape memory Ni2MnGa shape memory alloy, Transactions of the Materials Research Society of Japan, 28[2] (2003), 245-246.
6) 福田隆、掛下知行，鉄基強磁性形状記憶合金における磁場によるマルテンサイトバリアントの再配列と巨大歪，熱処理 43 (2003) 137-142.
7) T. Kakeshita and T. Fukuda, Conversion of Variants by Magnetic Field in Iron-Based Ferromagnetic Shape Memory Alloys, Materials Science Forum, 426-432 (2003), 2309-2314.
8) T. Fukuda, T. Sakamoto, T. Terai, T. Kakeshita and K. Kishio, Stability of B2-type structure and martensitic transformation in Ti-Ni shape memory alloys, J. Phys. IV France 112 (2003),685-688.
9) T. Kakeshita, T. Fukuda, T. Terai, T. Takeuchi and K. Kishio, Martensitic Transformation in Fe-based shape memory alloys under magnetic field, J. Phys. IV France 112 (2003), 93-100.
10) T. Sakamoto, T. Fukuda, T. Kakeshita, T. Takeuchi and K. Kishio, Influence of magnetic field direction on rearrangement of martensite variants in an Fe-Pd alloy, Mater. Trans. 44 (2003), 2495-2498.
11) T. Murata, T. Terai, T. Fukuda, T. Kakeshita and K. Kisho, Influence of grain boundary on magnetoresistance in hole doped manganites La0.7Ca0.3MnO3, La0.7Sr0.3MnO3 and (La0.75Y0.25)0.7Sr0.3MnO3, Mater. Trans. 44 (2003), 2589-2593
12) S. Yoshii, H. Nakanishi, T. Kakeshita and K. Kindo, Metamagnetism and magnetic phase diagrams of intermetallic compound DyAg, Mater. Trans. 44 (2003), 2582-2588.
13) T. Ohba, T. Fukuda, T. Tabata and T. Kakeshita, Neutron Scattering study on equi-atomic TiNi alloy, J. Phys. IV France 112 (2003), 639-642.
14) C.Uyeda, K.Tanaka and R.Takashima, Stabilization of the Position of a Solid Body isolated in Micro-Gravity and Field Induced Rotational Oscillation Caused by Diamagnetic Anisotropy Jpn.J. Appl. Phys., 42,(2003) L1236-1228.
15) C.Uyeda and K.Tanaka, Effective parameters on the magnetic alignment process of nonmagnetic inoroganic micro-crystals dispersed in a fluid medium, Trans.Mater.Res.Soc.Jpn.,28 (2003) 227-230.
16) C.Uyeda and K.Tanaka, Diamagnetic Anisotropy of Inorganic Oxides Correlated with the Directions of Chemical Bonds, J. Phys. Soc. Jpn.,72 (2003) 2334-2337
17) C.Uyeda M.Sakakibara and K.Tanaka, The Temperature Dependences of the Preferential Magnetic Alignment of the Magnetically Stable Axes Observed for Small Oxide Crystals Dispersed in a Fluid Medium, Jpn.J. Appl. Phys., 42 (2003) 581-L584.
18) C.Uyeda, M.Sakakibara and K.Tanaka, Temperature dependences of the magnetic rotation process of kaolinite micro-crystals containing paramagnetic impurity ions dispersed in liquid medium, Phys. Chem. Minerals,30 (2003),425-429.
19) C.Uyeda, T.Komatsu, M.Sakakibara and K.Tanaka, Magneto-Rotation Experiment of Diamagnetic Single-Crystals Suspended in the Gas Medium for Examining Dust Alignment in Interstellar Region. Astron. Astrophys. 400 (2003) 805-810

2004

1) T. Fukuda, T. Sakamoto, T. Kakeshita, T. Takeuchi and K. Kishio, Rearrangement of martensite variants in iron-based ferromagnetic shape memory alloys under magnetic field, Materials Transactions, 45 (2004), 188-192.
2) C.Uyeda, K.Tanaka and R.Takashima, Magnetic Alignment of Non-ferromagnetic Particles Caused by Paramagnetic and Diamagnetic Anisotropy Achieved at Low Field Intensity Due to Reduction of Temperature, Jpn.J. Appl. Phys., 42, (Part 1) (2004) 980-984.
3) C.Uyeda, K.Tanaka and R.Takashima, Magnetic Alignment of Micronsized Particles at Low Temperature Achieved on Particles Dispersed inHe Gas Medium, J. Phys. Soc. Jpn.,73 (2004) 296-497.
4) N. Okamoto, T. Fukuda, T. Kakeshita, T. Takeuchi and K. Kishio: Rearrangement of variants in Ni2MnGa under magnetic field, Science and Technology of Advanced Materials 5 (2004) 29-34
5) T. Sakamoto, T. Fukuda, T. Kakeshita, T. Takeuchi and K. Kishio : Giant magnetic field-induced strain due to rearrangement of variants in an ordered Fe3Pt, Science and Technology of Advanced Materials 5 (2004) 35-40
6) T. Fukuda, T. Sakamoto, T. Terai, T. Kakeshita and K. Kishio: Magnetization Process Associated with Rearrangement of Martensite Variants in Iron-Based Ferromagnetic Shape Memory Alloys, Mat. Res. Soc. Symp. Proc., 785 (2004) 421-426

7) T. Kakeshita and T. Fukuda: Control of microstructure by magnetic field in iron-based ferromagnetic shape memory alloys, Journal of Physics: Condensed Matter, 16 (2004) S5615-S5622
8) T. Murata, T. Terai, T. Fukuda, T. Kakeshita and K. Kishio]: Influence of Grain Boundary on Magnetoresistance in La0.7Ca0.3MnO3, Transactions of the Materials Research Society of Japan 29[7] (2004) 3099-3102.
9) T. Fukuda, T. Sakamoto, T. Inoue, T. Kakeshita and K. Kisho: Influence of Magnetic Field Direction on Recoverable Strain Due to Rearrangement of Variants in Fe3Pt, Transactions of the Materials Research Society of Japan 29[7] (2004) 3059-3060.
10) N. Okamoto, T. Fukuda, T. Kakeshita, T. Takeuchi and K. Kishio: Magnetic shear stress for the rearrangement of martensite variants in stoichiometric Ni2MnGa, Transactions of the Materials Research Society of Japan 29[7] (2004) 3061-3062.
11) T. Sakamoto, K. Yoshinaka, T. Fukuda, T. Kakeshita and K. Kishio: Rearrangement of Martensite Variants of Fe-31.2at.%Pd under Magnetic Field, Transactions of the Materials Research Society of Japan 29[7] (2004) 3057-3058.
12) T Terai, T Murata, T Fukuda and T Kakeshita: The influence of grain boundaries on the magnetoresistance in La0.7A0.3MnO3 (A = Ca, Sr) and La1.36Sr1.64Mn2O7, J. Phys.: Condens. Matter 16 (2004) S5801–S5806 PII: S0953-8984(04)79397-2
13) C.Uyeda, K.Tanaka and R. Takashima, Efficiency of Magnetic Alignment Detected for Non-magnetic Oxide Crystals Deriving from Individual Bonding Orbital, Trans. Matter. Res. Soc.Jpn. 29 (2004)1489.
14) K.Tanaka, C.Uyeda and R.Takashima, Development of a Method to Detect Magnetic Anisotropy with High Sensitivity in Micro-Gravity Condition, Trans. Matter. Res. Soc.Jpn. 29 (2004) 1221.
15) R.Takashima, K.Tanaka, and C.Uyeda, Magnetic Alignment of Nonmagnetic Mica Crystals Achieved at Low Field Intensity Due to High Concentration of Paramagnetic Ions, Trans. Matter. Res. Soc.Jpn. 29 (2004) 1056.

2005

1) M-S. Choi, T. Fukuda and T. Kakeshita, Anomalies in Physical Properties Related to the Stability of the B2-phase in Ti-Ni-Co Shape Memory Alloys, Materials Science Forum, 475-479 (2005) 1977-1982.
2) T. Kakeshita, T. Fukuda and T. Sakamoto, Magnetic Field-Induced Strain of Martensite and Parent Phases in a Ferromagnetic Shape Memory Iron-Palladium Alloy, Materials Science Forum, 475-479 (2005) 1999-2004.
3) N. Okamoto, T Fukuda, T Kakeshita and K Kishio, Temperature Dependence of Rearrangement of Martensite Variants in a Ferromagnetic Shape Memory Alloy Ni2MnGa, Materials Science Forum 475-479 (2005) 2021-2024.
4) M-S Choi, T. Fukuda, T. Kakeshita, Anomalies in resistivity, magnetic susceptibility and specific hat in iron-doped Ti-Ni shape memory alloys, Scripta Materialia 53 (2005) 869-873.
5) T. Sakamoto, T. Fukuda, T. Kakeshita and K. Kishio, Rearrangement of martensite variants under magnetic field applied along [001], [011] and [111] directions in Fe-31.2mol%Pd
International Journal of Applied Electromagnetics and Mechanics, 21 (2005) 163-169
6) J-h Kim, T. Taniguchi, T. Fukuda and T. Kakeshita, Effect of Hydrostatic Pressure on P-14M-2M and P-2M Martensitic Transformations in Single Crystalline Ni-Mn-Ga Ferromagnetic Shape Memory Alloys, Materials Transactions 46 (2005) 1928-1932
7) 阪本辰顕、福田隆、掛下知行, 強磁性形状記憶合金 Fe-31.2mol%Pd の一軸結晶磁気異方性定数ならびに双晶変形応力, 日本金属学会誌 69 (2005) 649-653.
8) T. Ohba, N. Miyamoto, K. Fukuda, T. Fukuda, T. Kakeshita and K. Kato, Fundamental structure of a Ni2MnGa intermediate phase having an orthorhombic structure, Smart Materials and Structures 14 (2005) S197-S200.
9) C.Uyeda, M.Skakibara, K.Tanaka and R.Takashima: Magnetic Alignment Experiment of Fine Graphite-Crystals Dispersed in He Gas Oriented to Study Alignment of Crystalline-Axes of Nano-sized Non-magnetic Particles. J. Electron Microscopy 43 (2005) 1-5
10) C.Uyeda, R. Takashima and K. Tanaka: Magneto-Rotation of Nonmagnetic Micro-crystals Caused by Diamagnetic Anisotropy, Appl. Phys. Lett., 28 (2005) 094103-1-3.
11) C Uyeda, R Takashima and K Hiraoka: Magnetic Alignment of Nonmagnetic Mica Crystals Achieved at Low Field Intensity Due to High Concentration of Paramagnetic Ions, Jpn. J. Appl. Phys. Pt2 44 (2005) L371.

2006

1) J-h Kim, T. Fukuda and T. Kakeshita, A new phase induced in Ni2MnGa by uniaxial stress, Scripta Materialia 54 (2006) 585-588.
2) J-h Kim, F. Inaba, T. Fukuda and T. Kakeshita, Effect of magnetic field on martensitic transformation temperature in Ni-Mn-Ga ferromagnetic shape memory alloys, Acta Materialia 54 (2006) 439-499.
3) M.-S Choi, T. Fukuda, T. Kakeshita and H. Mori, Incommensurate-commensurate transition and nanoscale domain-like structure in iron doped Ti-Ni shape memory alloys, Philosophical Magazine 86 (2006) 67-78.
4) T. Terai, N. Tamai, T. Fukuda and T. Kakeshita, Microstructure Formed by Charge Ordering Transition in Pr0.55Ca0.45MnO3 and Nd0.5Sr0.5MnO3, Materials Science Forum 512 (2006) 223-226
5) J-h Kim, T. Fukuda, T. Kakeshita, Martensitic transformation of Ni-Mn-Ga Alloys under Magnetic Field and Hydrostatic Pressure, Materials Science Forum, 512 (2006) 189-194.
6) M-S Choi, J. Ogawa, T. Fukuda and T. Kakeshita, Stability of the B2-type structure of Ti-Ni-Fe and Ti-Ni-Co shape memory alloys, Materials Science Forum, 512 (2006) 233-238.
7) T. Murata, T. Terai, T. Fukuda and T. Kakeshita, Magnetic Phase Diagram in Layered Perovskite Manganite La2-2xSr1+2xMn2O7 ($0.313 \leq x \leq 0.350$), Materials Science Forum, 512 (2006) 183-188.
8) T. Sakamoto, T. Fukuda and T. Kakeshita, Influence of Magnetic Field Direction and Temperature on Rearrangement of Martensite Variants in Fe-31.2at.%Pd, Materials Science Forum, 512 (2006) 201-204.
9) N. Okamoto, T. Fukuda, T. Kakeshita and T. Takeuchi, Magnetocrystalline anisotropy and twinning stress of 10M and 2M martensites in Ni-Mn-Ga system, Materials Science Forum, 512 (2006) 195-200.
10) C.Uyeda R. Takashima and K. Tanaka, Magneto-Rotation of Nonmagnetic Micro-crystals Caused by Diamagnetic Anisotropy, Appl. Phys. Lett.,86 (2005) 094103 1-3.
11) C. Uyeda, M. Mamiya, R. Takashima, T. Abe, H. Nagai and T. Okutani, Diamagnetic anisotropy detected by a magnetic oscillation in a drop capsule without suspending crystals with fiber, Jpn. J. Appl. Phys. 45 (2006) L124-127
12) C. Uyeda, T. Abe and R. Takashima, Magnetic anisotropy of ordinary crystals without spontaneous magnetic moments detected by rotational oscillations in a reduced field produced by a horseshoe magnet, Jpn. J. Appl. Phys. 46 (2006) 1397-1399.

国際会議

2003

1) T. Fukuda, T. Sakamoto, T. Terai, T. Kakeshita and K. Kisho, Magnetization process associated with rearrangement of martensite variants in iron-based ferromagnetic shape memory alloys, 2003 MRS Fall Meeting, Dec. 4 (2003), Boston.
2) T. Kakeshita and T. Fukuda, Effect of Magnetic Field on Rearrangement of Martensite Variants in Ferrous Shape Memory Alloys, IUMRS-ICAM 2003, Oct. 9 (2003), Yokohama.
3) T. Sakamoto, K. Yoshinaka, T. Fukuda, T. Kakeshita and K. Kishio, Rearrangement of Martensite Variants of Fe-31.2Pd under Magnetic Field, IUMRS-ICAM 2003, Oct. 9 (2003), Yokohama.
4) T. Fukuda, T. Sakamoto, T. Inoue, T. Kakeshita, Orientation Dependence of Magnetic Field Induced Strain in Fe3Pt Ferromagnetic Shape Memory Alloy, IUMRS-ICAM 2003, Oct. 9 (2003), Yokohama.
5) N. Okamoto, Y. Nakamura, T. Fukuda, T. Kakeshita, T. Takeuchi and K. Kishio, Rearrangement of Martensite Variants of Stoichiometric Ni2MnGa under Magnetic Field, IUMRS-ICAM 2003, Oct. 9 (2003), Yokohama.
6) T. Kakeshita, T. Fukuda and T. Terai, Conversion of Variants by Magnetic Field in Iron-Based Ferromagnetic Shape Memory Alloys, Thermec'2003, Madrid, Spain, July 7-11 (2003).
7) C.Uyeda, K.Tanaka and R. Takashima, Efficiency of Magnetic Alignment Detected for Non-magnetic Oxide Crystals Deriving from Individual Bonding Orbital, IUMRS Oct.8-13 (2003) Yokohama
8) K.Tanaka, C.Uyeda, M.Sakakibara and R.Takashima, Development of a Method to Detect Magnetic Anisotropy with High Sensitivity in Micro-Gravity Condition, IUMRS Oct.8-13 (2003) Yokohama
9) R. Takashima C.Uyeda and K.Tanaka, Magnetic Alignment of Micron-Sized Particles at Low Temperature Achieved on Particles Dispersed in He Gas, IUMRS Oct.8-13 (2003) Yokohama.

2004

1) T. Kakeshita, Rearrangement of martensite variants in iron-based ferromagnetic shape memory alloys under magnetic field, Workshop on interplay of magnetism and structure of functional materials, Feb. 10-13, Benasque, Spain.
2) T. Fukuda and T. Kakeshita, Anomalies in magnetic susceptibility, electrical resistivity, and heat

capacity of Ti-Ni with B2-type structure, Workshop on interplay of magnetism and structure of functional materials, Feb. 10-13, Benasque, Spain.
3) T. Kakeshita, Martensitic transformation in some ferrous alloys under magnetic field, International workshop on materials analysis & processing in magnetic field, Mar. 17 (2004), Tallahassee, FL, USA.
4) T. Sakamoto, T. Fukuda, T. Kakeshita and K. Kishio, Influences of Magnetic Field and External Stress on Rearrangement of Martensite Variants in Fe-Pd, The First International Symposium on Intelligent Artifacts and Bio-systems (1st INABIO), Sendai, Japan, Feb. 24-25 (2004).
5) T. Sakamoto, T. Fukuda and T.Kakeshita: Magnetostriction of Fe-Pd and Fe3Pt with tweed structure, XIII International materials research congress (Aug. 2004, Cancun).
6) T. Fukuda and T. Kakeshita, Condition for rearrangement of martensite variants under magnetic field in ferromagnetic shape memory alloys, XIII International materials research congress (Aug. 2004, Cancun).
7) Jae-hoon Kim, T. Fukuda and T. Kakeshita: Effect of magnetic field on martensitic transformation temperature in Ni-Mn-Ga alloys, XIII International materials research congress (Aug. 2004, Cancun).
8) Mi Seon Choi, T. Fukuda and T. Kakeshita: Anomalies in Physical Properties Related to the Stability of the B2-phase in Ti-Ni-Co Shape Memory Alloys, The Fifth Pacific Rim International Conference on Advanced Materials and Processing (Nov. 2-5, 2004 Beijing).
9) T.Kakeshita, T. Fukuda and T. Sakamoto, Magnetic Field-Induced Strain of Martensite and Parent Phases in a Ferromagnetic Shape Memory Iron-Palladium Alloy: The Fifth Pacific Rim International Conference on Advanced Materials and Processing (Nov. 2-5, 2004 Beijing).
10) Nariaki Okamoto, T. Fukuda, T. Kakeshita and Kohji Kishio: Temperature Dependence of Rearrangement of Martensite Variants in a Ferromagnetic Shape Memory Alloy Ni2MnGa, The Fifth Pacific Rim International Conference on Advanced Materials and Processing (Nov. 2-5, 2004 Beijing).

2005

1) T. Kakeshita, T. Fukuda and T. Takeuchi, Energy evaluation for twinning plane movement driven by magnetic field in ferromagnetic shape memory alloys, Int. Conf. on Martensitic Transformations, June 14-17 (2005), Shanghai.
2) T. Fukuda, T. Kakeshita and K. Kindo, Effect of high magnetic field and uniaxial stress at cryogenic temperatures on phase stability of some austenitic stainless steels, Int. Conf. on Martensitic Transformations, June 14-17 (2005), Shanghai.
3) T. Terai, N. Tamai, T. Fukuda and T. Kakeshita, Crystallographic domain structures associated with charge ordering transition in $Pr_{0.55}Ca_{0.45}MnO_3$ and $Nd_{0.5}Sr_{0.5}MnO_3$, Int. Conf. on Martensitic Transformations, June 14-17 (2005), Shanghai.
4) T. Sakamoto, T. Fukuda and T. Kakeshita, Influence of temperature on rearrangement of martensite variants by magnetic field in Fe_3Pt, Int. Conf. on Martensitic Transformations, June 14-17 (2005), Shanghai.
5) J-h Kim, T. Fukuda and T. Kakeshita, Effects of magnetic field and hydrostatic pressure on martensitic transformation temperature of Ni-Mn-Ga ferromagnetic shape memory alloys, Int. Conf. on Martensitic Transformations, June 14-17 (2005), Shanghai.
6) M-S Choi, J. Ogawa, T. Fukuda and T. Kakeshita, Stability of the B2-type structure and R-phase transformation behavior of Fe or Co doped Ti-Ni alloys, Int. Conf. on Martensitic Transformations, June 14-17 (2005), Shanghai.
7) N. Okamoto, T. Fukuda, T. Kakeshita and T. Takeuchi, Magnetocrystalline anisotropy constant and twinning stress in martensite phase of Ni-Mn-Ga, Int. Conf. on Martensitic Transformations, June 14-17 (2005), Shanghai.
8) T. Ohba, M. Mitsuka, T. Fukuda, T. Kakeshita and M. Tanaka, Martensitic Transformation in FePd alloy revealed by synchrotron radiations, Int. Conf. on Martensitic Transformations, June 14-17 (2005), Shanghai.
9) J-h Kim, T. Fukuda, T. Kakeshita, Martensitic transformation of single crystalline Ni_2MnGa under compressive stress, E-MRS Fall meeting, Sep 5-9 (2005) Warsaw Poland.
10) T. Kakeshita and T. Fukuda, Energy Evaluation for Twinning Plane Movement under Magnetic Field in Ferromagnetic Shape Memory Alloys, E-MRS Fall meeting, Sep 5-9 (2005) Warsaw Poland.
11) T. Fukuda and T. Kakeshita, Selection of variants by magnetic field in some ferromagnetic alloys, Int. Symp. on Magneto-Science 2005, Nov.14-17 (2005) Yokohama.
12) T. Kakeshita, and T. Fukuda, Martensitic Transformation and Rearrangement of Varians in Some Ferromagnetic Shape Memory Alloys under Magnetic Field, 2005 MRS Fall Meeting, Nov. 27 (2005) Boston.

13) T. Kakeshita and T. Fukuda, Control of crystallographic domains by magnetic field in some ferromagnetic alloys, Pacific Chem 2005, Dec. 17 (2005) Waikiki.
14) R. Takashima, T. Abe and C. Uyeda, Magnetic Alignment of Magnetic Silicate Crystals Achieved at Low Field Intensities below 1 mT in Star Formation Regions Caused by Paramagnetic Impurity Ions. Int. Symp. on magnetic field effects on materials, Nov. 11-12 (2005) Yokohama.
15) T. Abe, R. Takashima1 and C. Uyeda, The Role of Water Molecules and Hydrogen Bonds on Magnetic Alignments Observed for Popular Diamagnetic Crystals Including Hexagonal Ice. Int. Symp. on magnetic field effects on materials, Nov. 11-12 (2005) Yokohama.
16) C. Uyeda, M. Mamiya, R. Takashima, T. Abe, H. Nagai and T. Okutani, Detection of Small Magnetic Anisotropy using Micro-gravity and Diamagnetic Anisotropy Deriving From a Single Chemical Bond in Inorganic Oxides. Int. Symp. on magnetic field effects on materials, Nov. 11-12 (2005) Yokohama.

解説・書籍等

2004

1) 掛下知行：期待される強磁性形状記憶合金，金属，74, No.2 (2004) 127-131.

2005

1) 掛下知行、福田隆：鉄基合金のマルテンサイト変態に及ぼす磁場効果，鉄と鋼，91 (2005) 363-375.
2) 福田隆、掛下知行、竹内徹也：強磁性形状記憶合金における磁場によるマルテンサイトバリアントの再配列と巨大歪，まてりあ 44(2005) 285-291.
3) 土谷浩一、及川勝成、福田隆、掛下知行：ホイスラー型強磁性形状記憶合金，まてりあ 44 (2005) 642-647.

2006

1) T. Kakeshita and T. Fukuda Magnetic field-induced martensitic transformation in ferrous alloys, Magneto-Science, Kodansha-Springer, (in print).

(7) 研究課題キ

雑誌論文

2003

1) H. Morita, F. Matsubayashi, and A. Nozue, Photochemical sensitization and magnetic field effect on ultrafine particle formation from a gaseous mixture of glyoxal and carbon disulfide, Mol. Phys., 101 (2003) 2569-2574.
2) H. Morita, H. Nomura, and Y. Kita, Photochemical fine particle formation from gaseous ternary mixtures under visible light irradiation, J. Photopolym. Sci. Technol., 16 (2003) 109-114.
3) H. Yonemura, S. Moribe, K. Hayashi, M. Noda, H. Tokudome, S. Yamada, N. Nakamura, Photo-induced intramolecular electron-transfer reactions in carbazole-fullerene and phenothiazine-fullerene linked compounds in benzene and benzonitrile as studied by fluorescence, transient absorption, time-resolved EPR, and magnetic field effects, Appl. Magn. Reson., 23 (2003) 289-307.

2004

1) H. Morita, T. Kumagai, and Z. Bastl, Magnetic field effect on photochemical thin film formation from a gaseous mixture of trimethyl(2-propynyloxy)silane and glyoxal, J. Photopolym. Sci. Technol., 17 (2004) 53-59.
2) H. Yonemura, H. Nobukuni, S. Moribe, S.Yamada, Y. Fujiwara, Y. Tanimoto, Magnetic field effects on the decay rates of triplet biradical photogenerated from intramolecular electron-transfer in a zinc-tetraphenylporphyrin-fullerene linked compound, Chem. Phys. Lett., 358 (2004) 417-422.
3) S. Moribe, H. Yonemura, and S. Yamada, Temperature dependence on magnetic field effects on the decay rates of biradical photogenerated from intramolecular electron-transfer in a phenothiazine-C_{60} linked compound, Chem. Phys. Lett., 398 (2004) 427-433.
4) H. Inaba , T. Saitou, K. Tozaki, and H. Hayashi, Effect of the magnetic field on the melting transition of H_2O and D_2O measured by a high resolution and super-sensitive differential scanning calorimeter, J. Appl.

Phys., 96 (2004) 6127-6132.

2005

1) H. Morita, K. Semba , Z. Bastl , J. Šubrt, and J. Pola, N_2 laser-induced formation of copolymeric ultrafine particles in a gaseous tetraethenylgermane-carbon disulfide mixture, J. Photochem. Photobiol. A: Chem., 171 (2005) 21-26.

2) H. Morita and H. Ishikura, Morphological control of deposits from a gaseous mixture of allyltrimethylsilane and iron pentacarbonyl, J. Photopolym. Sci. Technol., 18 (2005) 193-198.

3) Y. Mouri, Y. Fujiwara, T. Aoki, H. Yoshida, K. Naka, Y. Aoki, H. Yonemura, S. Yamada, T. Haino, Y. Fukazawa, and Y. Tanimoto, High magnetic field effects on biradical lifetimes: evaluation of magnetic field dependence and chain length dependence using calculated g and hyperfine tensors, Bull. Chem. Soc. Jpn., 78 (2005) 804-813.

4) S. Wang, K. Tozaki, H. Hayashi and H. Inaba, Nano-watt stabilized DSC and its applications, J. Therm. Anal. Cal., Vol. 79 (2005) 605-613.

5) H. Hayashi, C. Nonaka, K. Tozaki, H. Inaba, and C. Uyeda, Effect of the magnetic field on the ferroelectric transition of KD2PO4 measured by a high resolution and super-sensitive differential scanning calorimeter, Thermochimica Acta 431 (2005) 200-204.

6) H. Hayashi, K. Tozaki, C. Ikeuchi, and H. Inaba, Phase transitions in dipalmitoylphosphatidylcholine - water and dipalmitoylphosphatidylcholine - CaCl2 aqueous solution system by means of a high resolution and high-sensitive differential scanning calorimeter, Thermochimica Acta 431 (2005) 205-211.

7) M. Zeng, H. Hayashi, and H. Inaba, Simultaneous measurements of dielectric constant and heat flux on the phase transition of a single crystalline BaTiO3, Thermochimica Acta 439 (2005) 135-141.

2006

1) H. Morita, R. Nozawa, Z. Bastl , J. Šubrt , and J. Pola, Photochemical synthesis of ultrafine organosilicon particles from trimethyl(2-propynyloxy)silane and carbon disulfide, J. Photochem. Photobiol. A: Chem., 179 (2006) 142-148.

2) H. Morita, R. Nozawa, and Z. Bastl, Magnetic field effect on photochemical synthesis of ultrafine organosilicon particles from a gaseous mixture of trimethyl(2-propynyloxy)silane and carbon disulphide, Mol. Phys., 104 (2006) (in press).

3) H. Morita, Y. Takeyasu, H. Okamura, and H. Ishikawa, Magnetic field effect on gas-phase synthesis of metal-containing ultrafine particles from iron pentacarbonyl and carbon disulfide, Sci. Technol. Advanced Materials, 7 (2006), (in press).

4) S. Moribe, H. Yonemura, and S. Yamada, Photoinduced electron-transfer and magnetic-field effects on the decay rates of photogenerated biradicals in a phenothiazine-C_{60} linked compound with six methylene groups: temperature dependence, Comptes Rendus Chimie 9 (2006) 247–253.

5) H. Yonemura, N. Kuroda, S. Moribe, and S. Yamada, Photoinduced electron-transfer and magnetic field effects on the dynamics of the radical pair in a C_{60} cluster–phenothiazine system, Comptes Rendus Chimie 9 (2006) 254–260.

6) H. Yonemura, S. Harada, S. Moribe, S. Yamada, H. Nakamura, Y. Fujiwara, and Y. Tanimoto, Magnetic field effects and time-resolved EPR studies on photogenerated biradical from intramolecular electron transfer reactions in zinc-tetraphenylporphyrin-C_{60} linked compounds: contribution of relaxation mechanism due to spin-spin relaxation, Mol. Phys. 104 (2006) (in press).

7) M. Minohara, K. Tozaki, H. Hayashi, and H. Inaba, Effect of the magnetic field on the melting transition of Ga and In measured by a nW-stabilized differential scanning calorimeter, J. Therm. Anal. Cal. (2006) (in press).

国際会議

2003

1) H. Yonemura, S. Moribe, N. Kuroda, K. Hayashi, S. Yamada, H. Nakamura, Y. Araki, and O. Ito, Photoinduced electron transfer reactions, magnetic field effects on the decay process of charge-separated state, and time-resolved EPR spectra in fullerene-donor systems, 203rd Meeting of the Electrochemical Society, April 27-May 2 (2003) Paris, France.

2) S. Moribe, H. Yonemura, M. Noda, K. Hayashi, and S. Yamada, Photoinduced intramolecular electron-transfer reactions in phenothiazine-fullerene linked compounds as studied by fluorescence, transient absorption, magnetic field effects, and time-resolved EPR, 5th CMC-Kyushu Chemistry Symposium,

May 9 (2003) Seoul, Korea.
3) H. Yonemura, S. Moribe, H. Nobukuni, M. Noda, K. Hayashi, and S. Yamada, Magnetic field effects on the decay rates of triplet biradical photogenerated from intramolecular electron-transfer in donor-fullerene linked systems, XXIst International Conference on Photochemistry, July 26-31 (2003) Nara, Japan.
4) Y. Fujiwara, J. Hamada, Y. Tanimoto, H. Yonemura, S. Moribe, H. Nobukuni, and S. Yamada, High magnetic field effect on lifetimes of biradicals generated by photo-induced intramolecular electron transfer in electron donor-acceptor (C60) linked compounds, XXIs[t] International Conference on Photochemistry, July 26-31 (2003) Nara, Japan.
5) S. Moribe, M. Noda, H. Yonemura, and S. Yamada, Magnetic field effect on photogenerated biradicals in phenothiazine-fullerne linked compounds, XXIst International Conference on Photochemistry, July 26-31 (2003) Nara, Japan.
6) Y. Fujiwara, J. Hamada, Y. Tanimoto, H. Yonemura, S. Moribe, H. Nobukuni, and S. Yamada, High magnetic field effects on lifetimes of biradicals generated by photo-induced intramolecular electron transfer in donor-acceptor (C60) linked compounds, The 8th International Symposium on Spin and Magnetic Field Effects in Chemistry and Related Phenomena, September 21-26 (2003), the Carolina Inn in Chapel Hill, North Carolina, USA.

2004
1) S. Moribe, H. Yonemura, and S. Yamada, Magnetic field effects on intramolecular electron-transfer reactions in phenothiazine-C_{60} linked compounds: effects of spacer-chain length and temperature, 15th International Conference on Photochemical Conversion and Storage of Solar Energy, July 4-9 (2004) Paris, France.
2) H. Yonemura, N. Kuroda, S. Moribe, and S. Yamada, Photoinduced electron-transfer and magnetic field effects on the dynamics of radical pair photogenerated between C_{60} cluster and phenothiazine, 15th International Conference on Photochemical Conversion and Storage of Solar Energy, July 4-9 (2004) Paris, France.
3) S. Moribe, H. Yonemura, and S. Yamada, Magnetic field effects on photogenerated biradical in phenothiazine-C_{60} linked compounds: dependence of spacer chain length and temperature, The 1st International Symposium on Functional Innovation of Molecular Informatics, October 13-15 (2004) Fukuoka, Japan.
4) H. Inaba, S. Wang, K. Tozaki, and H. Hayashi, Nano-watt stabilized DSC for the measurements with high resolution and high sensitivity, The 18th IUPUC International Conference on Chemical Thermodynamics, August 17-21 (2004) Beijing, China.
5) H. Inaba, T. Saitou, M. Minohara, K. Tozaki, and H. Hayashi, Magnetic effect on the phase transitions of diamagnetic substances measured by a nW-stabilized DSC, 13th International Conference on Thermal Analysis and Calorimetry, September 12-19 (2004) Chia Laguna, Italy.
6) H. Inaba, S. Wang, K. Tozaki, and H. Hayashi, Performance of a nano-watt stabilized DSC, 13th International Conference on Thermal Analysis and Calorimetry, September 12-19 (2004) Chia Laguna, Italy.

2005
1) H. Morita, R. Nozawa, Z. Bastl, and J. Pola, Magnetic field effect on chemical compositions of ultrafine particles produced from a gaseous mixture of organosilicon compound and CS_2, Spin Chemistry Meeting (SPM) 2005, Sep. 11-17 (2005) Oxford, UK.
2) H. Morita and S. Kanaya, Excitation wavelength dependence and magnetic field effect on ultrafine particle formation from a gaseous mixture of glyoxal and CS_2, Spin Chemistry Meeting (SPM) 2005, Sep. 11-17 (2005) Oxford, UK.
3) H. Morita, H. Tonooka, and Y. Okano, Magnetic field effect on morphology of photochemical products from a gaseous mixture of trimethylsilylacetylene and iron pentacarbonyl, International Symposium on Magneto-Science 2005 (ISMS2005), Nov. 14-17 (2005) Yokohama, Japan.
4) H. Morita, H. Ishikura, and H. Tonooka, Morphological control of photochemical products deposited from gaseous molecules, International Chem. Congress of Pacific Basin Societies (Pacifichem2005), Dec. 16 (2005) Honolulu, Hawaii, U.S.A.
5) H. Morita, A. kasai, Y. Takeyasu, and K. Abe, Magnetic field effect on gas-phase synthesis of metal-containing ultrafine particles, International Chem. Congress of Pacific Basin Societies (Pacifichem2005),

Dec. 17 (2005) Honolulu, Hawaii, U.S.A.
6) H. Yonemura, S. Moribe, S. Harada, S. Yamada, Y. Fujiwara, Y. Mouri, J. Hamada, and Y. Tanimoto, Magnetic field effects on the decay rates of photogenerated biradical in donor-C_{60} linked compounds: contribution of spin-spin relaxation mechanism, Spin Chemistry Meeting 2005, Sep. 11-17 (2005) Oxford, UK.
7) H. Yonemura, N. Kuroda, Y. Wakita, and S. Yamada, Magnetic field effects on photoelectrochemical reactions of modified electrodes with nanocluster of C_{60}-phenothiazine system, The 12th International Conference on Unconventional Photoactive Systems, Oct. 2-6 (2005) Sendai, Japan.
8) S. Moribe, H. Yonemura, S. Yamada, and S. Tero-Kubota, Photoinduced intramolecular electron transfer reactions and magnetic field effects on the photogenerated biradical in phenothiazine-C_{60} linked systems, 2005 Korea-Japan Symposium on Frontier Photoscience "Photochemistry and Nanotechnorogy", Oct. 7-11 (2005) Busan, Korea.
9) H. Yonemura, Y. Yomamoto, S. Yamada, Y. Fujiwara, and Y. Tanimoto, Magnetic orientation and organization of single-walled carbon nanotubes or their composite materials using polymer wrapping, International Symposium on Magneto-Science 2005 (ISMS 2005), Nov. 14-17 (2005) Yokohama, Japan.
10) Y. Yamamoto, H. Yonemura, S. Yamada, Y. Fujiwara, and Y. Tanimoto, Magnetic alignment of single-walled carbon nanotubes/polymer composites and photoelectrochemical properties, The 12th Molecular System Symposium, Nov. 17-18 (2005) Kyushu University, Japan.
11) H. Yonemura, Y. Yomamoto, S. Yamada, Y. Fujiwara, and Y. Tanimoto, Orientation and organization of composite materials based on single-walled carbon nanotubes by use of strong magnetic fields as a new tool, International Chem. Congress of Pacific Basin Societies (Pacifichem2005), Dec. 15-20 (2005), Honolulu, Hawaii, U.S.A.

2006
1) H. Yonemura, S. Moribe, S. Harada, S. Yamada, Y. Mouri, J. Hamada, Y. Fujiwara, and Y. Tanimoto, Novel magnetic field effects on the decay rates of photogenerated biradical in donor-C_{60} linked compounds, XXIst IUPAC Symposium on Photochemistry, April 2-7 (2006), Kyoto, Japan. (発表予定)
2) Y. Yomamoto, H. Yonemura, S. Yamada, Y. Fujiwara, and Y. Tanimoto, Magnetic orientation and photo- electorochemical reaction of single-walled carbon nanotube/conjugated polymer composites, XXIst IUPAC Symposium on Photochemistry, April 2-7 (2006), Kyoto, Japan. (発表予定)

解説・書籍等
2003
1) H. Yonemura, S. Moribe, H. Nobukuni, M. Noda, K. Hayashi, S. Yamada, H. Nakamura, Y. Araki, and O. Ito, Photoinduced electron-transfer reactions, magnetic field effects on the lifetimes of charge-separated state, and time-resolved EPR spectra in donor-fullerene systems, Fullerenes, 13, 175-186 (The Electrochemical Society) (2003).

2004
1) 米村弘明、ドナー - C_{60} 連結化合物の光誘起電子移動反応及び光電極反応の磁場制御, 電子スピンサイエンス, Vol. 2 (2004) pp.74 -79.
2) 森田　浩、金属ナノ粒子の合成・調製、コントロール技術と応用展開（米澤　徹　監修）第6章　第3節：金属ナノ粒子の配列・固定化・パターニング技術：二次元配列と磁場制御技術、pp. 112-120、技術情報協会、(Dec. 22, 2004).

2005
1) 米村弘明、磁場印加による電子移動過程制御と新規光機能ナノ材料の創製, 電気化学および工業物理化学、Vol. 78 No. 6, (2005) pp.450-454.
2) 稲場秀明、東崎健一、林英子、王紹蘭、ナノワット安定化 DSC の開発とその応用、熱測定 32 No.2, 77-85 (2005).

2006
1) 米村弘明、ナノ構造と光特性に及ぼす強磁場効果、化学と教育、Vol. 54, No. 1, (2006) pp. 20-23.
2) 米村弘明、有機または無機ナノ粒子を用いた薄膜の作製と光機能の磁場制御、Material Stage, 5月号(2006)（印刷中）.

3) H. Morita, Magnetic field effects on photo-induced ultrafine particle formation in gas phase, Magneto-Science, Kodansha-Springer, (in print).
4) H. Yonemura, Magnetic field effects in photo-sensitive electrodes, Magneto-Science, Kodansha-Springer, (in print).
5) H. Inaba, Magnetic field effects on the phase transitions in diamagnetic materials, Magneto-Science, Kodansha-Springer, (in print).

(8) 研究課題ク

雑誌論文

2003

1) Q.-K.Yu, Y.Miyakita, S.Nakabayashi, and R.Baba, Magnetic Field Effect on Electrochemical Oscillations during Iron Dissolution, Electrochem.Comm. 5 (2003) 321-324.
2) E.D. Mishina, N.E. Sherstyuk, V.I. Stadnichuk, K.A. Vorotilov, V.A. Vasilev, A.S. Sigov, O.M. Zhigalina, N. Ohta, S. Nakabayshi, Ferroelectrics templated in nanoporous silicon membranes, Ferroelectrics, 286, 205-211 (2003).
3) E. Mishina, Q.-K. Yu, T. Tamura, H. Sakaguchi, A. Karantonis, and S. Nakabayashi, Kinetic profile of adsorption and self-assembling of thiophene oligomers studied by optical second harmonic generation, Surf. Sci. 544, 269-277 (2003).
4) E.D.Mishina, N. Tanimura, S. Nakabayashi, O.A. Aktsipetrov, M. Downer, Photomodulated second harmonic generation at silicon-silicon oxide interface: from modeling to application, Jap. J. Appl. Phys. 42, Part1, 6731 (2003).
5) E. Mishina,, T. Tamura, H. Sakaguchi, and S. Nakabayashi, Kinetics of adsorption and self-assembling of thiophene and dodecanethiol studied by optical second harmonic generation, Chemistry Letters, 32, 652-653 (2003).
6) F. D. Morrison, Y. Luo, I. Szafraniak, V. Nagarajan, R. B. Wehrspohn, M. Steinhart, J. H. Wendroff, N. D. Zakharov, E. D. Mishina, K. A. Vorotilov, A.S. Sigov, S. Nakabayashi, M. Alexe, R. Ramesh, and J. F. Scott, Ferroelectric nanotubes, Rev. Adv. Mat. Sci. 4, 1-9 (2003).
7) A. Karantonis, M. Pagitsas, Y. Miyakita, S. Nakabayashi, From Excitatory to Inhibitory Connections in networks of Discrete Electrochemical Oscillators, J.Phys.Chem.B, 107, 14622–14630 (2003).
8) F. Iwata, K. Mikage, H. Sakaguchi, M. Kitao and A. Sasaki, Current-sensing scanning near-field optical microscopy using a metal probe for nanometer-scale observation of electrochromic film, J. Microscopy, 210,(2003) 241-246.
9) T. Matsumura, H. Sakaguchi, Y. Shimoyama, Formation kinetics and structure of self-assembled poly(3-alkylthiophene) films on gold surface, Journal of Materials Science: Materials in Electronics, 14, (2003) 353-356.
10) Bin Zhao, L.A. Guzman, Kaoru Ogawa and Kenji Shimizu, Effect of Magnetic Field on the Growth Rate of L-Alanine Crystal, J. Chem. Eng. Japan, 36, 8, 959-962 (2003)

2004

1) H. Hosoda, H. Mori, N. Sogoshi, A. Nagasawa and S. Nakabayashi, Refractive Indices of Water and Aqueous Electrolyte Solutions under High Magnetic Fields, J.Phys.Chem.B 108 (2004) 1461-1464.
2) V. Moshnyaga, A. Giske and K Samwer, E. Mishina, T. Tamura, and S.Nakabayashi, A. Belenchuk, O. Shapoval, and L. Kulyuk "Giant negative photoconductivity in La0.7Ca0.3MnO3 thin films," J.Appl.Phys. 95, 7360-7362 (2004).
3) A. Karantonis, M. Pagitsas, Y. Miyakita and S. Nakabayashi, In-phase, anti-phase and fractured synchrony in ring networks of coupled relaxiation electrochemical oscillators, J.Phys.Chem.B., 108 5836 (2004).
4) E. Mishina, T. Tamura, H. Sakaguchi, L.Kulyuk, S.Nakabayashi, Photoluminescence studies of oligothiophene self-assembled monolayers at low excitation energy, J. Chem. Phys., 120,9763 -9768(2004).
5) K. Kitajima, T. Fujita, N. Sogoshi, S. Nakabayashi, Synthesis of Magnetic Composite Particles of g-Fe2O3@SiO2 and the Comtrolof the Structural Color of the Colloidal Crystal by Magnetic Fields, ChemLett.1106-1107 (2004)
6) Elena D. Mishina, Vladimir I. Stadnichuk, Alexandr S. Sigov, Yuriy I. Golovko, Vladimir M.

Mukhorotov, S.Nakabayashi, H. Masuda, D. Hashizume and A. Nakao, Ferroelectriv nano-structure suputtered an alumina membranes, Physica E, 25, 35-41 (2004).
7) Elena D.Mishina, Galina A. Tsirlina, Elena V. Timofeeva, Nataliya E. Sherstyuk, Marina I.Borzenko, N. Tanimura, S. Nakabayashi, O. A. Petrii, Adlayers of Keggin type polytungstate anions on platinum: electrochemically invisible being' and manifestations of molecular upd', J. Phys. Chem. B (2004) 108, 17096-17105.
8) E. Mishina, T. Tamura, H. Sakaguchi, L. Kulyuk and S. Nakabayashi, Photoluminescence Studies of Oligothiophene Self-assembled Monolayers at Low Excitation Energy, Journal of Chemical Physics, 120, pp.9763 -9768 (2004).
9) H. Sakaguchi, H. Matsumura and H. Gong, Electrochemical Epitaxial Polymerization of Single Molecular Wires, Nature Materials, 3, pp.551-557 (2004).
10) K. Ogawa, L.A. Guzman and K. Shimizu, Surface Topography of Growing L-Alanine Crystal in Magnetic Field, J. Chem. Eng. Japan, 37, 6, 791-795 (2004).
11) Bin Zhao, L. A. Guzman, K. Ogawa and K. Shimizu, Effect of Magnetic Gradient on the Growth Rate of L-alanine Crystal, IEEE Transactions on Applied Superconductivity, 14, 2, 1596-1599 (2004)
12) K. Ogawa, L.A. Guzman and K. Shimizu, Surface Topography of Growing L-Alanine Crystal in Magnetic Field, J. Chem. Eng. Japan, 37, 6, 791-795 (2004).
13) Bin Zhao, L. A. Guzman, K. Ogawa and K. Shimizu, Effect of Magnetic Gradient on the Growth Rate of L-alanine Crystal, IEEE Transactions on Applied Superconductivity, 14,2, 1596-1599 (2004)

2005
1)Y. Miyakita, S. Nakabayashi, A. Karantonis, Spatiotemporal Coding in an Electrochemical Oscillator Network, Phys.Rev.E, 71, 056207 1-9(2005).
2) M. Fujita, Y. Miyakita, N. Sogoshi, S. Nakabayashi, M. Ishii, Electrochemical Deposition of Stacked Layers of Cu2O/Cu/Cu2O and Rendering of Structural Colors, Trans. Mat. Res. Soc. Jpn. 30(4), 1041-1044 (2005).
3)Y. Terui, M.i Fujita, Y. Miyakita, N. Sogoshi, and S. Nakabayashi, Photoluminescence of Electrochemically-Deposited Granular Cu2O Films, Trans. Mat. Res. Soc. Jpn. 30(4), 1049-1052 (2005).
4) A. Karantonis, M. Pagitas, Y. Miyakita, S. Nakabayashi, Manupilation of Spatio-temporal Patterns in Networks of Relaxation Electrochemical Oscillators, Electrochem. Acta., 50, 5056 (2005).
5) H. Sakaguchi, H. Matsumura, H. Gong and A. Abouelwafa, Direct visualization of the formation of single-molecule conjugated copolymers, Science, 310, (2005) 1002-1006.
6) B. Q. Xu, X. L. Li, X. Y. Xiao, H. Sakaguchi and N. J. Tao, Electromechanical and conductance switching properties of single oligothiophene molecules, Nano Letters, 5(7), (2005) 1491-1495.

2006
1) A.s Karantonis, M. Pagitas, Y. Miyakita, S. Nakabayashi, Synchronization Phenomena in Networks of Coupled Relaxation Electrochemical Oscillators, Journal of Bifurcation and Chaos (2006) (in press).

国際会議
2003
1) A. Karantonis, M. Pagitsas, Y. Miyakita and S. Nakabayashi, Primitive information manipulation by networks of coupled relaxation electrochemical oscillators, Dynamics Days 2003 Europe, P-31, Sep. 24-27 (2003) University of the Balearic Islands, Spain.

2004
1) Y. Miyakita, A. Karantonis and S. Nakabayashi, Spatiotemporal Dynamics in Networks of Discrete Electrochemical Oscillators, Dynamics Days 2004, Jan. 2-5(2004) North Carolina, USA.
2) K. Kitajima, N. Sogoshi, and S. Nakabayashi, Magnetic tuning of colloidal crystal color, Particles 2004 Particle Synthesis, Characterization, and Particle-Based Advanced Materials, Mar. 6-9 (2004) Orlando, Florida.
3) S. Nakabayashi, Refractive Indices of Water and Aqueous Electrolyte Solutions Under High Magnetic Fields, International Workshop on Materials Analysis and Processing in Magnetic Fields, Mar. 17-19 (2004) Tallahassee, Florida.
4) Moshnyaga, A. Giske and K Samwer, E. Mishina, T. Tamura, and S. Nakabayashi, A. Belenchuk, O. Shapoval, and L. Kulyuk, Giant negative photoconductivity in $La_{0.7}Ca_{0.3}MnO^{-3}$ thin films, 9-th Joint MMM-InterMag Conference, (2004)Anahiem.

2005
1) S. Nakabayashi, International Symposium on Next-generation nanotechnology on MEMS and Nano/Bio Technology, Towards Iron Brain/; Ensamble functions of the non-linear electrochemical oscillators, Dec9/2005 NTT Musashino R&D Center.

2006
1) H. Sakaguchi, Electrochemical epitaxial polymerization of single-molecular wires, Handai Nanoscience & Nanotechnology Int. Symp., Jan. 30-Feb.1 (2006) Osaka (Invited).
2) S.Nakabayashi, Water in the high magnetic field, effects for the bulk and adsorbed molecules, MAP2, March 19-22(2006) Grenoble.

解説・書籍等
2003
1) 坂口浩司, 光とナノ技術を用いる単一分子電気計測, 分析化学, 52, (2003) 383-392.
2) 坂口浩司, 光と金属探針を用いる単一分子電気計測, 電気化学および工業物理化学, 71, (2003) 131-135.
3) 宮北康之、カラントニス・アントニス、中林誠一郎, 連成非線形電気化学振動子；集団挙動と神経系ネットワークの相関, 電気化学および工業物理化学, 71, 332-336 (2003).

2004
1) 小川薫、清水健司、磁場環境でのＬ－アラニンの結晶成長、日本海水学会誌 58, 5, 462-474 (2004).
2) 小川薫、清水健司、光センサーおよび磁場を利用して形態制御した結晶をつくる、化学工学 68, 12, 726-728 (2004).
3) 中林誠一郎、宮北康之, A. Karantonis, 電極表面の非線形現象, 表面化学, 25, 104-109 (2004)

2005
1) 坂口浩司, 電気を流すプラスチックの単一分子細線, 化学と工業, 58(3), 233-234 (2005).
2) 曽越宣仁、中林誠一郎、強磁場下での水の溶液物性と電気化学, Electrochemistry, 73, 445-449 (2005.
3) 坂口浩司, 次世代電子デバイスとして期待されるナノレベル細線の制御技術, 工業材料, 53(9), (2005) pp.43-45.
4) S.Nakabayashi and N.Sogoshi, "Refractive Indices of Water and Aqueous Electrolyte Solutions under High Magnetic Fields" in "Materials Processing in Magnetic Fields" Edited by H.Wada and H.J.Schneider-Muntau, World Scientific (2005).

2006
1) 中林誠一郎、曽越宣仁、水と強磁場との相互作用；屈折率に見る水素結合ネットワークへの磁場効果, 化学と教育, 54, 8-11, (2006).
2) 坂口浩司、導電性ナノワイヤー, 「ナノオプティクス・ナノフォトニクス」, フロンティア出版, 分担執筆 (印刷中).
3) 坂口浩司、ナノレベルの極微配線技術, 「進化する有機半導体」エヌティーエス出版, 分担執筆, 印刷中.
4) S.Nakabayashi and N,Sogoshi magnetic field effects on optical properties of water and aqueous electrolyte solutions, in Magneto-Science, Kodansha-Springer, (in print).

９．特許

1) 発明者：米村弘明，山本裕一，山田淳，谷本能文，藤原好恒，発明の名称：繊維状材料の配列材料の製造方法，及び，繊維状材料の配列材料，特願 2005-256890 号，出願年月日：平成 17 年 9 月 5 日．
2) 発明者：勝木明夫，発明の名称：磁化率勾配による境界面制御下での反応方法，特願：NI0500036，出願年月日：平成 17 年 9 月 29 日．
3) 発明者：植田千秋，公開特許：微結晶体の配向方法及び微結晶配向集合体の製造方法，特開 2005-162563，公開日：平成 17 年 6 月 23 日．
4) 発明者：上村太一，杉谷雅夫，熊倉昌義，木村恒久，発明の名称：磁場を用いたパターン形成方法および電子装置の製造方法，特開 2005-317930，出願年月日：平成 17 年 3 月 15 日，取得年月日：平成 17 年 11 月 10 日．
5) 発明者：山登正文，武喜郎，木村恒久，発明の名称：磁場配向した結晶性高分子組成物の製造方法，特開 2005-68249，出願年月日：平成 15 年 8 月 21 日，取得年月日：平成 17 年 3 月 17 日．
6) 発明者：渡會仁，木村恒久，飯国良規，発明の名称：キャピラリ電磁泳動吸脱着クロマトグラフィおよびその装置，特開 2005-17214，出願年月日：平成 15 年 6 月 27 日，取得年月日：平成 17 年 1 月 20 日．
7) 発明者：櫻井伸一，辻佳宏，木村恒久，山登正文，木村史子，発明の名称：配向したシリンダー構造を有するブロック共重合体膜およびその製造方法，特願 2005-326221，出願年月日：平成 17 年 11 月 10 日．
8) 発明者:木村 恒久，吉野真司，出願人:木村 恒久，発明の名称：磁場による精密配向体の製造方法，特許出願 2004－242818，出願年月日:平成 16 年 8 月 23 日，特許公開 2006－57055，公開日:平成 18 年 3 月 2 日．

１０．主催した学術会合

(1) 第１回領域全体会議 2003/09/06（実施計画、研究計画の確認、東京都，国際文化会館，参加者 50 名）.
(2) 第１回公開シンポジウム 2003/12/19（テーマ「強磁場でなにができるか」，東京都，日本化学会会館，参加者 100 名）.
(3) 第１回研究会 2004/03/05（平成 15 年度研究成果報告、東京都，国際文化会館，参加者 50 名）.
(4) 第２回研究会 2004/07/09-10（集中討論テーマ「水は磁場と相互作用するか」，長野県，松本市浅間温泉文化センター，参加者 104 名）.
(5) 分子構造総合討論会 2004 シンポジウム「磁気科学の最前線」2004/09/28(広島県，広島国際会議場，参加者約 100 名，分子構造総合討論会に協賛）.
(6) 磁気科学合同シンポジウム 2004 および第 2 回公開[強磁場新機能]公開シンポジウム 2004/12/01-03（テーマ「高磁気力の世界」，神奈川県，横浜国立大学教育文化センター，参加者 204 名，新磁気科学研究会と共催）.
(7) 第３回研究会 2005/03/04（集中討論テーマ「結晶・組織材料の方向を磁場でそろえる・強磁場での新機能創出」，神奈川県，横浜国立大学大学院工学研究棟、参加者 65 名）.
(8) 第４回研究会 2005/07/01（集中討論テーマ「ナノデバイスと磁場」，千葉県、千葉大学けやき会館，参加者 70 名）.
(9) International Symposium on Magneto-Science 2005 (ISMS2005)2005/11/14-17(神奈川県，横浜国立大学教育文化センター，新磁気科学研究会と共催）磁気科学合同シンポジウム 2005 および第３回公開[強磁場新機能]公開シンポジウム）（参加者 200 名）.
(10) 第２回領域全体会議 2006/03/03（最終成果の評価，東京都，学士会館，参加者 60 名）.